

**Effect of 3'-fluoro substitution and loop modification in
2'-phosphodiester-linked thrombin-binding aptamer
(TBA) on its structure and function**

Thesis Submitted to AcSIR

For the Award of the Degree of

DOCTOR OF PHILOSOPHY

In

CHEMICAL SCIENCES



By

Manisha Nilkanth Aher

(Registration Number: 10CC17J26024)

Under the guidance of

Dr. Moneesha Fernandes

Co-Supervisor

Dr. Vaijayanti A. Kumar

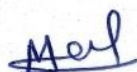
**Division of Organic Chemistry,
CSIR-National Chemical Laboratory,
Pune, India.**

July, 2020

CERTIFICATE

This is to certify that the work incorporated in this Ph.D. thesis entitled “**Effect of 3’-fluoro substitution and loop modification in 2’-phosphodiester-linked thrombin-binding aptamer (TBA) on its structure and function**” submitted by **Mrs. Manisha Nilkanth Aher** to Academy of Scientific and Innovative Research (**AcSIR**) in fulfillment of the requirements for the award of the Degree of Doctor of Philosophy, embodies original research work under our supervision. We further certify that this work has not been submitted to any other University or Institution in part or full for the award of any degree or diploma. Research material obtained from other sources has been duly acknowledged in the thesis. Any text, illustration, table etc., used in the thesis from other sources, have been duly cited and acknowledged.

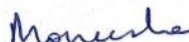
It is also certified that this work done by the student, under our supervision, is plagiarism free.



Manisha Nilkanth Aher

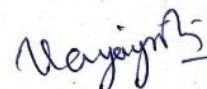
(Research Student)

AcSIR Enrolment No.
10CC17J26024



Dr. Moneesha Fernandes

(Research Supervisor)



Dr. Vaijayanti Kumar

(Research Co-Supervisor)


Date - 09/07/2020

Place - CSIR-NCL, Pune

Declaration

I hereby declare that the this thesis entitled, “**Effect of 3'-fluoro substitution and loop modification in 2'-phosphodiester-linked thrombin-binding aptamer (TBA) on its structure and function**” submitted for the degree of Doctor of Philosophy to the **Academy of Scientific and Innovative Research (AcSIR)** has been carried out by me at the Organic Chemistry Division, CSIR-National Chemical Laboratory, Pune-411008, India, under the supervision of **Dr. Moneesha Fernandes (Supervisor)** and **Dr. Vaijayanti A. Kumar (Co-Supervisor)**. Any material as has been obtained by other sources has been duly acknowledged in this thesis. I declare that the present work or any part thereof has not been submitted to any other university or institute for the award of any degree or diploma.

Date: 09/07/2020
CSIR-National Chemical Laboratory
Pune - 411008


Manisha Nilkanth Aher
(Research Student)

Dedicated to My Family



Acknowledgement

Any human accomplishment is the culmination of numerous contributions and endeavors. The present thesis is no exception. My thesis would not have been possible without the support, guidance and help of several individuals who in one way or another contributed and extended their valuable assistance in my journey towards completion of this phase in my life. I wish to thank all the people whose assistance was a milestone in the completion of my thesis.

It gives me immense pleasure to express my deep sense of gratitude to my research supervisor Dr. Moneesha Fernandes for her advice, guidance, support and encouragement during every stage of this work. I do sincerely acknowledge freedom rendered to me by her for independent thinking, planning and executing the research. Throughout my thesis writing period, she provided encouragement, sound advice, good teaching. Her receptive attitude will always remain a source of inspiration for me.

I have utmost gratitude to my co-supervisor Dr. Vaijayanti Kumar for her incessant guidance, perspicacious thoughts, constructive criticism, wonderful analysis and her great efforts to explain things clearly and simply. Her enthusiasm, patience and accomplishments for teaching, research and life in general have been truly inspirational. It has been a great opportunity to work under such an experienced and caring teacher. It was a challenging time but you made it easier. I couldn't have done it without you.

I would also like to thank my DAC members, Dr. Narendra Kadoo, Dr. Ashish Bhattacharya and Dr. M. Muthukrishnan for their insightful suggestion, encouragement and evaluation of my research work.

My sincere thanks to Dr. Anil Kumar for all the help during the course of this work. I gratefully acknowledge Mrs. Anita Gunjal, for encouragement and especially for teaching me handling of the DNA synthesizer for oligonucleotide synthesis.

I owe my deepest gratitude to Dr. R. A. Joshi, Dr. (Mrs.) R. R. Joshi and Dr. (Mrs.) V. S. Pore who provided me an opportunity to join their team as project assistance. Their valuable advice, friendly help, kind support and encouragement gave me untiring help during my stay in NCL. Their endorsement is beyond any words. I am thankful for their love and support. I also extend my sincere thanks to Dr. C. V. Ramana for enlightening me the first glance of research.

I take this opportunity to offer my sincere appreciation to Dr. G. J. Sanjayan and Dr. N. P. Argade for their support in all the ways.

I am grateful to my friend Dr. Namrata Erande, who has been my support system during all these years. Her constant piece of advice helped me to stay on track of work. She has always been available for discussion, proposal writing, experimental design, manuscript corrections, and what not. This work was not possible without her constant support and help.

I take this opportunity to express my deep sense of gratitude and heartfelt thanks to Dr. Ayesha Khan, Professor, Department of chemistry, Savitribai Phule Pune University, Pune, for her unconditional support and kindness.

I am also very much thankful to Dr. Shanta Kumari and group members for their excellent support in MALDI-TOF and HRMS analysis. The kind support from NMR group and the LC-MS facility, Organic Chemistry Division are also greatly acknowledged. Thanks to Dr. Rajesh Gonnade for the X-ray analysis. I would like to express my whole hearted thanks to Mr. Gati Nayak, Senior technical officer, library for his active help and providing me the opportunity to utilize their resources for completion of this thesis.

My sincere thanks to Student Academic Office and Division of Organic Chemistry at CSIR-NCL for their help. I would extend my sincere thanks to Vaishali, Komal and Vijaya for support at crucial times, for the smooth documentation process and help during my doctoral studies.

Acknowledgement

I extend my sincere thanks to Head of Organic Chemistry Division and Director, CSIR-National Chemical Laboratory, Pune for providing all necessary infrastructural facilities to complete my work successfully. Financial support from CSIR in the form of SRF is duly acknowledged.

I would like to take this opportunity to thank Dr. Atul Kulkarni, Director, Jankalyan blood bank, Pune and Mr. Milind Jituri for guidance and initial help to carry out anticoagulation experiments.

Thanks to all my labmates Komal, Harsha, Dr. Ragini, Aniket, Atish, Sanyami, Jayesh and Preeti for kind co-operation for maintaining a warm and cheerful atmosphere in the lab. Thanks for the endless discussions, cheerful company and for the wonderful times we shared, specially evening tea, birthday parties and outside lunch and dinner parties. I admire the co-operation of my lab seniors who have taught me many things. I thank Dr. Anjan, Dr. Venu, Dr. Manoj, Dr. Harshit, Dr. Tanaya, Dr. Seema, Dr Kiran, Dr. Govind, and Dr. Amit. I thank Mr. Bhumkar and Mr. Gurav for the laboratory assistance.

I would like to express my thanks and appreciation to my friends Dr. Savita Shingote and Dr. Lalita Roy for motivating me towards my goal.

I extend huge thanks to my M.Sc friends Mrs. Sarika Mohite Patil and Dr. Suparn Tambe for their kind help in my societal project (NCL-403).

I am especially thankful to my friend Mrs. Sandhya Jagdale and Dr. Arun Jagdale for unconditional support and help which they provided like a family.

I feel great sense of gratitude for my teacher Bonde madam (Mrs. Kalpana Bonde) from my graduation days; who made me a better, more thoughtful person

I owe my reverential gratitude to my parents, Aai and Anna for inspiring me, believing in me and supporting me at each important stage of my life. They have been my teachers since childhood, right from nursery. It is their teachings that have made me capable enough to be able to write a PhD thesis today.

It is impossible to express my sense of gratitude for my Mother in law (Tai) and Father in law (Nana) in mere words. I wish to thank them for their encouragement and unconditional support.

Words fall short to thank my brothers Dada (Pravin), Lalit and my sister Surekha, and brothers-in law- Machhindra and Yogesh and sisters-in-law Arunatai, Chhaya, Anita and Minakshi for their never ending encouragement and support

And most of all, I owe my deepest gratitude to my husband, Dr. Nilkanth Aher, for his affection, encouragement, understanding and patience. He supported me without any complaint or regret that enabled me to complete my Ph.D. thesis. My thesis acknowledgement would be incomplete without thanking my son, Om (Sharvil), whose smiling face always made me happy, I owe you lots and lots fun hours. Words can never say how grateful I am to both of you.

At last but not the least, I thank whole heartedly, the omnipotent God, for His kindness because I firmly believe that it is He who has shown me the path to reach where I am today. His constant blessings have helped me stride through the troubled waters and always stand firm behind me. I truly appreciate everyone's help and I thank the ones whose contribution I may not have mentioned here because every little contribution provided by anyone was crucial for the completion of this study.

Manisha Nilkanth Aher

Contents

General remark	i
Abbreviation	iii
Abstract	vi

Chapter 1

1	Introduction to Guanine-rich nucleic acid aptamers with a focus on the Thrombin binding aptamer (TBA)	
1.1	Introduction to nucleic acids: A structural overview.....	1
1.2	Base pairing and structures of DNA.....	2
1.2.1	The double helix.....	2
1.2.2	Triplex structure.....	2
1.2.3	Quadruplex structure -The 'G-quadruplex'.....	3
1.3	Sugar puckering in nucleotides	3
1.3.1	Steric effect	4
1.3.2	Stereoelectronic effect	4
1.3.2.1	Anomeric effect	5
1.3.2.2	Gauche effect.....	5
1.4	Base-stacking.....	6
1.5	Isonucleic Acids.....	6
1.6	Sugar ring conformations in 3'-5' Vs 2'-5'-linked oligomers.....	7
1.7	Quadruplex-forming DNA	8
1.7.1	G-quadruplex structure	9
1.7.2	Variations on the G-quadruplex theme (Polymorphism)	10
1.7.2.1	Strand stoichiometry.....	10
1.7.2.2	Strand polarity polymorphism.....	10
1.7.2.3	Glycosidic torsion angle variation.....	11
1.7.2.4	Connecting loops.....	11
1.8	Quadruplex stability dependence on metal ions.....	12
1.9	Aptamers: An emerging class of therapeutics.....	12
1.10	The G-quadruplex in aptamers.....	14
1.10.1	Anticoagulation aptamer target: Thrombin (Master enzyme of hemostasis)	14

1.10.2	Thrombin binding aptamer (TBA) – More than a simple aptamer...	15
1.10.3	TBA- Thrombin interaction.....	16
1.10.4	TBA quadruplex stability, dependence on cations.....	16
1.11	Modifications in TBA	17
1.11.1	Modifications in the G tetrads.....	17
1.11.2	Sugar modification.....	18
1.11.3	Sugar-phosphate backbone modification in TBA loops	20
1.12	Solid-phase synthesis of oligonucleotides: Brief history and application in oligonucleotide synthesis.....	23
1.13	Tools and techniques for structural and stability studies of nucleic acid complexes and higher-ordered G-quadruplexes.....	25
1.13.1	UV-spectroscopy.....	25
1.13.2	Circular Dichroism (CD)	26
1.13.3	Polyacrylamide gel electrophoresis (PAGE)	27
1.13.4	MALDI TOF Mass Spectrometry	28
1.13.5	High-performance liquid chromatography (HPLC)	28
1.14	Present work.....	29
1.15	References.....	32

Chapter 2

2	S/N-type frozen 3'-Deoxy, 3'-fluoro nucleosides in non-genetic 2'-5'-linked thrombin binding aptamer (<i>iso</i>TBA)	
2.1	Introduction.....	40
2.2	Sugar ring conformation of C2' and C3' fluoro substituted (α/β) nucleos(t)ides.....	41
2.3	Rationale, design and objectives of the present work.....	43

Section A

Synthesis of S/N-type-frozen 3'-deoxy-3'-ribo/xylo fluoro thymidine (^RT^F and ^XT^F) and 3'-deoxy-3'-ribo/xylo fluoro uridine (^RU^F and ^XU^F) nucleosides

2.4	Present work	47
2.4.1	Synthesis of S-type monomer: 3'-Deoxy-3'-ribofluoro thymidine phosphoramidite (^R T ^F) and 3'-Deoxy-3'-ribofluoro uridine phosphoramidite (^R U ^F).....	47
2.4.1.1	Synthesis of 3-deoxy-3-fluoro-1- <i>O</i> -methyl-2- <i>O</i> - acetyl - 5- <i>O</i> -benzoyl- ribofuranoside	48

2.4.1.2	Synthesis of 3'-deoxy-3'-ribofluoro thymidine phosphoramidite monomer (^R T ^F).....	49
2.4.1.3	Synthesis of 3'-deoxy-3'-ribofluoro uridine phosphoramidite monomer (^R U ^F)	50
2.4.2	Synthesis of N-type monomer: 3'-Deoxy-3'-xylofluoro thymidine phosphoramidite (^X T ^F) and 3'-Deoxy-3'-xylofluoro uridine phosphoramidite (^X U ^F)	51
2.4.2.1	Synthesis of 3-deoxy-3-fluoro-1,2,5-tri- <i>O</i> -acetyl-D-xylofuranose	51
2.4.2.2	Synthesis of 3'-deoxy-3'-xylofluoro thymidine phosphoramidite monomer (^X T ^F)	53
2.4.2.3	Synthesis of 3'-deoxy-3'-xylofluoro uridine phosphoramidite monomer(^X U ^F)	53
2.4.3	Preliminary study of sugar pucker using ¹ H NMR <i>J</i> _{1'2'} coupling constant	54
2.4.4	X-ray crystal structure of modified nucleoside analogue, 3'-deoxy-3'-fluoro-2'-hydroxy-thymidine (^R T ^F)	55

Section B

3'-Deoxy, 3'-fluoro nucleosides in the thrombin binding aptamer (TBA): Evaluation of stability and activity

2.4.5	Synthesis of TBA, <i>iso</i> TBA and modified <i>iso</i> TBA variants, their purification and characterization.....	60
2.4.6	Evaluation of G-quadruplex formation and stability in the presence of monovalent ions by circular dichroism spectroscopy.....	62
2.4.6.1	G-quadruplex topology.....	62
2.4.6.2	Evaluation of G-quadruplex thermal stability using CD spectroscopy.....	63
2.4.7	Formation of G-quadruplex in the presence of thrombin	65
2.4.8	Antithrombin effect of modified aptamers.....	67
2.4.9	Stability of oligonucleotides towards exonucleases	68
2.5	Key highlights of this study.....	70
2.6	Conclusion.....	70
2.7	Experimental.....	71
2.7.1	Experimental procedures and spectral data.....	71
2.7.2	Oligonucleotide synthesis.....	92
2.7.3	Purification and characterization.....	92
2.7.3.1	High-performance liquid chromatography.....	92

2.7.3.2	Polyacrylamide gel electrophoresis study.....	92
2.7.3.4	MALDI-TOF characterisation.....	93
2.8	Biophysical technique-CD spectroscopy.....	93
2.9	Thrombin time measurements for clotting inhibition (antithrombin effect)..	93
2.10	Exonuclease stability study.....	94
2.11	Appendix A.....	95
2.12	References.....	156

Chapter 3

3	Truncated loops in 3'-5' linked TBA Vs 2'-5' linked <i>iso</i>TBA: Effect on quadruplex topology and thrombin binding	
3.1	Introduction.....	162
3.2	Rationale and objectives of the present work.....	162
3.3	Present work, results and discussion.....	165
3.3.1	Synthesis of TBA, <i>iso</i> TBA and TBA/ <i>iso</i> TBA variants with truncated loops, their purification and characterization.....	165
3.3.2	Evaluation of G-quadruplex formation and topology using circular dichroism spectroscopy.....	166
3.3.3	Evaluation of G-quadruplex thermal stability using circular dichroism spectroscopy.....	171
3.3.4	Evaluation of G-quadruplex topology by UV-Thermal Difference Spectra.....	174
3.3.5	Polyacrylamide Gel Electrophoresis (PAGE) study.....	175
3.3.6	Binding with Thrombin (Chaperone Effect of Thrombin)	177
3.3.7	Nuclease stability study-Exonuclease stability.....	181
3.4	Key highlights of this study.....	183
3.5	Conclusions.....	183
3.6	Experimental	184
3.6.1	Synthesis of oligonucleotides, Purification and characterization....	184
3.6.2	Biophysical techniques.....	184
3.4.2.1	CD spectroscopy.....	184
3.4.2.2	UV experiments for Thermal difference spectra.....	184
3.6.3	Polyacrylamide gel electrophoresis (PAGE) experiments.....	185
3.6.4	Snake venom phosphodiesterase stability experiments.....	185
3.7	Appendix B.....	186
3.8	References.....	192

Chapter 4

4	Effect of 2'-5' and 3'-5' linkages in the loop region of TBA and <i>iso</i>TBA respectively, on G-quadruplex stability and function	
4.1	Introduction	196
4.2	Sugar phosphate backbone linkages in G - quadruplexes	197
4.3	Rationale and objectives of the present work.....	199
4.4	Present work, results and discussion.....	200
4.4.1	Synthesis of TBA, <i>iso</i> TBA and modified TBA variants with mixed backbone, their purification and characterization.....	200
4.4.2	Evaluation of G-quadruplex formation in the presence of monovalent cations by circular dichroism spectroscopy.....	201
4.4.3	Evaluation of G-quadruplex thermal stability using CD spectroscopy	204
4.4.3.1	CD Thermal stability in presence of K ⁺ ions.....	204
4.4.3.2	CD Thermal stability in the presence of Na ⁺ ions.....	206
4.4.4	Formation of G-quadruplex in the presence of thrombin	206
4.4.5	Antithrombin effect of chimeric aptamers.....	209
4.4.6	Stability of oligonucleotides towards exonuclease and endonuclease	210
4.4.6.1	Exonuclease resistance.....	210
4.4.6.2	Endonuclease resistance.....	212
4.5	Key highlights of this study.....	215
4.6	Conclusion.....	215
4.7	Experimental.....	216
4.7.1	Synthesis of oligonucleotides, Purification and characterization....	216
4.7.2	Endonuclease stability.....	216
4.8	Appendix C.....	217
4.9	References.....	225

- All the reagents were purchased from Sigma-Aldrich and used without further purification.
- DMF, ACN, were dried over P₂O₅ and CaH₂ respectively and stored by adding 4 Å molecular sieves. Pyridine, TEA were dried over KOH and stored on KOH.
- Reactions were monitored by TLC. TLCs were run in either Petroleum ether with appropriate quantity of EtOAc or DCM with an appropriate quantity of MeOH for most of the compounds. TLC plates were visualized with UV light and/or by spraying perchloric acid solution and heating.
- Usual reaction work up involved sequential washing of the organic extract with water and brine followed by drying over anhydrous Na₂SO₄ and evaporation of the solvent under vacuum. Column chromatographic separations were performed using silica gel 60-120 mesh (Merck) or 200- 400 mesh (Merck) and using the solvent systems EtOAc/Petroleum ether or MeOH/DCM. TLC was run using pre-coated silica gel GF254 sheets (Merck 5554).
- ¹H and ¹³C NMR spectra were obtained using Bruker AC-200, AC-400 and AC-500 NMR spectrometers. The chemical shifts (δ/ppm) are referred to internal TMS for ¹H and chloroform-*d* for ¹³C NMR. ¹H NMR data are reported in the order of chemical shift, multiplicity (s, singlet; d, doublet; t, triplet; br, broad; br s, broad singlet; m, multiplet and/ or multiple resonance), number of protons.
- Mass spectra were recorded on a Q Exactive Hybrid Quadrupole Orbitrap Mass spectrometer (Thermo Fisher Scientific).
- DNA oligomers were synthesized on CPG solid support using Bioautomation MerMade 4 synthesizer. The 2'-deoxy-3'-phosphoramidites were obtained from ChemGenes and 3'-deoxy-2'-phosphoramidites from Glen Research. Universal columns procured from Bioautomation.
- RP-HPLC on C-18 column using Waters system (waters Delta 600e quaternary solvent delivery system, 2998 photodiode array detector and Empower2 chromatography software)
- MALDI-TOF spectra were recorded on a SCIEX TOF/TOF 5800 system, and the matrix used for analysis was THAP (2, 4, 6-trihydroxyacetophenone) /Ammonium citrate (2:1).

- UV experiments were carried out on a Varian Cary 300 UV-Visible spectrophotometer equipped with a Peltier-controlled cell holder.
- CD spectra were recorded on a Jasco J-815 spectropolarimeter equipped with a Peltier-controlled cell holder.

μL	Microliter
μM	Micromolar
A	Adenine
A	Absorbance
Å	Angstrom
Ac_2O	Acetic anhydride
ACE	Acetone
ACN	Acetonitrile
AcOH	Acetic acid
ADA	Allose-diacetonide
aq.	Aqueous
Bz	Benzoyl
C	Cytosine
Calc.	calculated
Cat.	Catalytic/catalyst
CD	Circular Dichroism
Conc.	Concentrated
CPG	Controlled Pore Glass
DEPT	Distortionless Enhancement by Polarization Transfer
DCA	Dichloroacetic acid
DCM	Dichloromethane
DAST	Diethylammonium sulphur trifluoride
DMTr-Cl	4, 4'-dimethoxytrityl chloride
DIPEA/DIEA	Diisopropylethylamine
DMAP	4',4'-Dimethylaminopyridine
DMF	<i>N,N</i> -dimethylformamide
DMSO	<i>N,N</i> -Dimethyl sulfoxide
DNA	2'-deoxyribonucleic acid
ds	Double stranded
DI	Deionized
3D	Three Dimensional
EDTA	Ethylenediaminetetraacetic acid
EtOH	Ethanol
EtOAc	Ethyl acetate
g	gram
G	Guanine

GDA	Glucose-diacetonide
h	Hours
HIV	Human Immuno Difficiency Virus
HPLC	High Performance Liquid Chromatography
Hz	Hertz
HRMS	High Resolution Mass Spectrometry
L	liter
LCMS	Liquid Chromatography-Mass Spectrometry
LNA	Locked Nucleic Acids
MALDI-TOF	Matrix Assisted Laser Desorption-Time-Of-Flight
MeOH	Methanol
MF	Molecular formula
mg	milligram
MHz	Megahertz
min	minutes
M	Molar
mL	milliliter
mM	millimolar
mmol	millimoles
MS	Mass spectrometry
MW	Molecular weight
N-type	North type
ng	nongenetic
nm	Nanometer
NMR	Nuclear Magnetic Resonance
Obsd.	Observed
ONs	Oligonucleotides
ORTEP	Oak Ridge Thermal Ellipsoid Plot Program (molecular modeling)
ppm	Parts per million
PO-oligo	Phosphodiester-oligomer
PS-oligo	Phosphorothioate-oligoer
Py	Pyridine
PNA	Peptide Nucleic Acid
Pet-ether	Petroleum ether
PCC	Pyridinium chlorochromate

RNA	Ribose Nucleic Acid
R _f	Retention factor
RP	Reversed Phase
rt	Room temperature
RP-HPLC	Reversed Phase-HPLC
ss	Single stranded
s	Second
SVPD	Snake Venom Phosphodiesterases
T	Thymine
TBA	Thrombin binding aptamer
TEAA	Triethyl ammonium acetate
TEA/Et ₃ N	Triethylamine
TFA	Trifluoroacetic acid
THAP	2', 4', 6'-trihydroxyacetophenone
TLC	Thin layer chromatography
TMSOTf	Trimethylsilyltrifluoromethanesulfonate
TNA	α-L-Threose nucleic acid
<i>T_m</i>	Melting temperature
U	Uracil
UV-Vis	Ultraviolet-Visible
XRD	X-ray Diffraction

Name of the Candidate:	Ms. Manisha Nilkanth Aher
AcSIR Enrolment No. & Date:	Ph. D. in Chemical Sciences (10CC17J26024); January 2017
Title of the Thesis:	Effect of 3'-fluoro substitution and loop modification in 2'-phosphodiester-linked thrombin-binding aptamer (TBA) on its structure and function
Research Supervisor:	Dr. Moneesha Fernandes
Research Co-Supervisor:	Dr. Vaijayanti A. Kumar

Abstract

The Thesis entitled "**Effect of 3'-fluoro substitution and loop modification in 2'-phosphodiester-linked thrombin-binding aptamer (TBA) on its structure and function**" has been divided into four chapters.

Chapter 1: Introduction to Guanine-rich nucleic acid aptamers with focus on the Thrombin binding aptamer (TBA)

Chapter 2: S/N-type frozen 3'-deoxy, 3'-fluoro nucleosides in non-genetic 2'-5' linked thrombin binding aptamer (*iso*TBA)

Section A: Synthesis of S/N-type-frozen 3'-deoxy-3'-ribo/xylofluoro thymidine (^RT^F and ^XT^F) and 3'-deoxy-3'-ribo/xylofluoro uridine (^RU^F and ^XU^F) nucleosides

Section B: 3'-deoxy 3'-fluoronucleosides in the thrombin binding aptamer (TBA): Evaluation of stability and activity

Chapter 3: Truncated loops in 3'-5' linked TBA Vs 2'-5' linked *iso*TBA: Effect on quadruplex topology and thrombin binding

Chapter 4: Effect of 2'-5' and 3'-5' linkages in the loop region of TBA and *iso*TBA respectively, on G quadruplex stability and function

Chapter 1: Introduction to Guanine-rich nucleic acid aptamers with focus on the Thrombin binding aptamer (TBA)

This chapter briefly describes the structure of nucleic acids, the different kinds of hydrogen bonding between the canonical nucleobases and the sugar puckering in nucleic acids. The common higher order nucleic acid structures and parameters that control the stability of these structures are presented.

The recent two decades have seen significant work in the field of aptamer technology mainly focused on G-quadruplex forming aptamers. A particular folded

sequence which specifically binds to a target biomolecule is termed as an aptamer. Guanine-rich DNA/RNA aptamers can fold into three-dimensional G-quadruplex structures by stacking of two or more guanine quartets upon each other, and are constructed by one, two or four guanine-rich oligonucleotide strands. G-quadruplex strand orientation and polymorphism is discussed in this chapter. The thrombin-binding aptamer 5'-GGTTGGTGTGGTTGG-3' (TBA) is a G-quadruplex forming 15 mer DNA oligonucleotide. It was discovered by the SELEX process, selectively binds to thrombin (enzyme in the blood coagulation process) and inhibits its action. This chapter presents a brief review about the research focused on the development of new TBA derivatives with improved anticoagulant properties as well as the use of TBA as a model compound for the study of quadruplex structure.

The principles of tools and techniques for structural and stability studies of nucleic acid complexes including higher-ordered G-quadruplexes, such as UV-spectroscopy, Circular Dichroism (CD) spectroscopy, Polyacrylamide gel electrophoresis (PAGE), MALDI TOF mass spectrometry are outlined.

Chapter 2: S/N-type frozen 3'-deoxy, 3'-fluoro nucleosides in non-genetic 2'-5' linked thrombin binding aptamer (*iso*TBA)

The 2'-5' linked ONs (figure 1) are a unique class of oligonucleotides for potential therapeutic applications since they exhibit high resistance to nuclease digestion.

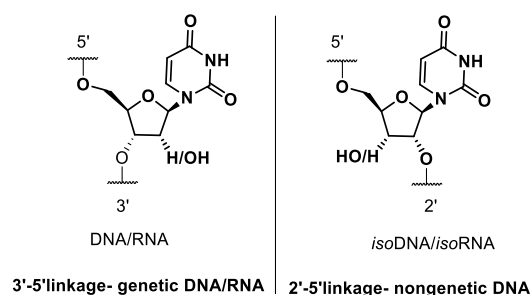


Figure1: Structures of natural DNA, RNA and *iso*DNA

We planned the synthesis of conformationally frozen nucleosides and their incorporation in 3'-deoxy-2'-5'-ONs (*iso*TBA) in order to improve the thermal stability and nuclease resistance of G-quadruplex forming *iso*TBA. As there is no conclusive experimental evidence in the literature for the preferred sugar geometries in *iso*TBA strands, we selected in this work to study either nucleoside analogues that would be in either N-type or S-type frozen conformation (figure 2).

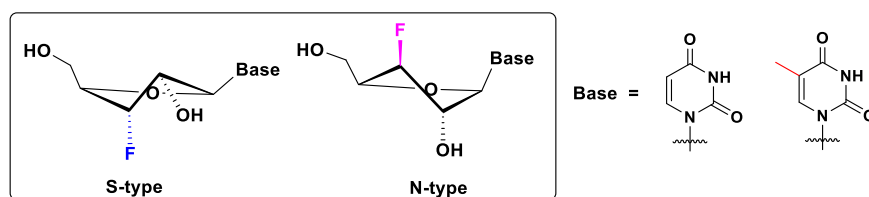
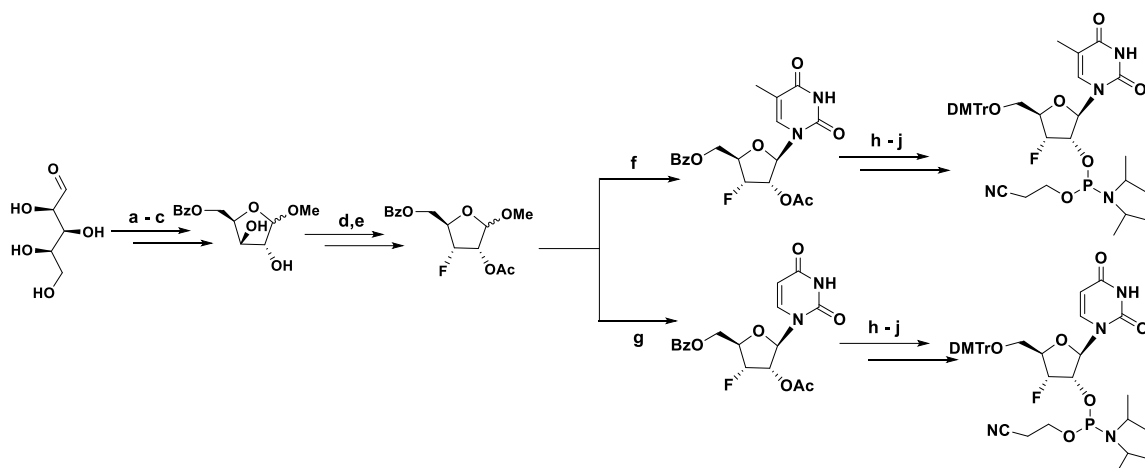


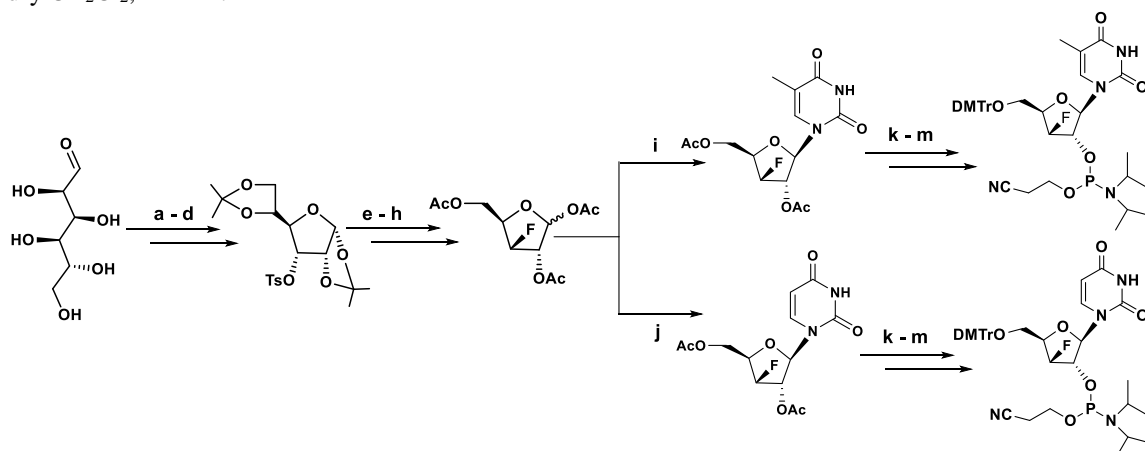
Figure 2: Sugar puckering for 3'-deoxy-3'-fluoro ribo/xylo nucleoside

Section A: Synthesis of S/N-type-frozen 3'-deoxy-3'-ribo/xylofluoro thymidine ($R^T F$ and $X^T F$) and 3'-deoxy-3'-ribo/xylofluoro uridine ($R^U F$ and $X^U F$) nucleosides

Herein, we report the synthesis and conformational analysis of monomers frozen in the N-type or S-type sugar conformation (Schemes 1&2). The synthesis of N-type frozen monomer is briefly outlined in Scheme 1 starting from D-xylose, while the synthesis of the S-type frozen monomer is outlined in Scheme 2, starting from D-glucose.



Scheme 1: a) Acetone, conc. H_2SO_4 , Na_2CO_3 ; b) $BzCl$, dry CH_2Cl_2 , $0^\circ C$; c) I_2 , MeOH, reflux; d) DAST, dry CH_2Cl_2 ; e) Ac_2O , pyridine; f) N,O-Bis (trimethylsilyl) acetamide, TMS-Triflate, thymine, ACN, reflux; g) N, O-Bis (trimethylsilyl) acetamide, TMS-Triflate, uracil, ACN, reflux; h) aq. NH_3 , MeOH: H_2O (4:1), $50^\circ C$; i) DMTr-Cl, DMAP, pyridine; j) 2-cyanoethyl-N,N-diisopropylchlorophosphine, dry CH_2Cl_2 , DIPEA.



Scheme 2: a) $CuSO_4$, acetone, conc. H_2SO_4 (cat.); b) PCC, dry CH_2Cl_2 , molecular sieves; c) $NaBH_4$, MeOH: H_2O (4:1); d) $TsCl$, pyridine; e) KF , acetamide, $210^\circ C$; f) $AcOH:H_2O$ (1:1), $50^\circ C$; g) $NaIO_4$, MeOH, $NaBH_4$; h) Ac_2O , $AcOH$, Conc. H_2SO_4 ; i) N, O-Bis (trimethylsilyl) acetamide, TMS-Triflate, thymine, ACN, reflux; j) N, O-Bis (trimethylsilyl) acetamide, TMS-Triflate, uracil, ACN, reflux; k) aq

NH₃, MeOH:H₂O (4:1), 50°C; l) DMTr-Cl, DMAP, pyridine; m) 2-cyanoethyl-N,N-diisopropylchlorophosphine, dry CH₂Cl₂, DIPEA.

Conformational analysis of the nucleoside analogues:

The sugar conformations of S/N-type conformationally frozen 3'-deoxy-3'-fluoro ribo/xylothymidine nucleosides (^RT^F and ^XT^F) and 3'-deoxy-3'-fluoro ribo/xyloouridine nucleosides (^RU^F and ^XU^F) were compared based on the homonuclear ³J_{H1'-H2'} coupling constants. The % S for 3'-deoxy-3'-fluoro-2'-hydroxy-thymidine (^RT^F) and 3'-deoxy-3'-fluoro ribouridine (^RU^F) were found to be 91.5 % and 97 % respectively. This shows that these compounds are frozen in the S-type conformation whereas the % S for 3'-deoxy-3'-fluoro-2'-hydroxy-xylothymidine (^XT^F) and 3'-deoxy-3'-fluoro-xyloouridine (^XU^F) were found to be 2.9 % and 0.15 % respectively, indicating N-type sugar conformation. X-ray crystal structure analysis of 3'-deoxy-3'-fluoro-2'-hydroxy-thymidine (^RT^F) revealed that it crystallizes in the orthorhombic space group P2₁2₁2₁ with two unique molecules, A and B, in the asymmetric unit (Figure 3). The furanose ring conformations of molecules A and B of ^RT^F are ²T₃ (P = 170.2°, v_{max} = 36.1°) and ²E (P = 164.3°, v_{max} = 38.8°), indicating a C2'-endo puckered sugar conformation (S-type).

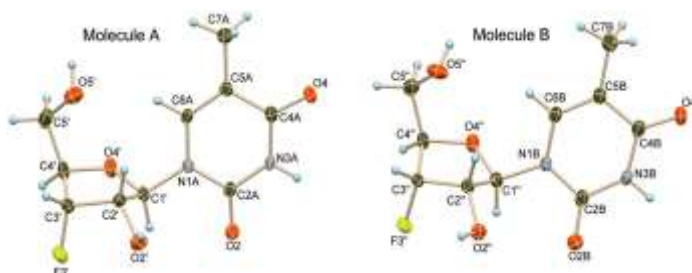


Figure 3: ORTEP drawing for the molecular structure of 3'-deoxy-3'-fluoro-2'-hydroxy-thymidine (^RT^F); molecules A and B are the two different conformers observed.

Section B: 3'-deoxy 3' fluoronucleosides in the thrombin binding aptamer (TBA):

Evaluation of stability and activity

In this section, the incorporation of monomers with N-type or S-type sugar conformation in *iso*TBA is reported, with a study of the effects in terms of their quadruplex forming possibility and consequently anti-thrombin activity.

We chose the 3'-deoxy-2'-5'-linked *iso*TBA (Figure 1), as it exhibits high stability against cellular enzymes. The four phosphoramidite derivatives of monomers 3'-deoxy-3'-ribo/xylofluoro thymidine (^RT^F and ^XT^F) and 3'-deoxy-3'-ribo/xylofluoro uridine (^RU^F and ^XU^F) (Figure 4) were incorporated into 2'-5' linked *iso*TBA in the central loop at position T⁷ and T⁹ or both.

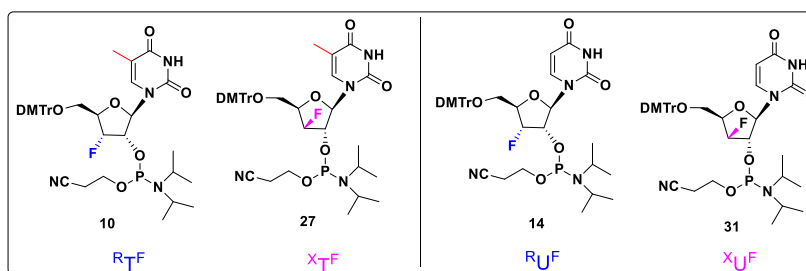


Figure 4: Phosphoramidate monomer for this study

Evaluation of G-quadruplex formation and stability in the presence of monovalent ions by circular dichroism spectroscopy

CD spectra recorded for all oligomers (Table 1) in the presence potassium ions displayed the characteristic signals corresponding to the antiparallel G-quadruplex topology. The thermal stability studies of modified *iso*TBA analogues showed an enhancement in thermal stability compared to the parent *iso*TBA but less stability as compared to TBA.

Table 1[#]: TBA, *iso*TBA, modified oligomers used in the present work and their CD- T_m in 10 mM K phosphate buffer (pH 7.2), containing 100 mM KCl.

Entry no.	Sequence code	Sequence	T_m °C in K^+ (ΔT_m) [*]
1.	TBA	5'-GGTTGGTGTGGTTGG-3'	50 (+16)
2.	<i>iso</i> TBA	5'-GGTTGGTGTGGTTGG-2'	34
3.	<i>iso</i> TBA ^{R^TF} -7	5'-GGTTGG ^{R^TF} GTGGTTGG 2'	37 (+3)
4.	<i>iso</i> TBA ^{R^TF} -79	5'-GGTTGG ^{R^TF} G ^{R^TF} GGTTGG- 2'	38 (+4)
5.	<i>iso</i> TBA ^{R^TF} -9	5'-GGTTGGTG ^{R^TF} GGTTGG- 2'	35 (+1)
6.	<i>iso</i> TBA ^{X^TF} -7	5'-GGTTGG ^{X^TF} GTGGTTGG- 2'	40 (+6)
7.	<i>iso</i> TBA ^{X^TF} -79	5'-GGTTGG ^{X^TF} G ^{X^TF} GGTTGG- 2'	42 (+8)
8.	<i>iso</i> TBA ^{X^TF} -9	5'-GGTTGGTG ^{X^TF} GGTTGG 2'	35 (+1)
9.	<i>iso</i> TBA ^{R^UF} -7	5'-GGTTGG ^{R^UF} GTGGTTGG -2'	37 (+3)
10.	<i>iso</i> TBA ^{R^UF} -79	5'-GGTTGG ^{R^UF} G ^{R^UF} GGTTGG -2'	36 (+2)
11.	<i>iso</i> TBA ^{R^UF} -9	5'-GGTTGGTG ^{R^UF} GGTTGG -2'	35 (+1)
12.	<i>iso</i> TBA ^{X^UF} -7	5'-GGTTGG ^{X^UF} GTGGTTGG -2'	35 (+1)
13.	<i>iso</i> TBA ^{X^UF} -79	5'-GGTTGG ^{X^UF} G ^{X^UF} GGTTGG-2'	36 (+2)
14.	<i>iso</i> TBA ^{X^UF} -9	5'-GGTTGGTG ^{X^UF} GGTTGG- 2'	36 (+2)

[#] The number in the sequence name indicates the position of the modified nucleotide unit in the central loop. ^{*} Values in parentheses indicate the difference in T_m (ΔT_m) w.r.t. *iso*TBA.

G-quadruplex formation in the presence of thrombin without monovalent cations

In water, all the modified sequences showed maxima at ~ 260 nm. We performed CD experiments with all the sequences of the study, in the presence of increasing

concentrations of thrombin at 4 °C. We observed an increase in the CD signal amplitude near 290 nm upon incremental addition of thrombin.

Antithrombin effect of modified oligomers

The effect of thrombin binding on the anti-thrombin activity of the 3'-fluoro modified *iso*TBA variants was assessed by carrying out a clotting assay. From Figure 7, it can be seen that in comparison to the reference, the fluoro modified *iso*TBA oligomers had a better anti-thrombin activity; however, in comparison to the TBA and *iso*TBA, the fluoro modified *iso*TBA oligomers showed a lower anti-thrombin activity, the highest activity being observed for the parent TBA (Figure 5).

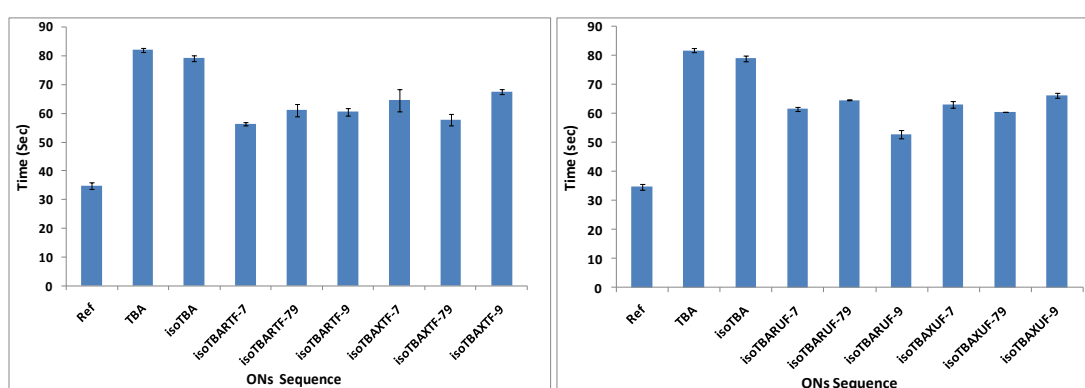


Figure 5: Antithrombin activity measurement using fibrinogen from human plasma and bovine thrombin.

Stability of the modified and unmodified 2'-5'-linked oligonucleotides towards snake venom phosphodiesterase (SVPD):

The stability of unmodified and modified 2'-5'-linked oligonucleotides towards the 3'-exonuclease, snake venom phosphodiesterase (SVPD) was examined. We exposed *iso*TBA^{XTF}-79 as a representative oligomer, to snake venom phosphodiesterase. We found that the stability of TBA was very low; it was immediately cleaved within 2 min, whereas both *iso*TBA and *iso*TBA^{XTF}-79 were found to be digested much slower; even after 60 min, nearly 40 % of both oligomers were intact (Figure 6).

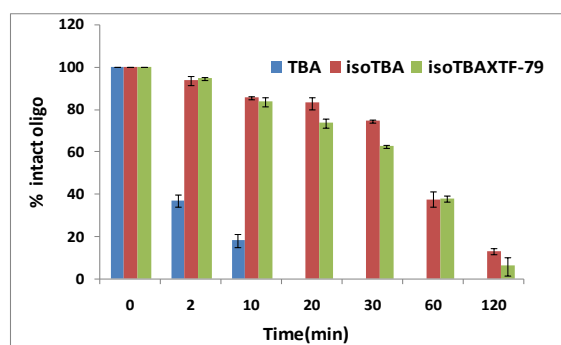


Figure 6: RP-HPLC at different time points upon SVPD digestion.

Conclusion: Incorporation of S-type and N-type conformationally frozen monomers (3'-deoxy, 3'-fluoro thymidine/uridine) in *iso*TBA with a 2'-5'-backbone is reported for the first time. Newly reported *iso*TBA analogues showed antiparallel quadruplex topology with an enhancement in thermal stability compared to the parent *iso*TBA and better nuclease stability as compared to the natural 3'-5'-linked TBA.

Chapter 3: Truncated loops in 3'-5' linked TBA Vs 2'-5' linked *iso*TBA: Effect on quadruplex topology and thrombin binding

Classification of G- quadruplex topology can be done into three groups which are parallel (group I), mixed or hybrid (group II) and antiparallel (group III) based on the orientation of the polyG strands and the preference of a *syn* or an *anti* glycosidic bond angle (GBA) of guanine. Various factors affect the topology and stability of G-quadruplexes, such as loop length, type of nucleobase in the loop, glycosidic bond angle of guanine. This chapter summarizes the synthesis of 3'-5' linked TBA and 2'-5' linked *iso*TBA variants (listed in Table 2) with truncated loops, their quadruplex formation and topology studies.

Evaluation of G-quadruplex topology and thermal stability using CD spectroscopy

Table2: TBA and *iso*TBA loop modified sequences and their CD analysis

Sequence code	Sequence	Topology
TBA232(7)	5' GGTTGGTGTGGTTGG 3'	Antiparallel
TBA222(6)	5' GGTTGGTTGGTTGG 3'	Hybrid or mixture of antiparallel and parallel
TBA131(5)	5' GGTGGTGTGGTGG 3'	Hybrid or mixture of antiparallel and parallel
TBA111(3)	5' GGTGGTGGTGG 3'	Parallel
<i>iso</i> TBA232(7)	5' GGTTGGTGTGGTTGG 2'	Antiparallel
<i>iso</i> TBA222(6)	5' GGTTGGTTGGTTGG 2'	Hybrid or mixture of antiparallel and parallel
<i>iso</i> TBA131(5)	5' GGTGGTGTGGTGG 2'	Hybrid or mixture of antiparallel and parallel
<i>iso</i> TBA111(3)	5' GGTGGTGGTGG 2'	Parallel

The quadruplex formation of all the TBA and *iso*TBA sequences was studied by CD spectroscopy at a higher salt concentration and increased strand concentrations. We observed that in the case of TBA, as the loop length decreased from 232(7) to 111(3), the quadruplex topology changed from antiparallel to parallel structures. In case of *iso*TBA sequences, irrespective of loop length, all the modified *iso*TBA sequences (with extended N-type conformation of nucleotides) containing 222(6), 131(5) or even 111(3) loop nucleotides, exhibited antiparallel G-quadruplex conformation.

Antiparallel G-quadruplexes of *iso*TBA showed a decrease in thermal stability with decreasing loop length. The oligomer (TBA 111) with the shortest loop, existed in

the parallel multimolecular quadruplex conformation, and consequently showed the highest thermal stability compared to all other sequences.

Table 3: TBA and *iso*TBA loop-modified sequences and their CD- T_m at 295 nm at varying salt and strand concentrations.

Oligomer code	T_m (°C) at 5 μ M, with 100 mM KCl		T_m (°C) at 20 μ M, with 100 mM KCl		T_m (°C) at 5 μ M, with 500 mM KCl	
	Heat	Cool	Heat	Cool	Heat	Cool
TBA232(7)	50	50	48	48	54.2	52.3
TBA111(3)	55 ^a	45 ^a	59.5 ^a	52.5 ^a	63.8 ^a	53 ^a
<i>iso</i> TBA232(7)	37	37	34	34	40	41
<i>iso</i> TBA222(6)	32	32	34.2	32.5	40	39.5
<i>iso</i> TBA131(5)	32	32	33.6	32.2	36.1	37.8
<i>iso</i> TBA111(3)	22	20	20	20	21.5	19.1

^a indicates the CD- T_m values at 260 nm while other values are at 295 nm

G quadruplex topology confirmation by UV-Thermal Difference Spectra

For TBA 111(3), the values of TDS factor ($\Delta A_{240} \text{ nm} / \Delta A_{295} \text{ nm}$) appeared well above 4, indicating a group I parallel quadruplex, while the TDS factor of un-edited TBA232(7) was below 2, characteristic of antiparallel quadruplexes (group III) (Figure 7a).

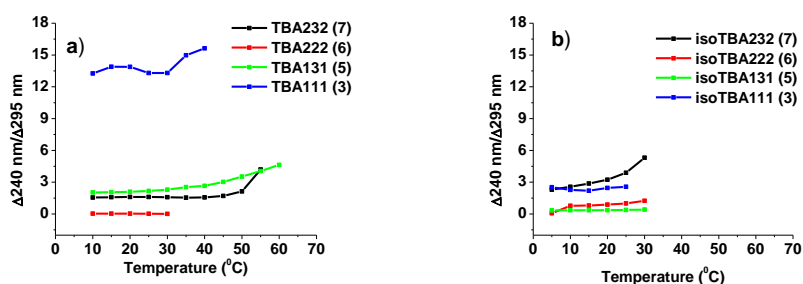


Figure 7: a) TDS factor of TBA oligomers and b) TDS factor of *iso*TBA oligomers

The TDS factor of all the *iso*TBA sequences of the study was characteristic of antiparallel G-quadruplex topology (Figure 7b). These results confirm the correct assignment of parallel/antiparallel quadruplex structures in concurrence with the CD signatures.

Polyacrylamide Gel Electrophoresis Experiments

A denaturing gel electrophoresis the mobility of the oligonucleotides displayed molecular weight- and charge- dependency and marginally higher mobility were seen for TBA111(3) and *iso*TBA111(3), as expected. The non-denaturing gel (Figure 8) clearly brought out the differences caused by the differing loop length on the quadruplex topology. The 15-mer sequences showed similar mobility corresponding to the unimolecular antiparallel quadruplex. TBA222(6) showed the bands corresponding to a

unimolecular quadruplex and highly retarded major band of suggesting multimolecular quadruplexes were observed for TBA111(3). *iso*TBA222(6), *iso*TBA131(5) and *iso*TBA111(3) were observed as single bands corresponding to the unimolecular complexes.

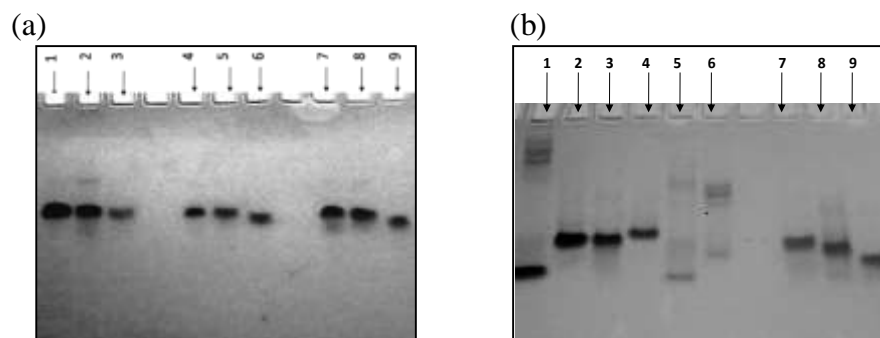


Figure 8: (a) Denaturing polyacrylamide gel mobility assay Lane1- Scrambled TBA (5'-GGTGGTGGTTGTGGT-3') Lane2-TBA232(7), Lane3-*iso*TBA232(7), Lane4-TBA222(6), Lane5-TBA131(5), Lane6-TBA111(3), Lane7-*iso*TBA222(6), Lane8-*iso*TBA131(5), Lane9-*iso*TBA111(3). (b) Non-denaturing polyacrylamide gel mobility assay Lane1-Scrambled TBA (5'-GGTGGTGGTTGTGGT-3'), Lane2-TBA232(7), Lane3-*iso*TBA232(7), Lane4-TBA222(6), Lane5- TBA131(5), Lane6-TBA111(3), Lane7-*iso*TBA222(6), Lane8-*iso*TBA131(5), Lane9-*iso*TBA111(3).

Binding with Thrombin (by the Chaperone Effect of Thrombin)

We performed CD experiments in the presence of increasing concentrations of thrombin to study the chaperone effect of thrombin. All the 3'-5'-linked TBA oligomers (except TBA) with decreasing loop lengths did not show any change in the CD spectrum. In the case of all *iso*TBA oligomers, upon incremental addition of thrombin, an increase in the CD amplitude near 295 was observed, indicating the ability of thrombin to assist the folding of these oligomers into the typical quadruplex structure known for TBA. The strength of the TBA232 (7) G-quadruplex:thrombin complex was the highest.

Table 4: CD data showing the chaperone effect of thrombin on the TBA and *iso*TBA loop-modified sequences and T_m values of the resulting quadruplexes.

Sequence code	+ Thrombin		Binding to thrombin	T_m (°C) with thrombin Heat/cool
	Maxima	Minima		
TBA232 (7)	298, 248	278-268	Yes	22/22
<i>iso</i> TBA232(7)	290, 245	265	Yes	13/13
<i>iso</i> TBA222(6)	291, 250	265	Yes	<10/<10
<i>iso</i> TBA131(5)	296, 248	272	Yes	<10/<10
<i>iso</i> TBA111(3)	260	295	No	-

Nuclease stability study-Exonuclease stability

We treated TBA and *iso*TBA131, with snake venom phosphodiesterase (SVPD) that has predominantly 3'-exonuclease activity. The 2'-5'-linked *iso*TBA131 was digested much slower compared to the control TBA. The half-life of *iso*TBA131 was

found to be ~30 min (Figure 9) whereas TBA was completely digested within 10 min at 37°C.

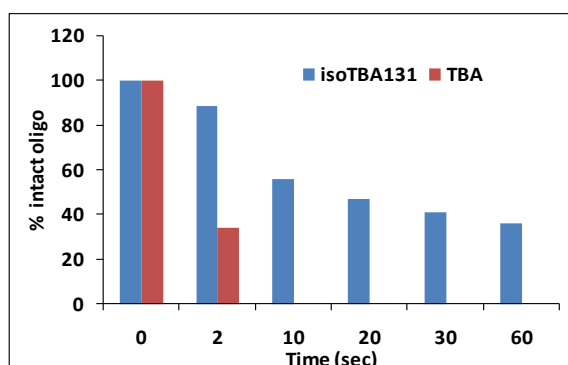


Figure 9: Stability of the aptamers *isoTBA131* and TBA towards SVPD enzyme.

Conclusion: In this Chapter, we reported the topology and thermal stability of all the TBA and *isoTBA* oligomers. The 2'-5'-linked *isoTBA* oligomers were found to be amenable to form antiparallel G-quadruplex structures, independent of loop length. The decreasing loop-length however, adversely affected the stability of the regioisomeric antiparallel quadruplexes, and consequently, reduced their binding to thrombin.

Chapter 4: Effect of 2'-5' and 3'-5' linkages in the loop region of TBA and *isoTBA* respectively, on G quadruplex stability and function.

The 3'-deoxy-2'-5'-linked non-genetic *isoDNA* exhibits high stability against cellular enzymes. Efforts toward improving stability to nucleases and thermal stability of thrombin binding aptamer have mostly focused on the introduction of modified nucleosides, or on changing the number of residues in the loop/stem regions. There are only a few reports pertaining to modification of the phosphodiester internucleoside linkage. This chapter summarizes the synthesis of chimeric oligomers with 3'-5'-(TBA) and 2'-5'-phosphodiester-linked (*isoTBA*) backbones in which the loop region is modified with 2'-5'-phosphodiester linkages and 3'-5'- phosphodiester linkages respectively. The stability and structural topology of the quadruplex and its effect on anti-clotting ability as well as stability towards nuclease with reference to the control 3'-5'-linked TBA was investigated.

Evaluation of G-quadruplex formation and stability in the presence of monovalent ions by circular dichroism spectroscopy

All the TBA and *isoTBA* oligomers (listed in Table 5) were synthesized using SPS methodology. The G-quadruplex formation and their stability were studied by CD spectroscopy in the presence of K⁺ and Na⁺. The unmodified TBA, *isoTBA* and loop-

modified variants were found to exhibit a strong, positive maximum CD absorbance at 290 nm and minimum near 260 nm, which correspond to the antiparallel G-quadruplex topology for 3'-5'-DNA, and as reported for TBA.

Table 5: TBA, *iso*TBA, modified oligomers used in the present work and their CD- T_m in K^+ / Na^+ ions in 10 mM K/ Na- phosphate buffer (pH 7.2) containing 100 mM KCl/NaCl and thrombin.

Sequence code	Sequence	T_m °C in $K^+(\Delta T_m)^*$	T_m °C in $Na^+(\Delta T_m)^*$	T_m °C of thrombin(T_m) [*]
TBA	5'-GGTTGGTGTGGTTGG-3'	50	21	22
TBA232	5'-GGttGGtgtGGttGG-3'	20 (-30)	15 (-6)	nd
TBA202	5'-GGttGGTGTGGttGG-3'	29 (-21)	18 (-3)	nd
TBA030	5'-GGTTGGtgtGGTTGG-3'	33 (-17)	25 (+4)	nd
TBA200	5'-GGttGGTGTGGTTGG-3'	38 (-12)	13 (-8)	nd
TBA002	5'-GGTTGGTGTGGttGG-3'	38 (-12)	18 (-3)	nd
<i>iso</i> TBA	5'-ggttggtgtggttg-2'	34 (-16)	19 (-2)	13 (-9)
<i>iso</i> TBA232	5'-ggTTggTGTggTTgg-2'	48 (-2)	36 (+13)	18 (-4)
<i>iso</i> TBA202	5'-ggTTggtgtggTTgg-2'	54 (+4)	43 (+22)	26 (+4)
<i>iso</i> TBA030	5'ggttggTGTggttg-2'	33 (-17)	20 (-1)	12 (-10)
<i>iso</i> TBA200	5'-ggTTggtgtggttg-2'	45 (-5)	39 (+18)	10 (-12)
<i>iso</i> TBA002	5'-ggttggtgtggTTgg-2'	44 (-6)	30 (+9)	11 (-11)

* Values in parentheses indicate the difference in T_m (ΔT_m) w.r.t. native TBA, nd is not determinable.

G-quadruplex formation in the presence of thrombin

Chimeric TBA oligomers with 2'-5'- linkages in loops showed maxima near 280 nm in water, but upon incremental addition of thrombin showed a slight shift of maxima near 290 nm and a negligible amplitude change in the CD signal near 290 nm. In contrast, for *iso*TBA oligomers with 3'-5'-linked loop regions G-quadruplex structure was not observed in water. However, upon incremental addition of thrombin, a marked change was observed, with a concomitant increase in CD amplitude near 295 nm. The effect of thrombin binding on the anti-thrombin activity was examined. It can be seen that in comparison to the TBA oligomers, the *iso*TBA oligomers had a lower anti-thrombin activity, with the highest activity being observed for the parent TBA. TBA202, with 2'-5'-linked T³T⁴ and T¹²T¹³ loops showed similar clotting time to TBA. Except for TBA202, all other oligomers showed decrease in anti-thrombin activity relative to the parent oligomer (Figure 10).

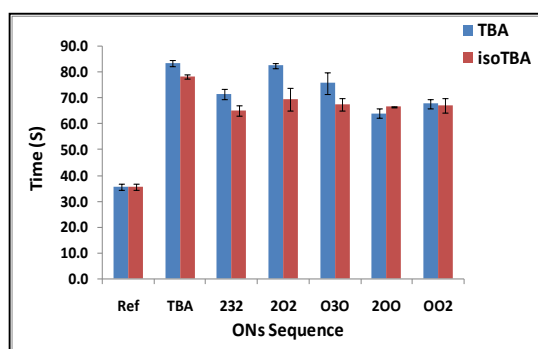


Figure 10: Antithrombin activity measurement using fibrinogen from human plasma and bovine thrombin. Ref indicates the clotting time measured with fibrinogen and thrombin in the absence of any added oligomer.

Stability of oligonucleotides towards endonuclease and exonuclease

A comparative study of TBA002 and *iso*TBA002 against hydrolytic cleavage by SVPD (Figure 11a) and S1 nuclease digestion (Figure 11b) of TBA, *iso*TBA, TBA202 and *iso*TBA202 was done. Compared to native TBA, *iso*TBA oligomers showed better stability to nucleases.

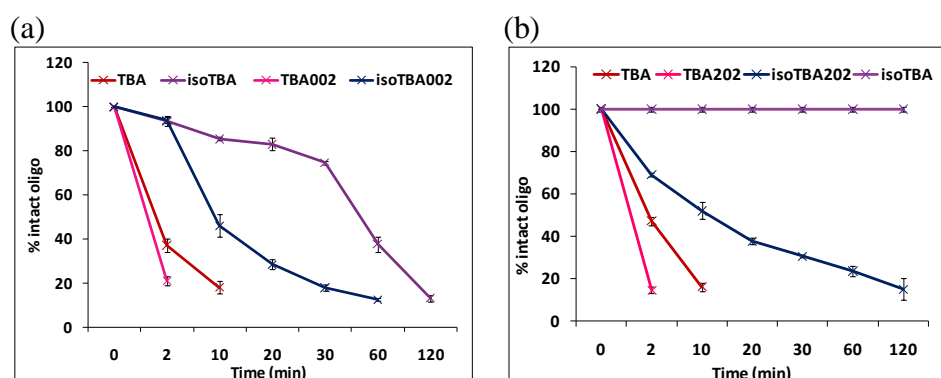
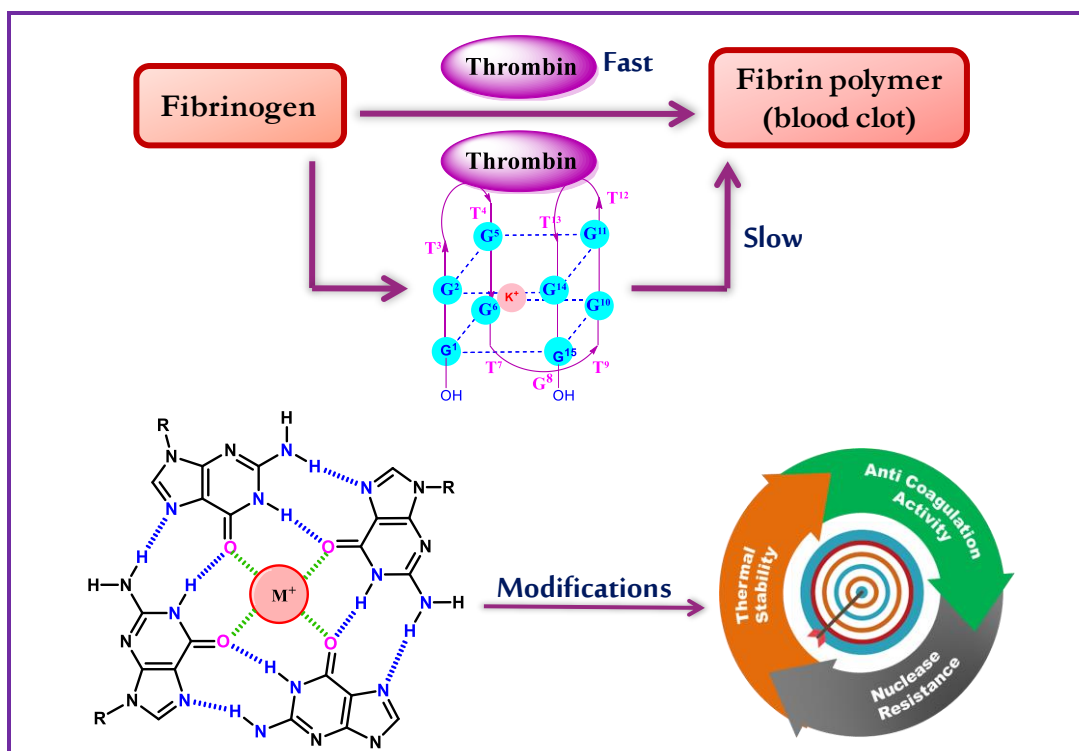


Figure 11: RP- HPLC at several time points for (a) SVPD and (b) S1 endonuclease

Conclusion: A new class of chimeric thrombin-binding aptamers were found to be similar to the native DNA aptamer (TBA) both in terms of structure as well as function. The *iso*TBA sequences showed better nuclease stability against exonuclease and endonuclease which could prove beneficial in applications in biological systems where a longer half-life is desired.

Chapter 1

Introduction to Guanine-rich nucleic acid aptamers with a focus on the Thrombin binding aptamer (TBA)



Nucleic acid aptamers are single-stranded DNA or RNA or modified nucleic acids that are able to fold into unique three-dimensional structures and able to bind to small molecules, peptides, proteins with selectivity, specificity and affinity. G-quadruplexes are a unique class of highly ordered nucleic acid structures. G-quadruplex structures are stable and detectable in human genomic DNA and perform important regulatory functions in many biological processes. The regular occurrence of quadruplex structures in the genome suggests the designing of potential drug molecules based on DNA/RNA G-quartets. A thrombin binding aptamer (TBA), a 15-mer DNA oligonucleotide, 5'-GGTTGGTGTGGTTGG-3' was found to inhibit fibrin-clot formation by binding to the thrombin protein with high selectivity and affinity. This chapter presents a concise review about the research focused on the development of new TBA derivatives with improved thermal stability, Nuclease resistance and anticoagulant properties as well as the use of TBA as a model compound for the study of quadruplex structures.

1.1 Introduction to nucleic acids: A structural overview

Nucleic acids are present in all forms of life on Earth. These are the most important class of biopolymers dominating modern biomolecular science since double-helical structure was brought to the light by Watson and Crick.¹ Deoxyribonucleic acid (DNA) and Ribonucleic acid (RNA) are essential parts of our genetic make-up and are comprised of nucleoside units connected through phosphodiester linkages (Figure 1). Each nucleoside is a micromolecular component and consists of a heterocyclic nitrogenous base (purine or pyrimidine) and a β -D-pentafuranose sugar moiety. In DNA, the sugar is deoxyribose, while in RNA it is ribose. Both nucleic acids, DNA and RNA contain the heterocyclic bases adenine (A), cytosine (C) and guanine (G); while thymine (T) only occurs in DNA and uracil (U) is found in RNA. The presence or absence of the 2'-OH group in RNA or DNA respectively dictates structural differences as well as their chemical behaviour.

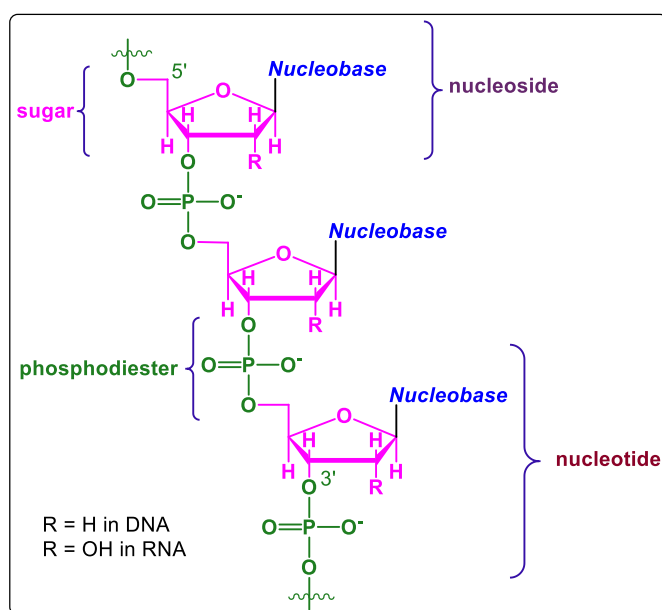


Figure 1: Basic structure of natural DNA and RNA

The backbone of natural nucleic acids is formed by 3'- to 5'- phosphodiester linkages. The nucleic acids that function in encoding, transmitting and expressing genetic information, therefore are referred to as genetic nucleic acids. In most cases, DNA carries the genetic information and RNA functions as a messenger to convert the genetic information into amino acid sequences, which form proteins.

1.2 Base pairing and structures of DNA

1.2.1 The double helix

The modern era of molecular biology began in 1953 after discovery of the double-stranded helical structure of DNA. DNA predominantly consists of two associated polynucleotide strands held together by hydrogen bonding often described as the double helix. The two strands have an antiparallel orientation i.e., one strand runs in the 5'→3' direction while the other in the 3'→5'. The basis of the structural features of DNA is the strong hydrogen bonding between specific Watson–Crick base-pairs. G:C pair has three hydrogen bonds; A:T pair has two hydrogen bonds (Figure 2).

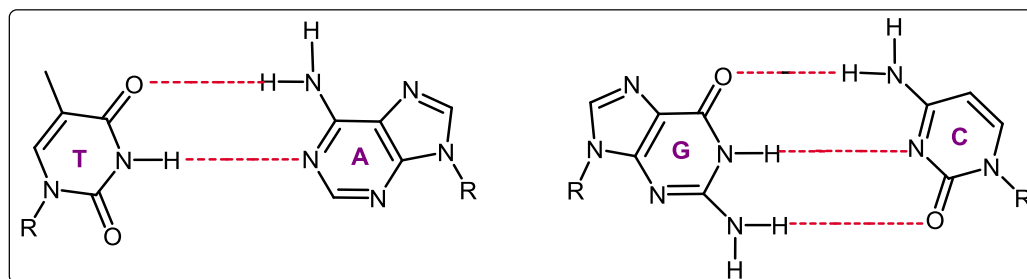


Figure 2: Watson-Crick (W-C) base-pairing

1.2.2 Triplex structure

Triple-helical nucleic acid structures² are known since 1957 which are formed by Hoogsteen³ base pairing. The double-helical DNA binds to the third strand and forms a triplex structure via Hoogsteen base pairing, which makes use of N7 of the purine as acceptor and C6 amino group of adenine or C6 oxo group of guanine as a donor or acceptor respectively for hydrogen bonding with the corresponding pyrimidine (Figure 3).

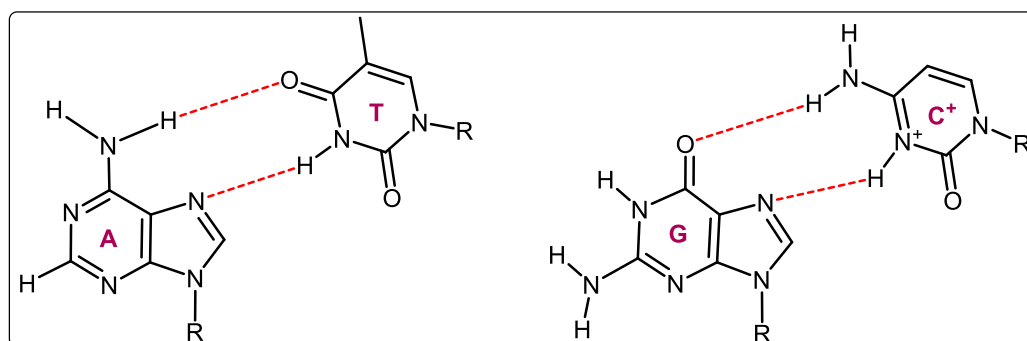


Figure 3: Hoogsteen hydrogen-bonding

1.2.3 Quadruplex structure - The 'G-quadruplex'

Both the ends of the eukaryotic chromosomes are protected by repetitive units of specific sequences known as telomeres, that are crucial for genome integrity, play an important role in cellular ageing and cancer.⁴ The extreme terminal part of telomeric DNA is either G-rich or C-rich and forms the unusual structures known as quadruplexes. Two types of quadruplexes are formed depending on the major nucleobase involved in their formation. Four-stranded G-quadruplex structure is formed by guanine-rich strands which involves planar G-tetrads of four guanines associated through Hoogsteen hydrogen bonding^{5, 6} (Figure 4a), while i-motifs are also four-stranded structures, but are formed by intercalation of cytosine-cytosine⁺ base pairs between cytosine-rich strands (Figure 4b).⁷

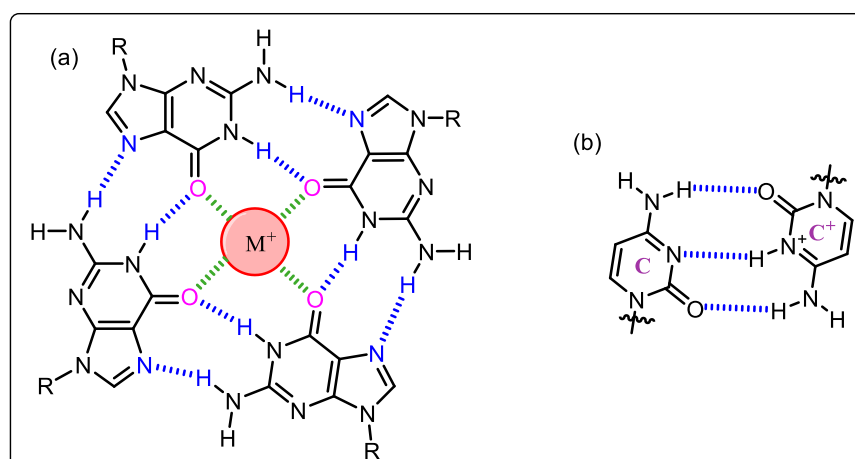


Figure 4: (a) G-tetrads of G-quadruplexes and (b) C:C⁺ hydrogen-bonding of i-motif quadruplexes

1.3 Sugar pucker in nucleotides

The pentafuranose sugar moiety in nucleotides minimizes non-bonded stereo-electronic interactions between substituents by puckering. The system reduces its energy by puckering. Displacement of C2' and C3' carbons from the median plane of C1'-O4'-C4' causes '*puckering*' of the planar sugar moiety. The *endo* face is that in which the atom of the sugar is placed on the same side as the nucleobase and C5' carbon (above the median plane), while the *exo* face is that in which the atom is placed on the opposite side of the nucleobase (below the median plane). In C2'-*endo* conformation the *endo*-displacement of C2' is greater than the *exo*-displacement of C3', and vice versa for C3'-*endo* conformation (Figure 5).⁸

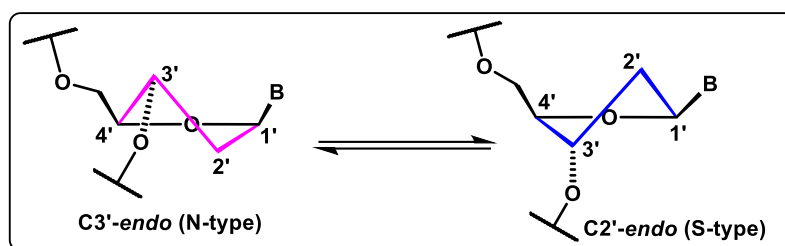


Figure 5: N-type and S-type sugar pucker

The sugars in DNA favour the 3'-*exo*, 2'-*endo* twist form (often referred to as *South* or S-type conformation), whereas sugars in RNA are predominantly in the 3'-*endo*, 2'-*exo* twist form (often referred to as *North* or N-type conformation) under physiological conditions. In solution, the sugar moiety exists in rapid equilibrium between Northern and Southern conformations as defined in the pseudorotational cycle⁹ and the energy barrier between both conformations is very low. The predominance of one conformation of sugar is governed by stereoelectronic effects like *anomeric* and *gauche* effects.¹⁰

1.3.1 Steric effect

In β -D-nucleosides, the S-type sugar conformation is energetically favoured as compared to its N-type counterpart. In the S-type pseudorotamer, the nucleobase is oriented pseudo-equatorially, causing less steric conflicts with other substituents on the pentafuranose moiety, and in case of the N-type nucleoside, the nucleobase orientation is pseudo-axial, which leads to more steric conflicts. Consequently, the two-state N \leftrightarrow S pseudorotational equilibrium shifts towards the S-type conformation (Figure 6).

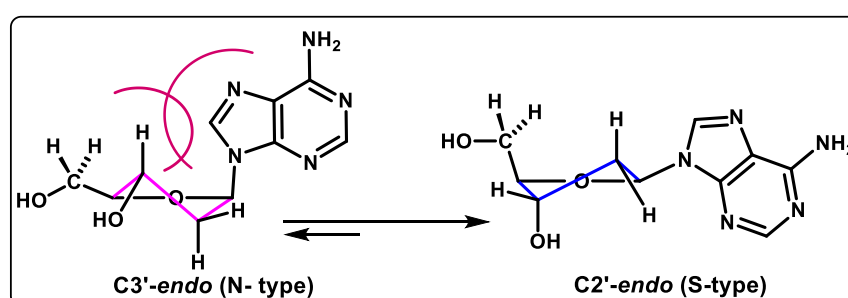


Figure 6: The steric interactions of nucleobase in the South \leftrightarrow North equilibrium in DNA

1.3.2 Stereoelectronic effect

The sugar conformation is dictated by stereoelectronic effects, which mainly involves the *anomeric* and *gauche* effects.¹⁰ The conformational equilibrium of

nucleosides and nucleotides is influenced by these *anomeric* and *gauche* effects.

1.3.2.1 Anomeric effect

The *anomeric* effect is defined as a stereoelectronic effect; in cyclohexane or cyclopentane ring a heteroatomic substituent adjacent to the heteroatom favours axial orientation rather than the less hindered equatorial orientation, which is significant in determining conformational preferences of glycosides. The presence of a nucleobase at the C1' position of the furanose sugar ring of nucleosides exerts optimal *anomeric* effect in O4'-*exo* conformation (antiperiplanar orientation of Lp-O4'-C1'-N) but this conformation is not favourable due to large steric interaction between exocyclic 5'-CH₂OH and the nucleobase.

In nucleosides and nucleotides, N-type conformation is energetically favoured than S-type conformation in terms of anomeric effect alone where the *anomeric* effect is caused by the stabilizing interaction between the unshared electron pair of the endocyclic oxygen of the sugar ring and the exocyclic glycosidic C-N bond (Figure 7). Thus, the *anomeric* effect is strongest in N-type pseudorotamers (C3'-*endo* conformation).

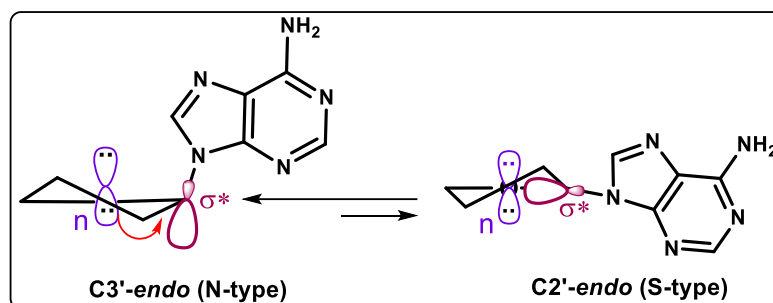


Figure 7: O4'-C1'-N9 *anomeric* effect in adenosine as an example of a purine nucleos(t)ides in terms of molecular orbital overlap

1.3.2.2 Gauche effect

The “*gauche effect*” is seen when the torsion angle between two vicinal groups is 60° and influences sugar ring conformation. In 2'-deoxyribonucleosides, the stronger *gauche effect* of fragment [O3'-C3'-C4'-O4'] favours the S-type conformation whereas; the *gauche effect* of fragment [O2'-C2'-C1'-O4'] stabilizes the N-type conformation in ribonucleosides. The *gauche* effect is a major factor that controls sugar conformation rather than *anomeric* effect.¹¹

1.4 Base-stacking

The strands in DNA are held together by hydrogen bonds (base pairing between the nucleotides of two complementary strands) and hydrophobic interactions (stacking interaction among two adjacent aromatic nucleobases),¹² that occurs when two or more bases appear to have parallel ring planes. These interactions are mainly a combination of Van der Waals and dipole-dipole interactions. Stacking interactions among aromatic bases is the crucial force responsible for stabilization of DNA and RNA 3D structures like duplexes, triplexes, quadruplexes and stem-loop structures by minimizing contact with water. As the purines and pyrimidines are aromatic, π - π -stacking interactions minimize solvent exposure of the base surfaces, leading to the face-to-face stacking of bases and base-pairs. The degree of stabilization afforded by base-stacking depends on the DNA sequence. Sugar pucker has an impact on base stacking tendency, as it influences nucleobase orientation. Studies have implied that the North-type sugar conformation (*C3'-endo*) causes the nucleobase to be pseudoaxially oriented, that leads to more efficient base-stacking, as opposed to the case in sugars with the South-type conformation (*C2'-endo*), where the nucleobase is pseudoequatorial.

1.5 Isonucleic Acids

IsoDNA or *isoRNA*, in this thesis, refer to DNA or RNA that have regioisomeric 2'-5'-phosphodiester linkages instead of 3'-5'-phosphodiester linkages. They are different from native DNA or RNA (Figure 8). The 2'-5'-linked constitutional isomers are known to form duplexes *via* Watson–Crick base-pair association and do not encode genetic information, thus are called non-genetic nucleic acids.¹³

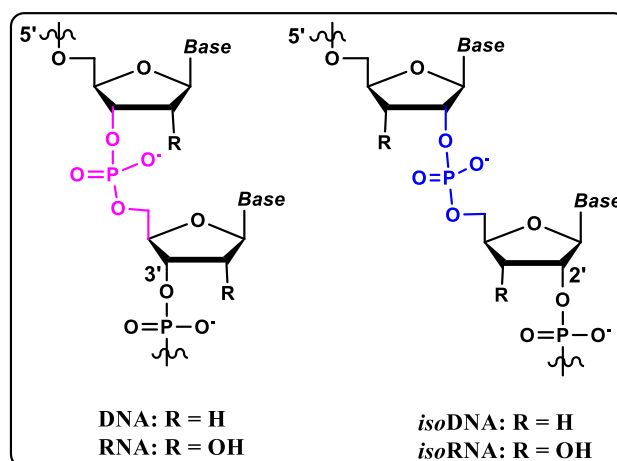


Figure 8: 3'-5'-DNA/RNA and 2'-5'-*isoDNA/isoRNA*

During non-enzymatic oligonucleotide synthesis, the 2'-5'-linkage is the major product,¹⁴ in comparison to 3'-5'-linkages. The higher reactivity of the 2'-OH group than the 3'-OH group leads to the formation of the 2'-5'-linkage rather than the 3'-5'-linkage.¹⁵ Therefore, the 2'-5'-linkage might have been a primary substitute of the natural 3'-5'-linkage in evolution. However, the 3'-5' linkages were selected during evolution probably because the rate of hydrolysis of 3'-5' linkages is slower than 2'-5' linkages¹⁶ and 2'-5'-linked oligonucleotides have low helix-forming ability.

1.6 Sugar ring conformations in 3'-5' Vs 2'-5'-linked oligomers

In the single-stranded 3'-deoxy, 2'-5'-linked oligomer, the 3'-*endo* (N-type) sugar conformation is preferred due to *gauche* and *anomeric* (stereoelectronic) effects exerted by the 2'-hydroxy group (Figure 9).

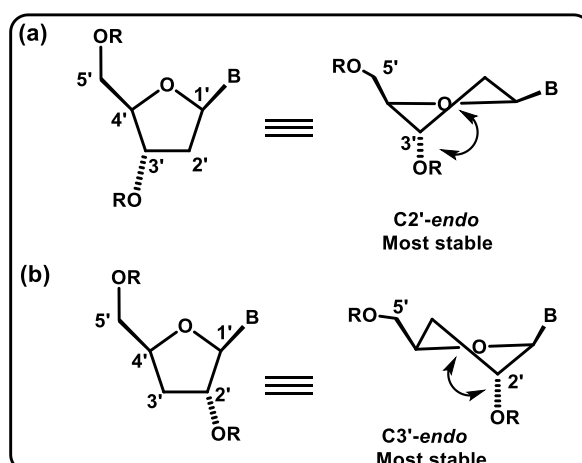


Figure 9: (a) S-type (*C2'-endo*) sugar conformation DNA and (b) N-type (*C3'-endo*) sugar conformation in 2'-5'-linked *iso*DNA.

In 2'-5'-linked *isonucleic* acids, the internucleotide linkage changes from C3' to C2'. This leads to an increase in the number of internucleotide bonds from six (in 3'-5'-linked DNA) to seven (in 2'-5'-linked DNA). The 2'-5'-linkages maintain an extended backbone geometry with the *C3'-endo* sugar conformation whereas the 3'-5' linkages maintain extended backbone geometry with the *C2'-endo* sugar conformation (Figure 10).

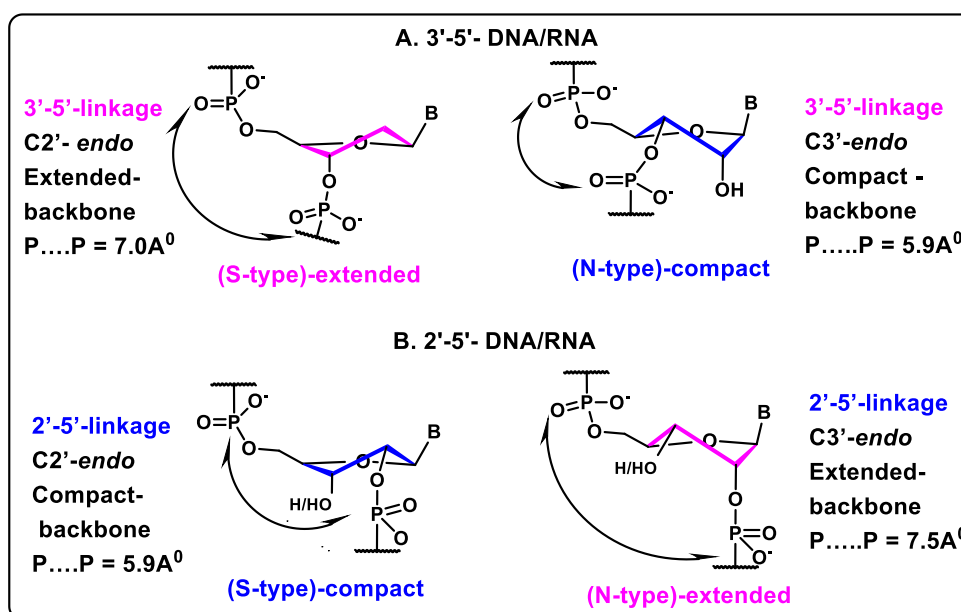


Figure 10: 3'-5'-DNA/RNA and 2'-5'-*iso*DNA/*iso*RNA in compact and extended conformations showing their inverse relationship

1.7 Quadruplex-forming DNA

The most common image of DNA is a duplex formed by hydrogen bonding between complementary A:T and G:C base pairs connected by the phosphodiester backbone. For years, DNA has been recognized only as a molecule for genetic information storage, but accumulated experimental data in the last few decades indicated the dynamic properties of this macromolecule to catalyze and control biological processes. To carry out diverse biological processes, with the canonical duplex structure, other non-canonical and polymorphic nucleic acid structures such as triplex, hairpin and higher-order structures like G-quadruplexes are necessary.

The story of quadruplex DNA-It started with a Bang!¹⁷ Near the beginning of the last century (1898) Ivar Christian Bang¹⁸ discovered viscous gel formation by guanosine and its derivatives in water. More than 50 years later, in 1962, X-ray diffraction data explained its particular behaviour. It was proposed that guanine bases associated in tetrameric arrangement¹⁹ and the structure was termed as a guanine tetrad. The square co-planar arrangement of guanine bases is formed by the Hoogsteen hydrogen bonding that entail N1, N7, O6 and C2-N of each guanine and every guanine base acts both as a donor and acceptor of hydrogen bonds. The four-stranded motif is formed by stacking of planar G-tetrads on each other which is termed as G-quadruplex.

The significance of G-quadruplexes was overlooked for more than two decades and guanine quadruplexes had remained as a structure in search of function. In early 1987, ground-breaking work performed by Blackburn et al.²⁰ identified that at the end of the chromosomes, G-rich recurrent sequences are located and thereafter, interest in the structural arrangement of G-quadruplexes was sparked. Guanine-rich segments present widely in biologically significant regions of the genome that are associated with regulatory activity like gene promoter regions,^{21,22} immunoglobulin switch regions⁶ and telomeres.²³ Several quadruplex-binding proteins have been discovered and some of them assist the quadruplex formation.²⁴ Various pharmacologically important molecules like perylenes, cationic porphyrins and 2,6-diamido anthraquinones facilitate the formation and stabilization of G-quadruplexes, and are considered plausible selective inhibitors of telomerase, a potential target for anticancer therapy.²⁵

1.7.1 G-quadruplex structure

G-quadruplexes are four-stranded right-handed helical structures formed from guanine-rich sequences. Four guanine bases are arranged in a cyclic manner in a G-tetrad through hydrogen-bonding that involves the Hoogsteen face of each guanine with the Watson-Crick face of the adjacent guanine (Figure 4a).

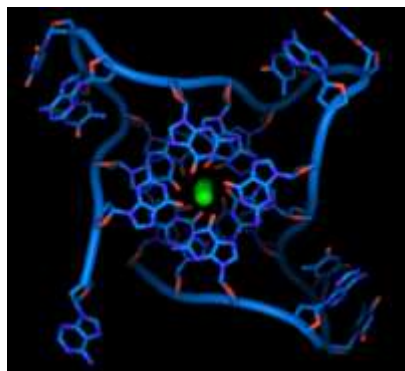


Figure 11: The G-quadruplex stacked structure arising from G-rich sequences.

(<http://www.molecularstation.com/molecular-biology-images/>)

Two or more G-tetrads can stack on one another with a helical twist of 30° and a diameter of 25 \AA and are stabilized by monovalent cations coordinated to the O6 oxygen atoms of the guanines, and sandwiched between the base-stacks. The overall quadruplex structure is stabilized by cations as they neutralize the electrostatic repulsion between the guanine O6 atoms (Figure 4a and Figure 11).

1.7.2 Variations on the G-quadruplex theme (Polymorphism)

Not all G-rich sequences have the tendency to form a G-quadruplex structure, but G-rich sequences are an important requirement for G-quadruplex formation. Fundamental basis for G-quadruplex polymorphism are length of nucleic acid sequence, strand polarity, glycosidic torsion angle variation and connecting loops.

1.7.2.1 Strand stoichiometry

The folding of a quadruplex is determined by the length of nucleic acid sequence that participates in G-tetrad formation. Four separate strands create a tetramolecular quadruplex by short sequences with a single consecutive stretch of three or more guanine bases (Figure 12a).

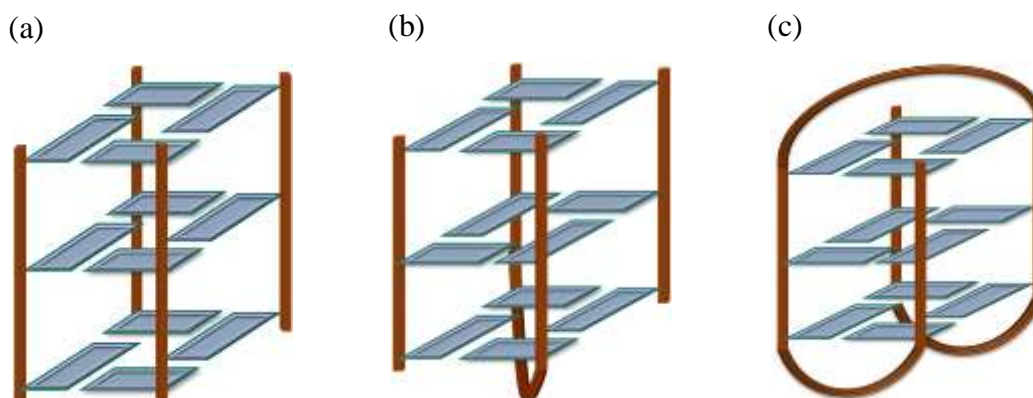


Figure 12: Stoichiometries of the G-quadruplex structure (a) Tetramolecular (b) Bimolecular (c) Unimolecular

A bimolecular quadruplex structure is formed by longer sequences comprising two consecutive stretches of three or more guanine bases and the guanine regions are separated by one or more bases (Figure 12b). A sequence that can form a quadruplex structure by folding upon itself and consisting of four distinct G-runs is called a unimolecular (intramolecular) quadruplex (Figure 12c).²⁶

1.7.2.2 Strand polarity polymorphism

Strand polarity is another fundamental basis of structural variation in G-quadruplexes; the strands which form a G-quadruplex can assemble in four ways, as shown in Figure 13. Thus, the strands may be (a) all parallel, (b) three parallel one antiparallel, (c) two pairs of adjacent parallel strands and (d) alternating parallel and antiparallel strands.

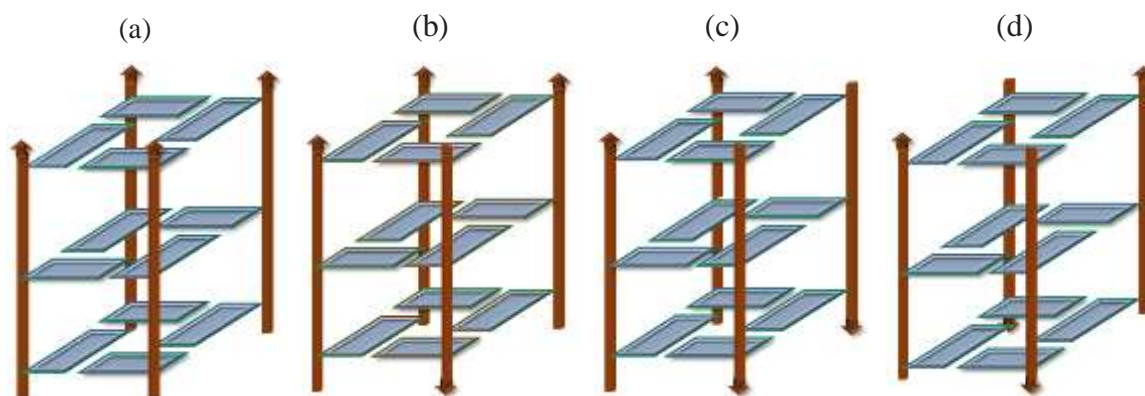


Figure 13: Different strand polarity arrangements in G-quadruplexes

1.7.2.3 Glycosidic torsion angle variation

The guanine nucleobases associated in a G-tetrad are found to be in both *syn* and *anti* conformations, (Figure 14) though restraints apply to neighbouring guanines of the same tetrad. In all parallel quadruplexes, the orientation of all nucleobases is either *syn* or *anti* whereas mixed *syn*- and *anti* orientation of nucleobases is present in antiparallel quadruplexes. When all the strands are oriented parallel, the groove widths are equal, glycosidic torsion angles are all *syn* / all *anti*, whereas antiparallel alignment of strands generates both wide and narrow grooves as glycosidic torsion angles are mixed *syn* and *anti*.²⁷

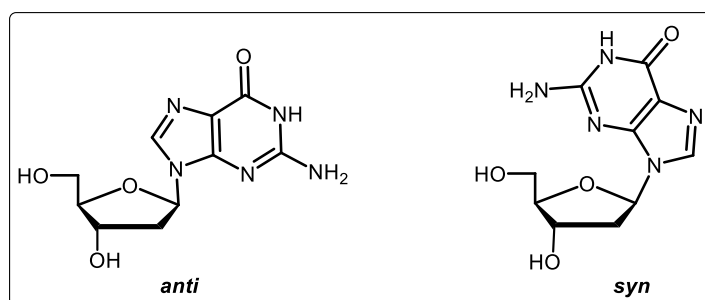


Figure 14: *anti* and *syn* conformations of guanosine

1.7.2.4 Connecting loops

The loops that connect guanine tracts generally make three different types of connections, according to which, they may be (i) lateral loops, that connect adjacent bases of the same tetrad, join adjacent strands and bases share hydrogen bonds, (ii) diagonal loops link bases of the same tetrad and join opposite antiparallel strands but

bases do not share hydrogen bonds and (iii) propeller loops that link nucleobases of adjacent parallel strands that are not in the same tetrad (Figure 15).

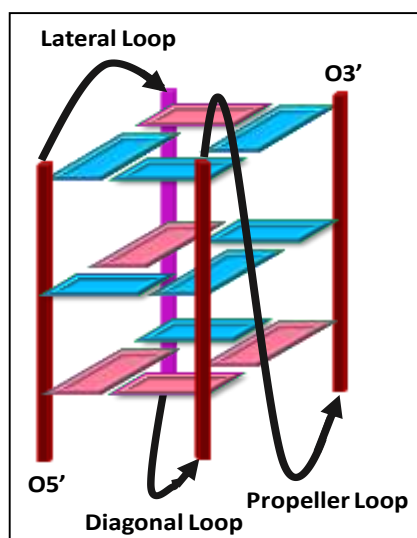


Figure 15: G-quadruplex linking loop motifs (black arrows). Backbone strand polarity: parallel (brown) and antiparallel (purple). Glycosidic torsion angles: *anti*-conformation (pink) and *syn*-conformation (blue).

1.8 Quadruplex stability dependence on metal ions

Arnott et al.²⁸ for the first time, demonstrated the dependence of quadruplex formation on metal ion coordination to the guanine O6 carbonyl oxygen. The negatively charged cavity between the G-tetrads can be stabilized through coordination to a cation (Figure 4a & 11). Several monovalent cations such as K^+ , Na^+ , Li^+ , Rb^+ , Cs^+ , etc., and also divalent cations such as Mg^{2+} , Ba^{2+} , Ca^{2+} , Sr^{2+} etc. are known to influence the G-quadruplex structure.²⁹ The non-metal cation, NH_4^+ is also able to induce stable G-quadruplexes. Most of the studies explored the role of K^+ and Na^+ ions on G-quadruplex structure and stability as both ions are physiologically important ions.

1.9 Aptamers: An emerging class of therapeutics

Nucleic acid ligands termed as aptamers are single-stranded DNA or RNA or modified nucleic acids that are able to fold into unique three-dimensional structures and able to bind to an extensive range of molecular targets including proteins, small molecules, ions, whole cell bacteria and viruses. The shape-forming feature of the oligonucleotide imparts high selectivity, specificity and affinity towards the target. Aptamers⁵ are generally synthetic oligonucleotides and particularly designed for binding to a specific target, often referred as chemical antibodies, however, natural aptamers also

exist in riboswitches. They bind to their target of interest via van der Waals forces, electrostatic interactions, hydrogen bonding and shape complementarity.³⁰ Aptamers can distinguish between minor structural variations probably arising due to differing chirality or presence and absence of a small functional group. The term 'aptamer' was first introduced by Ellington and Szostak.³¹ In the 1990s, the groups of Gold³² and Szostak³¹ independently demonstrated an *in vitro* selection and amplification technique for the isolation of oligonucleotides able to bind non-nucleic acid targets with high affinity and specificity from a large pool of random sequences. This process of selection is known as SELEX (Systematic *E*volution of *L*igands by *EX*ponential enrichment, Figure 16).

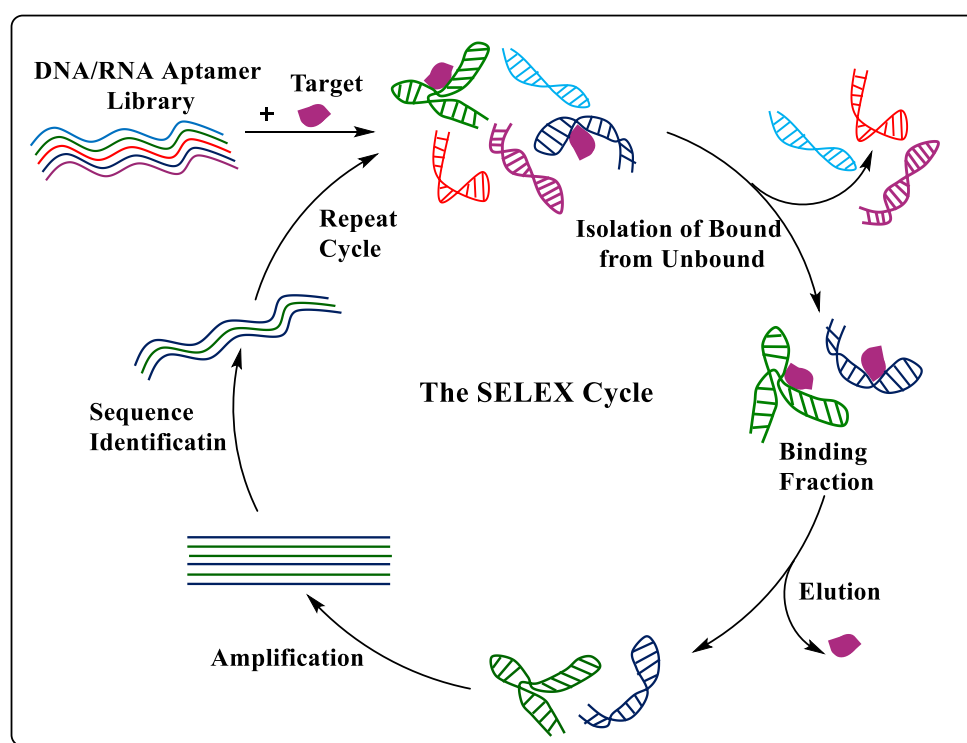


Figure 16: Schematic representation of SELEX (Systematic *E*volution of *L*igands by *EX*ponential enrichment).

Aptamers act in a similar way to antibodies but have superior features like smaller size (~10 fold) than antibody, can be chemically modified, longer shelf life, which makes their use attractive in diverse diagnostic, therapeutic and imaging applications. During the past 30 years, more than a hundred extremely selective and strong binding nucleic acid aptamers have been developed for various molecular targets. The first aptamer based drug approved by US FDA in 2004 was Pegaptanib sodium (Macugen) for the treatment of age related macular degeneration.³³

1.10 The G-quadruplex in aptamers

G-rich oligonucleotides comprise a significant proportion of aptamers that display the ability to fold into stable G-quadruplex structures that enable molecular recognition of their ligands. G-quadruplex-forming aptamers have several advantages over unstructured oligonucleotides,³⁴ like chemical and thermodynamic stability, enhanced resistance to nuclease degradation and increased cellular uptake.³⁵ The enhanced stability of the G-quadruplex structure is advantageous for improving electrostatic interactions with positively charged target proteins due to the negatively charged nature of the backbone.

Aptamers exhibit different structural arrangements that account for their binding efficiency and selectivity towards targets. Information about the G-quadruplex structure is essential for the development of G-quadruplex aptamers so that modification can be done for the improvement of their function. Thrombin binding aptamer (TBA) is one of the most comprehensively studied G-quadruplex aptamers.³⁶ Till date many G-quadruplex forming aptamers against various human pathologies have been studied, for example, AS1411 is anticancer aptamer to prevent tumor growth, antiviral aptamers like ISIS 5320, T30177 against HIV, targeting the gp 120 protein, antithrombin aptamer RE 31, RA 36 binding with exosite of thrombin, GVEGF aptamer as an antifungal agent. Besides targeting protein binding and function regulation, aptamers have been used as aptasensors to mediate analytic detection in diseases such as Alzheimer's disease, diabetes and Wilson's disease.³⁷

1.10.1 Anticoagulation aptamer target: Thrombin (Master enzyme of hemostasis)

Thrombin is a central key regulatory enzyme in the process of hemostasis. It is a multifunctional serine protease enzyme and has both procoagulant and anticoagulant functions,³⁸ generated from its inactive precursor prothrombin by factor Xa. Fibrinogen is a soluble protein which is converted into insoluble fibrin, building block of blood clot by the action of thrombin.³⁹ Therefore thrombin is a primary target in the development of anticoagulation therapy. Bock and co-workers³⁶ first used thrombin as the protein target, to choose the first single-stranded DNA aptamer. One of the most explored targets for aptamer binding is thrombin. Thereafter at least four aptamers, which are TBA (G15D, HTQ and HD1), a 15-mer ssDNA of the sequence (5'-GGTTGGTGTGGTTGG)³⁶,

HD22 (HTDQ) a 29-mer ssDNA aptamer of the sequence (5'-AGTCCGTGGTAGGGCAGGTTGGGGTGACT-3'),⁴⁰ NU172 (ARC2172), a 26-mer ssDNA of the sequence (5'-CGCCTAGGTTGGGTAGGGTGGTGGCG-3')⁴¹ and Toggle-25 (TOG25), a 25-mer RNA aptamer of the sequence (5'-GGGAACAAAGCUGAAGUACUUACCC-3')⁴² and their modified analogues were reported. The significant structural features of thrombin are a) a deep active site cleft and b) two positively charged surfaces, exosites I and II. Fibrinogen binds to the exosite I of thrombin and exosite II is the heparin binding site of thrombin. A number of thrombin-binding DNA aptamers have been developed during recent years, but probably TBA is one of the finest.

1.10.2 Thrombin binding aptamer (TBA) – More than a simple aptamer

Along with the design of new aptamers, a lot of attempts have been devoted to the modification of well-known aptamers, with the aim of improvement in affinity, selectivity and stability to overcome potential drawbacks. The pentadecameric thrombin-binding aptamer (TBA, 5'-GGTTGGTGTGGTTGG-3') is probably one of the best-known DNA aptamers. It has been extensively studied and well-characterized for its spatial organization and interaction with thrombin. The thrombin-TBA pair has been used as a model structure in the design of various drugs and diagnostics due to the relative ease of evaluation of binding efficacy in biological environment.⁴³ The binding interaction of TBA with thrombin shows inhibition in its function due to which blood clotting time decreases, that can be identified through a simple in vitro test ('thrombin time test').⁴⁴

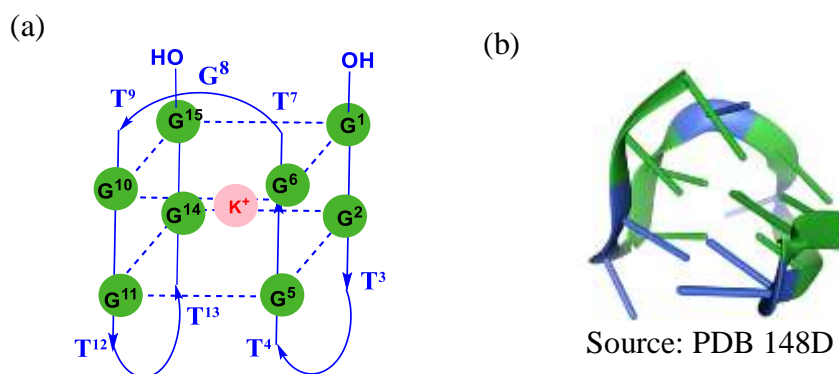


Figure 17: (a) Unimolecular Antiparallel Quadruplex structure of TBA (b) 3D structure of Thrombin binding aptamer⁴⁵

NMR and X-ray structural studies revealed the 3D structure of TBA, It folds into an intramolecular antiparallel G-quadruplex that consists of two G-quartets (G^1, G^6, G^{10}, G^{15} and G^2, G^5, G^{11}, G^{14}) that are connected by two TT loops and a central TGT loop in a chair-like conformation (Figure 17).⁴⁶

Guanines in the same quartet exhibit alternating 5'-*syn-anti-syn-anti*-3' conformation with respect to the glycosidic bond angle. All ribose sugar puckers are predominantly in South (*S*-type, *C2'-endo*) conformation. The nucleobases in the loop- G^8 and all thymines ($T^3, T^4, T^7, T^9, T^{12}$ and T^{13}) display *anti* conformation of the glycosidic torsion angle. The crystallographic image reported by Padmanabhan et al.⁴⁷ showed that the central TGT loop and lateral TT loops spanned the wide and narrow grooves respectively.

1.10.3 TBA- Thrombin interaction

The two lateral TT loops (T^3, T^4 and T^{12}, T^{13}) of TBA are particularly important for the interaction with exosite I of α thrombin, and act as a pincer-like system.⁴⁸ (Figure 18) T^4 and T^{13} are mainly engaged in polar interactions while T^3 and T^{12} associated with amino acid residues His71, Arg75, Tyr76, Arg77, Asn78, Ile79 and Tyr117 in the exosite I of thrombin through hydrophobic interaction. Studies done by Yeates and coworkers⁴⁶ suggested that the TGT loop is in the vicinity of the exosite II of an adjacent thrombin molecule.

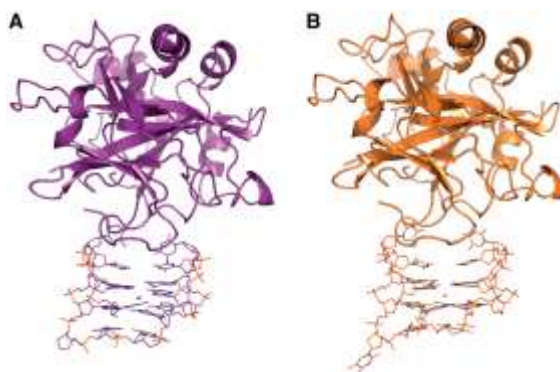


Figure 18: G-quadruplex structure of the thrombin binding aptamer, X-ray structure when bound to thrombin A) in the presence of Na^+ and B) in the presence of K^+ .⁴⁸

1.10.4 TBA quadruplex stability, dependence on cations

Together with the primary nucleotide sequence, the environmental conditions and in particular, cations are also responsible for G quadruplex formation and its topology.

The central negatively charged cavity can coordinate to a variety of cations with different radii which significantly influences the stability as well as topology of the folded G-quadruplex structure. Various measurements showed that the two G-tetrad planes formed by the eight guanine moieties created a cavity in which metal ion fits through coordination with four O6 atoms of each plane. The thrombin binding aptamer (TBA), in the presence of K^+ , folds into a unimolecular antiparallel G-quadruplex. Potassium is usually proved to be ideal for G-quadruplexes and leads to enhanced G-quadruplex stability.⁴⁹ A combination of various techniques such as CD spectroscopy, UV spectroscopy, Nuclear magnetic resonance spectroscopy (NMR), X-ray, Fluorescence spectroscopy, isothermal titration calorimetry and electrospray ionization mass spectrometry (ESI-MS) has been used to study the impact on the stability and thermodynamics of the monovalent and divalent metal ions in the formation of the 3D structures of the TBA complexes.⁵⁰ The monovalent cation NH_4^+ and divalent cations Mn^{2+} , Pb^{2+} , Ba^{2+} and Sr^{2+} were found to result in stable intramolecular quadruplex structures^{51,52} with even greater stability than K^+ , whereas Li^+ , Na^+ , Mg^{2+} , Cs^+ and Ca^{2+} formed less stable complexes that could be detected at low temperatures.⁵³ TBA is able to bind thrombin even in ion-deficient conditions, when thrombin acts as a molecular chaperone and assists the formation of the TBA quadruplex.⁵⁴

1.11 Modifications in TBA

1.11.1 Modifications in the G tetrads

It has been speculated that the stability and rigidity of TBA are crucial for thrombin-TBA interaction. In the past several chemical and structural modifications have been attempted to achieve the goal of improving its biological activity. The first and possibly most popular approach for TBA optimization is chemical modification. The most widely applied strategy is the systematic substitution by chemically modified nucleotides with unique structural characteristics or physicochemical properties. This aptamer has accordingly been subjected to several chemical modifications. The main purposes were to: (a) enhance its affinity to thrombin; (b) improve its thermal stability under physiological conditions; (c) make it resistant to degradation in biological environments; and (d) focus on aptamer–target interaction studies.

The various chemical modifications are classified depending on the position in G-tetrads or loops. Modifications involving the replacement of sugar units, phosphate groups as well as nucleobase have been reported.

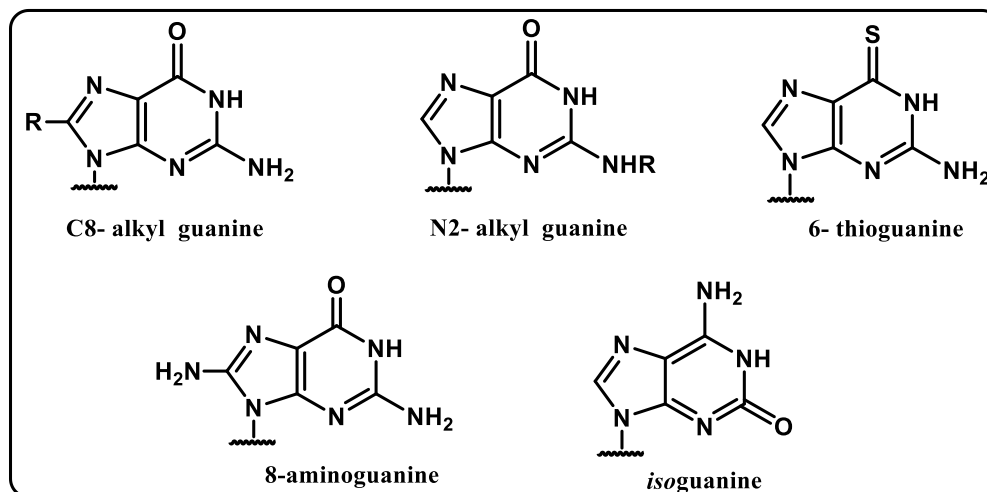


Figure 19: Modified guanines in TBA tetrads

Some of the modifications that are analogues of guanine and have been introduced in the G-tetrads are summarized in Figure 19, like C8-methylguanine, N2-alkyl guanine,⁵⁵ 6-thioguanine,⁵⁶ 8-aminoguanine⁵⁷ and *isoguanine*.⁵⁸

He et al.⁵⁵ reported the effect of replacement of guanines in the G-tetrad by the N2- and C8-alkyl substituted G residues.⁵⁵ It produced different effects on thrombin activity. Introduction of a small group such as methyl or propynyl at the C8 positions of *syn* Gs showed enhancement in the activity, probably due to the stabilization of a chair like structure, while steric hindrance caused by a large substituent group, like phenyl or ethynyl decreased the activity. Inhibition of quadruplex formation due to Hoogsteen hydrogen bonding destabilization was observed when guanines in the G-tetrads were substituted by 6-thioguanine. Probably this is due to decreased electro-negativity and increased radius of sulphur as compared to oxygen.⁵⁶ 8-Aminoguanine reduced the strength of stacking interactions, but the TBA quadruplex structure was not altered, and thus had only a small destabilization effect on the TBA quadruplex. Nallagatla et al.⁵⁸ substituted guanine by *isoguanine* in all possible positions of TBA, and found that three of the modified aptamers carrying one single *isoguanine* at position G¹, G⁸ or G¹⁰ showed greater binding affinity for thrombin than the unmodified TBA.

1.11.2 Sugar modification

TBA is characterized by nucleotides with a *C2'-endo* (South, *S*) sugar pucker. Several researchers demonstrated that alteration in the sugar puckering of the nucleoside in the loops of TBA influences the folding ability of TBA. Most substitutions with LNA, (2'-O-4'-C-methylene-linked ribonucleotide) with the *C3'-endo* sugar conformation led to a reduction of anticoagulant activity.⁵⁹ Eritja et al.⁶⁰ reported the effect on quadruplex stability of North-nucleoside, uridine (U) and 2'-fluorouridine (FU) in the loop regions of TBA (Figure 20).

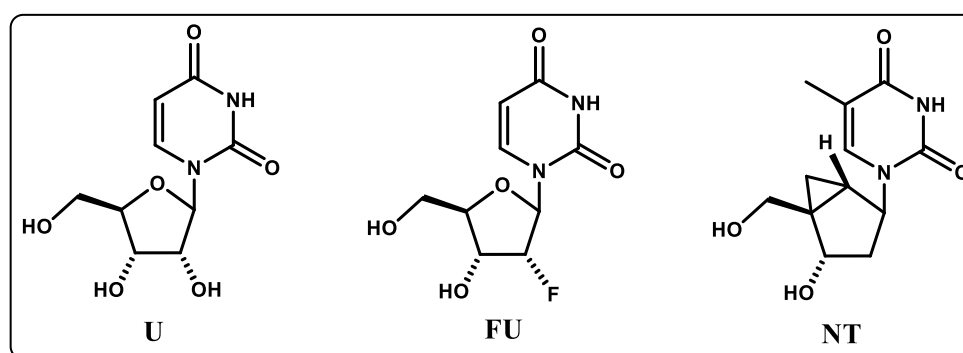


Figure 20: Nucleoside modifications- uridine (U), 2'-deoxy-2'-fluorouridine (FU) and North-methanocarbathymidine (NT)

Damha and co-workers examined the impact of 2'-deoxy-2'-fluoroarabinonucleoside residues (2'-F-araN) on TBA.⁶¹ 2'-F-araN confers a DNA-like South conformation to nucleotides. Incorporation of 2'-F-araN G or T residues was found to stabilize the TBA quadruplex; when introduced in the loop, binding with thrombin was improved by 4-5-fold. In addition, enhancement in thermal stability and better nuclease resistance were seen.⁶¹ Wengel's group investigated the modified variants of TBA, one at a time substituted with a UNA monomer in each possible position, and recognized a single position (position 7) out of 15 investigated, that showed improvement in anticoagulant activity.⁶² The substitution of four thymine residues (T³, T⁷, T⁹ or T¹³) by 4-thio-dU resulted in a modified TBA analogue which showed 3-fold enhancement in anticoagulant activity.⁶³ Studies from our group showed a single 2'-OMe chemical modification in the loop region to be able to favourably affect the topology and stability of TBA and its binding with thrombin.⁶⁴ Guan et al.⁶⁵ explored the impact of sugar pucker and glycosidic torsion angles on the TBA quadruplex structures by

substituting 2'-*O*-methyl nucleotide which possesses a C3'-*endo* sugar pucker. TBA has been modified by incorporation of unlocked nucleic acid (UNA), 3'-amino-modified UNA and abasic three-carbon spacer (spacer-C3) by Veedu and co-workers (Figure 21).⁶⁶ All three modifications were incorporated at loop positions T³, T⁷ or T¹², out of which, spacer-C3 introduction at the T⁷ loop position exhibited notable enhancement in thermal stability and anticoagulation activity.⁶⁶

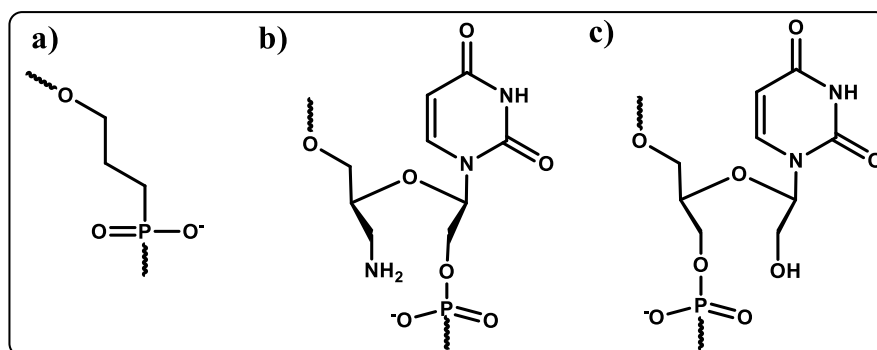


Figure 21: Structure of the three monomer modifications a) spacer-C3, b) amino-UNA and c) UNA

1.11.3 Sugar-phosphate backbone modification in TBA loops

The loop regions of TBA, particularly the TT loops are reported to be important for the folding of the aptamer and interaction with its target, thrombin.⁴⁸ Efforts towards improving stability to nucleases have focused on backbone modifications. Different phosphate-modified linkers have been reported including the phosphorothioate, methyl phosphonate,⁶⁷ formacetal⁵⁵ and triazole⁶⁸ linkages (Figure 22). Phosphorothioate linkages in the stem region resulted in decreased thermal stability, but in the TT loop, caused increased nuclease stability, while retaining the thermal stability and anticoagulant activity.⁴⁴ Methyl phosphonates caused a large destabilization of the G-quadruplex.⁶⁷ Replacement of the negatively charged phosphodiester by the neutral formacetal linkage⁵⁵ had not much effect on the thrombin inhibitory activity. The triazole internucleotide linkage led to a decrease in thermal stability of the resulting quadruplexes but increased their resistance to nucleolytic digestion.

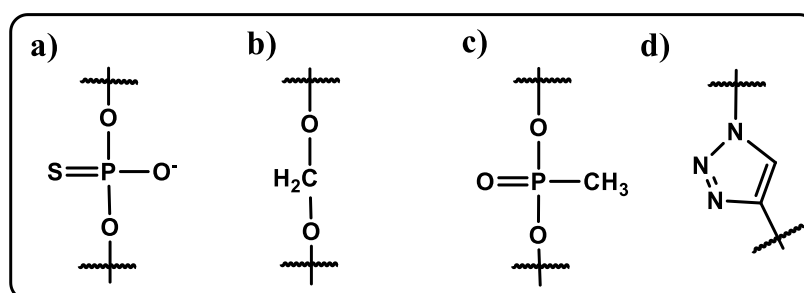


Figure 22: Chemical structure of modified internucleotide phosphate a) phosphorothioate, b) formacetal, c) methyl phosphonate and d) triazole internucleoside linkages

Significant impact of strand polarity inversion⁶⁹ (Figure 23) on thermal stability and thrombin affinity was seen, but decreased thrombin inhibition was observed

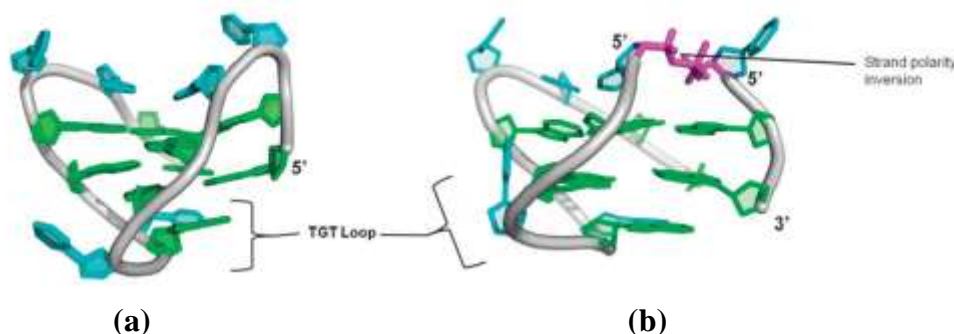


Figure 23: NMR solved structures of the (a) thrombin binding aptamer (TBA) [PDB Id 148D] and (b) modified TBA with strand-polarity inversion [PDB Id 2IDN]. (Collie, G. W., Parkinson, G. N., *Chem. Soc. Rev.*, 2011, 40, 5867.)

Another interesting work has focused on TBA analogues consisting of an extra residue added at both the ends or only at the 3'-end of native TBA, connected through 3'-3' or 5'-5' phosphodiester bonds⁷⁰ (Figure 24). The TT loops involved in interaction with thrombin were thus, not affected by this straightforward modification.

Among the modified TBA derivatives, TBA-A (5'-G¹G²T³T⁴G⁵G⁶T⁷G⁸T⁹G¹⁰G¹¹T¹²T¹³G¹⁴G¹⁵-3'-3'-A¹⁶) characterized by enhancement in the thrombin-binding affinity compared to TBA, showed the highest increase in the melting temperature (+11 °C). Molecular modelling studies showed that TBA-A with the extra 3'-3' adenosine allowed a very efficient additional stacking interaction at the 3'-end.

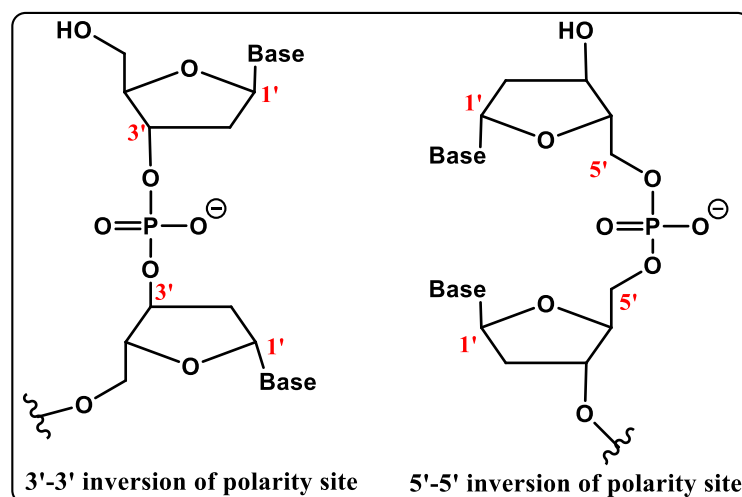


Figure 24: The chemical structures of the 3'-3' and 5'-5' inversion of polarity sites.

The folding patterns of an isosequential TBA RNA sequence⁷¹ showed formation a multimolecular parallel G-quadruplex in contrast to the unimolecular antiparallel G-quadruplex structure of TBA. Tang and Shafer⁷² examined the impact of a single nucleoside conformation on the folding topology by selective replacement of dG by rG in the TBA sequence. Depending on the position of the ribo- or deoxyribo-nucleotides, whether the oligomers with a mixed DNA/RNA backbone folded in a DNA-like or RNA-like quadruplex structure was evaluated. Our group earlier reported *iso*TBA,⁷³ where the 3'-5'-phosphodiester backbone was replaced by the isomeric 2'-5'-phosphodiester backbone throughout the TBA oligomer (Figure 25), that was able to retain the unimolecular antiparallel quadruplex topology of TBA. *Iso*TBA was shown to bind to thrombin and exhibit anticoagulant properties, though to a lower degree than TBA. Recently we developed TBA analogues with substitutions at loop positions by 4'-methoxymethyl threofuranosyl thymidine (4'-MOM-T), where substitution at the T⁷ position was found to show enhanced thermal stability, anticoagulation activity and nuclease resistance.⁷⁴

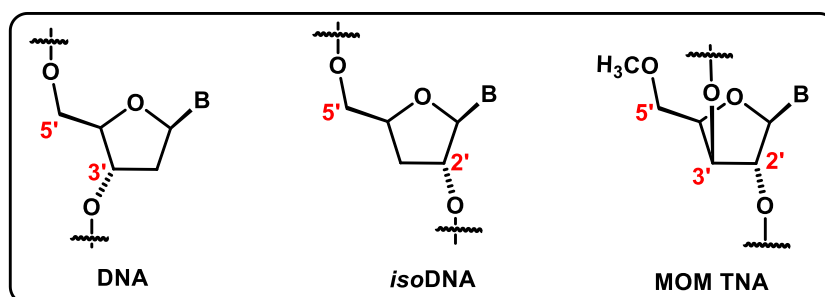


Figure 25: Structures of natural DNA, *iso*DNA, and 4'-methoxymethyl -TNA

Many strategies for improving the stability and the target affinity of the thrombin binding aptamer have been exploited. Results from the literature provide insights into specific interactions between TBA and thrombin and provide a better knowledge of the subtle characteristics involved in TBA and thrombin interaction.

1.12 Solid-phase synthesis of oligonucleotides: Brief history and application in oligonucleotide synthesis.

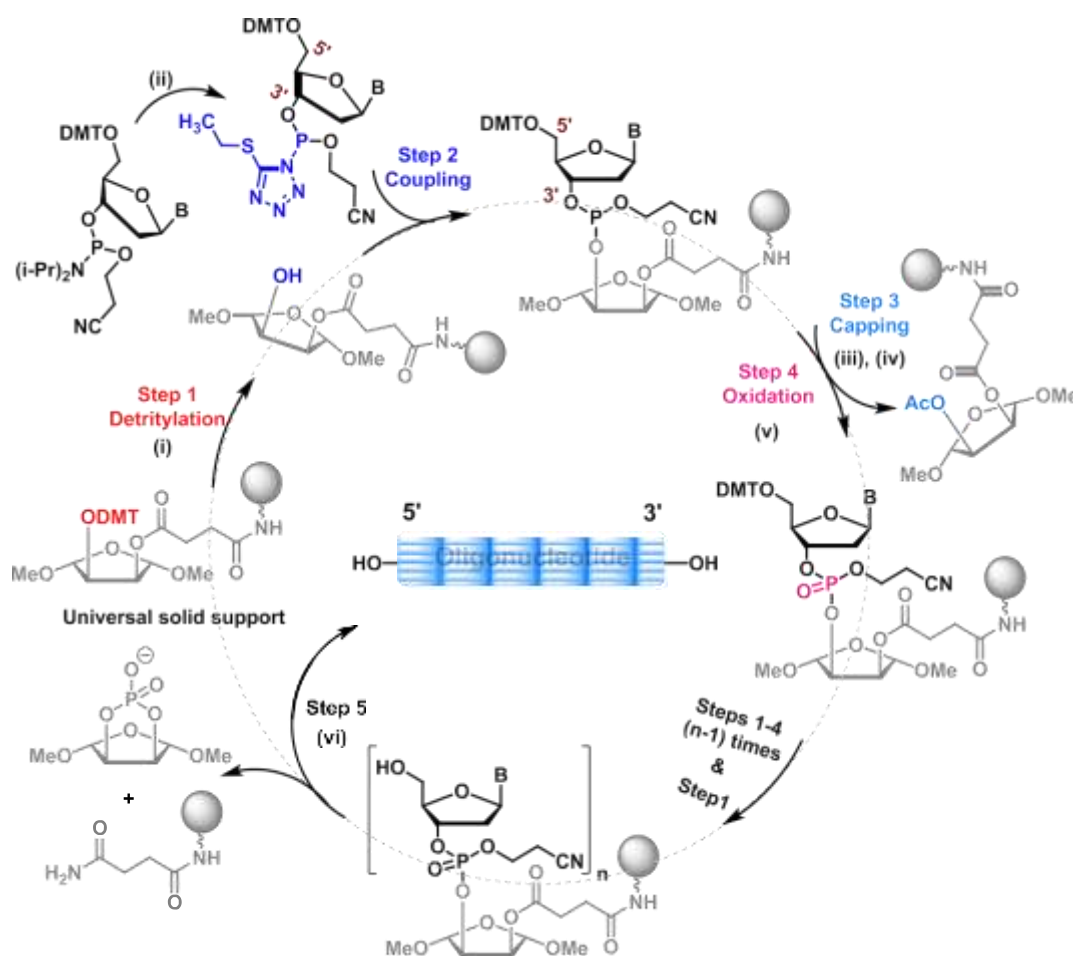
Solid-phase synthesis is a commonly used method for the synthesis of peptides and oligonucleotides. In 1960, it was invented by Bruce Merrifield, who received the Nobel Prize in 1984. This synthesis is performed on a solid support like controlled pore glass or polystyrene. Several methods have been developed for oligonucleotide synthesis in solution phase. In the early 1950s, Michelson and Todd⁷⁵ pioneered the H-phosphonate and phosphate triester approach, later Har Govind Khorana's group⁷⁶ developed the phosphodiester method. In the 1960s the phosphotriester⁷⁷ approach was developed by a group led by R. Letsinger and in the 1970s, a reinvestigation of the phosphotriester method was done by the same group and they developed the phosphite triester⁷⁸ approach. Each of these methods has its drawbacks. In the early 1980s, Marvin Caruthers⁷⁹ provided a breakthrough and pioneered the phosphoramidite method that was enhanced with the solid support and automation and proved to be the Gold standard method for oligonucleotide synthesis.

Synthesis

Two types of solid supports can be used to perform oligonucleotide synthesis. One of them is the standard support with a nucleosidic unit that becomes the 3'-end residue, as the synthesis is carried out in 3'→5' direction, another type is the universal solid support, which has an abasic sugar unit instead of the 3'-nucleoside unit, and does not form a part of the final oligonucleotide. The benefit of using the universal support is that four different supports (depending on whether the desired oligonucleotide has A/ T/ G or C at the 3'-end) for DNA synthesis are not necessary and another key benefit is that 3'-end modified oligomer synthesis can be done only on universal solid support which is not feasible on conventional standard supports.

Phosphoramidite oligonucleotide synthesis proceeds in the 3'→5' direction, and is outlined in Scheme 1. The synthesis is performed by the sequential addition of protected

nucleotide residues. It involves a four-step cycle comprising 1) detritylation 2) coupling 3) capping and 4) oxidation. At the beginning of typical oligonucleotide synthesis, the 4,4'-dimethoxytrityl group of the support-bound nucleoside is removed by treatment with 3% trichloroacetic acid (step 1). Once the DMT group is removed, the activated phosphoramidite monomer is added. Activation of the phosphoramidite monomer is achieved by treatment with a 0.25 M solution of 5-(S-ethyltetrazole) in CH_3N (step 2). The activated phosphoramidite moiety of this added monomer reacts with the free 5'-hydroxy group on the solid support to produce a one-nucleotide-extended oligonucleotide on the support, bound by a phosphate triester linkage. The unreacted 5'-OH groups of nucleosides on the support are blocked by capping as their acetate derivatives, achieved using acetic anhydride and *N*-methylimidazole in pyridine (step 3). The newly formed phosphotriester (P(III)) is unstable to acid and therefore is transformed to stable P(V) state by oxidation using iodine with water and pyridine (step 4).



Reagents and conditions: (i) 3% TCA in DCM (ii) 0.25 M 5-(S-ethyltetrazole) in ACN (iii) 10% N-methylimidazole in THF 0.1 M (iv) Ac₂O/Py (v) I₂/Py/H₂O/THF (vi) aq. NH₃, 55 °C.

Scheme 1: The sequence of chemical reactions involved in the solid phase synthesis of oligonucleotides on a universal support

Repetition of this cycle, once for each nucleotide, produces the desired oligonucleotide sequence. In the post-synthesis treatment, cleavage from the solid support is done by aqueous ammonia treatment. The protecting groups of exocyclic amino groups of the nucleobases and inter-nucleoside β -cyanoethyl phosphate protection were also removed in aqueous ammonia treatment. Purification of the crude oligomer was done by RP-HPLC and characterization by MALDI-TOF mass spectrometry.

1.13 Tools and techniques for structural and stability studies of nucleic acid complexes and higher-ordered G-quadruplexes

1.13.1 UV-spectroscopy

The heterocyclic bases of nucleic acids absorb ultraviolet light, and the λ_{\max} for all nucleobases lies between 250 nm to 280 nm because of the π - π^* transitions associated with purine and pyrimidine bases. Estimation of nucleic acid concentration can therefore, be done by measuring the absorbance at 260 nm in aqueous solution. The concentration can then be determined by using the Beer-Lambert law,

$$A = Ecl$$

Where, E = extinction coefficient, c = the concentration and l = the length of the cuvette.

To monitor the folding and unfolding patterns of nucleic acids in solution, UV absorption spectroscopy is widely used. As with duplex formation, the quadruplex formation also can be inferred from UV spectroscopy studies. The formation of the G-quadruplex structure is accompanied by an increase in absorbance at 295 nm. Thermal denaturation experiments can provide information about the thermal stability of DNA/RNA complexes such as duplexes, triplexes or quadruplexes. The denaturation/renaturation of quadruplex at different temperatures can be monitored by recording absorbance at 295 nm. Melting studies for G-quadruplexes⁸⁰ can be performed on a UV-visible spectrophotometer by recording the absorbance at 295 nm with increasing temperature. The melting temperatures (T_m) can be obtained from the absorbance versus temperature curves. Recording a UV absorbance scan at different

temperatures can be used to generate a thermal difference spectrum (TDS). Subtraction of the spectral scan of the sample at a temperature below (e.g., 10 °C) from that above (e.g., 90 °C) the melting temperature results in the TDS. The TDS is reported to provide a fingerprint of G-quadruplex topologies.⁸¹

The TDS shape illustrates the intricate details of base-stacking interactions that occur peculiarly within each nucleic acid structure type. TDS offers an easy and quick method for obtaining structural information of nucleic acids.

1.13.2 Circular Dichroism (CD)

Circular dichroism is an absorption spectroscopic technique based on differential absorption of left- and right- circularly polarized light due to structural asymmetry. It has been extensively used to investigate structural aspects of optically active chiral molecules, biological molecules, and their interactions with metal ions and other molecules. The value in CD arises from the ability to show conformational changes in molecules. The spectrum resulting from an ordered structure may have both positive and negative signals; lack of regular structure results in zero CD amplitude. The phenomenon of CD is very sensitive to the secondary structures of biomolecules like proteins, DNA and RNA, so it has very special significance in the characterization of biomolecules. There are three sources of chirality in nucleic acids which are the asymmetric sugar, the helicity of the secondary structure adopted by the nucleic acid and the long-range tertiary ordering of DNA in some environments. In nucleic acids, the heterocyclic bases are achiral but are the principal chromophores.⁸² CD spectroscopy is one of the most significant tools and is a frequently-utilized method for studies of G-quadruplexes. It is a well-known technique for studying the polymorphism of G-quadruplexes. In the case of G-quadruplexes, two determining factors are the source of spectra in CD spectroscopy 1) differential G-tetrad polarity, and 2) differential folding geometry. G-tetrad polarity means directional orientation and can be defined in terms of strand orientation and stacking orientation.

In parallel quadruplexes, all nucleobases are either *syn* oriented or *anti* oriented and have the same stacking polarity (head-to-head). However, in antiparallel quadruplexes, nucleobases are alternately *syn* or *anti* oriented and has the opposite polarity stacking (head-to-tail). In the case of G-quadruplexes, the characteristic

differences in the CD spectra are very much dependent on the folding topology which is related to *syn* or *anti* glycosidic bond angles and orientation of nucleobases. The different orientation of strands results in parallel, mixed parallel-antiparallel or antiparallel topology. It is possible to differentiate between particular G-quadruplex topologies, as parallel quadruplexes exhibit strong positive CD maxima at 260 nm, while antiparallel quadruplexes show a characteristic signals positive at 295 nm and negative at 260 nm. In addition to the topology, denaturation/renaturation of quadruplexes at different temperatures can be monitored by recording the amplitude at 295 nm in CD spectroscopy.⁸³ Melting studies for G-quadruplexes can be performed by CD by monitoring the changes with increasing temperature. Ellipticity versus temperature curves can provide the melting temperature (T_m) of the quadruplex (Figure 26).

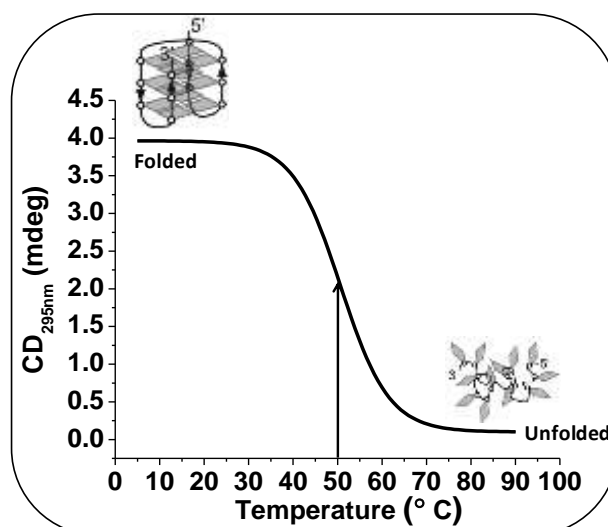


Figure 26: Representative CD thermal melting spectra

In most cases of intramolecular quadruplexes, hysteresis is not observed. Most bimolecular quadruplexes fold much faster, consequently shows hysteresis between their melting and annealing profiles. G-quadruplex topology of DNA as well as RNA has been studied by CD Spectroscopy. This is an outstandingly advantageous tool in this area.⁸⁴

1.13.3 Polyacrylamide gel electrophoresis (PAGE)

Several methods exist for the purification of oligonucleotides; among these, polyacrylamide gel electrophoresis (PAGE) is widely used for purification and to study complex formation in DNA/RNA. It separates the molecules on the basis of their electric

charge, size and secondary or tertiary structure. Denaturing gel electrophoresis is used for purification of DNA where denaturing agent such as urea is used. It is possible to separate and purify an oligonucleotide of 'n' base-pairs from a failure sequence of 'n-1' base-pairs or others by means of PAGE. Depending on the percentage of polyacrylamide used, denaturing polyacrylamide gels can separate oligonucleotides from 2 to 300 bases in length. In the gel, molecules may be run in their native state, preserving the molecule's higher-order structure. Non-denaturing or native gel can be utilized to distinguish structural changes in oligomers. The rapid recognition of folded and unfolded single-stranded DNA states can be easily carried out under native conditions.

1.13.4 MALDI-TOF Mass Spectrometry

Matrix-assisted laser desorption/ionization time-of-flight (MALDI-TOF) mass spectrometry can be successfully utilized for the analysis of biomolecules like DNA, RNA proteins and peptides due to its ease and speed of analysis. It is a two-step soft ionization technique, in which the first step is desorption triggered by pulses of laser light (nitrogen laser, 337 nm) to vaporize the matrix, heavy absorption of UV laser by matrix leads to the ablation of the upper layers of the matrix. In the second step, oligomer molecules are ionized in a hot cloud. In time-of-flight (TOF), ionized oligomer molecules are accelerated by the electric field to the same kinetic energy and then the time taken by them to reach the detector is measured. With the same charge and same kinetic energy, their velocities, and the TOF are dependent only on their masses, lighter ions travel faster, heavier ions travel slowly. The mass spectrum is recorded as ion flux versus time. The matrix is a crystalline material of low molecular weight; typically used matrices are 3, 5-dimethoxy-4-hydroxycinnamic acid, 2', 4', 6' trihydroxy acetophenone (THAP), and 2, 5 dihydroxybenzoic acid. MALDI-TOF analysis can be used to confirm the identity and integrity of a synthesized oligonucleotide sequence and can be used at multiple stages during oligonucleotide synthesis to reveal potential problems during synthesis.

1.13.5 High-performance liquid chromatography (HPLC)

High-performance liquid chromatography (HPLC) is an efficient method that has been used conventionally for the analysis and purification of synthetic oligonucleotides. For the purification of oligonucleotides, reverse phase RP-HPLC and anion exchange

chromatography is routinely used. Anion exchange HPLC separates oligonucleotides on the basis of charge differences using ion exchange resin containing positively charged groups. Cationic resin binds to negatively-charged molecules; increasing the ionic strength of the mobile phase reduces the interaction between ONs and cationic stationary phase so that shorter ONs elutes first and the longer, highly charged ONs elutes later.

RP-HPLC separates oligonucleotides on the basis of difference in hydrophobicity. Crude oligonucleotides contain terminated shorter sequences that differ from the desired oligonucleotide in hydrophobicity. RP-HPLC uses a nonpolar stationary phase. Mixtures of organic solvents and aqueous buffers are used as the mobile phase for elution. In the present work of this thesis, RP-HPLC has been used for the purification of oligonucleotides. Aqueous ammonium acetate and acetonitrile were used as solvents for elution. Molecules with a greater degree of hydrophobicity are eluted more slowly and polar compounds are eluted first with a gradient of increasing acetonitrile in aqueous buffer. Further, degradation of single-stranded nucleic acid oligomers can be examined by RP-HPLC. The amount of intact oligonucleotides can be estimated from the area under the peak. A plot of the amount of intact oligonucleotide Vs time, provides an idea of the half-life of the oligonucleotide under the specified experimental conditions.

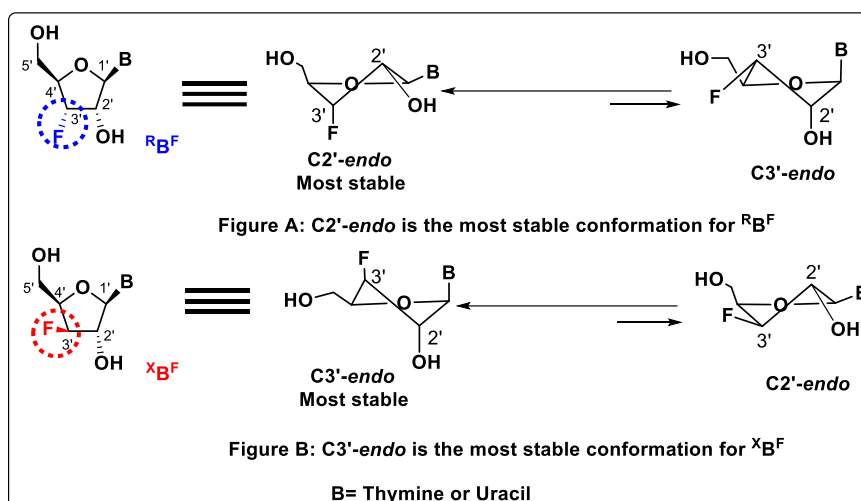
1.14 Present work

Chapter 1: Introduction to Guanine-rich nucleic acid aptamers with a focus on the Thrombin binding aptamer (TBA)

Aptamers are chemically synthesized short oligonucleotide sequences that bind to their targets with high selectivity, specificity and affinity. The thrombin-binding aptamer, 5'-GGTTGGTGTGGTTGG-3' (TBA) is a 15mer guanine-rich sequence that forms an antiparallel G quadruplex structure. It was discovered by the SELEX process and selectively binds to thrombin (enzyme in the blood coagulation process), inhibiting its action. TBA is a strong anticoagulant in vitro and has a short in vivo half-life which makes it an ideal anticoagulant for cardiopulmonary bypass surgeries. Currently, heparin is the most widely used anticoagulant, for which TBA is a promising alternative. This chapter presents a brief review about the research focused on the development of new TBA derivatives with improved anticoagulant properties as well as the use of TBA as a model compound for the study of quadruplex structures.

Chapter 2: S/N-type frozen 3'-deoxy, 3'-fluoro nucleosides in non-genetic 2'-5' linked thrombin binding aptamer (*iso*TBA).

The highly electronegative nature of the fluorine substitution in different orientations on the sugar ring imparts very different electronic effects that in turn influence the sugar ring conformations. 3'-xylo and 3'-ribo configured 3'-fluoro, 3'-deoxy nucleosides are frozen in the N-type and S-type geometry, respectively (Figure A & B). In this chapter, we report the synthesis of 3'-deoxy-3'-ribo/xylo fluoro thymidine ($^R\text{T}^F$ and $^X\text{T}^F$) and 3'-deoxy-3'-ribo/xylo fluoro uridine ($^R\text{U}^F$ and $^X\text{U}^F$) nucleosides, their incorporation into the TBA oligomer and compare the effects of these frozen sugar geometries on the resulting G-quadruplexes.



This chapter is divided into two sections

Section A: Synthesis of S/N-type-frozen 3'-deoxy-3'-ribo/xylo fluoro thymidine ($^R\text{T}^F$ and $^X\text{T}^F$) and 3'-deoxy-3'-ribo/xylo fluoro uridine ($^R\text{U}^F$ and $^X\text{U}^F$) nucleosides.

This section describes the synthesis of 3'-deoxy-3'-ribo ($^R\text{T}^F$ and $^R\text{U}^F$) and 3'-deoxy-3'-xylo fluoro ($^X\text{T}^F$ and $^X\text{U}^F$) nucleosides from D-xylose and D-glucose respectively as appropriately protected phosphoramidite derivatives which are suitable for solid-phase oligonucleotide synthesis of TBA.

Section B: 3'-Deoxy-3'-fluoro nucleosides in the thrombin binding aptamer (TBA): Evaluation of stability and activity.

In this section we describe the synthesis of *iso*TBA variants bearing the 3'-deoxy, 3'-fluoro modified units in loop positions and biophysical evaluation studies of their

effect on the stability of the quadruplex structure and anticoagulation properties. Incorporation of S-type and N-type conformationally frozen monomers (3'-deoxy, 3'-fluoro thymidine/uridine) in *iso*TBA with a 2'-5'-backbone is reported for the first time. These newly reported *iso*TBA analogues showed antiparallel quadruplex topology with an enhancement in thermal stability compared to the parent *iso*TBA and better nuclease stability as compared to the natural 3'-5'-linked TBA.

Chapter 3: Truncated loops in 3'-5' linked TBA Vs 2'-5' linked *iso*TBA: Effect on quadruplex topology and thrombin binding

The loop length, as well as the nature and identity of nucleotides in the loop region, control the topology and stability of the quadruplex structures. This chapter summarizes the synthesis of 3'-5' linked TBA and 2'-5' linked *iso*TBA variants with truncated loops and the effect on the quadruplex topology and thrombin binding properties. The 2'-5'-linked *iso*TBA sequences of the present study were found to form antiparallel G-quadruplex structures, independent of the loop length in the presence of K⁺ ions. The extended backbone geometry as a result of the 2'-5' linkages helps to reduce the strain of the shortened loops compared to 3'-5' linkages and allows the formation of unimolecular folded structures. This result is in contrast to previously reported studies of 3'-5'-phosphodiester-linked G-quadruplexes where reducing the loop length resulted in a change from an antiparallel to a parallel quadruplex structural topology. The decreasing loop-length in the *iso*TBA sequences, however, adversely affected the thermal stability of the quadruplexes.

Chapter 4: Effect of 2'-5' and 3'-5' linkages in the loop region of TBA and *iso*TBA respectively, on G-quadruplex stability and function

The 3'-deoxy-2'-5'-linked non-genetic *iso*DNA exhibits high stability against cellular enzymes and therefore it is a promising alternative nucleic acid for developing DNA therapeutics. This chapter summarizes the synthesis of oligomers with 3'-5'-(TBA) and 2'-5'-phosphodiester-linked (*iso*TBA) backbones in which the loop regions are systematically replaced by 2'-5'- and 3'-5'- phosphodiester linkages respectively. We found that substitution of the 2'-5' linkage in *iso*TBA with the 3'-5' linkage resulted in a strong stabilization of the quadruplex structure. The *iso*TBA sequences showed better nuclease stability against exonuclease as well as endonuclease.

1.15 References

1. Watson, J. D.; Crick, F. H. C., Molecular Structure of Nucleic Acids: A Structure for Deoxyribose Nucleic Acid. *Nature* **1953**, *171* (4356), 737-738.
2. Felsenfeld, G.; Davies, D. R.; Rich, A., Formation of a three-stranded polynucleotide molecule. *J. Am. Chem. Soc.* **1957**, *79* (8), 2023-2024.
3. Hoogsteen, K., The crystal and molecular structure of a hydrogen-bonded complex between 1-methylthymine and 9-methyladenine. *Acta. Cryst.* **1963**, *16* (9), 907-916.
4. Greider, C. W., Telomerase activity, cell proliferation, and cancer. *Proc. Natl. Acad. Sci. USA* **1998**, *95* (1), 90-92.
5. Sundquist, W. I.; Klug, A., Telomeric DNA dimerizes by formation of guanine tetrads between hairpin loops. *Nature* **1989**, *342* (6251), 825-829.
6. Sen, D.; Gilbert, W., Formation of parallel four-stranded complexes by guanine-rich motifs in DNA and its implications for meiosis. *Nature* **1988**, *334* (6180), 364-366.
7. Gehring, K.; Leroy, J. L.; Guéron, M., A tetrameric DNA structure with protonated cytosine-cytosine base pairs. *Nature* **1993**, *363* (6429), 561-565.
8. Sundaralingam, M., Stereochemistry of nucleic acids and their constituents. IV. Allowed and preferred conformations of nucleosides, nucleoside mono-, di-, tri-, tetraphosphates, nucleic acids and polynucleotides. *Biopolymers* 1969, *7* (6), 821-860.
9. Mathé, C.; Périgaud, C., Recent Approaches in the Synthesis of Conformationally Restricted Nucleoside Analogues. *Eur. J. Org. Chem.* **2008**, *2008* (9), 1489-1505.
10. Plavec, J.; Tong, W.; Chattopadhyaya, J., How do the gauche and anomeric effects drive the pseudorotational equilibrium of the pentofuranose moiety of nucleosides? *J. Am. Chem. Soc.* **1993**, *115* (21), 9734-9746.
11. Thibaudeau, C.; Chattopadhyaya, J., *Stereoelectronic effects in nucleosides and nucleotides and their structural implications*. Uppsala University Press Uppsala: 1999; p 91-506.
12. Yakovchuk, P.; Protozanova, E.; Frank-Kamenetskii, M. D., Base-stacking and base-pairing contributions into thermal stability of the DNA double helix. *Nucleic Acids Res.* **2006**, *34* (2), 564-574.
13. Dougherty, J. P.; Rizzo, C. J.; Breslow, R., Oligodeoxynucleotides that contain 2',5" linkages: synthesis and hybridization properties. *J. Am. Chem. Soc.* **1992**, *114* (15), 6254-6255.

14. Sulston, J.; Lohrmann, R.; Orgel, L. E.; Miles, H. T., Nonenzymatic synthesis of oligoadenylates on a polyuridylic acid template. *Proc. Natl. Acad. Sci. USA* **1968**, *59* (3), 726-733.
15. Orgel, L. E.; Lohrmann, R., Prebiotic chemistry and nucleic acid replication. *Acc. Chem. Res.* **1974**, *7* (11), 368-377.
16. Dhingra, M. M.; Sarma, R. H., Why do nucleic acids have 3'5' phosphodiester bonds? *Nature* **1978**, *272* (5656), 798-801.
17. Lagnado, J., The story of quadruplex DNA – it started with a Bang! *Biochem. (lond)* **2013**, *35* (2), 44-46.
18. (a) Bang, I., Z., *Biochem.* **1910**, *26*, 293-311; (b) Bang, I., Z. , *Physiol. Chem.* **1898**, (26), 133-159.
19. Gellert, M.; Lipsett, M. N.; Davies, D. R., Helix formation by guanylic acid. *Proc. Natl. Acad. Sci. USA* **1962**, *48* (12), 2013-2018.
20. Henderson, E.; Hardin, C. C.; Walk, S. K.; Tinoco, I., Jr.; Blackburn, E. H., Telomeric DNA oligonucleotides form novel intramolecular structures containing guanine-guanine base pairs. *Cell* **1987**, *51* (6), 899-908.
21. Evans, T.; Schon, E.; Gora-Maslak, G.; Patterson, J.; Efstratiadis, A., S1-hypersensitive sites in eukaryotic promoter regions. *Nucleic Acids Res.* **1984**, *12* (21), 8043-8058.
22. Kilpatrick, M.; Torri, A.; Kang, D.; Engler, J.; Wells, R., Unusual DNA structures in the adenovirus genome. *J. Bio. Chem.* **1986**, *261* (24), 11350-11354.
23. Blackburn, E. H., Telomeres: no end in sight. *Cell* **1994**, *77* (5), 621-623.
24. Giraldo, R.; Suzuki, M.; Chapman, L.; Rhodes, D., Promotion of parallel DNA quadruplexes by a yeast telomere binding protein: a circular dichroism study. *Proc. Natl. Acad. Sci. USA* **1994**, *91* (16), 7658-7662.
25. Han, H.; Hurley, L. H., G-quadruplex DNA: a potential target for anti-cancer drug design. *Trends pharmacol. sci.* **2000**, *21* (4), 136-142.
26. Simonsson, T., G-quadruplex DNA structures--variations on a theme. *Biol. Chem.* **2001**, *382* (4), 621-628.
27. Collie, G. W.; Parkinson, G. N., The application of DNA and RNA G-quadruplexes to therapeutic medicines. *Chem. Soc. Rev.* **2011**, *40* (12), 5867-5892.

28. Arnott, S.; Chandrasekaran, R.; Marttila, C. M., Structures for polyinosinic acid and polyguanylic acid. *Biochem. J.* **1974**, *141* (2), 537-543.
29. Bhattacharyya, D.; Mirihana Arachchilage, G.; Basu, S., Metal Cations in G-Quadruplex Folding and Stability. *Front. in Chem.* **2016**, *4* (38), 1-14.
30. Nimjee, S. M.; Rusconi, C. P.; Sullenger, B. A., Aptamers: An Emerging Class of Therapeutics. *Annu. Rev. Med.* **2005**, *56* (1), 555-583.
31. Ellington, A. D.; Szostak, J. W., In vitro selection of RNA molecules that bind specific ligands. *Nature* **1990**, *346* (6287), 818-822.
32. Tuerk, C.; Gold, L., Systematic evolution of ligands by exponential enrichment: RNA ligands to bacteriophage T4 DNA polymerase. *Science* **1990**, *249* (4968), 505-510.
33. Viores, S. A., Pegaptanib in the treatment of wet, age-related macular degeneration. *Int. J. Nanomed.* **2006**, *1* (3), 263-268.
34. Gatto, B.; Palumbo, M.; Sissi, C., Nucleic acid aptamers based on the G-quadruplex structure: therapeutic and diagnostic potential. *Curr. Med. Chem.* **2009**, *16* (10), 1248-1265.
35. Choi, E. W.; Nayak, L. V.; Bates, P. J., Cancer-selective antiproliferative activity is a general property of some G-rich oligodeoxynucleotides. *Nucleic Acids Res.* **2010**, *38* (5), 1623-1635.
36. Bock, L. C.; Griffin, L. C.; Latham, J. A.; Vermaas, E. H.; Toole, J. J., Selection of single-stranded DNA molecules that bind and inhibit human thrombin. *Nature* **1992**, *355* (6360), 564-566.
37. Roxo, C.; Kotkowiak, W.; Pasternak, A., G-Quadruplex-Forming Aptamers—Characteristics, Applications, and Perspectives. *Molecules* **2019**, *24* (20), 3781.
38. (a) Narayanan, S., Multifunctional roles of thrombin. *Ann Clin Lab Sci* **1999**, *29* (4), 275-280; (b) Di Cera, E., Thrombin as procoagulant and anticoagulant. *J. Thromb. Haemost.* **2007**, *5 Suppl 1*, 196-202.
39. Coughlin, S. R., Thrombin signalling and protease-activated receptors. *Nature* **2000**, *407* (6801), 258-264.
40. Tasset, D. M.; Kubik, M. F.; Steiner, W., Oligonucleotide inhibitors of human thrombin that bind distinct epitopes. *J. mol. biol.* **1997**, *272* (5), 688-698.
41. Stefano, L.; Raimondo De, C., Nucleotide-Derived Thrombin Inhibitors: A New Tool for an Old Issue. *Cardiovasc. & Hematol. Agents Med. Chem.* **2009**, *7* (1), 19-28.

-
42. White, R.; Rusconi, C.; Scardino, E.; Wolberg, A.; Lawson, J.; Hoffman, M.; Sullenger, B., Generation of species cross-reactive aptamers using "toggle" SELEX. *Mol. Ther.* **2001**, *4* (6), 567-573.
 43. Manoharan, M.; Akinc, A.; Pandey, R. K.; Qin, J.; Hadwiger, P.; John, M.; Mills, K.; Charisse, K.; Maier, M. A.; Nechev, L., Unique gene-silencing and structural properties of 2'-fluoro-modified siRNAs. *Angew. Chem., Int. Ed.* **2011**, *50* (10), 2284-2288.
 44. Zaitseva, M.; Kaluzhny, D.; Shchyolkina, A.; Borisova, O.; Smirnov, I.; Pozmogova, G., Conformation and thermostability of oligonucleotide d (GGTTGGTGTGGTTGG) containing thiophosphoryl internucleotide bonds at different positions. *Biophys. chem.* **2010**, *146* (1), 1-6.
 45. Schultze, P.; Macaya, R. F.; Feigon, J., Three-dimensional solution structure of the thrombin-binding DNA aptamer d(GGTTGGTGTGGTTGG). *J. mol. biol.* **1994**, *235* (5), 1532-1547.
 46. Kelly, J. A.; Feigon, J.; Yeates, T. O., Reconciliation of the X-ray and NMR structures of the thrombin-binding aptamer d(GGTTGGTGTGGTTGG). *J. mol. biol.* **1996**, *256* (3), 417-422.
 47. Padmanabhan, K.; Padmanabhan, K.; Ferrara, J.; Sadler, J. E.; Tulinsky, A., The structure of alpha-thrombin inhibited by a 15-mer single-stranded DNA aptamer. *J. Biol. Chem.* **1993**, *268* (24), 17651-17654.
 48. Russo Krauss, I.; Merlino, A.; Randazzo, A.; Novellino, E.; Mazzearella, L.; Sica, F., High-resolution structures of two complexes between thrombin and thrombin-binding aptamer shed light on the role of cations in the aptamer inhibitory activity. *Nucleic Acids Res.* **2012**, *40* (16), 8119-8128.
 49. Lu, M.; Guo, Q.; Kallenbach, N. R., Thermodynamics of G-tetraplex formation by telomeric DNAs. *Biochemistry* **1993**, *32* (2), 598-601.
 50. Zavyalova, E.; Tagiltsev, G.; Reshetnikov, R.; Arutyunyan, A.; Kopylov, A., Cation Coordination Alters the Conformation of a Thrombin-Binding G-Quadruplex DNA Aptamer That Affects Inhibition of Thrombin. *Nucleic Acid Ther.* **2016**, *26* (5), 299-308.
 51. Chen, F. M., Strontium(2+) facilitates intermolecular G-quadruplex formation of telomeric sequences. *Biochemistry* **1992**, *31* (15), 3769-3776.

-
52. Smirnov, I.; Shafer, R. H., Lead is unusually effective in sequence-specific folding of DNA. *J. mol. biol.* **2000**, *296* (1), 1-5.
53. Vairamani, M.; Gross, M. L., G-quadruplex formation of thrombin-binding aptamer detected by electrospray ionization mass spectrometry. *J. Am. Chem. Soc.* **2003**, *125* (1), 42-43.
54. Nagatoishi, S.; Tanaka, Y.; Tsumoto, K., Circular dichroism spectra demonstrate formation of the thrombin-binding DNA aptamer G-quadruplex under stabilizing- cation-deficient conditions. *Biochem. Biophys. Res. Commun.* **2007**, *352* (3), 812-817.
55. He, G.-X.; Krawczyk, S. H.; Swaminathan, S.; Shea, R. G.; Dougherty, J. P.; Terhorst, T.; Law, V. S.; Griffin, L. C.; Coutré, S.; Bischofberger, N., N2- and C8-Substituted Oligodeoxynucleotides with Enhanced Thrombin Inhibitory Activity in Vitro and in Vivo. *J. Med. Chem.* **1998**, *41* (13), 2234-2242.
56. Marathias, V. M.; Sawicki, M. J.; Bolton, P. H., 6-Thioguanine alters the structure and stability of duplex DNA and inhibits quadruplex DNA formation. *Nucleic Acids Res.* **1999**, *27* (14), 2860-2867.
57. López de la Osa, J.; González, C.; Gargallo, R.; Rueda, M.; Cubero, E.; Orozco, M.; Aviñó, A.; Eritja, R., Destabilization of Quadruplex DNA by 8-Aminoguanine. *ChemBioChem* **2006**, *7* (1), 46-48.
58. Nallagatla, S. R.; Heuberger, B.; Haque, A.; Switzer, C., Combinatorial synthesis of thrombin-binding aptamers containing iso-guanine. *J. Comb. Chem.* **2009**, *11* (3), 364-369.
59. Bonifacio, L.; Church, F. C.; Jarstfer, M. B., Effect of locked-nucleic acid on a biologically active G-quadruplex. A structure-activity relationship of the thrombin aptamer. *Int. J.Mol. Sci.* **2008**, *9* (3), 422-433.
60. Aviñó, A.; Mazzini, S.; Ferreira, R.; Gargallo, R.; Marquez, V. E.; Eritja, R., The effect on quadruplex stability of North-nucleoside derivatives in the loops of the thrombin-binding aptamer. *Bioorg. Med. Chem.* **2012**, *20* (14), 4186-4193.
61. Peng, C. G.; Damha, M. J., G-quadruplex induced stabilization by 2'-deoxy-2'-fluoro-D-arabinonucleic acids (2'F-ANA). *Nucleic Acids Res.* **2007**, *35* (15), 4977-4988.
62. Pasternak, A.; Hernandez, F. J.; Rasmussen, L. M.; Vester, B.; Wengel, J., Improved thrombin binding aptamer by incorporation of a single unlocked nucleic acid monomer. *Nucleic Acids Res.* **2011**, *39* (3), 1155-1164.

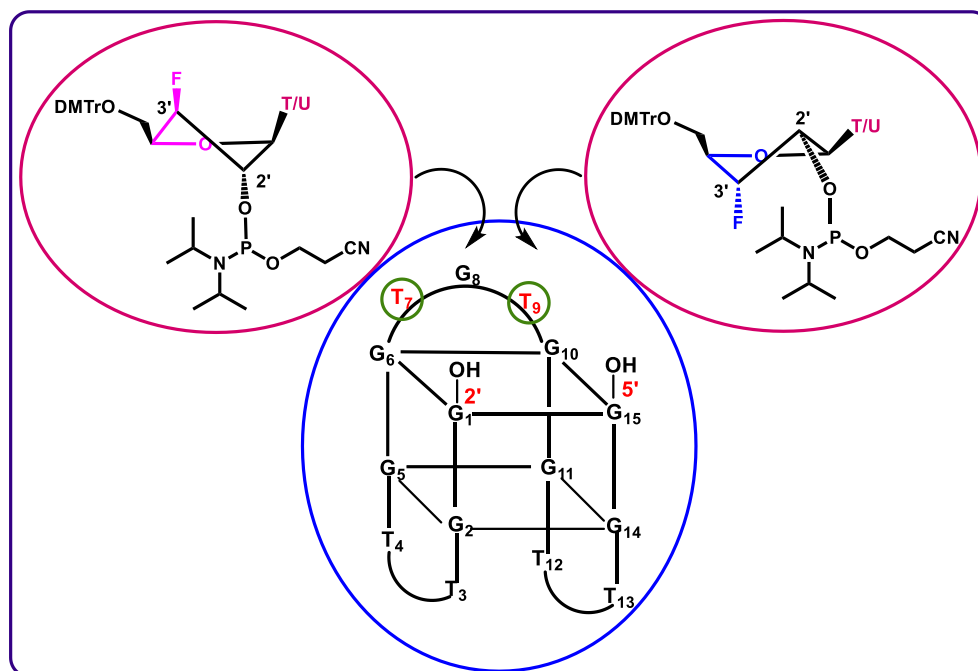
-
63. Mendelboum Raviv, S.; Horvath, A.; Aradi, J.; Bagoly, Z.; Fazakas, F.; Batta, Z.; Muszbek, L.; Harsfalvi, J., 4-Thio-deoxyuridylate-modified thrombin aptamer and its inhibitory effect on fibrin clot formation, platelet aggregation and thrombus growth on subendothelial matrix. *J. Thromb. Haemostasis* **2008**, *6* (10), 1764-1771.
64. Awachat, R.; Wagh, A. A.; Aher, M.; Fernandes, M.; Kumar, V. A., Favorable 2'-substitution in the loop region of a thrombin-binding DNA aptamer. *Bioorg. Med. Chem. Lett.* **2018**, *28* (10), 1765-1768.
65. Zhao, X.; Liu, B.; Yan, J.; Yuan, Y.; An, L.; Guan, Y., Structure variations of TBA G-quadruplex induced by 2'-O-methyl nucleotide in K⁺ and Ca²⁺ environments. *Acta Biochim. Biophys. Sin.* **2014**, *46* (10), 837-850.
66. Aaldering, L. J.; Poongavanam, V.; Langkjaer, N.; Murugan, N. A.; Jørgensen, P. T.; Wengel, J.; Veedu, R. N., Development of an Efficient G-Quadruplex-Stabilised Thrombin-Binding Aptamer Containing a Three-Carbon Spacer Molecule. *ChemBioChem* **2017**, *18* (8), 755-763.
67. Sacca, B.; Lacroix, L.; Mergny, J.-L., The effect of chemical modifications on the thermal stability of different G-quadruplex-forming oligonucleotides. *Nucleic Acids Res.* **2005**, *33* (4), 1182-1192.
68. Varizhuk, A. M.; Tsvetkov, V. B.; Tatarinova, O. N.; Kaluzhny, D. N.; Florentiev, V. L.; Timofeev, E. N.; Shchyolkina, A. K.; Borisova, O. F.; Smirnov, I. P.; Grokhovsky, S. L., Synthesis, characterization and in vitro activity of thrombin-binding DNA aptamers with triazole internucleotide linkages. *Eur.J.Med. Chem.* **2013**, *67*, 90-97.
69. Martino, L.; Virno, A.; Randazzo, A.; Virgilio, A.; Esposito, V.; Giancola, C.; Bucci, M.; Cirino, G.; Mayol, L., A new modified thrombin binding aptamer containing a 5'-5' inversion of polarity site. *Nucleic Acids Res.* **2006**, *34* (22), 6653-6662.
70. Virgilio, A.; Amato, T.; Petraccone, L.; Filosa, R.; Varra, M.; Mayol, L.; Esposito, V.; Galeone, A., Improved thrombin binding aptamer analogues containing inversion of polarity sites: structural effects of extra-residues at the ends. *Org. Bio.Chem.* **2016**, *14* (32), 7707-7714.
71. Joachimi, A.; Benz, A.; Hartig, J. S., A comparison of DNA and RNA quadruplex structures and stabilities. *Bioorg.Med.Chem.* **2009**, *17* (19), 6811-6815.

72. Tang, C.-F.; Shafer, R. H., Engineering the quadruplex fold: nucleoside conformation determines both folding topology and molecularity in guanine quadruplexes. *J. Am. Chem. Soc.* **2006**, *128* (17), 5966-5973.
73. Gunjal, A. D.; Fernandes, M.; Erande, N.; Rajamohanan, P. R.; Kumar, V. A., Functional isoDNA aptamers: modified thrombin binding aptamers with a 2'-5'-linked sugar-phosphate backbone (isoTBA). *Chem. Commun.* **2014**, *50* (5), 605-607.
74. Varada, M.; Aher, M.; Erande, N.; Kumar, V. A.; Fernandes, M., Methoxymethyl Threofuranosyl Thymidine (4'-MOM-TNA-T) at the T7 Position of the Thrombin-Binding Aptamer Boosts Anticoagulation Activity, Thermal Stability, and Nuclease Resistance. *ACS Omega* **2020**, *5* (1), 498-506.
75. (a) Michelson, A. M.; Todd, A. R., Nucleotides part XXXII. Synthesis of a dithymidine dinucleotide containing a 3': 5'-internucleotidic linkage. *J. Chem. Soc.* **1955**, (0), 2632-2638; (b) Hall, R. H.; Todd, A.; Webb, R. F., 644. Nucleotides. Part XLI. Mixed anhydrides as intermediates in the synthesis of dinucleoside phosphates. *J. Chem. Soc.* **1957**, (0), 3291-3296.
76. Gilham, P. T.; Khorana, H. G., Studies on Polynucleotides. I. A New and General Method for the Chemical Synthesis of the C5'-C3' Internucleotidic Linkage. Syntheses of Deoxyribo-dinucleotides¹. *J. Am. Chem. Soc.* **1958**, *80* (23), 6212-6222.
77. Letsinger, R. L.; Mahadevan, V., Stepwise Synthesis of Oligodeoxyribonucleotides on an Insoluble Polymer Support. *J. Am. Chem. Soc.* **1966**, *88* (22), 5319-5324.
78. Letsinger, R. L.; Finnan, J. L.; Heavner, G. A.; Lunsford, W. B., Nucleotide chemistry. XX. Phosphite coupling procedure for generating internucleotide links. *J. Am. Chem. Soc.* **1975**, *97* (11), 3278-3279.
79. Matteucci, M. D.; Caruthers, M. H., Synthesis of deoxyoligonucleotides on a polymer support. *J. Am. Chem. Soc.* **1981**, *103* (11), 3185-3191.
80. Mergny, J.-L.; Lacroix, L., UV Melting of G-Quadruplexes. *Curr. Protoc. Nucleic Acid Chem.* **2009**, Chapter 17, 17.1.
81. Mergny, J.-L.; Li, J.; Lacroix, L.; Amrane, S.; Chaires, J. B., Thermal difference spectra: a specific signature for nucleic acid structures. *Nucleic Acids Res.* **2005**, *33* (16), e138-e138.

82. Elzagheid, M. I.; Viazovkina, E.; Damha, M. J., Synthesis of Protected 2'-Deoxy-2'-fluoro- β -D-arabinonucleosides. *Curr. Protoc. Nucleic Acid Chem.* **2002**, *10* (1), 1.7.1-1.7.19.
83. Gray, D. M.; Wen, J.-D.; Gray, C. W.; Repges, R.; Repges, C.; Raabe, G.; Fleischhauer, J., Measured and calculated CD spectra of G-quartets stacked with the same or opposite polarities. *Chirality* **2008**, *20* (3-4), 431-440.
84. Paramasivan, S.; Rujan, I.; Bolton, P. H., Circular dichroism of quadruplex DNAs: applications to structure, cation effects and ligand binding. *Methods* **2007**, *43* (4), 324-331.

Chapter 2

S/N-type frozen 3'-Deoxy, 3'-fluoro nucleosides in non-genetic 2'-5'-linked thrombin binding aptamer (*iso*TBA)



The anticoagulant thrombin binding aptamer folds into antiparallel G-quadruplex structure. The TBA loops (T₃T₄, T₁₂T₁₃ and T₇G₈T₉) are crucial for the recognition and binding to thrombin. Various chemically modified TBA analogues consisting of conformationally restricted nucleotides (e.g. LNA, 2'F-ANA, 2'FRNA and North-methanocarbothymidine) in which the sugar moieties are locked/ frozen in a specific sugar pucker are reported and that are significant in terms of binding properties with thrombin as well as their stability to nucleases. Fluorine substitution in different orientations has a strong influence on the conformational preferences of the furanose ring of the nucleic acid. In the stereoisomers, 3'-deoxy-3'-fluoro xylonucleoside and 3'-deoxy-3'-fluoro ribonucleoside, the opposite configuration of fluorine at the 3'-carbon freezes the sugar in the opposing N-type and S-type conformations respectively. We have introduced N-type and S-type conformationally frozen nucleosides in the central TGT loop of *iso*TBA to understand the structural preferences of sugars. Biophysical experiments were carried out to study the structural implications of these modified *iso*TBA oligomers on the stability of quadruplexes.

2.1 Introduction

Fluorocarbohydrates constitute an important class of bioactive molecules which show antiviral, anticancer activity. Examples include the 2'-difluoro cancer drug, gemcitabine¹ and the 2',3'-dideoxyadenosine derivative, lodenosine.² 2'-Fluoro-5-methyl- β -D-arabinouridine (FMAU) showed activity against Herpes Simplex Virus (HSV).³ Its enantiomer, L-FMAU (clevudine), exhibits a more favourable therapeutic index than D-FMAU against Hepatitis B Virus (HBV) and Epstein-Barr Virus (EBV).⁴ Clofarabine is one of the most successful 2'-deoxy-2'-fluoroarabino nucleoside approved for the treatment of pediatric acute leukaemia by the FDA.⁵ Substitution of hydrogen by fluorine causes a change in the biological activity as well as enhances the chemical and metabolic stability of the fluorinated nucleosides.⁶ The synthesis and application of fluorinated oligonucleotide analogues have been extensively investigated in the context of antisense therapeutics. Watanabe and coworkers⁷ initially introduced pyrimidine 2'-deoxy-2'-fluoroarabino nucleosides into oligonucleotides. Since then, oligonucleotides containing derivatives of such fluorinated compounds remains an attractive area of research mainly focused on therapeutic application. A large volume of work in this field has been reported by Damha and coworkers. They synthesized oligomers containing nucleotides with the 2'-OH group of arabino nucleic acid (ANA) substituted by either 2'-ribofluoro- or 2'-arabino-fluoro group (Figure 1). These were found to have a major impact on the thermal stability of the derived 3'-5'-linked 2'-fluoro-DNA:RNA (2'F-RNA:RNA and 2'F-ANA:RNA)⁸ duplexes caused by the favourable influence of the 2'-fluoro group on the conformational preference of the sugar pucker. The 2'F-RNA-modified duplexes further showed enhancement in serum stability.⁹

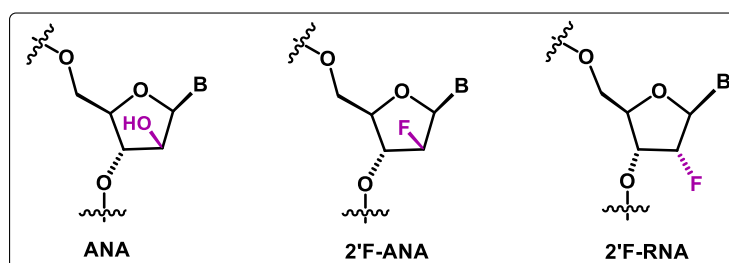


Figure 1: Arabinose and 2'-deoxy-2'-fluoroarabino/ribo nucleic acid (ANA, 2'F-ANA and 2'F-RNA)

2'-deoxy-2'-ribofluoro modification (2'F-RNA) has been utilized for the study of region-specific cleavage of RNA by RNase H,¹⁰ as modulators of RNA splicing.¹¹ 2'F-

RNA modified nucleic acids have been utilized for improving the properties of oligonucleotide aptamers, e.g., 2'-F-RNA-modified oligonucleotide aptamer approved by US FDA in 2004 is Macugen (pegaptanib),¹² for the treatment of age related macular degeneration

2.2 Sugar ring conformation of C2' and C3' fluoro substituted (α/β) nucleos(t)ides

The stronger *gauche* effect of the highly electronegative fluorine atom (O_{4'}-C1'-C2'-F_{2'} *gauche* effect) has a strong influence on both the electronic properties and stereochemical configuration of the adjacent group. Consequently, the fluorine substituent dictates the overall conformation of the furanose ring, so that 2'-deoxy-2'-fluoro nucleic acid in *ribo* configuration (2'-F-RNA) takes up a North-type sugar pucker (C3'-*endo* conformation) whereas 2'-deoxy-2'-fluoro nucleic acid in the *ara* configuration (2'-F-ANA) adopts a South-type (C2'-*endo* conformation) sugar pucker (Figure 2).

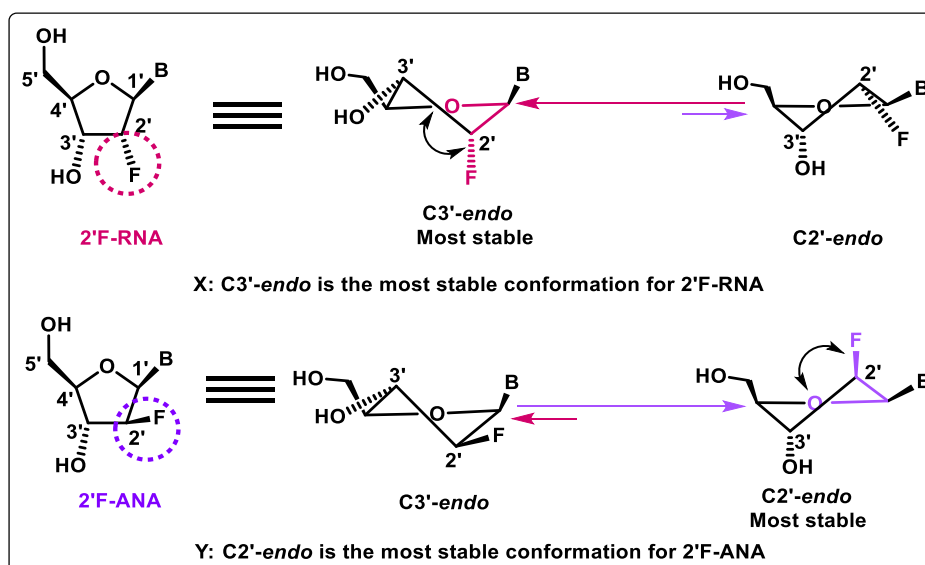


Figure 2: Sugar puckering equilibrium for 2'-F- RNA and 2'-F-ANA (**B** = Purine/pyrimidine)

3'-deoxy-3'-ribofluoro / xylofluoro uridine (Figure 3) represents another functional chemical modification, with a fluorine substituent at 3'-position of the sugar. These very interesting and novel studies were performed in our laboratory in which the effectiveness of the introduction of one or more unit of 3'-deoxy-3'-fluoro nucleosides in *iso*DNA (2'-5'-backbone) on the binding selectivity and affinity to complementary RNA

(*iso*DNA:RNA duplexes) and increased resistance to the degradation by nucleases was demonstrated.¹³

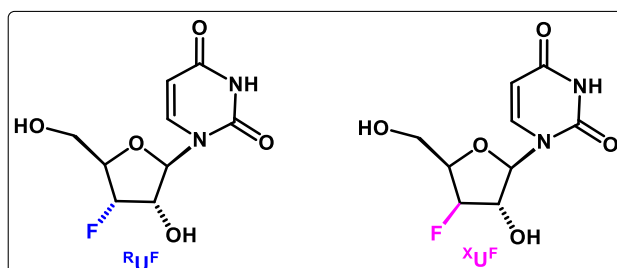


Figure 3: 3'-deoxy-3'-fluoro ribo/xylouridine ($^R\text{U}^F$ and $^X\text{U}^F$)

In the stereoisomers 3'-deoxy-3'-fluoro ribouridine and 3'-deoxy-3'-fluoro xylouridine, the differing orientation of fluorine at the 3'-carbon causes a distinct sugar pucker due to the dominating $\text{O}_4'\text{-C}_4'\text{-C}_3'\text{-F}_3'$ *gauche* effect. The 3'-deoxy-3'-fluoro xylouridine shows a strong preference for the $\text{C}_3'\text{-endo}$ (North) conformation whereas the 3'-deoxy-3'-fluoro ribouridine prefers the $\text{C}_2'\text{-endo}$ (South) conformation (Figure 4).

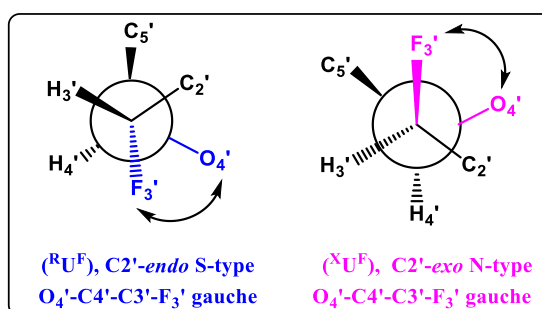


Figure 4: Fluorine-induced *gauche* effect is configuration-dependent

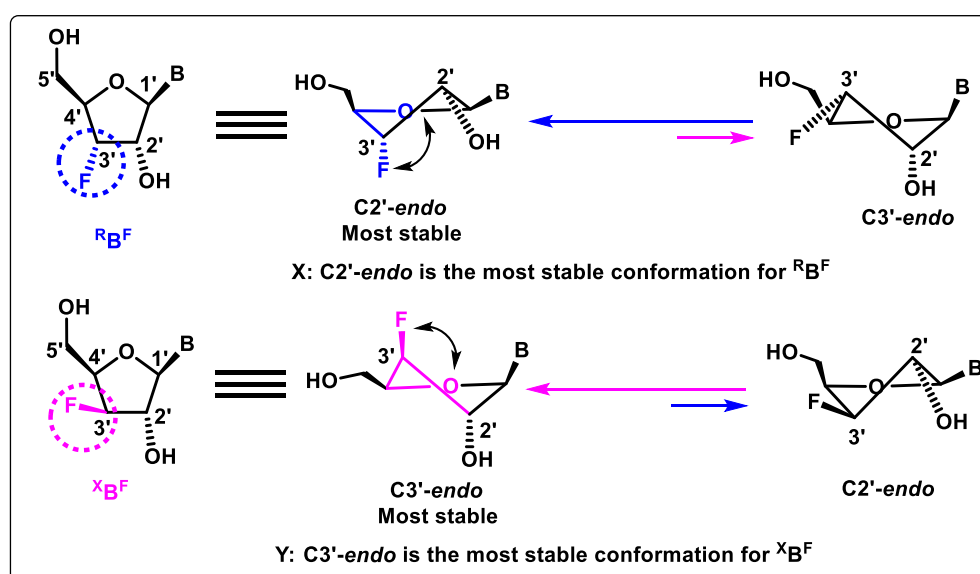


Figure 5: Sugar pucker equilibrium for $^R\text{B}^F$ and $^X\text{B}^F$. **B** =Thymine/Uracil

This is further clarified through Figure 5, which shows that the opposite configuration of fluorine in 3'-ribo and 3'-xylofuranose sugars freezes the sugar in the opposing S-type and N-type conformations respectively.

2.3 Rationale, design and objectives of the present work

DNA and RNA aptamers are short, single-stranded oligonucleotide entities that bind to the desired target typically discovered through a selection process known as SELEX.¹⁴ Many so-discovered therapeutically important guanine-rich aptamers show high affinity towards biologically important targets. Guanine-rich DNA/RNA aptamers can fold into three-dimensional structures to form G-quadruplexes by the stacking of two or more guanine quartets upon each other, and maybe constructed by one, two or four guanine-rich oligonucleotide strands.

In the recent past, G-quadruplexes have been received increasing attention due to their abundance *in vivo* and their role in meiosis, telomere maintenance, gene regulation¹¹ and also as aptamers for tumour-targeted drug delivery for cancer treatments.¹⁵ The G-quadruplex structures, their folding mechanism, protein binding to the quadruplex structures and ligands targeting the quadruplex over duplex were extensively studied by various experimental and theoretical studies.¹⁶ Examples include the thrombin-binding aptamer (TBA),¹⁷ anti-cancer¹⁸ and anti-HIV aptamers.¹⁹

The thrombin-binding aptamer is a 15-mer guanine-rich DNA oligomer (TBA; d(GGTTGGTGTGGTTGG)), that binds to thrombin,²⁰ a serine protease enzyme,²¹ and acts as a catalyst in the process of hemostasis in which insoluble cross-linked fibrin is formed. TBA shows remarkable anticoagulant properties *in vitro*. It adapts a unimolecular antiparallel quadruplex topology with two stacked G-tetrads and is associated with two external TT (T³T⁴ and T¹²T¹³) loops and one central TGT (T⁷G⁸T⁹) loop.²² The TBA loops are crucial for the recognition and binding of thrombin. Thymines in the loop display *anti* glycosidic bond configuration and all sugar puckers are predominantly of the South (*S*, C2'-*endo*) conformation.²³ G-quadruplexes have very specific requirements for glycosidic bond orientation and the sugar conformation, therefore are highly sensitive to sugar modifications. Understanding the driving forces that are responsible for the unique G-quadruplex fold of TBA is very essential for expanding the conformational landscape and for enhancing its target-specific properties.

Overwhelming efforts have been directed towards a better understanding of the folding topology and stability of TBA. One of the approaches is to selectively replace nucleotides with those possessing different structural characteristics or physicochemical properties. To improve the biophysical and biological properties of nucleic acids, a variety of chemical modifications have been reported in the past. Among these, various chemically modified oligonucleotides consisting of conformationally restricted nucleotides in which the sugar moieties are locked/ frozen in a specific sugar pucker are significant in terms of binding properties with target nucleic acids as well as their stability to nucleases. The primary target for such chemical modification has been the C2' position in the sugar ring. The relevant modifications in the sugar ring (Figure 6) and the resulting conformational changes are summarized here. 2'-Deoxy-2'-fluoro-D-arabino nucleotides (2'F-araN) show a strong preference for the C2'-endo (South) conformation, while 2'-Deoxy-2'-fluoro-ribonucleotides (2'F-RNA) prefer the C3'-endo (North) conformation.²⁴ 2'F-araN and 2'F-RNA differ only in the relative configuration of the fluorine atom at the C2' position of the sugar ring. Damha et al.²⁵ systematically introduced 2'F-araN in the TBA loops and observed an enhancement in the thermal stability as well as nuclease resistance. Eritja and co-workers studied the effect of substitution of thymidines situated in the loops of TBA by ribonucleotides (uridine or 2'-Deoxy-2'-fluorouridine) or by the conformationally-restricted pseudo nucleotide North-methanocarbothymidine.²⁶ 2'F-RNA and uridine were well-tolerated when incorporated in the T⁷ and T⁹ loop positions and both substitutions caused an increase in thermal stability of TBA ($\Delta T_m = +2$ °C in case of 2'F-RNA and $\Delta T_m = +4.9$ °C in case of uridine), whereas North-methanocarbothymidine in the same position resulted in strong destabilization ($\Delta T_m = -17$ °C). Replacement by 2'-deoxyribo-uridine having C2'-endo (South) sugar pucker in all loops of TBA resulted in strong stabilization ($\Delta T_m = +6$ °C) while Sacca et al.²⁷ reported that 2'-O-methyl ribonucleotides or ribonucleotides in all loops not only destabilized the TBA quadruplex, but also changed the quadruplex topology in case of methoxy substitution. A comparative analysis of all three modified TBA oligomers indicated that the thermal stability of the oligomer containing 2'-O-methyl ribonucleotide ($T_m = 34$ °C) was the least, while the oligomer containing deoxyribo-uridine showed the highest stability among the three oligomers, with a T_m of 54 °C, even more stable than unmodified TBA ($T_m = 48$ °C). This suggests the stabilizing

role of thymine substitution by uracil. Our research group recently reported the systematic replacement of single thymidine residues in the loop region of TBA by 2'-OMe-uridine. These studies revealed that the compact N-type sugar geometry of 2'-OMe derivatives in the loop regions stabilizes the TBA quadruplex when there is only one modification either in a TT loop or the TGT loop.²⁸

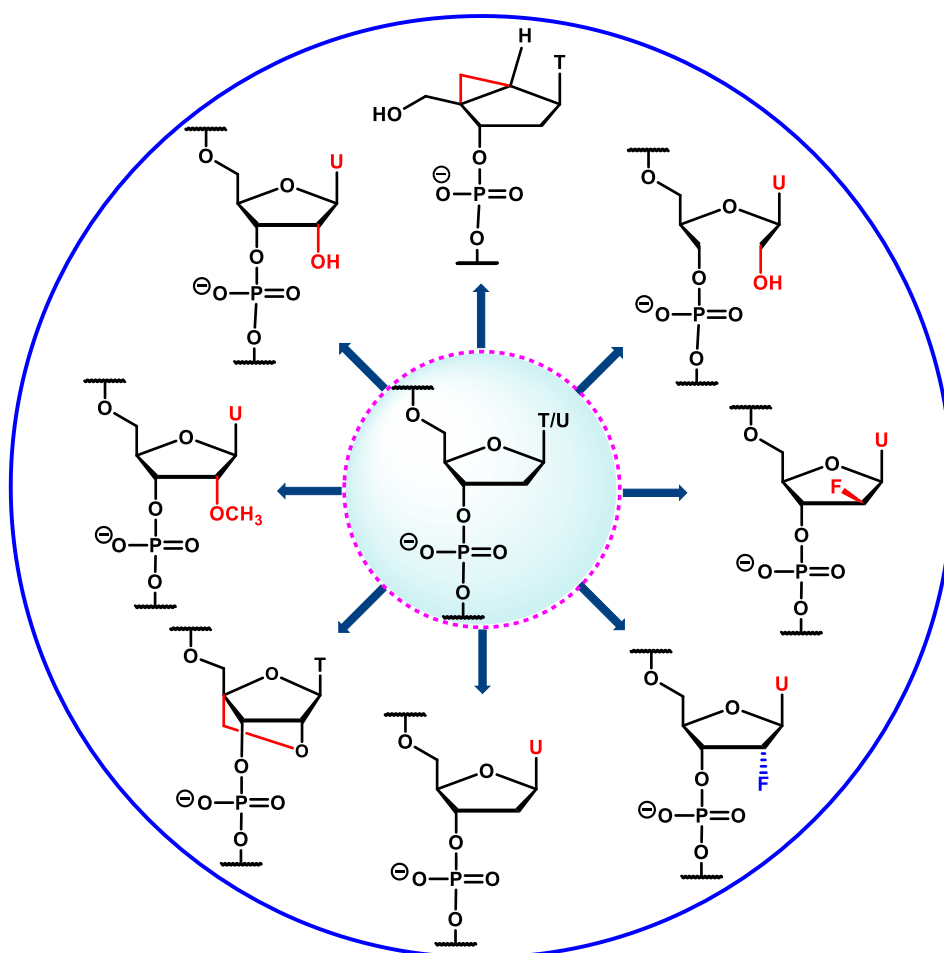


Figure 6: Summary of selective chemical modifications introduced into TBA

The substitution of G⁸ by LNA-G (2'-O-4'-C-methylene-linked ribonucleotide) with the C3'-endo sugar conformation improved the stability, but the substitution of T⁷ led to a reduction in thermal stability as well as anticoagulant activity.²⁹ Wengel's group reported 15 different variants of TBA derived from single substitutions with unlocked nucleic acid (UNA) at every possible position, where the oligomer with substitution at T⁷ position was found to be more capable of inhibiting blood clotting than the control TBA.¹⁰ Recently, we reported the 4'-methoxymethyl threose nucleic acid (4'-MOM-TNA) with a 2'-3'-linked backbone and C3'-endo sugar (North) conformation, where the

oligomer bearing a single 4'-MOM-TNA-T nucleotide substitution at the T⁷ position resulted in a quadruplex with enhanced thermal stability, anticlotting activity and nuclease resistance properties.³⁰ In general, the central TGT loop modifications are more tolerated, and modification at the T⁷ position has been shown to impart better quadruplex stability and anticoagulation activity.

The work included in this chapter is divided into two sections.

Section A: Synthesis of S/N-type-frozen 3'-deoxy-3'-ribo/xylo fluoro thymidine (^RT^F and ^XT^F) and 3'-deoxy-3'-ribo/xylo fluoro uridine (^RU^F and ^XU^F) nucleosides.

Section B: 3'-Deoxy-3'-fluoro nucleosides in the thrombin binding aptamer (TBA): Evaluation of stability and activity.

Section A

Synthesis of S/N-type-frozen 3'-deoxy-3'-ribo/xylo fluoro thymidine ($^R\text{T}^F$ and $^X\text{T}^F$) and 3'-deoxy-3'-ribo/xylo fluoro uridine ($^R\text{U}^F$ and $^X\text{U}^F$) nucleosides

2.4 Present work

In view of the demonstrated properties of fluoro-sugar-modified nucleotides and impact of central TGT loop on the stability of G quadruplex, we proposed to synthesize S/N-type conformationally frozen 3'-deoxy-3'-fluoro ribo/xylo thymidine nucleosides ($^R\text{T}^F$ and $^X\text{T}^F$) and 3'-deoxy-3'-fluoro ribo/xylo uridine nucleosides ($^R\text{U}^F$ and $^X\text{U}^F$) (Figure 7) and incorporate them into 2'-5'-linked *iso*TBA, with a view to improving its thermal stability. We had earlier reported the incorporation of these C3'-fluoro-nucleosides into duplex-forming oligomers,³¹ but their effect when incorporated in quadruplex-forming sequences have not yet been reported.

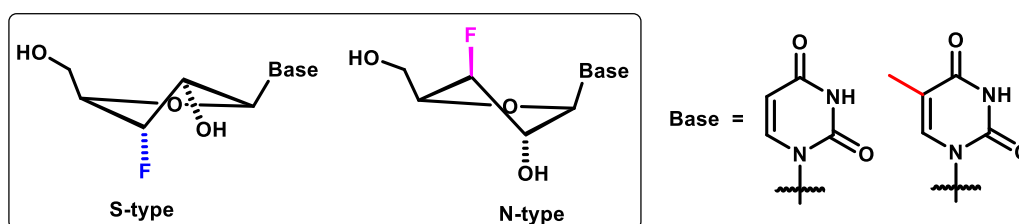


Figure 7: Sugar puckering of 3'-deoxy-3'-ribo/xylo fluoro nucleoside

2.4.1 Synthesis of S-type monomer: 3'-Deoxy-3'-ribofluoro thymidine phosphoramidite ($^R\text{T}^F$) and 3'-Deoxy-3'-ribofluoro uridine phosphoramidite ($^R\text{U}^F$)

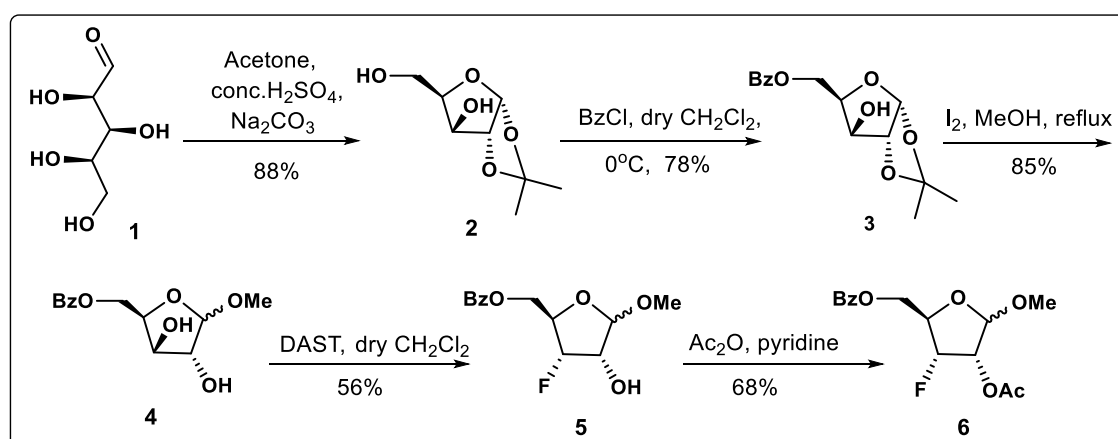
A lot of attention has been paid to the introduction of fluoro group into nucleosides; various efficient synthetic methodologies have been developed for the selective formation of C-F bond. Incorporation of α -F moiety at C3 position was reported in the literature. Opening of epoxide of methyl 2, 3-anhydro-D-lyxofuranoside using potassium hydrogen fluoride (KHF_2) used as a fluorinating agent in 1,2-ethanediol was reported by Taylor et al.³² Miyai and coworkers³³ reported the ring-opening of the epoxide, 9-(2,3-anhydro- β -D -lyxofuranosyl) adenine by KHF_2 . Epoxide opening appears to provide the best strategy to the synthesis of 3-F nucleoside since highly stereoselective scission of carbohydrate epoxides to the corresponding fluorohydrine has been observed. Mikhailopulo and coworkers³⁴ developed the synthesis of 3'-Deoxy-3'-

fluoro-ribonucleosides from D-xylose for all the nucleobases, where KHF_2 and NaF in ethylene glycol used for fluorination at C3 and the incorporation of the silylated bases at C1' position was done in presence SnCl_4 (Friedel-Crafts catalysts) and TMS-triflate (Lewis acid). Later on, the same group used DAST as a fluorinating reagent for the synthesis of 3'-Deoxy-3'-fluoro-ribonucleosides. Following the same synthetic route reported by Mikhailopulo et al.³⁵ in 1999, synthesis of ribofluoro nucleoside was accomplished. The synthesis of 3'-deoxy-3'-ribofluoro thymidine phosphoramidite was achieved from D-xylose as per the series of steps shown in Scheme 1 and Scheme 2a.

2.4.1.1 Synthesis of 3-deoxy-3-fluoro-1-O-methyl-2-O-acetyl-5-O-benzoyl-D-ribofuranoside

3-Deoxy-3-fluoro-1-O-methyl-2-O-acetyl-5-O-benzoyl-D-ribofuranoside **6** was prepared according to the reported procedure³⁵ outlined in Scheme 1 and used as the key glycosylating agent.

It was synthesized from D-xylose **1** by conversion to its monoacetonide derivative **2** (1, 2-O-isopropylidene- α -D-xylofuranose) using conc. H_2SO_4 and Na_2CO_3 in acetone with 88 % yield. Benzoylation to protect the primary hydroxyl group was achieved using benzoyl chloride and triethylamine in CH_2Cl_2 which yielded the 5-O-benzoyl derivative **3** in 78 % yield. Acetal cleavage and methylation were done in one pot by treating compound **3** with iodine in methanol under reflux conditions, which afforded a mixture of β - and α -D-xyloside anomers **4** in 85% yield.



Scheme 1: Synthesis of 3-deoxy-3-fluoro-1-O-methyl-2-O-acetyl-5-O-benzoyl-D-ribofuranose

Introduction of the C3- α -fluoro substituent was achieved by treating **4** with diethylaminosulfur trifluoride (DAST), a fluorinating reagent, at room temperature for

19 h, when 3-fluoro α - and β -D-ribosides **5** were obtained in 56 % yield along with arabino-difluoride **5a** and ribo epoxide **5b** as side-products (Figure 8).

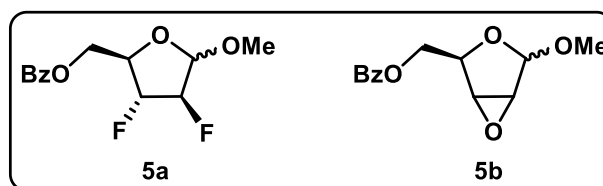
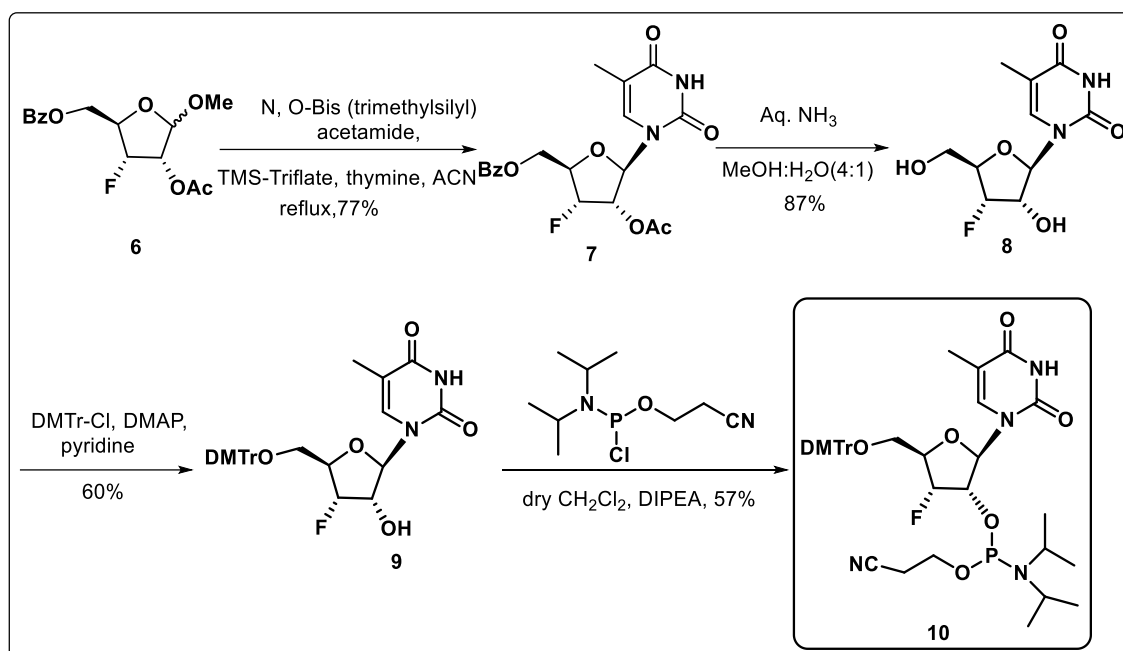


Figure 8: Side-products of fluorination reaction: **5a** arabino-difluoride and **5b** ribo-epoxide

The free secondary 2-hydroxy group of compound **5** was protected as its acetate derivative by using acetic anhydride to get the expected 3-deoxy-3-fluoro-1-*O*-methyl-5-*O*-benzoyl-2-*O*-acetyl-D-ribofuranose **6** in 68% yield. The substitution of the C1-OMe group in compound **6** by the nucleobase (thymine or uracil) was achieved by using the commonly known Vorbrüggen glycosylation reaction conditions.³⁶ The synthetic pathway for the S-type building block, 3'-deoxy-3'-ribofluoro thymidine phosphoramidite monomer ($^{\text{R}}\text{T}^{\text{F}}$) and 3'-deoxy-3'-ribofluoro uridine phosphoramidite monomer ($^{\text{R}}\text{U}^{\text{F}}$) from intermediate **6** is outlined in schemes 2a and 2b respectively.

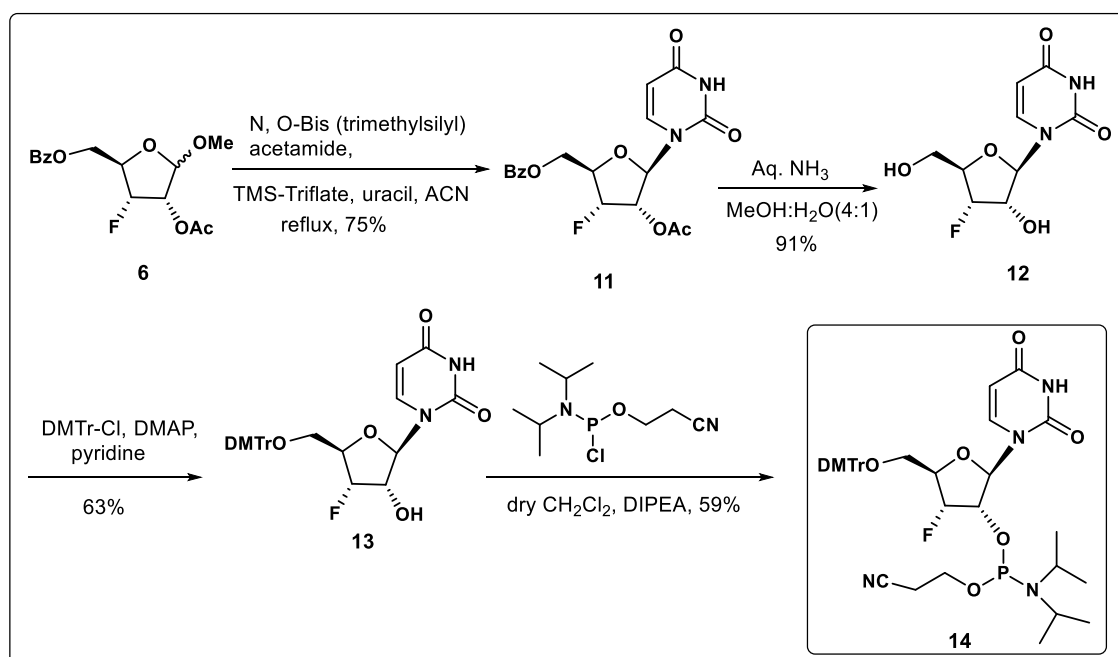
2.4.1.2 Synthesis of 3'-deoxy-3'-ribofluoro thymidine phosphoramidite monomer ($^{\text{R}}\text{T}^{\text{F}}$)

The coupling of an electrophilic sugar derivative and a nucleophilic silylated heterocyclic base in the presence of a Lewis acid to get N-glycosides is known as the Vorbrüggen glycosylation reaction. An anomeric mixture of 3-deoxy-3-fluoro-1-*O*-methyl-5-*O*-benzoyl-2-*O*-acetyl-D-ribofuranose **6** on treatment with bis(trimethylsilyl)acetamide, thymine and trimethylsilyl trifluoromethanesulfonate (TMS-triflate) under Vorbrüggen glycosylation conditions exclusively afforded the β -anomer of thymidine **7** due to the neighbouring group participation of the 2-*O*-acetyl group. Compound **7** on ammonolysis yielded 3'-deoxy-3'-fluoro ribothymidine **8** (87%). Protection of the primary hydroxyl group in compound **8** was achieved using DMTr-chloride and a catalytic amount of 4,4'-dimethylaminopyridine (DMAP) in anhydrous pyridine to obtain compound **9** in 60 % yield. Phosphitylation of the free 2'-hydroxyl group in **9** by treating with 2-cyanoethyl-N,N-diisopropyl chlorophosphine and N,N-diisopropylethylamine (DIPEA) under anhydrous conditions afforded the desired S-type thymidine phosphoramidite building block **10** (57%).

Scheme 2a: Synthesis of $R^T F$ monomer

2.4.1.3 Synthesis of 3'-deoxy-3'-ribofluoro uridine monomer ($R^U F$)

Using a similar reaction sequence to that shown in Scheme 2a, the 3'-deoxy-3'-ribofluoro ribouridine ($R^U F$) monomer **14** was synthesized from an anomeric mixture of 3-deoxy-3-fluoro-1-O-methyl-5-O-benzoyl-2-O-acetyl-D-ribofuranose **6** as shown in Scheme 2b.

Scheme 2b: Synthesis of $R^U F$ monomer

2.4.2 Synthesis of N-type monomer: 3'-Deoxy-3'-xylofluoro thymidine phosphoramidite ($^X\text{T}^F$) and 3'-Deoxy-3'-xylofluoro uridine phosphoramidite ($^X\text{U}^F$)

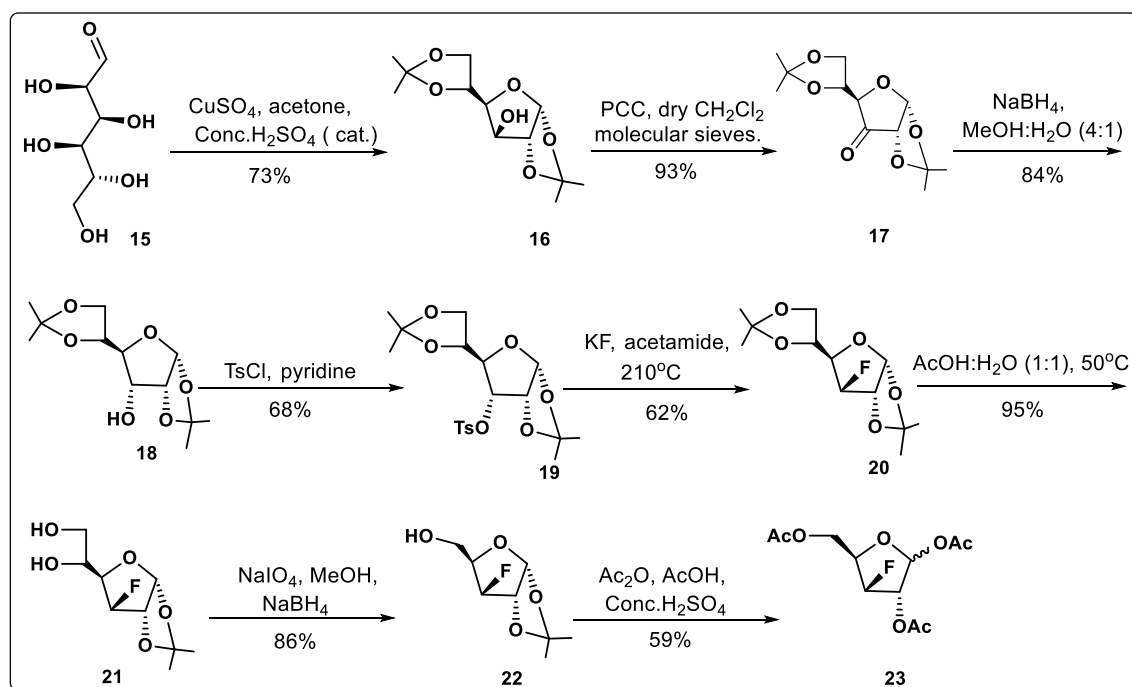
One of the methods applied by which 3- β -fluorine in pentafuranose is substituted for secondary hydroxyl group has been done by opening of 2'-3'- α -epoxide ring by fluoride ion. Robins et al.³³ reported the opening of 2'-3'- α -epoxide of adenosine 2',3'-ribo-epoxide by TBAF in acetonitrile afforded 3'-xylofluoro furanosyl nucleosides. Wright et al.³⁷ reported fluorination of methyl 2,3-anhydro-5-*O*-benzyl- β -D-ribofuranoside by the treatment with KHF_2 in ethylene glycol which afforded the mixture of the 3'- and 2'-fluoro-D-arabinofuranoside with the 3'- β -fluoro isomer as the major product. Webber et al.³⁸ reported nucleophilic displacement of the tosylate group at C-3 of 1,2:5,6-di-*O*-isopropylidene- α -D-allofuranose (ADA) by TBAF in acetonitrile. Fox and coworkers³⁹ also developed another approach for fluorination where KF in acetamide at temperature ~ 210 °C used as a fluorinating agent for the nucleophilic displacement of tosyloxy group at C-3. Tewson and Welch⁴⁰ done fluorination reaction of the same non-tosylated sugar with DAST avoided additional step of tosylation of C3-hydroxyl. Fluorinated product was isolated by vacuum distillation. An efficient synthesis of fluorinated nucleosides was developed by Komiotis et al.⁴¹ from glucose diacetone (GDA) where KF is used for fluorination and Vorbrüggen glycosylation for base attachment. In this work, we have followed the same synthetic route reported by Komiotis and coworkers with some modification. The synthesis of 3'-deoxy-3'-xylofluoro thymidine phosphoramidite was achieved from D-glucose as per the series of steps shown in Scheme 3 and Scheme 3a.

2.4.2.1 Synthesis of 3-deoxy-3-fluoro-1, 2, 5-tri-*O*-acetyl-D-xylofuranose

3-deoxy-3-fluoro-1,2,5-tri-*O*-acetyl-D-xylofuranose **23** was prepared from D-glucose by a literature-reported procedure⁴¹ detailed in Scheme 3 and used as a key glycosylating intermediate in the synthesis of the N-type monomer. 1,2:5,6-di-*O*-isopropylidene- α -D-glucofuranose (glucose diacetone, GDA) **16** was obtained from D-glucose **15** in 73% yield by using acetone in the presence of catalytic amount of conc. H_2SO_4 and anhydrous CuSO_4 . GDA **16** was oxidized by using pyridinium chlorochromate (PCC) in dry DCM to give keto compound **17** in 93 % yield, which was further stereoselectively reduced by sodium borohydride (NaBH_4) in $\text{MeOH}:\text{H}_2\text{O}$ to get

allose diacetone (ADA) **18** (84%). Tosylation of the hydroxyl group in **18** using tosyl-Cl in pyridine afforded the corresponding 1,2:5,6-di-*O*-isopropylidene-3-*O*-toluenesulphonyl- α -D-allofuranose **19** in 68% yield. Fluorination at C-3 carbon was achieved by S_N2 displacement of the tosyloxy group, that was carried out by using KF in acetamide at ~210 °C to obtain C-3 β -fluorinated compound **20** (62%). 3-deoxy-3-fluoro-1,2-*O*-isopropylidene- α -D-glucofuranose **21** was obtained in 95% yield by selective hydrolysis of the *O*-isopropylidene group using AcOH:H₂O (1:1) at 50 °C.

Oxidation of compound **21** by NaIO₄ resulted in an aldehyde which was further reduced by sodium borohydride to afford 3-deoxy-3-fluoro-1,2-*O*-isopropylidene- α -D-xylofuranose **22** (86%). In situ deprotection of the 1,2-acetonide in **22**, followed by acetylation using acetic acid and Ac₂O in the presence of catalytic amount of concentrated H₂SO₄ gave an anomeric mixture of the triacetate, 3-deoxy-3-fluoro-1,2,5-tri-*O*-acetyl-D-xylofuranose **23** in 59% yield. Substitution of the C1'-OAc group by the nucleobase (thymine or uracil) was achieved by using the well-known Vorbrüggen glycosylation reaction conditions.³⁶

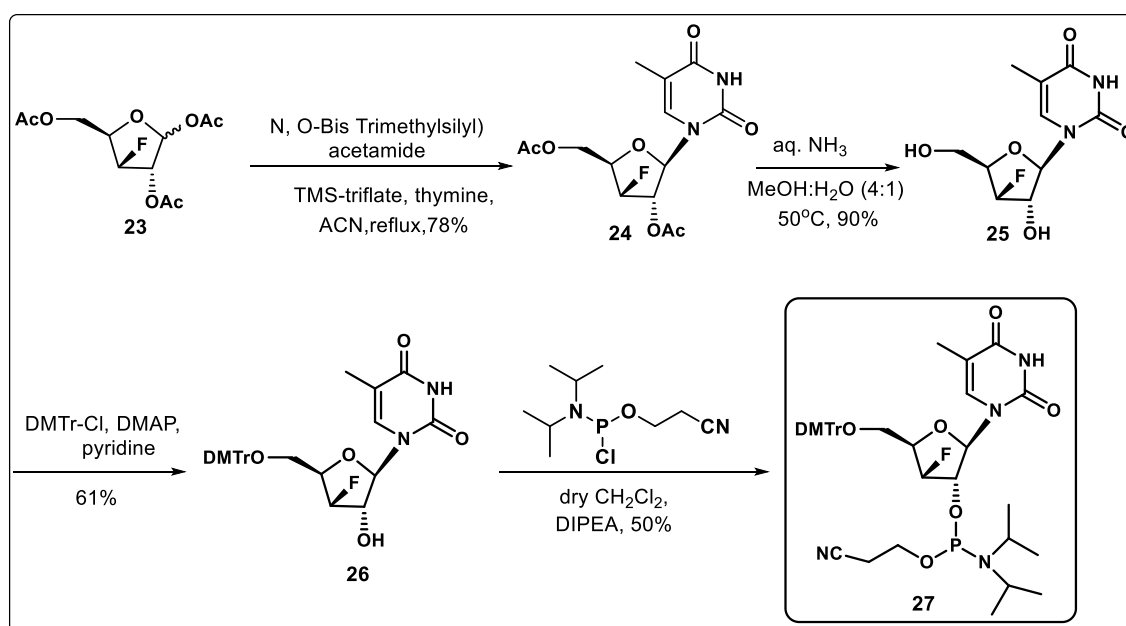


Scheme 3: Synthesis of 3-deoxy-3-fluoro-1, 2, 5-tri-*O*-acetyl-D-xylofuranose

The synthesis of N-type building blocks 3'-deoxy-3'-xylofluoro thymidine phosphoramidite monomer (^XT^F) and 3'-deoxy-3'-xylofluoro uridine phosphoramidite monomer (^XU^F) from intermediate **23** is outlined in Schemes 3a and 3b respectively.

2.4.2.2 Synthesis of 3'-deoxy-3'-xylofluoro thymidine phosphoramidite monomer ($^X\text{T}^F$)

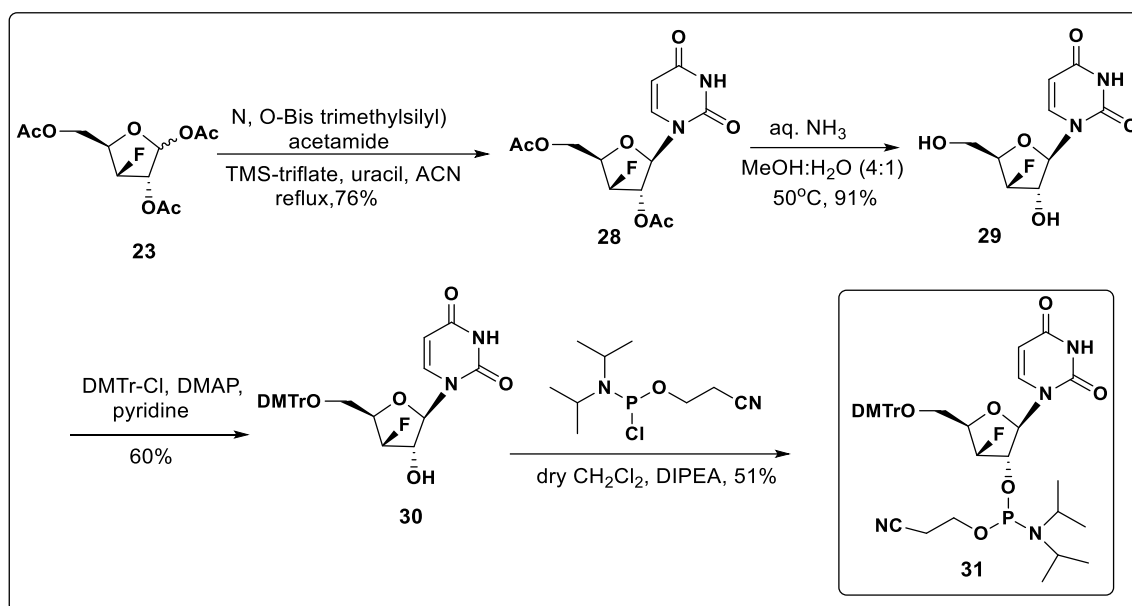
An anomeric mixture of 3-deoxy-3-fluoro-1,2,5-tri-O-acetyl-D-xylofuranose **23** when subjected to the Vorbrüggen glycosylation coupling on treatment with bis(trimethylsilyl)acetamide, thymine and TMS-triflate, exclusively afforded the β -anomer of thymidine **24** due to the neighbouring group participation of the 2-O-acetyl group. Compound **24** on ammonolysis yielded 3'-deoxy-3'-fluoro xylothymidine **25** (90%). Protection of the primary hydroxyl group in compound **25** was performed using DMTr-chloride and a catalytic amount of 4,4'-dimethylaminopyridine (DMAP) in anhydrous pyridine to obtain compound **26** (61%). Phosphitylation of the free 2'-hydroxyl group by treatment using 2-cyanoethyl-N,N-diisopropyl chlorophosphine and N,N-diisopropylethylamine (DIPEA) under anhydrous conditions afforded the desired N-type thymidine phosphoramidite building block **27** (50%).



Scheme 3a: Synthesis of $^X\text{T}^F$ monomer

2.4.2.3 Synthesis of 3'-deoxy-3'-xylofluoro uridine phosphoramidite monomer ($^X\text{U}^F$)

Using a similar reaction sequence as described above for $^X\text{T}^F$, 3'-deoxy-3'-fluoro xylouridine ($^X\text{U}^F$) monomer **31** was synthesized from an anomeric mixture of 3-deoxy-3-fluoro-1,2,5-tri-O-acetyl-D-xylofuranose **23** as shown in Scheme 3b.

Scheme 3b: Synthesis of $^X\text{U}^{\text{F}}$ monomer

Purification of all the compounds was done by column chromatography and characterization by ^1H , ^{13}C , ^{19}F & ^{31}P NMR as applicable and HRMS analysis.

2.4.3 Preliminary study of sugar pucker using ^1H NMR $J_{1'2'}$ coupling constant

The S- and N- conformation of natural and modified sugar moieties exist in equilibrium in solution; the conformation of a nucleoside can be determined from the coupling constants of the sugar ring protons in the ^1H NMR spectrum. The sugar conformations of S/N-type conformationally frozen 3'-deoxy-3'-fluoro ribo/xylothyridine nucleosides ($^{\text{R}}\text{T}^{\text{F}}$ and $^{\text{X}}\text{T}^{\text{F}}$) and 3'-deoxy-3'-fluoro ribo/xyloouridine nucleosides ($^{\text{R}}\text{U}^{\text{F}}$ and $^{\text{X}}\text{U}^{\text{F}}$) were compared (Table 1) based on the homonuclear $^3J_{\text{H}1'-\text{H}2'}$ coupling constants. The % S conformation of nucleoside unit was calculated from the value of H1'-H2' NMR coupling constants as earlier reported.⁴² A simple equation for the calculation of the percentage of S conformation is shown in equation (A). A coupling constant value between 6-9 Hz represents the S-type sugar pucker whereas lower J value between 0-3 Hz is characteristic of the N-type sugar pucker.

$$S (\%) = 100 \times (J_{1'2'} - 1)/6.9 \quad (\text{A})$$

The % S for 3'-deoxy-3'-fluoro-2'-hydroxy-thymidine **8** and 3'-deoxy-3'-fluoro ribouridine **12** were found to be 91.5 % and 97 % respectively. This shows that compound **8** and **12** are frozen in S-type conformation whereas the % S for 3'-deoxy-3'-

fluoro-2'-hydroxy-xylothymidine **25** and 3'-deoxy-3'-fluoro-xyloouridine **29** were found to be 2.9 % and 0.15 % respectively indicates N-type sugar conformation.

Table 1: Conformational analysis of the nucleosides using H1'-H2' coupling constants from ¹H NMR spectra

Nucleoside derivative	H1'-H2' coupling <i>J</i> in Hz	% S
3'-deoxy-3'-fluoro-2'-hydroxy-thymidine (8)	7.32	91.5
3'-deoxy-3'-fluoro-uridine (12)	7.7	97
3'-deoxy-3'-fluoro-2'-hydroxy-xylothymidine (25)	1.2	2.9
3'-deoxy-3'-fluoro-xyloouridine (29)	1.01	0.15

2.4.4 X-ray crystal structure of modified nucleoside analogue, 3'-deoxy-3'-fluoro-2'-hydroxy-thymidine (^RT^F)

The conformation of 3'-deoxy-3'-fluoro-2'-hydroxy-thymidine **8** was analyzed from the X-ray crystal structure. The estimation of the contribution of % S conformation for 3'-deoxy-3'-fluoro-2'-hydroxy-thymidine **8** from the H1'-H2' coupling constant gave a value of 91.5%. This indicates that compound **8** (^RT^F) shows a conformational equilibrium in aqueous solution. Hence, to verify the actual puckering of the furanose ring (N or S) in the crystalline state we investigated its single-crystal structure. The X-ray crystallographic data for compound ^RT^F has not been reported before. It has been reported that the presence of a hydroxy group at the C3' position produces an N-type sugar puckering.⁴³ We examined the effect of the replacement of the C3' hydroxy group by an F atom on the sugar puckering by X-ray crystallographic study. The four structural parameters are glycosidic torsion angle (χ), torsion angle (γ), the phase angle of pseudorotation (P) and the puckering amplitude (ν_{\max}), were calculated from X-ray crystallographic data which ultimately gives S-type and N-type population for each monomer in solid-state. The X-ray crystallographic data for 5-methyluridine (^RT^{OH}) (Figure 9) was reported earlier. The crystal structure of 3'-hydroxy-substituted 5-methyluridine (refcode MEURID)⁴³ was retrieved from the Cambridge Structural Database (CSD; Version 5.39)⁴⁴ in order to have a direct structural comparison between ^RT^{OH} and ^RT^F.

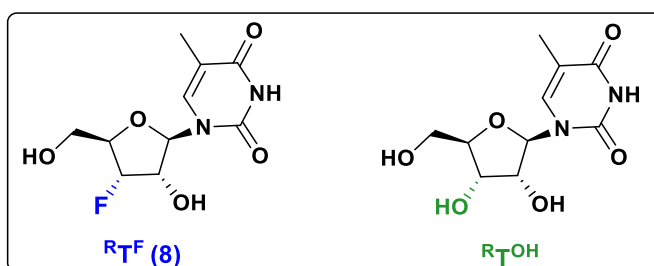


Figure 9: 3'-deoxy-3'-fluoro-2'-hydroxy-thymidine (R_{T^F}), 5-methyluridine ($R_{T^{OH}}$)

The compound R_{T^F} (8) was crystallized from methanol by slow evaporation. A single-crystal X-ray diffraction analysis was undertaken in order to investigate its crystal-state conformation. R_{T^F} crystallizes in the orthorhombic space group $P2_12_12_1$ with two unique molecules, A and B, in the asymmetric unit (Figure 10). In order to determine the conformational differences between the two conformers, molecules A and B were superimposed over the thymine moiety (Figure 11a).

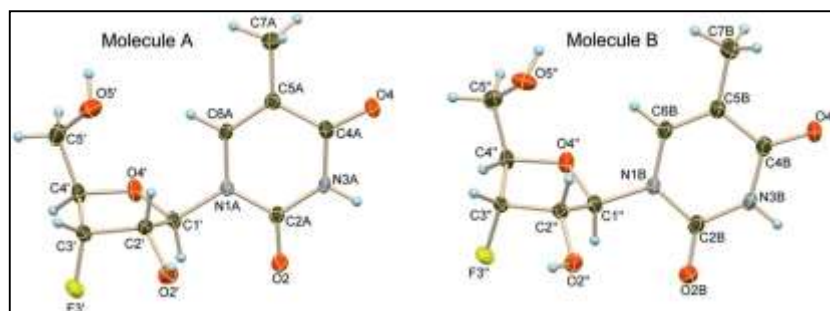


Figure 10: ORTEP drawing for the molecular structure of 3'-deoxy-3'-fluoro-2'-hydroxy-thymidine **8**, molecules A and B are the two different conformers of compound **8** (R_{T^F})

The structure overlay of molecule B of R_{T^F} and $R_{T^{OH}}$ is shown in Figure 11b. Both molecules show a significant change in the conformation of the furanose ring. The mode of puckering of the furanose ring of these two nucleosides is exactly the opposite. In R_{T^F} , C2' is found to be in the *endo* conformation (i.e., South, S), whereas in $R_{T^{OH}}$, C3' adopts an *endo* conformation (i.e., North, N).

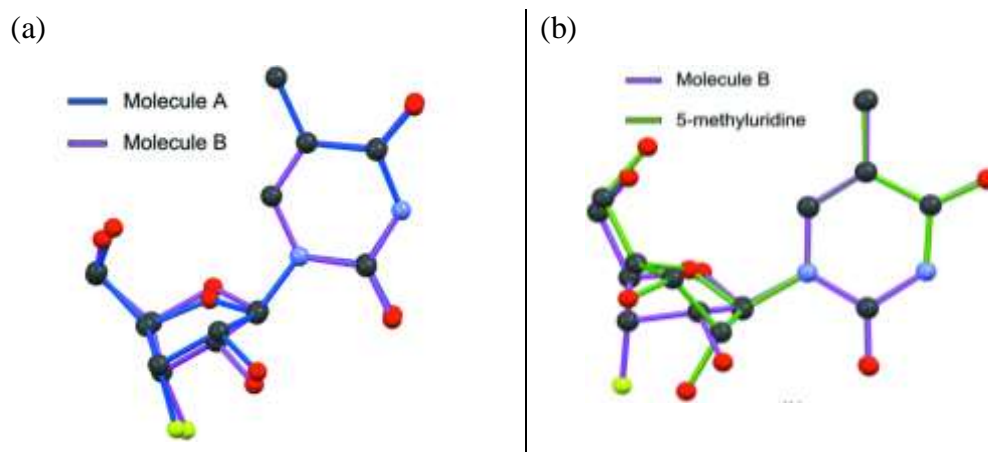


Figure 11: (a) X-ray crystal structure overlay of the two observed forms of compound $R^T^F(8)$ (b) Structure overlay of molecule B of compound, $R^T^F(8)$ and 5-methyluridine, R^T^OH retrieved from the CSD (refcode MEURID).

A comparison of the endocyclic torsion angles clearly reveals the differences caused by the F substituent at C3' position on the furanose ring puckering (Table 2). As shown in equation (B), the phase angle P is determined from the endocyclic torsion angles (v_0 – v_4). The v_{\max} value determines the deviation of the furanose ring from planarity, calculated from P and v_2 , as shown in equations (B) & (C).

$$\tan P = \frac{(v_4+v_1)-(v_3+v_0)}{2 v_2 (\sin 36^\circ + \sin 72^\circ)} \quad (\text{B})$$

$$v_{\max} = \frac{v_2}{\cos P} \quad (\text{C})$$

The furanose ring conformation can be characterized from the pseudorotation cycle where values of P (pseudoration phase angle) are plotted in combination with v_{\max} . (Figure 12).⁴⁵ The phase angle values range from 0° to 360° and are presented in multiples of 36° . The sugar can exist in a range of conformations- twist (T), envelope (E), based on the different relative phase angles as elucidated in the pseudorotation cycle. Twenty distinct envelope (E) and twist (T) conformations are found alternatively at every 18° . The E conformation is observed at odd multiples of 18° , and T is found at even multiples. For the majority of natural nucleosides, the value of P is either 18° (C3'-endo, N-type conformation) or 162° (C2'-endo, S-type conformation). In both regions, the values of v_{\max} range from 30 to 46° and, in the majority of cases, it falls around 38° .⁴⁶

Table 2: Geometrical parameters of the torsion angles ($^{\circ}$) and pseudorotation parameters ($^{\circ}$) of the furanose ring for molecules A and B of ${}^{\text{RTF}}$ and 5-methyluridine, ${}^{\text{RTOH}}$. (a) for anti, $\chi = 180^{\circ} \pm 90^{\circ}$, and for syn, $\chi = 0^{\circ} \pm 90^{\circ}$; (b) $\gamma^{\dagger} = 180^{\circ}$, $\gamma^{+} = 60^{\circ}$ and $\gamma^{-} = 60^{\circ}$; (c) for south S-type, $P = 180^{\circ} \pm 90^{\circ}$, and for north N-type, $P = 0^{\circ} \pm 90^{\circ}$; (d) data for 5-methyluridine (${}^{\text{RTOH}}$) was retrieved from the CSD (refcode MEURID).⁴³

Torsion Angle	3'-deoxy-3'-fluoro-2'-hydroxy-		5-methyluridine (${}^{\text{RTOH}}$)
	Molecule A	Molecule B	
$\nu_0 = [\text{C4}'\text{-O4}'\text{-C1}'\text{-C2}']$	-17.6 (2)	-22.3 (2)	2.5
$\nu_1 = [\text{O4}'\text{-C1}'\text{-C2}'\text{-C3}']$	33.3 (2)	37.1 (2)	-25.5
$\nu_2 = [\text{C1}'\text{-C2}'\text{-C3}'\text{-C4}']$	-35.5 (2)	-37.4 (2)	38.5
$\nu_4 = [\text{C1}'\text{-O4}'\text{-C4}'\text{-C3}']$	-5.6 (3)	-2.0 (2)	22.5
$\nu_3 = [\text{C2}'\text{-C3}'\text{-C4}'\text{-O4}']$	26.3(2)	25.2 (2)	-38.2
$\chi = [\text{C2}\text{-N1}\text{-C1}'\text{-O4}']$	-128.7 (2)	-134.4 (2)	-154
χ	<i>anti</i> ^a	<i>anti</i>	<i>anti</i>
$\gamma = [\text{C3}'\text{-C4}'\text{-C5}'\text{-O5}']$	54.8 (3)	56.1(3)	49.3
$\gamma^{\dagger}/\gamma^{+}/\gamma^{-}$ ^b	γ^{+}	γ^{+}	γ^{+}
Phase angle (P)	170.2	164.3	21.2
Puckering amplitude(ν_{max})	36.1	38.8	41.29
S or N ^c	S	S	N

The furanose ring conformations of molecules A and B of ${}^{\text{RTF}}$ (**8**) are ${}^2\text{T}_3$ ($P = 170.2^{\circ}$, $\nu_{\text{max}} = 36.1^{\circ}$) and ${}^2\text{E}$ ($P = 164.3^{\circ}$, $\nu_{\text{max}} = 38.8^{\circ}$), indicating a C2'-endo puckered sugar conformation (S-type). Conversely, for the ${}^{\text{RTOH}}$ molecule, the furanose ring conformation is ${}^3\text{E}$ ($P = 21.2^{\circ}$, $\nu_{\text{max}} = 41.29^{\circ}$) and the sugar conformation is C3'-endo (N-type) (Table 2).

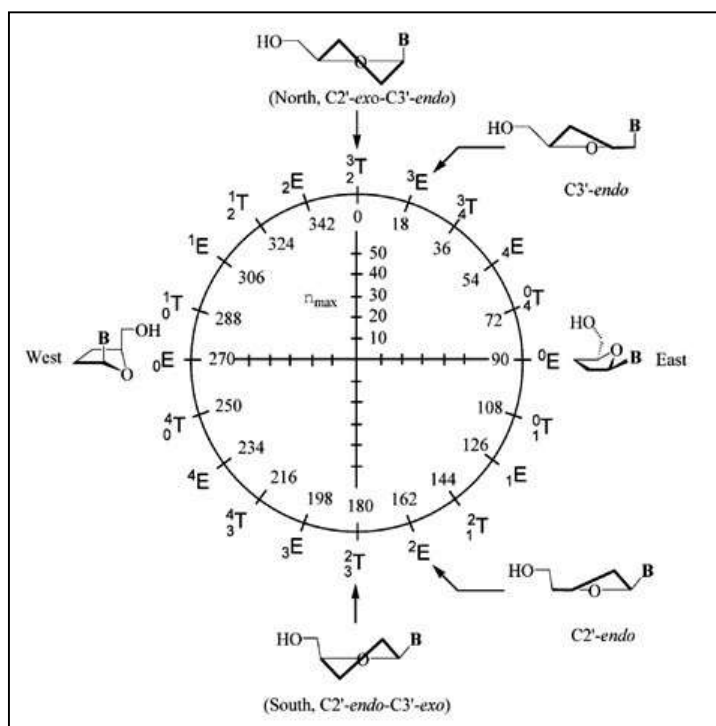


Figure 12: Pseudorotational cycle for nucleosides showing the characteristic North, South, East and West conformations. The radius of the cycle corresponds to v_{\max} . The units of P and v_{\max} values are degrees.

Envelope (E) and twist (T) forms alternate every 18° .^{45b}

From the crystal structure analysis of the C3'-fluoro substituted furanose ring, the S-type conformation of the sugar ring was confirmed, in contrast to the N-type conformation adopted by the C3'-hydroxy substituted sugar ring.

Section B

3'-Deoxy, 3'-fluoro nucleosides in the thrombin binding aptamer (TBA): Evaluation of stability and activity

2.4.5 Synthesis of TBA, *iso*TBA and modified *iso*TBA variants, their purification and characterization

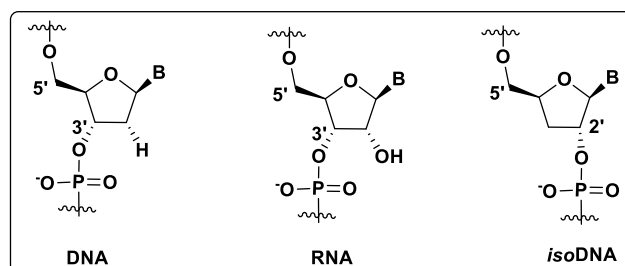


Figure 13: Structures of natural DNA, RNA and *iso*DNA

We chose the 3'-deoxy-2'-5'-linked *iso*TBA sequence (Figure 13) as it exhibits high stability against cellular enzymes.⁴⁷ The four phosphoramidite monomers 3'-deoxy-3'-ribo/xylo fluoro thymidine (R^T^F and X^T^F) and 3'-deoxy-3'-ribo/xylo fluoro uridine (R^U^F and X^U^F) (Figure 14) were incorporated into 2'-5' linked *iso*TBA in the central loop at position T⁷ and T⁹ or both.

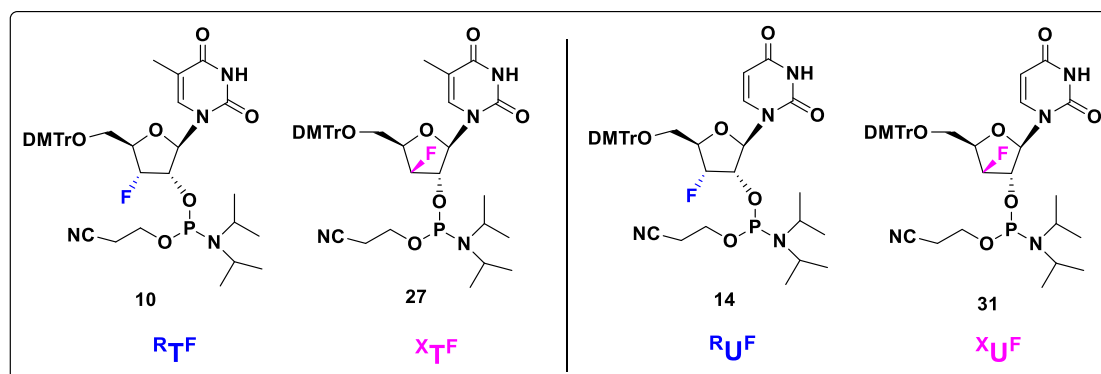


Figure 14: Phosphoramidite monomers for this study

All the *iso*DNA ONs (listed in Table 1) were synthesized on a Bioautomation MM4 DNA synthesizer using commercially available protected 3'-deoxy-thymidine-2'-phosphoramidite and 3'-deoxy-guanosine-2'-phosphoramidite by standard β -cyanoethyl phosphoramidite chemistry⁴⁸ using re-coupling for modified nucleotides. The synthesized oligonucleotides were cleaved from the solid support by aq. ammonia treatment at 55 °C. Purification of synthesized oligomer was done by RP-HPLC and

their integrity was confirmed by MALDI-TOF mass spectrometric analysis. The general scheme for solid-phase oligonucleotide synthesis is explained in Chapter 1, Scheme 1. The synthesized oligomeric sequences and their MALDI-TOF characterization data are listed in Table 1. Their purity was confirmed by RP-HPLC on a C18 column and polyacrylamide gel electrophoresis (Figure 15).

Table 3[#]: *iso*TBA and loop-modified oligomers used in the present work, MALDI-TOF mass spectrometric data.

Entry no.	Sequence code	Sequence	MALDI TOF Mass (Da)	
			M _{calcd.}	M _{obsd.}
1.	<i>iso</i> TBA	5'-GGTTGGTGTGGTTGG-2'	4726	4731
2.	<i>iso</i> TBA ^{RT^F} -7	5'-GGTTGG ^{RT^F} GTGGTTGG 2'-	4744	4750
3.	<i>iso</i> TBA ^{RT^F} -79	5'-GGTTGG ^{RT^F} ^{RT^F} GGTTGG- 2'	4762	4766
4.	<i>iso</i> TBA ^{RT^F} -9	5'-GGTTGGTGT ^{RT^F} GGTTGG- 2'	4744	4748
5.	<i>iso</i> TBA ^{XT^F} -7	5'-GGTTGG ^{XT^F} GTGGTTGG- 2'	4744	4755
6.	<i>iso</i> TBA ^{XT^F} -79	5'-GGTTGG ^{XT^F} ^{XT^F} GGTTGG- 2'	4762	4774
7.	<i>iso</i> TBA ^{XT^F} -9	5'-GGTTGGTGT ^{XT^F} GGTTGG 2'-	4744	4753
8.	<i>iso</i> TBA ^{RU^F} -7	5'-GGTTGG ^{RU^F} GTGGTTGG -2'	4730	4733
9.	<i>iso</i> TBA ^{RU^F} -79	5'-GGTTGG ^{RU^F} ^{RU^F} GGTTGG -2'	4734	4737
10.	<i>iso</i> TBA ^{RU^F} -9	5'-GGTTGGTGT ^{RU^F} GGTTGG -2'	4730	4730
11.	<i>iso</i> TBA ^{XU^F} -7	5'-GGTTGG ^{XU^F} GTGGTTGG -2'	4730	4731
12.	<i>iso</i> TBA ^{XU^F} -79	5'-GGTTGG ^{XU^F} ^{XU^F} GGTTGG-2'	4734	4738
13.	<i>iso</i> TBA ^{XU^F} -9	5'-GGTTGGTGT ^{XU^F} GGTTGG- 2'	4730	4742

[#]The number in the sequence name indicates the position of the modified nucleotide unit in the central loop.

Polyacrylamide gel electrophoresis was used to examine the purity of the synthesized oligomers using a 20% denaturing gel. All the 15-mer oligonucleotides showed similar mobility.

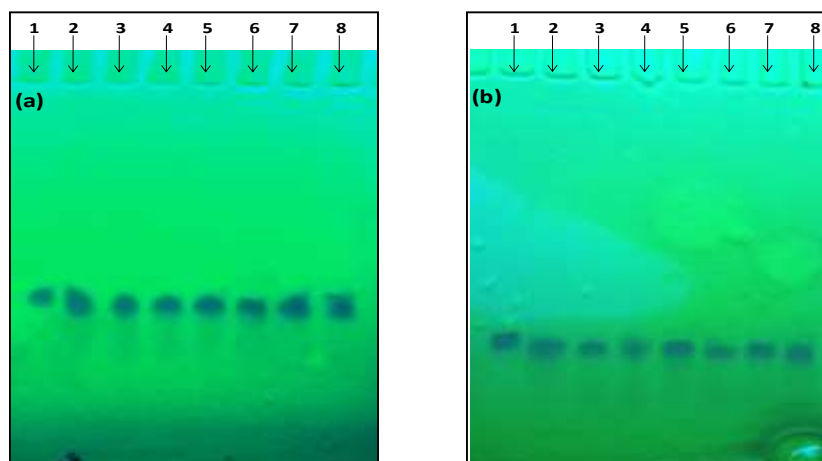


Figure 15: Denaturing gel electrophoresis analysis of TBA, *iso*TBA oligomers, indicating their purity. Strand concentration of TBA and *iso*TBA oligomers was 320 μ M and the gel was run in TBE buffer at 25 $^{\circ}$ C at 150V. The gel was visualized by UV- shadowing.

Figure 15(a): 1-TBA, 2-*iso*TBA, 3-*iso*TBA^{RT^F}-7, 4-*iso*TBA^{RT^F}-79, 5- *iso*TBA^{RT^F}-9, 6- *iso*TBA^{XT^F}-7, 7- *iso*TBA^{XT^F}-79, 8- *iso*TBA^{XT^F}-9

Figure 15(b): 1-TBA, 2-*iso*TBA, 3-*iso*TBA^{RU^F}-7, 4- *iso*TBA^{RU^F}-79, 5- *iso*TBA^{RU^F}-9, 6- *iso*TBA^{XU^F}-7, 7- *iso*TBA^{XU^F}-79, 8- *iso*TBA^{XU^F}-9

2.4.6 Evaluation of G-quadruplex formation and stability in the presence of monovalent ions by circular dichroism spectroscopy

The impact of the 3'-fluoro-modified units on the structural topology of TBA can be studied by CD spectroscopy. CD spectra were recorded for TBA, *iso*TBA and all modified oligomers to monitor the influence of the different sugar substitutions in the central loop of TBA on its overall topology. TBA is known to form an antiparallel G-quadruplex in the presence of K⁺ ions; the CD spectrum of TBA shows a CD maximum at 295 nm and a minimum at 265 nm, that are characteristic of antiparallel G-quadruplexes.⁴⁹

2.4.6.1 G-quadruplex topology

Firstly, we examined the effect of modification in the loop on the folding topology of all oligomers by CD spectroscopy in the presence of potassium ions. The CD spectra of these derivatives displayed the characteristic signals corresponding to the antiparallel G-quadruplex topology known for TBA and *iso*TBA at the same concentration.⁵⁰ All the modified oligomers showed two maxima at 292 nm and \sim 240 nm and minima at \sim 265 nm in presence of potassium ions (Figure 16), whereas the CD spectra recorded in water,

in the absence of any added cations, except in the case of TBA, failed to show any of these characteristic signals. TBA showed the characteristic antiparallel quadruplex signals even in water (Figure 17).

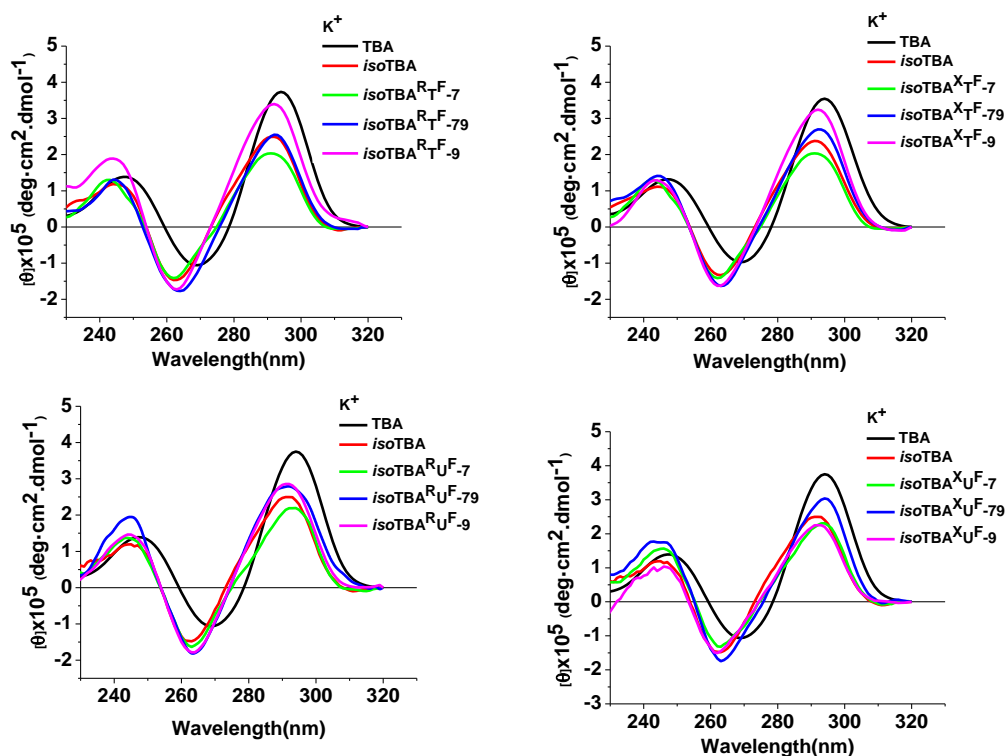


Figure 16: CD spectra of the TBA, *isoTBA* and modified *isoTBA* oligomers (5 μM) in the presence of K^+ ions. Spectra were recorded at 4 $^{\circ}\text{C}$ in 10 mM K-phosphate buffer, pH 7.2, containing 100 mM KCl.

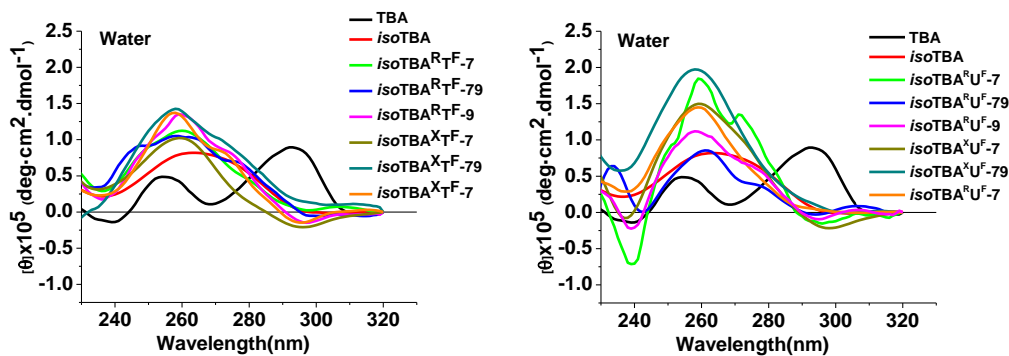


Figure 17: CD spectra of the TBA, *isoTBA* and modified *isoTBA* oligomers (5 μM) in water

2.4.6.2 Evaluation of G-quadruplex thermal stability using CD spectroscopy

Denaturation – renaturation profiles and melting temperature (T_m) can be monitored by CD spectroscopy at varying temperatures. The stability of the G-quadruplexes in the presence of K^+ ions was monitored by the temperature-dependent change in the amplitude of the CD signal at 295 nm for all oligomers.

Table 4: CD- T_m values of modified sequences in the presence of K^+ ions. ΔT_m represents melting difference compared to ^a *iso*TBA and ^b TBA

Entry	Sequence code	T_m ° C in	ΔT_m^a	ΔT_m^b
1.	TBA	50	+16	-
2.	<i>iso</i> TBA	34	-	-16
3.	<i>iso</i> TBA ^{RT^F} -7	35	+2	-15
4.	<i>iso</i> TBA ^{RT^F} -79	36	+2	-14
5.	<i>iso</i> TBA ^{RT^F} -9	36	+2	-14
6.	<i>iso</i> TBA ^{XT^F} -7	37	+3	-13
7.	<i>iso</i> TBA ^{XT^F} -79	36	+2	-14
8.	<i>iso</i> TBA ^{XT^F} -9	35	+1	-15
9.	<i>iso</i> TBA ^{RU^F} -7	40	+6	-10
10.	<i>iso</i> TBA ^{RU^F} -79	42	+8	-8
11.	<i>iso</i> TBA ^{RU^F} -9	35	+1	-15
12.	<i>iso</i> TBA ^{XU^F} -7	37	+3	-13
13.	<i>iso</i> TBA ^{XU^F} -79	38	+4	-12
14.	<i>iso</i> TBA ^{XU^F} -9	35	+1	-15

The results were compared with native TBA and *iso*TBA. In comparison to TBA (3'-5' linked backbone $T_m = 50$ °C), all the oligomers, including *iso*TBA ($T_m = 34$ °C) with 2'-5' linked backbone, were destabilized to a large extent ($\Delta T_m = -8$ °C to -15 °C). The extended backbone in *iso*TBA, together with the altered sugar pucker conformation could be the reason for the observed lower stability. The results are summarized in Table 4, and the melting plots are shown in Figure 18. As discussed above in the introduction, modification at T⁷ position has often been shown to be favourably tolerated in terms of quadruplex stability. In this study, we observed that substitution by 3'-deoxy-3'-ribofluoro uridine (with S-type sugar conformation) at T⁷ and T⁹ positions in *iso*TBA^{RU^F}-7 ($T_m = 40$ °C) and *iso*TBA^{RU^F}-79 ($T_m = 42$ °C) displayed remarkable enhancement in quadruplex stability by $+6$ °C and $+8$ °C respectively as compared to *iso*TBA. The effect of replacement of T⁷ by ^{RU^F} in oligomers *iso*TBA^{RU^F}-7 ($T_m = 40$ °C) and *iso*TBA^{RU^F}-79 ($T_m = 42$ °C) showed stabilization as compared to *iso*TBA^{RT^F}-7 ($T_m = 35$ °C), *iso*TBA^{RT^F}-79 ($T_m = 36$ °C). Sacca et al.²⁷ reported similar stabilization effect when thymidine was replaced by 2'-deoxyuridine at T⁷ position of TBA.

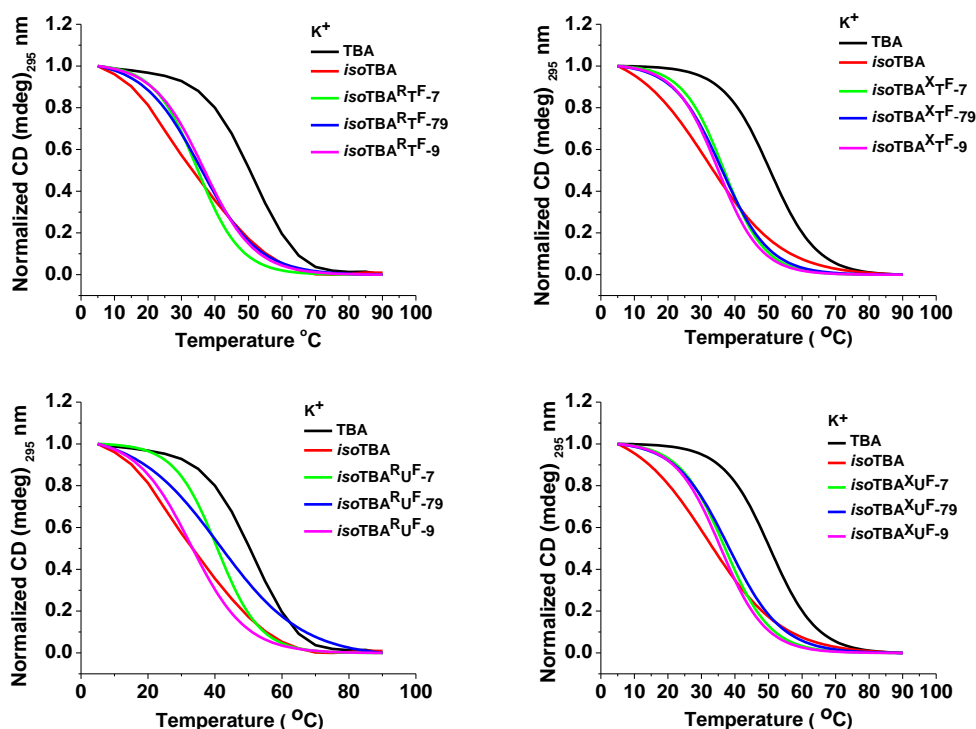


Figure 18: CD melting profiles of the TBA, *iso*TBA and modified *iso*TBA oligomers at a strand concentration of 5 μ M in 10 mM potassium phosphate buffer (pH 7.2) containing 100 mM KCl.

Substitution at T⁹ position by all modified monomers showed a modest stabilization by +1°C/+2°C, whereas moderate enhancement by +3°C/+4°C was observed in case of *iso*TBA^XU^F-7 and *iso*TBA^XU^F-79 oligomers with a 3'-xylofluoro uridine unit at T⁷ and T⁷T⁹ positions respectively in comparison to *iso*TBA.

2.4.7 Formation of G-quadruplex in the presence of thrombin

Thrombin may act as a molecular chaperone for the folding of TBA, as has been reported previously by Baldrich and O'Sullivan.⁵¹ Nagatoishi and co-workers⁵² showed that at low temperature, TBA forms an antiparallel G-quadruplex in the presence of thrombin and in the absence of any cation, which can be monitored through the CD amplitude at 295 nm. In our earlier studies, we observed that the *iso*TBA sequence was also able to attain the folded G-quadruplex topology by the chaperone activity of thrombin.⁵⁰ Therefore, we carried out CD experiments with the addition of thrombin, which was added incrementally to the individual oligomers at 4 °C. The CD spectrum of TBA in water, even in the absence of K⁺ or any other cation shows a CD maximum at 290 nm (Figure 19a). With the incremental addition of thrombin to TBA, we observed a increase in the CD signal amplitude with a concomitant shift towards 300 nm.

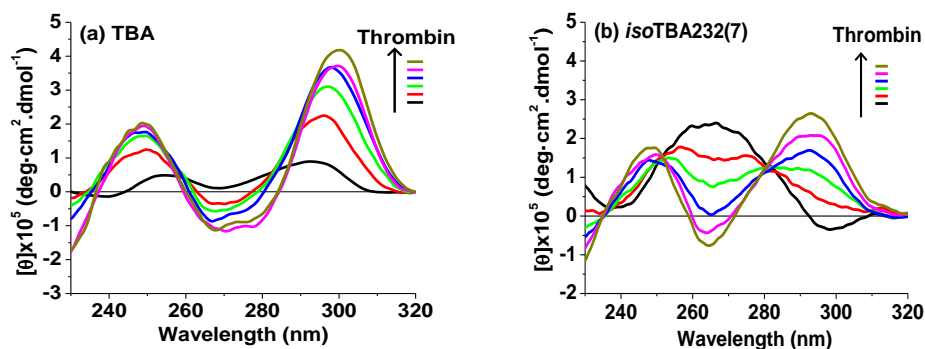


Figure 19: Changes in CD signal at 295 nm showing the chaperone effect of thrombin on (a) TBA and (b) *isoTBA*. Black: in water (No thrombin), Red: 0.44 μM , Green: 0.85 μM , Blue: 1.25 μM , Magenta: 1.63 μM , Dark yellow: 2 μM

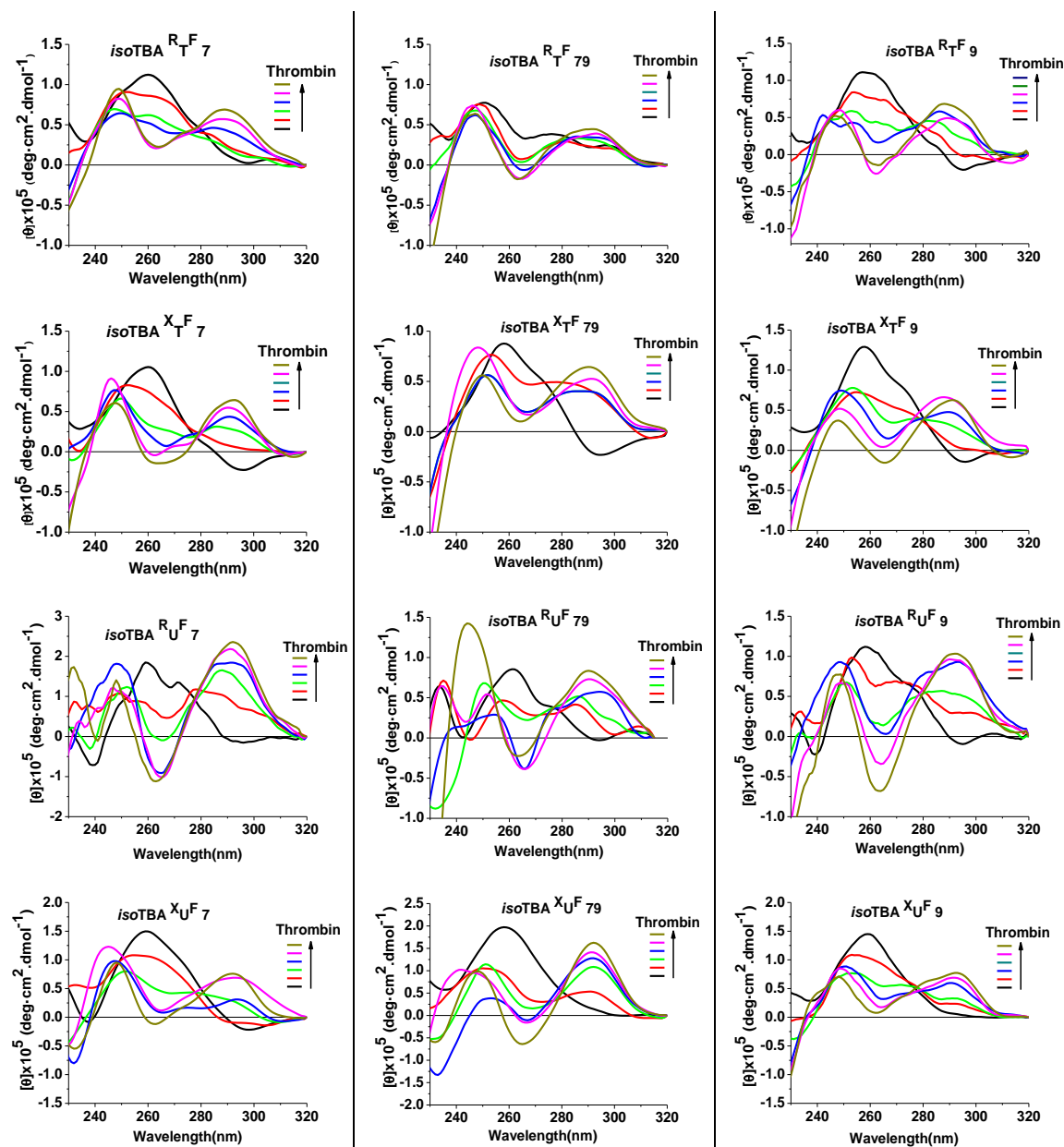


Figure 20: Changes in CD signal at 295 nm showing the chaperone effect of thrombin on the TBA and *iso*TBA loop-modified oligomers Black: in water (No thrombin), Red: 0.44 μ M, Green: 0.85 μ M, Blue: 1.25 μ M, Magenta: 1.63 μ M, Dark yellow: 2 μ M

In water, all the modified sequences showed maxima at \sim 260 nm (Figure 17). We performed CD experiments with all the sequences of the study, in the presence of increasing concentrations of thrombin at 4 $^{\circ}$ C (Figure 20). We observed an increase in the CD signal amplitude near 290 nm upon incremental addition of thrombin, in accordance with its chaperone effect.

2.4.8 Antithrombin effect of modified aptamers

Thrombin transforms fibrinogen to fibrin and that leads to coagulation.⁵³ The effect of thrombin binding on the anti-thrombin activity of the modified oligomers was assessed by carrying out a clotting assay and the inhibitory effect on thrombin-catalyzed fibrin polymerization (thrombin time/clotting time) was measured at 37 $^{\circ}$ C. The thrombin reagent was pre-incubated with the oligomer before addition to fibrinogen-containing saline and the time for clotting was measured using a STart Max Coagulation analyzer (Diagnostica Stago). The anti-thrombin activity reflects the additional time required for clotting in the presence of the oligomer, relative to the reference in the absence of any added oligomer.

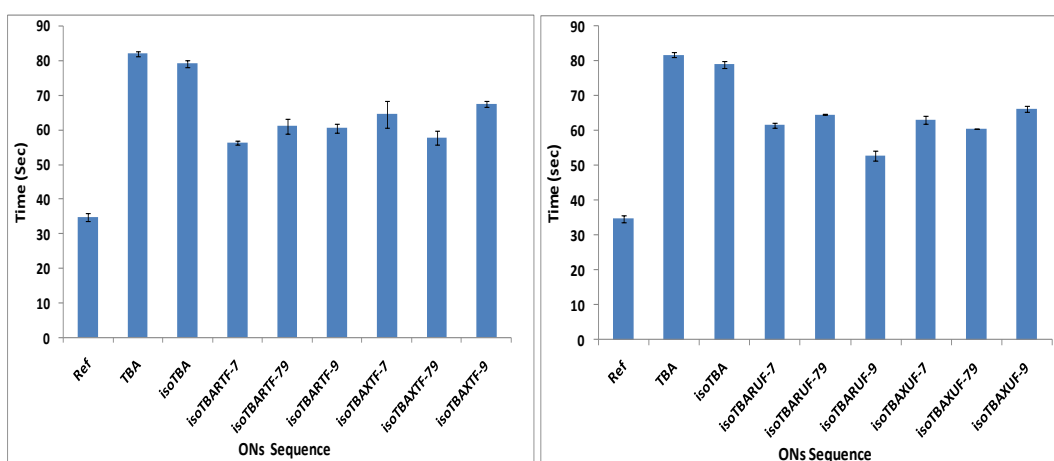


Figure 21: Antithrombin activity measurement using fibrinogen from human plasma and bovine thrombin. Error bars represent the standard deviation obtained from triplicate experiments. Ref indicates the clotting time measured with fibrinogen and thrombin in the absence of any added oligomer.

From Figure 21, it can be seen that in comparison to the reference, the fluoro modified *iso*TBA oligomers had a better anti-thrombin activity, however in comparison to the TBA and *iso*TBA the fluoro modified *iso*TBA oligomers had shown a lower anti-thrombin activity, the highest activity being observed for the parent TBA.

2.4.9 Stability of oligonucleotides towards exonucleases

Nuclease resistance of oligonucleotides is an essential aspect that decides the efficacy of oligonucleotides *in vivo*. Many strategies have been applied to develop the stability against nucleases without affecting the binding affinity of the aptamer and specificity to their target. C2'-modification in the sugar ring such as 2'-F-RNA, 2'-amino, 2'-methoxy, locked nucleic acid (LNA, ribonucleotide with methylene linkage between 2'-O and 4'-C of the sugar ring), unlocked nucleic acid (UNA, in which the bond between C2' and C3' carbons is absent) and 2'-F-ANA are some of the notable modifications that showed good nuclease resistance.

In addition to the enhancement of the thermal stability and thrombin affinity, another purpose of incorporation of our synthetic 3'-fluoro-modified units into 2'-5'-linked *iso*TBA was to increase the resistance of the resulting oligomers to degradation by nucleases. To test the enzymatic stability, we exposed *iso*TBA^{XTF}-79 as a representative oligomer, to snake venom phosphodiesterase, an enzyme which possesses predominantly 3'-exonuclease activity, and compared it to TBA and *iso*TBA.

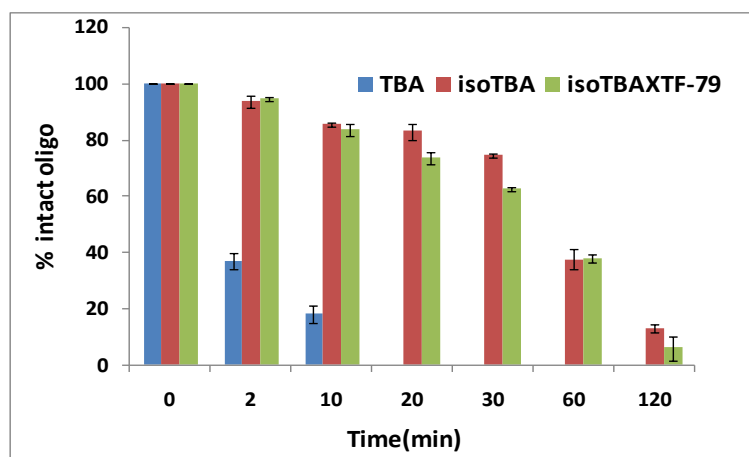


Figure 22: RP-HPLC at different time points upon SVPD digestion of oligonucleotides TBA, *iso*TBA and *iso*TBA^{XTF}-79. Experiments were done in duplicate and the error bars (standard deviation) are indicated.

We found that the stability of TBA was very low; it was rapidly cleaved within 2 min, whereas both *iso*TBA and *iso*TBA^{XTF}-79 were found to be digested much slower;

even after 60 min, nearly 40 % of both oligomers were intact (Figure 22). This reaction was monitored by HPLC analysis, by measuring the peak area of the intact oligomer at progressive time periods (Figures 22a, 22b and 22c).

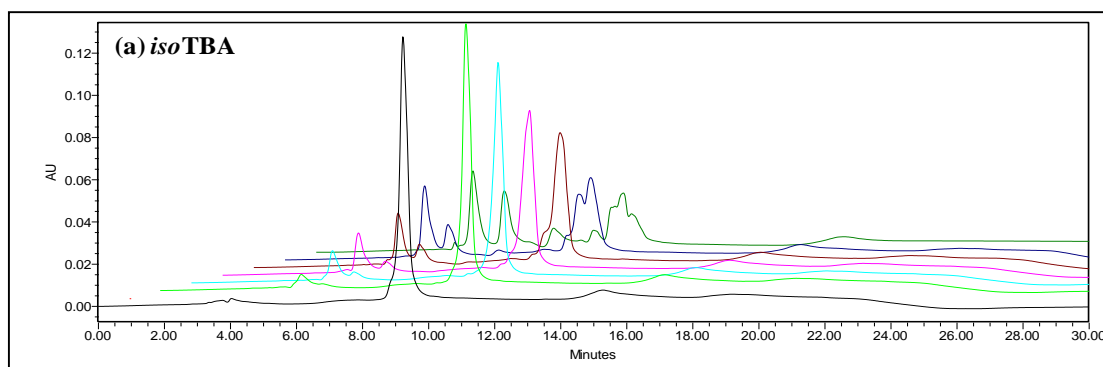


Figure 22a: HPLC profiles of *isoTBA*, towards SVPD at increasing time intervals. Black: without SVPD enzyme, Green: 2 min Cyan: 10 min, Magenta: 20 min, Brown: 30 min, Dark blue: 60 min, Dark Green: 120 min.

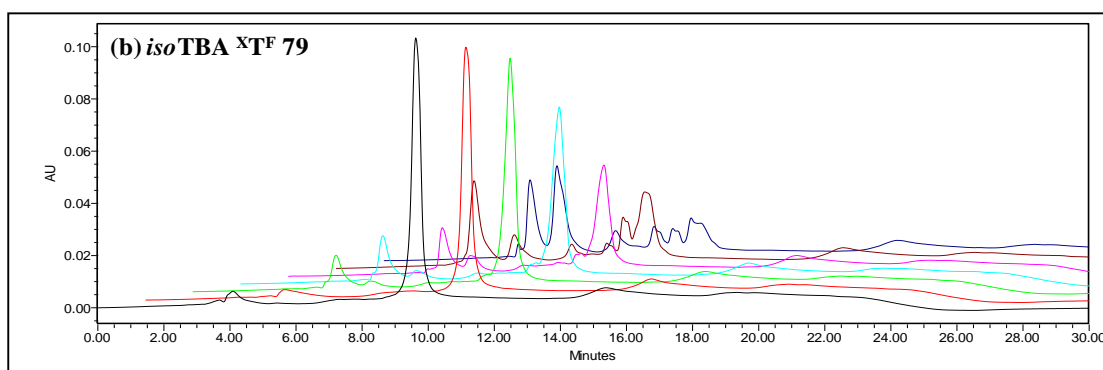


Figure 22b: HPLC profiles of *isoTBA^{XTF}-79*, towards SVPD at increasing time intervals. Black: without SVPD enzyme, Red: 2 min, Green: 10 min, Cyan: 20 min, Magenta:30 min, Brown:60 min, Dark blue: 120 min.

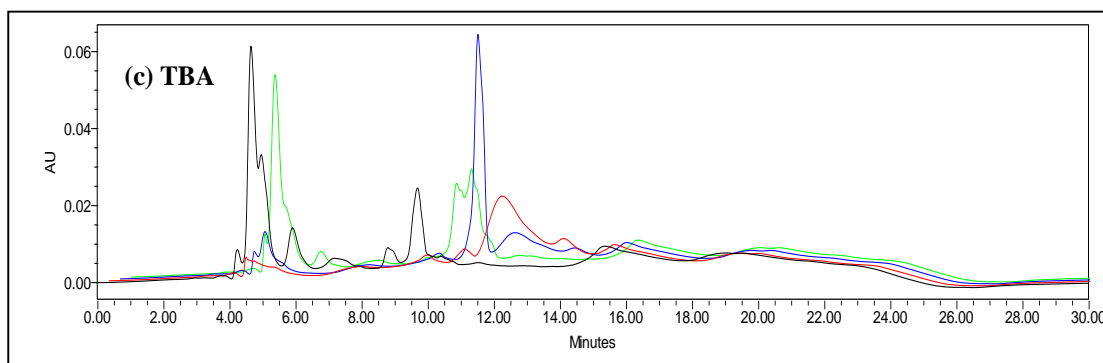


Figure 22c: HPLC profiles of TBA, towards SVPD at increasing time intervals. red: without SVPD enzyme, Blue: 2 min, Green: 10 min, Black: 20 min.

2.5 Key highlights of this study

- Synthesis of the 3'-deoxy-3'-fluoro ribo/xylo thymidine monomers ($^R\text{T}^F$ and $^X\text{T}^F$) 3'-deoxy-3'-fluoro ribo/xylo uridine monomers ($^R\text{U}^F$ and $^X\text{U}^F$) were done.
- These modified units were incorporated into *iso*TBA as single substitutions either at T⁷ or T⁹ position or at both T⁷ and T⁹ positions.
- CD spectroscopy studies in the presence of K⁺ ions showed that all *iso*TBA variants studied in this work were able to form unimolecular antiparallel G-quadruplexes, similar to native TBA.
- Thrombin-binding studies brought out the chaperone effect of thrombin on the quadruplex topology of individual oligomers.
- Antithrombin effect (anticoagulating ability) was examined, which revealed that fluoro modified *iso*TBA quadruplexes showed thrombin inhibition but exhibited lower anticoagulating ability in comparison to TBA and *iso*TBA.
- Enhanced stability to nucleases was shown by *iso*TBA and *iso*TBA $^X\text{T}^F$ -79 oligomers compared to TBA.

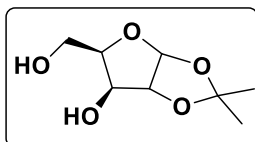
2.6 Conclusion

Incorporation of S-type and N-type conformationally frozen monomers (3'-deoxy, 3'-fluoro thymidine/uridine) in *iso*TBA with a 2'-5'-backbone is reported for the first time. Newly reported *iso*TBA analogues showed antiparallel quadruplex topology with an enhancement in thermal stability compared to the parent *iso*TBA and better nuclease stability as compared to TBA.

2.7 Experimental

2.7.1 Experimental procedures and spectral data

1, 2-*O*-Isopropylidene- α -D-xylofuranose (**2**)



Commercially available D-xylose compound **1** (15.0 g, 99.91 mmol) was dissolved in acetone (400 mL) containing conc. H₂SO₄ (15.0 mL, 268.68 mmol) with stirring at room temperature. After 30 min solution of Na₂CO₃ (19.0 g, 179.26 mmol) in H₂O (230 mL) was dropwise added within 30 min maintaining with external cooling to maintain the temperature below 20°C. After addition, the mixture was stirred for a further 3 h. Then, solid Na₂CO₃ (10.5 g, 99.07 mmol) was added till the neutral pH (pH = 7.0), Solid Na₂SO₄ was filtered off and washed with acetone, and the combined filtrates were concentrated under reduced pressure to yield 18.2 g of crude **2** contaminated with 5% of 1,2:3,5-di-*O*-isopropylidene- α -D-xylofuranose, and 5% of starting D-xylose. The crude compound **2** was purified by silica gel filtration using 30:1 DCM/MeOH and pure compound **2** was obtained as syrup, which crystallized on standing. Yield: 16.8 g, 88%.

Mol. Formula : C₈H₁₄O₅

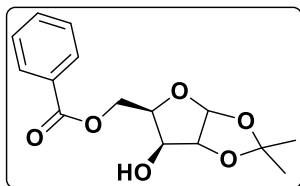
Exact Mass : 190.0841

HRMS: : 213.0734 (M + Na⁺)

¹H NMR : δ_{H} (ppm) 1.23 (s, 3H), 1.40 (s, 3H), 3.87 (br, 2H), 4.08–4.11 (m, 2H), 4.19 (br, 1H), 4.44 (d, $J = 3.5$ Hz, 1H), 4.63 (d, $J = 4.3$ Hz, 1H), 5.88 (d, $J = 3.5$ Hz, 1H)
(400MHz, CDCl₃)

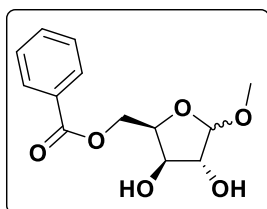
¹³C NMR : δ_{C} (ppm) 25.9, 26.4, 60.2, 75.5, 79.4, 85.1, 104.5, 111.5
(50MHz, CDCl₃)

¹³C-DEPT : δ_{C} (ppm) (CH/CH₃): 26.0, 26.4, 75.5, 79.5, 85.2, 104.5.
(50MHz, CDCl₃) (CH₂): 60.2

5-O-Benzoyl-1, 2-O-isopropylidene- α -D-xylofuranose (3)

Compound **2** (8 g, 42.06 mmol) and dry TEA (14.52 g, 20 mL, 143.49 mmol) was added into dry DCM (120 mL) under N₂ atmosphere with stirring. The reaction mixture was cooled to 0°C. A solution of benzoyl chloride (6.42 g, 5.3 mL, 45.62 mmol) in dry DCM (20 mL) was dropwise added to the reaction mixture at the same temperature. Reaction mixture was stirred for another 3 h. TLC indicated complete consumption of the starting material, DCM (100 mL) was added into the reaction mixture, washed with NaHCO₃ and H₂O, dried over Na₂SO₄, solvent was evaporated under reduced pressure. Crude product **3** was purified on a silica gel column chromatography using EtOAc/petether (2:8) as eluent. Yield: 9.7 g, 78%.

Mol. Formula	: C ₁₅ H ₁₈ O ₆
Exact Mass	: 294.1103
HRMS	: 317.0990 (M+Na ⁺)
¹H NMR (200MHz, CDCl ₃)	: δ_{H} (ppm) 1.33 (s, 3H), 1.52 (s, 3H), 3.35 (d, 1H), 4.17-4.18 (m, 1H), 4.35-4.44 (m, 2H), 4.61 (d, $J = 3.5\text{Hz}$, 1H, H-2), 4.76-4.87 (m, 1H), 5.97 (d, $J = 3.5\text{ Hz}$, 1H, H-1), 7.43-7.65 (m, 3H, Ar-H), 8.04-8.08 (m, 2H, Ar-H)
¹³C NMR (50MHz, CDCl ₃)	: δ_{C} (ppm) 26.1, 26.7, 61.4, 74.4, 78.5, 85.0, 104.7, 111.8, 128.5, 129.19, 129.8, 133.5, 167.3
¹³C-DEPT (50MHz, CDCl ₃)	: δ_{C} (ppm) (CH/CH ₃): 26.1, 26.7, 74.4, 78.5, 85.0, 104.7, 128.5, 129.9, 133.5, (CH ₂): 61.4

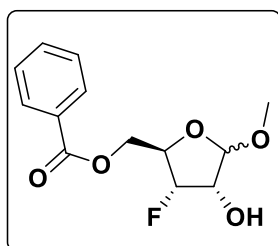
Methyl 5-O-benzoyl-D-xylofuranoside (4)

Compound **3** (9.3 g, 31.60 mmol) was dissolved into dry MeOH (150 mL), crystalline I₂ (1.8 g, 14.18 mmol) was added into the solution with stirring, and the mixture was refluxed for 4 h. Progress of reaction was monitored by TLC, after completion of the reaction, reaction mixture cooled to room temperature, the mixture was poured into saturated aqueous Na₂S₂O₃ solution (300 mL) and extracted with CHCl₃ (3 X 200 mL), the combined organic extract was washed with saturated NaCl solution (200 mL), dried over anhydrous Na₂SO₄. Solvent was evaporated under reduced pressure to yield oily

residue (8.5 g). This was purified on a silica gel column chromatography using pet ether/EtOAc (6:4) as solvent system. Compound **4** was obtained as a mixture of α/β isomer. Yield: 7.2 g, 85%.

Mol. Formula	: C ₁₃ H ₁₆ O ₆
Exact Mass	: 268.0947
HRMS	: 269.1016 (M+1)
¹H NMR ($\alpha+\beta$)	: δ_{H} (ppm) 3.43 & 3.53 (β : s, 2.25 H, OCH ₃ , α : s, 0.75H, (500MHz, OCH ₃), 4.19-4.27 (m, 2H), 4.39-4.75 (m, 3H), 4.92 & 5.07 (β : CDCl ₃) s, 0.3H, H-1, α : d, 0.7H, $J_{1'2'}$ = 4.27 Hz, H-1), 7.44-7.48 (m, 2H, Ar-H), 7.56-7.61(m, 1H, Ar-H), 8.04-8.09 (m, 2H, Ar-H)
¹³C NMR ($\alpha+\beta$)	: δ_{C} (ppm) 55.3, 56.1, 62.6, 64.3, 76.3, 76.5, 76.9, 77.9, 79.5, (125MHz, 80.8, 102.0, 108.6, 128.4, 128.5, 129.1, 129.8, 129.9, 129.9, CDCl ₃) 133.1, 133.4, 166.6, 166.9
¹³C-DEPT ($\alpha+\beta$)	: δ_{C} (ppm) (CH/CH ₃): 55.3, 56.1, 76.3, 76.5, 77.9, 77.9, 79.5, (125MHz, 80.8, 102.0, 108.6, 128.4, 128.5, 129.7, 129.7, 133.1, 133.4 CDCl ₃) (CH ₂): 62.6, 64.3

3-Deoxy-3-fluoro-1-O-methyl-5-O-benzoyl-D-ribofuranoside (**5**)

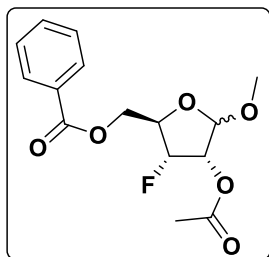


To a solution of compound **4** (2.3 g, 8.57 mmol) in dry DCM (50 mL), DAST (6.8 mL, 51.47 mmol) was added and the mixture was stirred at room temperature for 24 h. TLC examination revealed the appearance of the product and the disappearance of the starting material. After cooling to 0 °C, the reaction mixture was poured into saturated cold aqueous NaHCO₃ solution (100 mL), organic phase was separated and the aqueous phase extracted with DCM (3 X 100 mL), the combined organic extract was dried over Na₂SO₄ and evaporated under reduced pressure. Crude compound **5** was further purified by column chromatography using 6:4 petether/EtOAc solvent system to get pure compound **5**. Yield: 1.3 g, 56%.

Mol. Formula	: C ₁₃ H ₁₅ FO ₅
Exact Mass	: 270.0904
HRMS	: 293.0791 (M+Na ⁺)
¹H NMR ($\alpha+\beta$)	: δ_{H} (ppm) 3.33 & 3.48 (two S, 3H, OCH ₃ , $\alpha+\beta$), 4.24-4.26

(400MHz, CDCl ₃)	(m, 1H), 4.39-4.62 (m, 3H), 4.90-4.98 (m, 1H) 5.09-5.12 & 5.23-5.25 (dt, $J_{3',F} = 53.91$ Hz, 4.7 Hz, 2H), 7.42-7.58 (m, 3H, Ar-H), 7.97-8.07 (m, 2H, Ar-H)
¹³ C NMR ($\alpha+\beta$) (50MHz, CDCl ₃)	: δ_C (ppm) 55.4, 55.6, 63.6, 63.8, 64.0, 64.1, 72.1, 72.3, 74.2, 74.3, 78.1, 78.4, 80.3, 80.5, 89.4, 91.2, 91.3, 93.1, 102.2, 107.8, 107.9, 128.3, 128.5, 129.2, 129.5, 129.5, 129.6, 133.2, 133.3, 166.0, 166.2
¹³ C-DEPT ($\alpha+\beta$) (50MHz, CDCl ₃)	: δ_C (ppm) (CH/CH ₃): 55.5, 55.7, 72.1, 72.4, 74.1, 74.4, 78.1, 78.5, 80.1, 80.6, 88.5, 90.3, 92.2, 94.0, 102.2, 107.8, 107.9, 128.4, 128.5, 129.5, 129.6, 133.2, 133.4. (CH ₂): 63.6, 63.8, 64.0, 64.1
¹⁹ F NMR($\alpha+\beta$) (376MHz, CDCl ₃)	δ_F (ppm) -213.09, -195.38

3-Deoxy-3-fluoro-1-O-methyl-2-O-acetyl-5-O-benzoyl-D-ribofuranoside (6)

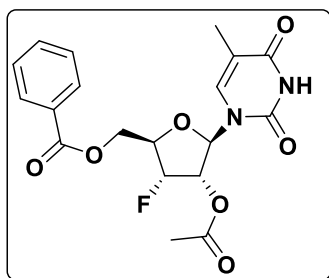


Acetic anhydride was added (1.07 mL, 11.32 mmol) to a solution of compound **5** (0.5 g, 1.850 mmol) in dry pyridine (25 mL). The mixture was stirred at room temperature for 3 h. Pyridine was removed under reduced pressure. The residue was dissolved in EtOAc (100 mL), washed with saturated NaHCO₃ (2 x 50 mL) and saturated aqueous NaCl (2 x 50 mL). The EtOAc layer was dried over Na₂SO₄, filtered and solvent was evaporated under reduced pressure to dryness. The crude compound **6** was purified by silica gel column chromatography using EtOAc/pet ether (2:8) to get pure compound **6** as yellow syrup. Yield: 0.392, 68%.

Mol. Formula	: C ₁₅ H ₁₇ FO ₆
Exact Mass	: 312.1009
¹ H NMR (200MHz, CDCl ₃)	: δ_H (ppm) 2.15 (s, 3H, OAc), 3.35 (s, 3H, OCH ₃), 4.42-4.57 (m, 3H), 4.98-5.38 (m, 3H), 7.43-7.58 (m, 3H, Ar-H), 8.06-8.08 (m, 2H, Ar-H)
¹³ C-NMR (50MHz, CDCl ₃)	: δ_C (ppm) 20.5, 55.6, 63.78-63.83 (d), 74.98-75.0 (d), 79.0-79.3 (d), 88.97, 90.89, 105.93-105.93 (d), 128.4, 129.5, 129.6, 133.2, 166.0, 169.7

¹³C-DEPT : δ_C (ppm) (CH/CH₃): 20.5, 55.6, 74.76-74.90 (d) 78.9-79.2 (d),
 (50MHz, CDCl₃) 88.9, 90.8 (d), 105.85-105.87 (d), 128.3, 129.6, 133.2. (CH₂):
 63.72-63.76 (d)

2'-O-Acetyl-5'-O-benzoyl-3'-deoxy-3'-fluoro-thymidine (7)



Compound **6** (0.6 g, 1.92 mmol) was added to solution thymine (0.29 g, 2.30 mmol) in dry acetonitrile (30 mL) under N₂ atmosphere. *N, O*-bis (trimethylsilyl acetamide) (0.94 mL, 3.84 mmol) was added to above reaction mixture at room temperature. The reaction mixture was refluxed for 1 h to give a clear solution and then cooled to room temperature. TMS-triflate (1.04 mL, 1.28 g, 5.75 mmol) was added to the reaction mixture and the resulting mixture was again refluxed for 3h. The reaction mixture was cooled to room temperature and concentrated to dryness under reduced pressure. Crude residue was dissolved in DCM (200 mL), washed successively with saturated aq. NaHCO₃ (3 X 100 mL) and H₂O (100 mL), dried over Na₂SO₄ and concentrated to dryness under reduced pressure and further purified by column chromatography using EtOAc/Pet ether (8:2) as solvent system. The pure compound **7** was collected as a white product. Yield: 0.60 g, 77%.

Mol. Formula : C₁₉H₁₉FN₂O₇

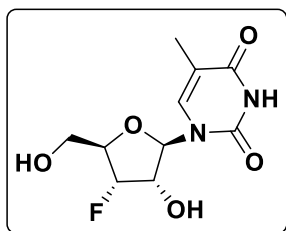
Exact Mass : 406.1176

HRMS : 429.1064 (M+Na⁺)

¹H NMR : δ_H (ppm) 1.57 (d, *J* = 1.14 Hz, 3H, CH₃), 2.18 (s, 3H), 4.49-4.77 (m, 3H), 5.26-5.53 (m, 2H), 6.25 (d, *J* = 7.33, 1H), 7.04 (d, *J* = 1.14 Hz, 1H), 7.46-7.67 (m, 3H, Ar-H), 8.04-8.09 (m, 2H, Ar-H), 9.30 (s, 1H).

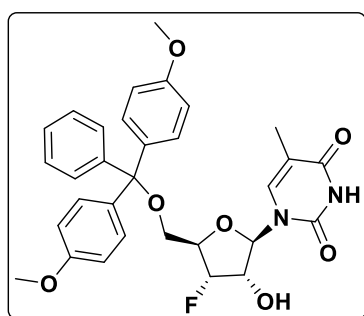
¹³C NMR : δ_C (ppm) 11.9, 20.4, 63.4-63.6 (d), 72.7-73.0 (d), 80.2-80.7 (d), (50MHz, CDCl₃) 85.9, 87.1, 90.9, 112.1, 128.8, 128.9, 129.5, 133.7, 134.8 150.5, 163.6, 165.8, 170.0

¹³C-DEPT : δ_C (ppm) (CH/CH₃): 11.9, 20.3, 72.6-72.9 (d), 80.1-80.6 (d), (50MHz, CDCl₃) 85.8, 87.0, 90.8, 128.7, 129.4, 133.7, 134.7 (CH₂): 63.4-63.5 (d)

3'-Deoxy-3'-fluoro-2'-hydroxy-thymidine (8)

Compound **7** (0.5g, 1.23 mmol) was dissolved in methanol (10 ml). The aqueous ammonia (5 mL) was added to a solution and stirred for 4 h at room temperature. TLC examination revealed the appearance of the product and disappearance of the starting material. The solvent was removed under reduced pressure to yield deprotected compound **8**. The crude product was further purified by column chromatography using DCM/MeOH (9:1) and the pure compound **8** was collected as a white solid and recrystallized using MeOH as a solvent. Yield: 0.28 g, 87%.

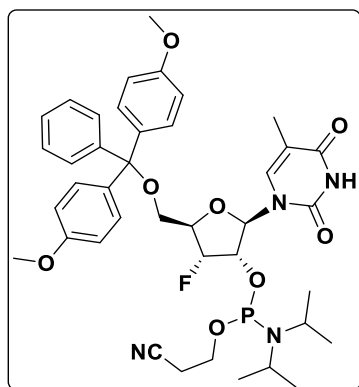
Mol. Formula	: C ₁₀ H ₁₃ FN ₂ O ₅
Exact Mass	: 260.0808
HRMS	: 283.0695 (M+Na ⁺)
¹H NMR (400MHz, D ₂ O)	: δ _H (ppm) 1.89 (s, 3H, CH ₃), 3.78-3.86 (m, 2H, H-5'a, H-5'b), 4.39-4.53 (m, 2H, H-2', H-4'), 5.02-5.17 (dd, <i>J</i> = 4.27 Hz, <i>J</i> _{3'F} = 53.71 Hz, 1H, H-3'), 6.04-6.06 (d, <i>J</i> _{1'2'} = 7.32 Hz, 1H, H-1'), 7.63 (s, 1H, H-6)
¹³C NMR (100MHz, CD ₃ OD)	: δ _C (ppm) 12.6, 62.5-62.6 (d), 74.5-74.7 (d), 84.9-85.2 (d), 88.4, 93.2-94.9 (d), 112.3, 138.1, 153.1, 166.4

5'-O-Dimethoxytrityl-3'-deoxy-3'-fluoro-2'-hydroxy-thymidine (9)

To a solution of compound **8** (0.514 g, 1.98 mmol) in pyridine (3.0 mL), 4, 4'-dimethoxy trityl chloride (0.803 g, 2.37 mmol) and cat. amount of DMAP (0.022 g, 0.18 mmol) was added. The reaction mixture was stirred at rt for 4h. The pyridine was removed under reduced pressure. The residue was dissolved in EtOAc (100 mL), washed with saturated NaHCO₃ (2 x 50 mL) followed by saturated aqueous NaCl (2 x 30 mL). The EtOAc layer was dried over Na₂SO₄, filtered and evaporated to dryness. The crude product was purified by silica gel (pre-neutralized with TEA) column chromatography using DCM/MeOH (9.7:0.3) afforded compound **9** as a white solid. Yield 0.67 g, 60%.

Mol. Formula	: C ₃₁ H ₃₁ FN ₂ O ₇
Exact Mass	: 562.2115
HRMS	: 585.2003 (M+Na ⁺)
¹H NMR	: δ _H (ppm) 1.47 (d, <i>J</i> = 0.98 Hz, 3H, CH ₃), 3.35-3.38 (dd, <i>J</i> = 1.96 Hz, 10.76 Hz, 1H, H-5'a), 3.53-3.56 (m, 1H, H-5'b), 3.80 (s, 6H), 4.43 (d, <i>J</i> = 28.12 Hz, 1H, H-4') 4.50-4.58 (m, 1H, H-2'), 5.00-5.15 (dd, <i>J</i> = 4.65 Hz, <i>J</i> _{3'F} = 54.78 Hz, 1H H-3'), 6.13 (d, <i>J</i> = 7.58 Hz, 1H, H-1'), 6.84 (d, <i>J</i> = 8.8 Hz, 4H, Ar-H), 7.23-7.37 (m, 9H), 7.55 (s, 1H, H-6), 8.35 (bs, 1H)
¹³C NMR	: δ _C (ppm) 11.7, 55.2, 62.9-63.0 (d), 74.7-74.8 (d), 82.1, 82.3, (100MHz, CDCl ₃) 87.3-87.5 (d), 91.8-93.6 (d), 111.9, 113.4, 127.4, 127.9, 128.1, 130.0, 134.8, 135.0, 143.9, 150.9, 158.8, 163.1
¹³C-DEPT	: δ _C (ppm) (CH/CH ₃): 11.7, 55.2, 74.7-74.8 (d), 82.1-82.3 (d), (100MHz, CDCl ₃) 87.3, 91.8-93.6 (d), 113.4, 127.3, 127.9, 128.1, 130.0, 135.1 CH ₂ : 62.9-63.0 (d)

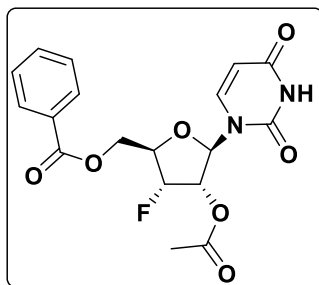
5'-*O*-Dimethoxytrityl-3'-deoxy-3'-fluoro-thymidinyl-2'-*O*-phosphoramidite (**10**)



Compound **9** (0.19 g, 0.34 mmol) was desiccated and co-evaporated with dry DCM and again dissolved in dry DCM (5 mL). Diisopropylethylamine (DIPEA) (0.23 mL, 1.34 mmol) was added to the ice-cooled solution under an argon atmosphere followed by 2-cyanoethyl-N, N-diisopropylchloro phosphine (0.09 mL, 0.403 mmol). After stirring the reaction mixture at room temperature for 3 h, TLC indicated complete consumption of the starting material. DCM was added to the reaction mixture, washed with saturated NaHCO₃ and H₂O, dried over Na₂SO₄, Solvent was evaporated under reduced pressure afforded a crude product **10** that was further purified by column chromatography on a silica gel (pre-neutralized with TEA) The pure compound **10** was eluted using 1:1 mixture of DCM/EtOAc and 1% TEA. Yield: 0.147 g, 57%.

Mol. Formula	: C ₄₀ H ₄₈ FN ₄ O ₈ P
Exact Mass	: 762.3194
HRMS	: 763.3271 (M+1)
³¹P NMR	: δ _H (ppm) 150.78, 152.02
(161MHz, CDCl ₃)	

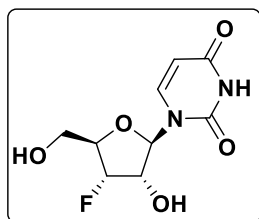
2'-O-Acetyl-5'-O-benzoyl-3'-deoxy-3'-fluorouridine (11)



Compound **6** (0.5 g, 1.60 mmol) was added to solution uracil (0.215 g, 1.92 mmol) in dry acetonitrile (30 mL) under N₂ atmosphere. *N, O*-bis (trimethylsilyl acetamide) (0.78 mL, 0.649 g, 3.19 mmol) was added to a reaction mixture at room temperature. The reaction mixture was refluxed for 1h to give a clear solution and then cooled to room temperature. TMS-

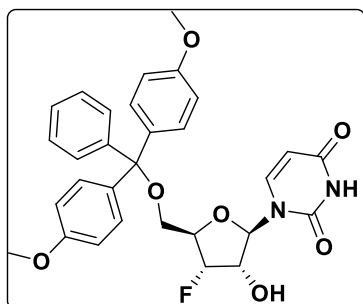
triflate (0.868 mL, 4.79 mmol) was added to the reaction mixture and the resulting mixture was again refluxed for 3h. The reaction mixture was cooled to room temperature and concentrated to dryness under reduced pressure. Crude residue was dissolved in DCM (200 mL), washed successively with saturated aq. NaHCO₃ (3 X 100 mL) and H₂O (100mL), dried over Na₂SO₄ and concentrated to dryness under reduced pressure and further purified by column chromatography using EtOAc/Pet ether (8:2) as solvent system. The pure compound **11** was collected as a white product. Yield: 0.47 g, 75 %.

Mol. Formula	: C ₁₈ H ₁₇ FN ₂ O ₇
Exact Mass	: 392.1020
HRMS	: 415.09 (M+Na ⁺)
¹H NMR	: δ _H (ppm) 2.18 (s, 3H, OAc), 4.54-4.71(m, 3H), 5.25-5.53 (m, (200MHz, 2H), 5.60 (d, <i>J</i> = 8 Hz, 1H, H-5), 6.15 (d, <i>J</i> = 6.9 Hz, 1H, H-1'), 7.25-7.29 (d, <i>J</i> = 8 Hz, 1H, H-6), 7.46-7.67 (m, 3H, Ar-H), 8.02-8.06 (m, 2H, Ar-H), 9.03 (bs, 1H,-NH)
¹³C NMR	: δ _C (ppm) 20.2, 63.2-63.3(d), 72.7-73.0 (d), 80.1-80.6 (d), 86.8, (50MHz, 90.6, 103.2, 128.6, 128.8, 129.4, 133.5, 139.6, 150.2, 163.3, CD ₃ OD) 165.8, 169.8 .
¹³C-DEPT	: δ _C (ppm)(CH/CH ₃): 20.2, 72.7-73.0(d), 80.1-80.5 (d), 86.8, 90.6, (50MHz, 103.2, 128.6, 129.35, 129.6, 133.5, 139.6. CH ₂ : 63.2-63.4 (d) CD ₃ OD)

3'-Deoxy-3'-fluoro-uridine (12)

To a solution of compound **11** (0.5g, 1.274 mmol) in methanol (10 ml). was added aqueous ammonia (5 mL), and the reaction mixture was stirred for 4h at room temperature. TLC examination revealed the appearance of the product and disappearance of the starting material. The solvent was removed under reduced pressure afforded deprotected compound **12**. The crude product was further purified by column chromatography using DCM/MeOH (9:1) and the pure compound was collected as a white solid. Yield: 0.284 g, 91%.

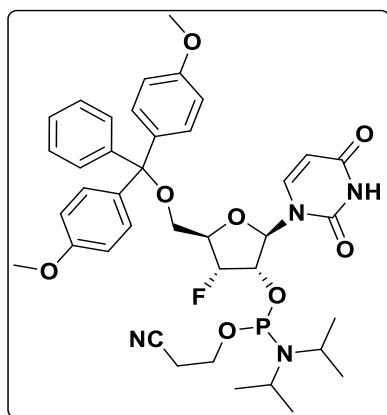
Mol. Formula	: C ₉ H ₁₁ FN ₂ O ₅
Exact Mass	: 246.0652
HRMS	: 269.0544 (M+Na ⁺)
¹H NMR (200MHz, CD ₃ OD)	: δ _H (ppm) 3.75-3.77 (m, 2H, H-5'a, H-5'b), 4.21-4.46 (m, 2H, H-2', H-4'), 4.84-5.15 (ddd, J _{3F} = 54.44 Hz, J = 4.5Hz, J = 0.7 Hz 1H, H-3'), 5.75 (d, J = 8 Hz, 1H, H-5), 6.06 (d, J _{1'2'} = 7.7 Hz, 1H, H-1'), 7.96 (d, J = 8 Hz, 1H, H-6)
¹³C NMR (50MHz, CD ₃ OD)	: δ _C (ppm) 62.4-62.6 (d), 74.6-74.9 (d), 84.9-85.4 (d), 88.6, 92.2-95.9 (d), 103.5, 142.5, 152.8, 166.1
¹³C-DEPT (50MHz, CD ₃ OD)	: δ _C (ppm)(CH/CH ₃): 74.6-74.9 (d), 84.9-85.4 (d), 88.6, 92.2-95.9 (d), 103.5, 142.5. CH ₂ : 62.4-62.6 (d)

5'-O-Dimethoxytrityl-3'-deoxy-3'-fluoro-uridine (13)

To a solution of compound **12** (0.250 g, 1.015 mmol) in pyridine (3.0 mL), 4, 4'-dimethoxy trityl chloride (0.41 g, 1.21 mmol) and cat. amount of DMAP (0.012 g, 0.098 mmol) was added. The reaction mixture was stirred at rt for 4h. The pyridine was removed under reduced pressure. The residue was dissolved in EtOAc (100 mL), washed with saturated NaHCO₃ (2 x 50mL) followed by saturated aqueous NaCl (2 x 30 mL). The EtOAc layer was dried over Na₂SO₄, filtered and evaporated to dryness. The crude product was purified by silica gel (pre-neutralized with TEA) column chromatography using DCM/MeOH (9.7:0.3) obtained compound **13** as a white solid. Yield: 0.351 g, 63%.

Mol. Formula	: C ₃₀ H ₂₉ FN ₂ O ₇
Exact Mass	: 548.1959
HRMS	: 571.1840 (M+Na ⁺)
¹H NMR (400MHz, CDCl ₃)	: δ _H (ppm) 3.42-3.50 (m, 2H), 3.79 (s, 6H), 4.37-4.53 (m, 2H), 4.95-5.23 (dd, <i>J</i> _{3',F} = 54.3 and <i>J</i> = 2.0 Hz, 1H), 5.44 (d, <i>J</i> = 8.0 Hz, 1H), 6.17 (d, <i>J</i> = 6.5 Hz, 1H), 6.86 (d, <i>J</i> = 8.8 Hz, 1H), 7.22-7.33 (m, 9H), 7.72 (d, <i>J</i> = 8.0 Hz, 1H), 9.89 (bs, 1H)
¹³C NMR (50MHz, CDCl ₃)	: δ _C (ppm) 55.2, 62.5-62.7 (d), 74.8-75.1 (d), 81.8-82.3 (d), 87.4, 90.0-93.7 (d), 103.1, 113.4, 127.3, 128.1, 128.1, 129.9, 130.0, 134.8, 134.9, 139.7, 143.9, 151.3, 158.7, 163.5
¹³C-DEPT (50MHz, CDCl ₃)	: δ _C (ppm) (CH/CH ₃): 55.2, 74.8-75.2 (d), 81.8-82.3 (d), 87.5, 90.1-93.7 (d), 103.1, 113.4, 127.3, 128.0, 128.1, 130.0, 139.8. (CH ₂): 62.6-62.8 (d)

5'-*O*-Dimethoxytrityl-3'-deoxy-3'-fluoro-uridiny-2'-*O*-phosphoramidite (**14**)



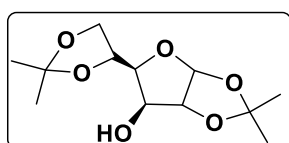
Compound **13** (0.15 g, 0.273 mmol) was desiccated and co-evaporated with dry DCM before reaction. Compound **13** was dissolved in dry DCM (5 mL). Diisopropylethylamine (DIPEA) (0.2 mL, 1.15 mmol) was added to the ice-cooled solution under an argon atmosphere followed by 2-cyanoethyl-N,N-diisopropylchlorophosphine (0.1 mL, 0.448 mmol). After stirring the reaction mixture at room temperature for 3h, TLC indicated complete consumption of the starting material DCM was added to the reaction mixture, washed with saturated NaHCO₃ and H₂O, dried over Na₂SO₄, Solvent was evaporated under reduced pressure afforded a the crude product **14** which was further purified by column chromatography on a silica gel (pre-neutralized with TEA) using 1:1 mixture of DCM/EtOAc containing 1% Et₃N as an eluent. Yield: 0.12g, 59 %.

Mol. Formula : C₃₉H₄₆FN₄O₈P

Exact mass : 748.3037

^{31}P NMR	: δ_{H} (ppm) 151.41, 152.51
(161MHz, CDCl_3)	
HRMS	: 749.3112 (M+H), 771.2930 (M+Na ⁺),

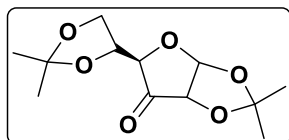
1, 2:5, 6-Di-*O*-isopropylidene- α -D-glucofuranose (**16**)



To a solution of D-glucose (10 g, 55.51 mmol) in dry acetone (130 mL), anhydrous CuSO_4 (18 g, 112.78 mmol) was added under N_2 atmosphere. Reaction mixture was cooled it to 0 °C in ice bath. After stirring for few minutes at ice-cold temperature, catalytic amount of conc. H_2SO_4 (0.6mL, 11.20 mmol) was added dropwise. Then reaction mixture was brought to room temperature and stirred for another 48 h. After which the reaction mixture was neutralized with saturated aqueous K_2CO_3 solution of and filtered using whatman filter paper. The filtrate was concentrated under reduced pressure and obtained solid compound was recrystallized using pet-ether afforded pure compound **16** as a white crystal. Yield: 10.5 g, 73%.

Mol. Formula	: $\text{C}_{12}\text{H}_{20}\text{O}_6$
Exact Mass	: 260.1260
HRMS	: 283.1150 (M+Na ⁺)
^1H NMR	: δ_{H} (ppm) 1.32 (s,3H), 1.37 (s,3H), 1.45 (s,3H), 1.50 (s,3H), (200MHz, CDCl_3) 3.96-4.21 (m, 3H), 4.30-4.39 (m, 2H), 4.54 (d, $J = 3.66$ Hz, 1H, H-2), 4.79 (bs, 1H), 5.95 (d, $J_{1,2} = 3.66$ Hz, 1H, H-1)
^{13}C NMR	: δ_{C} (ppm) 25.1, 26.1, 26.7, 26.8, 67.6, 73.4, 75.2, 81.0, 85.0, (50MHz, CDCl_3) 105.24, 109.7, 111.8
^{13}C-DEPT	: δ_{C} (ppm)(CH/CH ₃): 25.1, 26.1, 26.7, 26.8, 73.5, 75.2, 81.0, (50MHz, CDCl_3) 85.0, 105.2. (CH ₂): 67.6

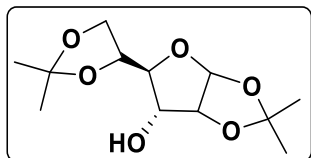
1, 2:5, 6-Di-*O*-isopropylidene- α -D-ribohexofuranose-3-ulose (**17**)



Pyridinium chlorochromate (15 g, 69.78 mmol) and powdered molecular sieve (30 g) were added to compound **16** (5 g, 19.35 mmol) in dry DCM (50 mL) and the mixture was stirred at rt for 6 h. The resulting suspension was diluted with diethyl ether (50mL), triturated and filtered through a silica gel bed (eluted with diethyl ether). The filtrate was concentrated

under reduced pressure obtained the crude compound **17** as white solid which was unstable and used as such for the next reaction. Yield 4.6 g, 93 %.

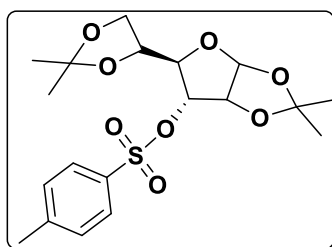
1, 2:5, 6-Di-*O*-isopropylidene- α -D-allofuranose (**18**)



Compound **17** (2.3 g, 8.905 mmol) was dissolved in mixture of MeOH (80 mL) and H₂O (20 mL) and cooled to 0 °C. To above solution NaBH₄ (0.948 g, 25.06 mmol) was added portionwise and solution stirred for another 2 h. The resulting solution was concentrated, and the crude material was dissolved in EtOAc (100 mL), and washed with H₂O (2 x 100 mL), dried over anhydrous Na₂SO₄ and solvent was evaporated under reduced pressure afforded compound **18** as white solid, which was used for the next reaction without any further purification. Yield: 1.94 g, 84 %.

Mol. Formula	:	C ₁₂ H ₂₀ O ₆
Exact Mass	:	260.1260
HRMS	:	283.1148 (M+Na ⁺)
¹H NMR (200MHz, CDCl ₃)	:	δ_{H} (ppm) 1.38 (s, 3H, CH ₃), 1.39 (s, 3H, CH ₃), 1.47 (s, 3H, CH ₃), 1.59 (s, 3H, CH ₃), 2.57 (d, $J = 8.34$ Hz, 1H, 3'-OH), 3.79-3.85 (dd, $J = 4.67, 8.46$, 1H), 3.98-4.13 (m, 3H), 4.28-4.37 (m, 1H), 4.60-4.65 (dd, $J = 4.0, 4.93$ Hz, 1H), 5.82 (d, $J = 3.79$ Hz, 1H, H-1)
¹³C NMR (50MHz, CDCl ₃)	:	δ_{C} (ppm) 25.2, 26.2, 26.4, 26.5, 65.7, 72.3, 75.4, 78.9, 79.5, 103.8, 109.7, 112.7
¹³C-DEPT (50MHz, CDCl ₃)	:	δ_{C} (ppm) (CH/CH ₃): 25.2, 26.2, 26.5, 26.5, 72.3, 75.4, 78.9, 79.5, 103.8. CH ₂ : 65.7

1, 2:5, 6-di-*O*-isopropylidene-3-*O*-*p*-toluenesulphonyl- α -D-allofuranose (**19**)

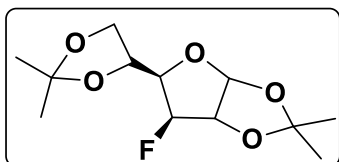


Compound **18** (1.9 g, 7.3 mmol) was dissolved in dry pyridine (8 mL) and cooled to 0 °C. *P*-toluene sulphonyl chloride (2.8 g, 14.68 mmol) was added in two portions and the reaction mixture was stirred for 4h. TLC indicated complete consumption of the starting material. The mixture was concentrated under reduced pressure and EtOAc (100 mL) was added into the residue obtained clear solution, washed with saturated Na₂HCO₃ (2 X 50 mL), H₂O (2 X

50 mL), and finally with saturated aqueous NaCl (1 X 20 mL). Then EtOAc layer dried over Na₂SO₄, filtered, and concentrated under reduced pressure. The crude product **19** was further purified by silica gel column chromatography using EtOAc/Pet ether (2:8) afforded a white solid of pure compound **19**. Yield: 2.06 g, 68 %.

Mol. Formula	: C ₁₉ H ₂₆ O ₈ S
Exact Mass	: 414.1348
HRMS	: 437.12 (M+Na ⁺), 453.097 (M+K ⁺)
¹H NMR	: δ _H (ppm)
(200MHz, CDCl ₃)	1.29 (s,3H), 1.30 (s,3H), 1.32 (s,3H), 1.53 (s,3H), 2.46 (s, 3H), 3.74-3.94 (m, 2H), 4.14-4.22 (m, 2H), 4.54-4.79 (m, 2H), 5.77 (d, J _{1,2} =3.15 Hz, 1H, H-1), 7.35 (d, 2H, J = 8Hz), 7.88 (d, 2H, J = 8 Hz)
¹³C NMR	: δ _C (ppm) 21.6, 25.0, 26.0, 26.5, 26.6, 65.1, 74.6, 76.5, 76.9,
(50MHz, CDCl ₃)	77.9, 103.7, 109.9, 113.6, 128.3, 129.6, 133.0, 145.2
¹³C-DEPT	: δ _C (ppm)(CH/CH ₃): 21.6, 25.0, 26.0, 26.6, 26.6, 74.5, 76.4,
(50MHz, CDCl ₃)	76.9, 77.9, 103.7, 128.3, 129.6. CH ₂ : 65.1

3-Deoxy-3-fluoro-1, 2:5, 6-di-*O*-isopropylidene- α -D-glucofuranose (**20**)

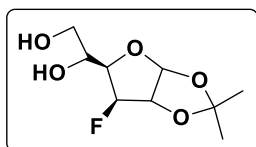


Compound **19** (2 g, 48.25 mmol), KF (3.5 g, 60.24 mmol), and acetamide (17.5 g, 296.26 mmol) were mixed heated to 210 °C (internal temperature), TLC examination revealed the appearance of the product and disappearance of the starting material (~15min). After 45 min, the dark reaction mixture was cooled to 70 °C and poured into a saturated solution of NaHCO₃ (50 mL). The mixture was filtered to separate insoluble tar. Both the tar and filtrate were extracted with diethyl ether (2 X 20 mL and 4 X 25 mL, respectively). The combined ether extract was washed with water (2 X 30 mL) dried with Na₂SO₄ and ether evaporation yielded under crude product as a yellow syrup which was further purified by column chromatography using EtOAc/Pet ether (2:8) as eluent. Pale-yellow syrup of pure compound **20** was obtained. Yield: 0.79g, 62%.

Mol. Formula	: C ₁₂ H ₁₉ FO ₅
Exact Mass	: 262.1217

HRMS	: 285.1107 (M+Na ⁺)
¹H NMR (400MHz, CDCl ₃)	: δ_{H} (ppm) 1.33 (s, 3H, CH ₃), 1.37 (s, 3H, CH ₃), 1.45(s, 3H, CH ₃), 1.51 (s, 3H, CH ₃), 4.02-4.16 (m, 3H), 4.27-4.32 (m, 1H), 4.68-4.72 (dd, $J = 3.75$ Hz, 10.76 Hz, 1H, H-2), 4.95-5.08 (dd, $J = 1.75$ Hz, $J_{3\text{F}} = 49.90$ Hz, 1H, H-3), 5.95 (d, $J = 3.75$ Hz, 1H, H-1)
¹³C NMR (50MHz, CDCl ₃)	: δ_{C} (ppm) 25.1, 26.1, 26.6, 26.8, 67.1, 71.8-71.9 (d), 80.4-80.8 (d), 82.1-82.8 (d), 91.9-95.6 (d), 105.1, 109.4, 112.3
¹³C-DEPT (50MHz, CDCl ₃)	: δ_{C} (ppm) (CH/CH ₃): 25.1, 26.1, 26.7, 26.8, 71.8-71.9 (d), 80.4-80.8 (d), 82.2-82.8 (d), 91.9-95.6 (d), 105.1. (CH ₂): 67.1
¹⁹F NMR (376MHz, CDCl ₃)	δ_{F} (ppm) -207.58

3-Deoxy-3-fluoro-1, 2-O-isopropylidene- α -D-glucofuranose (**21**)

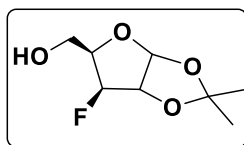


Compound **20** (0.5 g, 1.91 mmol) was added into a mixture of AcOH:H₂O (6:4) 10 mL. Reaction mixture was heated at 50 °C for 1 h. TLC indicated complete consumption of the starting material then reaction mixture was concentrated under reduced pressure and co-evaporated with toluene to remove traces of AcOH. Crude compound **21** as yellow syrup was obtained which was further purified by column chromatography using EtOAc /Pet ether (7:4) as eluent gave pure compound **21**. Yield 0.40 g, 95%.

Mol. Formula	: C ₉ H ₁₅ FO ₅
Exact Mass	: 222.0904
HRMS	: 245.0791 (M+Na ⁺)
¹H NMR (200MHz, CDCl ₃)	: δ_{C} (ppm) 1.33 (s, 3H, CH ₃), 1.50 (s, 3H, CH ₃), 3.70-3.99 (m, 3H), 4.06-4.26 (ddd, $J = 2.15$ Hz, 8.72 Hz, 28.93 Hz, 1H), 4.67-4.74 (dd, $J = 3.79$ Hz, 10.74 Hz, 1H), 4.97-5.23 (dd, $J = 2.02$ Hz, $J_{3\text{F}} = 49.77$ Hz, 1H, H-3), 5.97 (d, $J = 3.79$ Hz, 1H, H-1)
¹³C NMR (50MHz, CDCl ₃)	: δ_{C} (ppm) 26.1, 26.5, 64.0, 68.1-68.3 (d), 79.3-79.7(d), 81.9-82.6 (d), 92.1-95.8 (d), 105.0, 112.3

¹³C-DEPT : $\delta_c(\text{ppm})(\text{CH}/\text{CH}_3)$: 26.1, 26.5, 68.1-68.3 (d), 79.3-79.7 (d),
(50MHz, CDCl₃) 82.0-82.6 (d), 92.1-95.8 (d), 105.0. (CH₂): 64.0.

3-Deoxy-3-fluoro-1, 2-O-isopropylidene- α -D-xylofuranose (**22**)



The diol **7** (2.5g, 11.25 mmol) was added to a stirred solution of NaIO₄ (2.5 g, 11.25 mmol) in H₂O (37 mL) and MeOH (37 mL). Immediate precipitation of NaIO₃ was observed. After 1 h stirring at room temperature, any residual periodate was quenched with a drop of ethylene glycol. NaBH₄ (1 g, 26.43 mmol) was added to the reaction mixture and stirred for 1 h at room temperature. After completion of reaction (confirmed by TLC), reaction mixture was concentrated and then extracted with EtOAc (2 X 200mL). The organic layer was washed with brine solution, dried over Na₂SO₄, evaporated to dryness. Crude compound **22** was further purified by column chromatography with EtOAc/Pet-ether (4:6) gave pure compound as yellow syrup. Yield 1.87 g, 86%.

Mol. Formula : C₈H₁₃FO₄

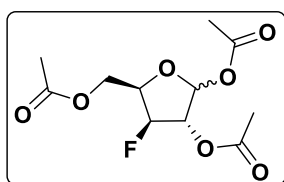
Exact Mass : 192.0798

¹H NMR : $\delta_H(\text{ppm})$ 1.33 (s, 3H, CH₃), 1.50 (s, 3H, CH₃), 2.07 (bs, 1H),
(200MHz, CDCl₃) 3.82-3.98 (m, 2H, H-5a, H-5b), 4.24-4.46 (m, 1H, H-4),
4.67-4.74 (dd, $J = 3.8$ Hz, 11.12 Hz, 1H, H-2), 4.85-5.12 (dd,
 $J = 2.02$ Hz, $J_{3,F} = 50.40$ Hz, 1H, H-3), 6.01 (d, $J = 3.8$ Hz,
1H, H-1)

¹³C NMR : $\delta_c(\text{ppm})$ 26.2, 26.6, 59.5-59.7 (d), 80.1-80.5 (d), 82.3-83.0
(50MHz, CDCl₃) (d), 92.2-95.8 (d), 104.8, 112.3

¹³C-DEPT : $\delta_c(\text{ppm})$ (CH/CH₃): 26.2, 26.6, 80.1-80.5 (d), 82.4-83.0 (d),
(50MHz, CDCl₃) 92.2-95.9 (d), 104.8. CH₂: 59.5-59.7 (d).

3-Deoxy-3-fluoro-1, 2, 5-tri-O-acetyl-D-xylofuranose (**23**)

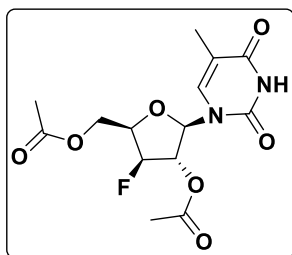


The 1, 2 acetonide of compound **22** (2 g, 10.41 mmol) was deprotected in situ and then acetylated with 50 mL mixture of Ac₂O:AcOH:H₂SO₄ (50:50:2, v/v). Reaction was monitored by TLC. After 3 h, anhydrous diethylether was added, followed by sodium acetate (10 g, 12.19 mmol). The mixture was filtered and the residue was washed with diethyl ether (2 X 50 mL). The combined solutions were co-evaporated with

toluene and the residue was further purified by column chromatography on silica gel compound **23** was eluted in using EtOAc/Pet-ether (2:8) obtained as thick yellow syrup. Yield: 1.7 g, 59%.

Mol. Formula	: C ₁₁ H ₁₅ FO ₇
Exact Mass	: 278.0802
HRMS	: 301.0696 (M+Na ⁺)
¹H NMR (α+β)	: δ _H (ppm) 2.07-2.12 (m, 9H, OAc) 4.18-4.67 (m, 3H, H-4, H-5a, H-5b), 4.93-5.20 (dd, <i>J</i> = 4.04 Hz, <i>J</i> _{3,F} = 50.3 Hz, 1H, H-3), 5.10-5.45 (m, 1H, H-2), 6.16 & 6.47-6.50 (α: d <i>J</i> = 4.3 Hz, 0.4H, H-1 β: s, 0.6H, H-1)
¹³C NMR (α+β)	: δ _C (ppm) 20.0, 20.2, 20.5, 20.7, 60.8, 61.1, 61.6, 61.9, 76.0, (50MHz, CDCl ₃) 76.2, 76.6, 78.4, 79.0, 80.2, 80.6, 90.2, 91.5, 93.0, 93.1, 94.0, 95.3, 98.4, 168.8, 169.1, 170.3
¹³C-DEPT (α+β)	: δ _C (ppm)(CH/CH ₃): 20.2, 20.5, 20.7, 20.9, 76.2, 76.4, 76.8, (50MHz, CDCl ₃) 78.6, 79.2, 80.4, 80.8, 90.4, 91.7, 93.3, 94.2, 95.5, 98.6. CH ₂ : 61.0, 61.2, 61.7, 62.0

2', 5'-Di-*O*-acetyl-3'-deoxy-3'-fluoro-xylothyridine (**24**)

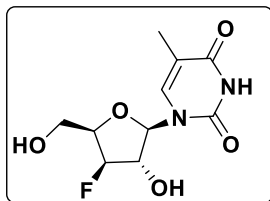


Compound **24** (0.45 g) was synthesized by using same Vorbrüggen glycosylation reaction using silylated thymine (0.273g, 2.16 mmol) from compound **23** (0.5 g, 1.80 mmol) accordingly as mentioned earlier for compound **7**. The pure compound **24** was collected as white foam. Yield: 0.48 g, 78 %.

Mol. Formula	: C ₁₄ H ₁₇ FN ₂ O ₇
Exact Mass	: 344.1020
HRMS	: 367.0903 (M+Na ⁺)
¹H NMR	: δ _H (ppm) 1.93 (d, <i>J</i> = 1.01 Hz, 3H, CH ₃), 2.11 (s, 3H, OAc), 2.14 (200MHz, CDCl ₃) (s, 3H, OAc), 4.23-4.51 (m, 3H), 4.93-5.29 (m, 2H), 6.12 (d, <i>J</i> = 2.4 Hz, 1H, H-1'), 7.15 (s, 1H, H-6), 9.58 (brs, 1H, NH)
¹³C NMR	: δ _C (ppm) 12.5, 20.4, 20.6, 60.3-60.5 (d), 78.6-78.9 (d), 79.0-79.5 (50MHz, CDCl ₃) (d), 87.9, 91.3-94.9 (d), 112.1, 134.4, 150.3, 163.7, 169.0, 170.4
¹³C-DEPT	: δ _C (ppm)(CH/CH ₃): 12.5, 20.4, 20.6, 78.6-78.9 (d), 79.0-79.5 (d),

(50MHz, CDCl₃) 87.9, 91.3-95.0 (d), 134.5, 134.6. CH₂: 60.4-60.6 (d).

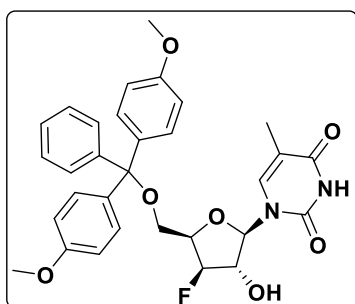
3'-Deoxy-3'-fluoro-2'-hydroxy-xylothyridine (25)



Compound **24** (0.5 g, 1.45 mmol) was dissolved in methanol (50 ml). The aqueous ammonia (5 mL) was added to a solution and stirred for 4 h at room temperature. TLC examination revealed the appearance of the product and disappearance of the starting material. The solvent was removed under reduced pressure afforded de-protected compound **25**. The crude product was further purified by column chromatography using DCM/MeOH (9:1) and the pure compound was collected as a white solid. Yield: 0.34 g, 90%.

Mol. Formula	: C ₁₀ H ₁₃ FN ₂ O ₅
Exact Mass	: 260.0808
HRMS	: 283.0694 (M+Na ⁺)
¹H NMR (400MHz, CD ₃ OD)	: δ _H (ppm) 1.83 (s, 1H, CH ₃), 3.93-4.02 (m, 2H, H-5'a, H-5'b), 4.36-4.46 (m, 1H), 4.50 (d, <i>J</i> = 15.26 Hz, 1H), 5.07 (d, <i>J</i> _{3'F} = 50.66 Hz, 1H, H-3'), 5.85 (d, <i>J</i> _{1'2'} = 1.2 Hz, 1H, H-1'), 7.49 (s, 1H, H-6)
¹³C NMR (50MHz, CD ₃ OD)	: δ _C (ppm) 12.7, 59.7-59.9 (d), 79.6-80.2 (d), 83.7-84.1 (d), 92.6, 94.9-98.5 (d), 111.4, 137.5, 137.6, 152.5, 166.5
¹³C-DEPT (50MHz, CD ₃ OD)	: δ _C (ppm) (CH/CH ₃): 12.7, 79.6-80.2 (d), 83.7-84.1 (d), 92.6, 94.9-98.5 (d), 137.5, 137.6. CH ₂ : 59.7-59.9

5'-O-Dimethoxytrityl-3'-deoxy-3'-fluoro-2'-hydroxy-xylothyridine (26)

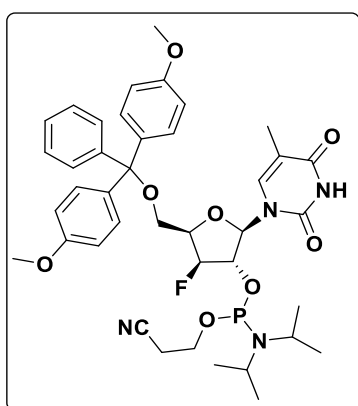


Compound **25** (0.35 g, 1.345 mmol) was dissolved in pyridine (3.0 mL), to this 4, 4'-dimethoxy trityl chloride (0.547 g, 1.61 mmol) and catalytic amount of DMAP (0.015 g, 0.123 mmol) was added. The reaction mixture was stirred at rt for 2h. Progress of reaction is followed by TLC, after completion of reaction, pyridine was removed under reduced pressure and residue was dissolved in EtOAc (100 mL), washed with saturated NaHCO₃ (2 x 50 mL) followed by saturated aqueous NaCl (2 x 30 mL). The

EtOAc layer was dried over Na_2CO_3 , filtered and evaporated to dryness. The crude product was purified by silica gel (pre-neutralized with TEA) column chromatography using DCM/MeOH (9.7:0.3) afforded compound **26** as a white solid. Yield: 0.46 g, 61%.

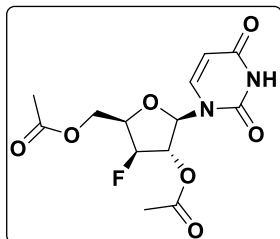
Mol. Formula	: $\text{C}_{31}\text{H}_{31}\text{FN}_2\text{O}_7$
Exact Mass	: 562.2115
HRMS	: 585.2005 ($\text{M}+\text{Na}^+$)
^1H NMR	: δ_{H} (ppm) 1.75 (s, 3H, CH_3), 2.97 (s, 1H), 3.44-3.59 (m, 2H, H-5'a, H-5'b), 3.76 (s, 6H, OCH_3), 4.47 (d, $J = 12.55$ Hz, 1H), 4.68 (d, $J = 32.88$ Hz, 1H), 4.94-5.06 (d, $J_{3\text{F}} = 51.45$ Hz, 1H, H-3') 5.90 (s, 1H), 6.83 (d, $J = 8.5$ Hz, 4H, Ar-H), 7.21-7.51 (m, 10 H, Ar-H, H-6)

5'-O-Dimethoxytrityl-3'-deoxy-3'-fluoro-xylofuranosyl-2'-O-phosphoramidite (**27**)



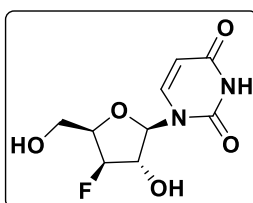
Compound **26** (0.3g, 0.533 mmol) was desiccated and co-evaporated with dry DCM and again dissolved in dry DCM (5 mL). Diisopropylethylamine (DIPEA) (0.038 mL, 2.153 mmol) was added to the ice-cooled solution under an argon atmosphere followed by 2-cyanoethyl- N, N-diisopropyl chlorophosphine (0.144 mL, 0.65 mmol) . After stirring the reaction mixture at room temperature for 3 h, TLC indicated complete consumption of the starting material DCM was added to the reaction mixture, washed with saturated NaHCO_3 and H_2O , dried over Na_2SO_4 , Solvent was evaporated under reduced pressure afforded a the crude product **27** which was further purified by column chromatography on a silica gel (pre-neutralized with TEA) using 1:1 mixture of DCM/EtOAc containing 1% Et_3N as a eluent. Yield: 0.205g, 50 %.

Mol. Formula	: $\text{C}_{40}\text{H}_{48}\text{FN}_4\text{O}_8\text{P}$
Exact Mass	: 762.3194
HRMS	: 763.3273 ($\text{M}+\text{H}$)
^{31}P NMR	: δ_{P} (ppm) 151.37, 153.39 (161MHz, CDCl_3)

2', 5'-di-O-acetyl-3'-deoxy-3'-fluoro-xylofuranosyluracil (28)

Compound **28** was synthesized by using same Vorbrüggen glycosylation reaction using silylated uracil 0.082 g, 0.73 mmol) from compound **23** (0.17 g, 0.61 mmol) accordingly as mentioned earlier for compound **11**. The pure compound **28** was obtained as white foam. Yield: 0.074 g, 76 %

Mol. Formula	: C ₁₃ H ₁₅ FN ₂ O ₇
Mol. Weight	: 330.27
ESI-MS	: 353.2080 (M+Na ⁺)
¹H NMR	: δ _H (ppm) 2.13 (s, 3H, OAc), 2.16 (s, 3H, OAc), 4.28-4.52 (m, (200MHz, CDCl ₃) 3H), 4.94-5.19 (dd, <i>J</i> = 2.15 Hz, <i>J</i> _{3F} = 51.16 Hz, 1H, H-3), 5.22-5.31(dd, <i>J</i> = 1.89 Hz, <i>J</i> _{3F} = 16.04 Hz, 1H, H-3), 5.82 (d, <i>J</i> = 8.21 Hz, 1H, H-5), 6.10 (d, <i>J</i> = 2.02 Hz, 1H, H-1'), 7.40 (d, <i>J</i> = 8.21 Hz, 1H, H-6), 9.47 (brs, 1H, NH)

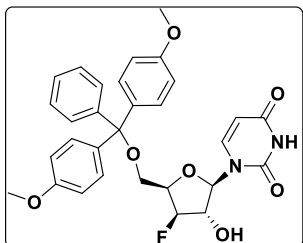
3'-Deoxy-3'-fluoro-xylofuranosyluracil (29)

Compound **28** (0.5g, 1.514 mmol) was dissolved in methanol (10 ml). The aqueous ammonia (5mL) was added to a solution and stirred for 4 h at room temperature. TLC examination revealed the appearance of the product and disappearance of the starting material. The solvent was removed under reduced pressure afforded diol compound **29**. The crude product was further purified on silica gel column chromatography using DCM/MeOH (9:1) which gave pure compound as a white solid. Yield: 0.34 g, 90%.

Mol. Formula	: C ₉ H ₁₁ FN ₂ O ₅
Exact Mass	: 246.0652
HRMS	: 269.0540 (M+Na ⁺)
¹H NMR	: δ _H (ppm) 3.85-4.01 (m, 2H, H-5'a, H-5'b), 4.26-4.49 (m, 2H, (200MHz, CD ₃ OD) 2H, H-2', H-4'), 4.83-5.10 (ddd, <i>J</i> _{3F} = 51.3 Hz, <i>J</i> = 1.01 Hz, <i>J</i> = 2.5 Hz, 1H, H-3'), 5.70 (d, <i>J</i> = 8Hz, 1H, H-5), 5.84 (d, <i>J</i> = 1.01 Hz, 1H, H-1'), 7.65 (d, <i>J</i> = 8 Hz, 1H, H-6)
¹³C NMR	: δ _C (ppm) 59.6-59.8 (d), 79.6-80.2 (d), 84.2-84.6 (d), 93.19- (50MHz, CD ₃ OD) 94.7 (d), 98.4, 102.4, 141.9-142.0 (d), 152.3, 166.4

¹³C-DEPT : δ_c (ppm) (CH/CH₃):79.6-80.2 (d), 84.2-84.6 (d), 93.1-94.7 (50MHz, CD₃OD) (d), 98.4, 102.4, 141.9-142.0 (d) . (CH₂): 59.6-59.8 (d)

5'-O-Dimethoxytrityl-3'-deoxy-3'-fluoro-xylofuranosyluracil (30)



To a stirred mixture of compound **29** (0.5 g, 2.03 mmol) and pyridine (3.0 mL), 4, 4'-dimethoxy trityl chloride (0.69 g, 2.03 mmol) and catalytic amount of DMAP (0.03 g, 0.24 mmol) was added. The reaction mixture was stirred at rt for 4 h. Reaction progress followed by TLC, after disappearance of starting material pyridine was removed under reduced pressure remaining residue was dissolved in EtOAc (100 mL), washed with saturated NaHCO₃ (2 x 50 mL) followed by saturated aqueous NaCl (2 x 30 mL). Organic layer was dried over Na₂SO₄, filtered and evaporated to dryness. The crude product was purified by silica gel (pre-neutralized with TEA) column chromatography using DCM/MeOH (9.7:0.3) compound **30** as a white solid. Yield 0.67 g, 60%.

Mol. Formula : C₃₀H₂₉FN₂O₇

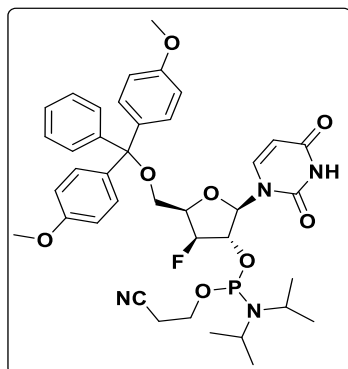
Mol. Weight : 548.1959

HRMS : 571.1855 (M+Na⁺)

¹H NMR : δ_H (ppm) 3.44-3.58 (m, 2H, H-5'a, H-5'b), 3.76 (s, 6H, (400MHz, CDCl₃) OCH₃), 4.42 (d, *J* = 13.14 Hz, 1H) 4.57-4.65 (m, 1H), 4.90-5.03 (dd, *J*_{3',F} = 51.41 Hz, *J* = 1.63 Hz, 1H, H-3), 5.58 (d, 1H, H5, *J* = 8.2 Hz), 5.83 (s, 1H, H-1'), 6.82 (d, *J* = 8.8, 4H, Ar-H), 7.18-7.47 (m, 10H, Ar-H, H-6)

¹³C NMR : δ_c (ppm) 55.2, 60.3-60.5 (d), 78.6-79.0 (d), 82.4-82.6 (d), (100MHz, CDCl₃) 86.5, 92.8, 94.0-95.7 (d), 101.7, 113.1, 126.9, 127.8, 128.1, 130.0, 130.1, 135.4-135.5, 139.8, 142.8, 144.4, 147.3, 148.22, 150.9, 158.5, 164.0.

¹³C-DEPT : δ_c (ppm) (CH/CH₃): 55.2, 78.6-79.0 (d), 82.4-82.5 (d), 92.7, (100MHz, CDCl₃) 94.0-95.7 (d), 101.7, 113.1, 126.9, 127.8, 128.1, 130.0, 130.1, 139.8, 142.8, 144.4, 147.3, 148.22, 158.5, (CH₂): 60.4-60.5 (d)

5'-O-Dimethoxytrityl-3'-deoxy-3'-fluoro-xylofuranosyl-2'-O-phosphoramidite (31)

Compound **30** (0.2g, 0.365 mmol) was desiccated and co-evaporated with dry DCM and dissolved in dry DCM (5 mL) followed by addition of Diisopropylethylamine (DIPEA) (0.19 mL, 1.09 mmol) under argon atmosphere. Reaction mixture was cooled to 0 °C, 2-cyanoethyl-N,N-diisopropyl chlorophosphine (0.16 mL, 0.72 mmol) was added above reaction mixture at 0°C. The reaction mixture

was stirred at room temperature for another 3 h; Completion of reaction was confirmed by TLC. After 3 h, 10 mL DCM was added to reaction mixture which was washed with saturated NaHCO₃ and H₂O, dried over Na₂SO₄, Solvent was evaporated under reduced pressure obtained crude product **31** which was further purified on a silica gel (pre-neutralized with TEA) column chromatography using 1:1 mixture of DCM/EtOAc containing 1% TEA afforded phosphoramidite derivative **31**. Yield 0.14g, 51 %.

Mol. Formula	: C ₃₉ H ₄₆ FN ₄ O ₈ P
Exact Mass	: 748.3037
HRMS(ESI)	: 749.3115 (M+H), 771.2932 (M+Na ⁺),
³¹P NMR	: δ _P (ppm) 151.46, 153.51
	(161MHz, CDCl ₃)

2.7.2 Oligonucleotide synthesis

Oligonucleotides both 3'-5' and 2'-5' were synthesized in-house on a Bioautomation Mermade-4 DNA synthesizer employing β -cyanoethyl phosphoramidite chemistry. The protected deoxyguanosine and thymidine phosphoramidites (used for 3'5' linkage) and 3'-dG-CE Phosphoramidite, 3'-dT-CE Phosphoramidites (used for 2'5' linkage) were obtained from ChemGenes corporation and 3' deoxy-2'-phosphoramidites were obtained from Glen Research and Innovasynth technologies. Universal columns procured from Bioautomation were used for 2'-5' oligomer synthesis. Oligonucleotides were cleaved from the column by using aq. ammonia at 60°C for 6 h and then concentrated. Oligonucleotides after post-synthetic treatment were desalted by passing through Pharmacia NAP-5 columns.

2.7.3 Purification and characterization

2.7.3.1 High-performance liquid chromatography

The purity of synthesized oligonucleotides was ascertained using RP-HPLC on a C18 column using a Waters system (Waters Delta 600e quaternary solvent delivery system and 2998 photodiode array detector and Empower 2 chromatography software). An increasing gradient of acetonitrile in 0.1M triethylammonium acetate (pH 7.0) was used and the eluent was monitored at 260 nm. [A = 5% ACN in TEAA (0.1M, pH 7); B = 30% ACN in TEAA (0.1M, pH 7.0)].

2.7.3.2 Polyacrylamide gel electrophoresis study

Polyacrylamide denaturing gel electrophoresis was used to examine the purity of synthesized oligomer using 20 % gel containing 7 M urea. For a pre-run or blank run, the gel plate assembly was placed in the gel run chamber and completely immersed in the 1X TBE buffer. Each well was loaded with 1 μ l of the bromophenol blue dye in 40% sucrose solution (1:1). Then 200V voltage was applied and the gel run was carried out for 1 hour until the marker dye had travelled down and washed out along with any unpolymerised gel.

Sample run and Gel visualization

Strand concentration of TBA, *iso*TBA oligomers were 320 μ M, 2 μ l solution was mixed with an equal volume of the formamide and loaded into the appropriately numbered wells. The marker dye was loaded in the first well to monitor the run. The gel

was run in TBE buffer at 25 °C with the voltage set at 150V for 30-40 minutes till the marker was visible at 3/4th the gel height. The gels after the run were washed with DI water and then were visualized by UV-shadowing.

2.7.3.4 MALDI-TOF characterisation

Synthesized oligonucleotides were characterized by MALDI-TOF Analysis. Mass spectra were recorded on SCIEX TOF/TOF 5800 system. A nitrogen laser (337nm) was used for desorption and ionization. The matrix used for analysis was THAP (2', 4', 6'-trihydroxyacetophenone), and diammonium citrate used as an additive. The sample was prepared by mixing 1µL oligomer (10-50 µM in DI H₂O) with 10 µL of THAP (0.55 M in EtOH) mixed well followed by 5µL diammonium citrate (0.1M in DI H₂O) again mixed well and then 1µL of the mixture was spotted on the metal plate. The metal plate was loaded to the instrument and the analyte ion were then accelerated by an applied high voltage in linear mode and detected as an electrical signal.

2.8 Biophysical technique-CD spectroscopy

CD spectra were recorded on Jasco J-815 CD Spectrometer equipped with a Jasco PTC-424S/15 Peltier system. 2 mm path-length quartz cuvettes were used for a sample volume 500 µL and strand concentration of 5 µM in 10mMol K (pH 7.2) containing 100 mM KCl. Oligomers prepared in buffer were annealed by heating at 90 °C for 5 minutes then slowly cooling to room temperature followed by refrigeration for 5 to 6 hours before use. Spectral scans were collected at 4 °C over a wavelength range 200- 320 nm at a scanning rate of 100 nm min⁻¹. CD melting was performed for the entire sample by monitoring the CD intensity at 295 nm against temperature over the range 5-90 °C. CD spectroscopy was also used to study the thrombin binding efficiency of the TBA/*iso*TBA oligomers. 10 uL of 0.5 NIH of Bovine thrombin (Tulip Diagnostics) was added to the oligomers at 5 min interval and their CD signal intensity at 295 nm was recorded with increasing thrombin concentration. Three scans were averaged for each sample.

2.9 Thrombin time measurements for clotting inhibition (antithrombin effect)

The inhibitory activity of the aptamers on thrombin-catalysed conversion of fibrinogen to fibrin (clotting) by TBA, *iso*TBA and modified *iso*TBA variants was

measured by a thrombin time assay. The time (in seconds) for clotting at 37 °C was measured on a a STart Max Coagulation analyzer (Diagnostica Stago). Each experiment was repeated at least thrice; the standard deviation was ± 1 °C. Each commercial reagent was re-constituted according to the manufacturer's protocols. Bovine thrombin (Tulip Diagnostics, 0.1 NIH unit) was pre-incubated with oligomers at 0.25 μM concentration for 2 min before addition to fibrinogen from human plasma (2.65 μM , Aldrich F-3897) and measurement of clotting time (thrombin time) was done according to the manufacturer's protocol.

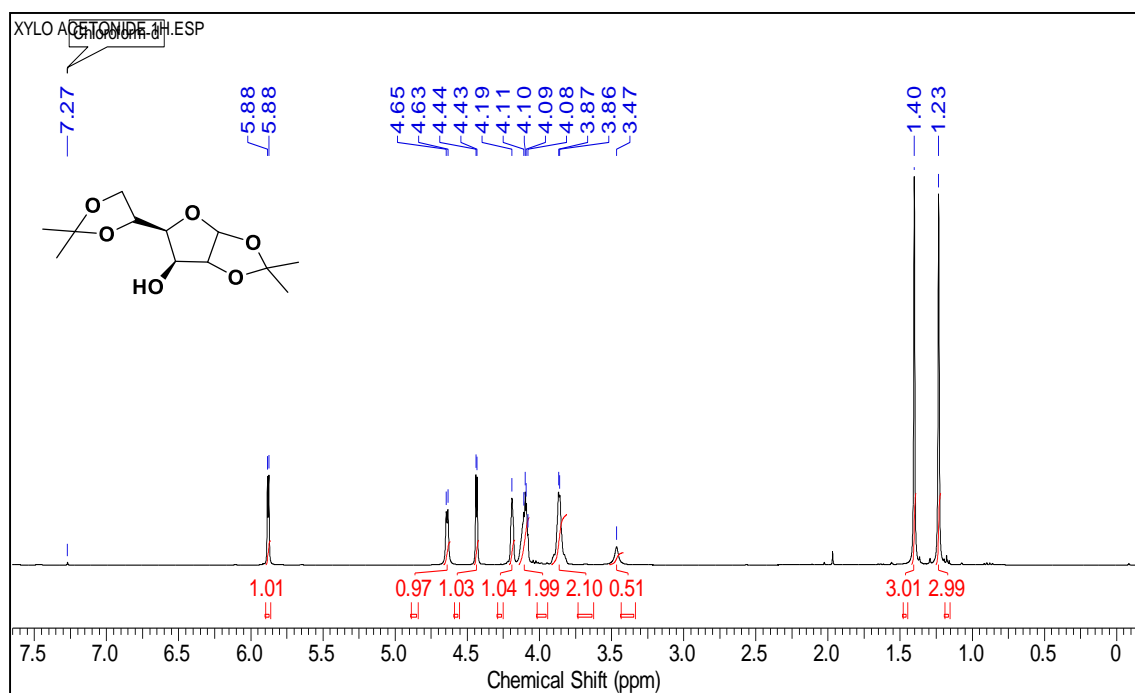
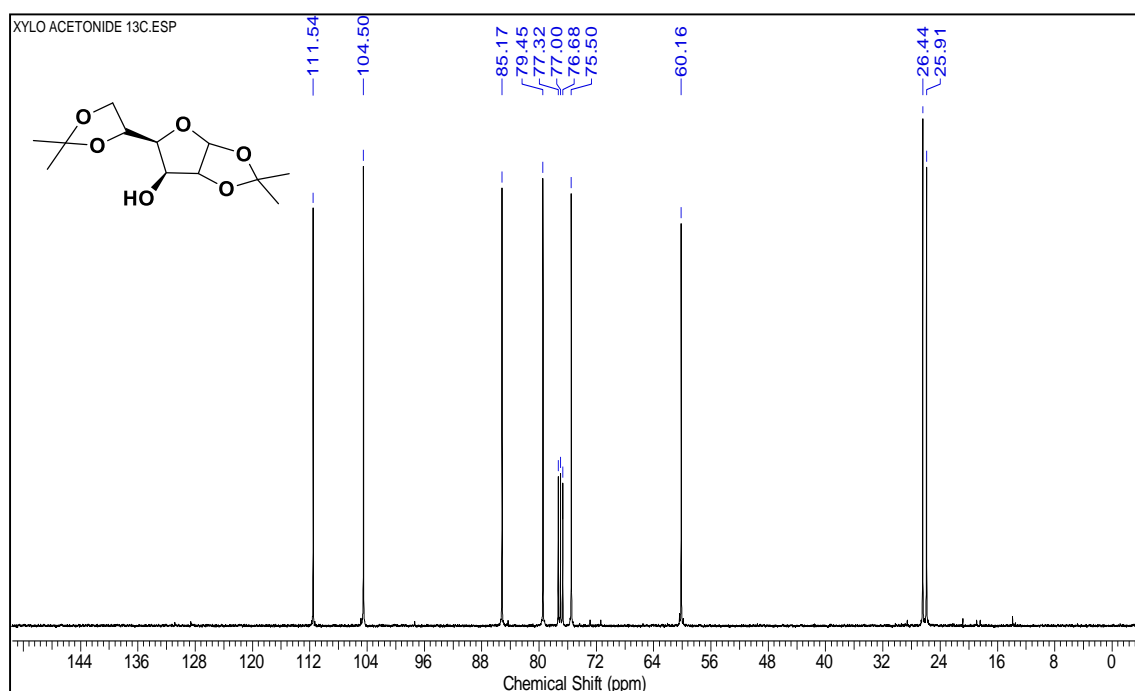
2.10 Exonuclease stability study

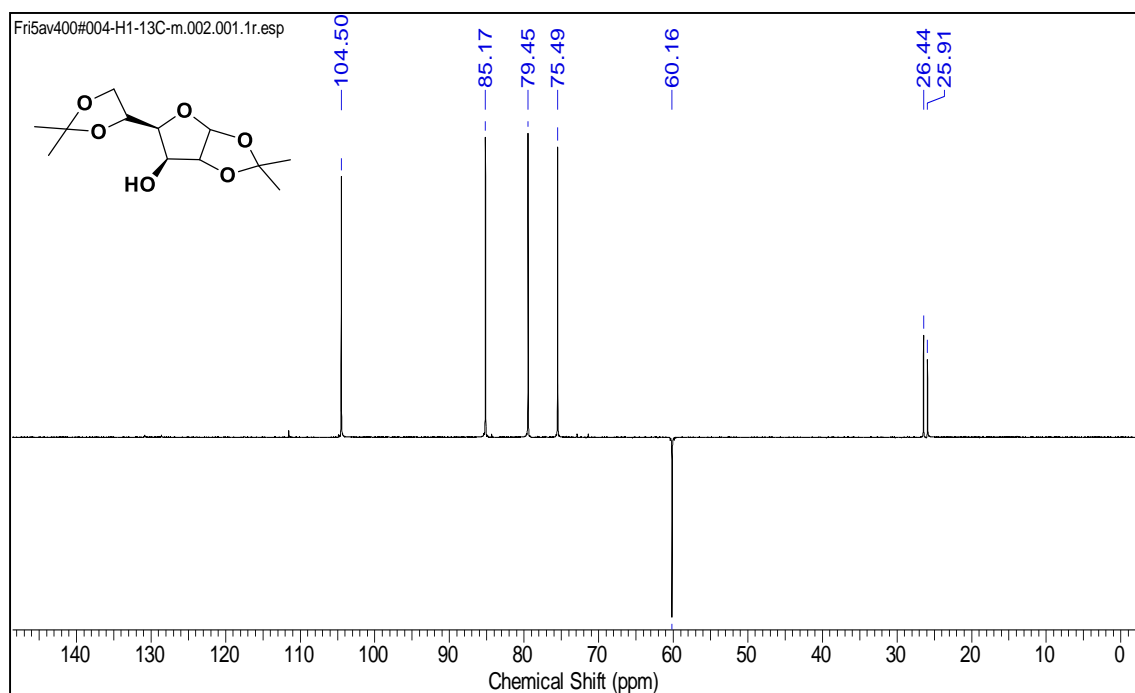
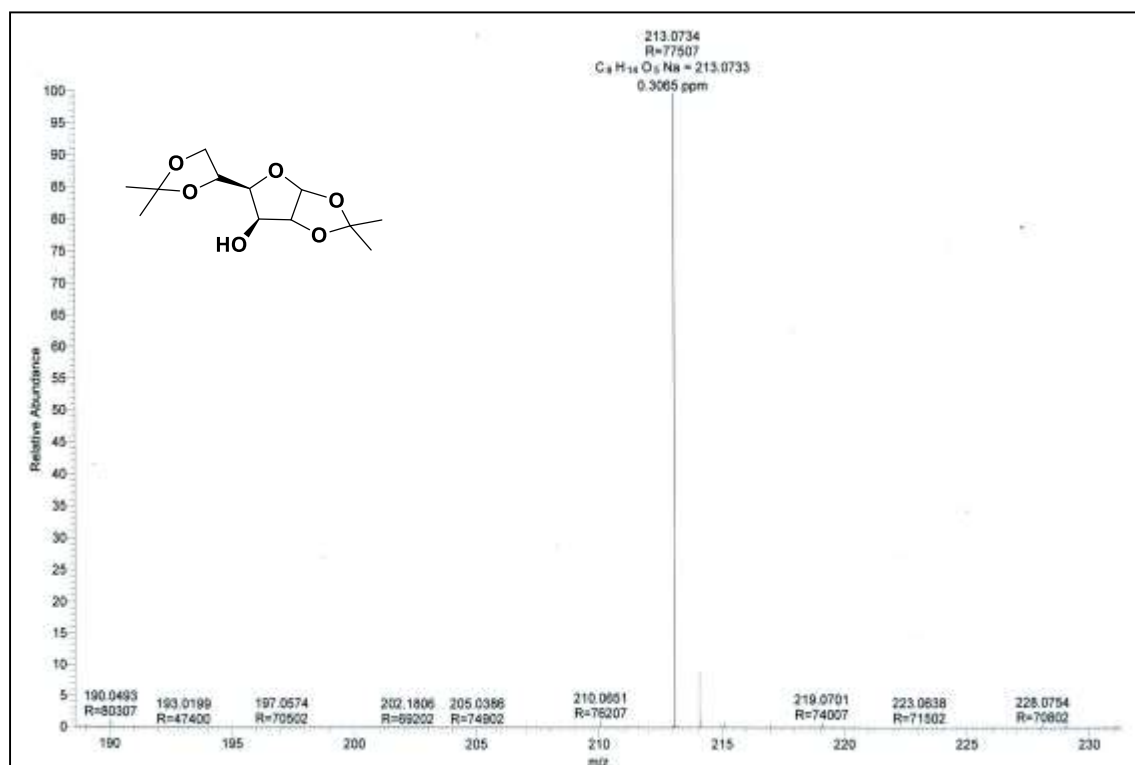
Stability of the oligonucleotides towards exo-nucleases SVPD (snake venom phosphodiesterase) was analyzed by RP-HPLC. 7.5 μM of oligonucleotide in 300 μL of Tris-HCl buffer (pH = 7.5, 10mM Tris-HCl, 8 mM MgCl_2) was incubated at 37 °C for 15 minutes. SVPD 1 $\mu\text{g}/100$ μL was added to the oligonucleotide and aliquots of 50 μL were removed at time intervals of 2, 10, 20, 30, 60, 120 minutes. Aliquots were kept at 90 °C for 2 minutes to inactivate nuclease and analysed by RP-HPLC using an increasing gradient of acetonitrile in triethylammonium acetate (A: 5% acetonitrile and B: 30% acetonitrile in 0.1N triethylammonium acetate, pH 7.0). The percent intact oligonucleotide (based on the peak area) was plotted against the time to show the degradation of oligomers with respect to time.

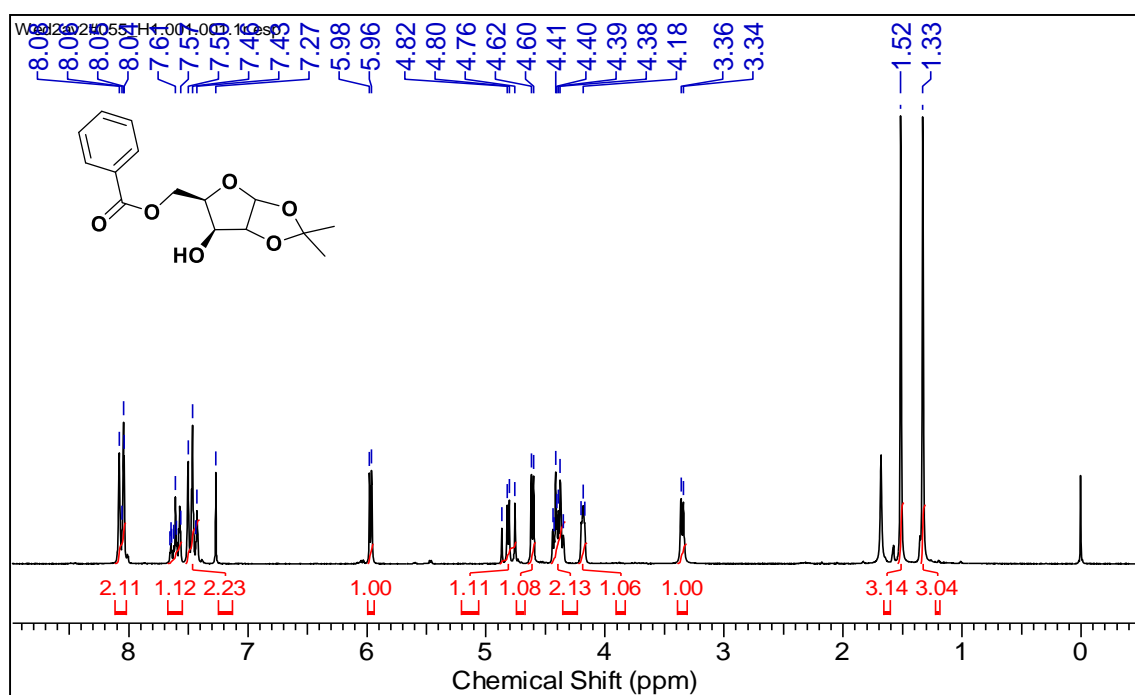
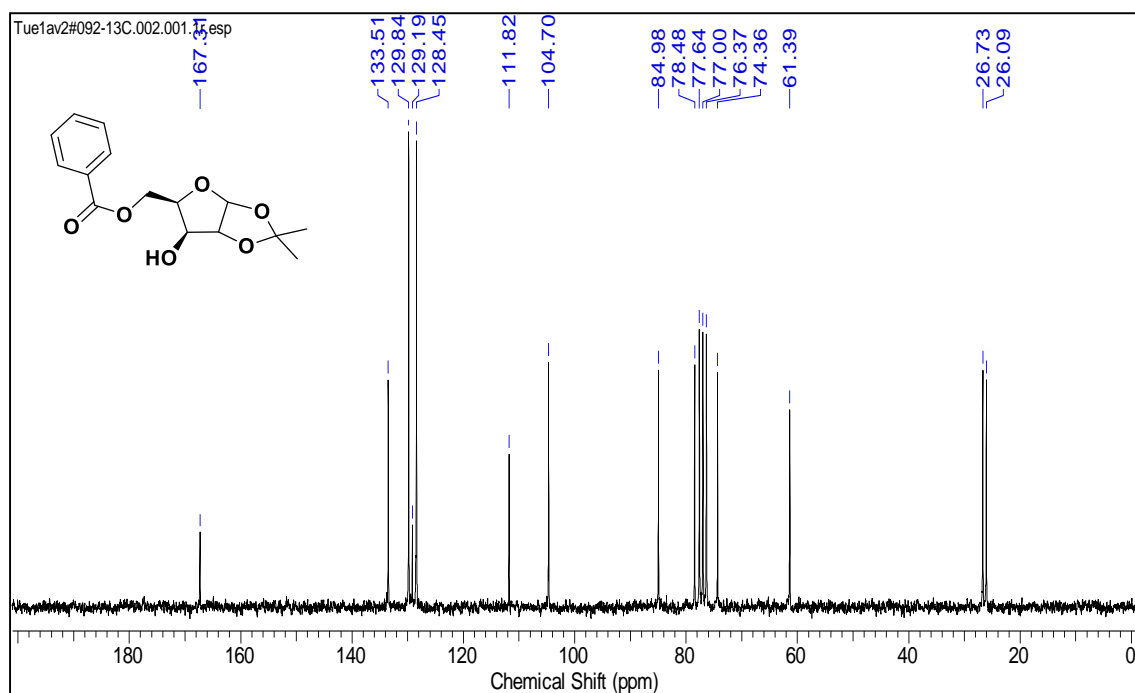
2.11 Appendix A

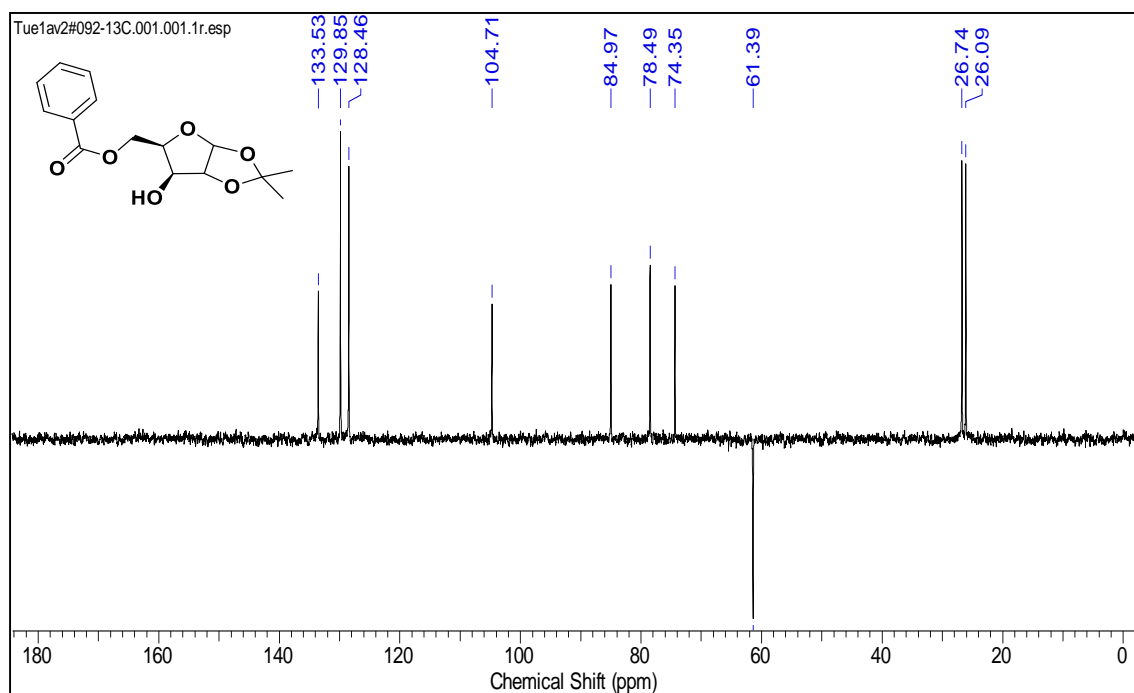
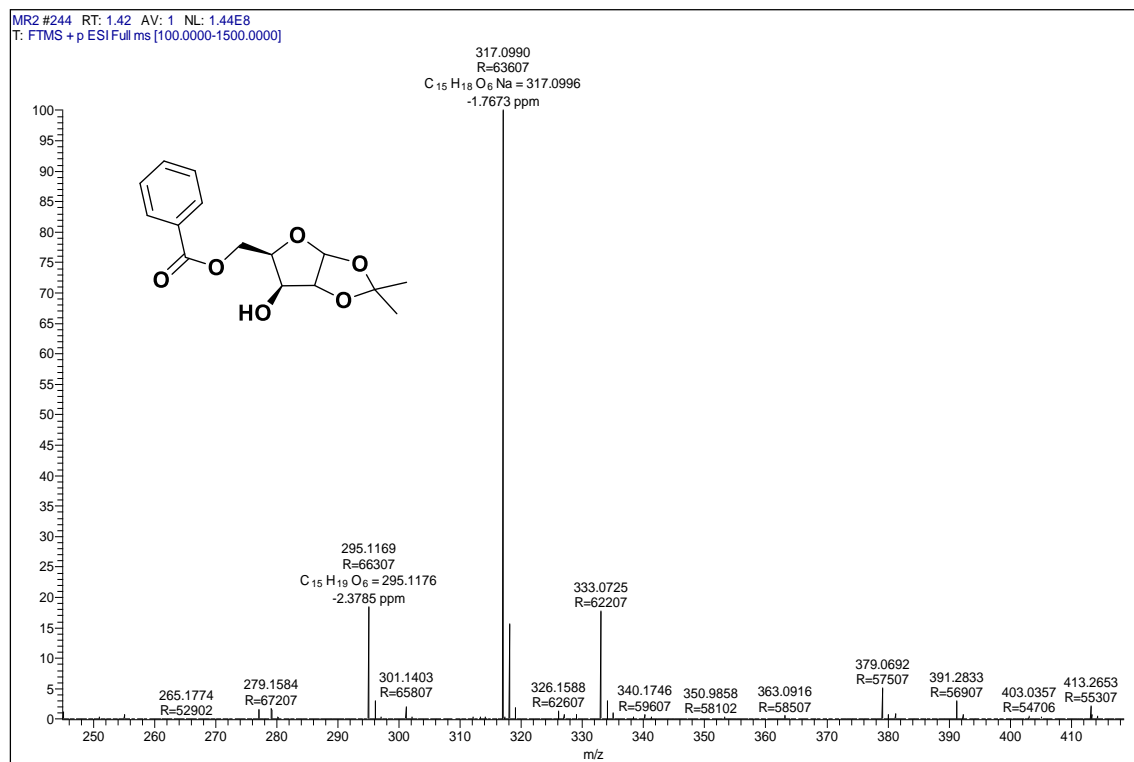
Compounds	Page Number
Compound 2: ^1H , ^{13}C , DEPT NMR and HRMS	97-98
Compound 3: ^1H , ^{13}C , DEPT NMR and HRMS	99-100
Compound 4: ^1H , ^{13}C , DEPT NMR and HRMS	101-102
Compound 5: ^1H , ^{19}F , ^{13}C , DEPT NMR and HRMS	103-105
Compound 6: ^1H , ^{13}C , DEPT NMR	105-106
Compound 7: ^1H , ^{13}C , DEPT NMR and HRMS	107-108
Compound 8: ^1H , ^{13}C NMR and HRMS	109-110
Compound 9: ^1H NMR and LCMS	110-112
Compound 10: ^{31}P NMR and HRMS	112-113
Compound 11: ^1H , ^{13}C , DEPT NMR and HRMS	113-115
Compound 12: ^1H , ^{13}C , DEPT NMR and HRMS	115-117
Compound 13: ^1H , ^{13}C , DEPT NMR and HRMS	117-119
Compound 14: ^{31}P NMR and HRMS	119-120
Compound 16: ^1H , ^{13}C , DEPT NMR and HRMS	120-122
Compound 18: ^1H , ^{13}C , DEPT NMR and HRMS	122-124
Compound 19: ^1H , ^{13}C , DEPT NMR and HRMS	124-126
Compound 20: ^1H , ^{19}F , ^{13}C , DEPT NMR and HRMS	126-128
Compound 21: ^1H , ^{13}C DEPT NMR and HRMS	129-130
Compound 22: ^1H , ^{13}C and ^{13}C DEPT NMR	131-132
Compound 23: ^1H , ^{13}C , DEPT NMR and HRMS	132-134
Compound 24: ^1H , ^{13}C , DEPT NMR and HRMS	134-136

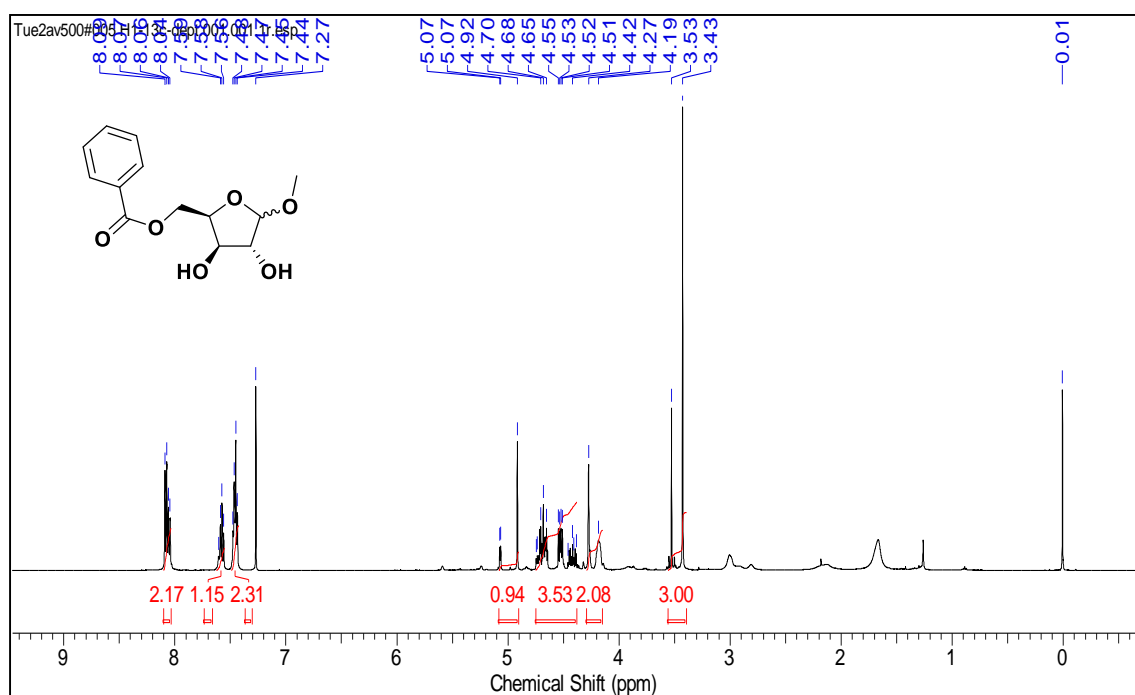
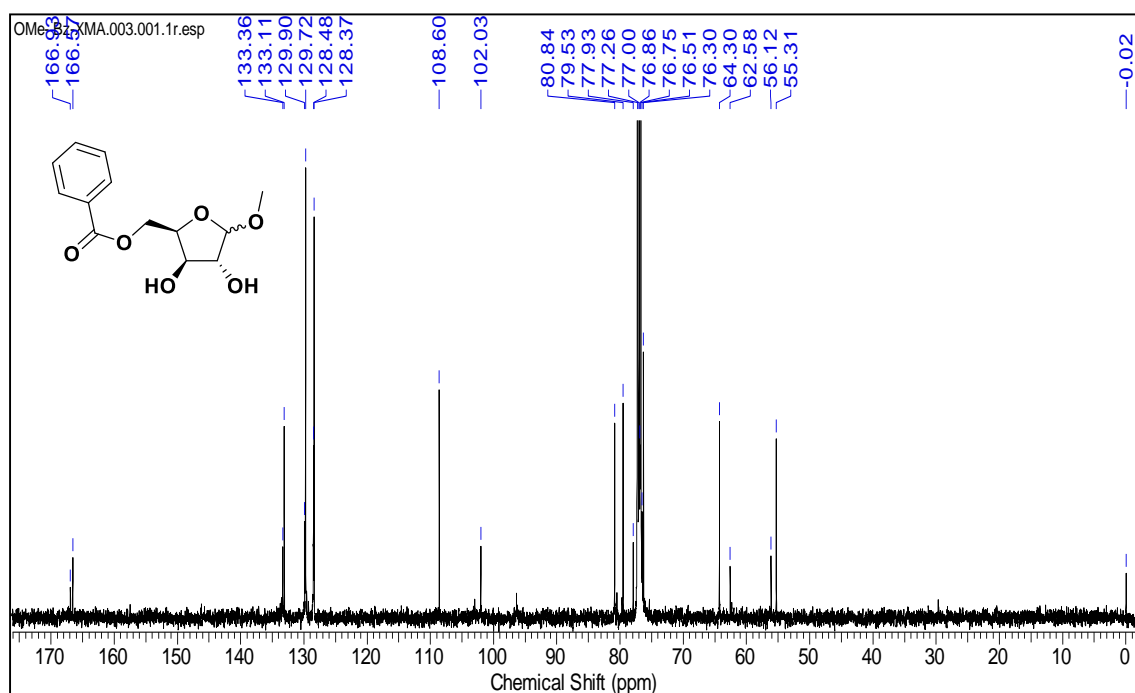
Compound 25: ^1H , ^{13}C DEPT NMR and HRMS	136-138
Compound 26: ^1H NMR and HRMS	138-139
Compound 27: ^{31}P NMR and HRMS	139-140
Compound 28: ^1H and LCMS	140-141
Compound 29: ^1H , ^{13}C , DEPT NMR and HRMS	141-143
Compound 30: ^1H , ^{13}C , DEPT NMR and HRMS	143-145
Compound 31: ^{31}P NMR and HRMS	145-146
HPLC chromatogram of TBA oligomers	147-150
MALDI-TOF spectra of TBA oligomers	151-155

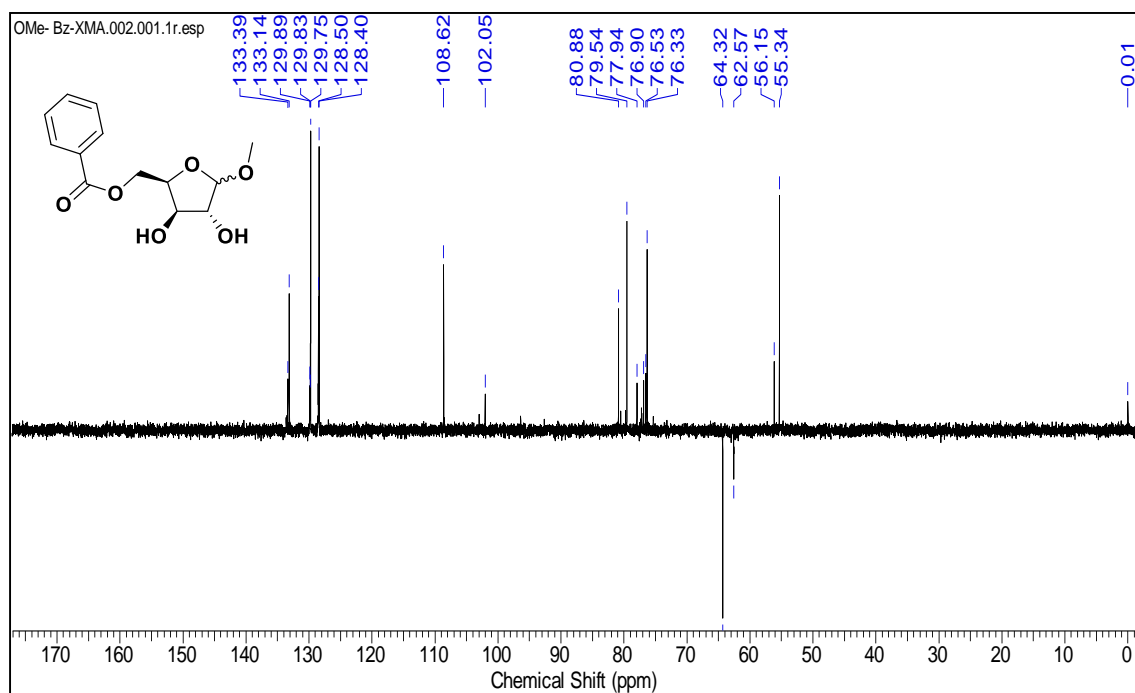
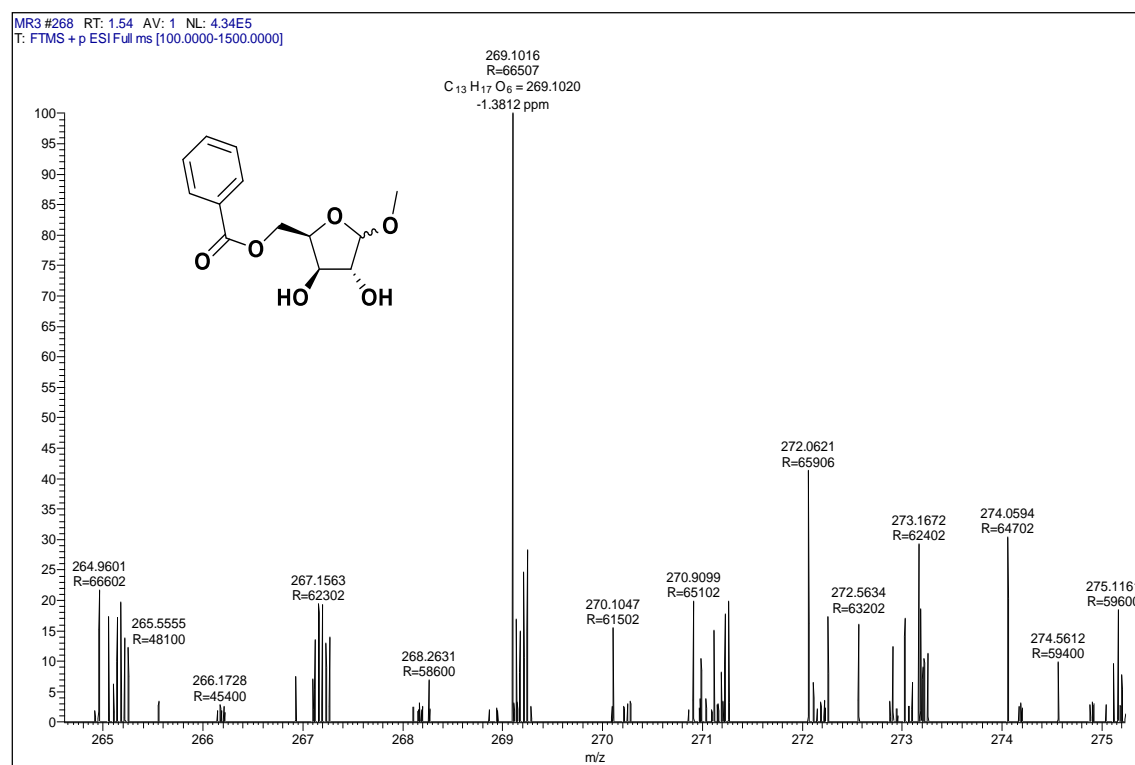
^1H NMR of compound 2 **^{13}C NMR of compound 2**

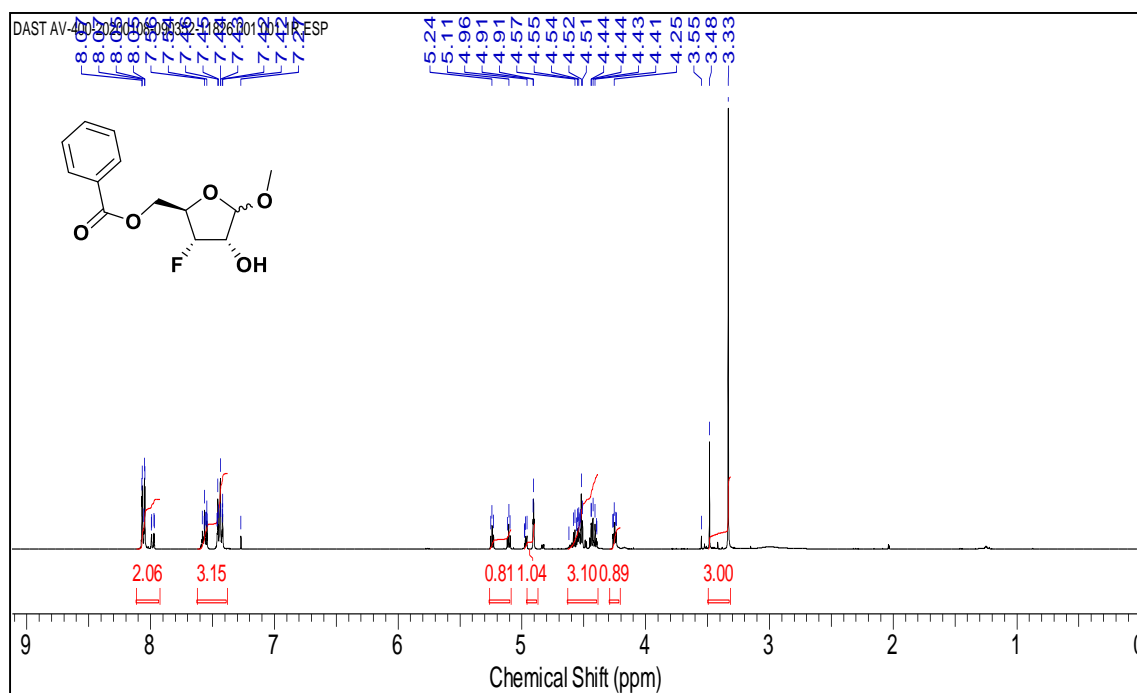
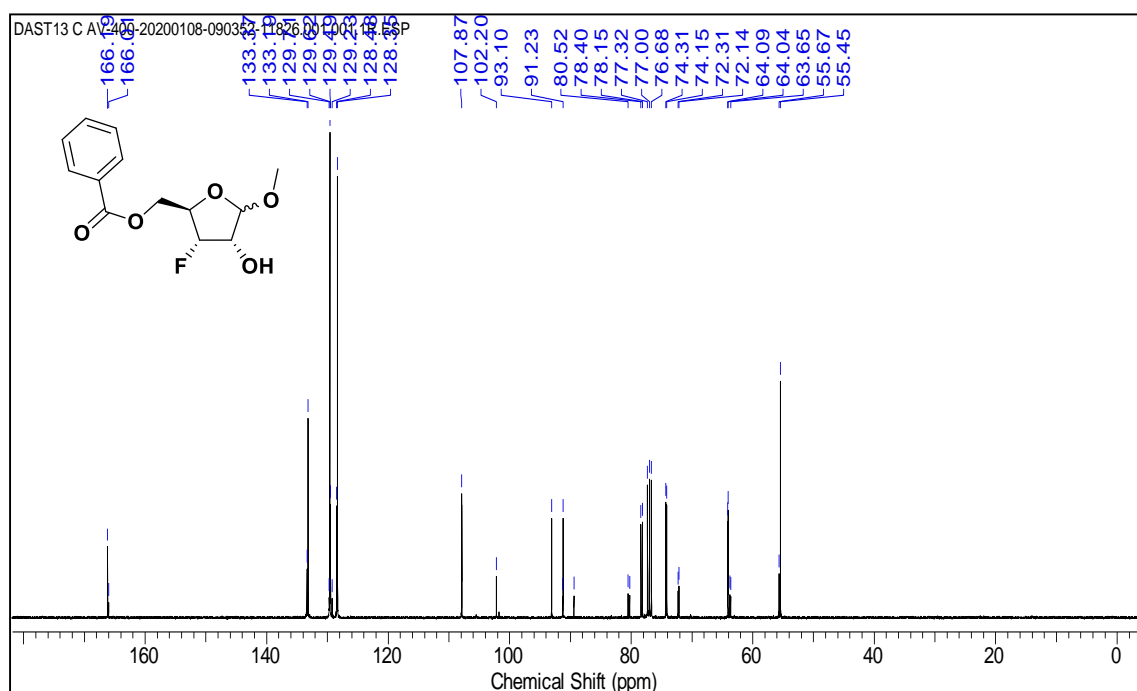
¹³C-DEPT of compound 2**HRMS spectrum of compound 2**

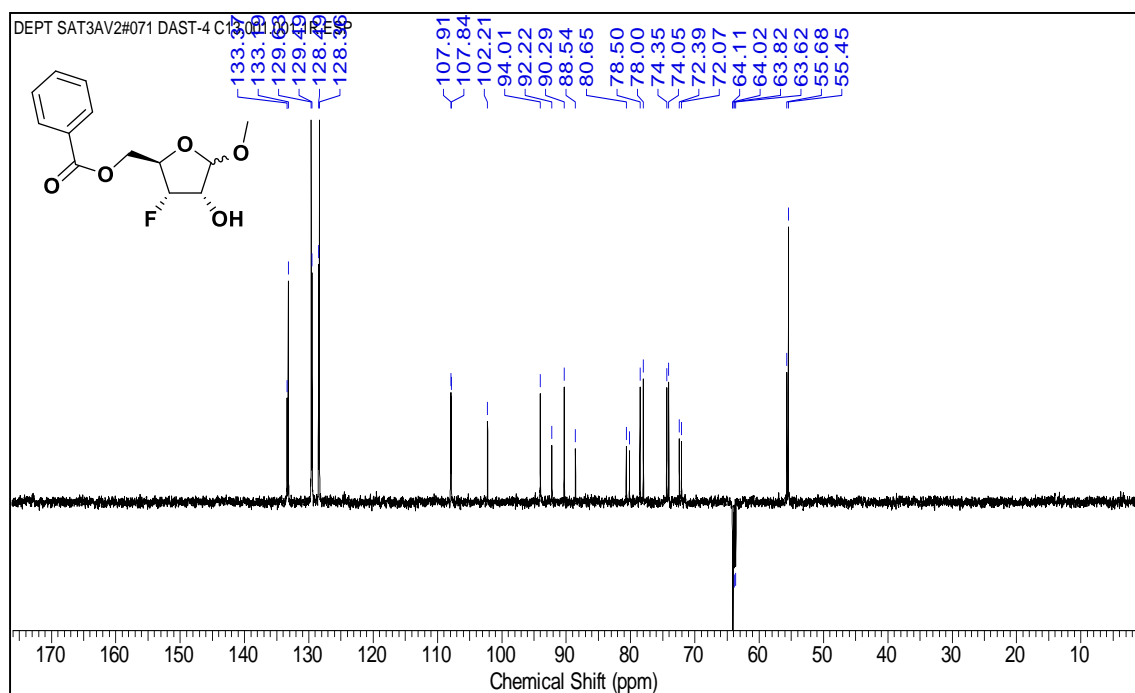
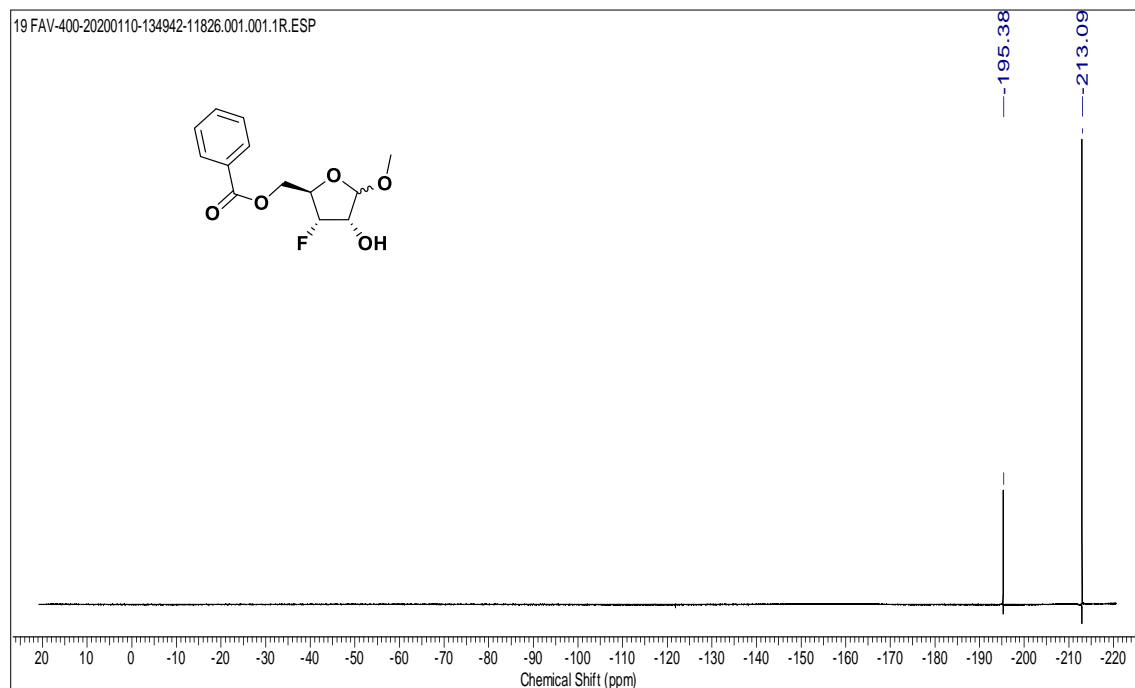
¹H NMR of compound 3**¹³C NMR of compound 3**

^{13}C -DEPT of compound 3**HRMS spectrum of compound 3**

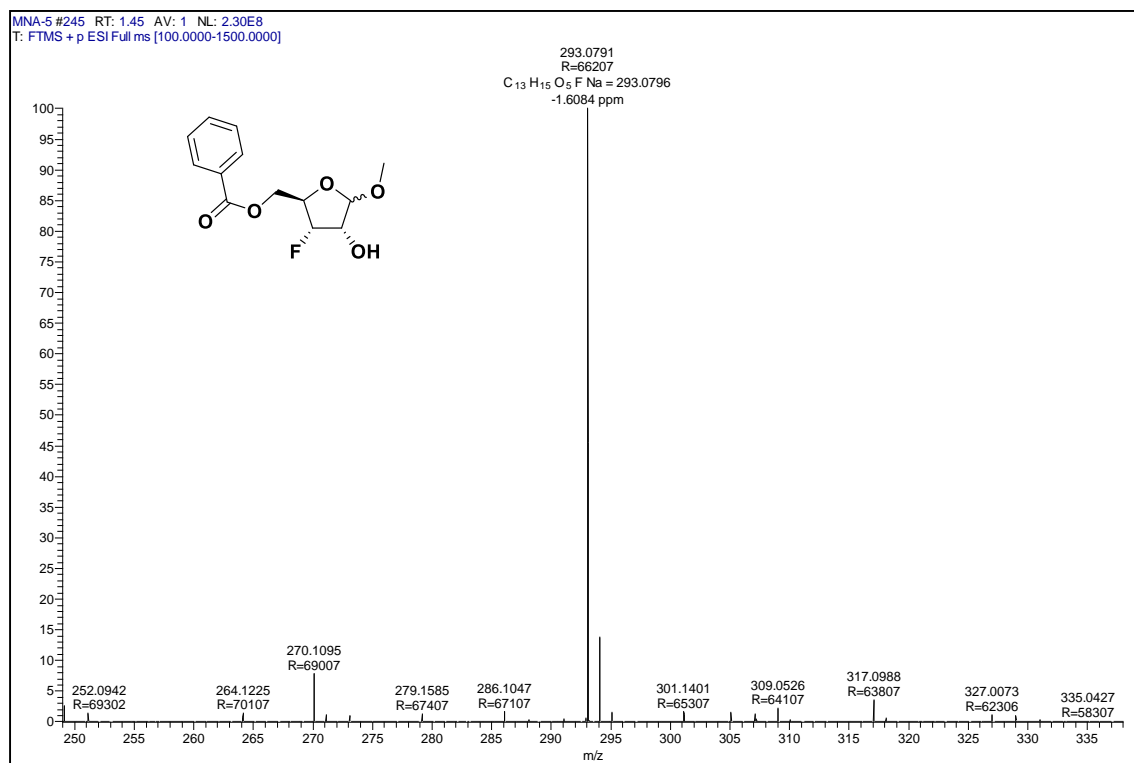
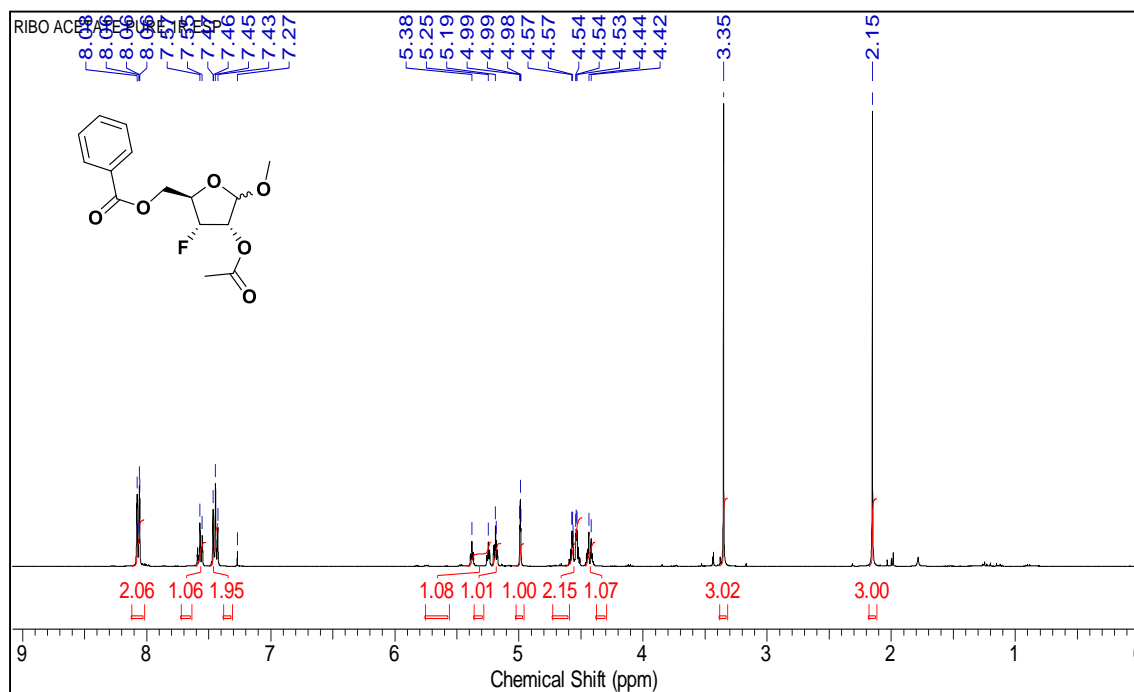
¹H NMR of compound 4**¹³C NMR of compound 4**

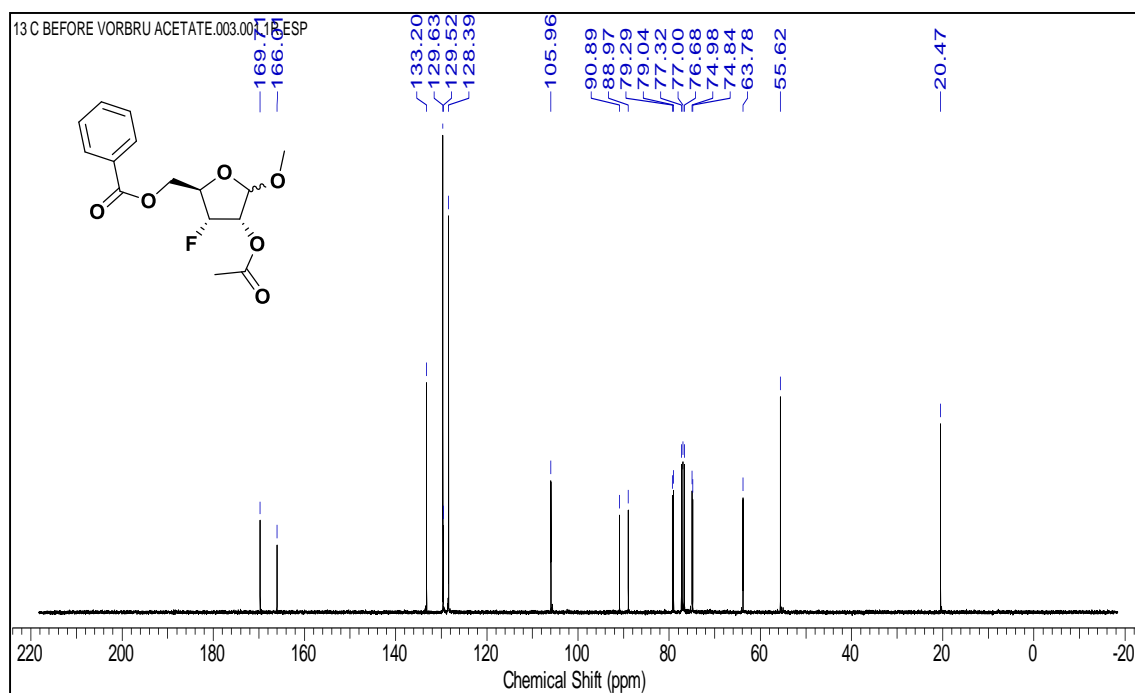
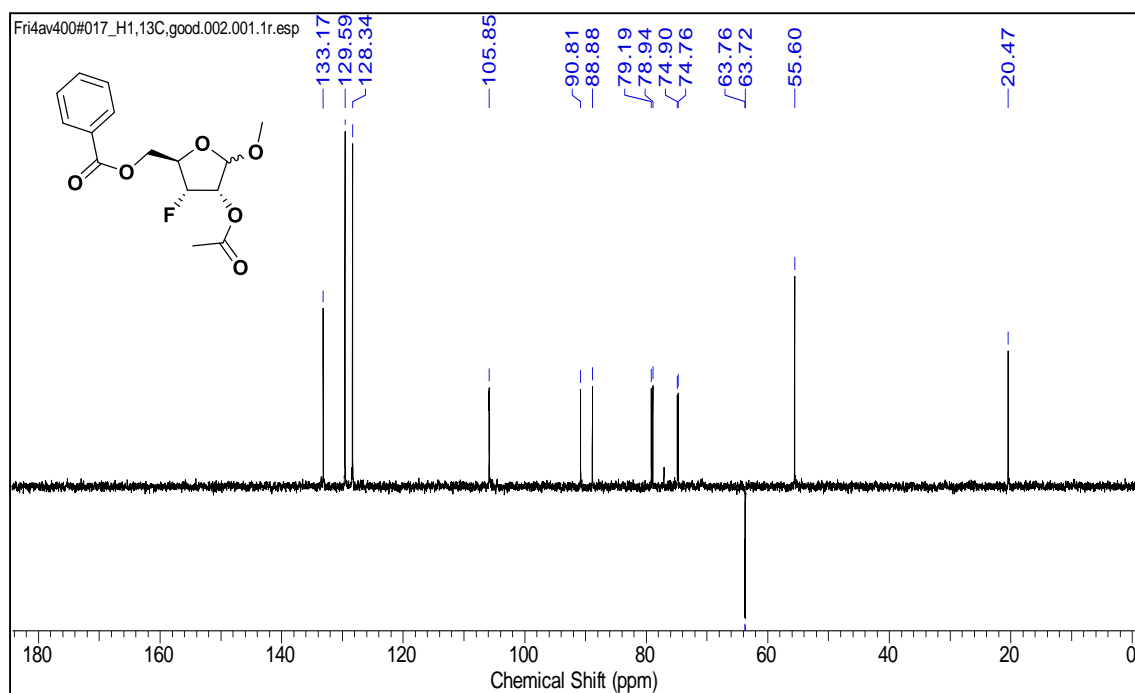
^{13}C -DEPT of compound 4**HRMS spectrum of compound 4**

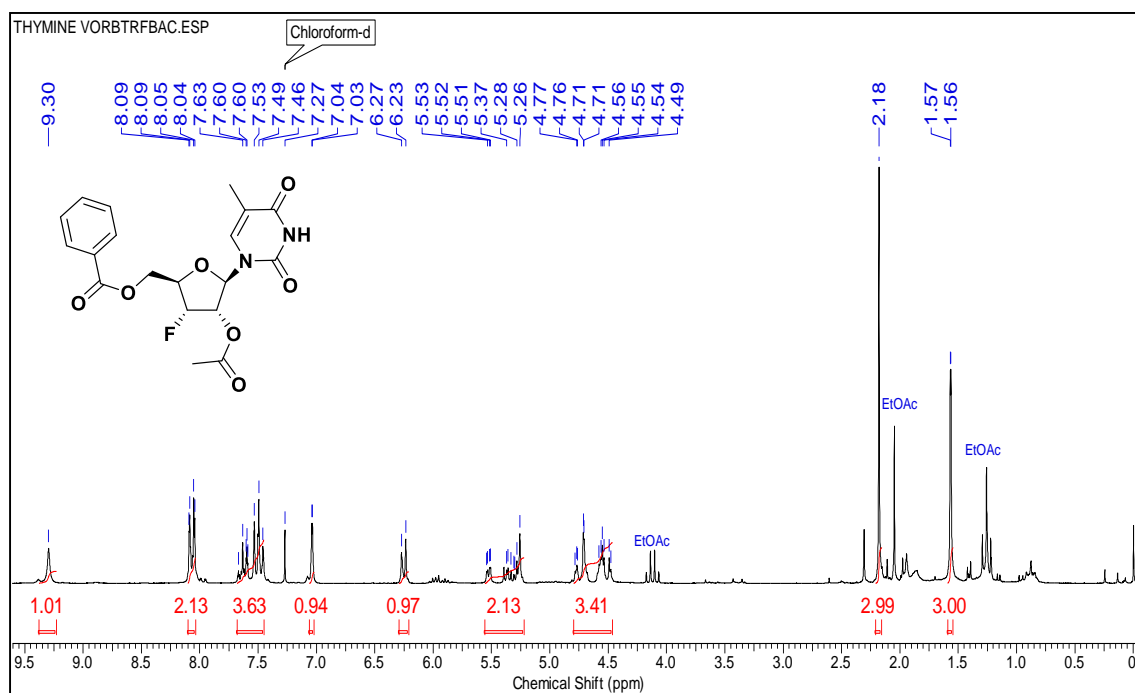
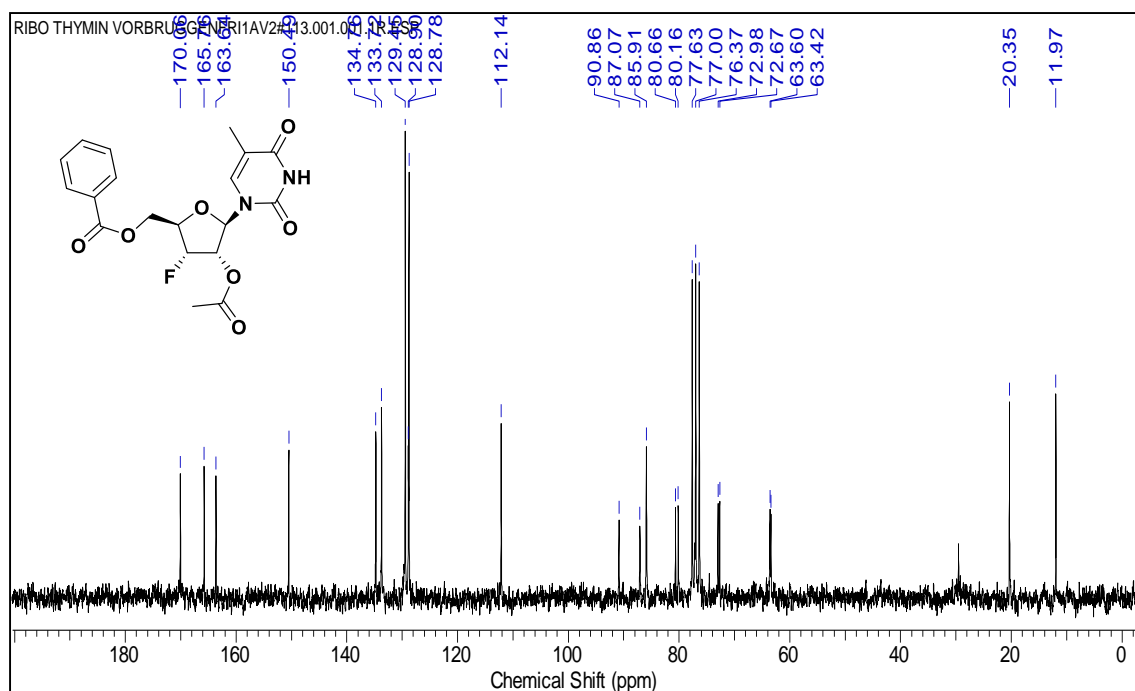
¹H NMR of compound 5**¹³C NMR of compound 5**

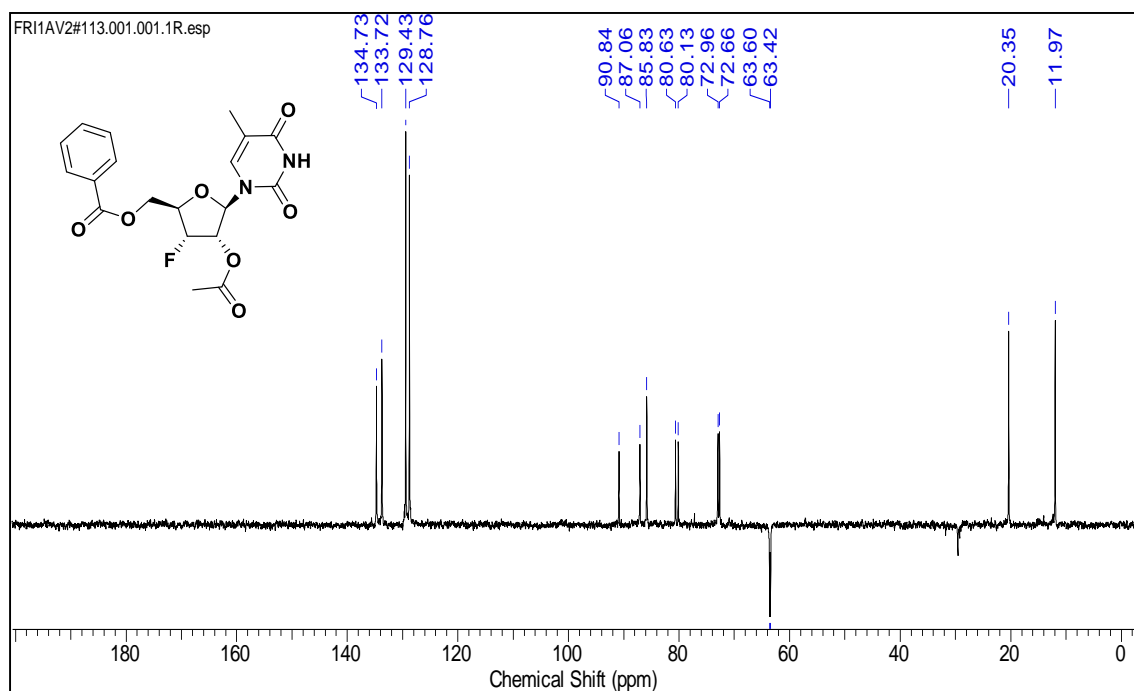
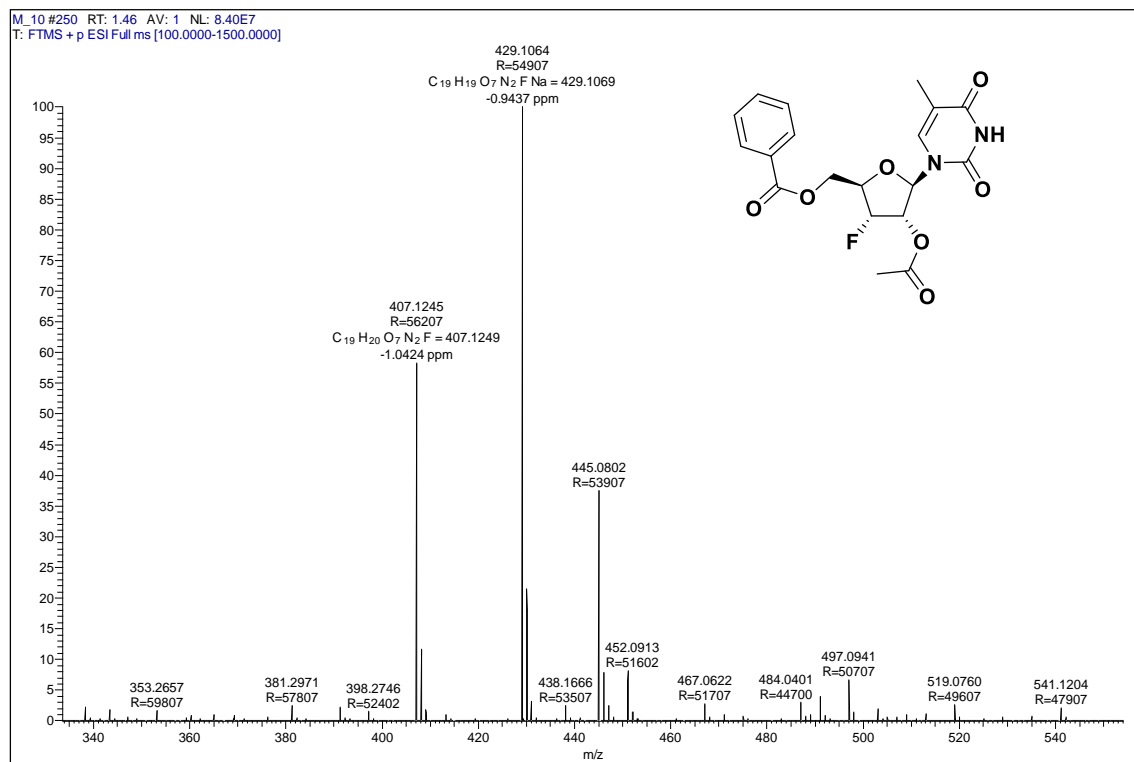
^{13}C -DEPT of compound 5 **^{19}F NMR of compound 5**

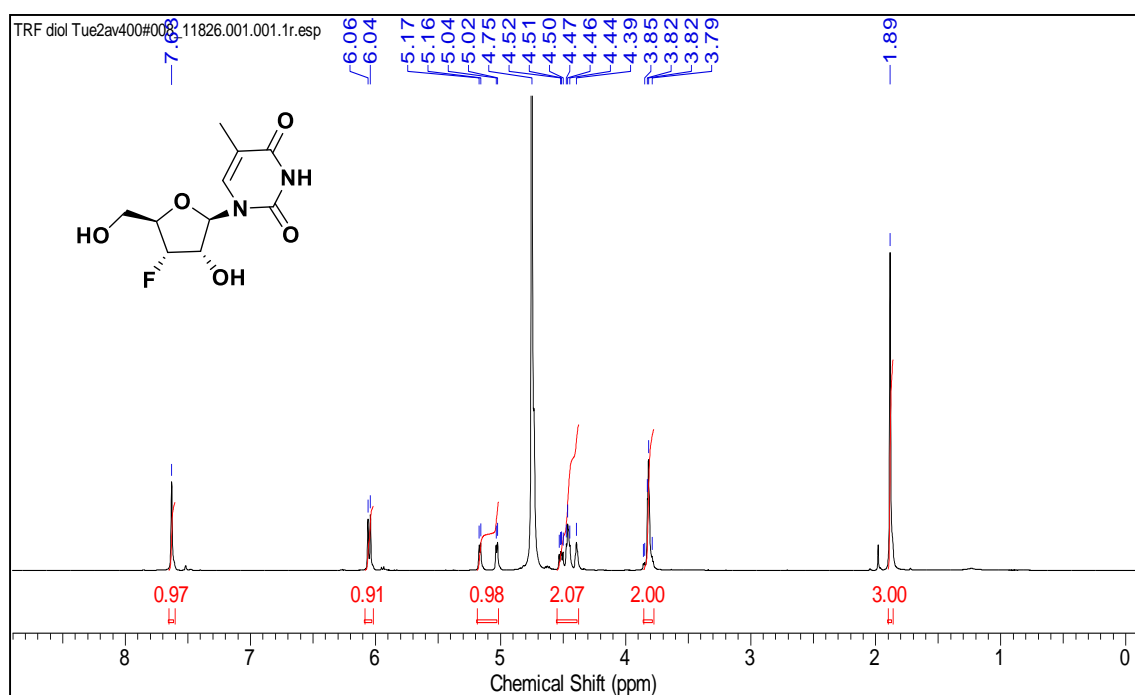
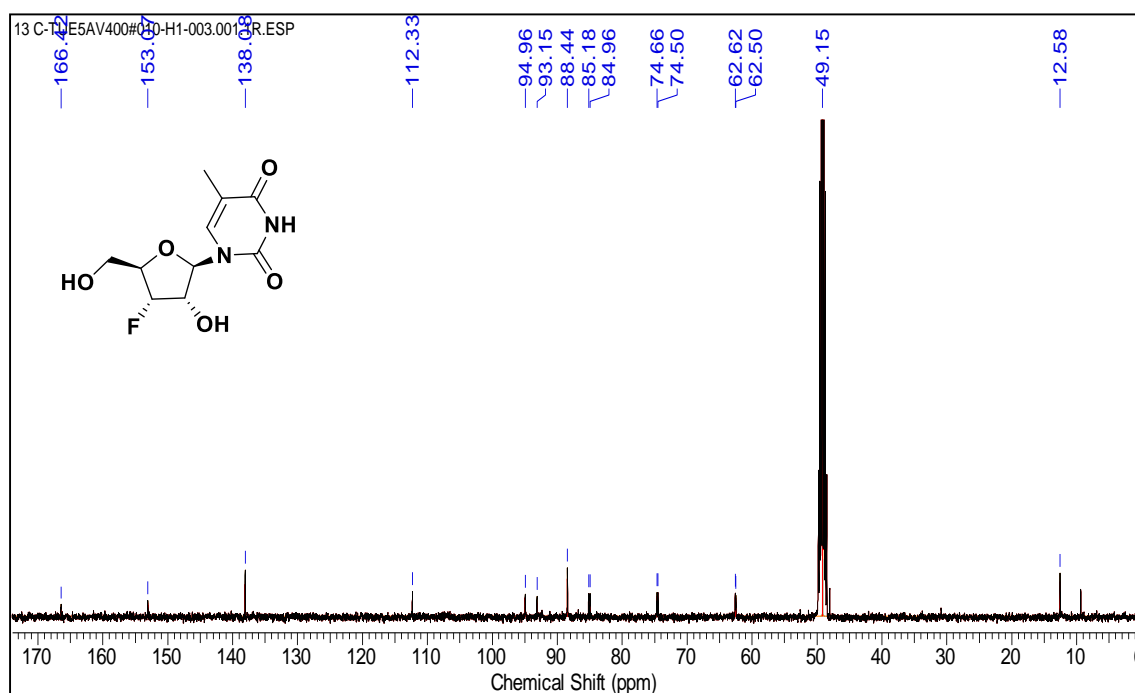
HRMS spectrum of compound 5

¹H NMR of compound 6

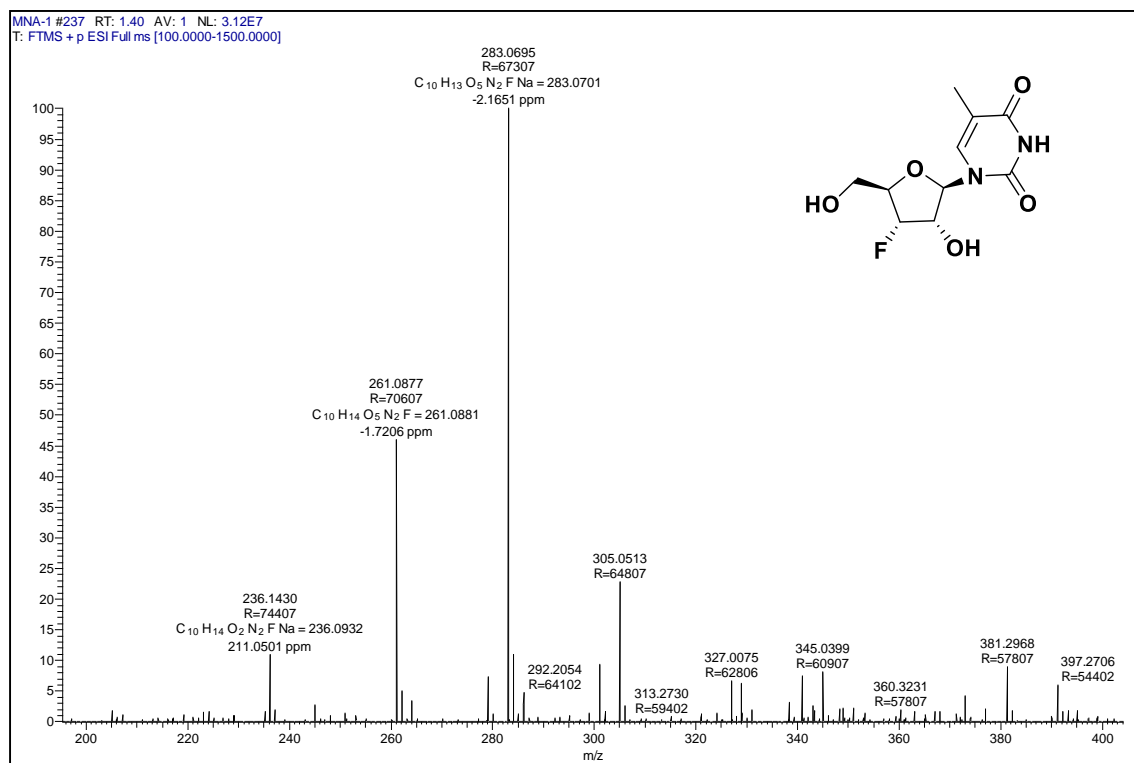
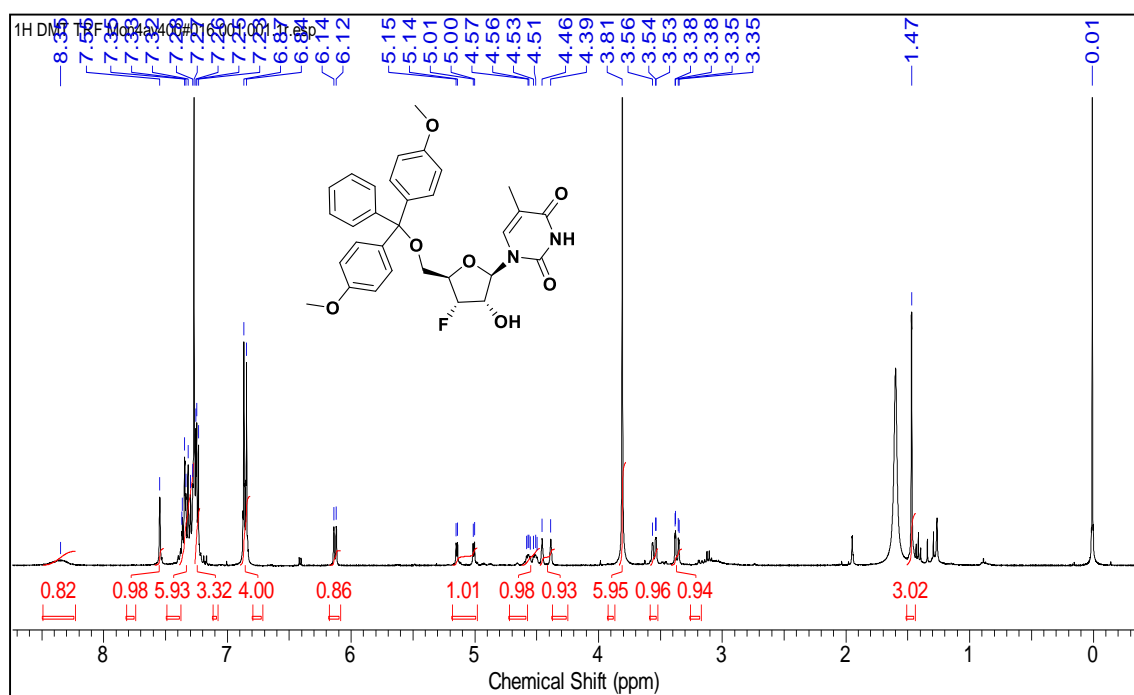
^{13}C NMR of compound 6 **^{13}C -DEPT of compound 6**

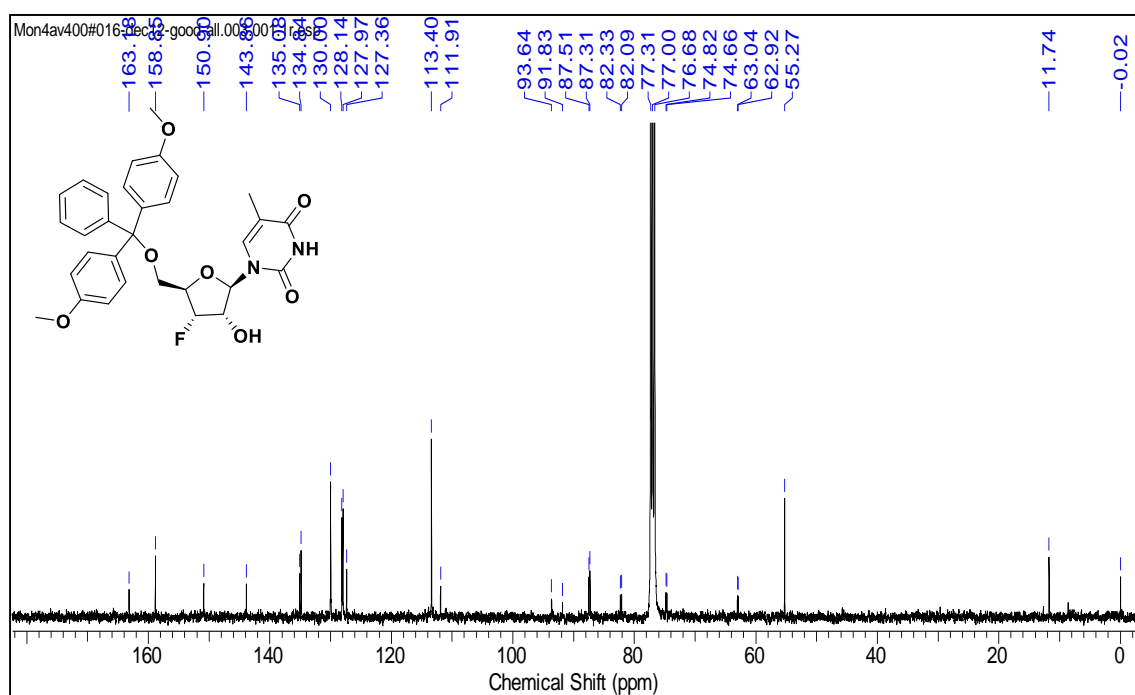
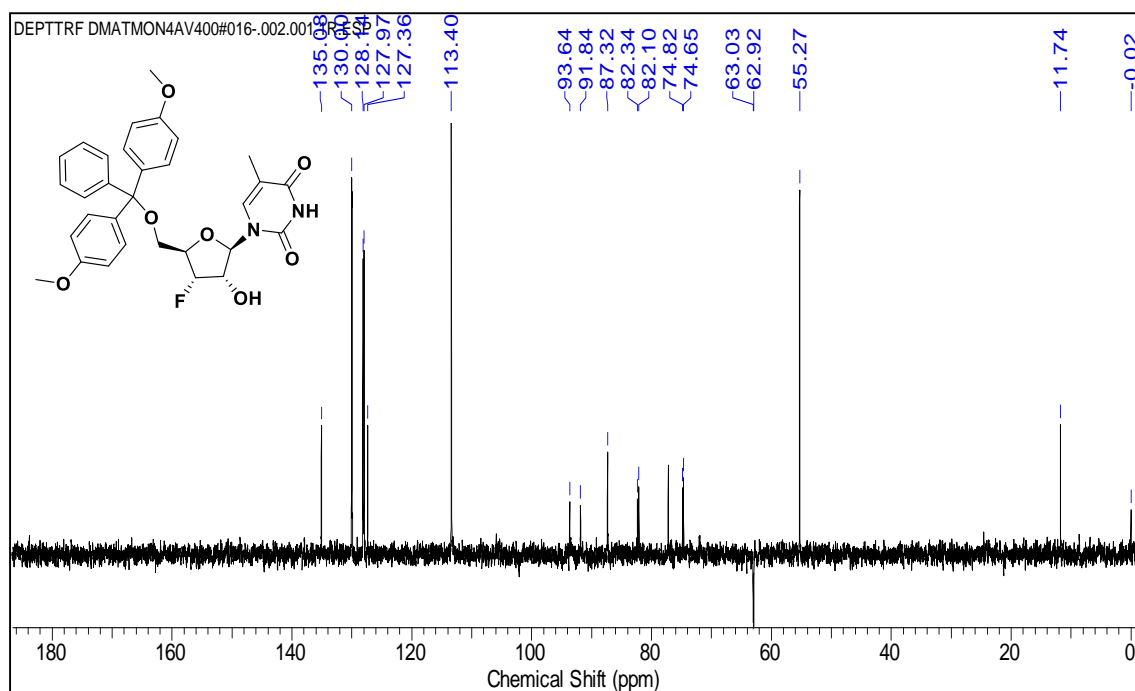
^1H NMR of compound 7 (CDCl_3) **^{13}C NMR of compound 7 (CDCl_3)**

^{13}C -DEPT of compound 7 (CDCl_3)**HRMS spectrum of compound 7**

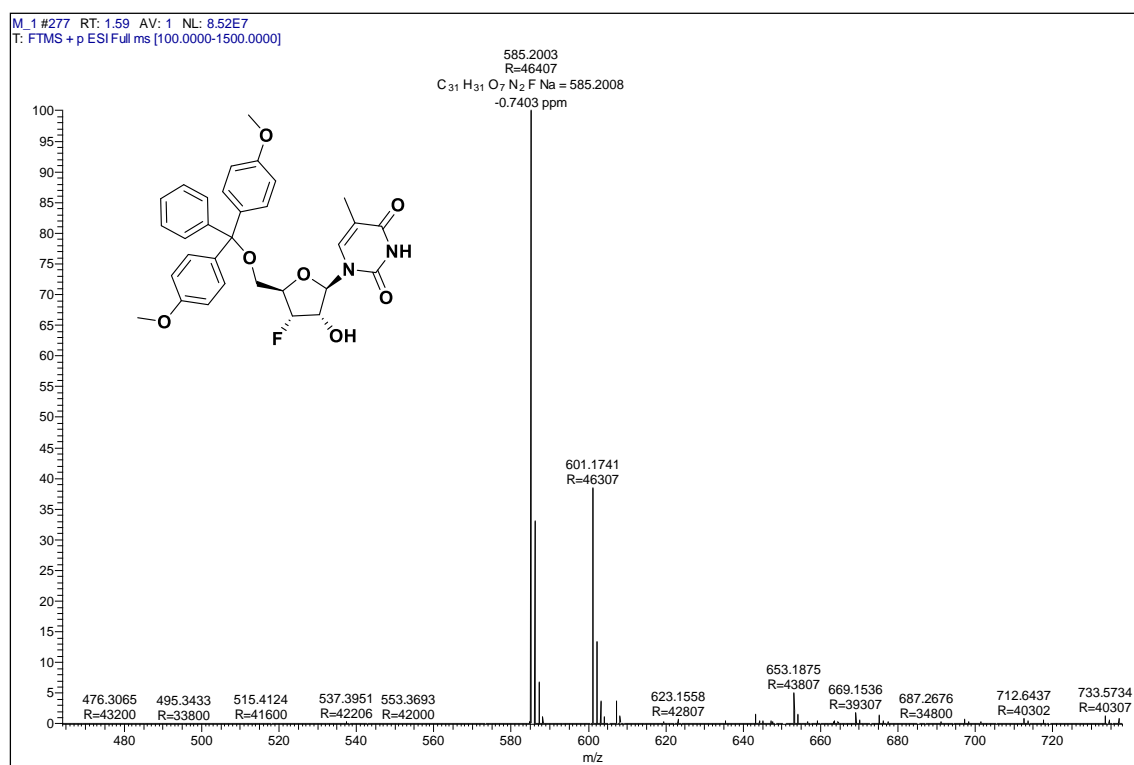
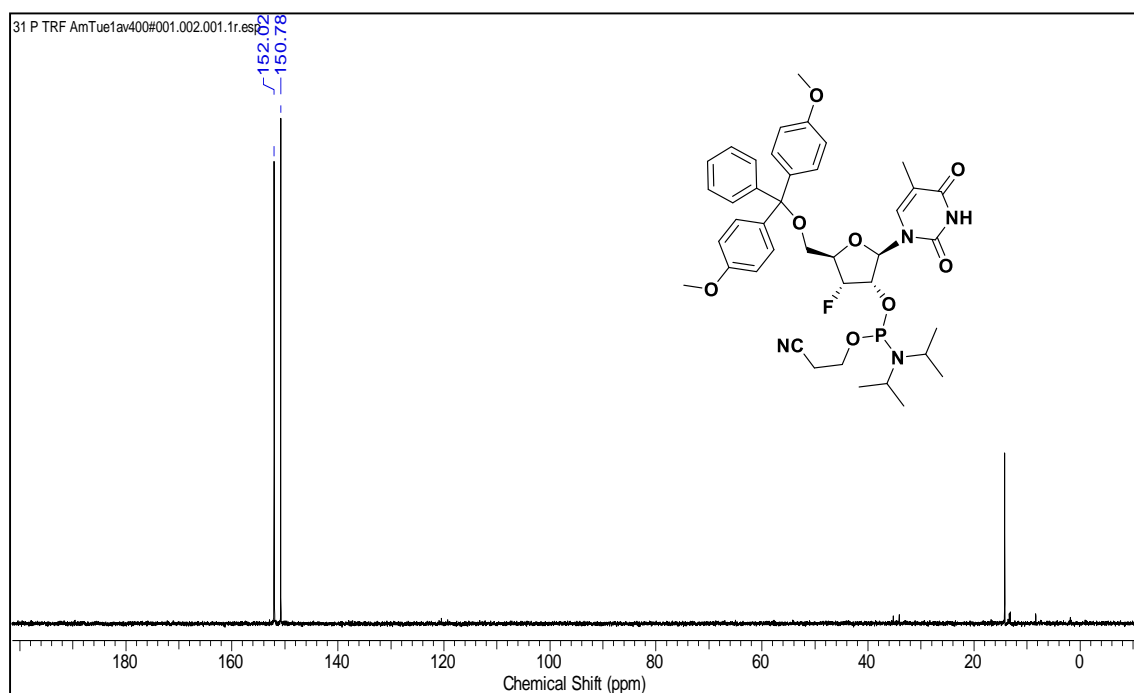
¹H NMR of compound 8 (D₂O)**¹³C NMR of compound 8 (CD₃OD)**

HRMS spectrum of compound 8

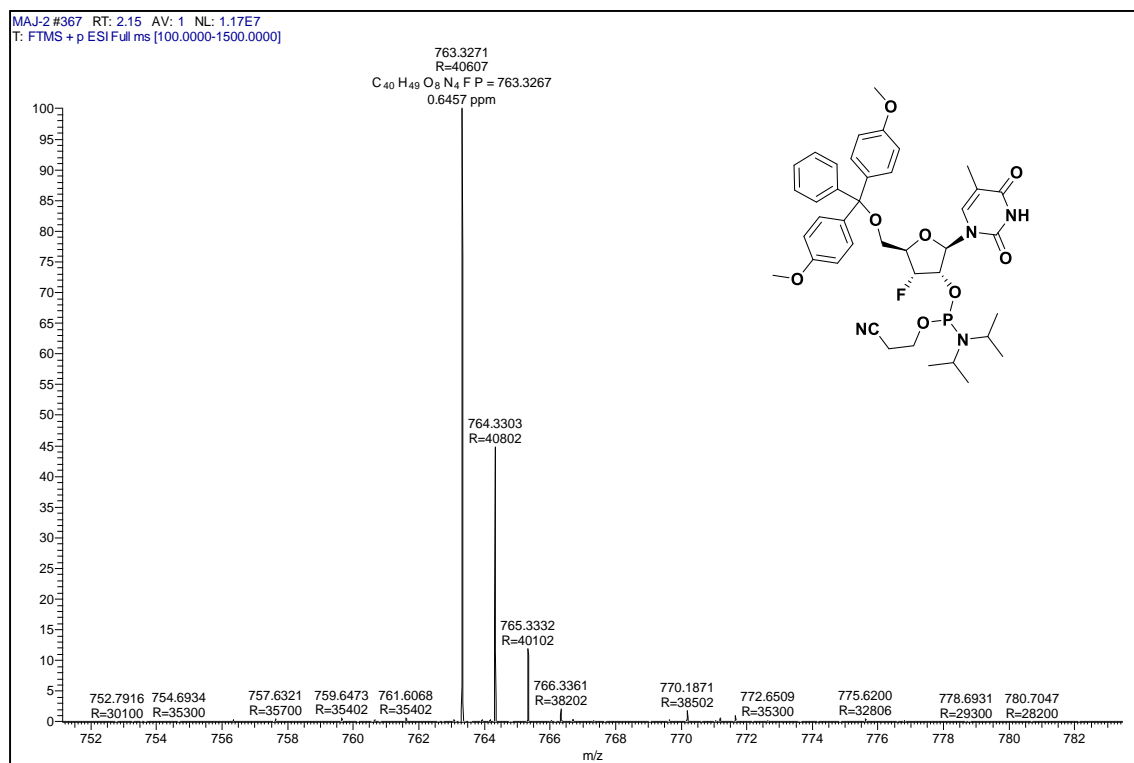
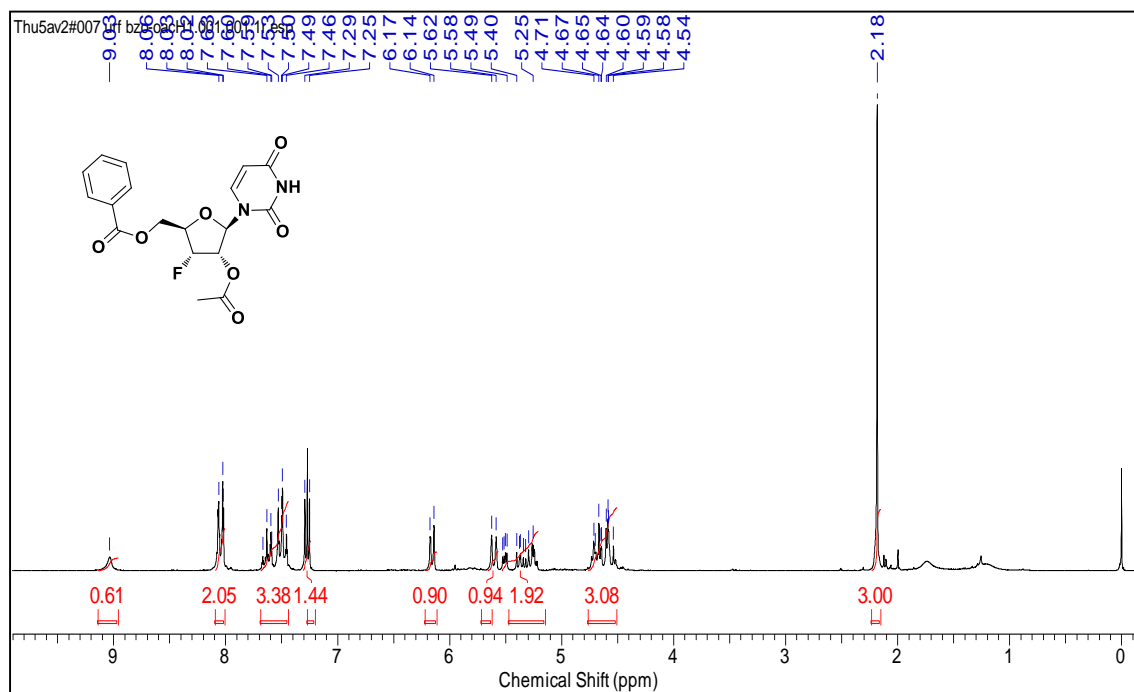
¹H NMR of compound 9 (CDCl₃)

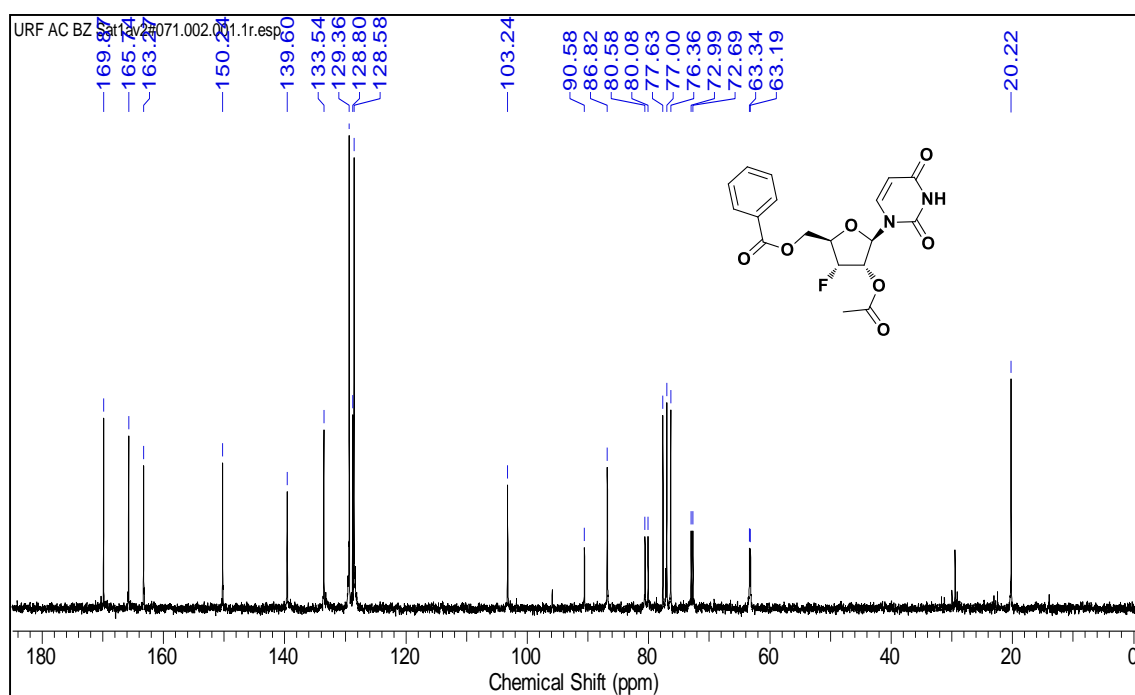
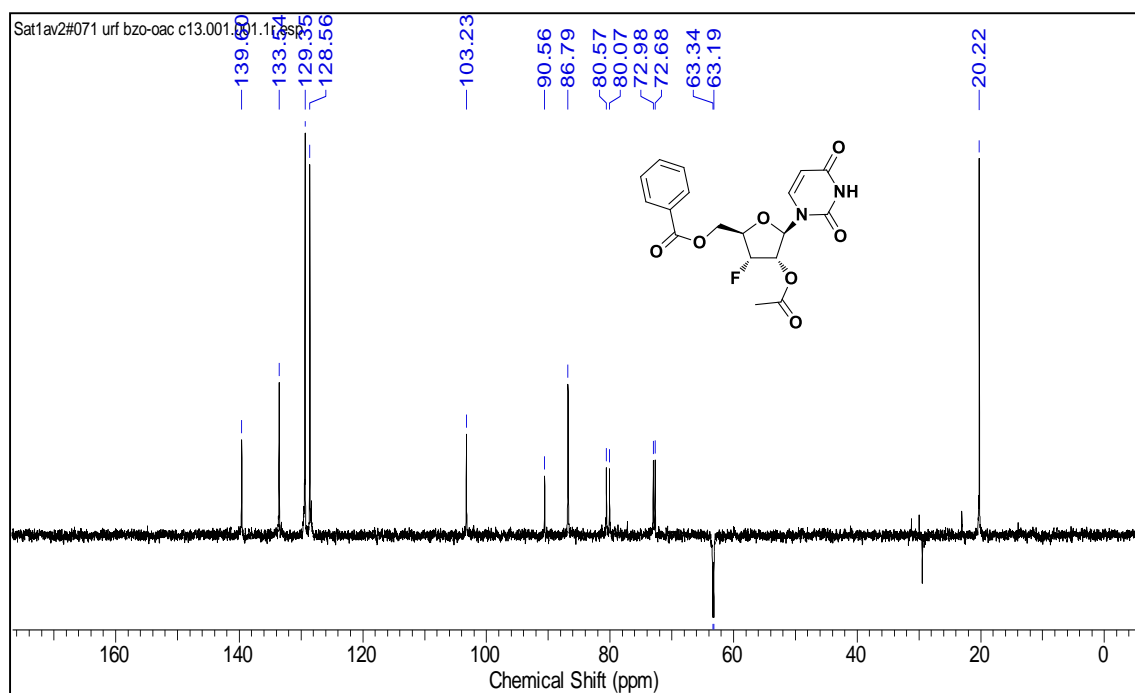
^{13}C NMR of compound 9 (CDCl_3) **^{13}C -DEPT of compound 9 (CDCl_3)**

HRMS spectrum of compound 9

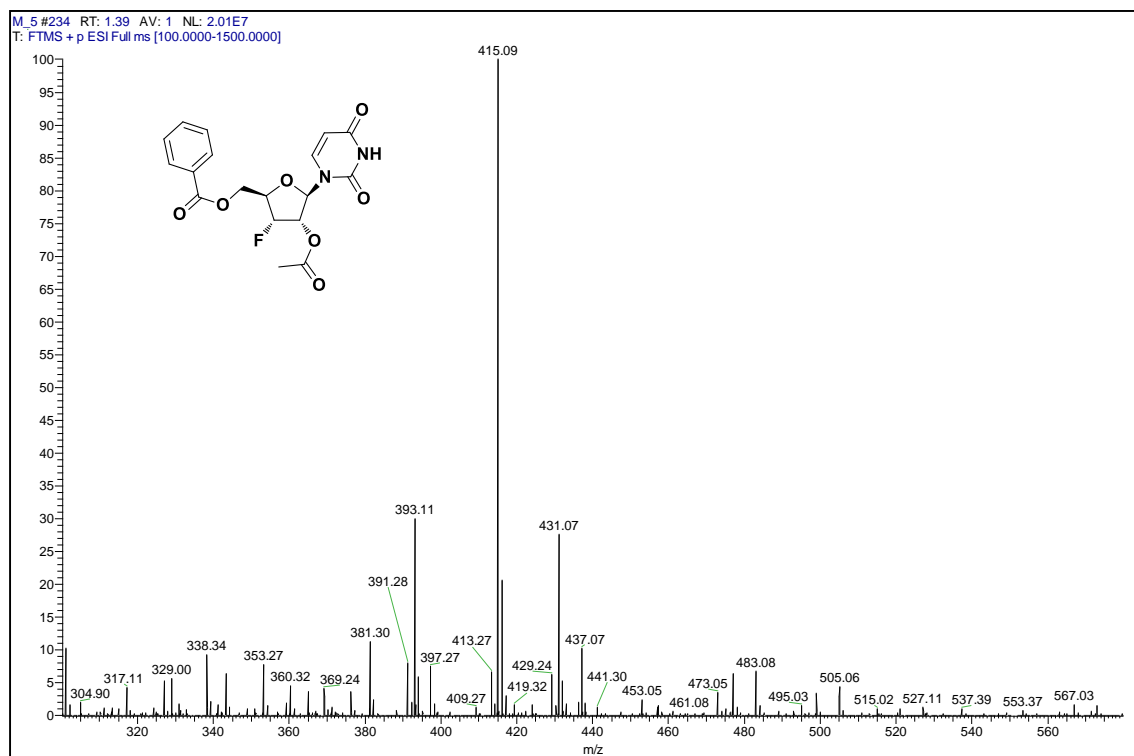
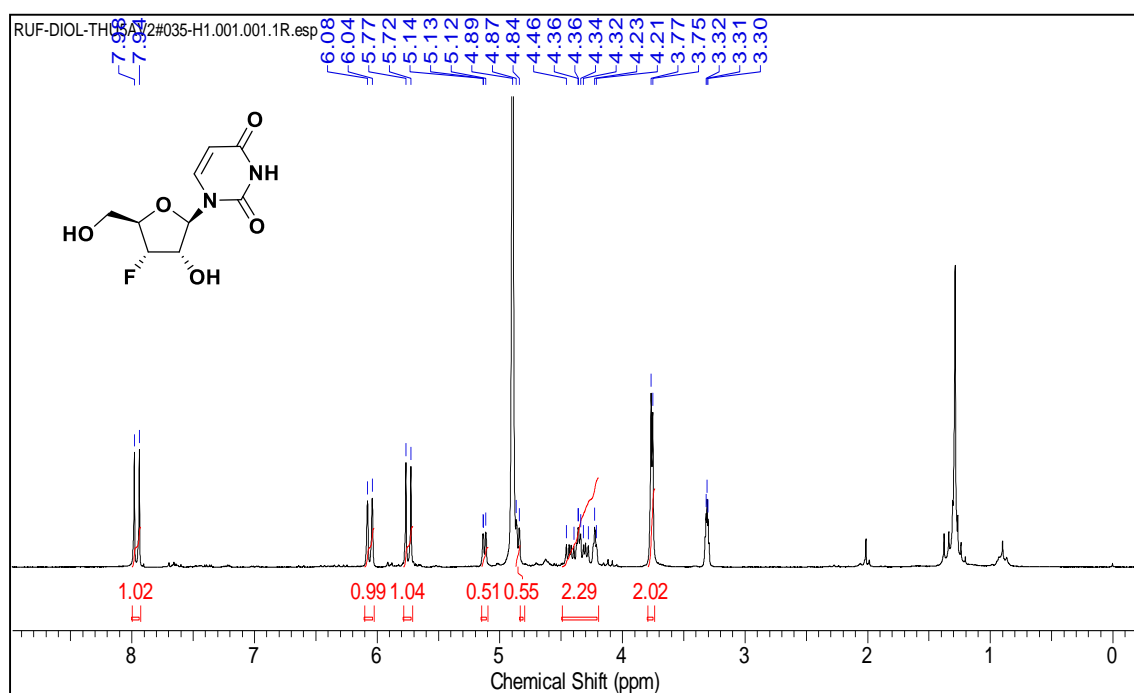
³¹P NMR of compound 10 (CDCl₃)

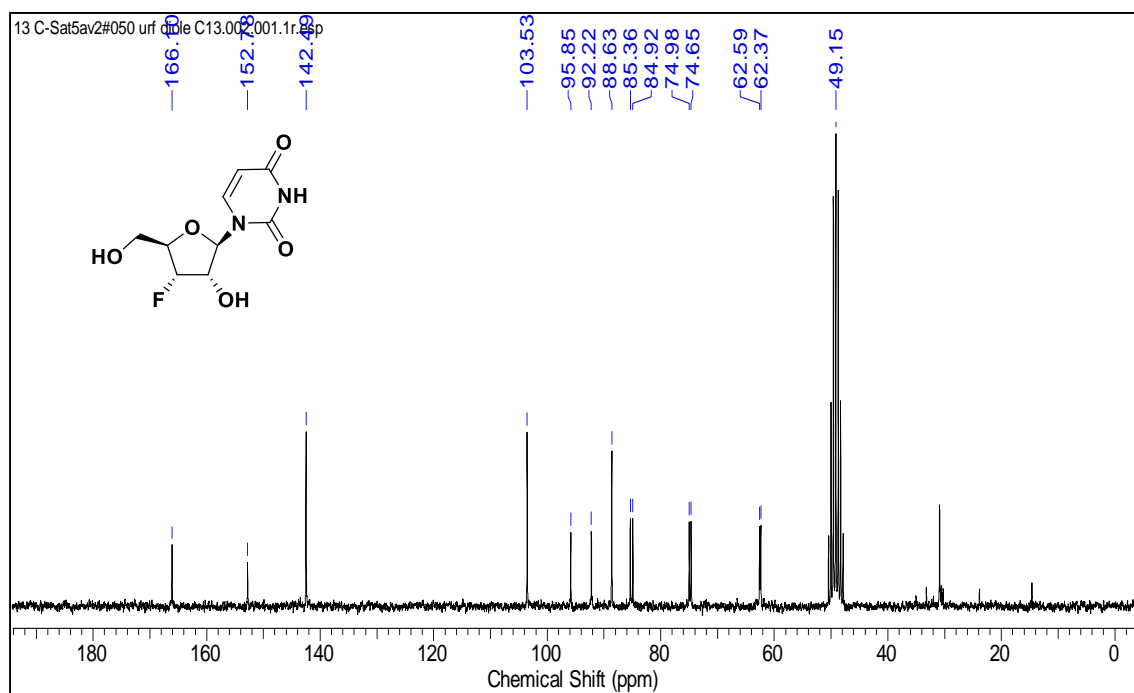
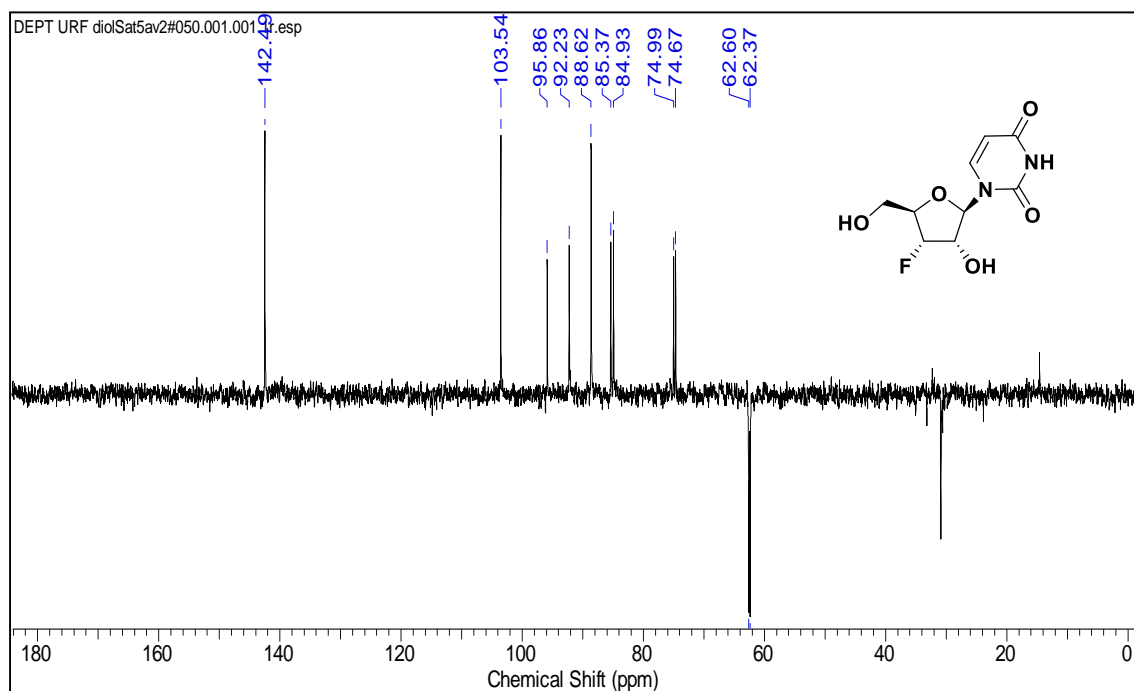
HRMS spectrum of compound 10

¹H NMR of compound 11 (CDCl₃)

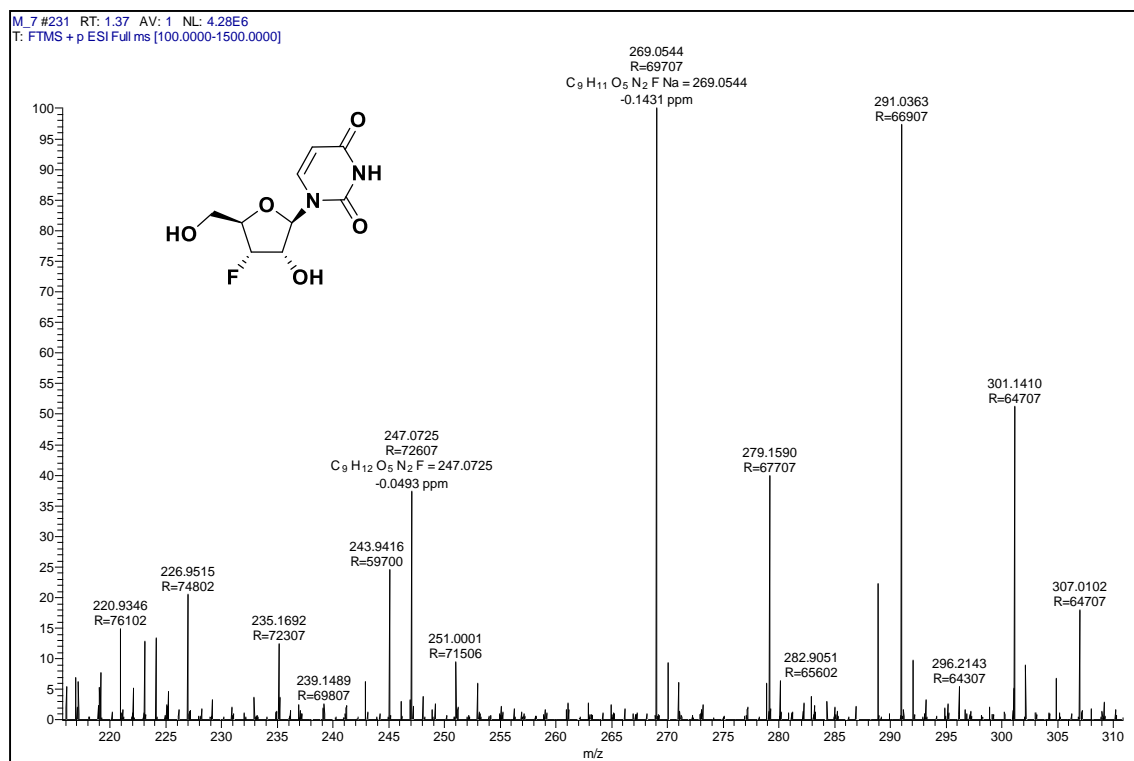
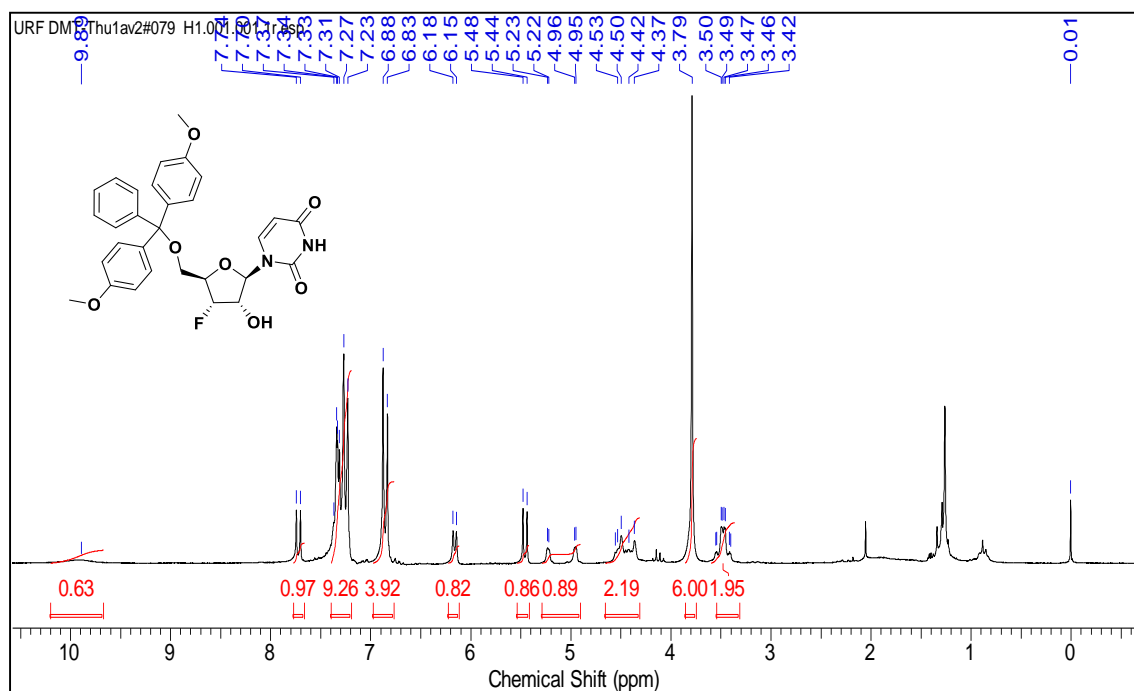
^{13}C NMR of compound 11 (CDCl_3) **^{13}C -DEPT of compound 11 (CDCl_3)**

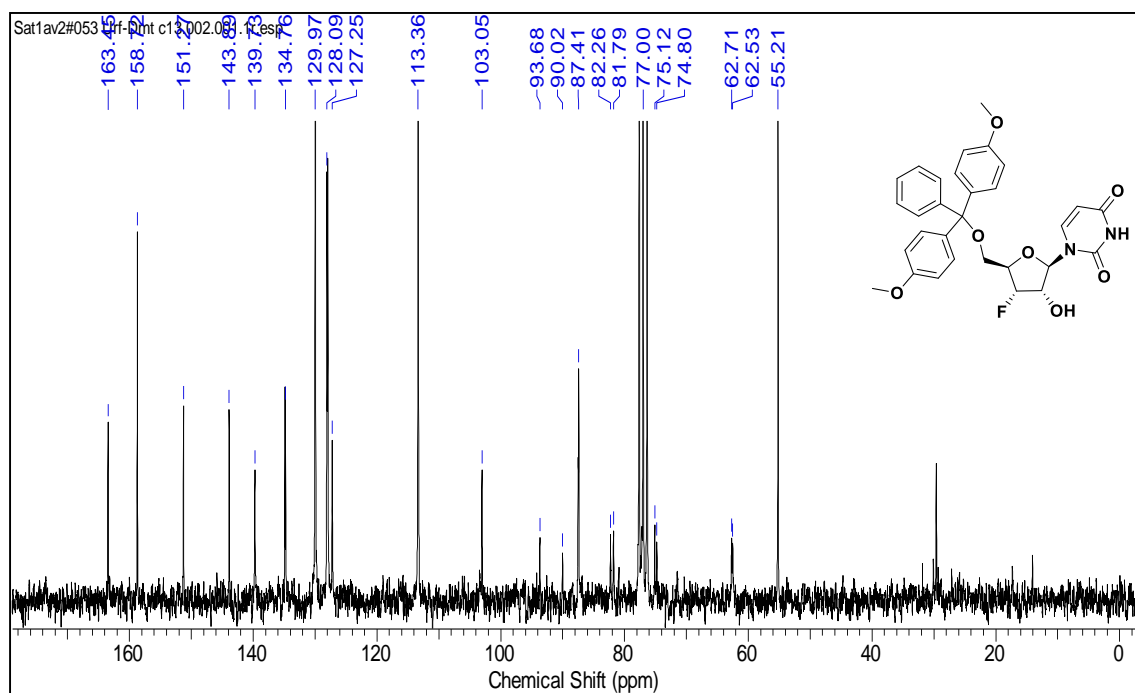
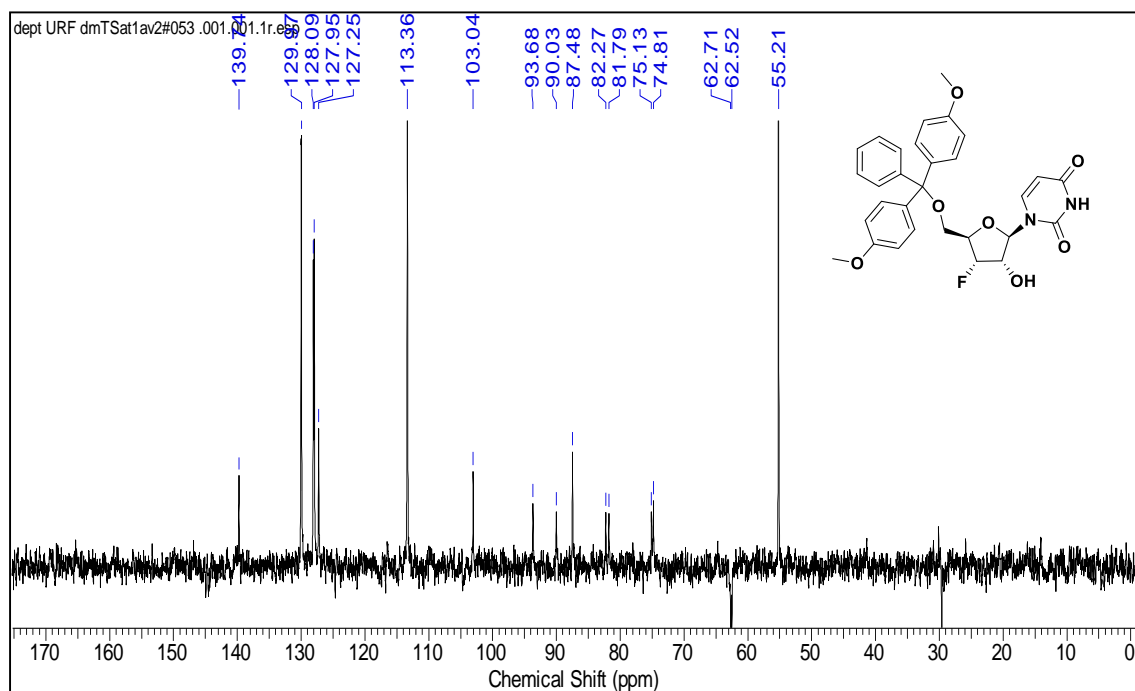
HRMS spectrum of compound 11

 ^1H NMR of compound 12 (CD_3OD)

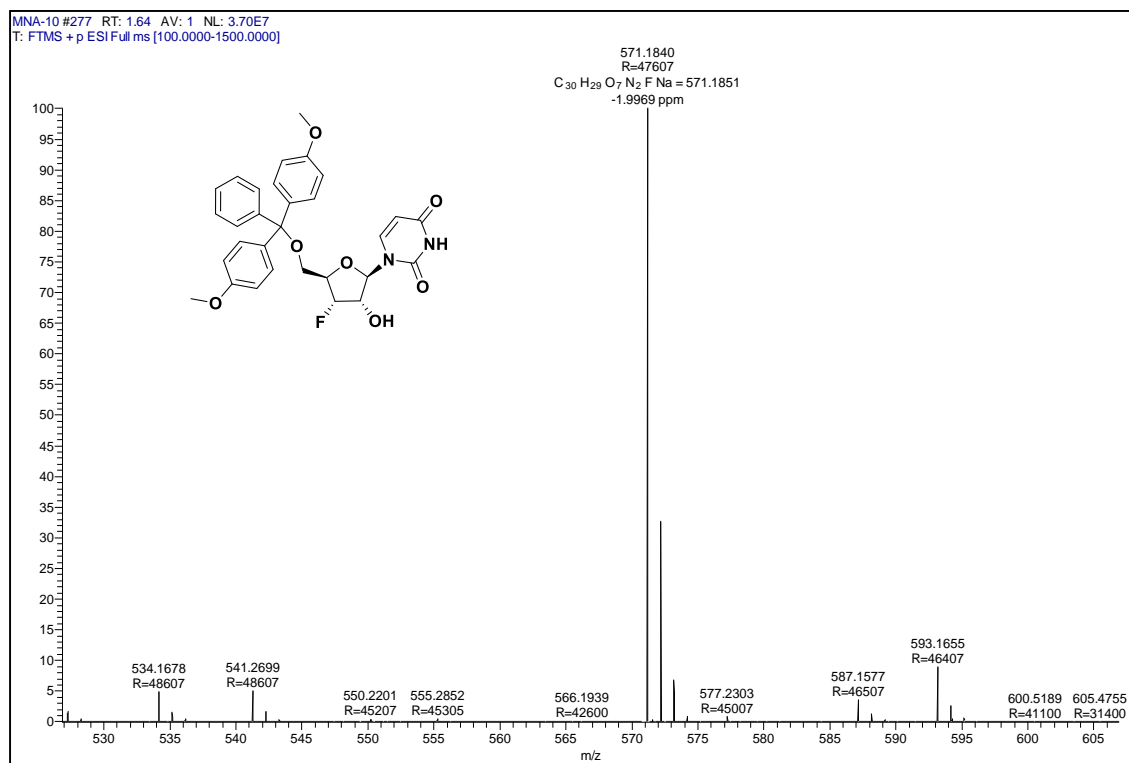
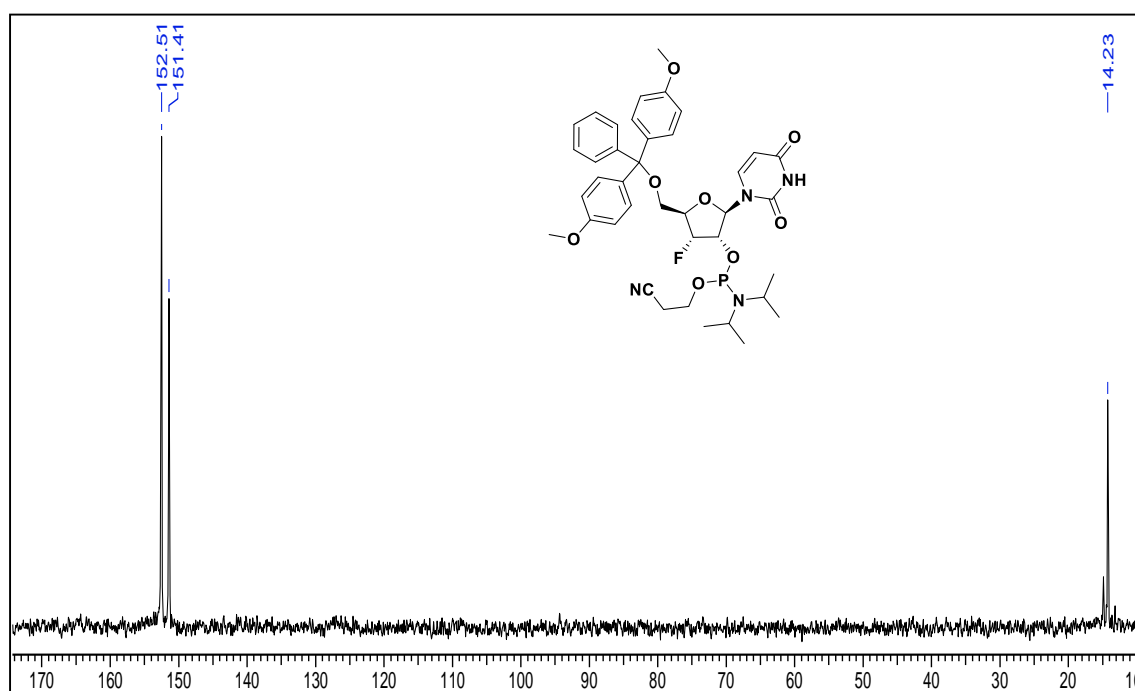
^{13}C NMR of compound 12 (CD_3OD) **^{13}C -DEPT of compound 12 (CD_3OD)**

HRMS spectrum of compound 12

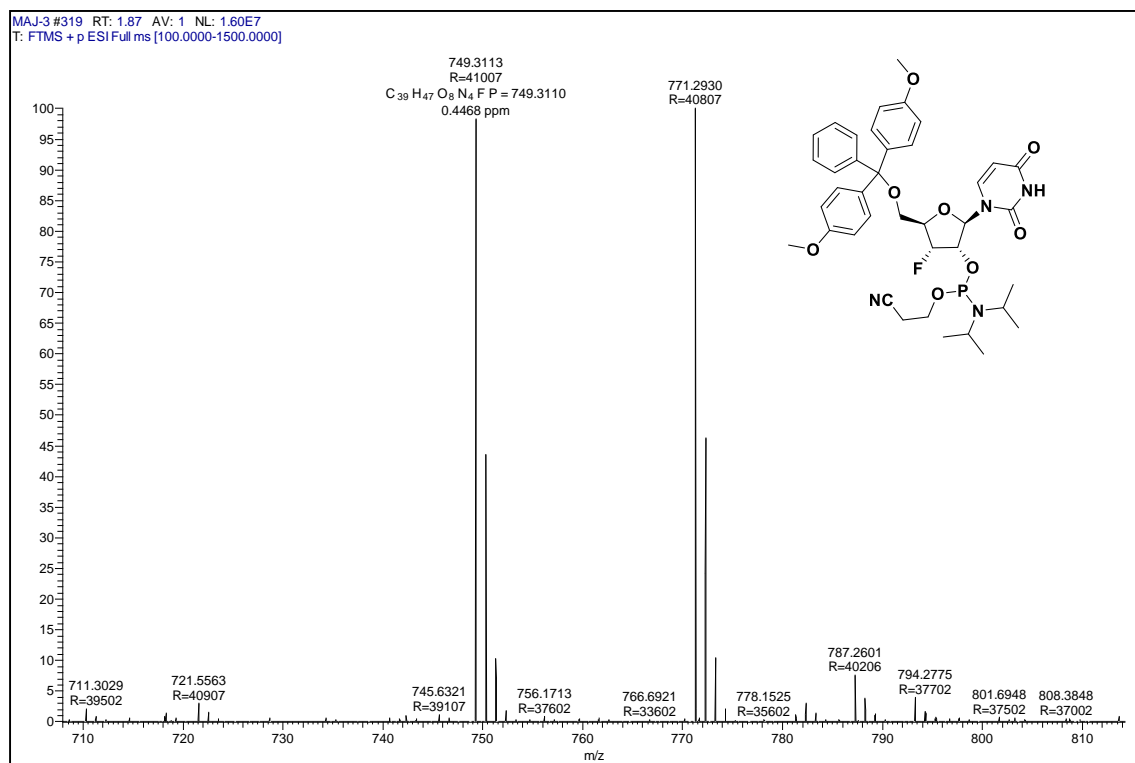
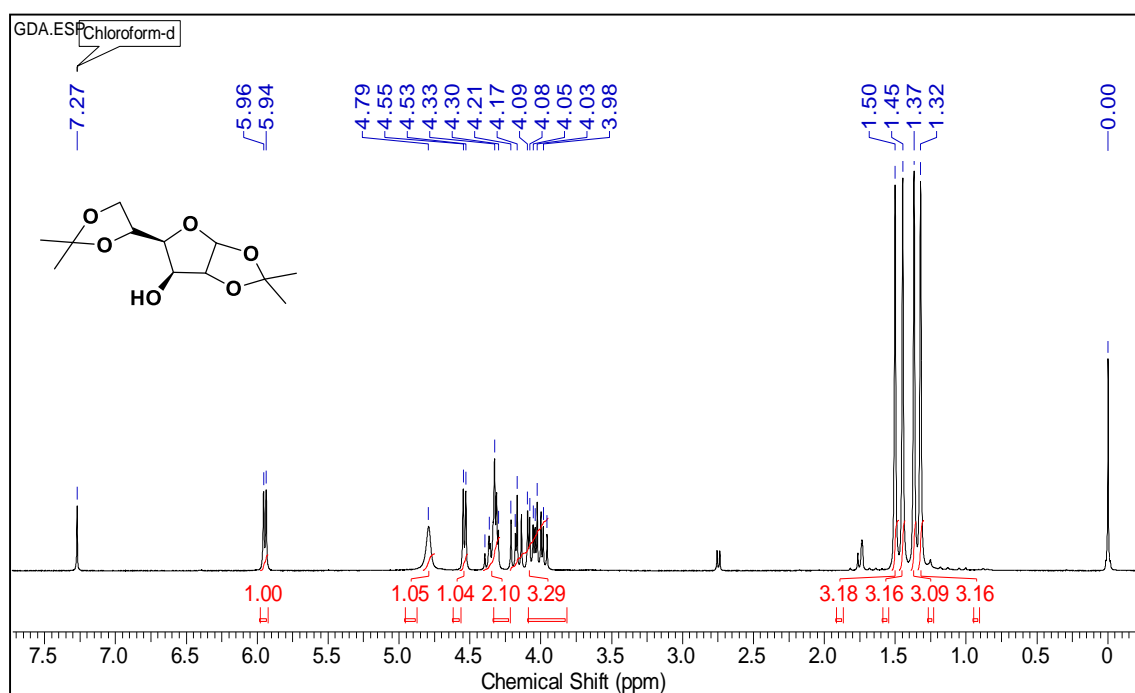
¹H NMR of compound 13 (CDCl₃)

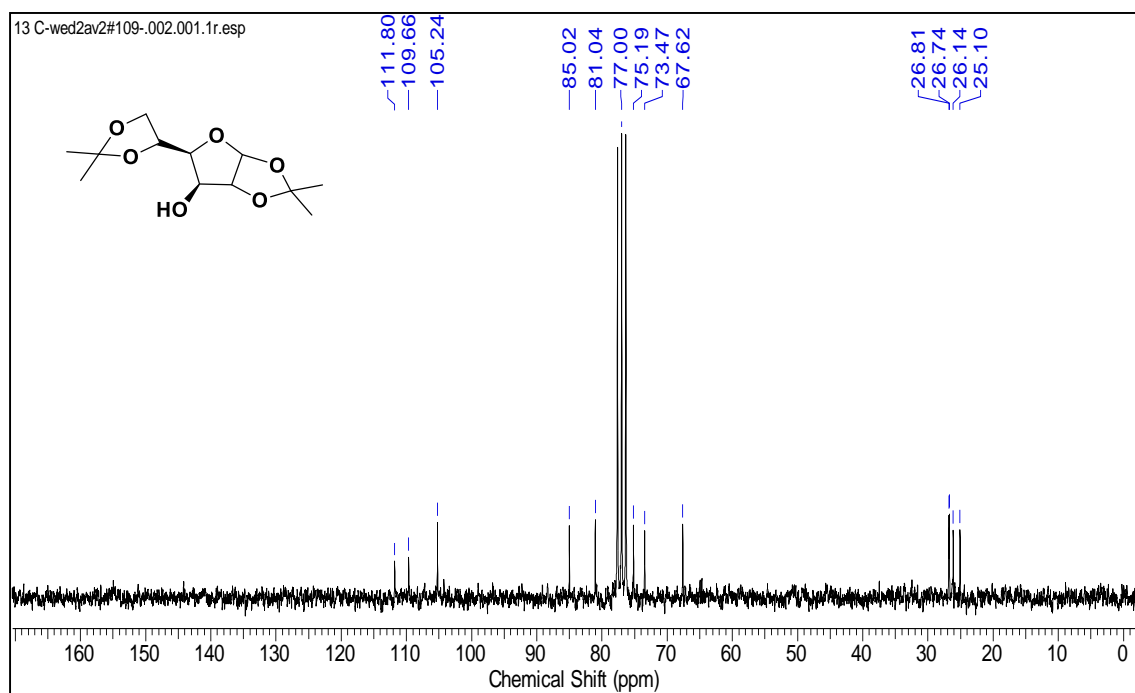
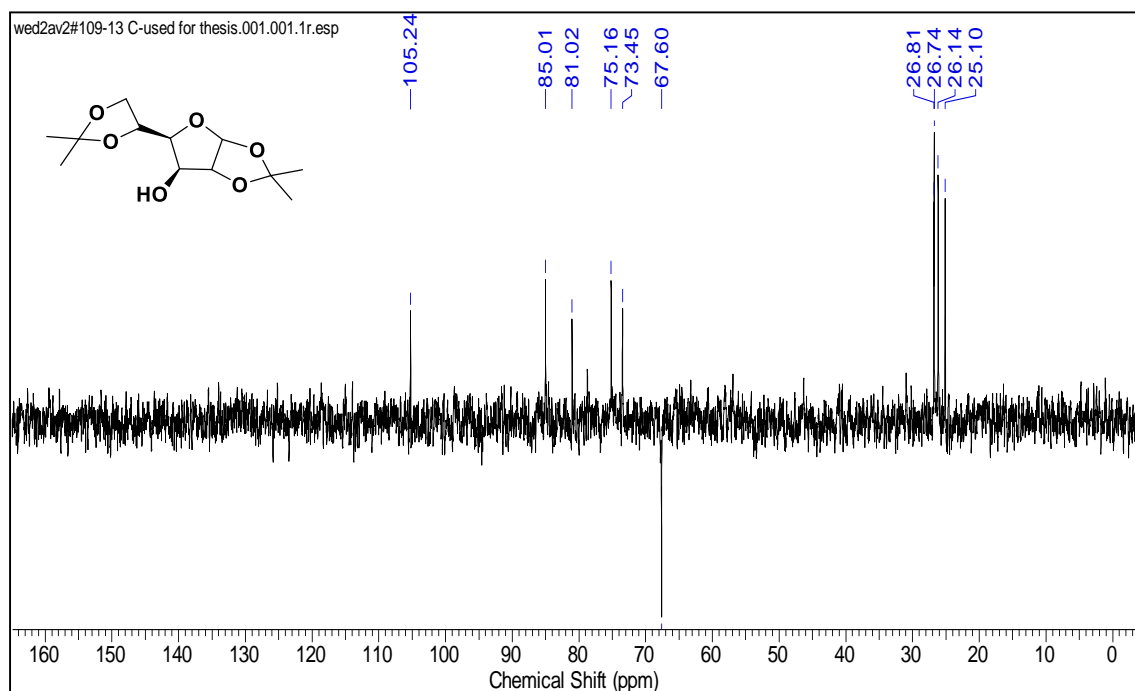
^{13}C NMR of compound 13 (CDCl_3) **^{13}C -DEPT of compound 13 (CDCl_3)**

HRMS spectrum of compound 13

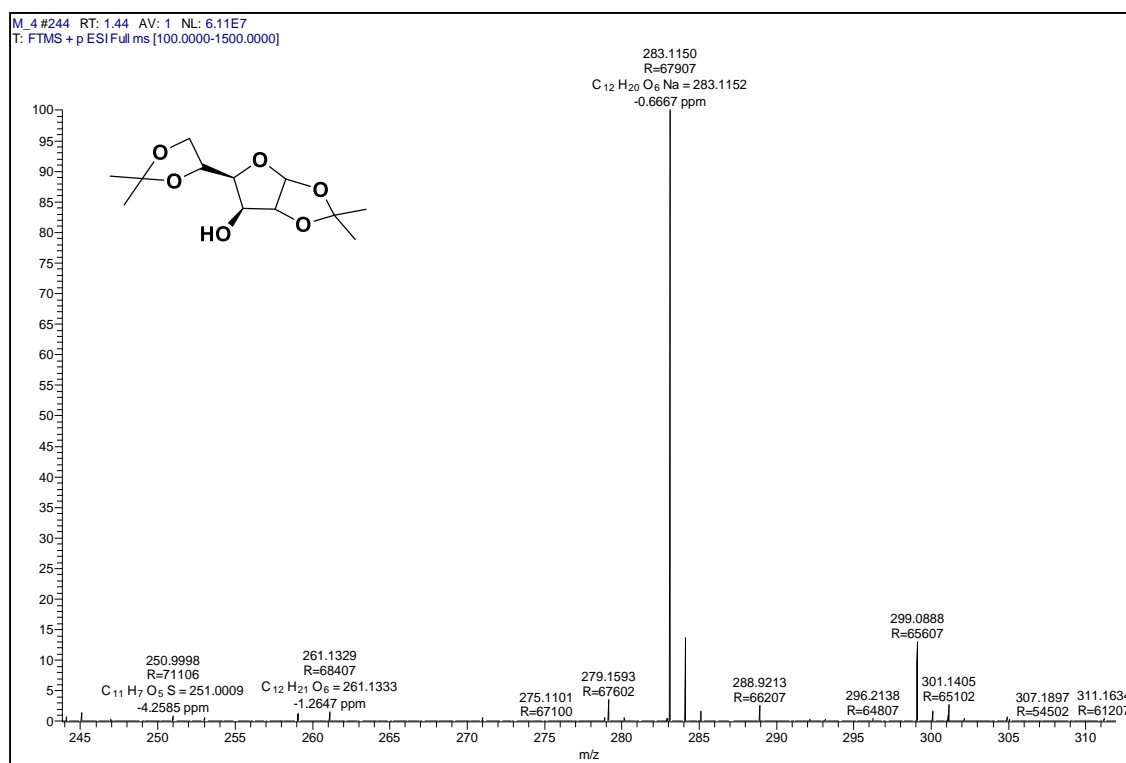
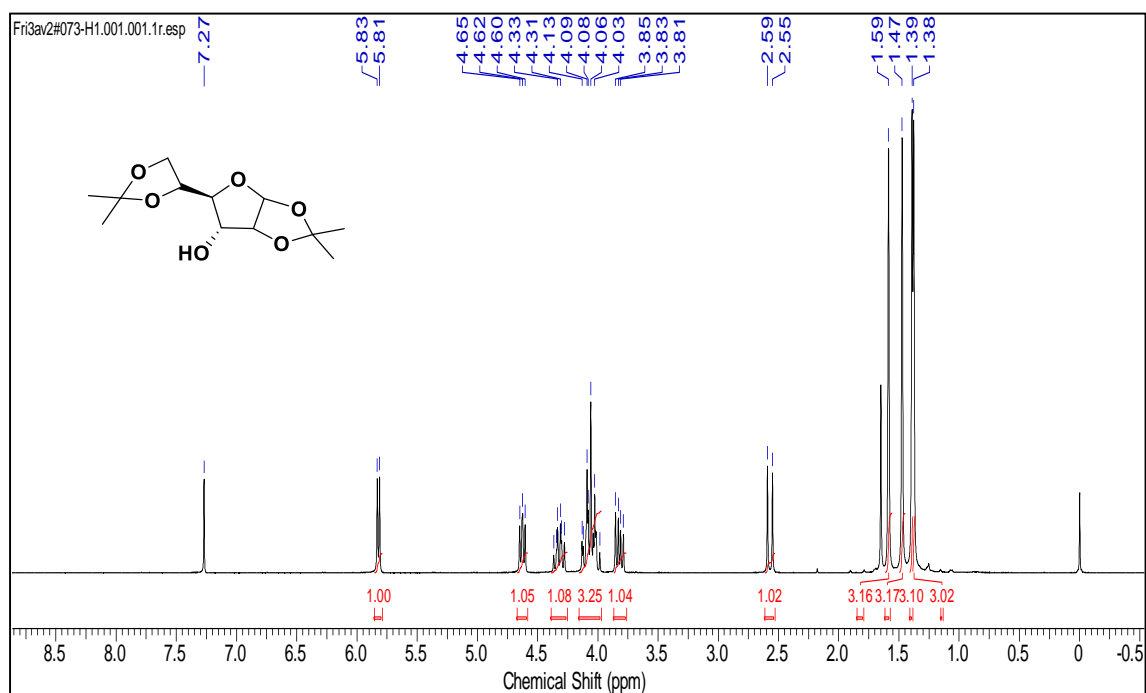
³¹P NMR of compound 14

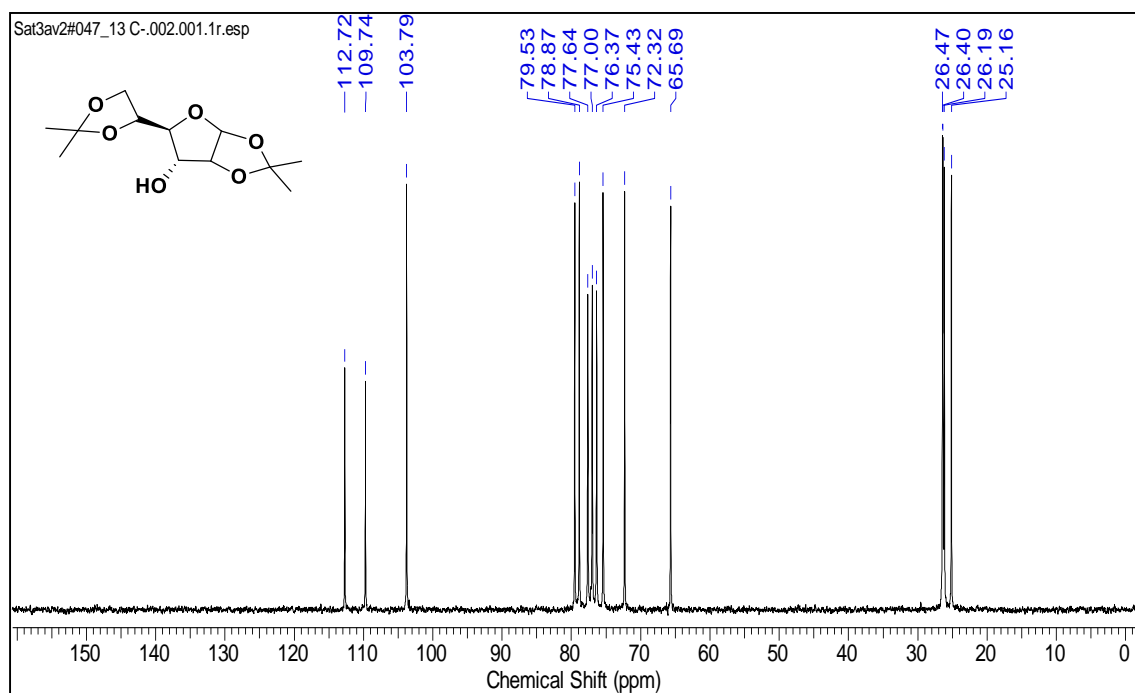
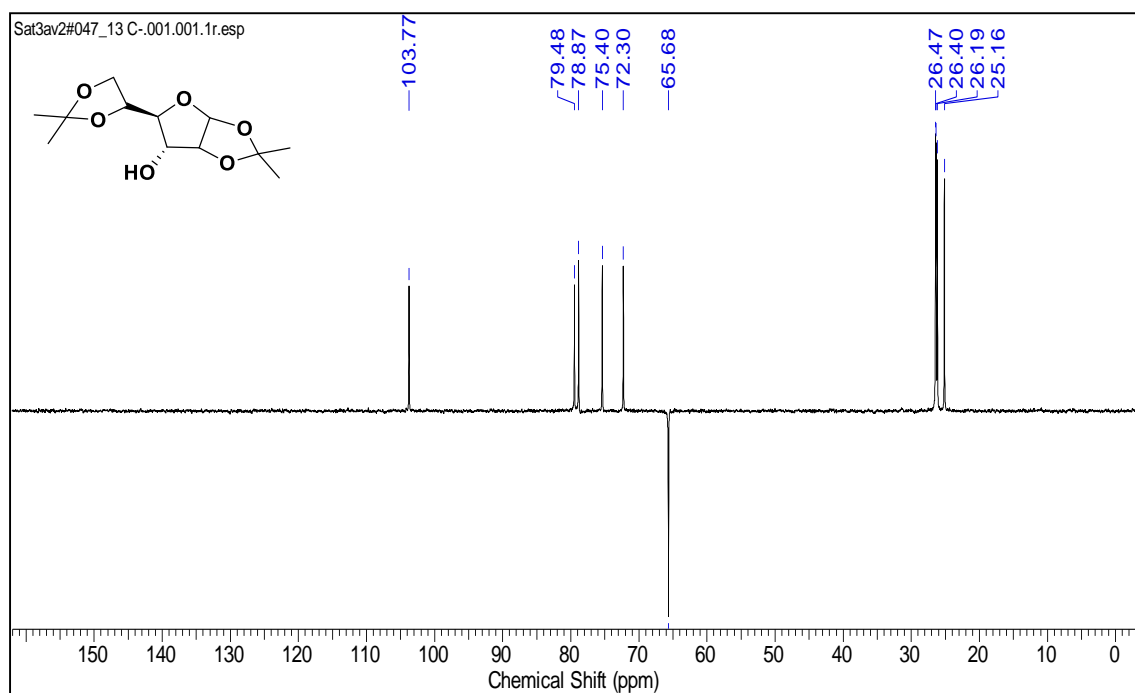
HRMS spectrum of Compound 14

¹H NMR of compound 16 (CDCl₃)

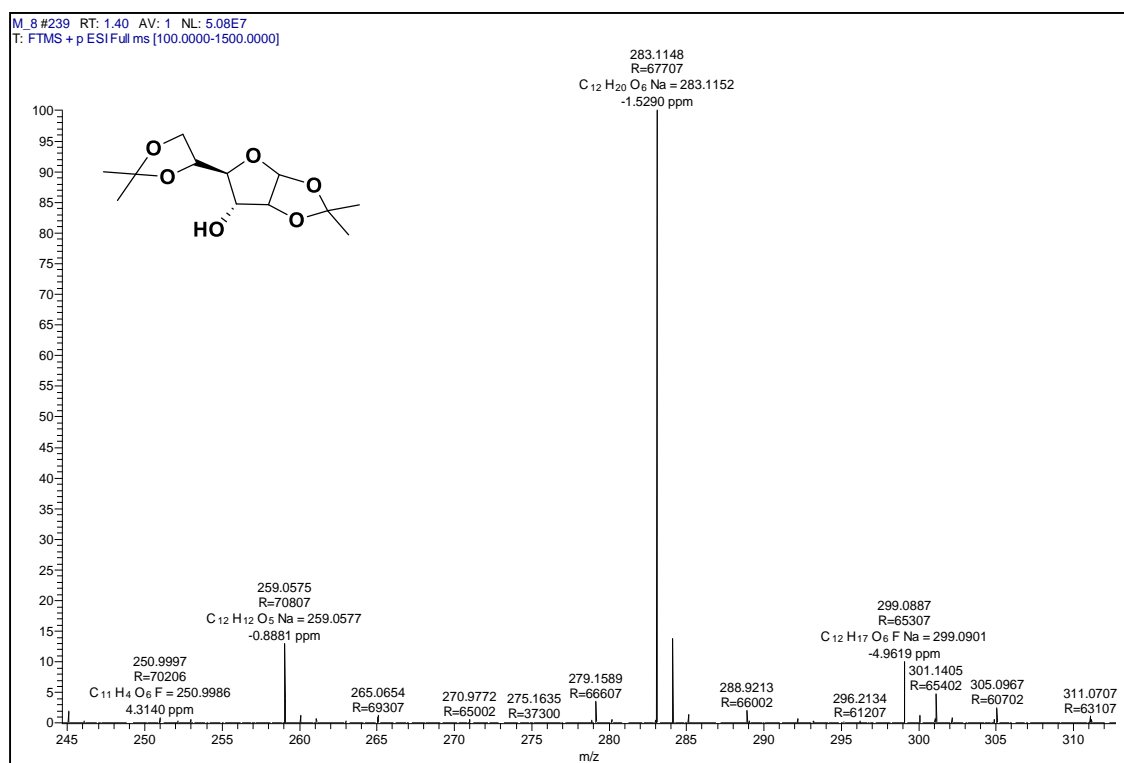
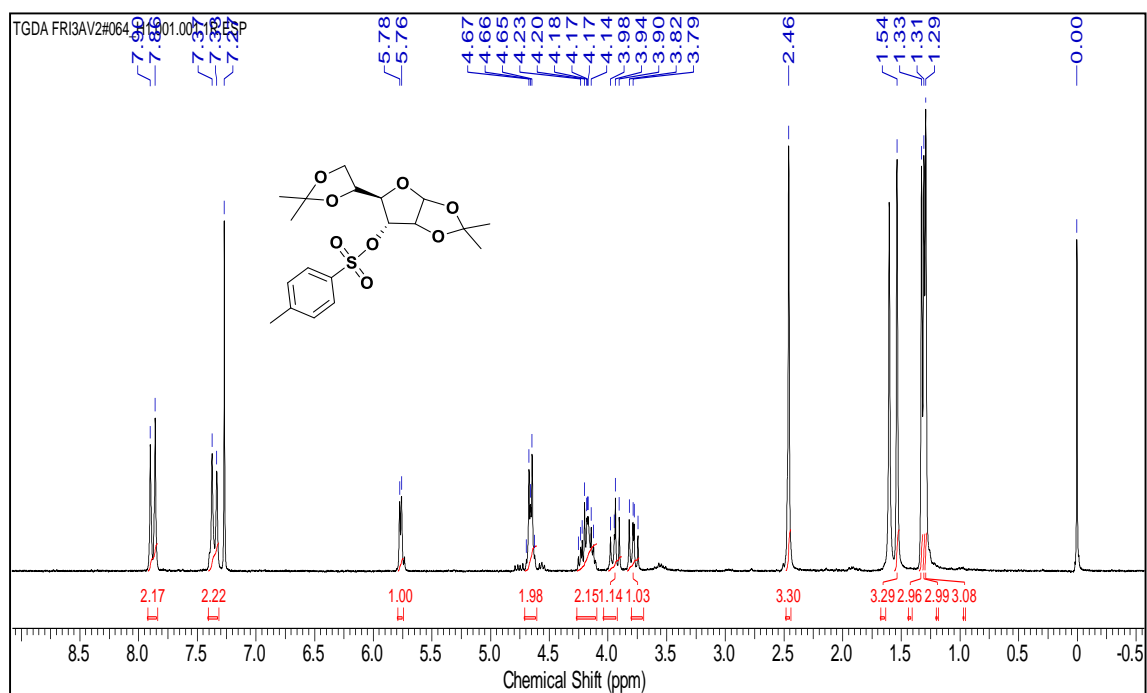
^{13}C NMR of compound 16 (CDCl_3) **^{13}C -DEPT of compound 16 (CDCl_3)**

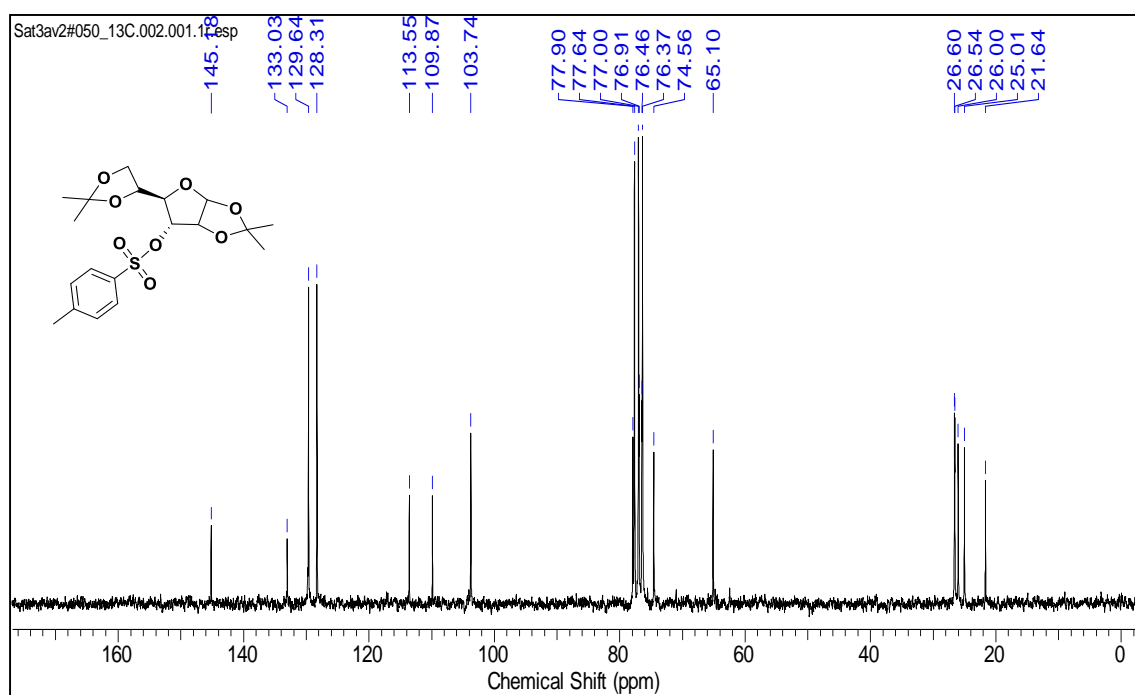
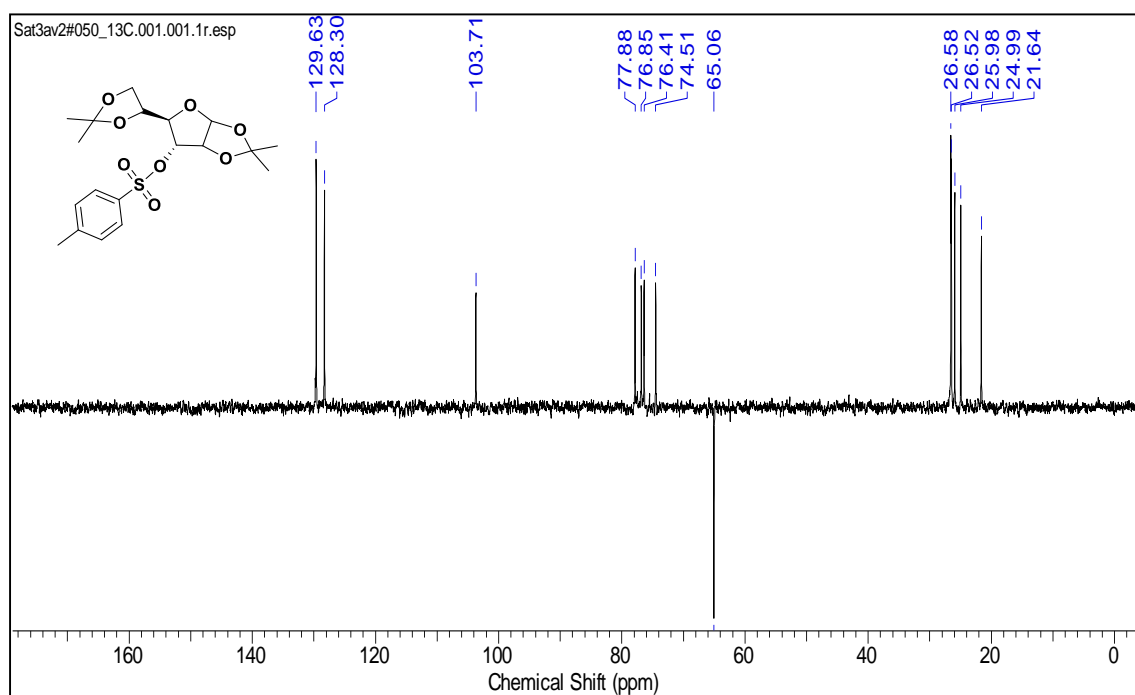
HRMS spectrum of compound 16

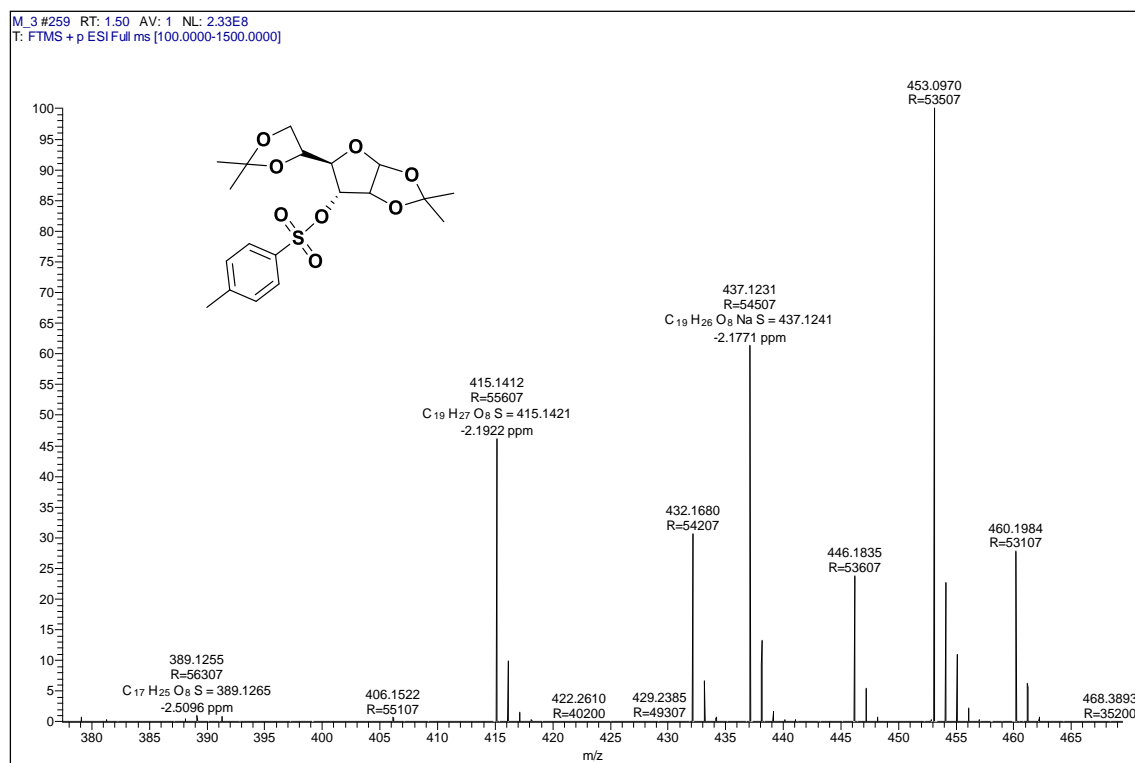
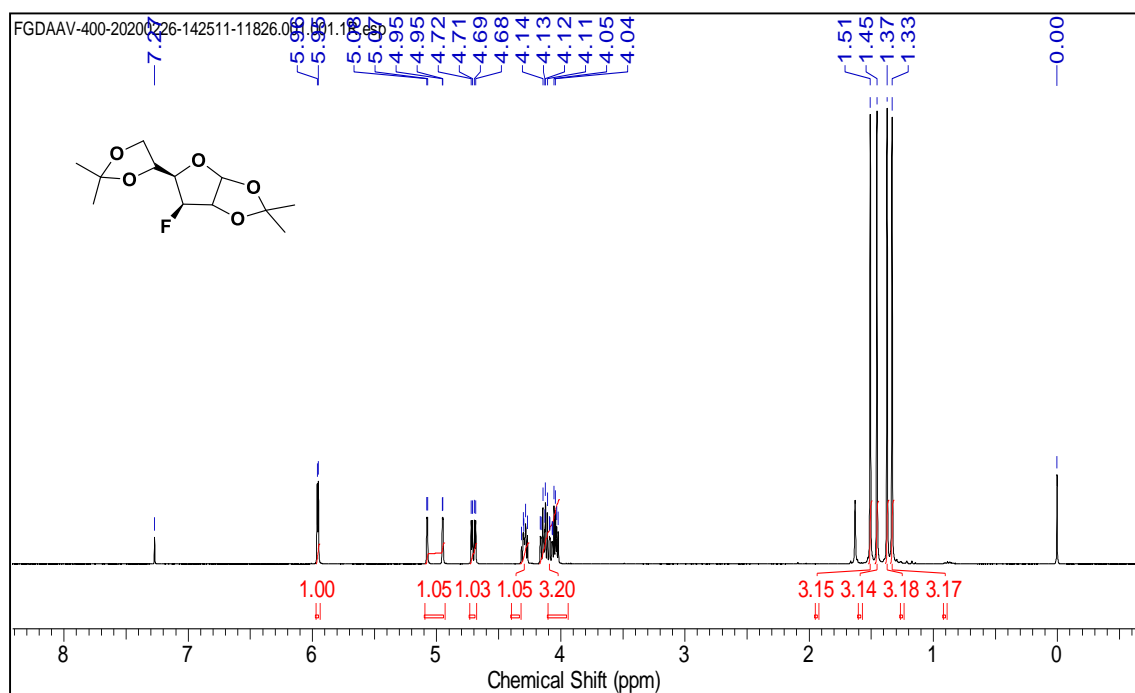
¹H NMR of compound 18 (CDCl₃)

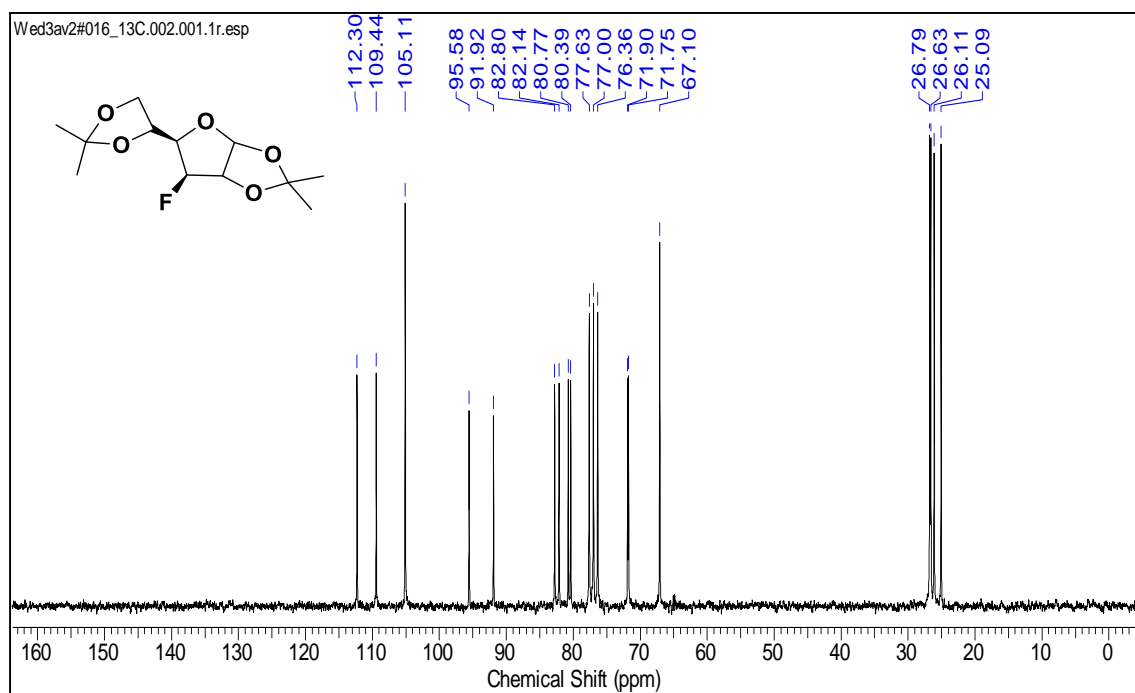
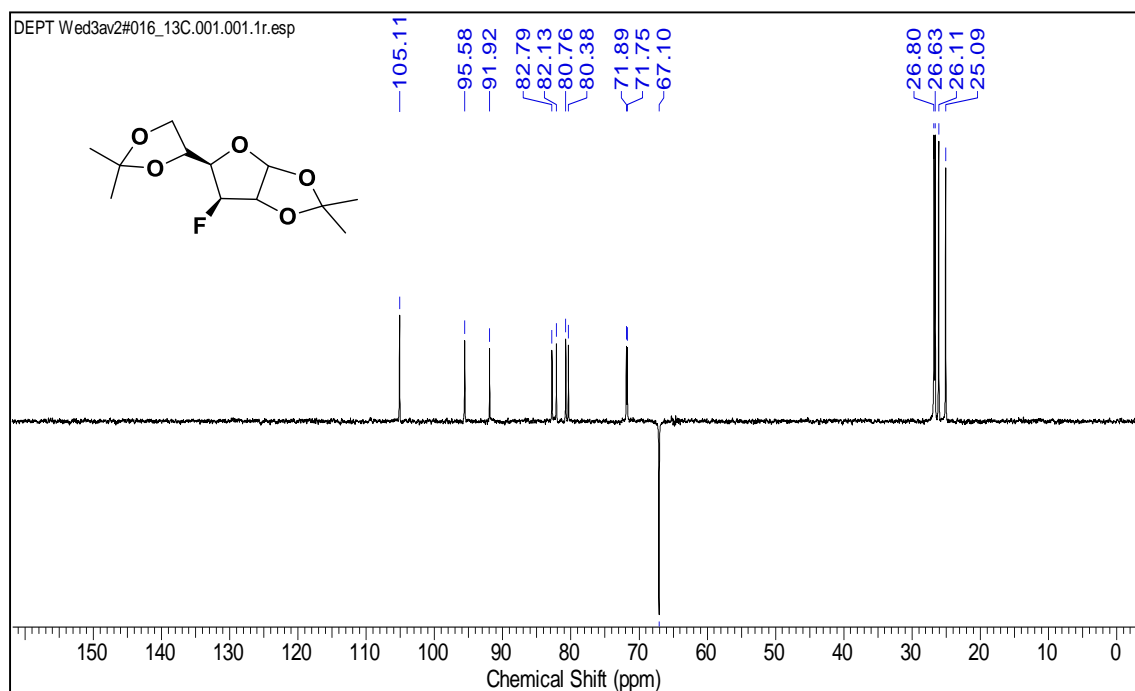
^{13}C NMR of compound 18 (CDCl_3) **^{13}C -DEPT of compound 18 (CDCl_3)**

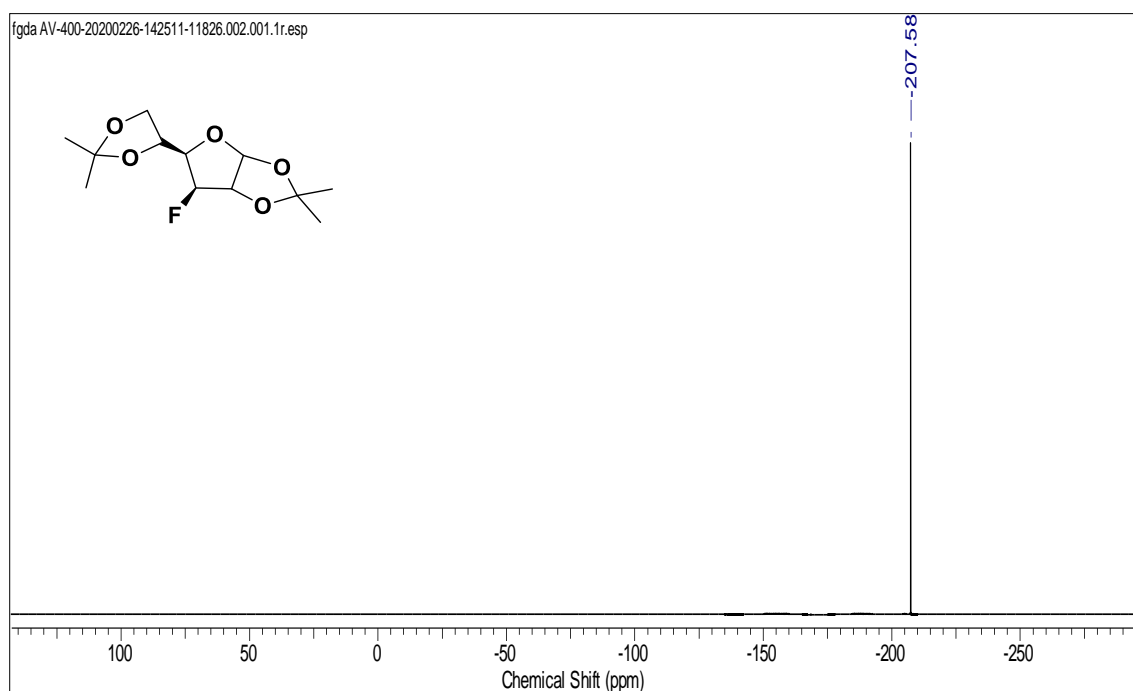
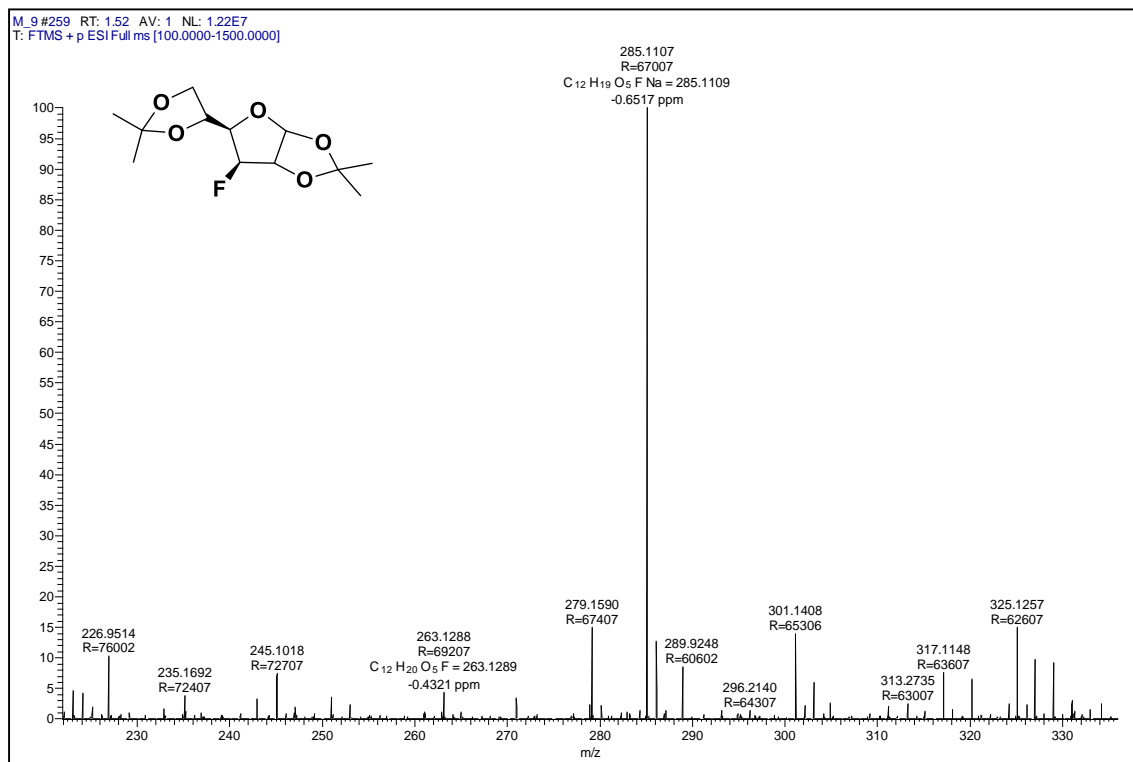
HRMS spectrum of compound 18

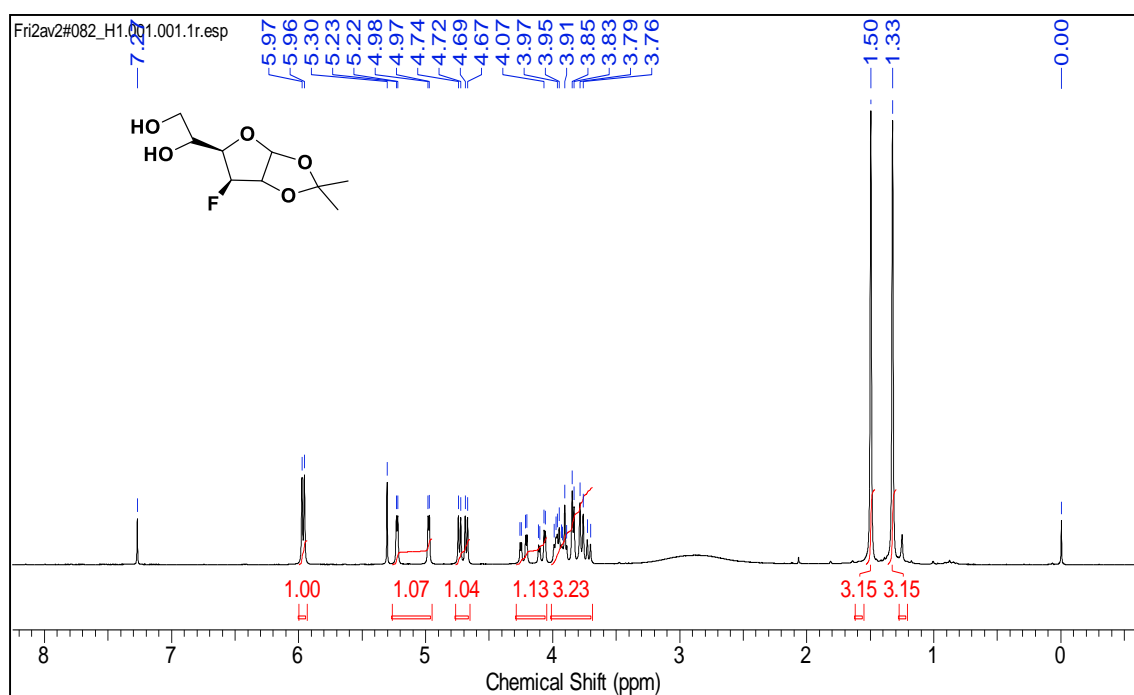
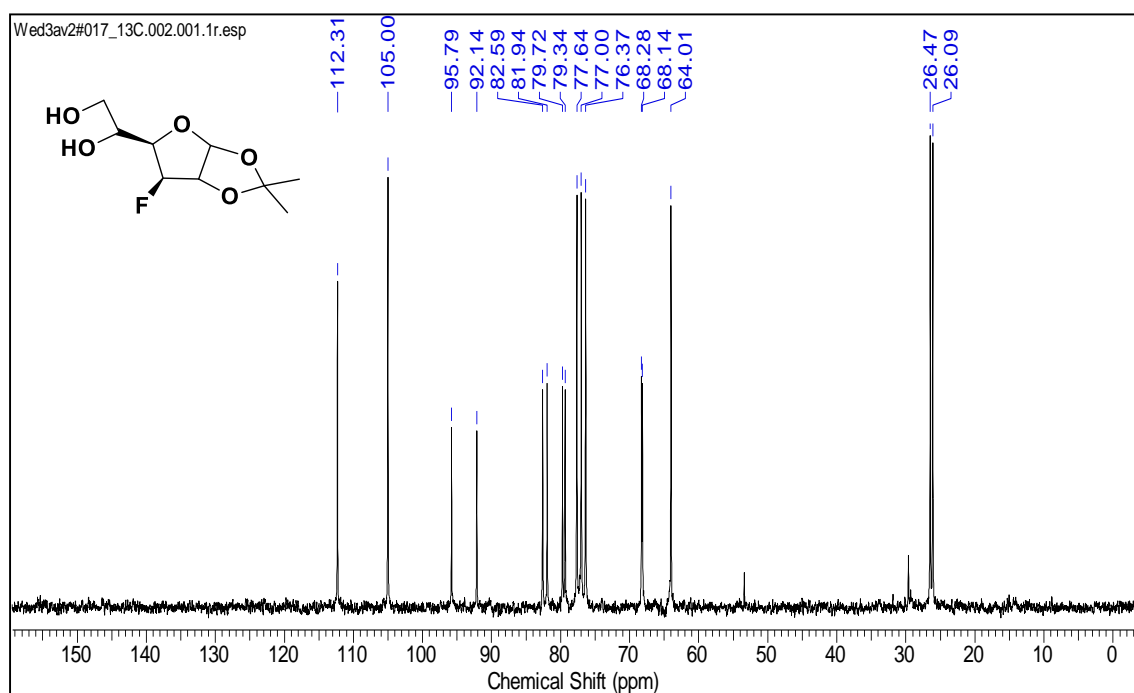
¹H NMR of compound 19 (CDCl₃)

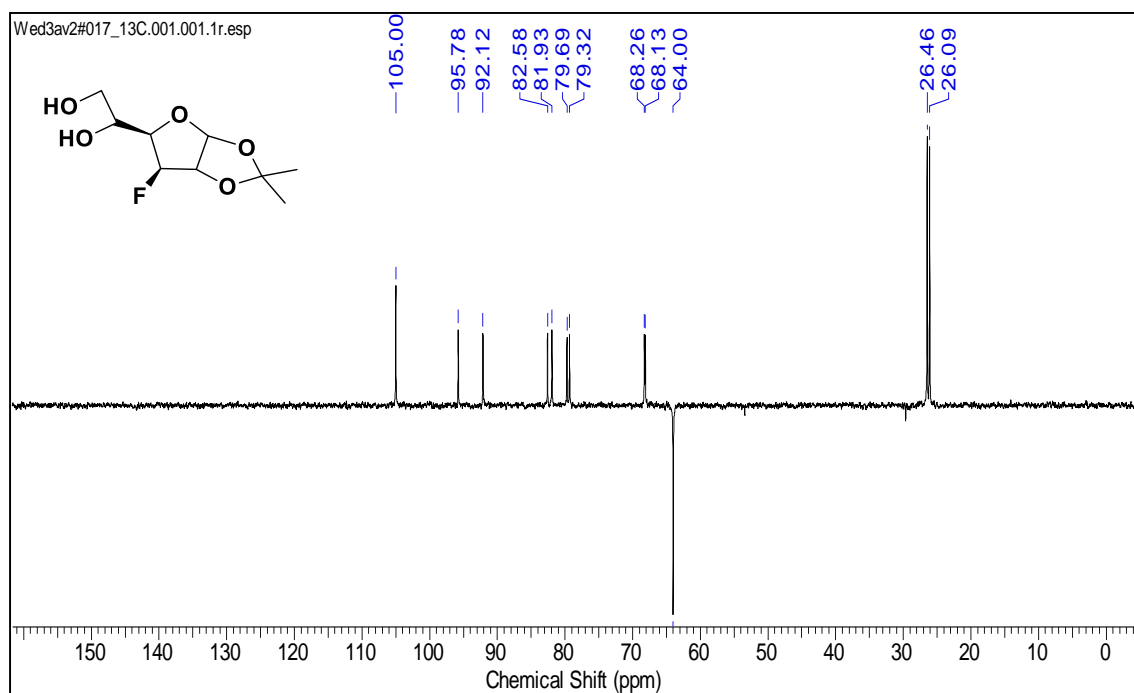
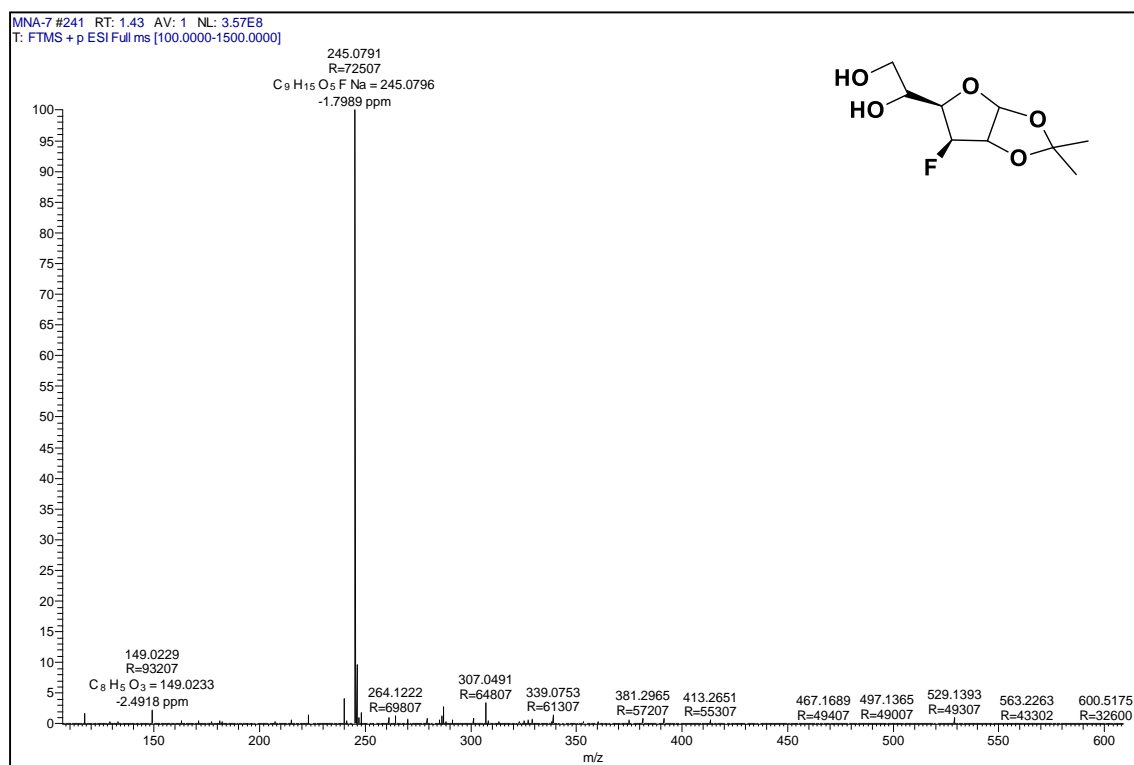
^{13}C NMR of compound 19 (CDCl_3) **^{13}C -DEPT of compound 19 (CDCl_3)**

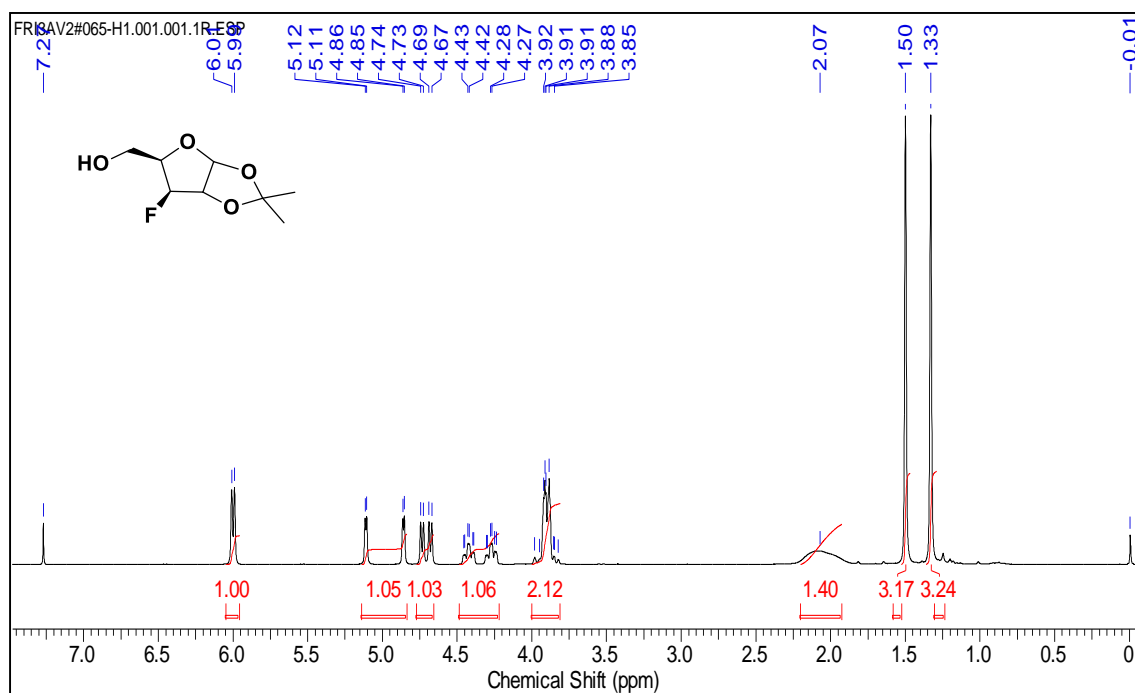
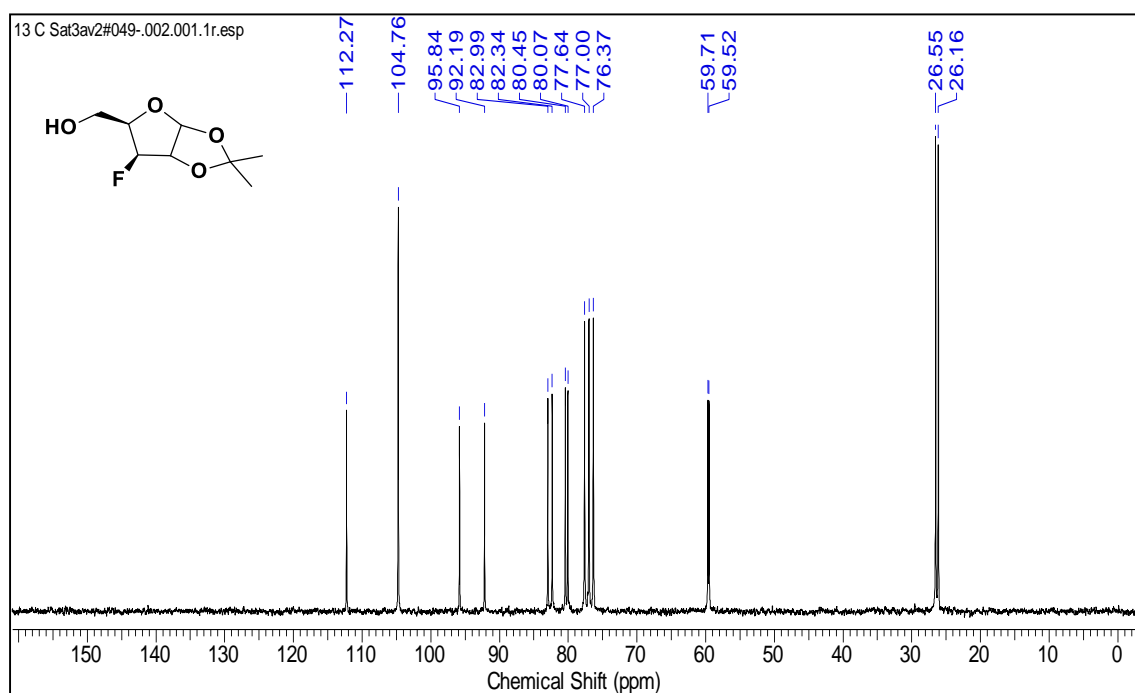
HRMS spectrum of compound 19 (CDCl₃)¹H NMR of compound 20 (CDCl₃)

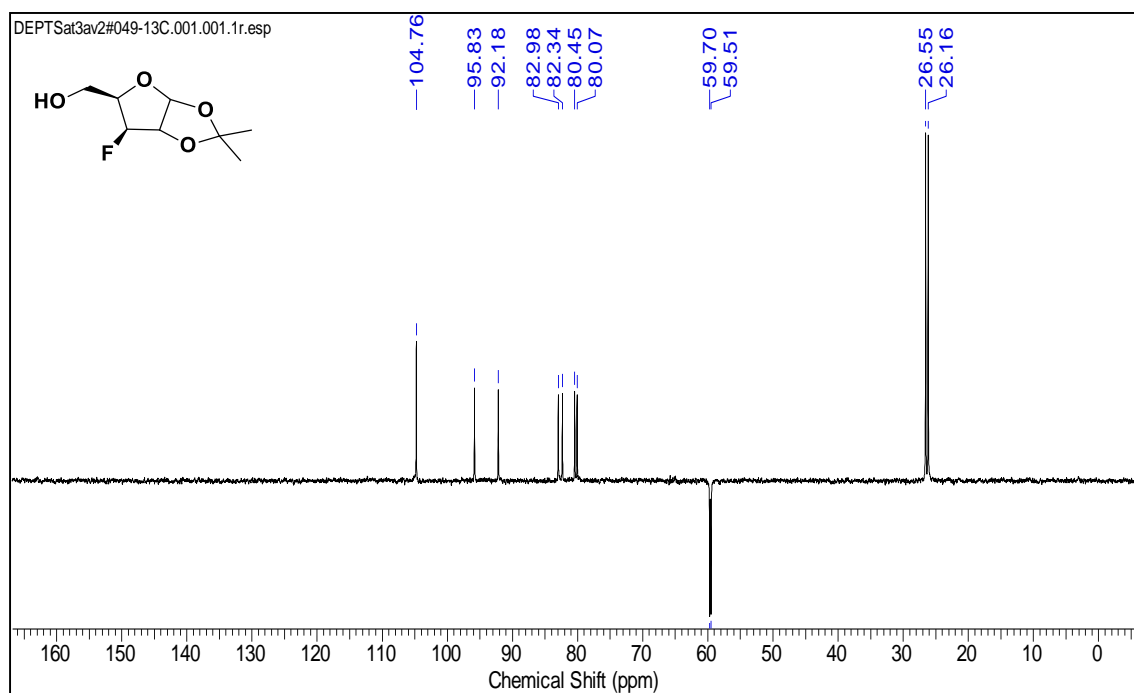
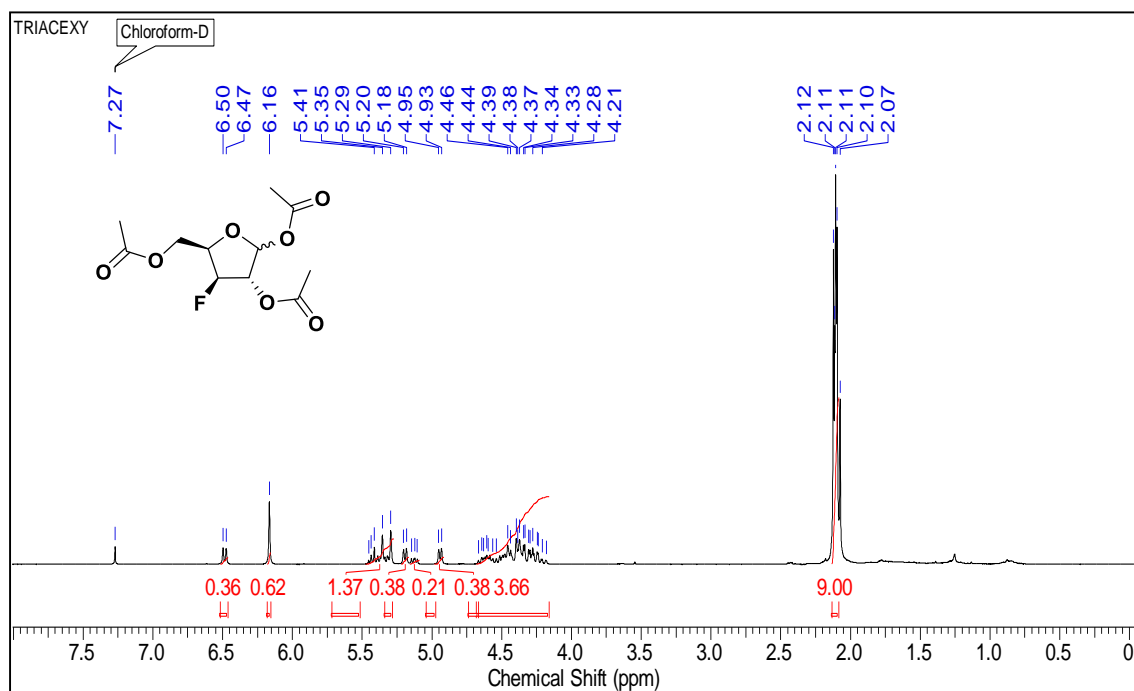
^{13}C NMR of compound 20 (CDCl_3) **^{13}C -DEPT of compound 20 (CDCl_3)**

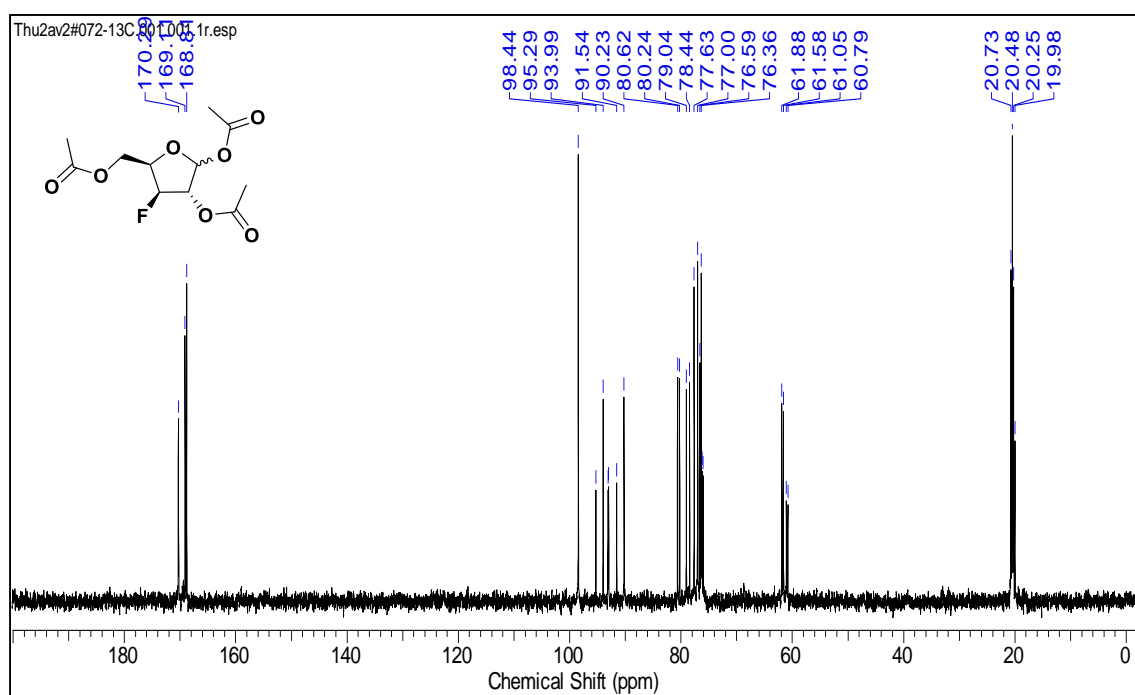
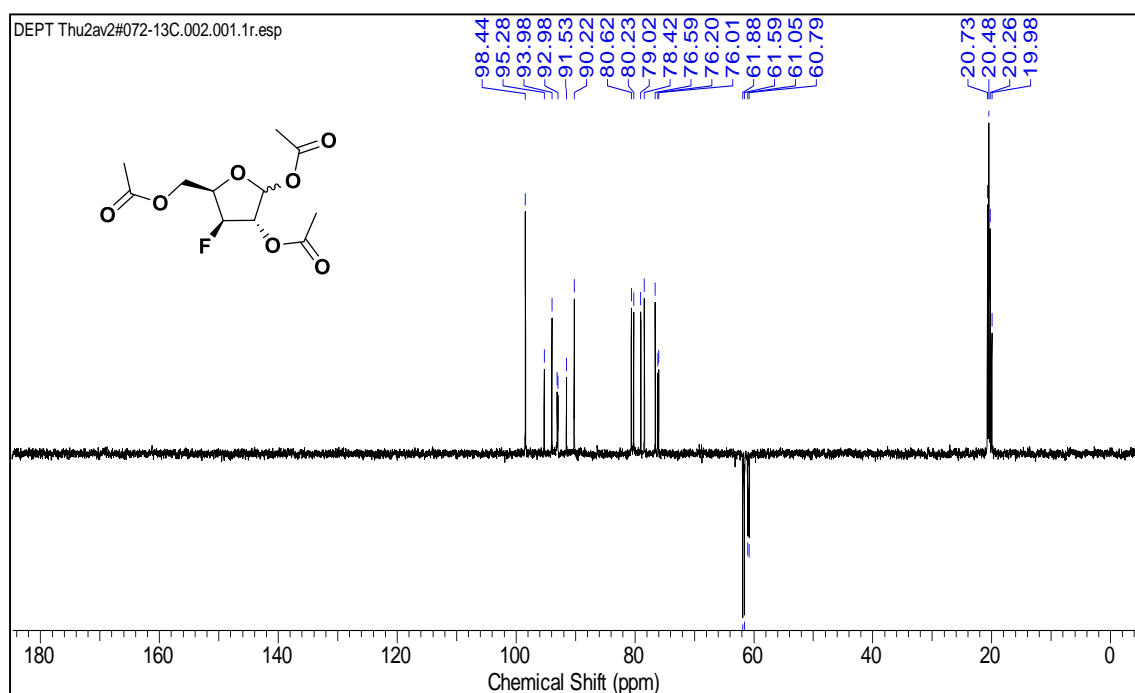
^{19}F NMR of compound 20 (CDCl_3)**HRMS spectrum of compound 20**

^1H NMR of compound 21 (CDCl_3) **^{13}C NMR of compound 21 (CDCl_3)**

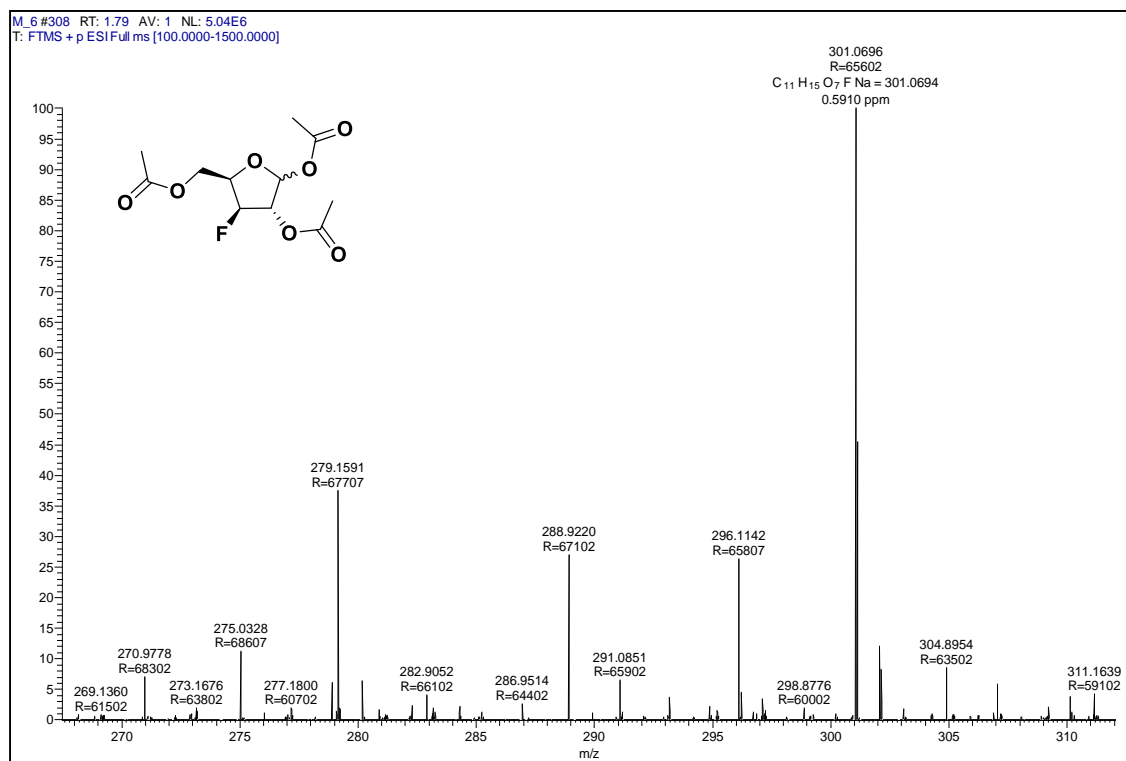
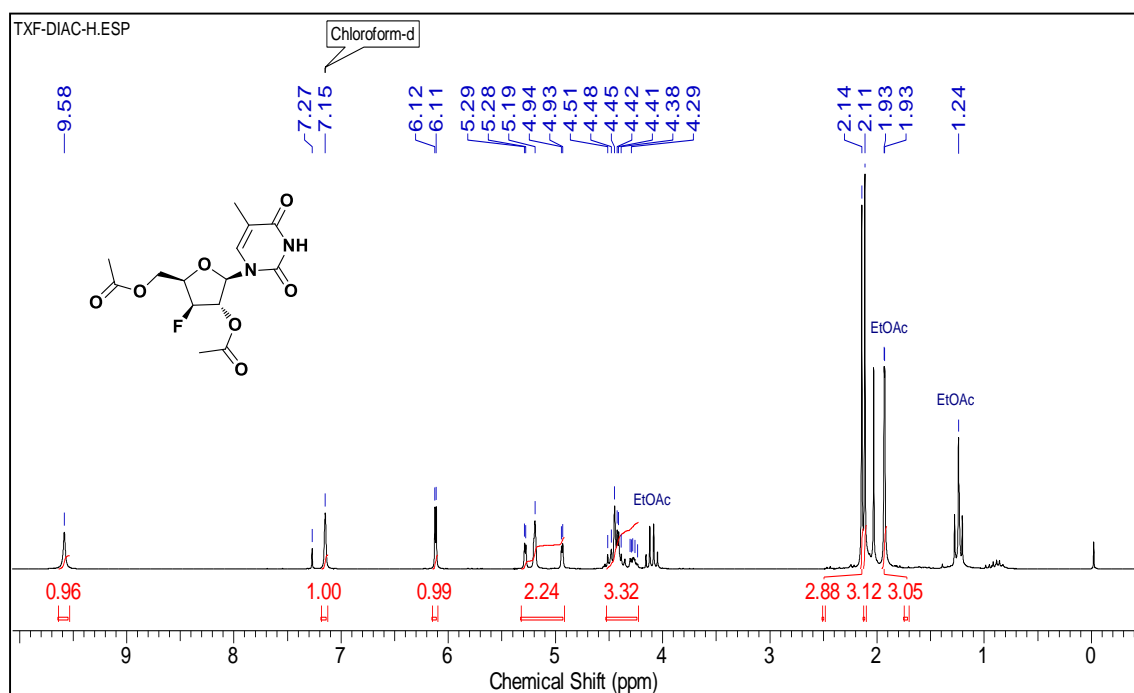
^{13}C -DEPT of compound 21 (CDCl_3)**HRMS spectrum of compound 21**

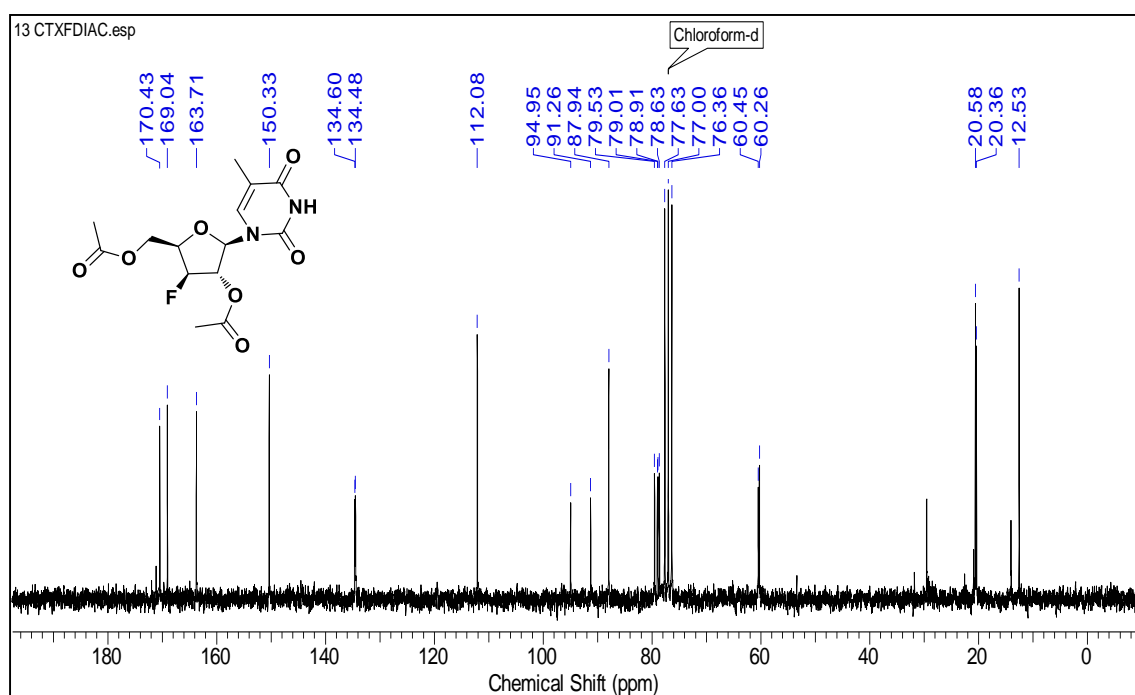
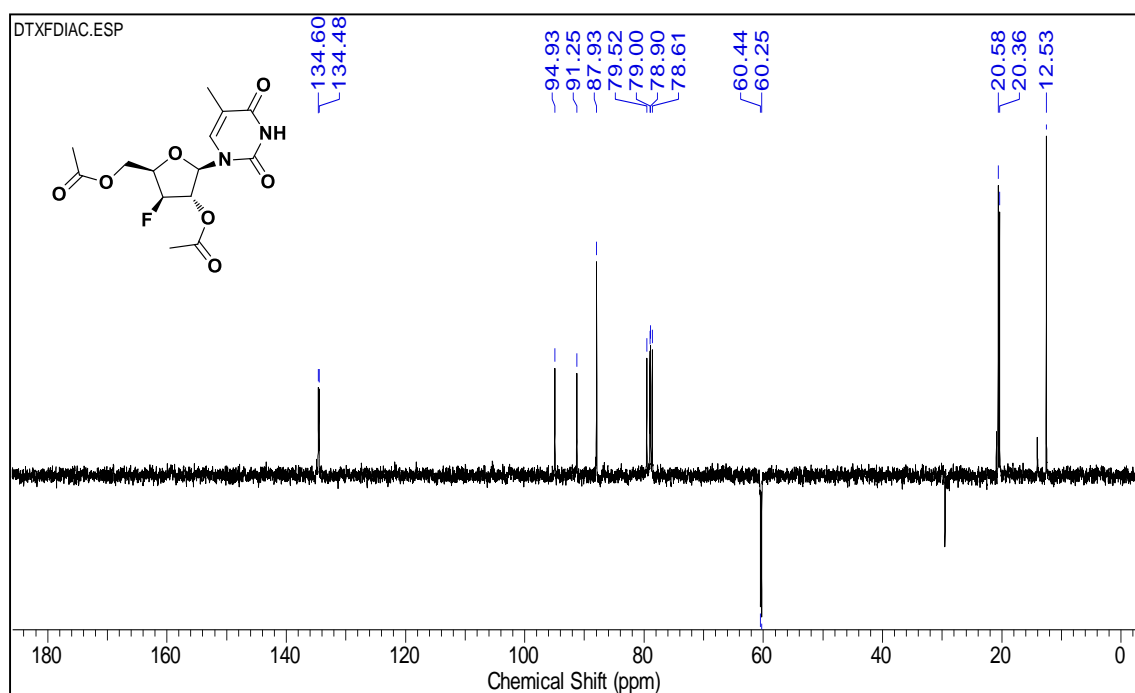
^1H NMR of compound 22 (CDCl_3) **^{13}C NMR of compound 22 (CDCl_3)**

^{13}C -DEPT of compound 22 (CDCl_3) **^1H NMR of compound 23 (CDCl_3)**

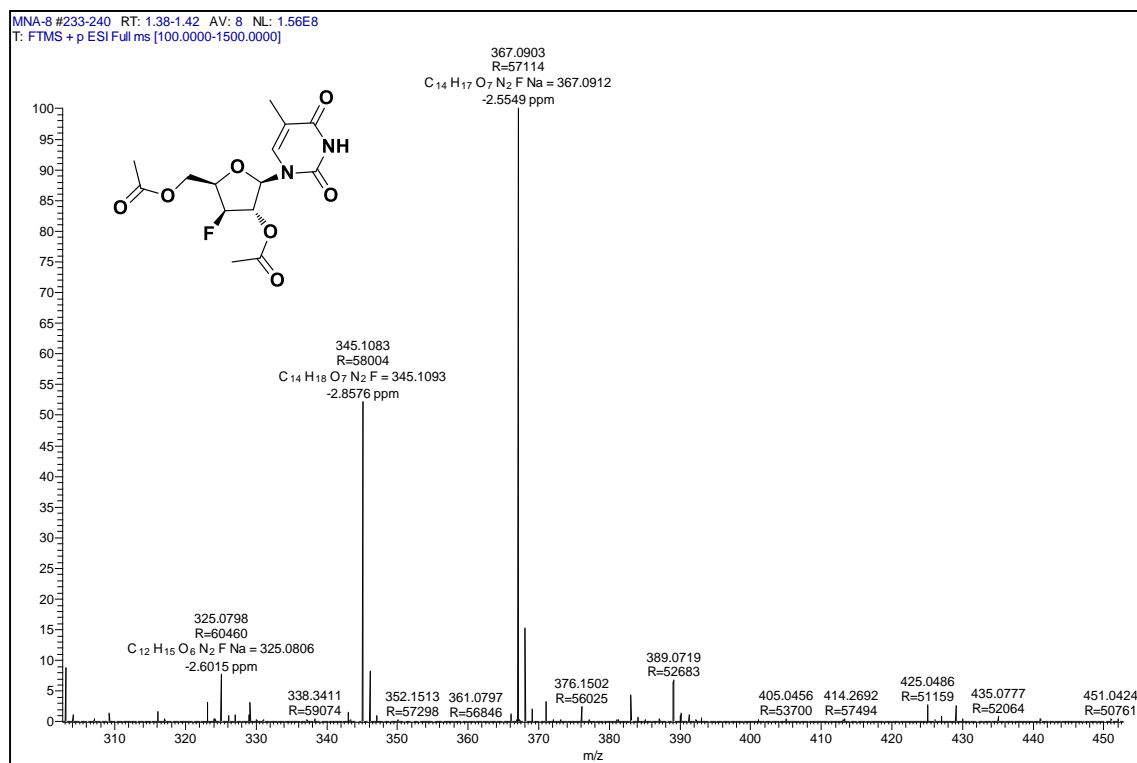
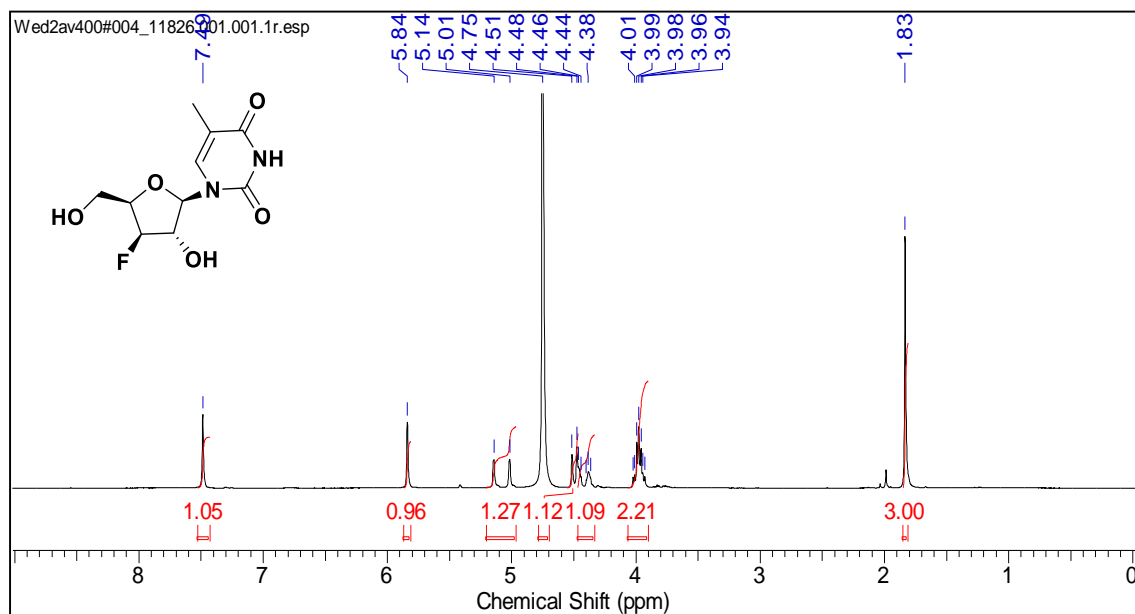
^{13}C NMR of compound 23 (CDCl_3) **^{13}C -DEPT of compound 23 (CDCl_3)**

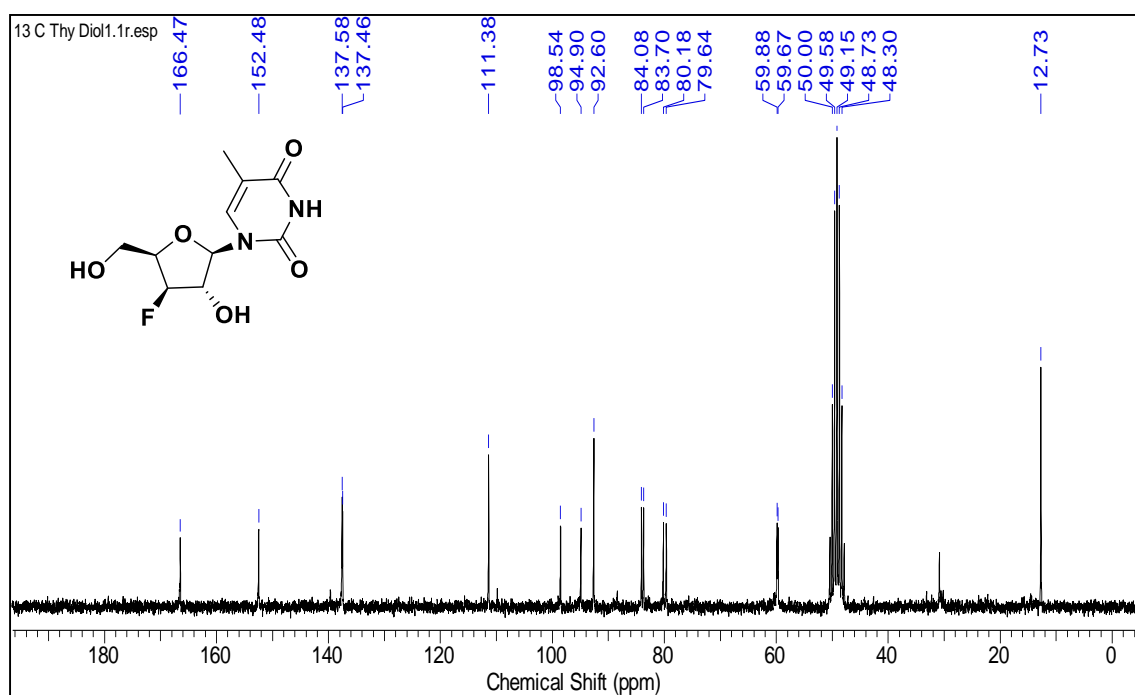
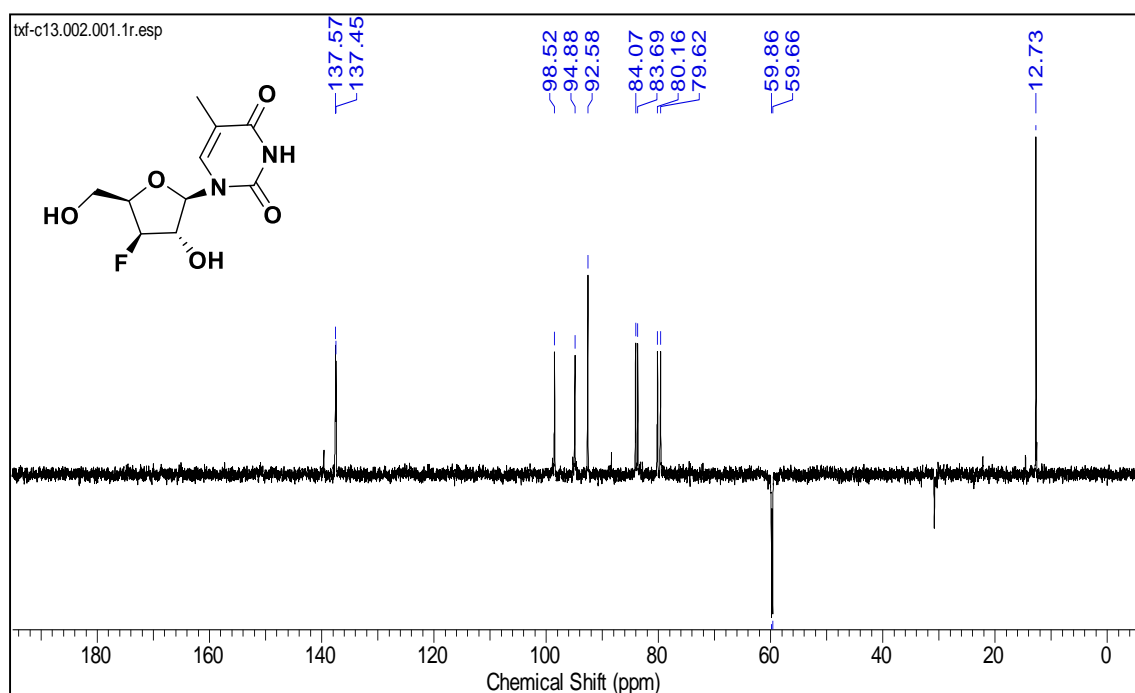
HRMS spectrum of compound 23

 ^1H NMR of compound 24 (CDCl_3)

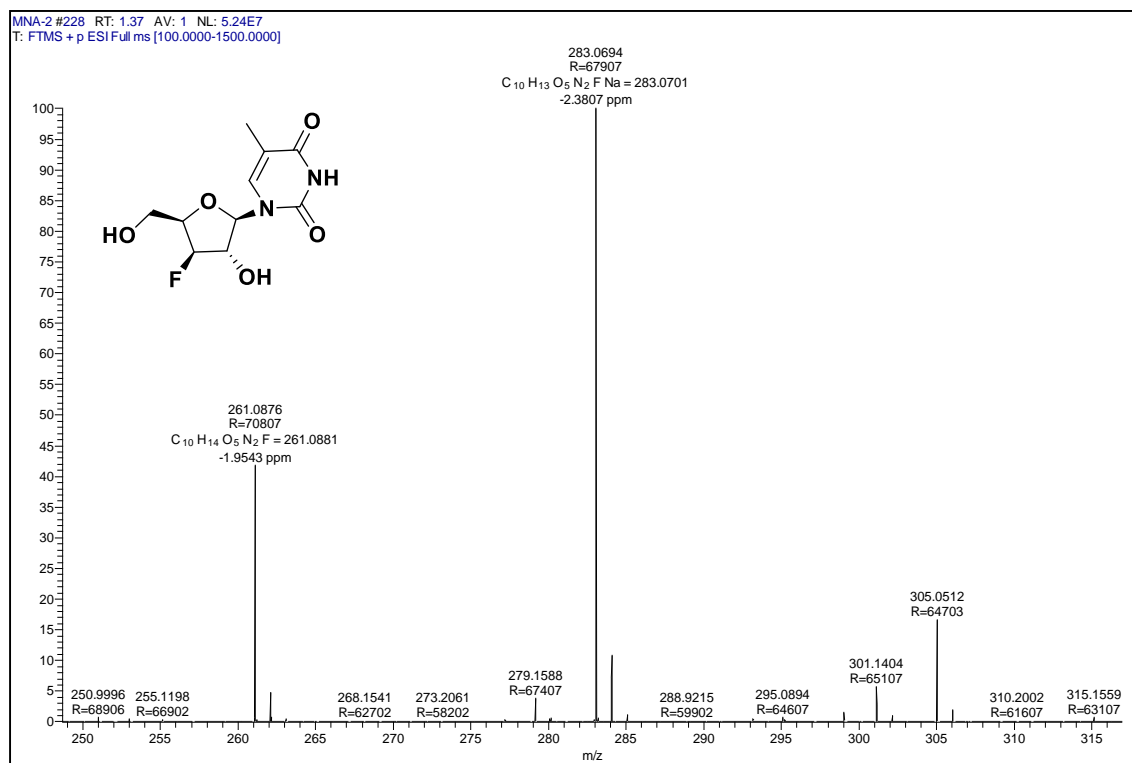
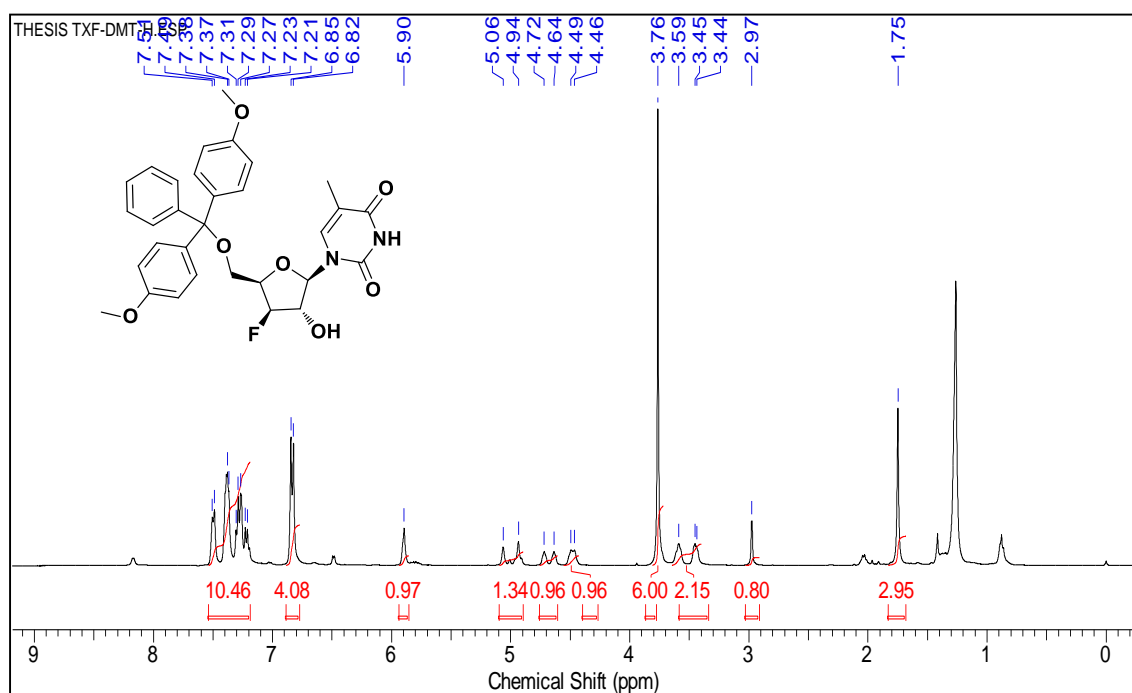
^{13}C NMR of compound 24 (CDCl_3) ^{13}C -DEPT of compound 24 (CDCl_3)

HRMS spectrum of compound 24

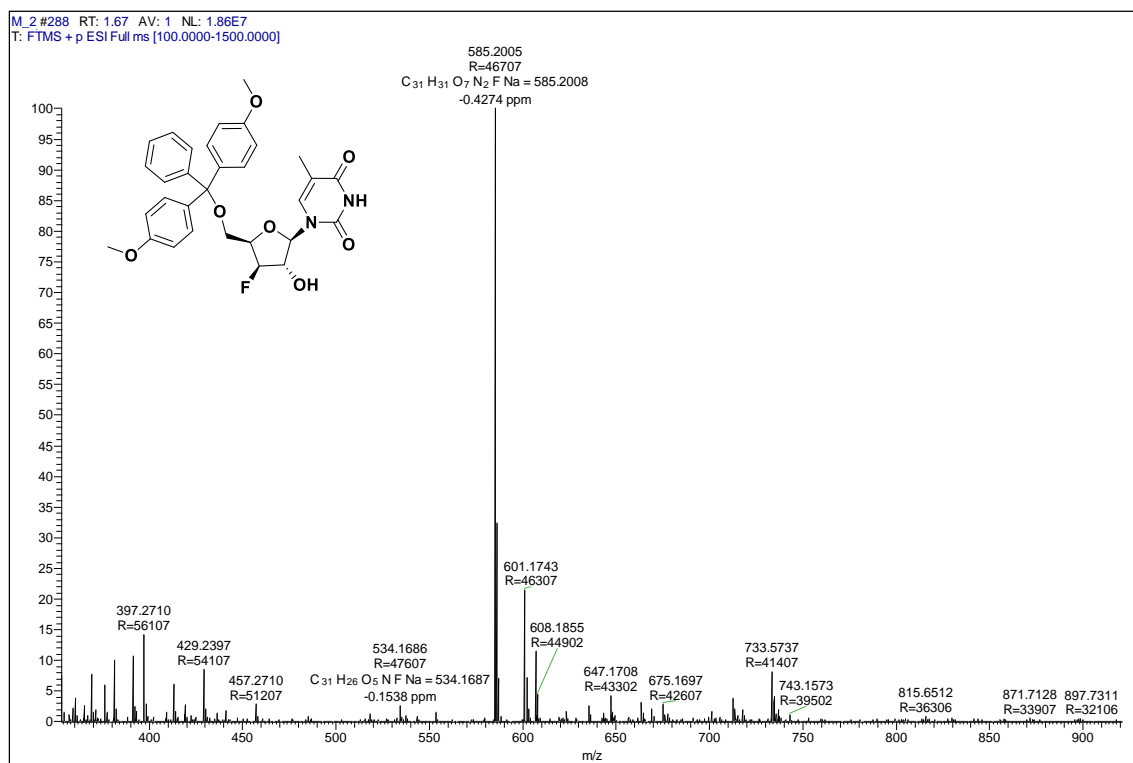
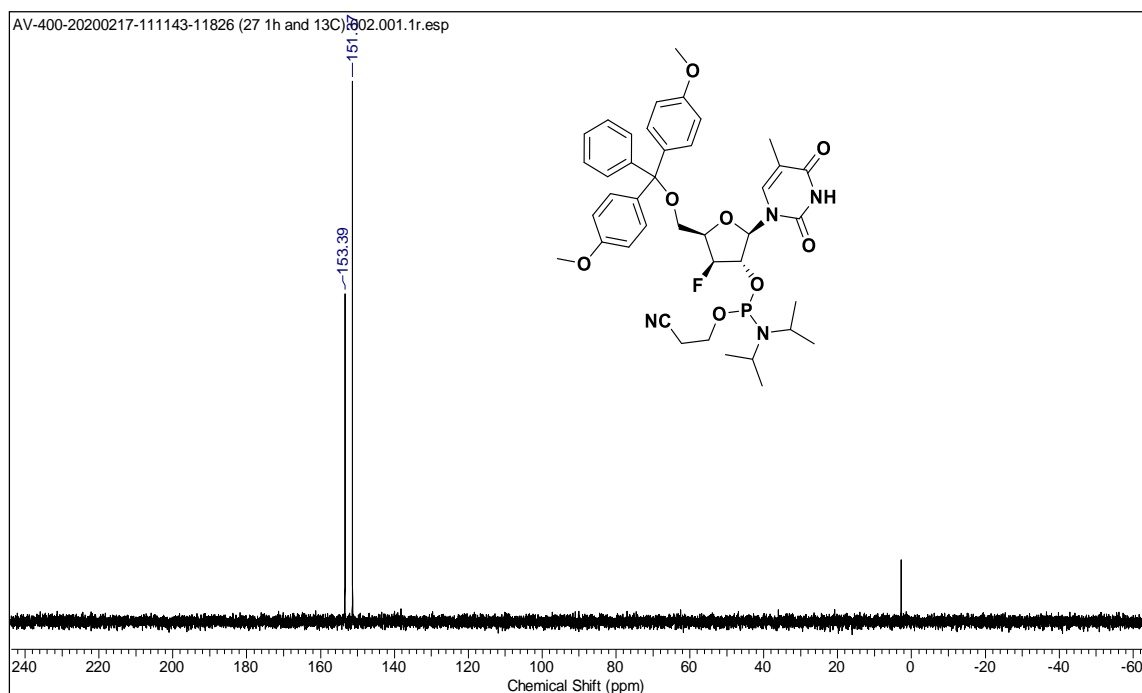
¹H NMR of compound 25 (CD₃OD)

^{13}C NMR of compound 25 (CD_3OD) **^{13}C -DEPT of compound 25 (CD_3OD)**

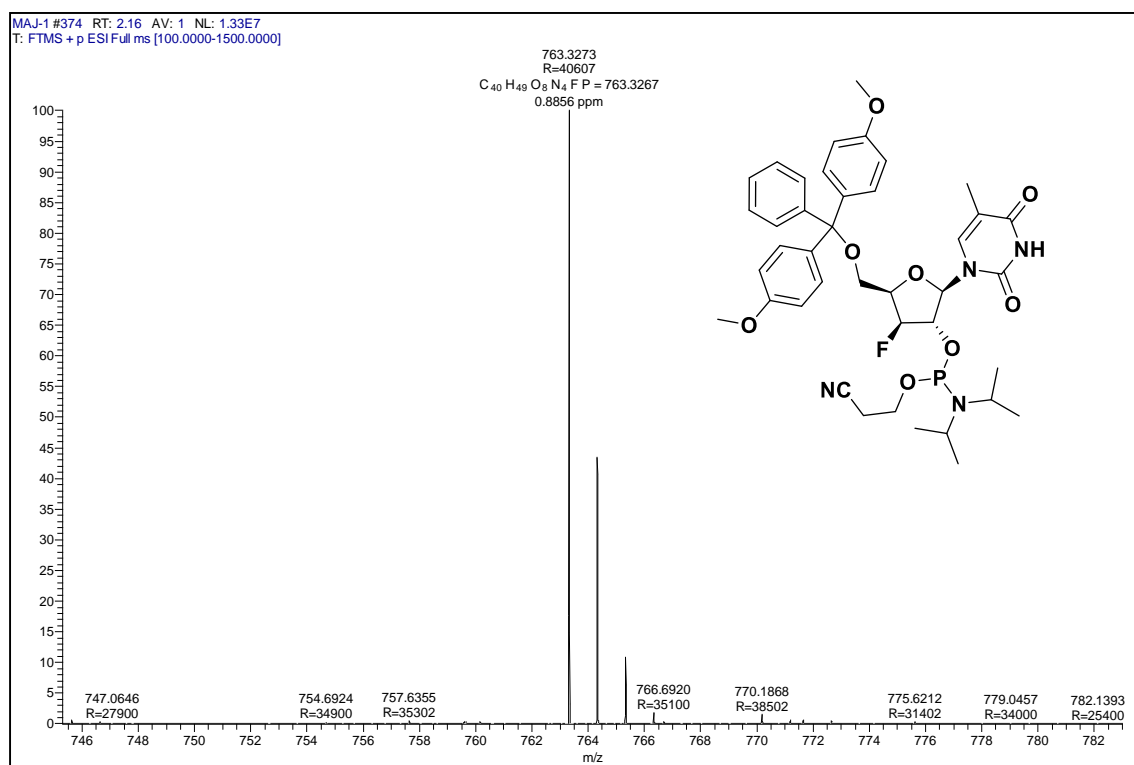
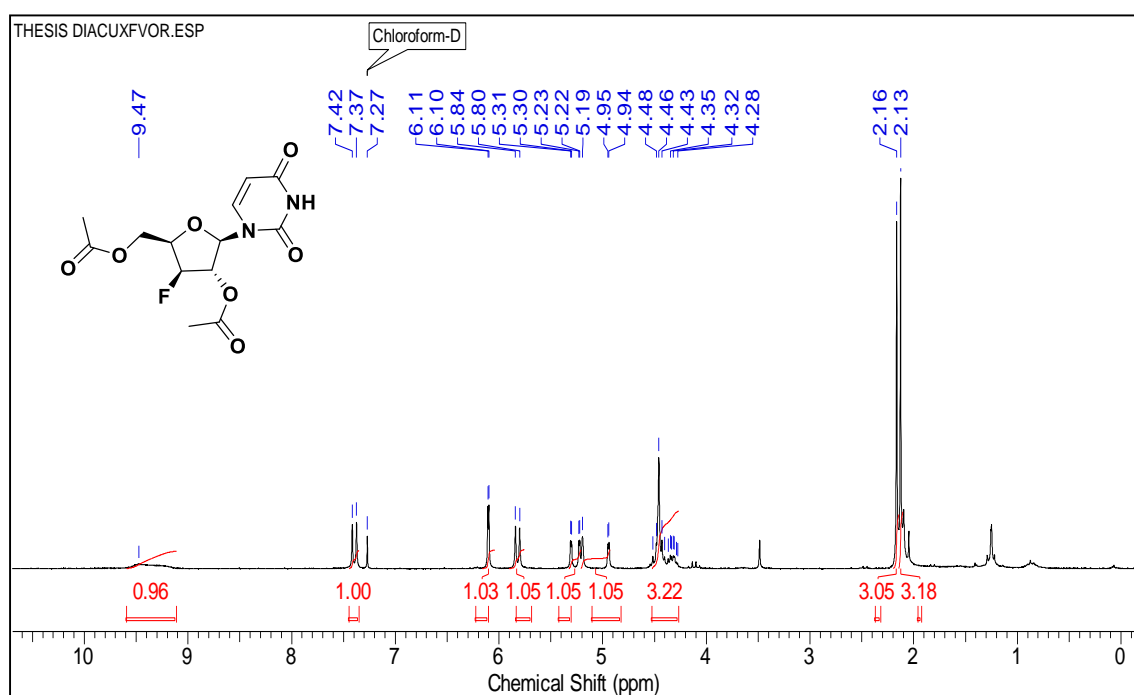
HRMS spectrum of compound 25

¹H NMR of compound 26 (CDCl₃)

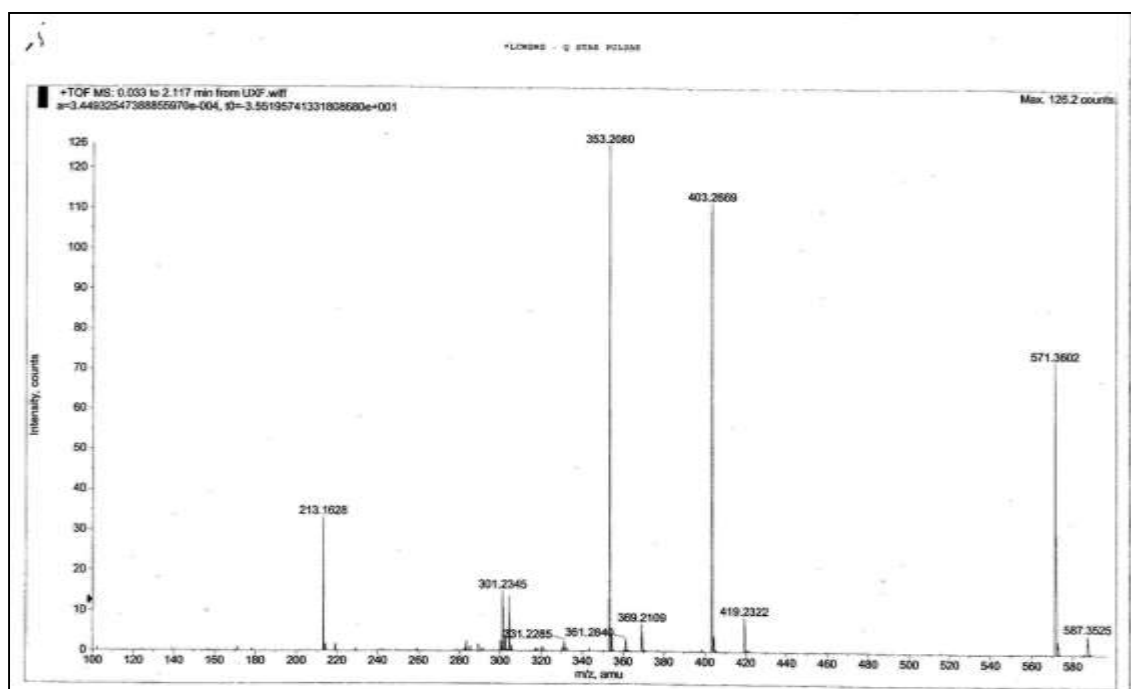
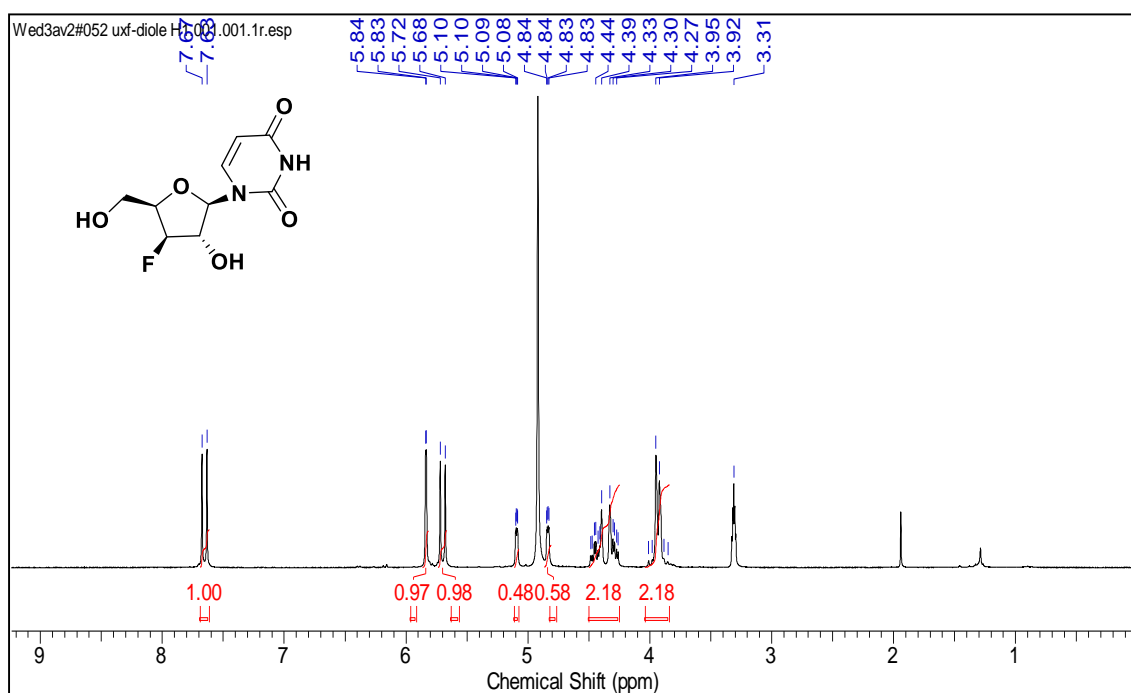
HRMS spectrum of compound 26

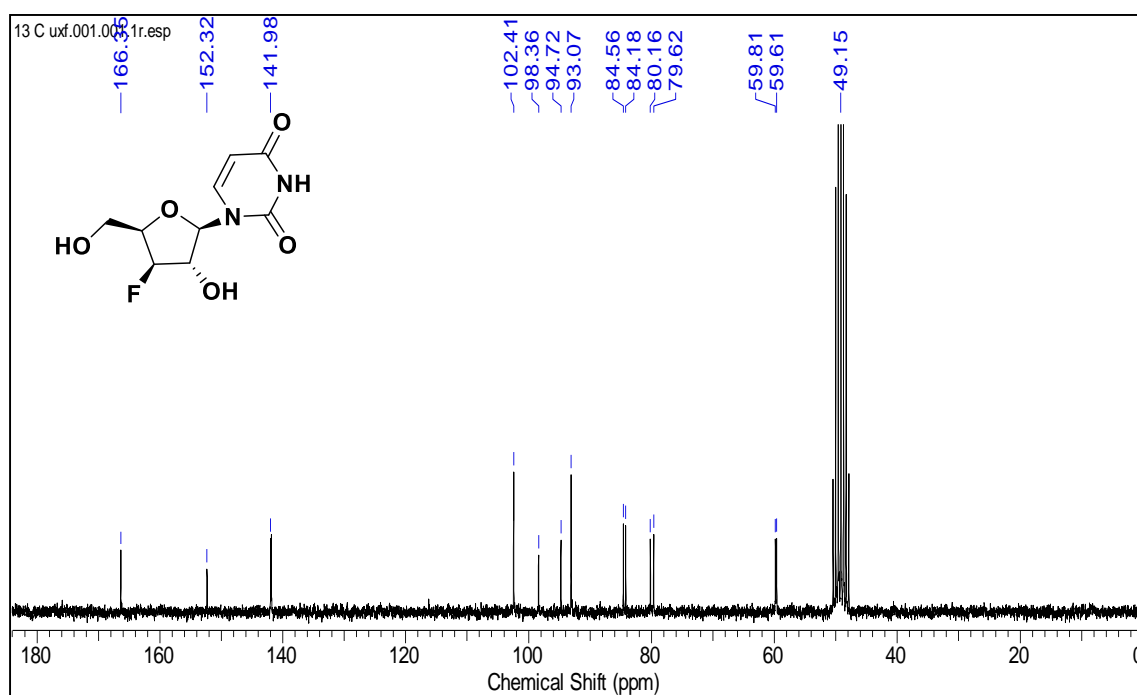
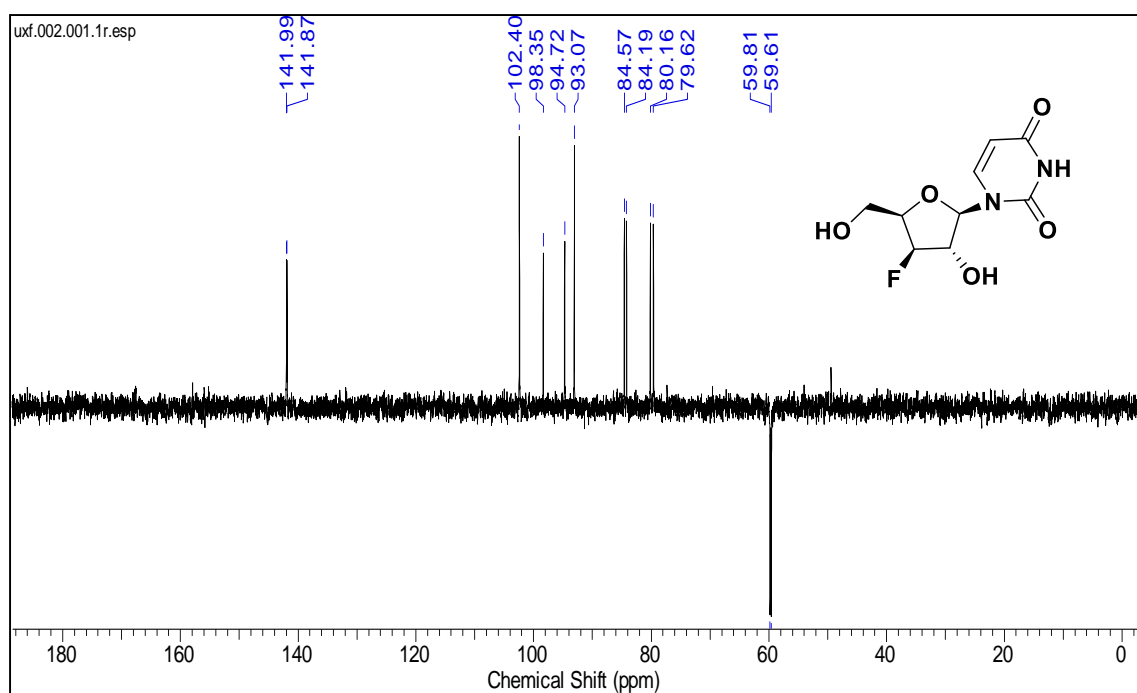
³¹P NMR of compound 27

HRMS spectrum of compound 27

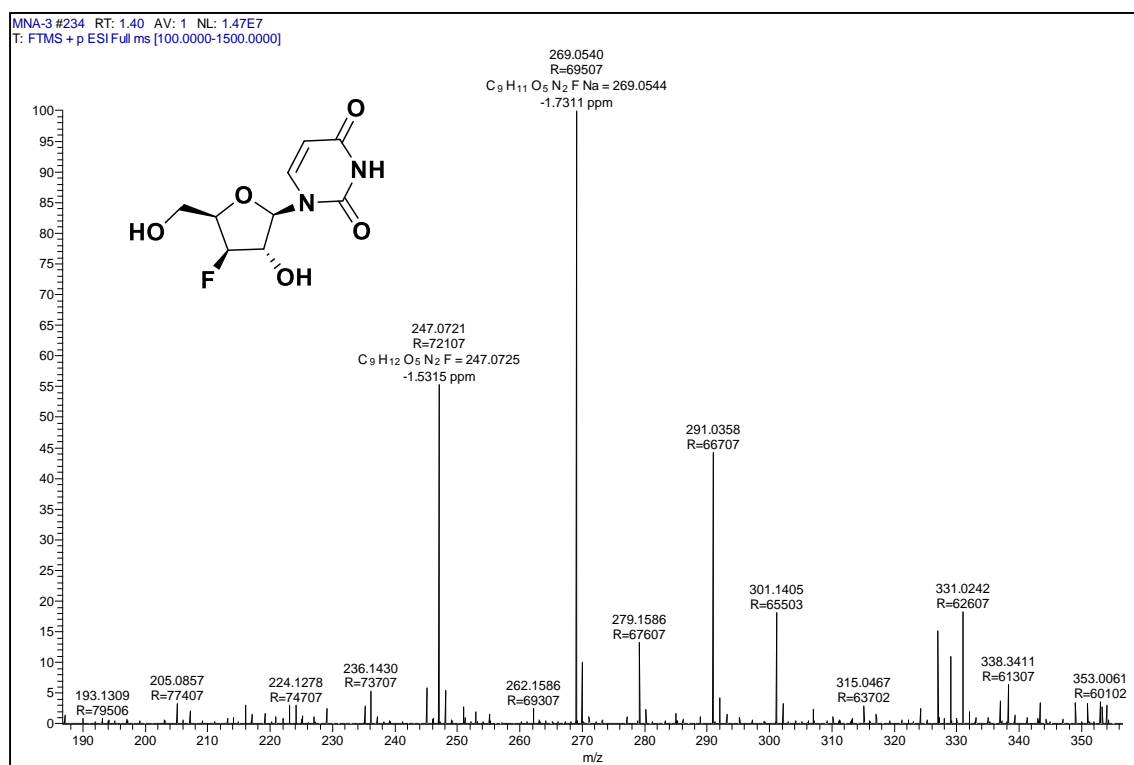
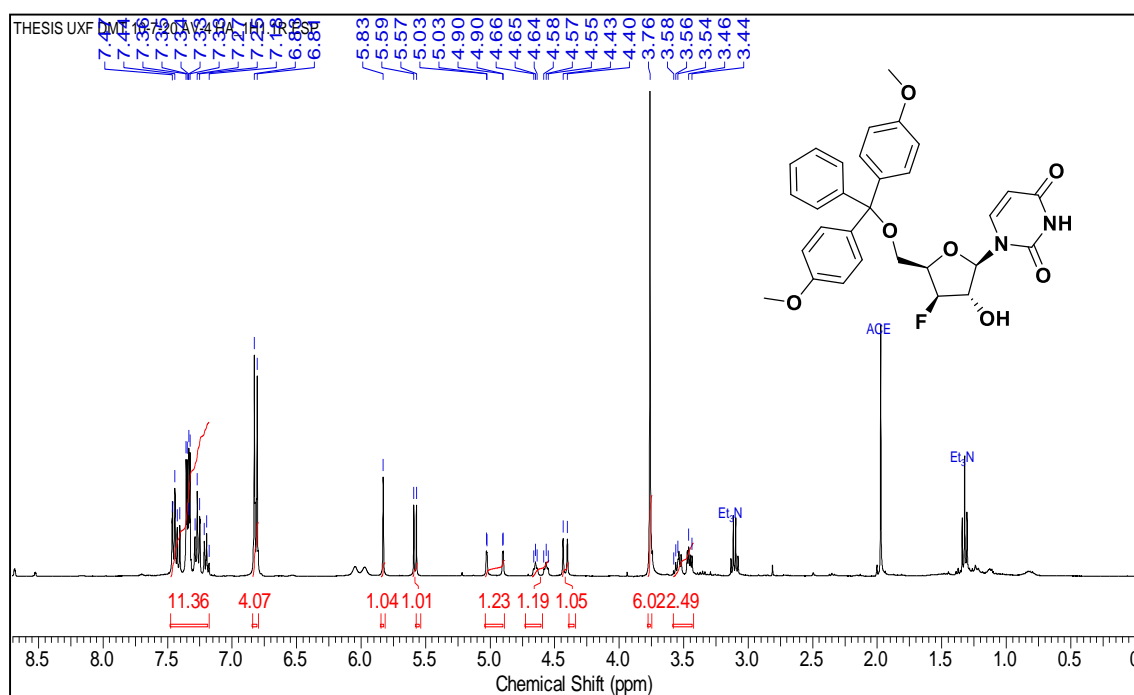
¹H NMR of compound 28 (CDCl₃)

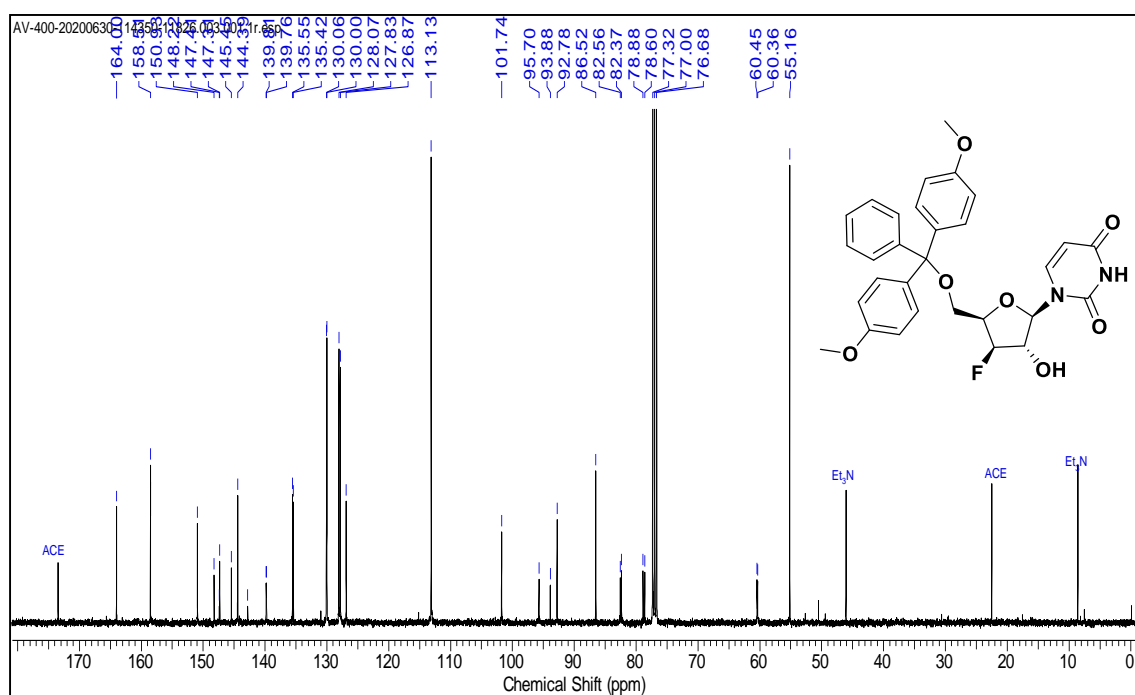
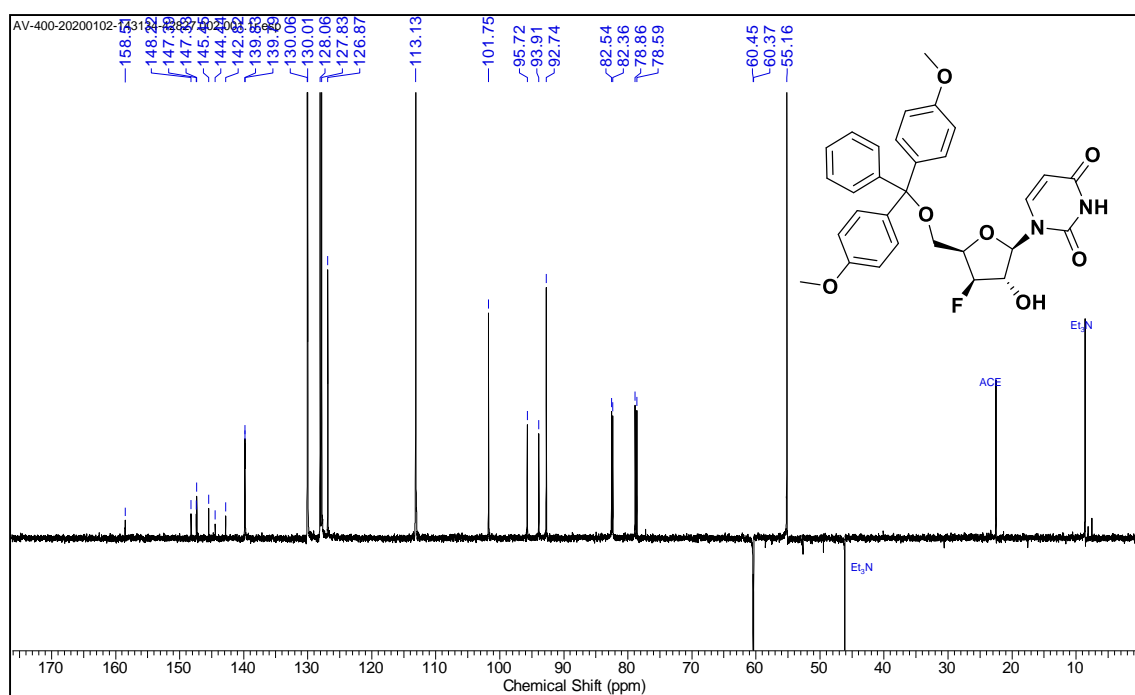
LCMS of compound 28

 ^1H NMR of compound 29 (CDCl_3)

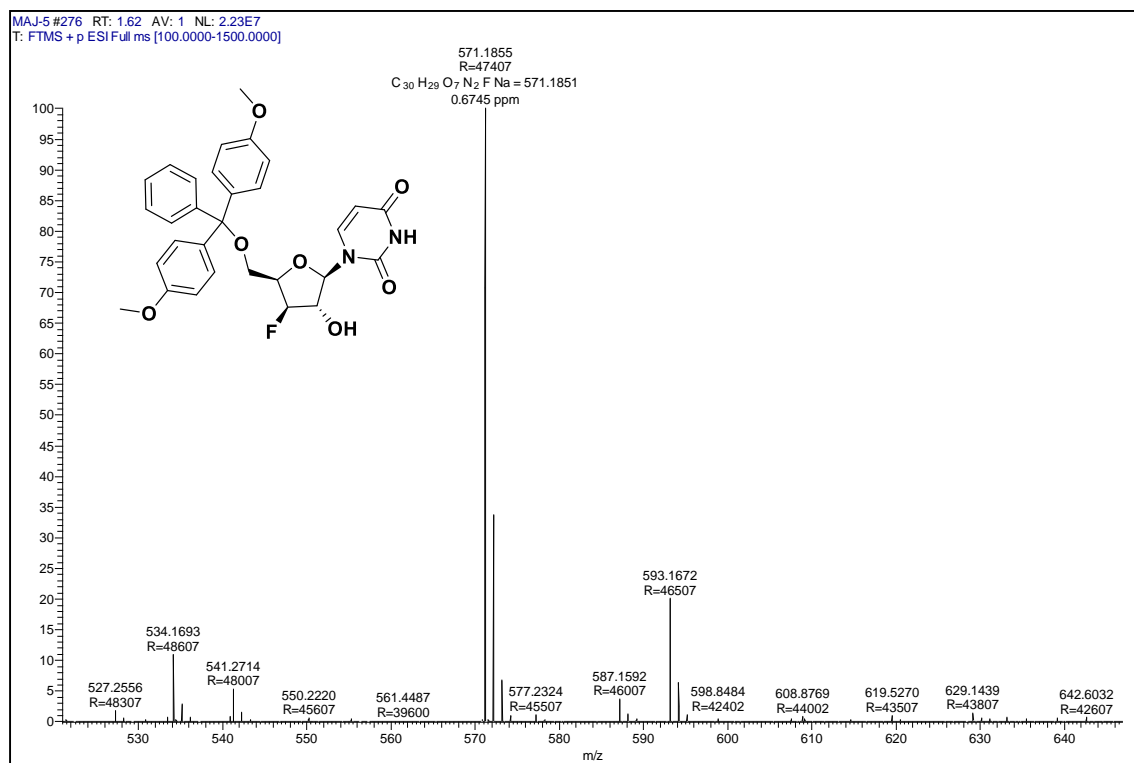
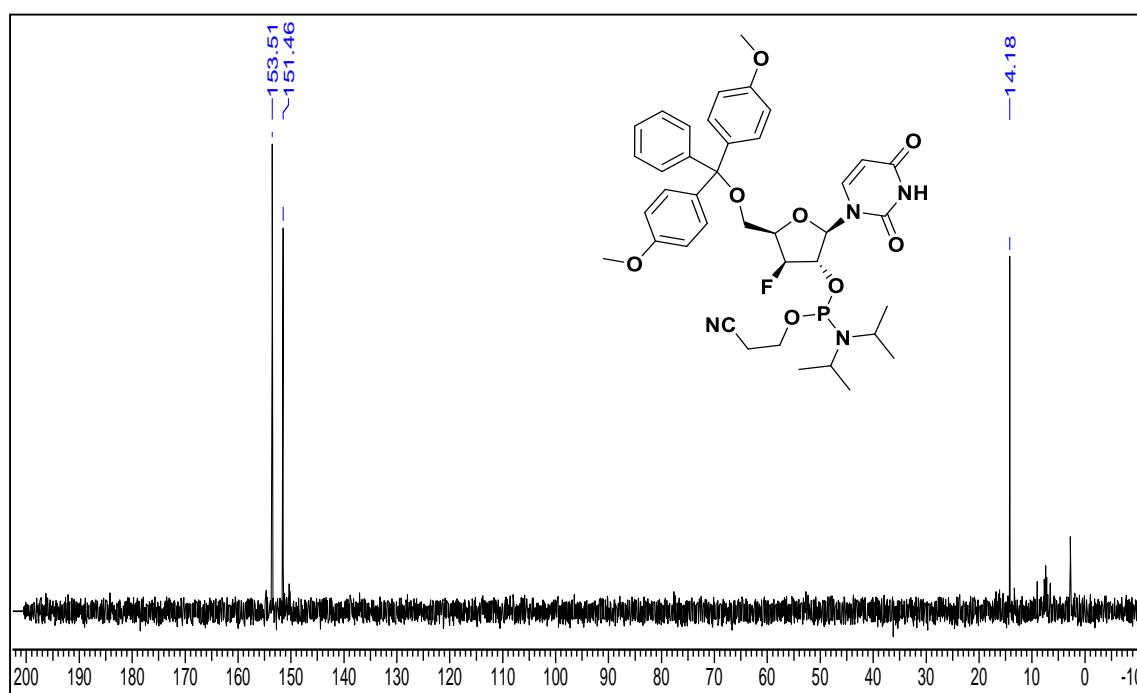
^{13}C NMR of compound 29 (CD_3OD) **^{13}C -DEPT of compound 29 (CD_3OD)**

HRMS spectrum of compound 29

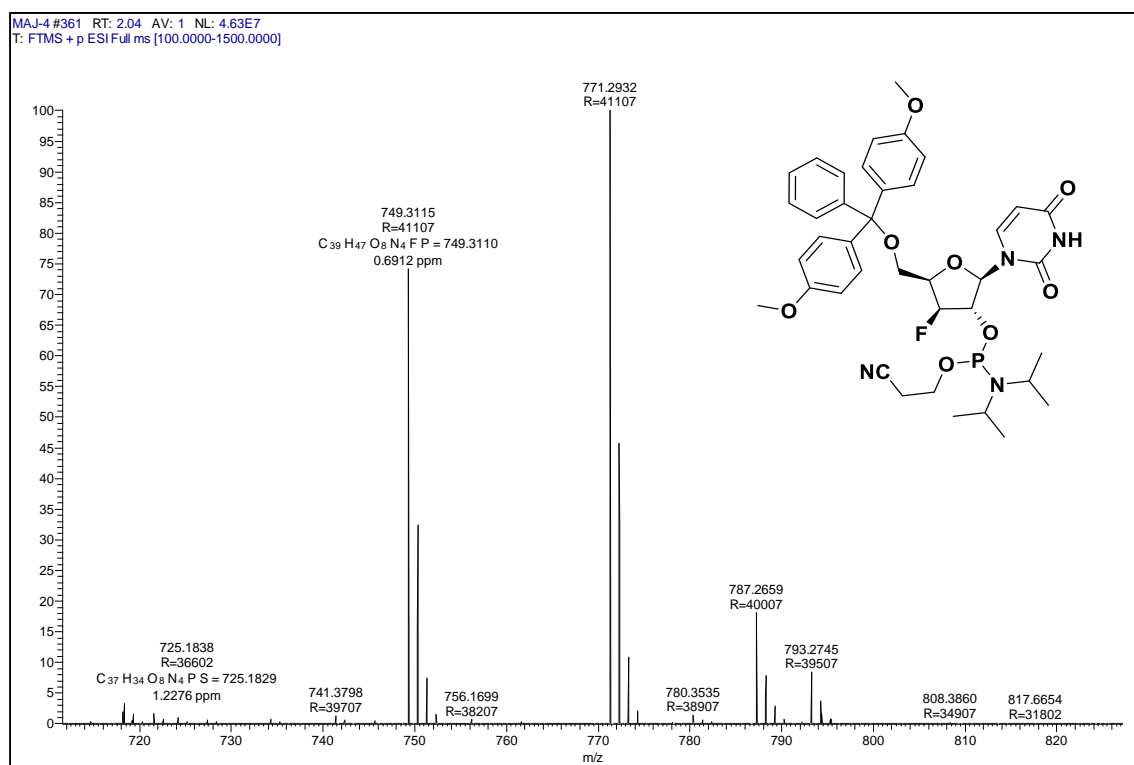
¹H NMR of compound 30 (CDCl₃)

^{13}C NMR of compound 30 (CDCl_3) **^{13}C -DEPT of compound 30**

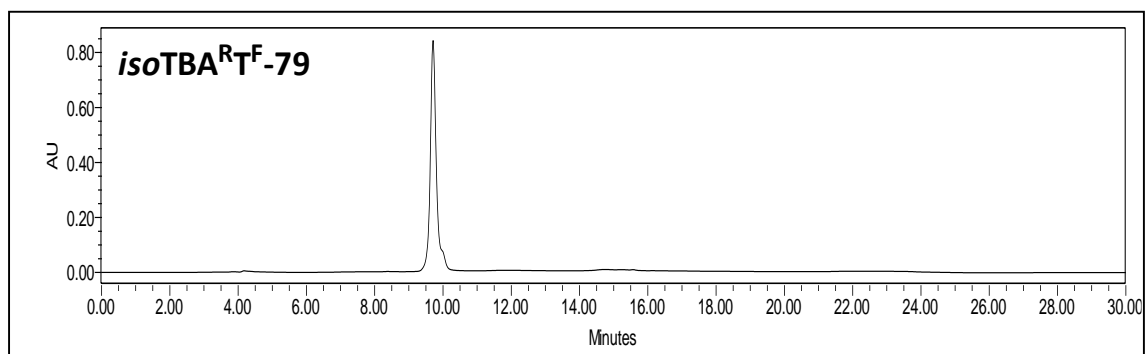
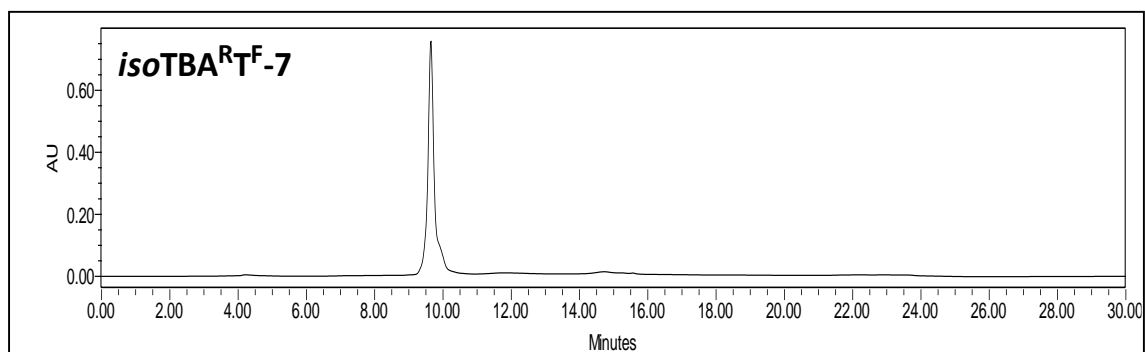
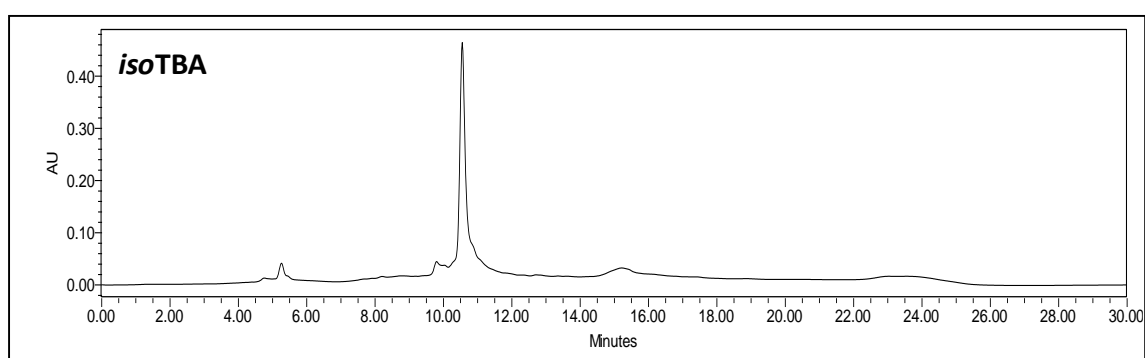
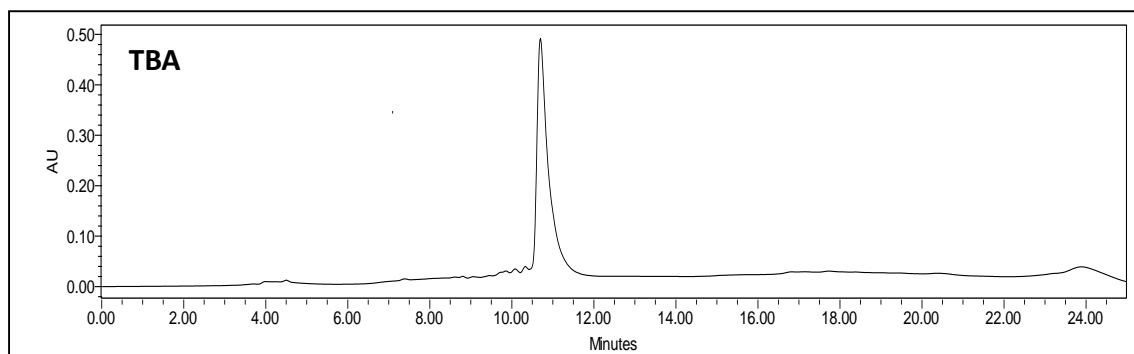
HRMS spectrum of Compound 30

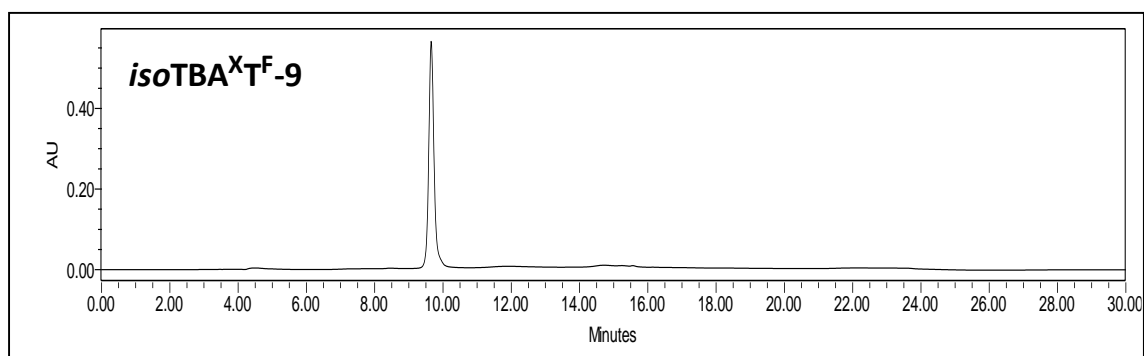
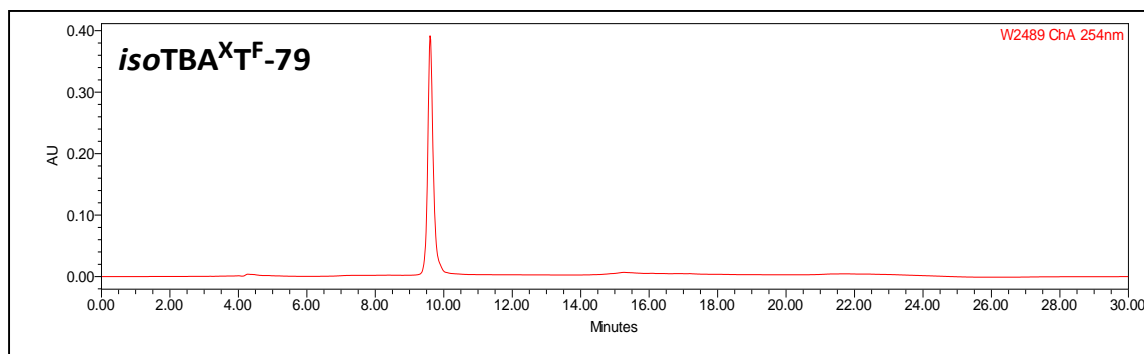
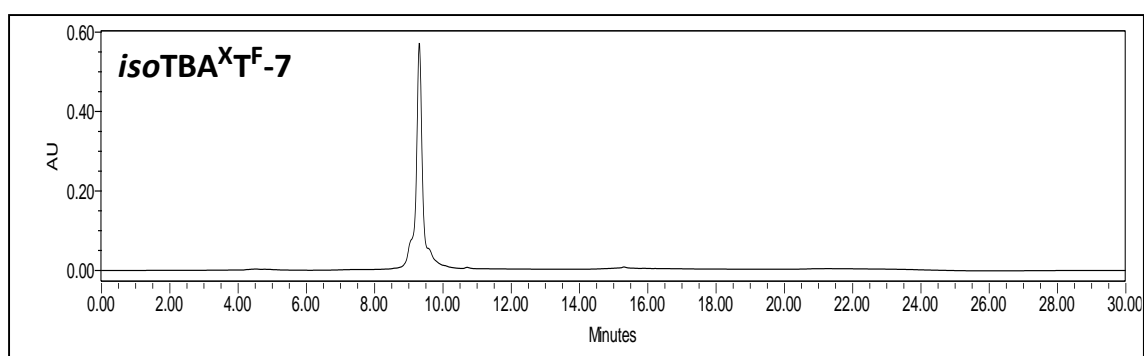
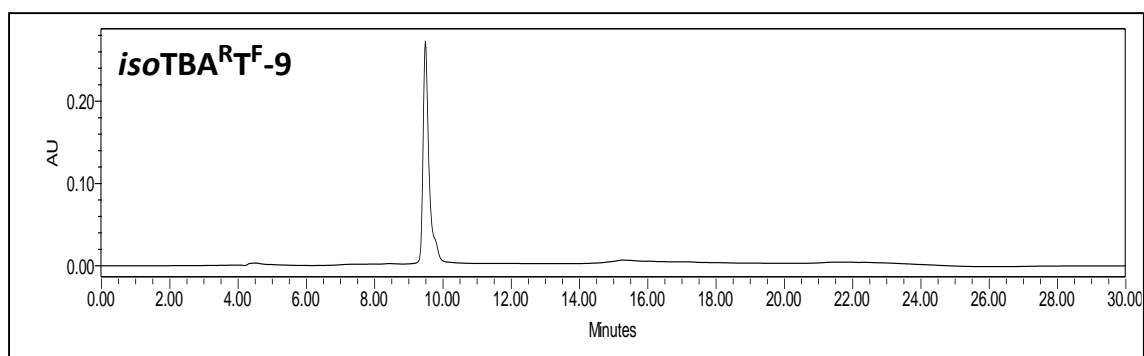
³¹P NMR of compound 31 (CDCl₃)

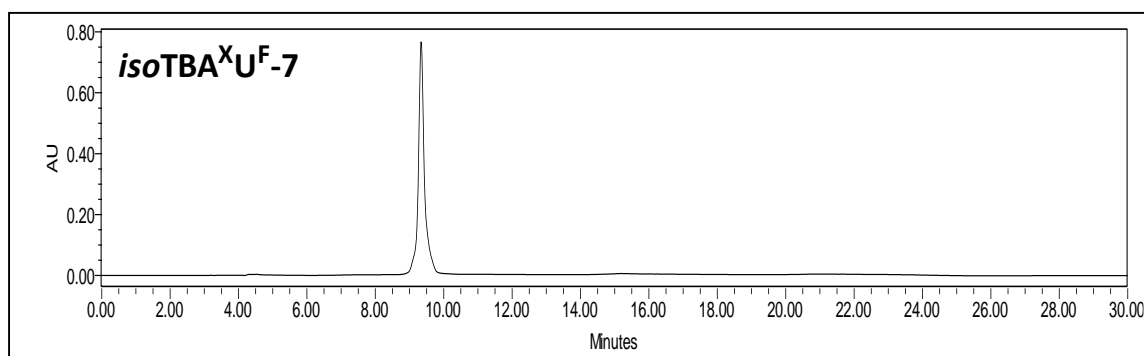
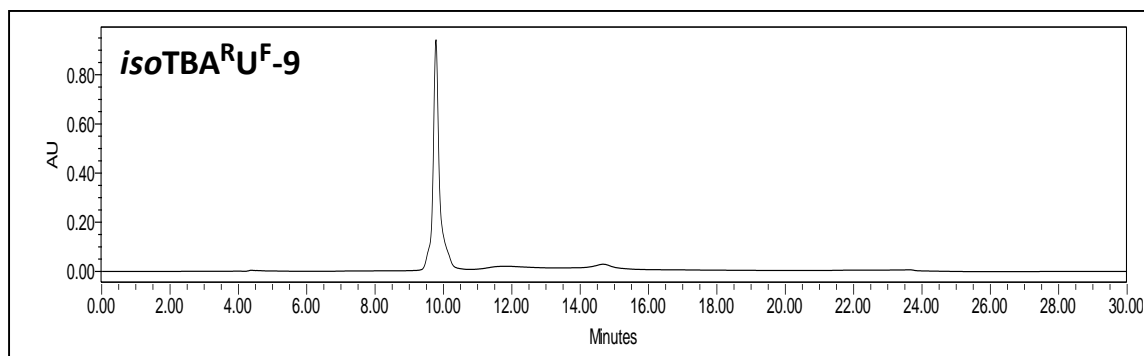
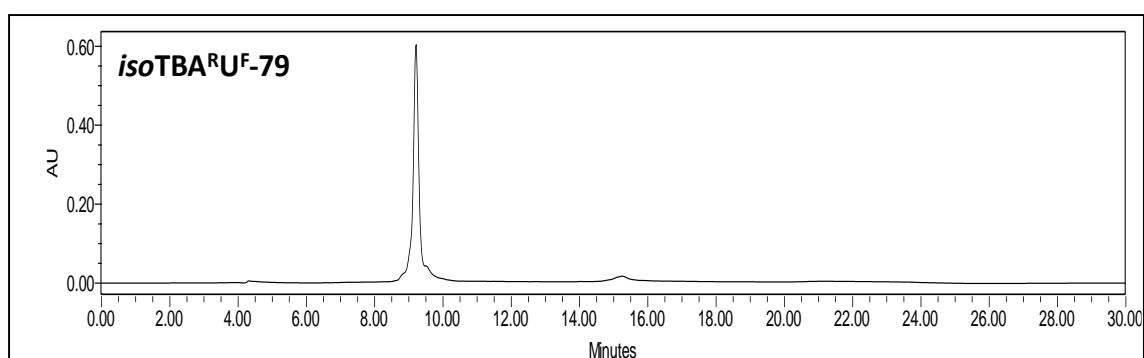
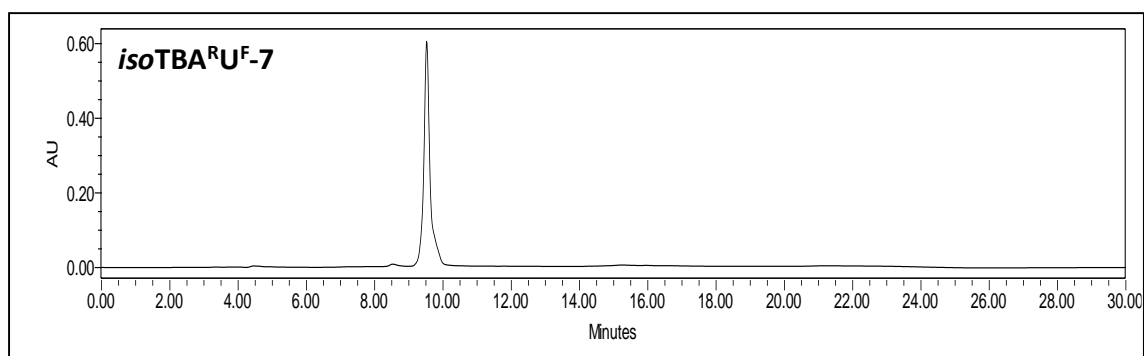
HRMS spectrum of Compound 31

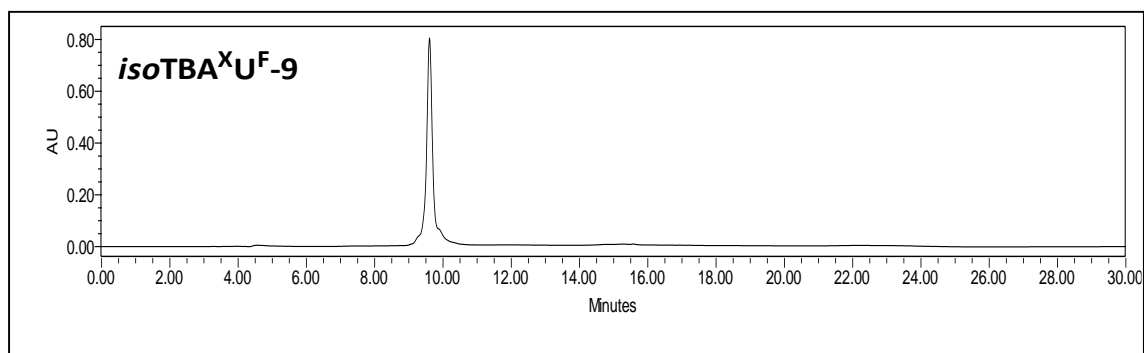
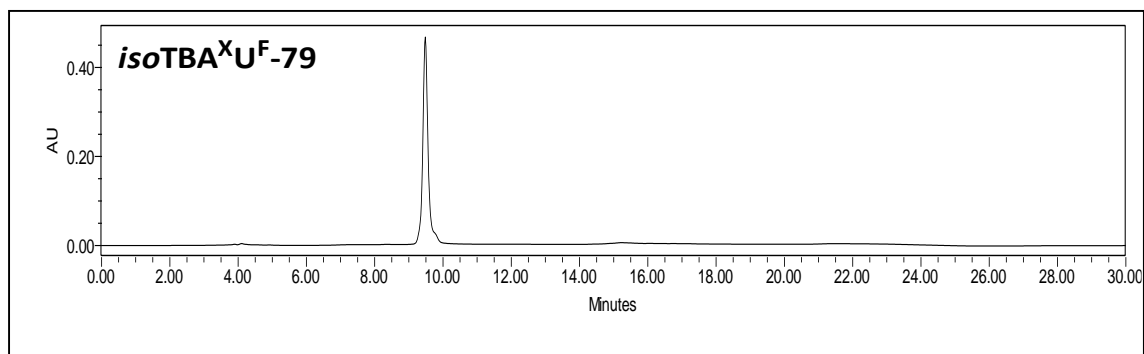


HPLC chromatograms of oligomers

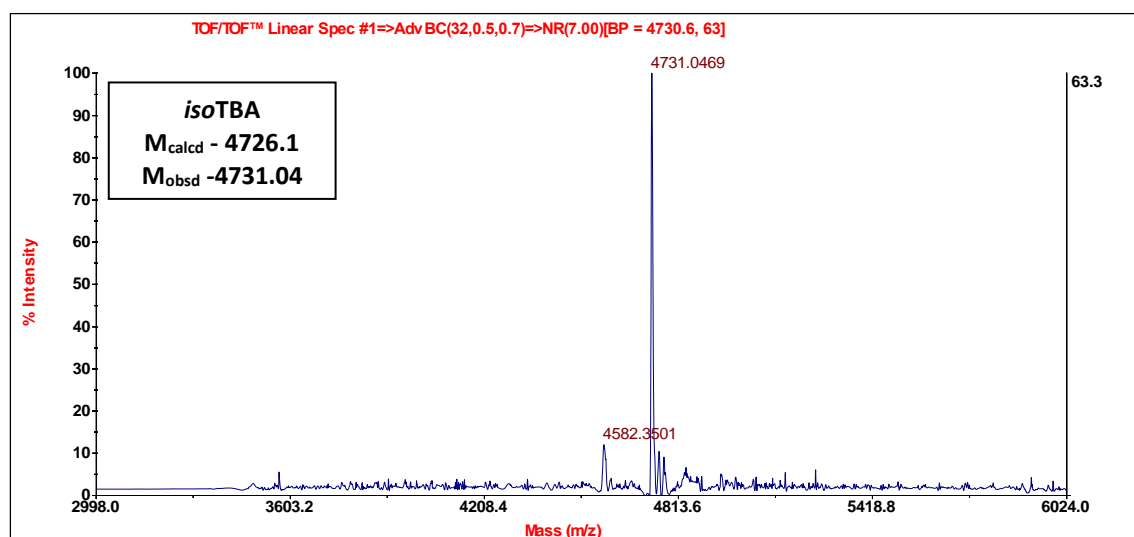
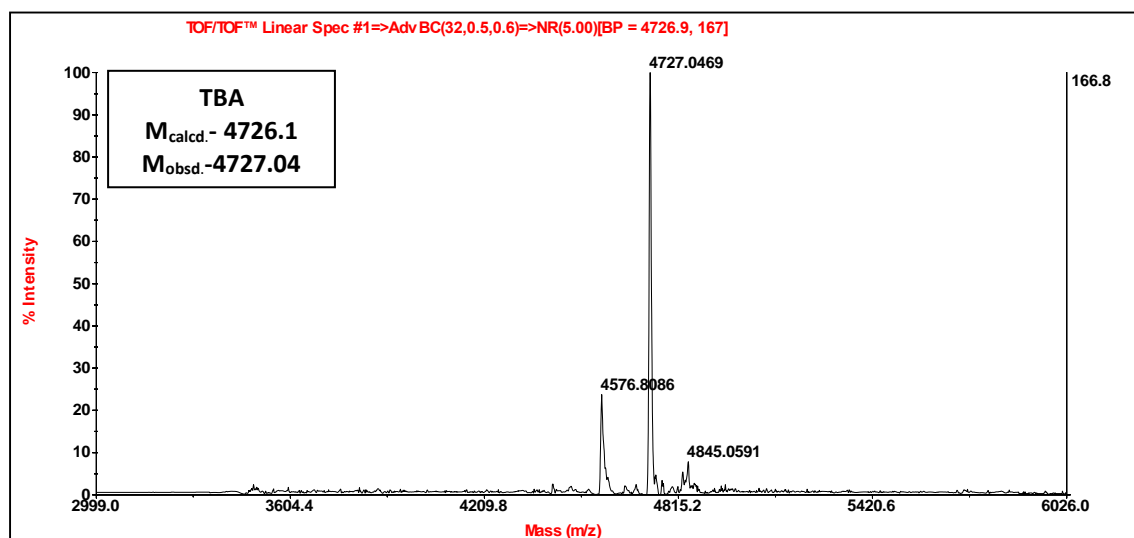


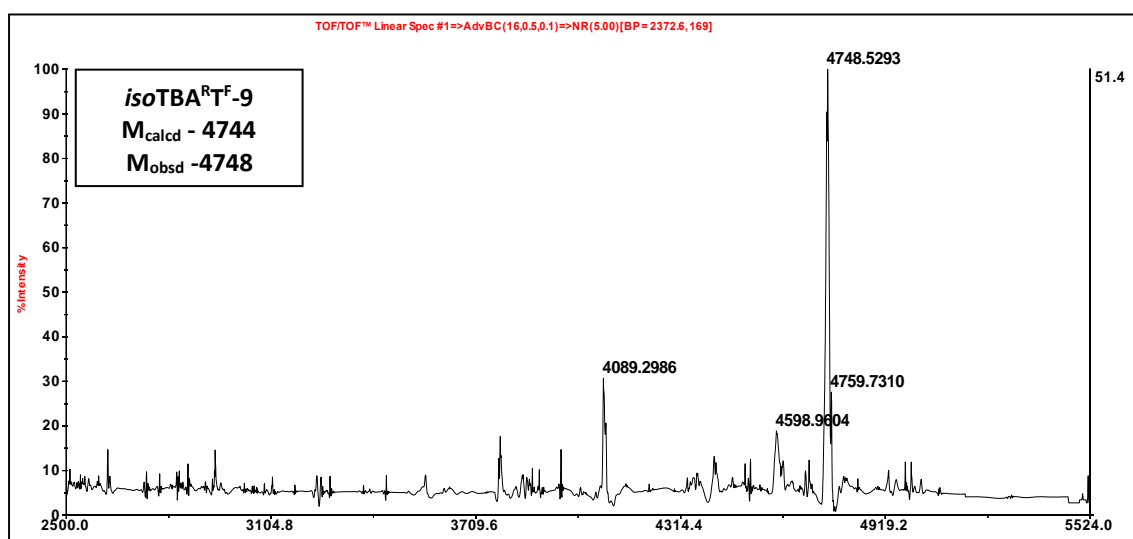
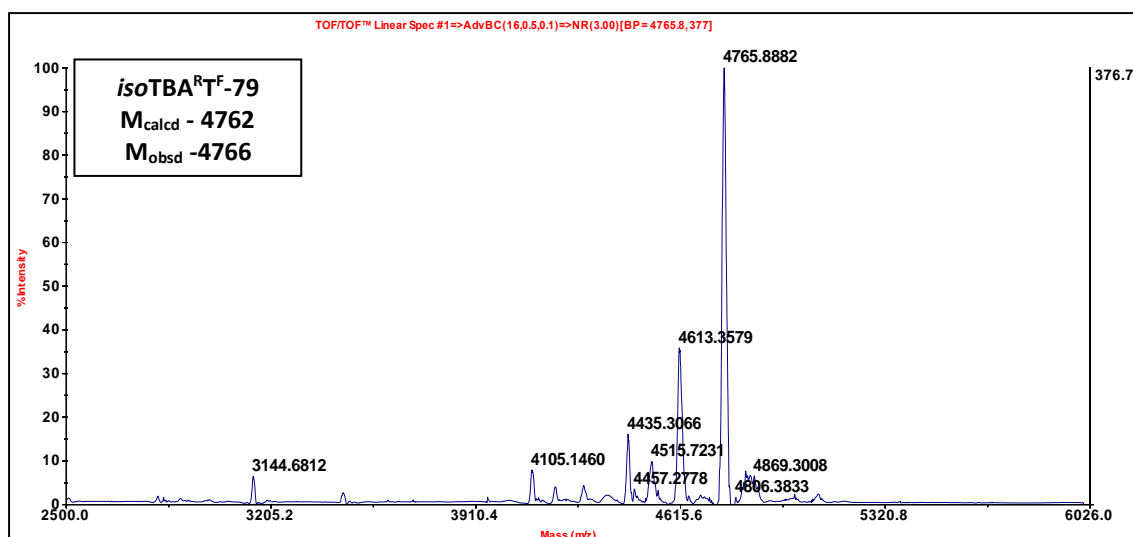
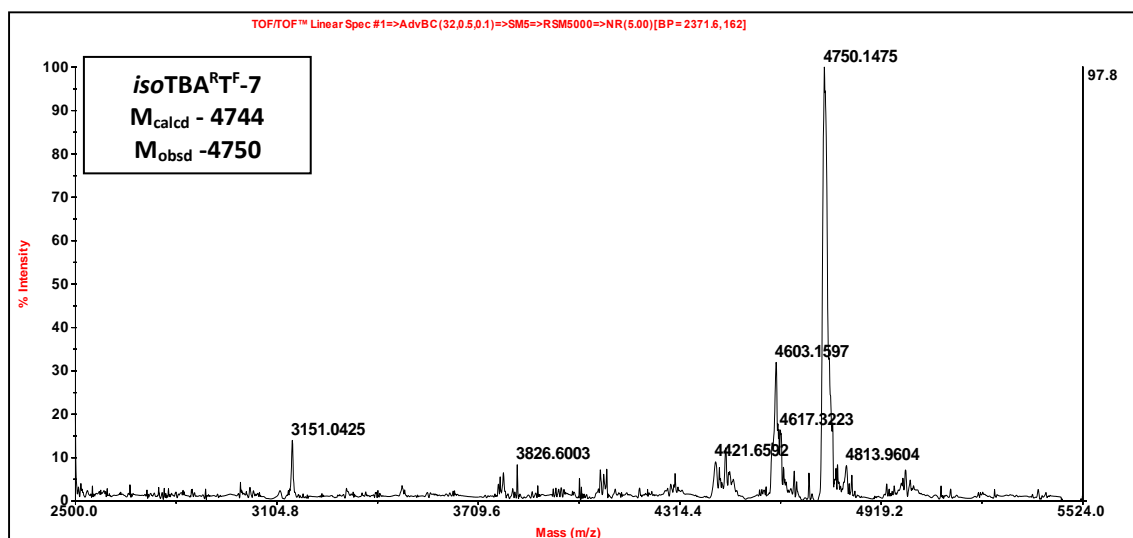


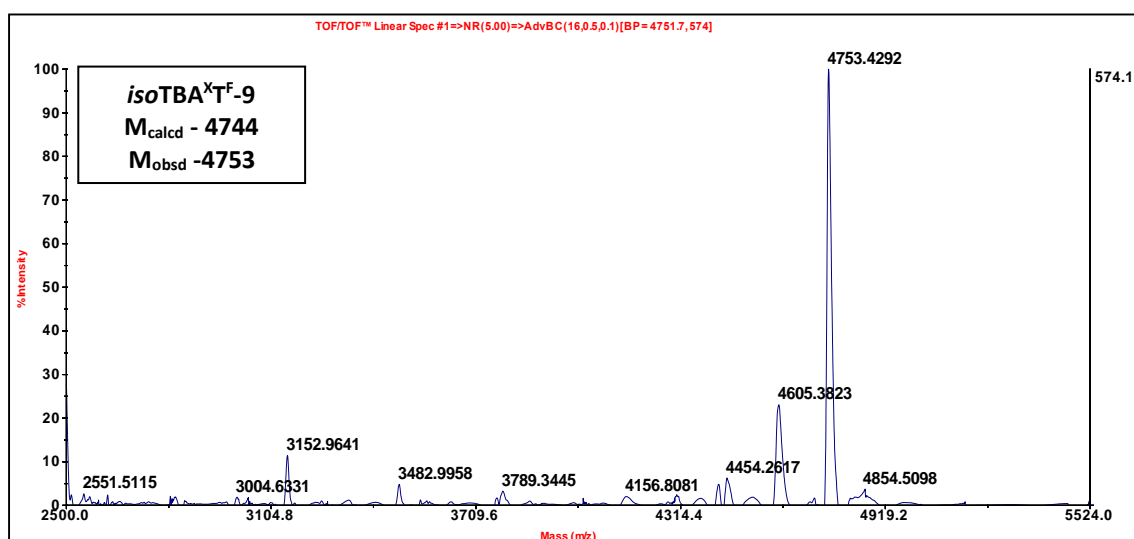
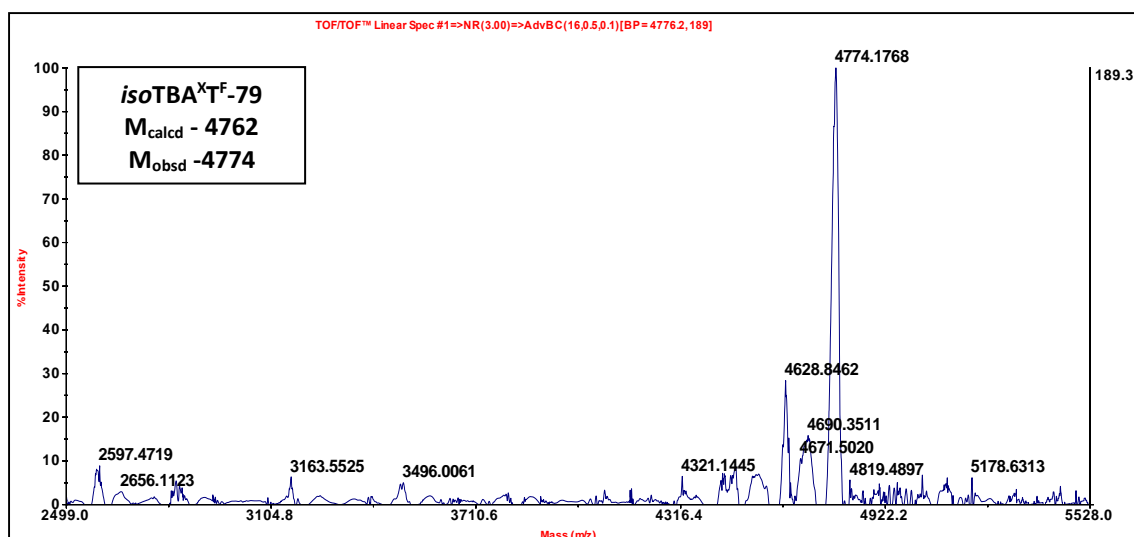
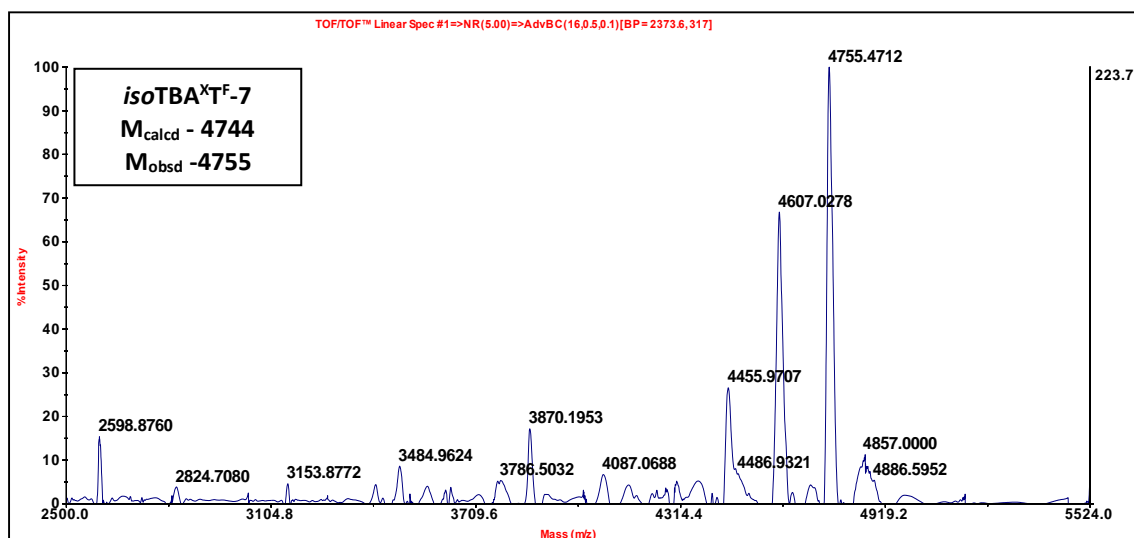


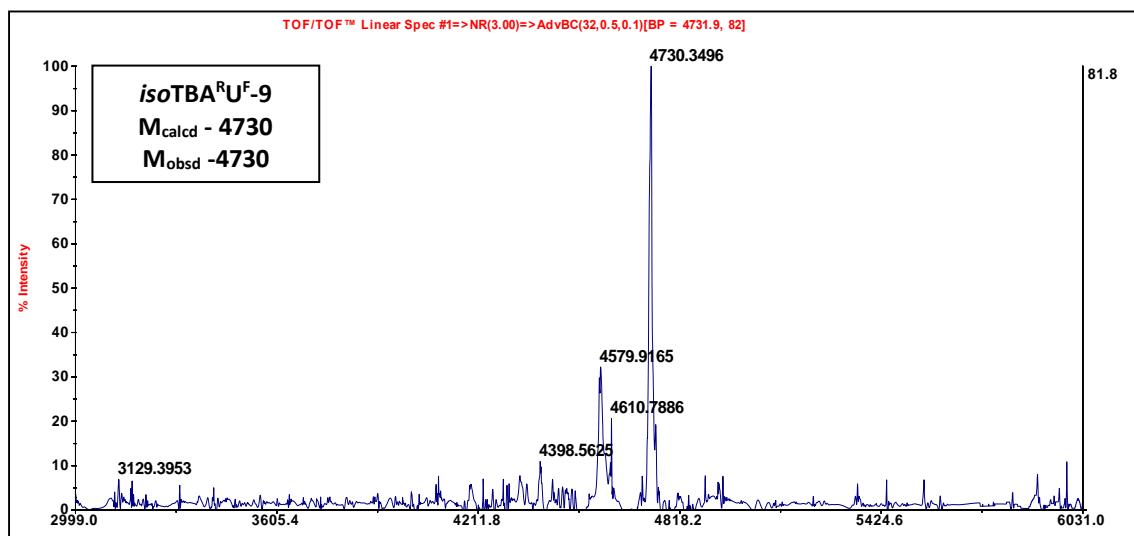
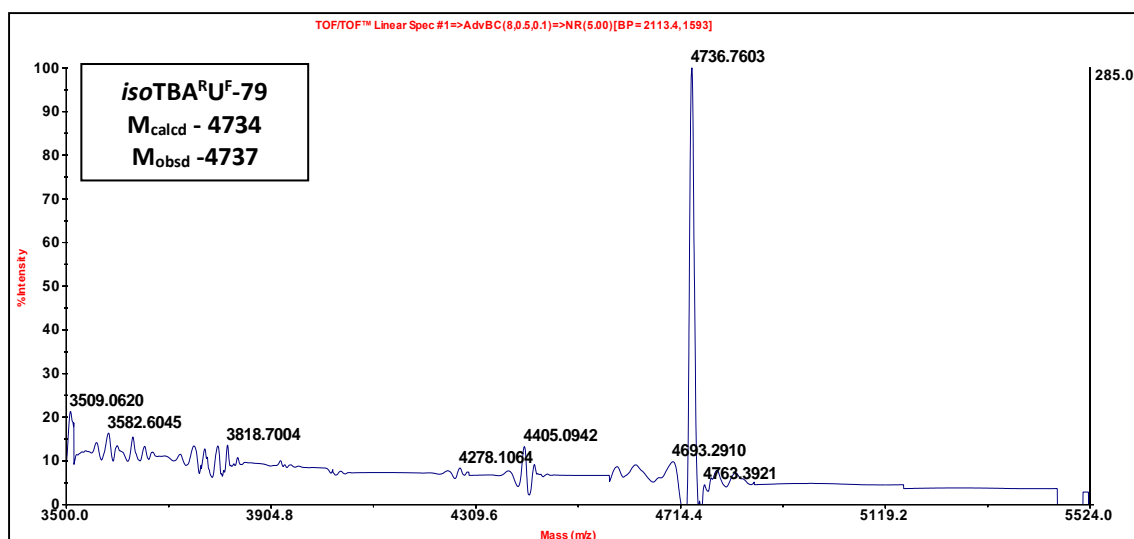
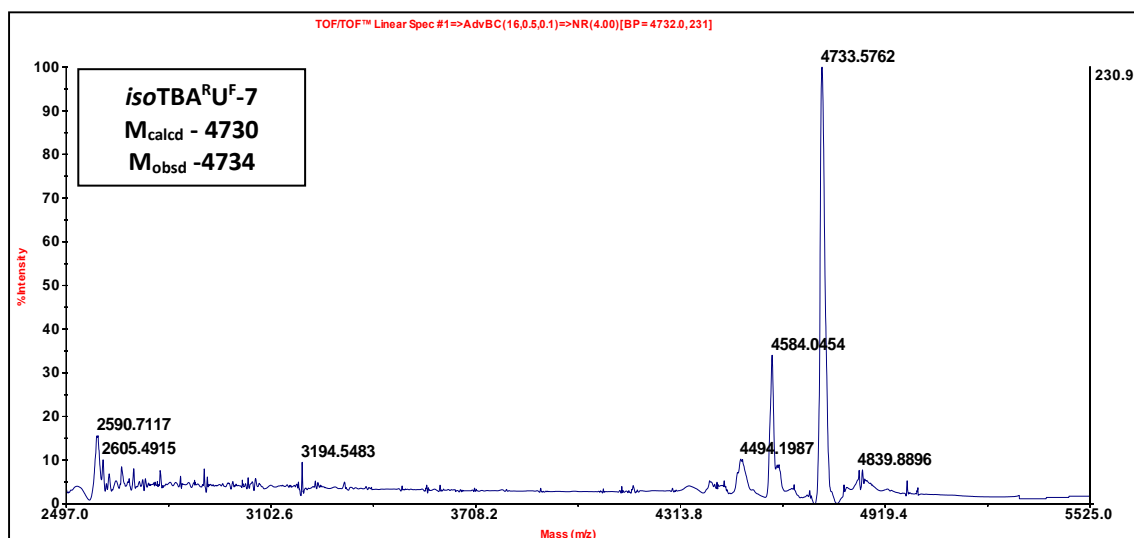


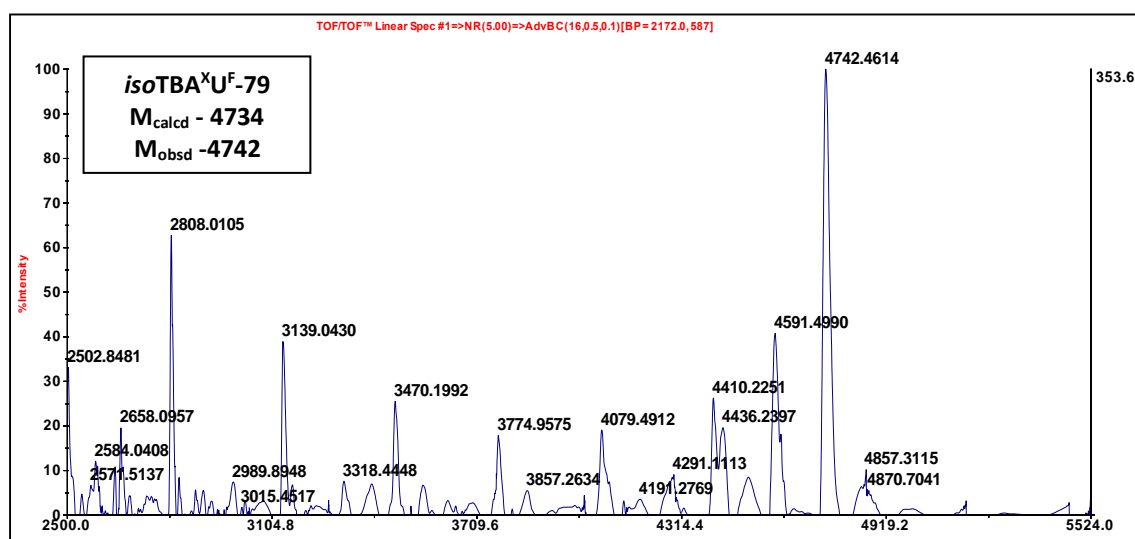
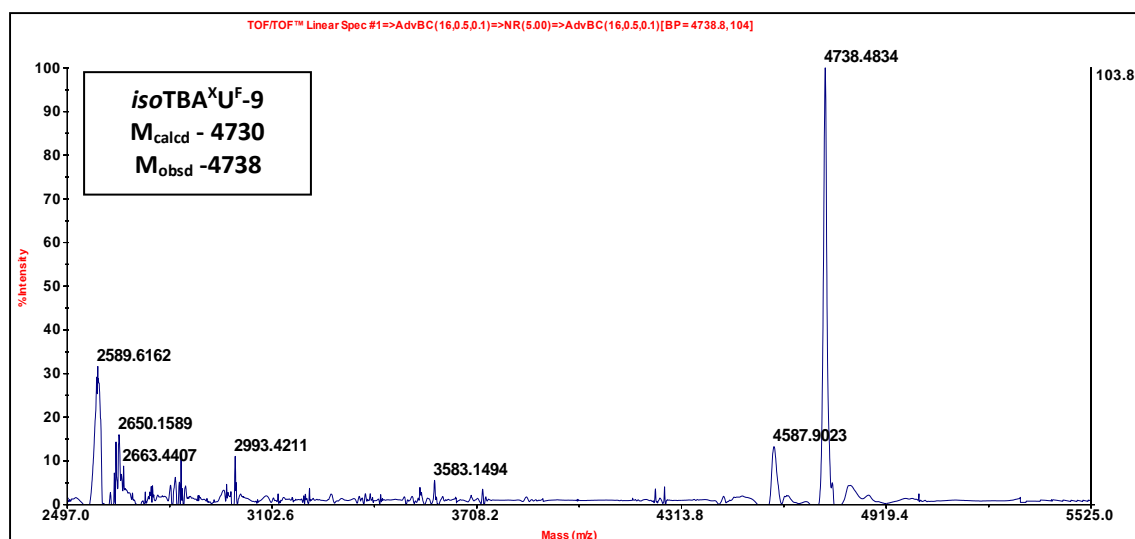
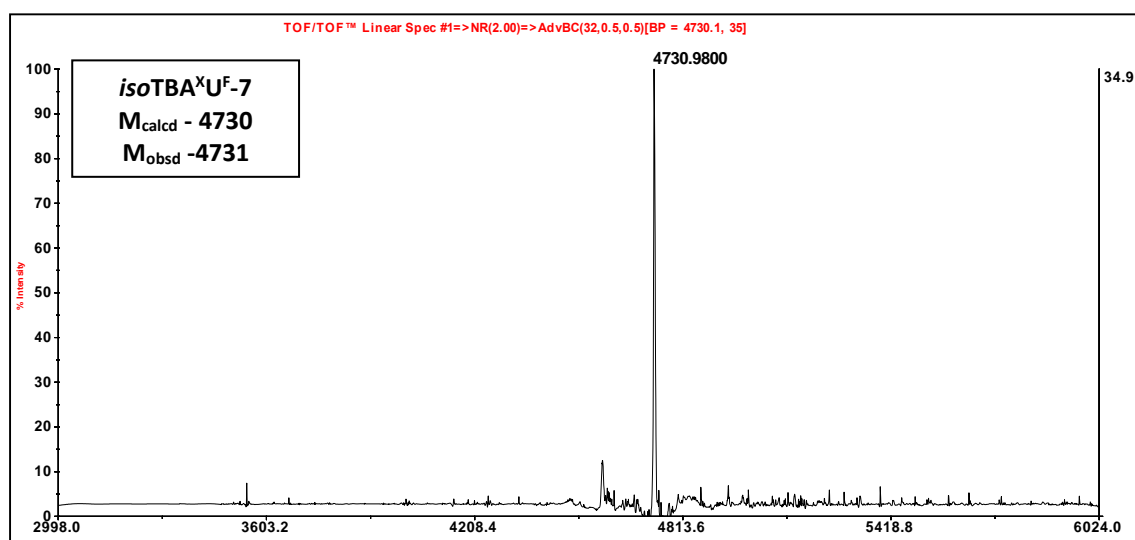
MALDI-TOF spectra of TBA oligomers











2.12 References

1. Hertel, L. W.; Boder, G. B.; Kroin, J. S.; Rinzel, S. M.; Poore, G. A.; Todd, G. C.; Grindey, G. B., Evaluation of the antitumor activity of gemcitabine (2',2'-difluoro-2'-deoxycytidine). *Cancer Res.* **1990**, *50* (14), 4417-4422.
2. Masood, R.; Ahluwalia, G. S.; Cooney, D. A.; Fridland, A.; Marquez, V. E.; Driscoll, J. S.; Hao, Z.; Mitsuya, H.; Perno, C.-F.; Broder, S., 2'-Fluoro-2', 3'-dideoxyarabinosyladenine: a metabolically stable analogue of the antiretroviral agent 2', 3'-dideoxyadenosine. *Mol. Pharmacol.* **1990**, *37*, 590-596.
3. Watanabe, K. A.; Reichman, U.; Hirota, K.; Lopez, C.; Fox, J. J., Nucleosides. 110. Synthesis and antiherpes virus activity of some 2'-fluoro-2'-deoxyarabinofuranosylpyrimidine nucleosides. *J. Med. Chem.* **1979**, *22* (1), 21-24.
4. Marcellin, P.; Mommeja-Marin, H.; Sacks, S. L.; Lau, G. K.; Sereni, D.; Bronowicki, J. P.; Conway, B.; Trepo, C.; Blum, M. R.; Yoo, B. C., A phase II dose-escalating trial of clevudine in patients with chronic hepatitis B. *Hepatology* **2004**, *40* (1), 140-148.
5. Bonate, P. L.; Arthaud, L.; Cantrell, W. R., Jr.; Stephenson, K.; Secrist, J. A., 3rd; Weitman, S., Discovery and development of clofarabine: a nucleoside analogue for treating cancer. *Nat. Rev. Drug Discovery* **2006**, *5* (10), 855-863.
6. (a) Stoeckler, J. D.; Bell, C. A.; Parks Jr, R. E.; Chu, C. K.; Fox, J. J.; Ikehara, M., C (2')-substituted purine nucleoside analogs: Interactions with adenosine deaminase and purine nucleoside phosphorylase and formation of analog nucleotides. *Biochem. pharmacol.* **1982**, *31* (9), 1723-1728; (b) Philips, F. S.; Feinberg, A.; Chou, T.-C.; Vidal, P. M.; Su, T.-L.; Watanabe, K. A.; Fox, J. J., Distribution, metabolism, and excretion of 1-(2-fluoro-2-deoxy- β -D-arabinofuranosyl) thymine and 1-(2-fluoro-2-deoxy- β -D-arabinofuranosyl)-5-iodocytosine. *Cancer Res.* **1983**, *43* (8), 3619-3627; (c) Sapse, A. M.; Snyder, G., Ab Initio Studies of the Antiviral Drug 1-(2-Fluoro-2-deoxy- β -D-arabinofuranosyl) thymine. *Cancer Invest.* **1985**, *3* (2), 115-121.
7. (a) Kois, P.; Tocik, Z.; Spassova, M.; Ren, W.-Y.; Rosenberg, I.; Soler, J. F.; Watanabe, K. A., Synthesis and Some Properties of Modified Oligonucleotides. II. Oligonucleotides Containing 2'-Deoxy-2'-fluoro- β -D-arabinofuranosyl Pyrimidine Nucleosides. *Nucleosides and Nucleotides* **1993**, *12* (10), 1093-1109; (b) Rosenberg, I.; Soler, J. F.; Tocik, Z.; Ren, W.-Y.; Ciszewski, L. A.; Kois, P.; Pankiewicz, K. W.;

- Spasova, M.; Watanabe, K. A., Synthesis of Oligodeoxynucleotides Containing the C-Nucleoside and 2'- Deoxy-2'-Fluoro-ara-Nucleoside Moieties by the H-Phosphonate Method. *Nucleosides and Nucleotides* **1993**, *12* (3-4), 381-401.
8. (a) Watts, J. K.; Martín-Pintado, N.; Gómez-Pinto, I.; Schwartzenruber, J.; Portella, G.; Orozco, M.; González, C.; Damha, M. J., Differential stability of 2'F-ANA•RNA and ANA•RNA hybrid duplexes: roles of structure, pseudohydrogen bonding, hydration, ion uptake and flexibility. *Nucleic Acids Res.* **2010**, *38* (7), 2498-2511; (b) Wilds, C. J.; Damha, M. J., 2'-Deoxy-2'-fluoro- β -d-arabinonucleosides and oligonucleotides (2'F-ANA): synthesis and physicochemical studies. *Nucleic Acids Res* **2000**, *28* (18), 3625-3635; (c) Watts, J. K.; Choubdar, N.; Sadalpure, K.; Robert, F.; Wahba, A. S.; Pelletier, J.; Mario Pinto, B.; Damha, M. J., 2'-Fluoro-4'-thioarabino-modified oligonucleotides: conformational switches linked to siRNA activity. *Nucleic Acids Res.* **2007**, *35* (5), 1441-1451.
9. Dowler, T.; Bergeron, D.; Tedeschi, A.-L.; Paquet, L.; Ferrari, N.; Damha, M. J., Improvements in siRNA properties mediated by 2'-deoxy-2'-fluoro- β - d - arabinonucleic acid (FANA). *Nucleic Acids Res.* **2006**, *34* (6), 1669-1675.
10. Pasternak, A.; Hernandez, F. J.; Rasmussen, L. M.; Vester, B.; Wengel, J., Improved thrombin binding aptamer by incorporation of a single unlocked nucleic acid monomer. *Nucleic Acids Res.* **2011**, *39* (3), 1155-1164.
11. Rigo, F.; Hua, Y.; Chun, S. J.; Prakash, T. P.; Krainer, A. R.; Bennett, C. F., Synthetic oligonucleotides recruit ILF2/3 to RNA transcripts to modulate splicing. *Nat. Chem. Bio.* **2012**, *8* (6), 555.
12. Vinores, S. A., Pegaptanib in the treatment of wet, age-related macular degeneration. *Int. J. Nanomed.* **2006**, *1* (3), 263-268.
13. Erande, N.; Gunjal, A. D.; Fernandes, M.; Gonnade, R.; Kumar, V. A., Synthesis and structural studies of S-type/N-type-locked/frozen nucleoside analogues and their incorporation in RNA-selective, nuclease resistant 2', 5' linked oligonucleotides. *Org. Bio. Chem.* **2013**, *11* (5), 746-757.
14. (a) Ellington, A. D.; Szostak, J. W., In vitro selection of RNA molecules that bind specific ligands. *Nature* **1990**, *346* (6287), 818-822; (b) Tuerk, C.; Gold, L., Systematic evolution of ligands by exponential enrichment: RNA ligands to bacteriophage T4 DNA polymerase. *Science* **1990**, *249* (4968), 505-510; (c)

- Robertson, D. L.; Joyce, G. F., Selection in vitro of an RNA enzyme that specifically cleaves single-stranded DNA. *Nature* **1990**, *344* (6265), 467-468.
15. Zhang, Y.; Hong, H.; Cai, W., Tumor-targeted drug delivery with aptamers. *Curr. Med. Chem.* **2011**, *18* (27), 4185-4194.
16. Cummins, L. L.; Owens, S. R.; Risen, L. M.; Lesnik, E. A.; Freier, S. M.; McGee, D.; Guinosso, C. J.; Cook, P. D., Characterization of fully 2'-modified oligoribonucleotide hetero- and homoduplex hybridization and nuclease sensitivity. *Nucleic Acids Res.* **1995**, *23* (11), 2019-2024.
17. Bock, L. C.; Griffin, L. C.; Latham, J. A.; Vermaas, E. H.; Toole, J. J., Selection of single-stranded DNA molecules that bind and inhibit human thrombin. *Nature* **1992**, *355* (6360), 564.
18. Qi, H.; Lin, C.-P.; Fu, X.; Wood, L. M.; Liu, A. A.; Tsai, Y.-C.; Chen, Y.; Barbieri, C. M.; Pilch, D. S.; Liu, L. F., G-Quadruplexes Induce Apoptosis in Tumor Cells. *Cancer Res.* **2006**, *66* (24), 11808-11816.
19. Wyatt, J. R.; Vickers, T. A.; Roberson, J. L.; Buckheit, R. W., Jr.; Klimkait, T.; DeBaets, E.; Davis, P. W.; Rayner, B.; Imbach, J. L.; Ecker, D. J., Combinatorially selected guanosine-quartet structure is a potent inhibitor of human immunodeficiency virus envelope-mediated cell fusion. *Proc. Natl. Acad. Sci. USA* **1994**, *91* (4), 1356-1360.
20. Wang, K. Y.; McCurdy, S.; Shea, R. G.; Swaminathan, S.; Bolton, P. H., A DNA aptamer which binds to and inhibits thrombin exhibits a new structural motif for DNA. *Biochemistry* **1993**, *32* (8), 1899-1904.
21. Coughlin, S. R., Thrombin signalling and protease-activated receptors. *Nature* **2000**, *407* (6801), 258-264.
22. (a) Macaya, R. F.; Schultze, P.; Smith, F. W.; Roe, J. A.; Feigon, J., Thrombin-binding DNA aptamer forms a unimolecular quadruplex structure in solution. *Proc. Natl. Acad. Sci. USA* **1993**, *90* (8), 3745-3749; (b) Padmanabhan, K.; Padmanabhan, K.; Ferrara, J.; Sadler, J. E.; Tulinsky, A., The structure of alpha-thrombin inhibited by a 15-mer single-stranded DNA aptamer. *J. Bio. Chem.* **1993**, *268* (24), 17651-17654.

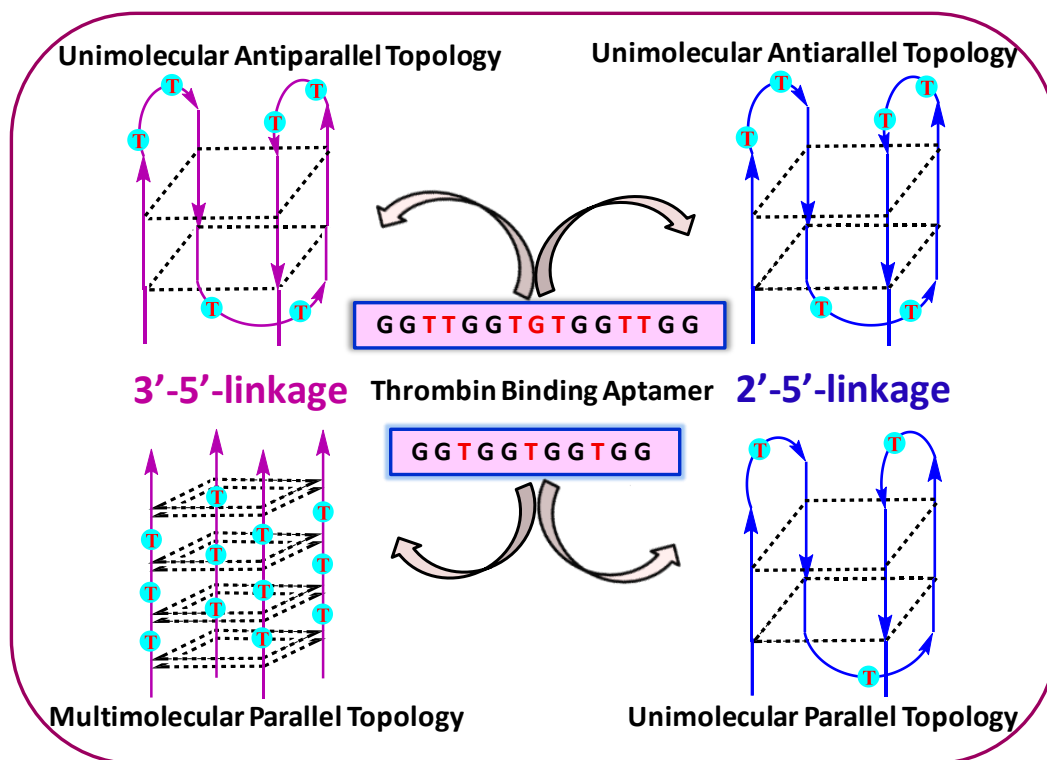
23. Schultze, P.; Macaya, R. F.; Feigon, J., Three-dimensional solution structure of the thrombin-binding DNA aptamer d(GGTTGGTGTGGTTGG). *J. Mol. Bio.* **1994**, *235* (5), 1532-1547.
24. Guschlbauer, W.; Jankowski, K., Nucleoside conformation is determined by the electronegativity of the sugar substituent. *Nucleic Acids Res.* **1980**, *8* (6), 1421-1433.
25. Peng, C. G.; Damha, M. J., G-quadruplex induced stabilization by 2'-deoxy-2'-fluoro-D-arabinonucleic acids (2'F-ANA). *Nucleic Acids Res.* **2007**, *35* (15), 4977-4988.
26. Aviñó, A.; Mazzini, S.; Ferreira, R.; Gargallo, R.; Marquez, V. E.; Eritja, R., The effect on quadruplex stability of North-nucleoside derivatives in the loops of the thrombin-binding aptamer. *Bioorg. Med. Chem.* **2012**, *20* (14), 4186-4193.
27. Sacca, B.; Lacroix, L.; Mergny, J.-L., The effect of chemical modifications on the thermal stability of different G-quadruplex-forming oligonucleotides. *Nucleic Acids Res.* **2005**, *33* (4), 1182-1192.
28. Awachat, R.; Wagh, A. A.; Aher, M.; Fernandes, M.; Kumar, V. A., Favorable 2'-substitution in the loop region of a thrombin-binding DNA aptamer. *Bioorg. Med. Chem. Lett.* **2018**, *28* (10), 1765-1768.
29. Bonifacio, L.; Church, F. C.; Jarstfer, M. B., Effect of locked-nucleic acid on a biologically active G-quadruplex. A structure-activity relationship of the thrombin aptamer. *Int. J. Mol. Sci.* **2008**, *9* (3), 422-433.
30. Varada, M.; Aher, M.; Erande, N.; Kumar, V. A.; Fernandes, M., Methoxymethyl Threofuranosyl Thymidine (4'-MOM-TNA-T) at the T7 Position of the Thrombin-Binding Aptamer Boosts Anticoagulation Activity, Thermal Stability, and Nuclease Resistance. *ACS Omega* **2020**, *5* (1), 498-506.
31. Erande, N.; Gunjal, A. D.; Fernandes, M.; Kumar, V. A., Probing the furanose conformation in the 2'-5' strand of iso DNA: RNA duplexes by freezing the nucleoside conformations. *Chem. Commun.* **2011**, *47* (13), 4007-4009.
32. Wright, J.; Taylor, N., Fluorocarbohydrates: Part XVI. The synthesis of 3-deoxy-3-flouro-D-xylose and 3-deoxy-3-flouro-β-D-arabinose. *Carbohydr. Res.* **1967**, *3* (3), 333-339.
33. Miyai, K.; Robins, R. K.; Tolman, R. L., Synthesis of 9-(3-deoxy-3-flouro-.beta.-D-arabinofuranosyl)adenine. *J. Med. Chem.* **1972**, *15* (10), 1092-1093.

-
34. Mikhailopulo, I. A.; Poopeiko, N. E.; Prikota, T. I.; Sivets, G. G.; Kvasyuk, E. I.; Balzarini, J.; De Clercq, E., Synthesis and antiviral and cytostatic properties of 3'-deoxy-3'-fluoro- and 2'-azido-3'-fluoro-2',3'-dideoxy-D-ribofuranosides of natural heterocyclic bases. *J. Med. Chem.* **1991**, *34* (7), 2195-2202.
35. Mikhailopulo, I. A.; Sivets, G. G., A Novel Route for the Synthesis of Deoxy Fluoro Sugars and Nucleosides. *Helv. Chim. Acta* **1999**, *82* (11), 2052-2065.
36. Niedballa, U.; Vorbrüggen, H., A General Synthesis of Pyrimidine Nucleosides. *Angew. Chem., Int. Ed. Engl.* **1970**, *9* (6), 461-462.
37. Wright, J. A.; Taylor, N. F.; Fox, J. J., Nucleosides. LX. Fluorocarbohydrates. 22. Synthesis of 2-deoxy-2-fluoro-D-arabinose and 9-(2-deoxy-2-fluoro-. alpha. and beta.-D-arabinofuranosyl) adenines. *J. Org. Chem.* **1969**, *34* (9), 2632-2636.
38. Foster, A. B.; Hems, R.; Webber, J. M., Fluorinated carbohydrates: Part I. 3-deoxy-3-fluoro-d-glucose. *Carbohydr. Res.* **1967**, *5* (3), 292-301.
39. Wright, J. A.; Taylor, N. F.; Fox, J. J., Nucleosides. LX. Fluorocarbohydrates. 22. Synthesis of 2-deoxy-2-fluoro-D-arabinose and 9-(2-deoxy-2-fluoro-.alpha. and .beta.-D-arabinofuranosyl)adenines. *J. Org. Chem.* **1969**, *34* (9), 2632-2636.
40. Tewson, T. J.; Welch, M. J., New approaches to the synthesis of 3-deoxy-3-fluoro-D-glucose. *J. Org. Chem.* **1978**, *43* (6), 1090-1092.
41. Tsoukala, E.; Agelis, G.; Dolinšek, J.; Botić, T.; Cencič, A.; Komiotis, D., An efficient synthesis of 3-fluoro-5-thio-xylofuranosyl nucleosides of thymine, uracil, and 5-fluorouracil as potential antitumor or/and antiviral agents. *Bioorg. Med. Chem.* **2007**, *15* (9), 3241-3247.
42. Obika, S.; Morio, K.-i.; Nanbu, D.; Imanishi, T., Synthesis and conformation of 3'-O,4'-C-methylenribonucleosides, novel bicyclic nucleoside analogues for 2',5'-linked oligonucleotide modification. *Chem. Commun.* **1997**, (17), 1643-1644.
43. Hunt, D. J.; Subramanian, E., The crystal structure of 5-methyluridine. *Acta Crystallogr., Sect. B* **1969**, *25* (10), 2144-2152.
44. Groom, C. R.; Bruno, I. J.; Lightfoot, M. P.; Ward, S. C., The Cambridge Structural Database. *Acta Crystallogr., Sec. B* **2016**, *72* (2), 171-179.
45. (a) Altona, C.; Sundaralingam, M., Conformational analysis of the sugar ring in nucleosides and nucleotides. New description using the concept of pseudorotation. *J. Am. Chem. Soc.* **1972**, *94* (23), 8205-8212; (b) Mathé, C.; Périgaud, C., Recent

- Approaches in the Synthesis of Conformationally Restricted Nucleoside Analogues. *Eur. J. Org. Chem.* **2008**, 2008 (9), 1489-1505.
46. De Leeuw, H. P. M.; Haasnoot, C. A. G.; Altona, C., Empirical Correlations Between Conformational Parameters in β -D-Furanoside Fragments Derived from a Statistical Survey of Crystal Structures of Nucleic Acid Constituents Full Description of Nucleoside Molecular Geometries in Terms of Four Parameters. *Isr. J. Chem.* **1980**, 20 (1-2), 108-126.
47. Elzagheid, M. I.; Viazovkina, E.; Damha, M. J., Synthesis of Protected 2'-Deoxy-2'-fluoro- β -D-arabinonucleosides. *Curr Protoc Nucleic Acid Chem* **2002**, 10 (1), 1.7.1-1.7.19.
48. Gait, M. J., *Oligonucleotide synthesis : a practical approach*. Rev. repr. ed.; Oxford : IRL press: 1984.
49. Karsisiotis, A. I.; Hessari, N. M. a.; Novellino, E.; Spada, G. P.; Randazzo, A.; Webba da Silva, M., Topological characterization of nucleic acid G-quadruplexes by UV absorption and circular dichroism. *Angew. Chem., Int. Ed. Engl.* **2011**, 50 (45), 10645-10648.
50. Gunjal, A. D.; Fernandes, M.; Erande, N.; Rajamohanan, P. R.; Kumar, V. A., Functional isoDNA aptamers: modified thrombin binding aptamers with a 2'-5'-linked sugar-phosphate backbone (*iso*TBA). *Chem. Commun.* **2014**, 50 (5), 605-607.
51. Baldrich, E.; O'Sullivan, C. K., Ability of thrombin to act as molecular chaperone, inducing formation of quadruplex structure of thrombin-binding aptamer. *Anal. Biochem.* **2005**, 341 (1), 194-197.
52. Nagatoishi, S.; Tanaka, Y.; Tsumoto, K., Circular dichroism spectra demonstrate formation of the thrombin-binding DNA aptamer G-quadruplex under stabilizing-cation-deficient conditions. *Biochem. Biophys. Res. Commun.* **2007**, 352 (3), 812-817.
53. Mann, K. G.; Jenny, R. J.; Krishnaswamy, S., Cofactor proteins in the assembly and expression of blood clotting enzyme complexes. *Annu. Rev. Biochem.* **1988**, 57, 915-956.

Chapter 3

Truncated loops in 3'-5' linked TBA Vs 2'-5' linked *iso*TBA: Effect on quadruplex topology and thrombin binding



G-quadruplexes are secondary structures formed from guanine rich nucleic acid sequences. The loop length, as well as the nature and identity of nucleotides in the loop region, control the topology and stability of the quadruplex structures. The relative arrangement of the strands can have different polarities. Strands can be parallel, antiparallel and mixed type. This chapter summarizes the synthesis of 3'-5' linked TBA and 2'-5' linked *iso*TBA variants with truncated loops and the effect on the quadruplex topology and thrombin binding properties. The 2'-5'-linked *iso*TBA sequences of the present study were found to form antiparallel G-quadruplex structures, independent of the loop length in the presence of K^+ ions. This result is in contrast to previously reported studies of 3'-5'-phosphodiester-linked G-quadruplexes where reducing the loop length resulted in a change from an antiparallel to a parallel quadruplex structural topology.

3.1 Introduction

Guanine rich aptamers exhibit a variety of folding patterns to form three dimensional structures known as G-quadruplexes that bind to the desired target. The high affinity with the target is derived from the fitting of the three-dimensional shape of the quadruplex to the binding site and an array of electrostatic/hydrogen bonding interaction possibilities created in the loop region, as a consequence of the folded structures. Classification of the G-quadruplex topology can be done into three groups which are parallel (group I), mixed or hybrid (group II) and antiparallel (group III) on the basis of orientation of the polyG strands and the preference of a *syn* or an *anti* glycosidic bond angle (GBA) of guanine¹ (Figure 1). In parallel (group I) quadruplexes, all the guanosine residues adopt the same GBA (all either *anti* or *syn*) and all the four strands have the same orientation. The mixed or hybrid (group II) quadruplexes contain both, sequences of guanosines with the same type of GBA (such as *anti-anti* and *syn-syn*), as well as different types (such as *syn-anti* and *anti-syn* steps). In contrast, antiparallel G-quadruplexes (group-III) exhibit both *anti* and *syn* guanines with *syn-anti* or *anti-syn* steps. As both group-II and group-III quadruplexes possess at least one of the four strands oriented antiparallel to the others, both are considered as types of antiparallel quadruplexes.

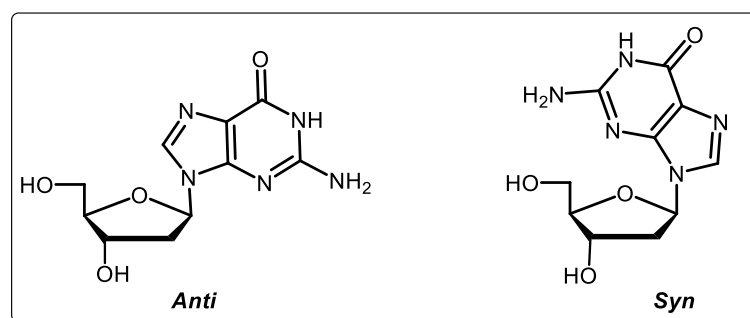


Figure 1: *anti* and *syn* conformations of the glycosidic bond angle in guanosine

3.2 Rationale and objectives of the present work

Various factors affect the topology and stability of G-quadruplexes, such as loop length, type of nucleobase in the loop, and glycosidic bond angle of guanosine.² Among all these, loops play a key role in determining the nature of the folding of G-quadruplexes. Fox and co-workers examined the properties of an intramolecular G-quadruplex where they replaced T with different nucleobases (adenine, cytosine, 1', 2'-

dideoxyribose). Their results suggested that not only loop length but also the loop nucleotide sequence affects quadruplex stability.³ Balasubramanian et al.² studied various G-quadruplex-forming sequences with varying loop lengths using UV and CD spectroscopy, molecular modeling and simulations to confirm that parallel is the only possible conformation for G-quadruplexes with shorter loops (i.e., the total number of nucleotides in the loops less than 6).

Multiple constructs of the G quadruplex-forming thrombin-binding aptamer (TBA) have been used to study G-quadruplex topology. The thrombin-binding aptamer (TBA; d(GGTTGGTGTGGTTGG)) binds to thrombin, an important protein in the blood coagulation cascade.⁴ The unimolecular structure of the G-quadruplex formed by TBA is well studied and is composed of two stacked G-quartets, two external TT loops and one central TGT loop, resulting in a chair-like conformation, stabilized by monovalent cations such as Na⁺ or K⁺.⁵ The TT loops were found to be sufficient to span the narrow grooves and the TGT loop sufficed to span the wider groove of the quadruplex. The two TT loops of the quadruplex are currently believed to interact with the thrombin anion exosite I in 1: 1 stoichiometry.⁶

Several chemical modifications of TBA are reported in the literature in the view of further optimizing its binding to thrombin and also to improve its stability⁷ against cellular nucleases. The nucleotides in the loop region as well as the length of the loop control the topology and stability of the quadruplex structures in general and also in the case of TBA.⁸ Shorter loop lengths (less than total 6 nucleotides in the loop) are known to destabilize the intramolecular, antiparallel G-quadruplexes such as TBA and allow only parallel intermolecular four-stranded G-quadruplex structures.² As a consequence, the thrombin-binding activity of TBA sequences in which the loops are short is adversely affected,⁹ whereas extension to TTT did not alter the topology but showed lower stability. Changes in the composition of loop or loop sequence have a substantial effect on the stability of the resulting structure.¹⁰ In contrast, releasing the rigidity in the loop region by introducing unlocked nucleic acid monomers and an abasic three-carbon spacer (spacer-C3) at selective positions in the loop region of TBA, e.g., at the T⁷ loop position caused an improvement in thermal stability and thrombin clotting time.¹¹

The 3'-deoxy-2'-5'-linked non-genetic *iso*DNA (Figure 2) exhibits high stability against cellular enzymes¹² and therefore it could be a promising alternative nucleic acid

for DNA therapeutics. Formation of duplex and triplex structures comprising *iso*DNA and complementary RNA is well-documented in the literature.¹³

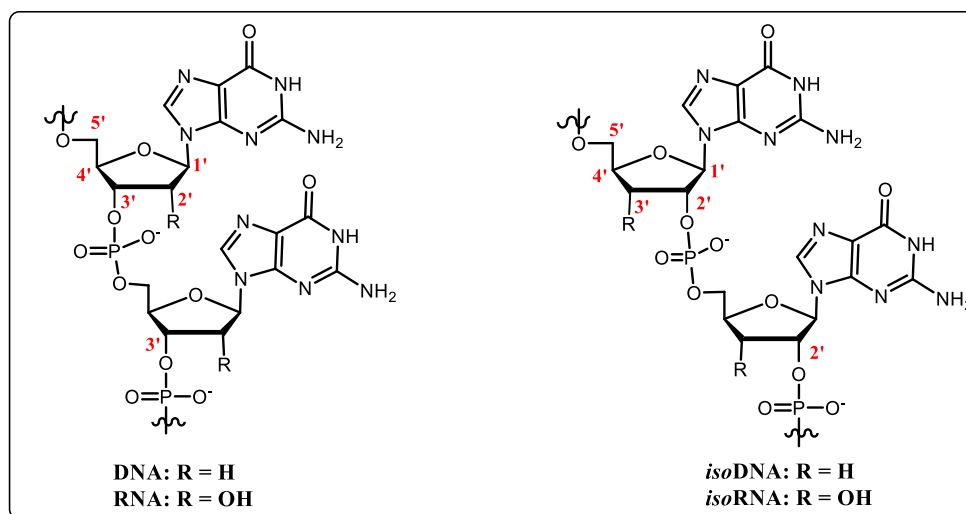


Figure 2: Genetic 3'-5'-linked DNA/RNA and non-genetic 2'-5'-linked *iso*DNA/*iso*RNA.

In a previous communication from our research group, we reported that employing these nuclease-resistant, homogeneous 2'-5' linkers in TBA (*iso*TBA) could also result in G-quadruplex structures that could exhibit the thrombin-binding property.¹⁴ In *iso*DNA, the phosphodiester linkage is C2'-C5' instead of C3'-C5' linkages present in native DNA (Figure 2). This leads to an increase in the number of bonds between O5' and phosphorus from six in DNA to seven in *iso*DNA. Also, the 2'-5' linkages maintain an extended backbone geometry as the *anomeric* effect and the O4'-C1'-C2'-O2' *gauche* effect on the substituted sugar favours N-type sugar conformation (Figure 3).¹⁵ This extended backbone with an increased number of bonds in *iso*TBA compared to TBA is probably responsible for the relatively less stable G-quadruplex structure compared to TBA.

As the nuclease resistant isomeric 2'-5'-linked *iso*TBA showed potential as an anticoagulant, we thought of exploring the possibilities of further stabilizing the quadruplex structure of *iso*TBA. Our group earlier reported that replacement of the central TGT loop by UGU loop stabilized the G-quadruplex structure of *iso*TBA.¹⁴ The 3'-hydroxy group in uridine would disfavour the extended N-type sugar conformation (Figure 3) compared to the 3'-deoxyuridine, due to the additional O4'-C4'-C3'-O3' *gauche* effect and exert rigidity in the TGT loop region due to compact S-type geometry of the sugar (Figure 3).

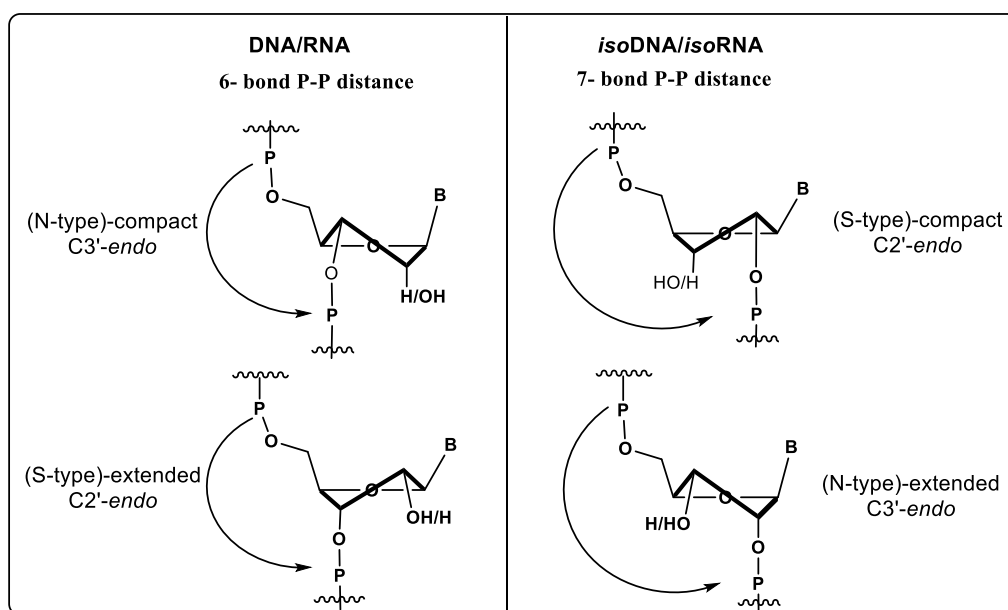


Figure 3: Extended and compact backbone geometry in DNA/RNA and *isoDNA/isoRNA*.

We, therefore, envisaged that unlike in TBA, *isoTBA* may benefit from decreasing the loop length and thought of exploring the effect of systematically decreasing the length in the loop region of *isoTBA*. For comparison, we also synthesized the earlier reported TBA sequences with decreasing loop length.¹⁰ This would enable us to study the effect of the reduced loop length on the topology of the G-quadruplexes formed by different *isoTBA*-like sequences and compare it with isosequential TBA.

3.3 Present work, results and discussion

3.3.1 Synthesis of TBA, *isoTBA* and TBA/*isoTBA* variants with truncated loops, their purification and characterization

We designed truncated loop TBA oligomers for the current study that consist of the 3'-5'-linked TBA and 2'-5'-linked *isoTBA* oligomers with shortened loop length (having the total number of loop residues 7, 6, 5 or 3). All the DNA and *isoDNA* ONs (listed in Table 1) were synthesized on a Bioautomation MM4 DNA synthesizer using commercially available protected 2'-deoxyguanosine-3'-phosphoramidite, 2'-deoxythymidine-3'-phosphoramidite, 3'-deoxy-thymidine-2'phosphoramidite and 3'-deoxy-guanosine-2'-phosphoramidite by standard β -cyanoethyl phosphoramidite chemistry.¹⁶ The synthesized oligonucleotides were cleaved from the solid support by aq. ammonia treatment at 55°C. Purification of synthesized oligomers was done by RP-

HPLC and their integrity was confirmed by MALDI-TOF mass spectrometric analysis. The general scheme for solid-phase oligonucleotide synthesis is explained in Chapter 1, Scheme 1. The synthesized oligomeric sequences and their MALDI-TOF characterization data are listed in Table 1.

The three-digit numbers in the sequence name are indicative of the number of residues in each loop, from 5'-end to the 3'/2'-end and the number in parentheses indicates the total number of loop residues. Thus, TBA232 (7) bears two residues in each TT loop and 3 residues in the central TGT loop, making the total number of loop residues 7. Loop residues are indicated in bold letters in the oligonucleotide sequence. sTBA is scrambled TBA sequence.

Table 1: TBA and *iso*TBA loop-modified oligomers, MALDI-TOF mass analysis

Entry no.	Sequence code	Sequence	MALDI-TOF Mass	
			$M_{\text{calcd.}}$	$M_{\text{obsd.}}$
1.	TBA232(7)	5'-GGT TGGTGTGGT TGG-3'	4726	4727
2.	TBA222(6)	5'-GGT TGGTTGGT TGG-3'	4396	4396
3.	TBA131(5)	5'-GGT TGGTGTGGT TGG-3'	4117	4116
4.	TBA111(3)	5'-GGT TGGTGGT TGG-3'	3484	3481
5.	<i>iso</i> TBA232(7)	5'-GGT TGGTGTGGT TGG-2'	4726	4731
6.	<i>iso</i> TBA222(6)	5'-GGT TGGTTGGT TGG-2'	4396	4392
7.	<i>iso</i> TBA131(5)	5'-GGT TGGTGTGGT TGG-2'	4117	4121
8.	<i>iso</i> TBA111(3)	5'-GGT TGGTGGT TGG-2'	3484	3483
9.	sTBA	5'-GGTGGTGGTTGTGGT-3'	4726	4730

3.3.2 Evaluation of G-quadruplex formation and topology using circular dichroism spectroscopy

CD spectroscopy is a primary characterization tool to analyze the nature of the G-quadruplex structure and is used to explore the parallel, mixed or hybrid and antiparallel G-quadruplex folding topology based on well-characterized CD patterns corresponding to the topology of the G-quadruplexes.¹⁷ The G-quadruplex structure is known to form

in presence of monovalent or divalent cations. To study the effect of K^+ on the topology, we recorded CD spectra in water (absence of any cation), and two different concentrations of potassium ions (K^+) (100 mM and 500 mM). Results are summarised in Table 2.

In the CD spectra of the loop-modified sequences in water, only the 15 mer TBA232(7) exhibited a weak positive signal at ~292 nm, showing its propensity for the formation of unimolecular antiparallel G-quadruplex even in the absence of cations. Except for TBA232(7), all the other loop modified TBA and *iso*TBA sequences were unable to adopt a quadruplex structure in the absence of cations (Figure 4). In the presence of monovalent K^+ ion (5 μ M strand concentration, 100 mM K^+ and 500 mM K^+ , Figure 4, Table 2), the unmodified 3'-5'-linked TBA232(7) showed maxima at 295 nm and minima at 265 nm, indicative of an antiparallel G-quadruplex.¹

Decreasing the loop length in TBA is known to disturb the unimolecular TBA quadruplex structure and the results were similar as reported earlier for TBA222(6) and TBA131(5).⁹ In these two oligomers which have intermediate loop length total of six/five residues respectively, the CD spectra showed two positive bands near 292 nm and 262 nm and a negative band at 235 nm indicating either a hybrid-type (group II) quadruplex conformation or the co-existence of parallel and antiparallel conformations. The 3'-5'-linked TBA111(3), having a total of three thymine residues, one in each of the three loops, and the shortest loop sequence studied, exhibited maxima and minima at 260 nm and 235 nm respectively indicating the group-I parallel G-quadruplex topology.¹⁰ Thus, in concurrence with the previous reports and loop-length phenomenon studied by Balasubramanian,¹⁸ we observed that in the case of TBA, as the loop length decreased from 232(7) to 111(3), the quadruplex topology changed from antiparallel to parallel structures. The shorter loop lengths could not support the quadruplex topology with antiparallel orientation (Figure 4a).

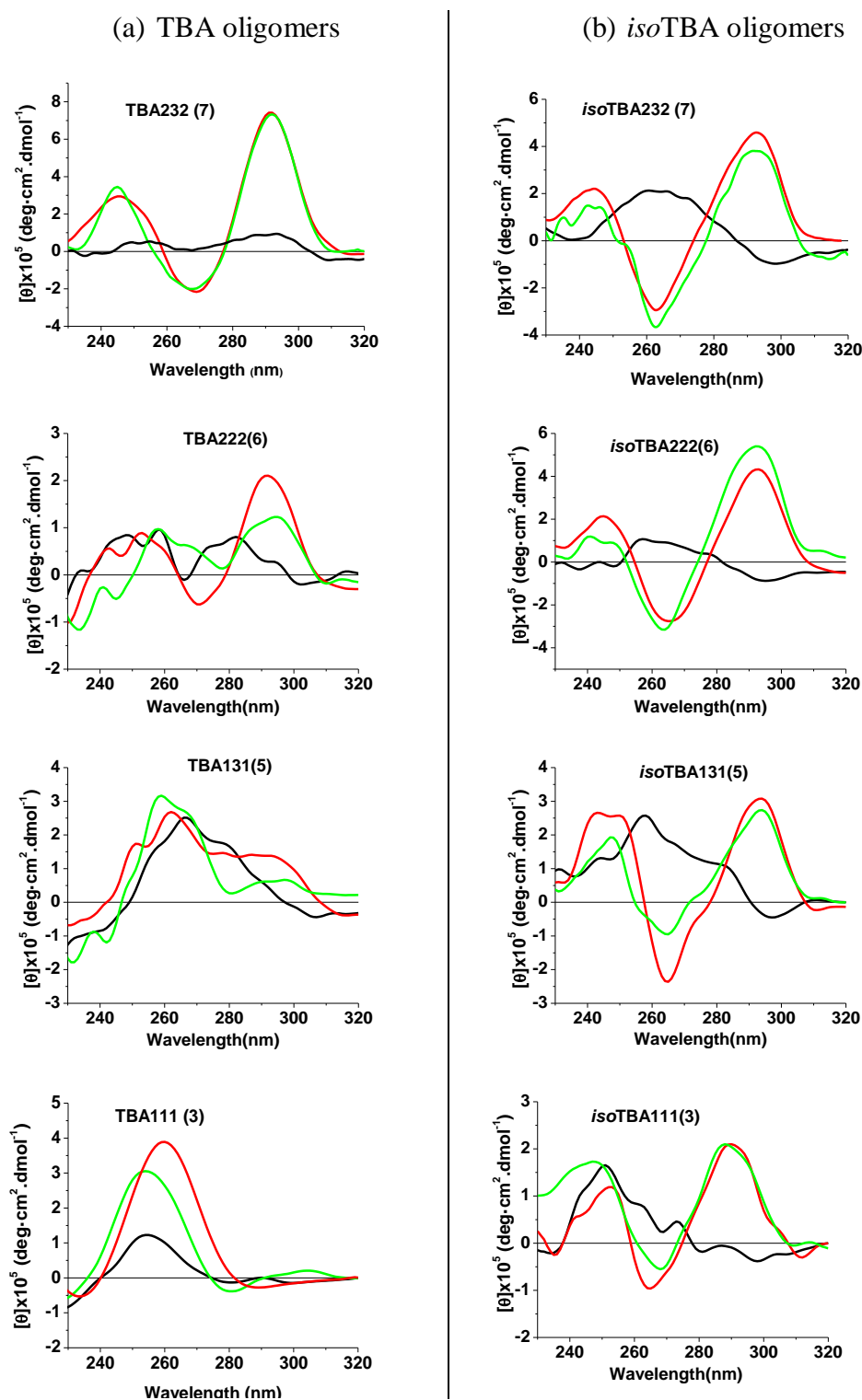


Figure 4: CD spectra of all the synthesized loop modified sequences (**Black**-5 μM in H_2O , **Red**-5 μM in buffer containing 100 mM K^+ , and **Green**-5 μM in buffer containing 500 mM K^+)

We further studied the CD spectra of the *iso*TBA sequences with shorter loops in comparison to TBA (Figure 4b). The results are tabulated in Table 2. Contrary to the results obtained for the loop-modified TBA, we observed that irrespective of loop length,

all the modified *iso*TBA sequences containing 222(6), 131(5) or even 111(3) loop nucleotides, exhibited a strong positive CD signal at 295 nm and minima at ~260 nm in the presence of K⁺ ions, characteristic of the antiparallel G-quadruplex conformation. In the case of 2'-5'-linked *iso*TBA, extended N-type conformation of nucleotides and presence of larger P-P distance^{15a} might relieve the strain caused by shorter loop lengths and allow the *iso*TBA to assume an antiparallel G-quadruplex structure. Another reason for the preferred antiparallel conformation for the *iso*TBA sequences could be the preferred *syn* and *anti* conformations for the 5'-end- and penultimate nucleobase respectively, of 2'-5'-linked oligomers, as evident from NMR¹⁹ and X-ray crystal structural studies.²⁰ This conformational restriction of 2'-5'-linked *iso*TBA oligomers may result in them not conforming to the 'all *syn*' or 'all *anti*' nucleobase conformation, a prerequisite for the formation of parallel quadruplex structures.

Table 2: TBA and *iso*TBA loop modified sequences and their CD analysis

code	5 μ M in H ₂ O at 5° C		5 μ M in 100 mM K ⁺ at 5° C		20 μ M in 100 mM K ⁺ at 5° C		5 μ M in 500 mM K ⁺ at 5° C		Topology
	Maxima	Minima	Maxima	Minima	Maxima	Minima	Maxima	Minima	
	(nm)	(nm)	(nm)	(nm)	(nm)	(nm)	(nm)	(nm)	
TBA232(7)	292	255	295,245	262	295, 245	262	292,245	262	Antiparallel
TBA222(6)	280, 250	265	292 ,252	270	292, 252	275	292, 252	275	Hybrid or mixture of antiparallel and parallel
TBA131(5)	280, 265	235	295, 275, 260	235	295, 275, 260	235	295, 275, 260	235	Hybrid or mixture of antiparallel and parallel
TBA111(3)	255	230	260	235	260	235	255	230	Parallel
<i>iso</i> TBA232(7)	260	295	295, 250	268	295, 250	268	295 , 240	260	Antiparallel
<i>iso</i> TBA222(6)	260	294	291, 243	265	291, 243	265	291 , 243	265	Antiparallel
<i>iso</i> TBA131(5)	280-258	298 , 230	292, 245	265	292-245	265	292, 245	265	Antiparallel
<i>iso</i> TBA111(3)	250	295	290, 250	265,	295, 245	265	290, 245	270,	Antiparallel

The CD patterns for all the TBA and *iso*TBA sequences were studied at a higher salt concentration (Figure 4) and at increased strand concentrations²¹ (Figure 5) to see if this affected the unique antiparallel nature of the G-quadruplexes formed by *iso*TBA sequences in comparison with those by TBA sequences. In the case of TBA232(7), only increase in the intensity of bands at 295 nm and 265 nm was seen, with the overall CD pattern remaining unchanged. In the loop-restricted TBA sequences TBA222(6), TBA131(5) and TBA111(3), the increased intensity of the CD signal at 260 nm was observed in the CD spectra at higher strand concentration, with decreasing loop length, indicating higher inclination to form parallel structures (Figure 5a). In contrast, the CD maximum at 260 nm corresponding to the parallel structure was not observed even at the higher salt or strand concentrations studied herein for 2'-5'-linked *iso*TBA sequences with reduced loop lengths (Figures 4b and 5b), confirming that these G-quadruplexes were indeed of antiparallel topology.

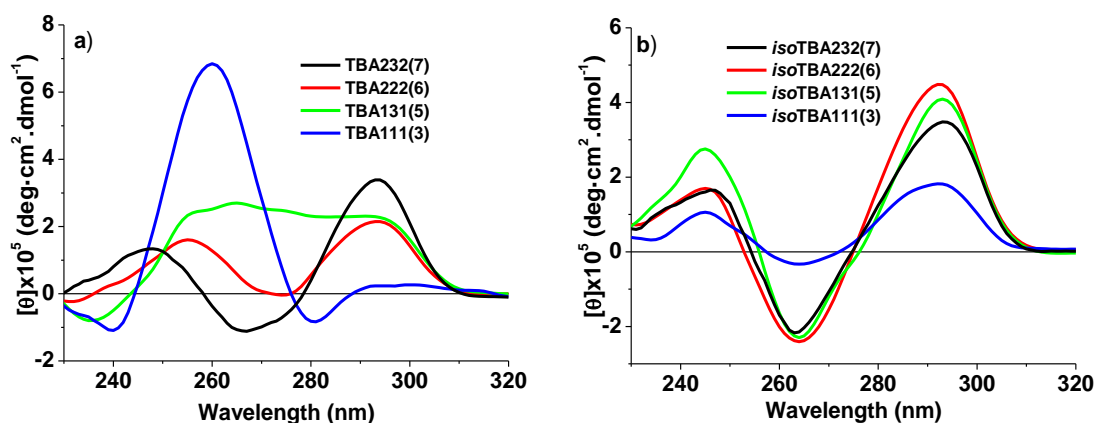


Figure 5: CD spectra of all the loop-modified sequences at 20 μ M concentration in 100 mM K^+ a) TBA sequences b) *iso*TBA sequences

3.3.3 Evaluation of G-quadruplex thermal stability using circular dichroism spectroscopy

The stability of the G-quadruplexes was followed by the temperature-dependent change in the amplitude of the CD signal at 295 nm for antiparallel quadruplexes formed by *iso*TBA oligomers in comparison with TBA232(7). The results were also compared with the change in the amplitude of the CD signal at 260 nm, for the parallel quadruplex formed by TBA111(3) (Table 3). At 5 μ M strand concentration in the presence of 100 mM K^+ , the *iso*TBA232(7) quadruplex was found to be less stable than the control TBA232(7) (Table 3, $\Delta T_m = -13$ °C, Figure 6a).¹⁴ All the other shorter loop-containing

antiparallel G-quadruplexes of *iso*TBA showed a decrease in stability with decreasing loop length. *Iso*TBA222(6) and *iso*TBA131(5) were equally stable, with T_m 5 °C less than that of *iso*TBA232(7) (Figure 7a). TBA111 (3), the oligomer with the shortest loop, existed in the parallel multimolecular quadruplex conformation, and consequently showed the highest thermal stability compared to all other sequences ($\Delta T_m = +5$ °C compared to TBA232(7)). In contrast, *iso*TBA111(3), containing the same number of nucleobases in the loops showed the lowest stability among all the sequences synthesized. Thus, although the extended 2'-5' linkages help to reduce the strain of the shortened loops in *iso*TBA111(3) compared to 3'-5' linkages and allow the formation of unimolecular folded structures, the quadruplex formed was less stable compared to the antiparallel quadruplexes formed by the other *iso*TBA and TBA oligomers.

Table 3: TBA and *iso*TBA loop-modified sequences and their CD- T_m at 295 nm at varying salt and strand concentrations. ^a indicates the CD- T_m values at 260 nm while all other values are at 295 nm

Oligomer code	T_m (°C) at 5 μ M, with 100 mM KCl		T_m (°C) at 20 μ M, with 100 mM KCl		T_m (°C) at 5 μ M, with 500 mM KCl	
	Heat	Cool	Heat	Cool	Heat	Cool
TBA232(7)	50	50	48	48	54.2	52.3
TBA111(3)	55 ^a	45 ^a	59.5 ^a	52.5 ^a	63.8 ^a	53 ^a
<i>iso</i> TBA232(7)	37	37	34	34	40	41
<i>iso</i> TBA222(6)	32	32	34.2	32.5	40	39.5
<i>iso</i> TBA131(5)	32	32	33.6	32.2	36.1	37.8
<i>iso</i> TBA111(3)	22	20	20	20	21.5	19.1

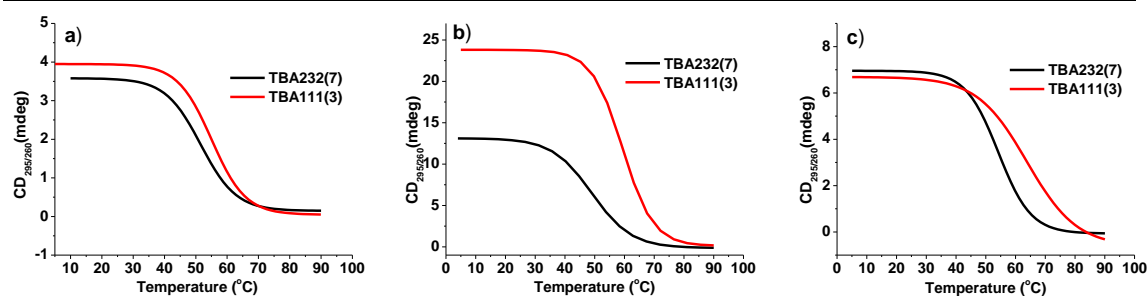


Figure 6: CD amplitude at 295 nm for TBA232 (7) and 260 nm TBA111(3) plotted versus temperature during heating to get T_m of TBA232(7) and TBA111(3) in presence of a) 5 μ M, in 100 mM KCl b) 20 μ M, in 100 mM KCl c) 5 μ M, in 500 mM KCl

The inter- Vs intramolecular nature of the quadruplexes was confirmed by carrying out CD melting experiments at a higher strand concentration (20 μM). The melting temperatures of all the *iso*TBA sequences were independent of concentration, similar to the TBA232(7) (at 5 μM and 20 μM ; Table 3, Figure 6b & 7b), confirming that these sequences indeed formed intramolecular (monomeric) folded structures.

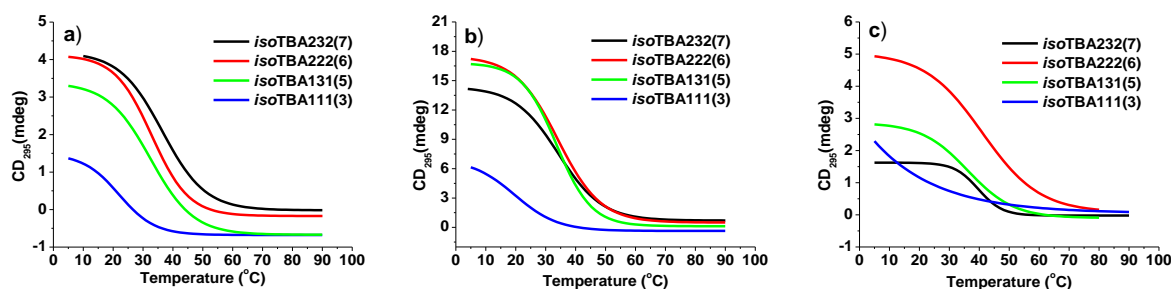


Figure 7: CD amplitude 295 nm versus temperature during heating to get T_m of *iso*TBA232(7), *iso*TBA222(6), *iso*TBA131(5) and *iso*TBA111(3) in presence of a) 5 μM , in 100 mM KCl b) 20 μM , in 100 mM KCl c) 5 μM , in 500 mM KCl

For all the CD melting experiments of antiparallel sequences, negligible hysteresis between the heating and the annealing curves was observed, again indicating unimolecular G-quadruplexes (Table 3, Figure 8 and Figure 9).²² The sequence TBA111(3), however, being a parallel multimolecular sequence melted at a higher temperature at 20 μM strand concentration. In the case of this sequence, appreciable hysteresis was also observed between the heating and cooling curves (Figure 8).

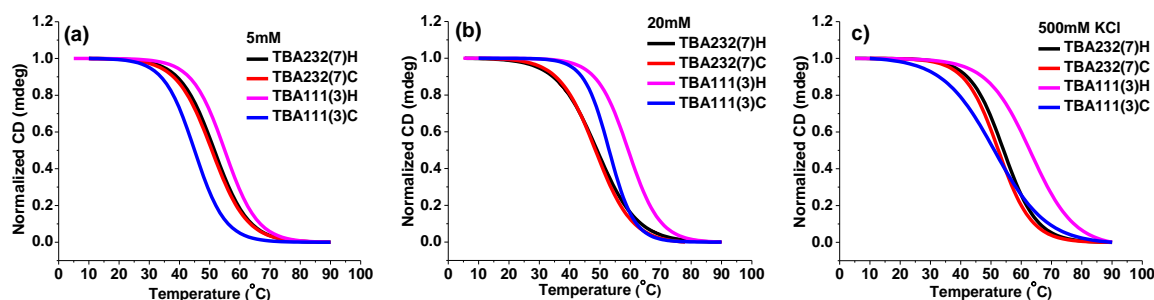


Figure 8: CD hysteresis CD amplitude at 295 nm for TBA232(7) and 260 nm TBA111(3) plotted versus temperature during heating and cooling experiments for TBA232(7), TBA111(3) in presence of a) 100 mM KCl at 5 μM strand concentration, b) 100 mM KCl at 20 μM strand concentration, and c) 500 mM KCl at 5 μM strand concentration. H= heating, C=cooling.

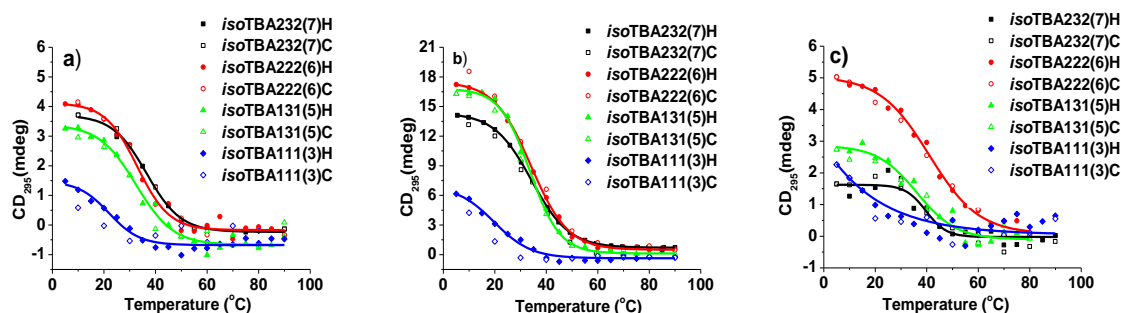


Figure 9: CD hysteresis CD amplitude at 295 nm versus temperature during heating and cooling experiments for *isoTBA232(7)*, *isoTBA222(6)*, *isoTBA131(5)* and *isoTBA111(3)* in presence of a) 100 mM KCl at 5 μ M strand concentration, b) 100 mM KCl at 20 μ M strand concentration, and c) 500 mM KCl at 5 μ M strand concentration. H= heating, C=cooling.

We further studied the CD melting of the *isoTBA* oligomers at a higher K^+ ion concentration of 500 mM. The T_m values of all the oligomers were found to be higher under these conditions, except in the case of *isoTBA111(3)*, where marginal destabilization was observed (Figures 6c & 7c).

3.3.4 Evaluation of G-quadruplex topology by UV-Thermal Difference Spectra

The thermal difference spectra (TDS) can be generated from the UV absorbance scans recorded at temperatures higher than and lower than that of the melting point of the quadruplexes. The TDS is known to provide a fingerprint of G-quadruplex topologies,²¹ and can be utilized to distinguish the different topologies of G-quadruplexes. To elucidate the topology of the G-quadruplexes of the synthesized loop-modified oligomers, we scanned their UV absorbance at different temperatures to generate the TDS. TDS were obtained by subtracting the spectral scan of the sample at temperatures below (i.e., 10 $^{\circ}$ C) and above (i.e., 90 $^{\circ}$ C) the melting temperatures (T_m s, Figure 10). The TDS factor is the ratio of $\Delta A_{240 \text{ nm}}/\Delta A_{295 \text{ nm}}$, where ΔA is the difference, at a given λ , between the absorbance above (i.e., 90 $^{\circ}$ C) and at a given temperature, T , below the melting temperature (where $T = 5$ $^{\circ}$ C, 10 $^{\circ}$ C, ..., etc. up to the melting temperature, T_m).¹

As the CD spectra for TBA232 (7) and TBA111 (3) showed maxima at 295 nm and 260 nm respectively, indicating two distinctly different G-quadruplex topologies, we first checked the TDS and TDS factor for these two oligomers (Figure 10a, and 10b). For TBA111(3), the values of TDS factor ($\Delta A_{240 \text{ nm}}/\Delta A_{295 \text{ nm}}$) appeared well above 4, indicating a group I parallel quadruplex, while the TDS factor of un-edited TBA232(7) was below 2, characteristic of antiparallel quadruplexes (group III).

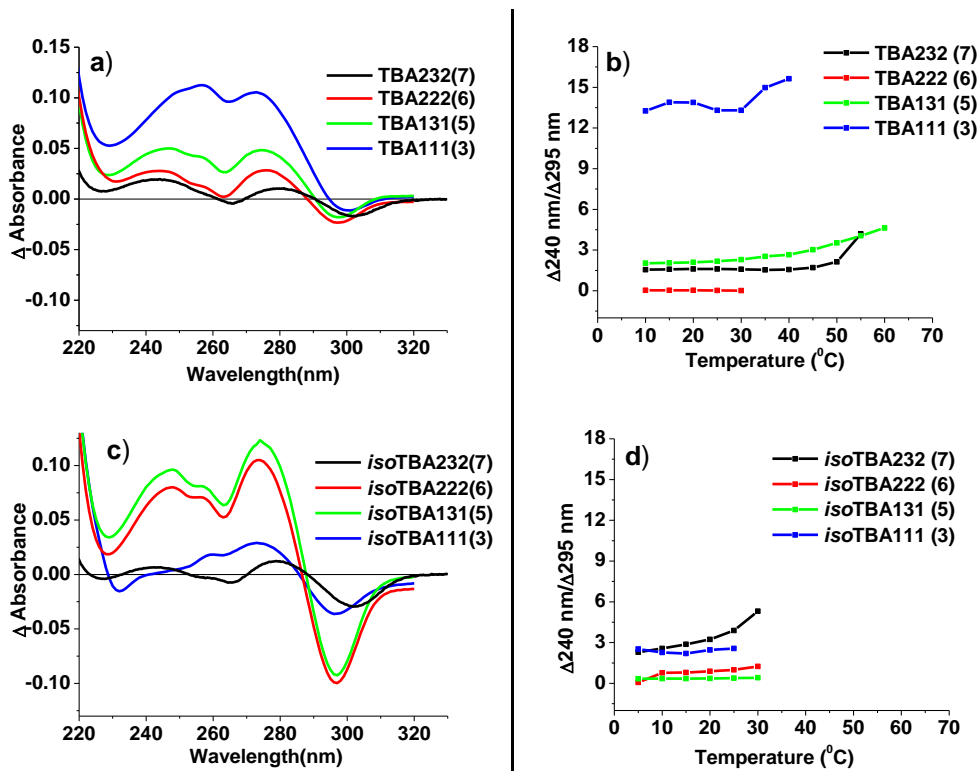


Figure 10: a) TDS of TBA oligomers, b) TDS factor of TBA oligomers c) TDS of *iso*TBA oligomers, d) TDS factor of *iso*TBA oligomers

Our observation that the TDS factor for both TBA222(6) and TBA131(5) was also below 2 was in concurrence with literature,¹ where it is reported that the TDS factor cannot differentiate group-II and group-III antiparallel quadruplexes. We conducted similar studies for the *iso*TBA sequences. The TDS factor of all the *iso*TBA sequences of the study was characteristic of antiparallel G-quadruplex topology (Figure 10c, Figure 10d). These results confirm the correct assignment of parallel/antiparallel quadruplex structures in concurrence with the CD signatures.

3.3.5 Polyacrylamide Gel Electrophoresis (PAGE) study

In a non-denaturing or native polyacrylamide gel, oligomers may be expected to preserve the higher-order structures, enabling one to distinguish them from single strands or differently ordered complexes. To confirm the structural and topological behaviour of the synthesized oligomers, we performed such a non-denaturing polyacrylamide gel retardation assay. A denaturing gel electrophoresis experiment was also carried out as a control. In the denaturing gel (Figure 11), the mobility of the oligonucleotides displayed molecular weight- and charge- dependency and marginally higher mobility was seen for TBA111(3) and *iso*TBA111(3), as expected.

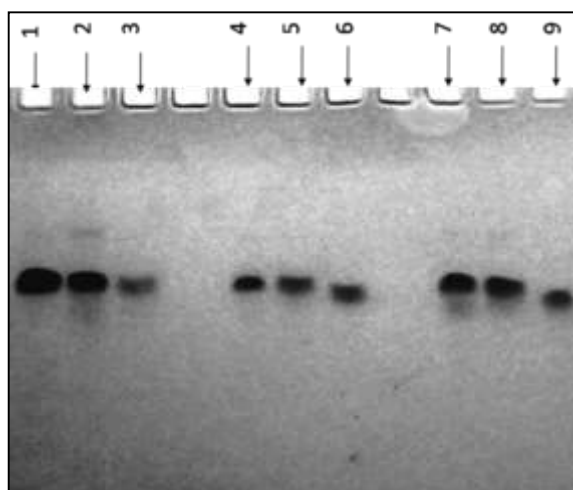


Figure 11: Denaturing polyacrylamide gel mobility assay of all the TBA and *iso*TBA oligomers. Lane1- Scrambled TBA (5'-GGTGGTGGTTGTGGT-3') Lane2-TBA232(7), Lane3-*iso*TBA232(7), Lane4-TBA222(6), Lane5-TBA131(5), Lane6-TBA111(3), Lane7-*iso*TBA222(6), Lane8-*iso*TBA131(5), Lane9-*iso*TBA111(3). The bands were visualized by UV-shadowing

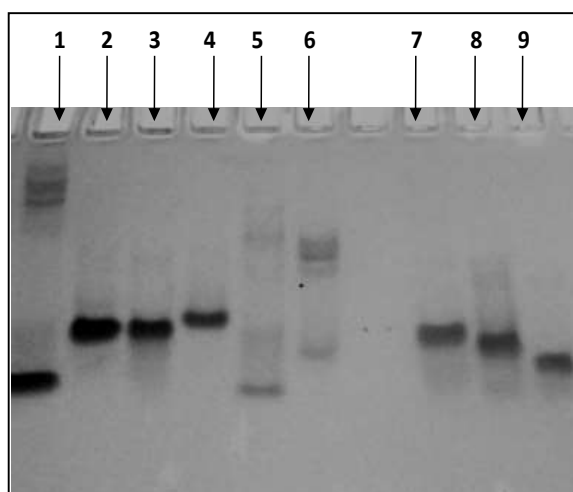


Figure 12 Non-denaturing polyacrylamide gel mobility assay of all the TBA and *iso*TBA oligomers. Oligomers were taken at 350 μ M concentration in potassium phosphate buffer (10 mM, pH 7.2); containing 500 mM KCl. Samples were annealed by heating at 90 $^{\circ}$ C for 2 min, followed by slow cooling to room temperature, and refrigeration for at least 2 h before the experiment. Lane1-Scrambled TBA (5'-GGTGGTGGTTGTGGT-3'), Lane2-TBA232(7), Lane3-*iso*TBA232(7), Lane4-TBA222(6), Lane5-TBA131(5), Lane6-TBA111(3), Lane7-*iso*TBA222(6), Lane8-*iso*TBA131(5), Lane9-*iso*TBA111(3). The bands were visualized by UV-shadowing.

The non-denaturing gel (Figure 12) clearly brought out the differences caused by the differing loop length on the quadruplex topology. The scrambled TBA sequence lacks the G-stretches required to form the typical unimolecular antiparallel TBA quadruplex but has the same nucleotide composition. The 15-mers TBA232(7) and *iso*TBA232(7), showed similar mobility corresponding to the unimolecular antiparallel quadruplex. TBA222 (6) showed the bands corresponding to a unimolecular quadruplex, although the CD spectrum indicated a hybrid structure for this sequence. Multiple bands were observed for the complex formed by TBA131 (5), suggesting the formation of different types of complexes. Highly retarded major bands of suggesting multimolecular quadruplexes were observed for TBA111 (3), as seen also in CD spectral studies. *Iso*TBA222 (6), *iso*TBA131(5) and *iso*TBA111(3) were observed as single bands corresponding to the unimolecular complexes, and no retarded bands were observed for these oligomers. Thus, the formation of unimolecular antiparallel quadruplexes in these cases was confirmed, as also seen from their CD spectral studies.

3.3.6 Binding with Thrombin (Chaperone Effect of Thrombin)

It has been shown previously that thrombin may act as a molecular chaperone for the folding of TBA232 (7).²³ Earlier studies from our group showed that the isomeric 2'-5'-linked *iso*TBA (*iso*TBA232(7)) also could be induced to attain a folded G-quadruplex by the chaperone activity of thrombin.¹⁴ We performed CD experiments with all the oligomers of the study, in the presence of increasing concentrations of thrombin at low temperature (Figure 13). In the case of native TBA232 (7), a CD maximum at 290 nm was observed even without thrombin or K⁺, revealing the preference for the G-quadruplex structure as discussed above. We observed an increase in the CD amplitude with a concomitant shift towards 300 nm upon incremental addition of thrombin. All the other 3'-5'-linked TBA oligomers with decreasing loop lengths did not show any change in the CD spectrum near 295 nm upon addition of thrombin, indicating the inability of thrombin to assist the folding of these oligomers into the typical quadruplex structure known for TBA (Figure 13b, 13c & 13d). On the other hand, in the case of all the 2'-5'-linked *iso*TBA oligomers, the CD maximum at 295 nm and thus, the G-quadruplex structure typical of TBA, was not evident in the absence of either thrombin or K⁺ ions. However, incremental addition of thrombin, showed the CD maximum at 295 nm appeared for *iso*TBA232(7), *iso*TBA222(6) and *iso*TBA131(5) (Figure 13e, 13f & 13g).

Isoelliptic points were observed at ~ 280 nm and ~ 255 nm in the case of *iso*TBA232(7) and *iso*TBA222 (6), indicating the two-state nature of the structural transition.²⁷ However, in the case of *iso*TBA111(3), thrombin was unable to induce the adoption of the antiparallel G-quadruplex structure (Figure 13h).

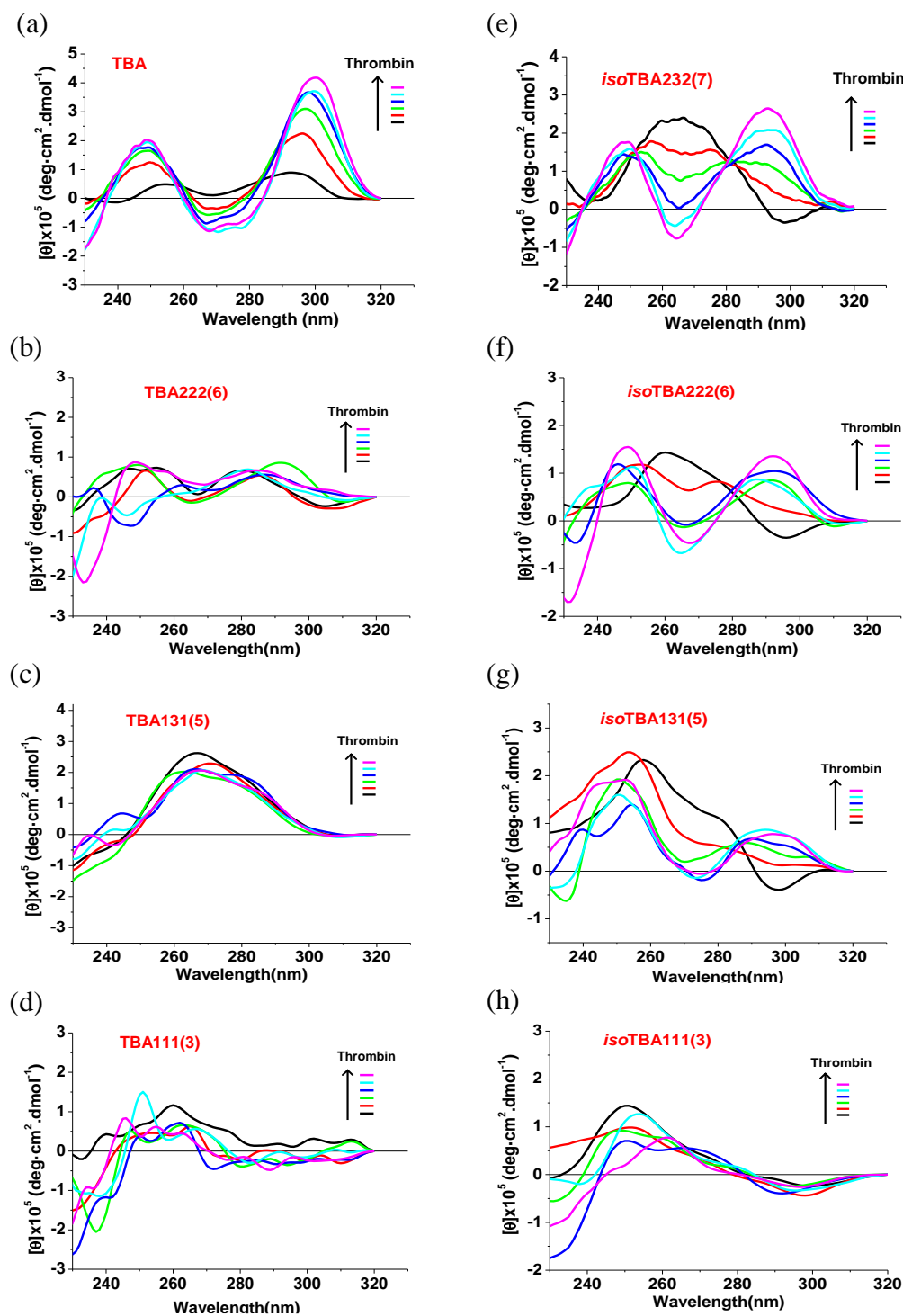


Figure 13: Changes in CD signal at 295 nm upon addition of thrombin Black: in water (No thrombin), Red: 0.44 μ M, Green: 0.85 μ M, Blue: 1.25 μ M, Cyan: 1.63 μ M, Magenta: 2 μ M

The temperature-dependent stability of these induced G-quadruplex structures was evaluated by recording the change in the CD amplitude at 295 nm with increasing temperature.

Table 4: CD data showing the chaperone effect of thrombin on the TBA and *iso*TBA loop-modified sequences and T_m values of the resulting quadruplexes. Oligomers were taken at 5 μ M strand concentration

Sequence code	+ Thrombin		Binding to thrombin	T_m ($^{\circ}$ C) with thrombin Heat/cool
	Maxima (nm)	Minima (nm)		
TBA232 (7)	298, 248	278-268	Yes	22/22
<i>iso</i> TBA232(7)	290, 245	265	Yes	13/13
<i>iso</i> TBA222(6)	291, 250	265	Yes	<10/<10
<i>iso</i> TBA131(5)	296, 248	272	Yes	<10/<10
<i>iso</i> TBA111(3)	260	295	No	-

The strength of the TBA232(7) G-quadruplex:thrombin complex was the highest with $T_m = 22$ $^{\circ}$ C, followed by *iso*TBA232 (7):thrombin ($T_m = 13$ $^{\circ}$ C), *iso*TBA222 (6):thrombin and *iso*TBA131 (5):thrombin ($T_m \leq 10$ $^{\circ}$ C for both oligomers).

Thrombin-binding studies of all the TBA and *iso*TBA oligomers were further carried out in buffer containing 100 mM KCl. The presence of K^+ ions ensured the restoration of the CD signal at 295 nm. Subsequent addition of thrombin led to negligible changes in the CD signal near 295 nm (Figure 14 and Figure 15). Melting studies of the so formed complexes revealed them to be as stable as with K^+ ions alone (Table 5).

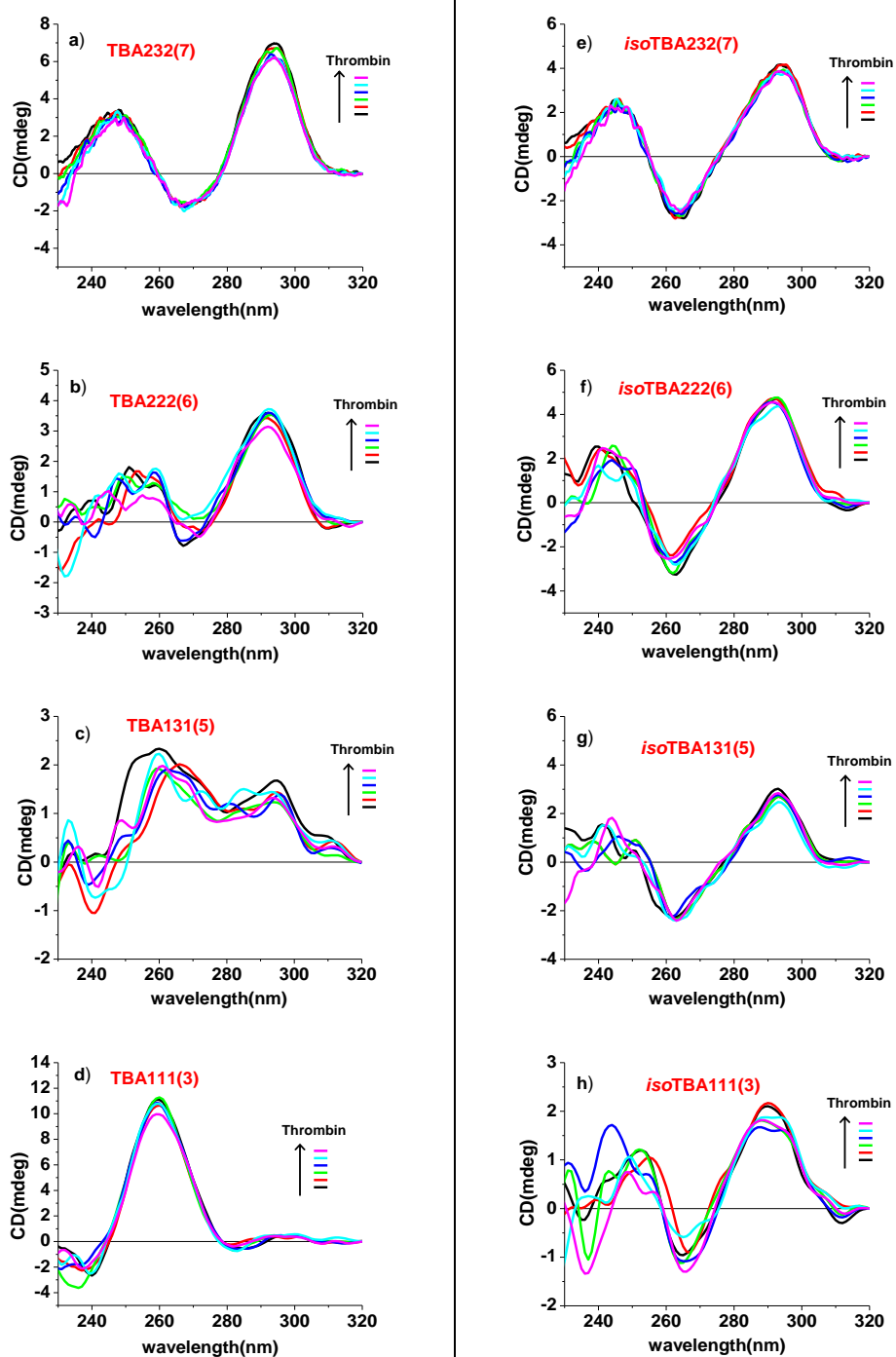


Figure 14: Changes in CD signal upon addition of thrombin for TBA and *iso*TBA sequences which annealed in 100 mM KCl a) TBA232(7), b) TBA222(6), c) TBA131(5), d) TBA111(3) e) *iso*TBA232(7), f) *iso*TBA222(6), g) *iso*TBA131(5), h) *iso*TBA111(3) Black:in water (No thrombin), Red: 0.44 μ M , Green: 0.85 μ M, Blue:1.25 μ M, Cyan: 1.63 μ M, Magenta: 2 μ M

Table 5: CD- T_m of TBA and *iso*TBA loop-modified oligomers, at 5 μ M strand concentration in the presence of 100 mM KCl, followed by the addition of thrombin. ^a indicates the CD- T_m values at 260 nm while all other values are at 295 nm.

Sequence code	T_m ($^{\circ}$ C)	
	Heat	Cool
TBA232(7)	53	53
TBA111(3)	60 ^a	48 ^a
<i>iso</i> TBA232(7)	38	38
<i>iso</i> TBA222(6)	34	34
<i>iso</i> TBA131(5)	34	31
<i>iso</i> TBA111(3)	<10	<10

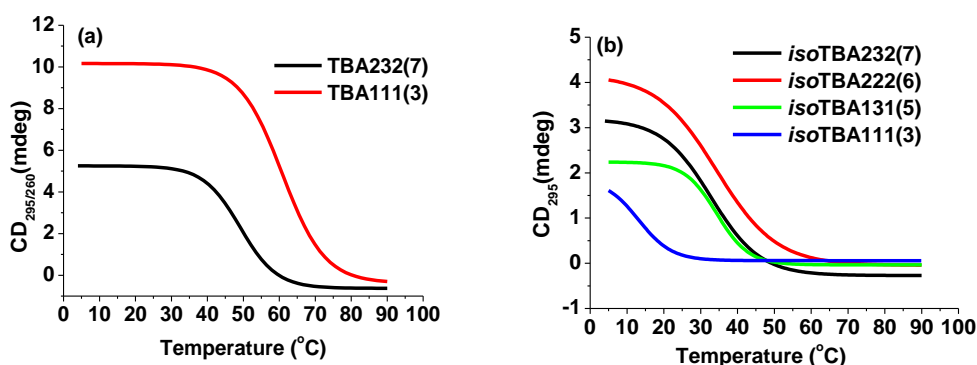


Figure 15: CD amplitude at 295 nm for all oligomers except TBA111(3), for which the CD amplitude was recorded at 260 nm, versus temperature. Oligomers taken at 5 μ M concentration were annealed in the presence of 100 mM KCl, followed by the addition of thrombin. (a) TBA232(7), TBA222(6), (b) *iso*TBA232(7), *iso*TBA222(6), *iso*TBA131(5) and *iso*TBA111(3)

3.3.7 Nuclease stability study-Exonuclease stability

To assess the nuclease stability of the 2'-5'-linked quadruplex-forming backbone as compared to the native TBA; we treated TBA and *iso*TBA131, as a representative example, with snake venom phosphodiesterase (SVPD) that has predominantly 3'-exonuclease activity (Figure 16). The 2'-5'-linked *iso*TBA131 was digested much slower compared to the control TBA. The reaction was monitored by HPLC (Figure 17). The half-life of *iso*TBA131 was found to be ~30 min whereas TBA was completely digested within 10 min at 37 $^{\circ}$ C. The observed higher stability of *iso*DNA oligomer as compared

to the control unmodified oligomer offers obvious advantages for applications in biological systems, where the control unmodified oligomer has a relatively low half-life.

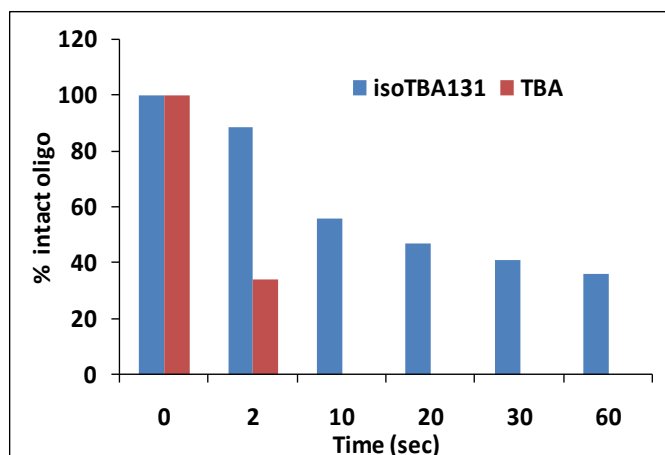


Figure 16: Stability of the aptamers *isoTBA131* (7.5 μM) and TBA-1 towards snake venom phosphodiesterase (SVPD) enzyme (0.02 mg/mL).

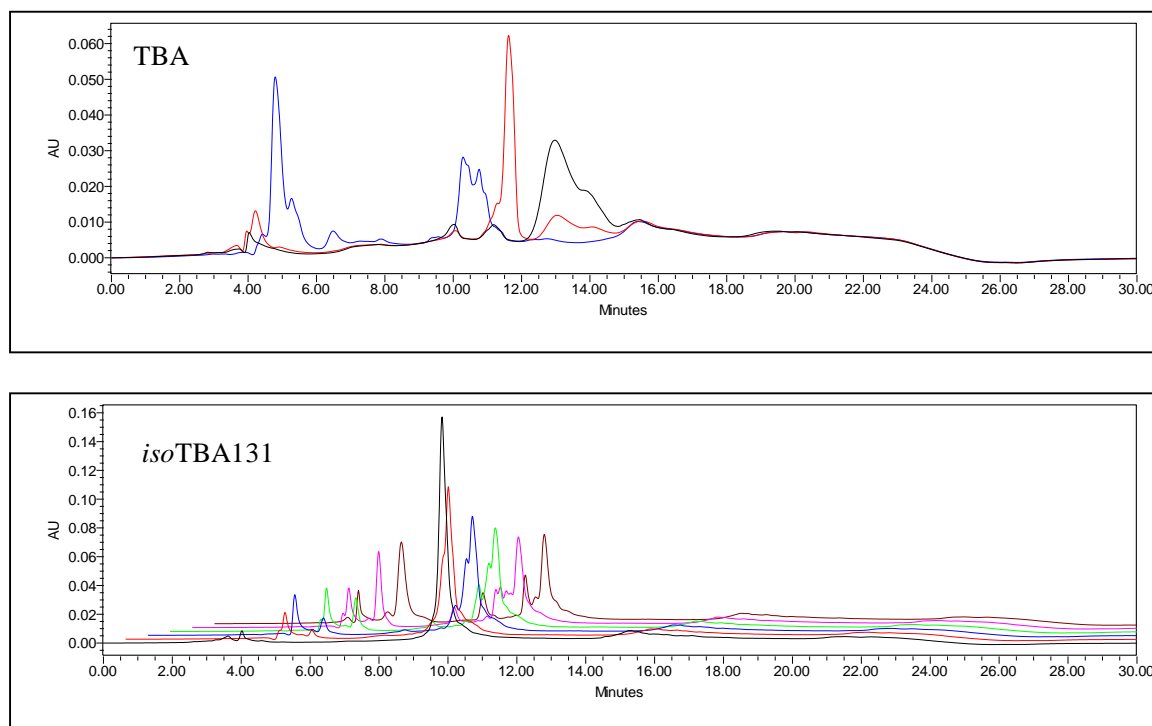


Figure 17: HPLC chromatograms of TBA and *isoTBA131* at increasing time intervals after exposure to SVPD. Black: without SVPD enzyme, Red: 2 min, Blue: 10 min, Green: 20 min, Magenta: 30 min, Brown: 60 min.

3.4 Key highlights of this study

- TBA and *iso*TBA variants with truncated loops were synthesized.
- CD spectroscopy studies were done in the presence of K⁺ ions was done at different strand concentration (5 μM and 20 μM) and different salt concentration (100 mM and 500 mM KCl) to evaluate the topology and molecularity of sequences with shorter loop length.
- Thermal difference spectra (TDS) obtained from UV spectroscopic studies elucidated the differences in the topology of the G-quadruplexes of the synthesized loop-modified oligomers.
- A polyacrylamide gel mobility shift assay was used to distinguish complexes of differing molecularity.
- Thrombin-binding studies brought out the chaperone effect of thrombin on the folding of the individual oligomers into quadruplexes and were studied by CD spectroscopy.
- Nuclease resistance study of *iso*TBA131 showed more stability to SVPD digestion than unmodified TBA131.

3.5 Conclusions

In this Chapter, we reported the topology and thermal stability of all the TBA and *iso*TBA oligomers using ultraviolet (UV) absorption, circular dichroism (CD) spectroscopy and gel electrophoresis. The 2'-5'-linked *iso*TBA oligomers were found to be amenable to form antiparallel G-quadruplex structures, independent of loop length. This result is in contrast to the previous study related to the natural 3'-5'-phosphodiester-linked G-quadruplexes where reducing the loop length resulted in changed antiparallel to parallel structural topology. The decreasing loop-length however, adversely affected the stability of the regioisomeric antiparallel quadruplexes, and consequently, reduced their binding to thrombin.

3.6 Experimental

3.6.1 Synthesis of oligonucleotides, purification and characterization

The regular procedures of oligonucleotide synthesis, their purification ((High-performance liquid chromatography) and MALDI-TOF characterization are same as discussed earlier in Chapter 2.

3.6.2 Biophysical techniques

3.6.2.1 CD spectroscopy

CD spectra were recorded on a Jasco J-815 CD spectrometer equipped with a Jasco PTC-424S/15 peltier system. 2 mm path-length quartz cuvettes were used for a sample volume 500 μ l and strand concentration of 5 μ M or 20 μ M in 10 mM K-phosphate buffer (pH 7.2) containing 100 mM and 500 mM KCl. Oligomers prepared in buffer were annealed by heating at 95 $^{\circ}$ C for 5 min, then slowly cooling to room temperature followed by refrigeration for 5 to 6 h before use. Spectral scans were collected at 4 $^{\circ}$ C over a wavelength range 200- 320 nm at a scanning rate of 100 nm/min. CD melting was performed for the entire sample by monitoring the CD intensity at 295 nm against temperature over the range 5-90 $^{\circ}$ C. Three scans were averaged for each sample. CD spectroscopy was also used to study the thrombin binding efficiency of the TBA/*iso*TBA oligomers of by recording their CD signal intensity at 295 nm with increasing thrombin concentration.

3.6.2.2 UV experiments for Thermal difference spectra

Thermal difference spectra (TDS) for all the TBA/*iso*TBA oligomers were obtained using a 10 mm quartz cell on a Varian Cary 300 Bio UV-Visible Spectrophotometer and AnalyticJena SPECORD $\text{\textcircled{R}}$ 200 plus, equipped with a peltier temperature controller and an scanning speed of 300 nm/min. The TBA oligomers at 5 μ M concentration were annealed in 10 mM potassium phosphate buffer, pH 7.5, containing 100 mM KCl. The oligomer concentration was calculated on the basis of the absorbance from molar extinction coefficients of the corresponding nucleobases of DNA/RNA. UV spectra over the 200 nm-320 nm range were recorded over a temperature range of 10 - 90 $^{\circ}$ C. 3 min equilibration period at each measurement was allowed to ensure homogeneous sample temperature. The auto zero function was applied

using the corresponding buffer at 10 °C. TDS factors were calculated as the absolute values of $\Delta A_{240 \text{ nm}}/\Delta A_{295 \text{ nm}}$, where ΔA_{λ} is the difference, at the given wavelength λ , between the absorbance above (95 °C) and below (15 °C) the melting temperature.

3.6.3 Polyacrylamide gel electrophoresis (PAGE) experiment

The quadruplex-forming ability and their topology difference study of the synthesized oligomers were assessed by denaturing and non-denaturing 20 % polyacrylamide gel electrophoresis. As reference scrambled TBA oligonucleotide sequence, viz., 5'-GGTGGTGGTTGTGGT-3' (15-mer) was used. For non-denaturing gel TBA and *iso*TBA oligomers were annealed in 10 mM K-phosphate buffer (pH 7.2) containing 100 mM KCl or 500 mM KCl prior to loading on the gel. The DNA oligomer control and samples (2 μ L, 350 μ M) were mixed with equal volume of 40% sucrose solution and loaded into the appropriately numbered wells. The gel was run at 10 °C at 150V for 120 min till the marker was visible at 3/4th the gel height. The gel was visualized by UV-shadowing. For denaturing gel experiments, 7 M urea was used as denaturant, and samples were mixed with equal volume of formamide for loading. The gel was run in 1X TBE buffer at 25 °C and at 150 V. The gels after the run were washed with DI water and then were visualized by UV-shadowing.

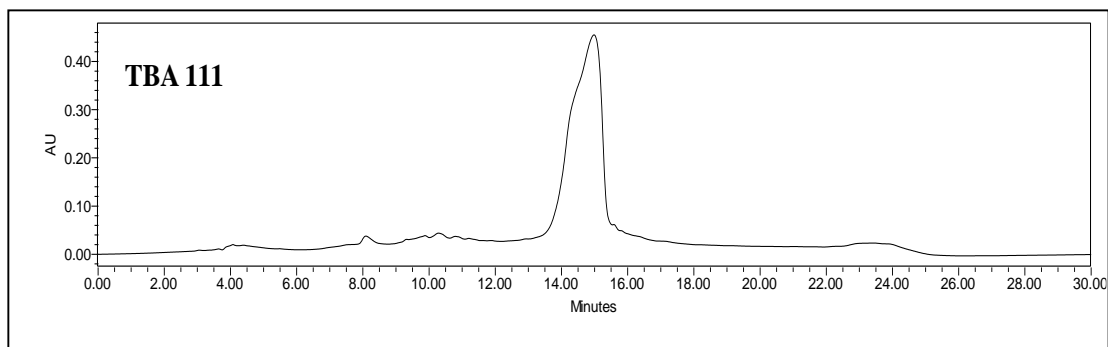
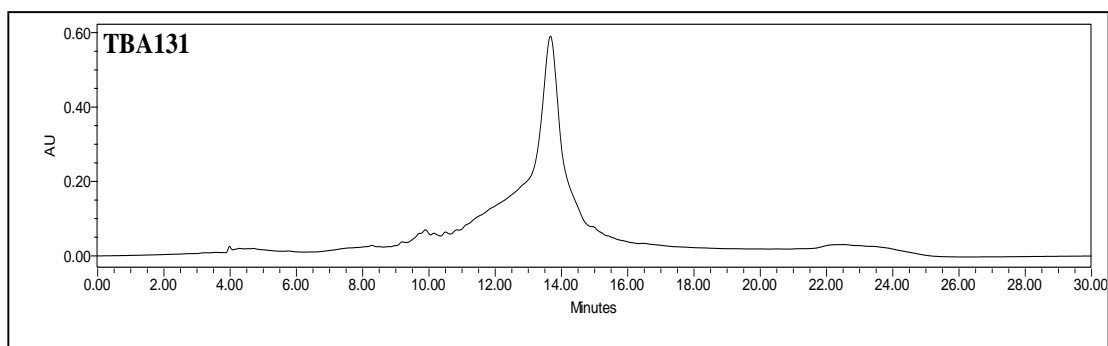
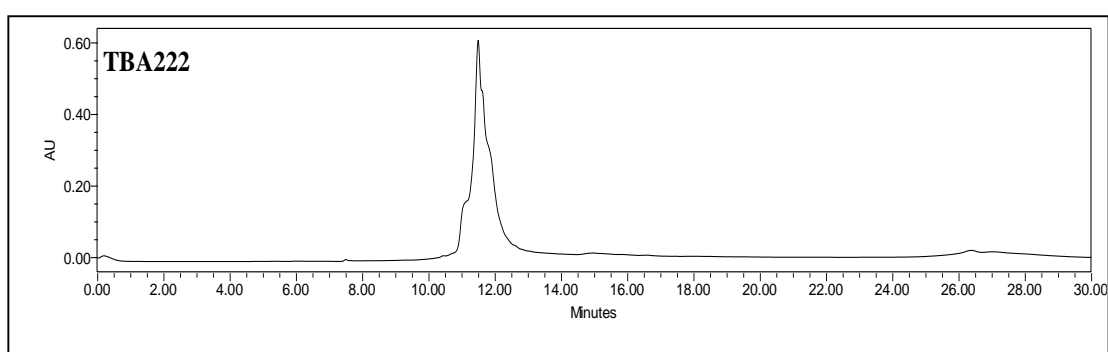
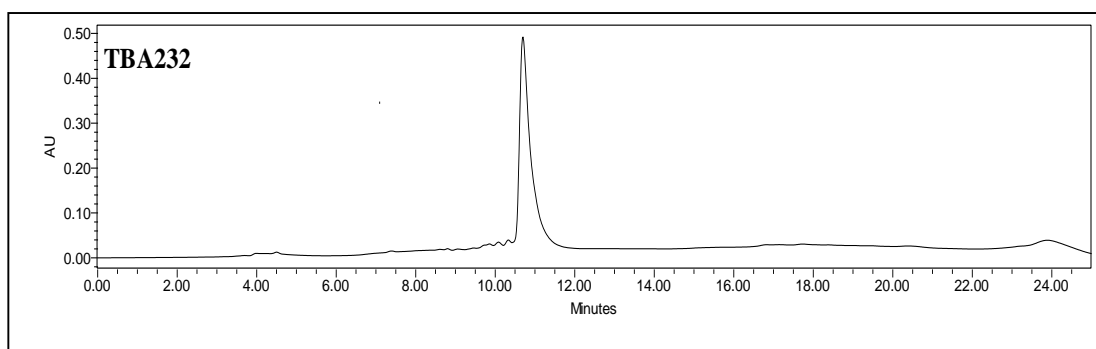
3.6.4 Snake venom phosphodiesterase stability experiments

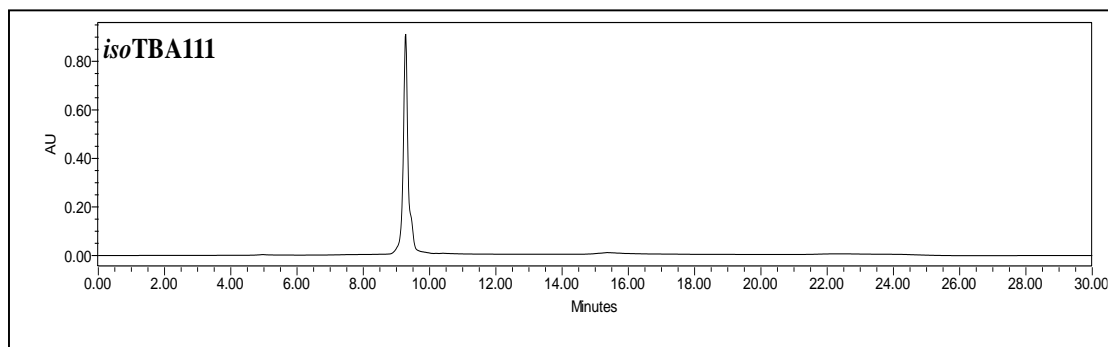
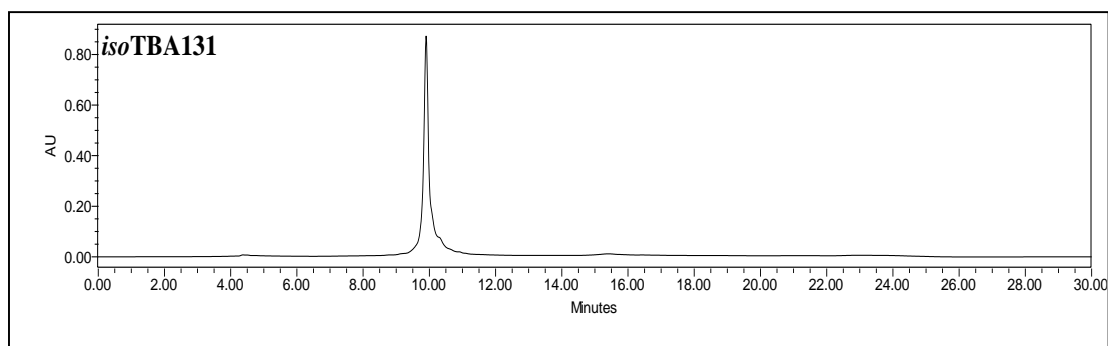
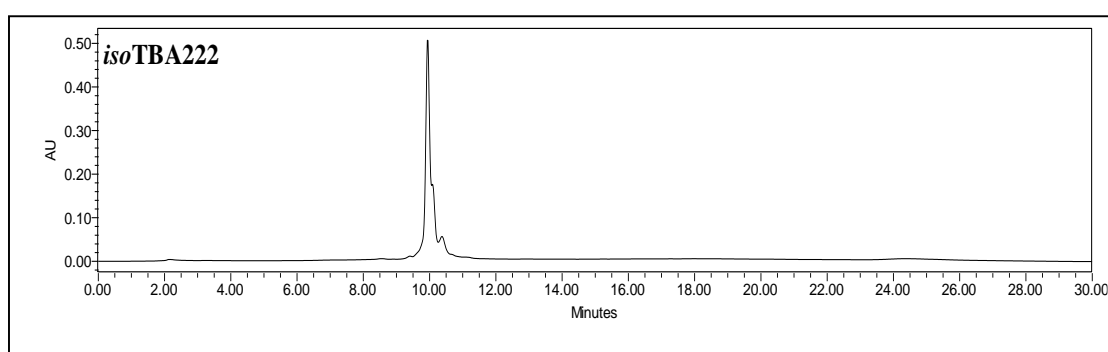
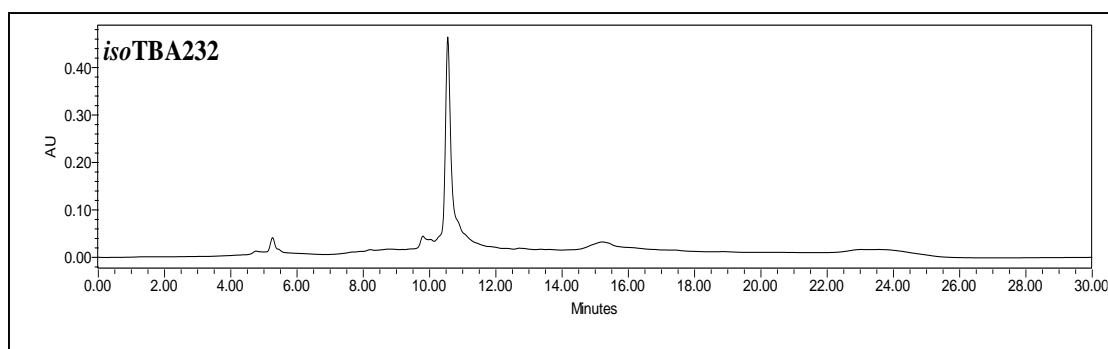
Enzymatic hydrolysis of the aptamers TBA, *iso*TBA131 (7.5 μ M) was carried out at 37 °C in 100 μ l Tris-HCl buffer (100 mM, pH 8.5, containing 15 mM MgCl₂, 100 mM NaCl) and SVPD (0.02 mg/ml). Aliquots were taken at pre-decided time intervals. Each aliquot was heated at 90 °C for 2 min to inactivate the nuclease. The intact oligomer in each aliquot was monitored by RP-HPLC were kept at 90 °C for 2 minutes to inactivate nuclease. Aliquots analysed by RP-HPLC using an increasing gradient of acetonitrile in triethylammonium acetate (A: 5% acetonitrile and B: 30% acetonitrile in 0.1N triethylammonium acetate, pH 7.0). The percentage of intact oligomer was plotted against time to show the degradation of oligomers with respect to time.

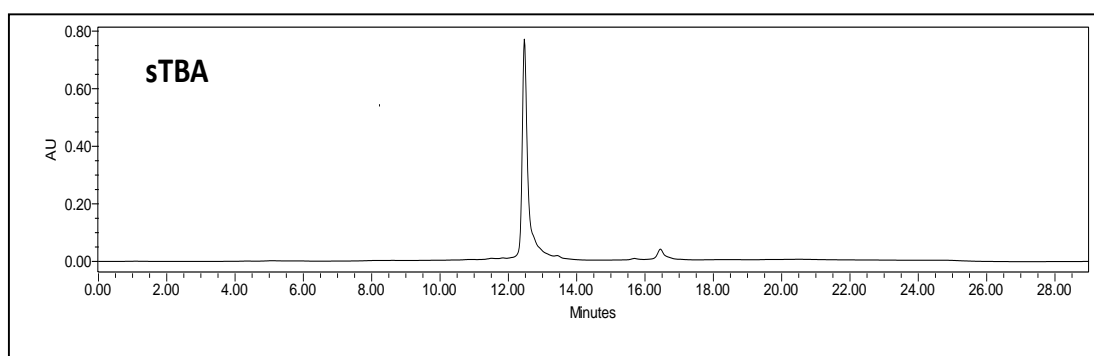
3.7 Appendix B

Description	Page No.
HPLC chromatogram of TBA oligomers	187
HPLC chromatogram of <i>iso</i> TBA oligomers	188
HPLC chromatogram of scrambled sequence sTBA=5'-GGTGGTGGTTGTGGT-3'	189
MALDI-TOF spectra of TBA oligomers	189-190
MALDI-TOF spectra of <i>iso</i> TBA oligomers	190-191
MALDI-TOF spectra of sTBA=5'-GGTGGTGGTTGTGGT-3'	192

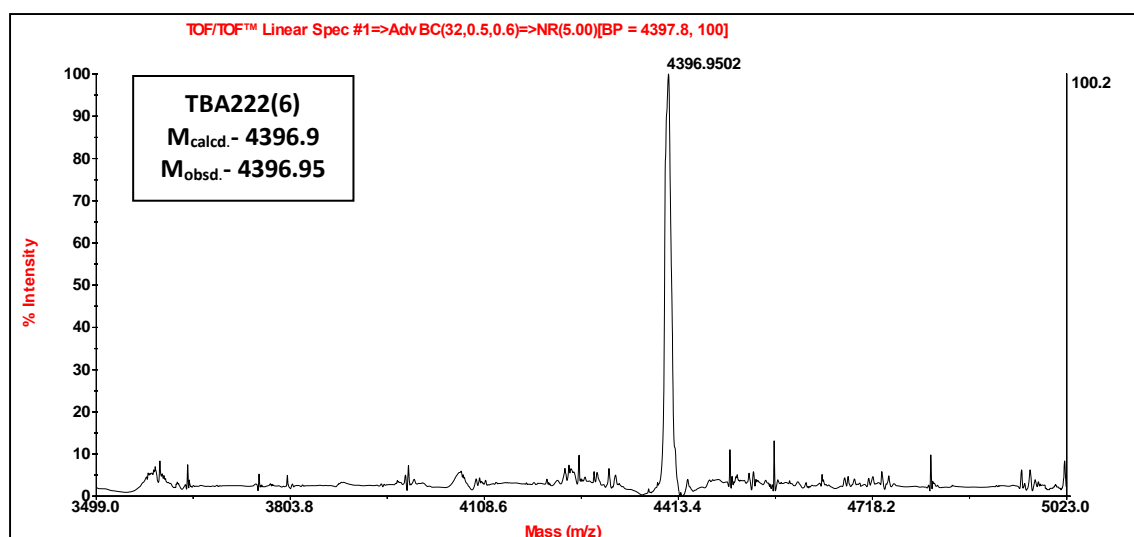
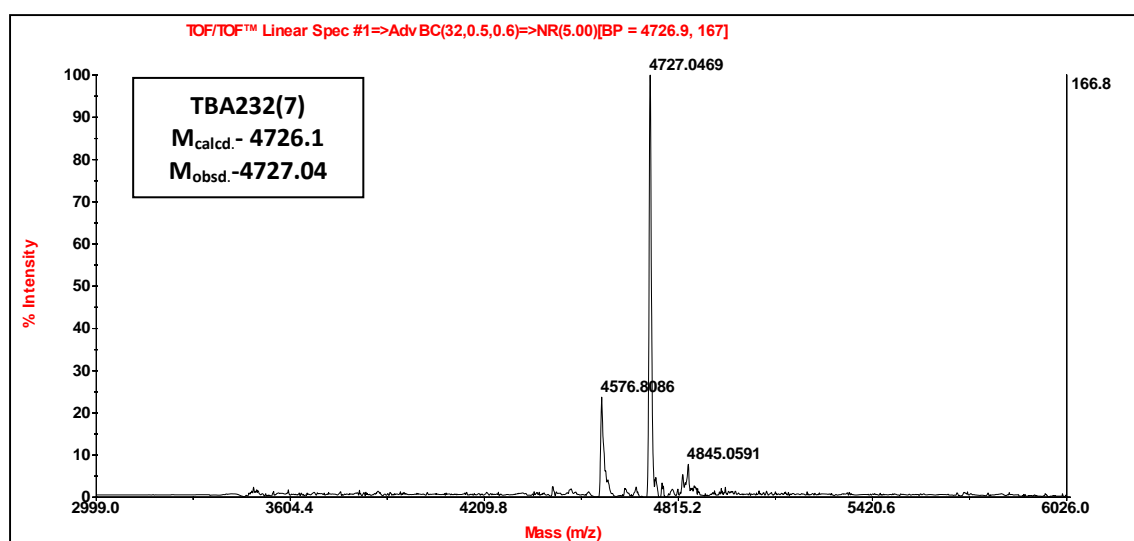
HPLC chromatograms of purified synthesized TBA oligomers

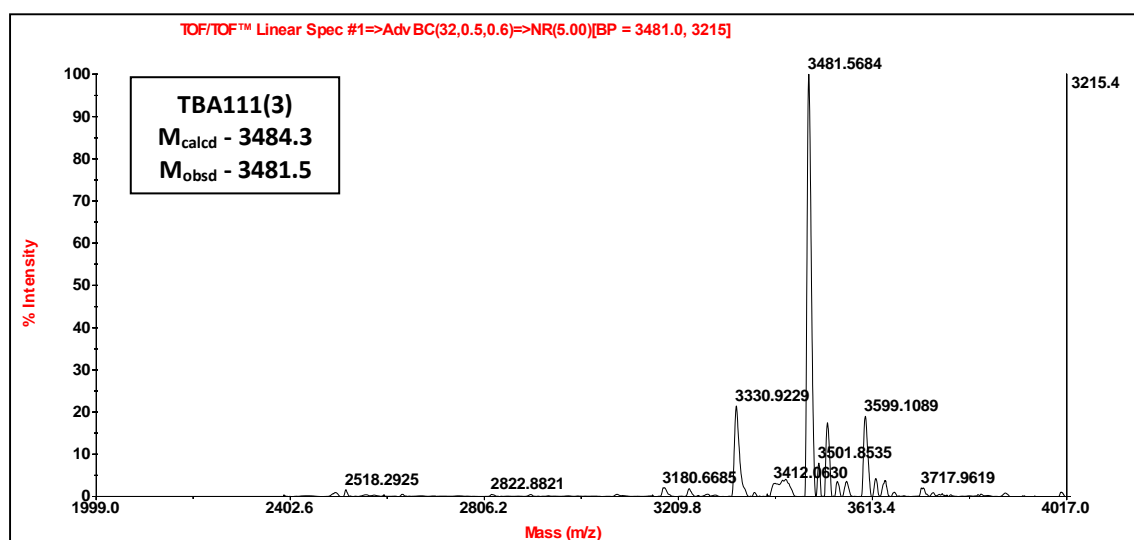
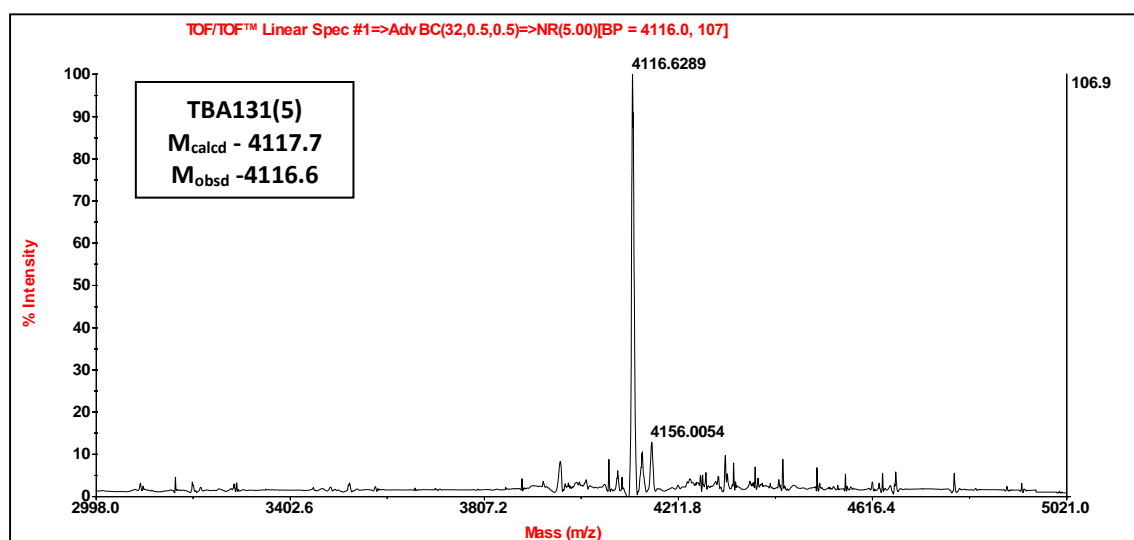


HPLC chromatograms of purified synthesized *iso*TBA oligomers

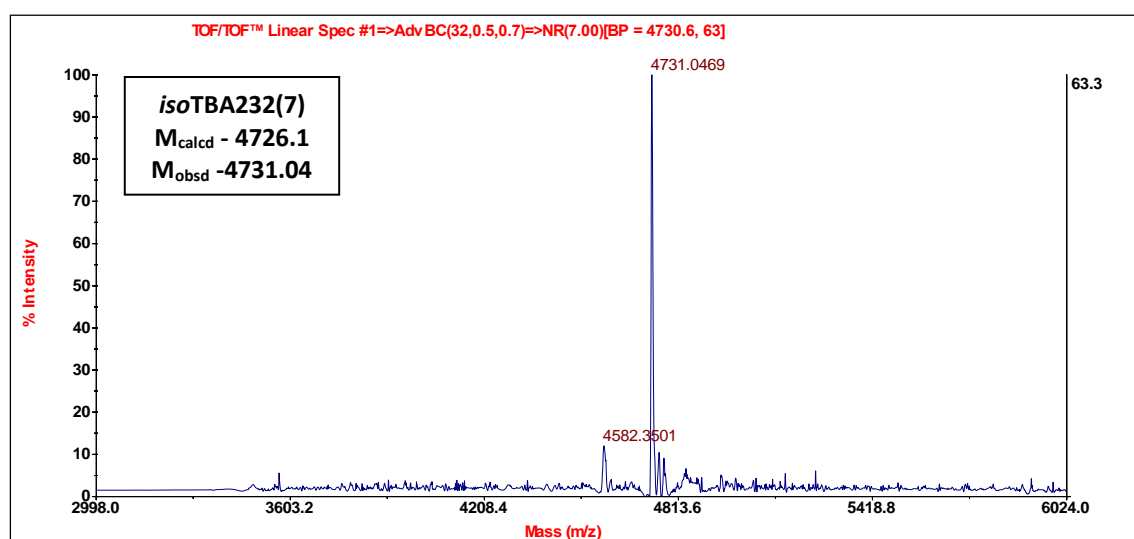


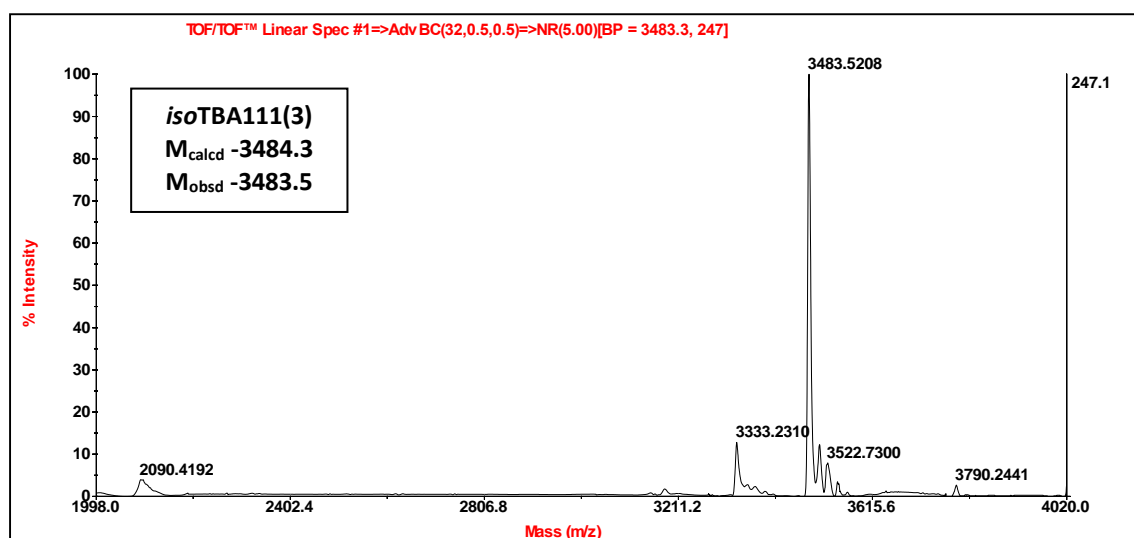
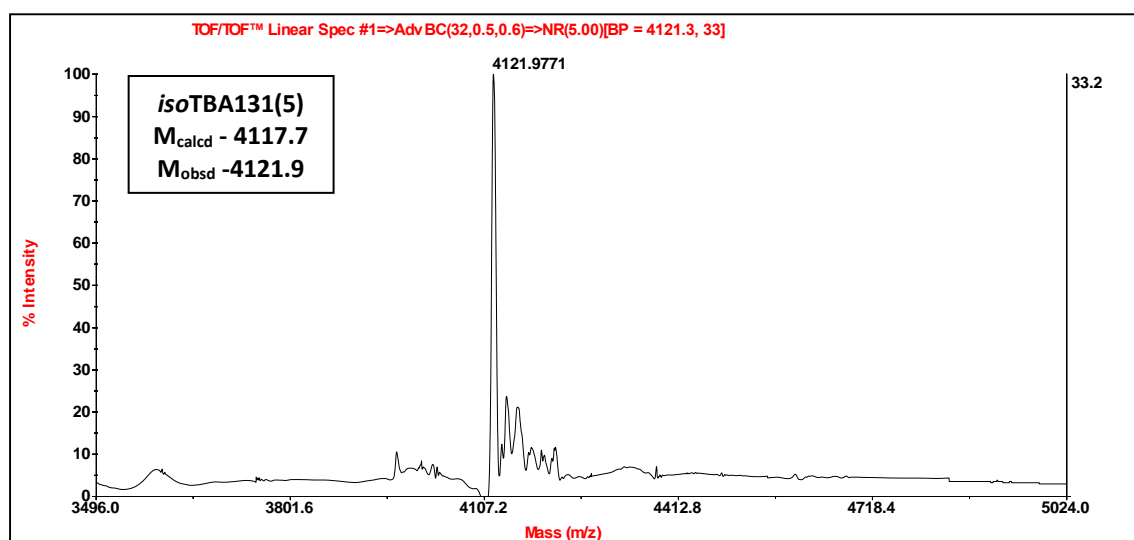
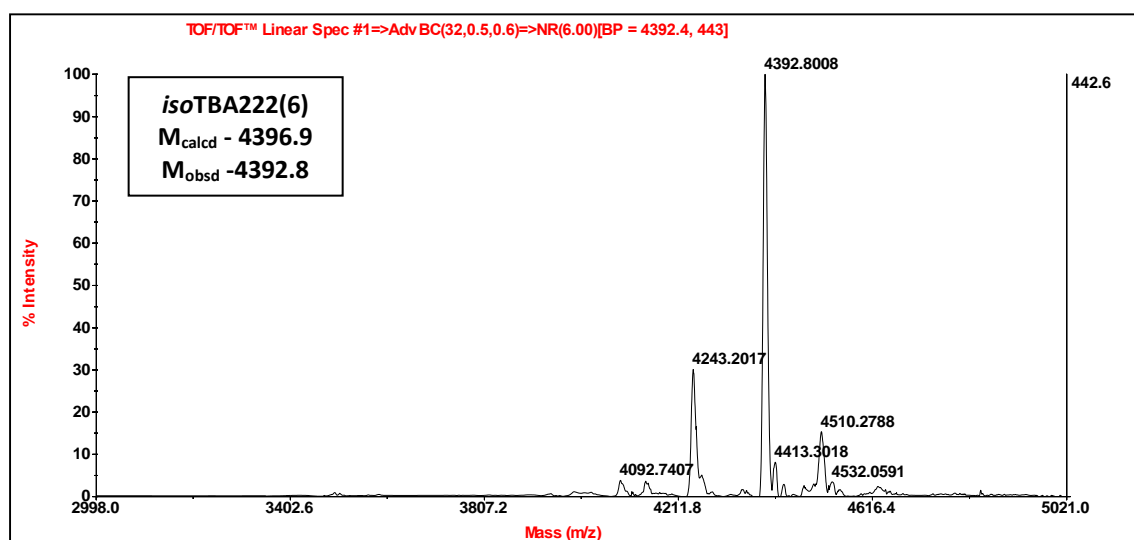
MALDI-TOF spectra of TBA oligomers



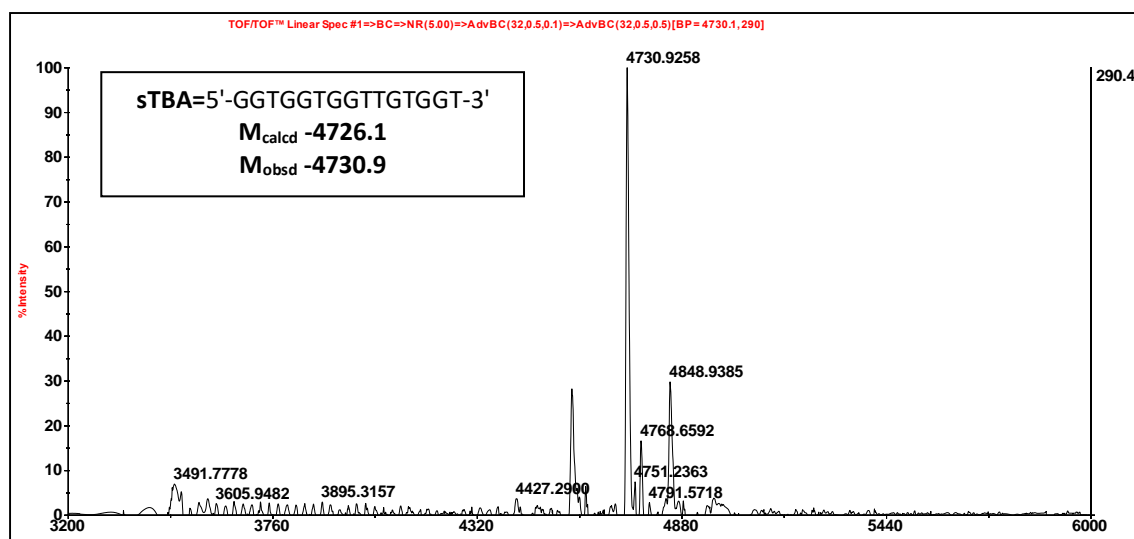


MALDI-TOF spectra of *iso*TBA oligomers





MALDI-TOF spectrum of scrambled TBA (sTBA)



3.8 References

1. Karsisiotis, A. I.; Hessari, N. M. a.; Novellino, E.; Spada, G. P.; Randazzo, A.; Webba da Silva, M., Topological characterization of nucleic acid G-quadruplexes by UV absorption and circular dichroism. *Angew. Chem., Int. Ed. Engl.* **2011**, *50* (45), 10645-10648.
2. Hazel, P.; Huppert, J.; Balasubramanian, S.; Neidle, S., Loop-length-dependent folding of G-quadruplexes. *J. Am. Chem. Soc.* **2004**, *126* (50), 16405-16415.
3. Rachwal, P. A.; Brown, T.; Fox, K. R., Sequence effects of single base loops in intramolecular quadruplex DNA. *FEBS Lett.* **2007**, *581* (8), 1657-1660.
4. Bock, L. C.; Griffin, L. C.; Latham, J. A.; Vermaas, E. H.; Toole, J. J., Selection of single-stranded DNA molecules that bind and inhibit human thrombin. *Nature* **1992**, *355* (6360), 564.
5. Kelly, J. A.; Feigon, J.; Yeates, T. O., Reconciliation of the X-ray and NMR structures of the thrombin-binding aptamer d(GGTTGGTGTGGTTGG). *J. Mol. Biol.* **1996**, *256* (3), 417-422.
6. Russo Krauss, I.; Merlino, A.; Randazzo, A.; Novellino, E.; Mazzarella, L.; Sica, F., High-resolution structures of two complexes between thrombin and thrombin-binding aptamer shed light on the role of cations in the aptamer inhibitory activity. *Nucleic Acids Res.* **2012**, *40* (16), 8119-8128.

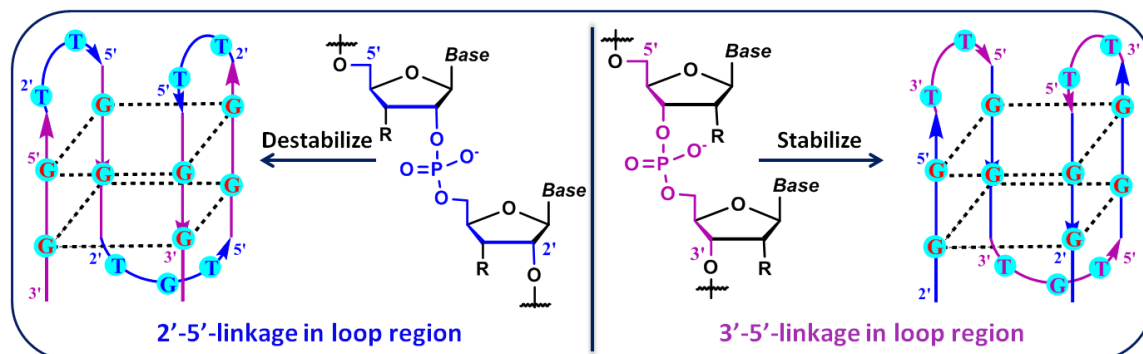
7. (a) Avino, A.; Fabrega, C.; Tintore, M.; Eritja, R., Thrombin binding aptamer, more than a simple aptamer: chemically modified derivatives and biomedical applications. *Curr. Pharm. Des.* **2012**, *18* (14), 2036-2047; (b) Sacca, B.; Lacroix, L.; Mergny, J.-L., The effect of chemical modifications on the thermal stability of different G-quadruplex-forming oligonucleotides. *Nucleic Acids Res.* **2005**, *33* (4), 1182-1192.
8. (a) Aviñó, A.; Portella, G.; Ferreira, R.; Gargallo, R.; Mazzini, S.; Gabelica, V.; Orozco, M.; Eritja, R., Specific loop modifications of the thrombin-binding aptamer trigger the formation of parallel structures. *FEBS J.* **2014**, *281* (4), 1085-1099; (b) Nagatoishi, S.; Isono, N.; Tsumoto, K.; Sugimoto, N., Loop residues of thrombin-binding DNA aptamer impact G-quadruplex stability and thrombin binding. *Biochimie* **2011**, *93* (8), 1231-1238.
9. (a) Joachimi, A.; Benz, A.; Hartig, J. S., A comparison of DNA and RNA quadruplex structures and stabilities. *Bioorg. Med. Chem.* **2009**, *17* (19), 6811-6815; (b) Smirnov, I.; Shafer, R. H., Lead is unusually effective in sequence-specific folding of DNA. *J. Mol. Biol.* **2000**, *296* (1), 1-5.
10. Smirnov, I.; Shafer, R. H., Effect of Loop Sequence and Size on DNA Aptamer Stability. *Biochemistry* **2000**, *39* (6), 1462-1468.
11. (a) Pasternak, A.; Hernandez, F. J.; Rasmussen, L. M.; Vester, B.; Wengel, J., Improved thrombin binding aptamer by incorporation of a single unlocked nucleic acid monomer. *Nucleic Acids Res.* **2011**, *39* (3), 1155-1164; (b) Aaldering, L. J.; Poongavanam, V.; Langkjaer, N.; Murugan, N. A.; Jørgensen, P. T.; Wengel, J.; Veedu, R. N., Development of an Efficient G-Quadruplex-Stabilised Thrombin-Binding Aptamer Containing a Three-Carbon Spacer Molecule. *ChemBioChem* **2017**, *18* (8), 755-763.
12. Kandimalla, E. R.; Manning, A.; Zhao, Q.; Shaw, D. R.; Byrn, R. A.; Sasisekharan, V.; Agrawal, S., Mixed backbone antisense oligonucleotides: design, biochemical and biological properties of oligonucleotides containing 2'-5'-ribo- and 3'-5'-deoxyribonucleotide segments. *Nucleic Acids Res.* **1997**, *25* (2), 370-378.
13. (a) Giannaris, P. A.; Damha, M. J., Oligoribonucleotides containing 2', 5'-phosphodiester linkages exhibit binding selectivity for 3', 5'-RNA over 3', 5'-ssDNA. *Nucleic Acids Res.* **1993**, *21* (20), 4742-4749; (b) Sheppard, T. L.; Breslow, R. C., Selective Binding of RNA, but Not DNA, by Complementary 2', 5'-Linked DNA. *J.*

- Am. Chem. Soc.* **1996**, *118* (40), 9810-9811; (c) Erande, N.; Gunjal, A. D.; Fernandes, M.; Gonnade, R.; Kumar, V. A., Synthesis and structural studies of S-type/N-type-locked/frozen nucleoside analogues and their incorporation in RNA-selective, nuclease resistant 2',5'-linked oligonucleotides. *Org. Biomol. Chem.* **2013**, *11* (5), 746-757; (d) Jung, K.-E.; Switzer, C., 2', 5'-DNA containing guanine and cytosine forms stable duplexes. *J. Am. Chem. Soc.* **1994**, *116* (14), 6059-6061; (e) Erande, N.; Gunjal, A. D.; Fernandes, M.; Kumar, V. A., Probing the furanose conformation in the 2'-5' strand of iso DNA: RNA duplexes by freezing the nucleoside conformations. *Chem. Commun.* **2011**, *47* (13), 4007-4009; (f) Sawai, H.; Seki, J.; Ozaki, H., Comparative Studies of Duplex and Triplex Formation of 2'-5' and 3'-5' Linked Oligoribonucleotides. *J. Biomol. Struct. Dyn.* **1996**, *13* (6), 1043-1051.
14. Gunjal, A. D.; Fernandes, M.; Erande, N.; Rajamohanan, P. R.; Kumar, V. A., Functional isoDNA aptamers: modified thrombin binding aptamers with a 2'-5'-linked sugar-phosphate backbone (*isoTBA*). *Chem. Commun.* **2014**, *50* (5), 605-607.
15. (a) Polak, M.; Manoharan, M.; Inamati, G. B.; Plavec, J., Tuning of conformational preorganization in model 2',5'- and 3',5'-linked oligonucleotides by 3'- and 2'-O-methoxyethyl modification. *Nucleic Acids Res.* **2003**, *31* (8), 2066-2076; (b) Premraj, B. J.; Raja, S.; Bhavesh, N. S.; Shi, K.; Hosur, R. V.; Sundaralingam, M.; Yathindra, N., Solution structure of 2', 5' d (G4C4) Relevance to topological restrictions and nature's choice of phosphodiester links. *Eur. J. Biochem.* **2004**, *271* (14), 2956-2966.
16. Gait, M. J., *Oligonucleotide synthesis : a practical approach*. Rev. repr. ed.; Oxford : IRL press: 1984.
17. (a) Vorlíčková, M.; Kejnovská, I.; Bednářová, K.; Renčiuk, D.; Kypr, J., Circular Dichroism Spectroscopy of DNA: From Duplexes to Quadruplexes. *Chirality* **2012**, *24* (9), 691-698; (b) Randazzo, A.; Spada, G. P.; da Silva, M. W., Circular dichroism of quadruplex structures. *Top. Curr. Chem.* **2013**, *330*, 67-86; (c) Gray, D. M.; Wen, J.-D.; Gray, C. W.; Repges, R.; Repges, C.; Raabe, G.; Fleischhauer, J., Measured and calculated CD spectra of G-quartets stacked with the same or opposite polarities. *Chirality* **2008**, *20* (3-4), 431-440.
18. Balasubramanian, S.; Neidle, S., G-quadruplex nucleic acids as therapeutic targets. *Curr. Opin. Chem. Biol.* **2009**, *13* (3), 345-353.

19. Krishnan, R.; Seshadri, T. P., Crystal structure of guanylyl-2',5'-cytidine dihydrate: An analogue of msDNA-RNA junction in *Stigmatella aurantiaca*. *Biopolymers* **1994**, *34* (12), 1637-1646.
20. Premraj, B.; Yathindra, N., Stereochemistry of 2', 5' nucleic acids and their constituents. *J. Biomol. Struct. Dyn.* **1998**, *16* (2), 313-328.
21. Mergny, J.-L.; Lacroix, L., Analysis of thermal melting curves. *Oligonucleotides* **2003**, *13* (6), 515-537.
22. Hatzakis, E.; Okamoto, K.; Yang, D., Thermodynamic Stability and Folding Kinetics of the Major G-Quadruplex and Its Loop Isomers Formed in the Nuclease Hypersensitive Element in the Human c-Myc Promoter: Effect of Loops and Flanking Segments on the Stability of Parallel-Stranded Intramolecular G-Quadruplexes. *Biochemistry* **2010**, *49* (43), 9152-9160.
23. (a) Baldrich, E.; O'Sullivan, C. K., Ability of thrombin to act as molecular chaperone, inducing formation of quadruplex structure of thrombin-binding aptamer. *Anal. Biochem.* **2005**, *341* (1), 194-197; (b) Nagatoishi, S.; Tanaka, Y.; Tsumoto, K., Circular dichroism spectra demonstrate formation of the thrombin-binding DNA aptamer G-quadruplex under stabilizing-cation-deficient conditions. *Biochem. Biophys. Res. Commun.* **2007**, *352* (3), 812-817.

Chapter 4

Effect of 2'-5' and 3'-5' linkages in the loop region of TBA and *iso*TBA respectively, on G-quadruplex stability and function



Regioisomeric nucleic acids with the 2'-5'-phosphodiester linkages compared to the 3'-5'-linkage are highly interesting biomolecules exhibits high stability against cellular enzymes and therefore it could be a promising alternative nucleic acid for DNA therapeutics. Formation of duplex and triplex structures comprising *iso*DNA and complementary RNA is well-documented in the literature. This chapter summarizes the synthesis of chimeric oligomers with 3'-5'-(TBA) and 2'-5'-phosphodiester-linked (*iso*TBA) backbones in which the loop regions are systematically replaced by 2'-5'- and 3'-5'- phosphodiester linkages respectively. We observed that substitution of the 2'-5' linkage in *iso*TBA with the 3'-5' linkage resulted in a strong stabilization of the quadruplex structure. The *iso*TBA sequences showed better nuclease stability against exonuclease as well as endonuclease.

4.1 Introduction

*Iso*DNA or *iso*RNA have regioisomeric 2'-5'-phosphodiester-linkages instead of 3'-5'-phosphodiester-linkages present in the native DNA or RNA (Figure 1). The 2'-5' linked constitutional isomers are known to form duplexes via Watson–Crick base pair association and are not used to encode genetic information; they are thus called non-genetic nucleic acids.¹ The 2'-5' *iso*DNA differentiates single-stranded DNA and RNA and forms duplexes exclusively with complementary 3'-5'-linked natural RNA, but with lower thermal stability compared to the DNA:DNA, DNA:RNA and RNA:RNA duplexes.²

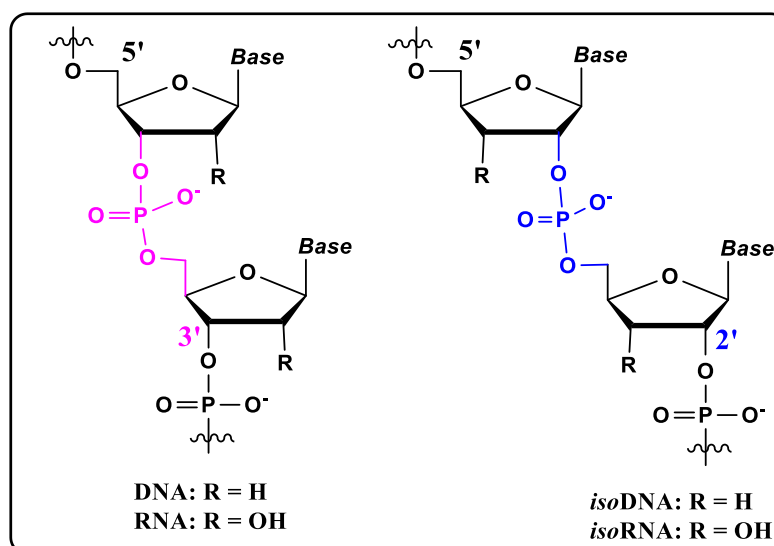


Figure 1: 3'-5'-DNA/RNA and 2'-5'-*iso*DNA/*iso*RNA

The non-genetic *iso*DNA oligomers are also known to form triplex structures. Sawai et al.³ and Damha and co-workers⁴ have done comparative studies of duplex and triplex formation of 2'-5'- and 3'-5'-linked oligonucleotides but higher-order structures involving the *iso*DNA backbone are not much explored. Higher-order structures like G-quadruplexes are getting more attention in the recent past because of their abundance *in vivo* their role in telomere maintenance, gene regulation and also for their therapeutic applications⁵ such as the anti-cancer,⁶ antithrombin⁷ and anti-HIV aptamers.⁸ The 3'-deoxy-2'-5'-linked non-genetic *iso*DNA exhibits high stability against cellular enzymes and therefore it can be a promising alternative for developing DNA therapeutics.

4.2 Sugar phosphate backbone linkages in G -quadruplexes

In the recent two decades, substantial research work has been done for the explication of the structural properties and biochemical functions of polymorphic G-quadruplex structures. Many backbone modifications of oligonucleotides involving the replacement of the phosphodiester group have been explored to study the topology and stability of different G quadruplex forming aptamers. The quadruplex structures with PNA backbone have been earlier reported by Datta and et al.⁹, that formed either four-stranded multimolecular structures or mixed bimolecular structures. Mergny and co-workers have done a systematic study of the thermal and conformational properties of phosphorothioates, methyl phosphonate, ribonucleotide backbone-modified G-quadruplex-forming oligonucleotides.¹⁰ Joachimi et al.¹¹ explored a variety of well-studied quadruplex-forming DNA sequences and corresponding RNA sequences for their quadruplex formation and stability. A guanine-rich 3'-2'-threose nucleic acid aptamer against thrombin was discovered by Chaput and co-workers.¹² From these examples, it is noticeable that the backbone element is a crucial guiding entity for maintaining the structure and function of any given nucleic acid oligomer.

The G-quadruplex forming thrombin binding aptamer (TBA)¹³ (5'-G¹G²T³T⁴G⁵G⁶T⁷G⁸T⁹G¹⁰G¹¹T¹²T¹³G¹⁴G¹⁵-3') has been broadly studied for its anticoagulant activity. It forms a unimolecular chair-like antiparallel G-quadruplex structure, which consists of two G quartets that are connected by two lateral TT loops and one central TGT loop. The loop regions of TBA, particularly the TT loops are reported to be important for the folding of the aptamer and interaction with its target, thrombin.¹⁴ Efforts toward improving its stability to nucleases and thermal stability¹⁵ have mostly focused on the introduction of modified nucleosides, or on changing the number of residues in the loop/stem regions. There are only a few reports pertaining to modification of the phosphodiester internucleoside linkage. These include the phosphorothioate,¹⁶ methyl phosphonate,¹⁰ formacetal¹⁷ and triazole¹⁸ linkages (Figure 2). Phosphorothioate linkages in the stem region caused decrease in thermal stability, but in the TT loop, caused increased resistance towards nucleases, while retaining the thermal stability and anticoagulant activity.¹⁶ Studies from Mergny's group also suggested that the incorporation of phosphorothioate bonds in all the guanines which are forming tetrads,¹⁰ the resulted modified TBA has shown less stability than the

unmodified TBA. Methyl phosphonates caused a large destabilization of the G-quadruplex.¹⁰ Replacement of the negatively charged phosphodiester by the neutral formacetal linkage¹⁷ had not much effect on the thrombin inhibitory activity in the case of mono substitutions, except for the T⁴-G⁵ and T¹³-G¹⁴ links when a large decrease in activity was observed. Multiple substitutions resulted in a decrease in thermal stability and activity, resulting from perturbations of the chair-like quadruplex fold. The triazole internucleotide linkage led to a decrease in thermal stability of the resulting quadruplexes but increased their resistance to nucleolytic digestion. It also had a negative effect on the anticoagulant activity, except in the case of the central loop modification, when the activity was comparable to the native TBA.¹⁸ The folding patterns of an isosequential TBA RNA sequence¹¹ showed the formation of a multimolecular parallel G-quadruplex in contrast to the unimolecular antiparallel G-quadruplex structure of TBA. Tang and Shafer¹⁹ examined the impact of single nucleoside conformation on the folding topology by selective replacement of dG by rG in TBA. Depending on the position of the ribo- or deoxyribo-nucleotides, oligomer with a mixed DNA/RNA backbone, folded in DNA-like or RNA-like quadruplex structures were evaluated.

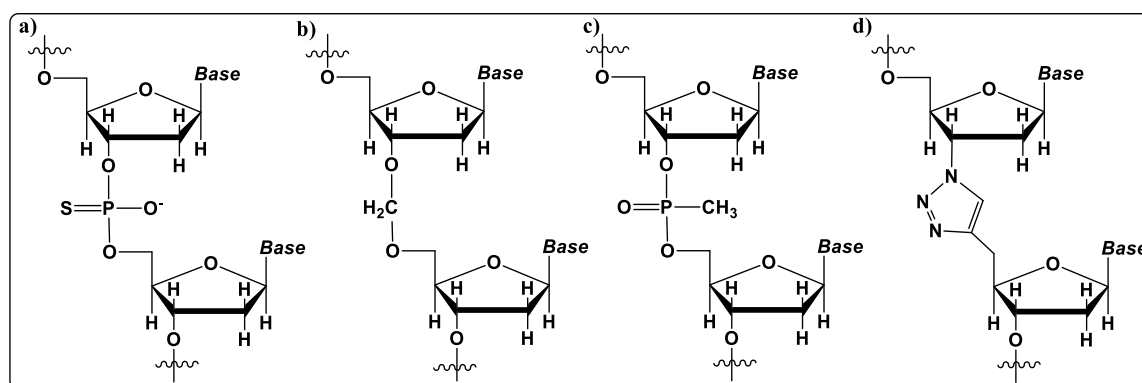


Figure 2: Dinucleotides showing a) phosphorothioate, b) formacetal, c) methyl phosphonate and d) triazole internucleoside linkages.

Our group earlier reported *iso*TBA, where the 3'-5'-phosphodiester backbone was replaced by the isomeric 2'-5'-phosphodiester backbone throughout the TBA oligomer (Figure 1),²⁰ that was able to retain the unimolecular antiparallel quadruplex topology of TBA, even when the total number of loop residues was significantly reduced.²¹ TBA was shown to bind to thrombin and exhibit anti-coagulant properties, though to a lower

degree than TBA. Recently, we developed TBA analogues, where the substitution of T⁷ by 4'-methoxymethyl threofuranosyl thymidine (4'-MOM-T) resulted in the enhancement of thermal stability, anticoagulation activity and nuclease resistance. Therefore, it is apparent that the backbone is the key factor to maintain the functional structural quadruplex topology of TBA.

4.3 Rationale and objectives of the present work

The 2'-5'-phosphodiester linkages give rise to a 7-atom backbone with an extended geometry resulting from the *anomeric* effect and the O4'-C1'-C2'-O2' *gauche* effect that favours the N-type sugar conformation,^{2e, 22} in comparison to the native 3'-5'-phosphodiester linkages, where the compact S-type of sugar pucker is favoured (Figure 3). We had previously found that the *iso*TBA structure was stabilized when the TGT loop was replaced by UGU.²⁰ The chimera of the present study were thus, designed to study the effect of differing preferred sugar pucker in the loop and stem regions of the quadruplex on the stability of the resulting quadruplex, and the consequences on the anticoagulant activity. The two TT loops of the quadruplex, being implicated in thrombin-binding to the exosite I, would be expected to have a larger impact on its function, in comparison to the TGT central loop, where minimal interactions with thrombin were observed in the crystal structure.¹⁴ The TGT loop, on the other hand, may be expected to mainly impact the thermal stability of the resulting quadruplex.

This chapter summarizes the synthesis of chimeric oligomers of TBA with 3'-5'- (TBA) and 2'-5'-phosphodiester-linked (*iso*TBA) backbones, in which the loop region is modified with 2'-5'-phosphodiester linkages and 3'-5'- phosphodiester linkages respectively. The impact of modification on thermal stability, nuclease stability and anticoagulation effect was studied.

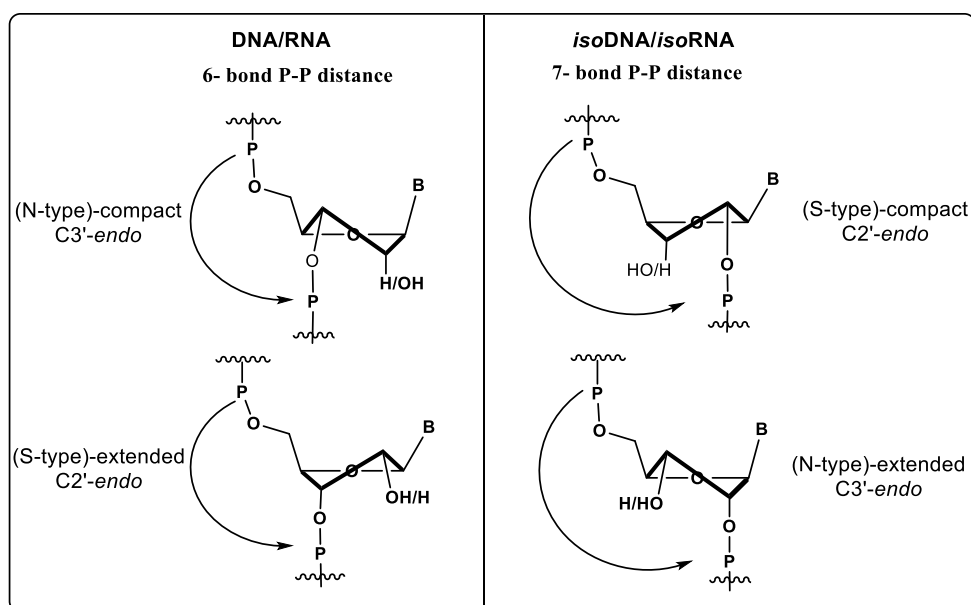


Figure 3: Extended and compact backbone geometry in DNA/RNA and *isoDNA/isoRNA*.

4.4 Present work, results and discussion

4.4.1 Synthesis of TBA, *isoTBA* and modified TBA variants with mixed backbone, their purification and characterization

We have chosen chimeric TBA oligomers for the current study that consists of the 3'-5'- and 2'-5'-phosphodiester linkages with the alternative 2'-5'- and 3'-5'-phosphodiester linkages respectively, in the loop regions. All the DNA and *isoDNA* ONs (listed in Table 1) were synthesized on a Bioautomation MM4 DNA synthesizer using commercially available protected 2'-deoxyguanosine-3'-phosphoramidite, 2'-deoxythymidine-3'-phosphoramidite, 3'-deoxy-thymidine-2'-phosphoramidite and 3'-deoxy-guanosine-2'-phosphoramidite by standard β -cyanoethyl phosphoramidite chemistry.²³ The general scheme for solid-phase oligonucleotide synthesis is explained in Chapter 1, Scheme 1.

The numbers in the oligomer names are indicative of the loop residues that were replaced with 2'-5'-linkages in TBA oligomers and 3'-5'-linkages in the *isoTBA* oligomers. Thus, in TBA232 all three loops bear 2'-5'-linkages; in TBA202, the T³T⁴ and T¹²T¹³ loops bear 2'-5'-linkages; in TBA030, TBA200 and TBA002, the T⁷G⁸T⁹, T³T⁴ and T¹²T¹³ loops respectively bear 2'-5'-linkages. Likewise, in *isoTBA*232, all three loops bear 3'-5'-linkages, while *isoTBA*202, *isoTBA*030, *isoTBA*200 and *isoTBA*002 bear 3'-5'-linkages in their T³T⁴ & T¹²T¹³, T⁷G⁸T⁹, T³T⁴ and T¹²T¹³ loops respectively.

The ONs were synthesized on a polystyrene solid support, and post-synthesis, were cleaved from the solid support by aq. ammonia treatment at 55°C. They were purified by RP-HPLC, their integrity was confirmed by MALDI-TOF mass spectrometric analysis and their purity was again confirmed by polyacrylamide gel electrophoresis (Figure 4).

Table 1: TBA, *iso*TBA and loop-modified oligomers used in the present work, MALDI-TOF mass spectrometric characterization.

Entry no.	Sequence code	Sequence	MALDI-TOF Mass	
			$M_{\text{calcd.}}$	$M_{\text{Obsd.}}$
1.	TBA	5'-GGTTGGTGTGGTTGG-3'	4726	4727
2.	TBA232	5'-GGtGGtGTGGtGG-3'	4726	4734
3.	TBA202	5'-GGtGGTGTGGtGG-3'	4726	4734
4.	TBA030	5'-GGTTGGtGTGGTTGG-3'	4726	4730
5.	TBA200	5'-GGtGGTGTGGTTGG-3'	4726	4731
6.	TBA002	5'-GGTTGGTGTGGtGG-3'	4726	4734
7.	<i>iso</i> TBA	5'-ggttggtgtggttg-2'	4726	4731
8.	<i>iso</i> TBA232	5'-ggTTggTGTggTTgg-2'	4726	4734
9.	<i>iso</i> TBA202	5'-ggTTggtgtggTTgg-2'	4726	4730
10.	<i>iso</i> TBA030	5'ggttggtGTggttg-2'	4726	4729
11.	<i>iso</i> TBA200	5'-ggTTggtgtggttg-2'	4726	4733
12.	<i>iso</i> TBA002	5'-ggttggtgtggTTgg-2'	4726	4725

^aThe upper case letters indicate 3'-5'-linked DNA, while lower case letters indicate 2'-5'-linked units.

Polyacrylamide gel electrophoresis was used to examine the purity of the synthesized oligomers using a 20% denaturing gel. All the 15-mer oligonucleotides showed similar mobility.



Figure 4: Denaturing gel electrophoresis of TBA, *iso*TBA oligomers, indicating their purity. Strand concentration of TBA and *iso*TBA sequences were 320 μ M and gel was run in TBE buffer at 25 $^{\circ}$ C at 150V. The gel was visualized by UV- shadowing.

1-TBA, 2-TBA232, 3-TBA202, 4-TBA030, 5-TBA200, 6-TBA002, 7-*iso*TBA, 8-*iso*TBA232, 9-*iso*TBA202, 10-*iso*TBA030, 11-*iso*TBA200, 12-*iso*TBA002

4.4.2 Evaluation of G-quadruplex formation in the presence of monovalent cations by circular dichroism spectroscopy

In the case of TBA, formation of quadruplex structure is dependent on metal ion coordination which has been investigated in the presence of ions like K^{+} and Na^{+} , when the equilibrium was found to shift towards quadruplex formation.¹⁴ The cation dependence can be observed between linear and folded unimolecular quadruplex conformation by CD spectroscopy. A positive CD signal at 295 nm and negative CD signal at 265 nm are a characteristic indication of antiparallel G-quadruplexes, such as TBA.²⁴

Firstly, we examined the effect of modification in the loops on the folding topology of TBA by CD spectroscopy in the presence of added monovalent cations like K^{+} , Na^{+} . We found that unmodified TBA and *iso*TBA aptamer and their loop-modified variants displayed a strong, positive maximum CD absorbance at 290 nm and a minimum near 260 nm, as reported²⁴ for TBA (Figures 5 and 6).

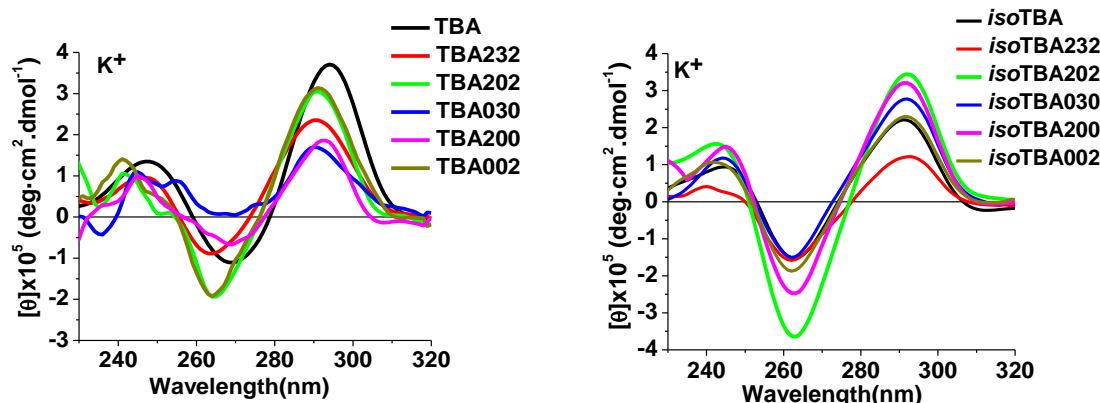


Figure 5: CD spectra of the TBA oligomers (5 μM) in the presence of K^+ ions. Spectra were recorded at 4 $^{\circ}\text{C}$ in 10 mM K phosphate buffer, pH 7.2, containing 100 mM KCl

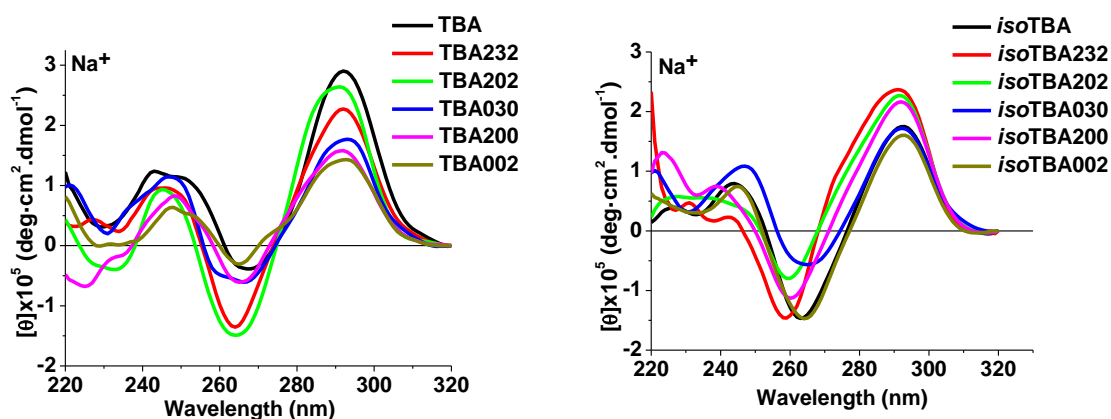


Figure 6: CD spectra of the TBA oligomers (5 μM) in the presence of Na^+ ions. Spectra were recorded at 4 $^{\circ}\text{C}$ in 10mM Na-phosphate buffer, pH 7.2, containing 100 mM NaCl

In the absence of added cations, the typical antiparallel fold was observed only for TBA, while the other oligomers including TBA with 2'-5'-linked loops and *iso*TBA with 3'-5'-linked loops did not display this characteristic CD signature for an antiparallel G-quadruplex (Figure 7).

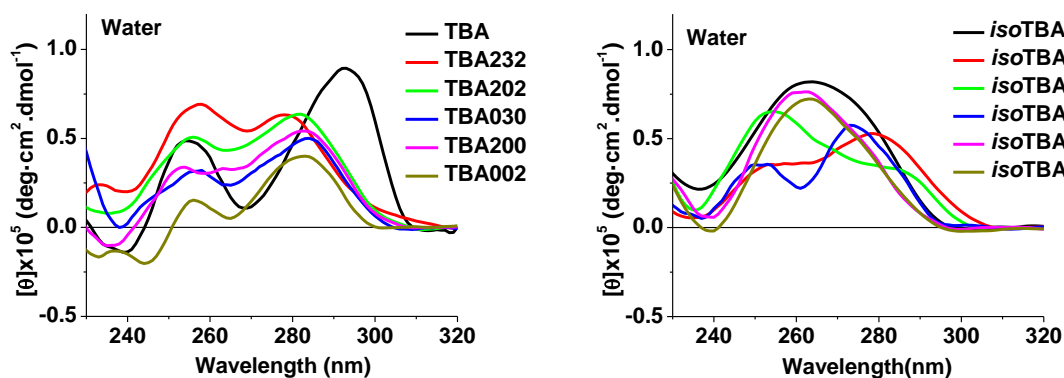


Figure 7: CD spectra of the TBA, *iso*TBA and modified oligomers (5 μM) in water.

4.4.3 Evaluation of G-quadruplex thermal stability using CD spectroscopy

The thermal stability of the quadruplex structures of all modified oligomers was further evaluated by monitoring the temperature-dependent variation in CD amplitude at 295 nm in the presence of K⁺ and Na⁺ ions. The melting profiles are displayed in Figure 8 and values are listed in Table 2.

Table 2: CD- T_m values of modified sequences in presence of K⁺ or Na⁺ ions. ΔT_m^a represents the melting difference compared to native TBA in K⁺ ion. ΔT_m^b represents melting difference compared to native TBA in Na⁺ ion

Entry No.	Sequence code	T_m ° C in K ⁺	ΔT_m^a	T_m ° C in Na ⁺	ΔT_m^b
1.	TBA	50	-	21	-
2.	TBA232	20	-30	15	-6
3.	TBA202	29	-21	18	-3
4.	TBA030	33	-17	25	+4
5.	TBA200	38	-12	13	-8
6.	TBA002	38	-12	18	-3
7.	<i>iso</i> TBA	34	-16	19	-2
8.	<i>iso</i> TBA232	48	-2	36	+13
9.	<i>iso</i> TBA202	54	+4	43	+22
10.	<i>iso</i> TBA030	33	-17	20	-1
11.	<i>iso</i> TBA200	45	-5	39	+18
12.	<i>iso</i> TBA002	44	-6	30	+9

4.4.3.1 CD Thermal stability in presence of K⁺ ions

Noteworthy, the *iso*TBA oligomers that contained 3'-5'-linked loops were found to be much stabler than the TBA oligomers that contained 2'-5'-linked loops (Figure 8). The TBA oligomer that contained homogeneous 3'-5'-linkages, on the other hand, displayed a significantly higher T_m (50 °C) than *iso*TBA (34 °C), its 2'-5'-linked counterpart. Alternative linkages in the TGT central loop were less tolerated than in the TT loops; TBA030 and *iso*TBA030 were destabilized by 17 °C and 1 °C respectively relative to the parent oligomers (TBA/*iso*TBA), in comparison to TBA200 ($\Delta T_m = -12$

°C), TBA002 ($\Delta T_m = -12$ °C), *iso*TBA200 ($\Delta T_m = +11$ °C) and *iso*TBA002 ($\Delta T_m = +10$ °C), where in fact, a stabilizing effect was observed with the *iso*TBA oligomers. This effect also extended to the oligomers with multiple loop replacements. Accordingly, TBA202 and TBA232 where two or all three loops bore 2'-5'-linkages were destabilized to a larger degree ($\Delta T_m = -21$ °C and -30 °C respectively), while *iso*TBA202 and *iso*TBA232 displayed T_m s of 54 °C ($\Delta T_m = +20$ °C) and 48 °C ($\Delta T_m = +14$ °C) respectively, clearly combining the destabilizing effect of the TGT loop linkage replacement with the stabilizing effect linkage replacement in the TT loops.

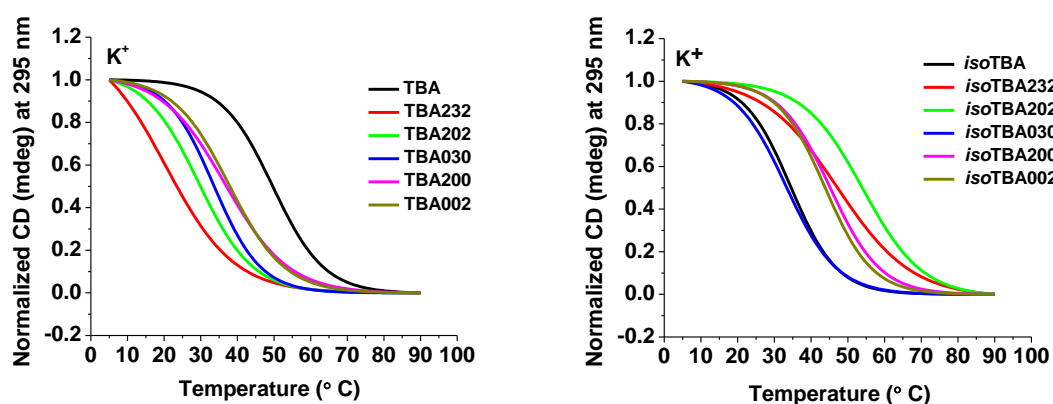


Figure 8: CD melting profiles of the TBA oligomers at a strand concentration of $5\mu\text{M}$ in 10 mM potassium phosphate buffer (pH 7.2) containing 100 mM KCl.

This indicates that the extended 2'-5'-phosphodiester backbone is more beneficial to the thermal stability when in the stem region of the quadruplex, while the more compact 3'-5'-phosphodiester backbone has a positive effect when in the loops, notably the TT loops. The 2'-5'-phosphodiester linkages give rise to a 7-atom backbone with an extended geometry, which imparts more flexibility to the backbone that could at least partly account for the destabilization of the quadruplexes with these linkages in the TBA loops.

Avino et al.^{15b} earlier reported modified thrombin binding aptamers carrying nucleosides in the north (N-type) conformation in loops of TBA, where they found that replacement of thymidines in TT loop by north nucleosides induced destabilization of the antiparallel quadruplex structure. The 2'-5'-linked nucleosides in this chapter are also known to adopt the N-type sugar conformation, and in consistence with the report of Avino et al.,^{15b} a destabilizing effect of these nucleosides was observed when they were included in the loop regions of TBA, notably the TT loops.

4.4.3.2 CD Thermal stability in the presence of Na⁺ ions

Melting studies of all oligomers in presence of sodium ions were carried out by CD spectroscopy (Figure 9). It is very well known that TBA forms unimolecular antiparallel quadruplex in the presence of Na⁺ ions,¹⁴ but of lower thermal stability than in the presence of K⁺ ions.

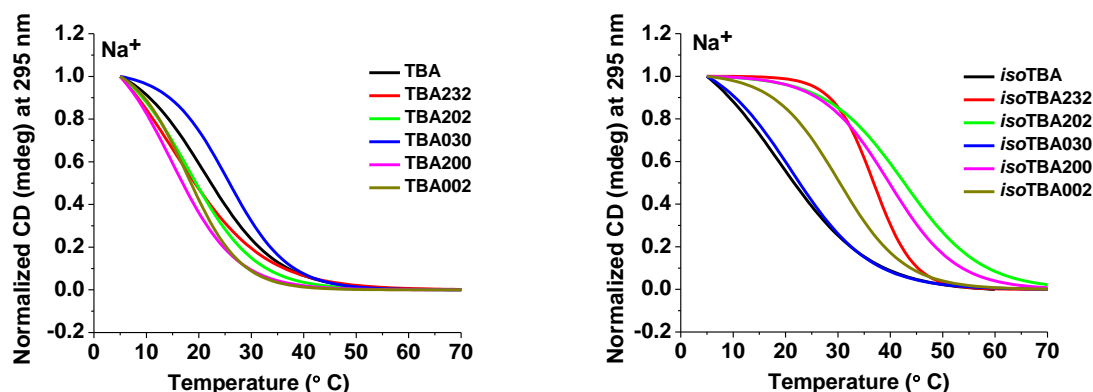


Figure 9: CD melting profiles of the TBA oligomers at a strand concentration of 5 μ M in 10 mM sodium phosphate buffer (pH 7.2) containing 100 mM NaCl.

All modified TBA oligomers that contained 2'-5'-linked loops (TBA232, TBA202, TBA200 and TBA002) showed lower stability than the TBA oligomer with homogeneous 3'-5'-linkages except TBA030, which showed +4 $^{\circ}$ C stabilization ($T_m = 25^{\circ}$ C). The *iso*TBA with a homogeneous 2'-5'-linked backbone ($T_m = 19^{\circ}$ C) and *iso*TBA030 ($T_m = 20^{\circ}$ C) were less stable compared to native TBA ($T_m = 21^{\circ}$ C). Interestingly, enhancement of thermal stability was observed in *iso*TBA oligomers with modification in lateral loops by 3'-5' linkages. *iso*TBA232, *iso*TBA202, *iso*TBA200 and *iso*TBA002 displayed an increase in stability in comparison to TBA with melting temperature difference (ΔT_m) of +13 $^{\circ}$ C, +22 $^{\circ}$ C, +18 $^{\circ}$ C and +9 $^{\circ}$ C respectively.

The thermal stability analysis has shown that changes in the conformation of the sugar pucker of the nucleotides present in loop regions, together with the flexibility/compactness of the backbone are crucial for determining the folding and stability of TBA.

4.4.4 Formation of G-quadruplex in the presence of thrombin

Thrombin can act as a molecular chaperone for the folding of TBA, as has been reported previously by Baldrich and O'Sullivan.²⁵ Nagatoishi and co-workers showed

that at low temperature, TBA forms an antiparallel G quadruplex in the presence of thrombin and in the absence of any cation,²⁶ which can be monitored through the CD amplitude at 295 nm. Therefore, we carried out CD experiments with addition of thrombin incrementally to the individual oligomers at 4 °C. The modified TBA oligomers were classified into two groups, based on their backbone. Melting experiments were performed and the data is summarized in Table 3.

Table 3: Melting data of the two groups of modified TBA oligomers.

Group I (3'-5' linkage)		Group II (2'-5' linkage)	
Sequence code	T_m °C of thrombin(ΔT_m) ^a	Sequence code	T_m °C of thrombin(ΔT_m) ^a
TBA	22	<i>iso</i> TBA	13 (-9)
TBA232	nd	<i>iso</i> TBA232	18 (-4)
TBA202	nd	<i>iso</i> TBA202	26 (+4)
TBA030	nd	<i>iso</i> TBA030	12 (-10)
TBA200	nd	<i>iso</i> TBA200	10 (-12)
TBA002	nd	<i>iso</i> TBA002	11 (-11)

Experiments were performed with strand concentration of 5 μ M in water containing 2.5 NIH Thrombin in 0.5 ml, ^a values in parentheses indicate the difference in T_m (ΔT_m) w.r.t. native TBA, nd is not determinable.

The CD spectra of group I oligomers showed a maximum near 280 nm in water, except in case of control TBA that displayed maxima at 290 nm, as it forms antiparallel G-quadruplex in water. While this chaperone effect was observed for TBA, the TBA oligomers with 2'-5'-linked loops (Group I) showed a slight shift of maxima near 290 nm and a negligible amplitude change in the CD signal near 290 nm. In contrast, for Group II *iso*TBA oligomers with 3'-5'-linked loop regions, G-quadruplex structure was not observed in the absence of thrombin. However, upon incremental addition of thrombin, a marked change was observed, with a concomitant increase in CD amplitude near 295 nm (Figure 10).

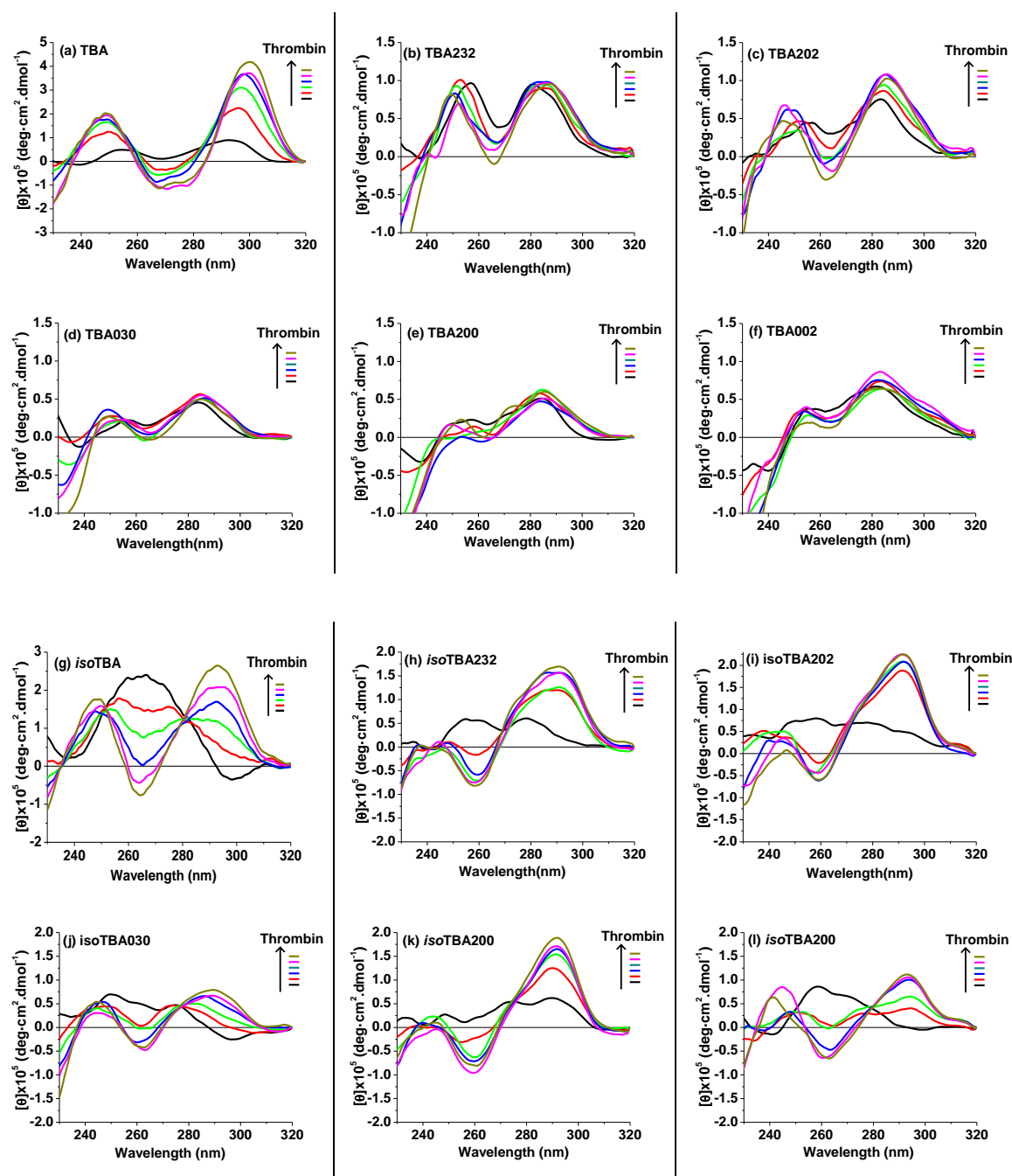


Figure 10: Changes in CD signal at 295 nm showing the chaperone effect of thrombin on the TBA and *iso*TBA loop-modified oligomers Black: in water (No thrombin), Red: 0.44 μ M, Green: 85 μ M, Blue: 1.25 μ M, Magenta: 1.63 μ M, Dark yellow: 2 μ M

The temperature-dependent stability of the thrombin-induced quadruplex structure was monitored by recording the CD amplitude at 295 nm with increasing temperature intervals (Figure 11). The strength of *iso*TBA202 G-quadruplex-thrombin was the highest with $T_m = 26^\circ\text{C}$ ($\Delta T_m = +4^\circ\text{C}$ stabilization compared to native TBA), followed

by thrombin complexes of TBA (22 °C), *iso*TBA232 ($T_m = 18$ °C), *iso*TBA ($T_m = 13$ °C) and *iso*TBA030, *iso*TBA200 and *iso*TBA002 ($T_m \sim 10$ -12 °C). For all oligomers in Group I, i.e., TBA sequences with 2'-5' linkages in the loops, binding with thrombin was not strong enough. Therefore, the melting temperature of their complexes with thrombin could not be determined. The above results suggest the requirement of compact geometry in the TT loops, but flexibility in the stem region for favourable thrombin-aptamer interaction.

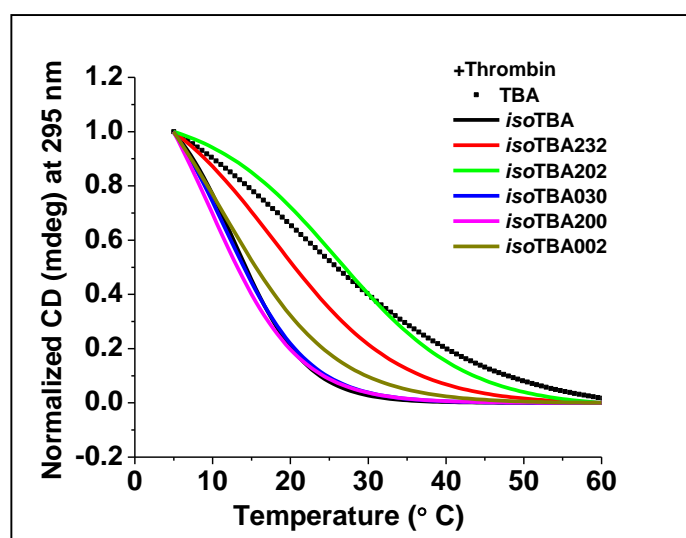


Figure 11: Melting data of G-quadruplex induced by thrombin. Thrombin concentration = 2 μ M, oligomer concentration = 5 μ M in 0.5 ml water.

4.4.5 Antithrombin effect of chimeric aptamers

Thrombin transforms fibrinogen to fibrin and that leads to coagulation.²⁷ The effect of thrombin binding on the anti-thrombin activity of the mixed backbone variants was assessed by carrying out a clotting assay and the inhibitory effect on thrombin-catalyzed fibrin polymerization (thrombin time/clotting time) was measured at 37 °C. The thrombin reagent was pre-incubated with the oligomer before addition to fibrinogen-containing saline and the time for clotting was measured using a SStart Max Coagulation analyzer (Diagnostica Stago). The anti-thrombin activity reflects the additional time required for clotting in the presence of the oligomer, relative to the reference in the absence of any added oligomer. From Figure 12, it can be seen that in comparison to the TBA oligomers, the *iso*TBA oligomers had a lower anti-thrombin activity, with the highest activity being observed for the parent TBA containing all 3'-5'-phosphodiester backbone linkages. TBA202, with 2'-5'-linked T³T⁴ and T¹²T¹³ loops showed similar

clotting time to TBA. Except for TBA202, in the case of all other oligomers, the introduction of alternative linkages in the loop regions led to a decrease in anti-thrombin activity relative to the parent oligomer.

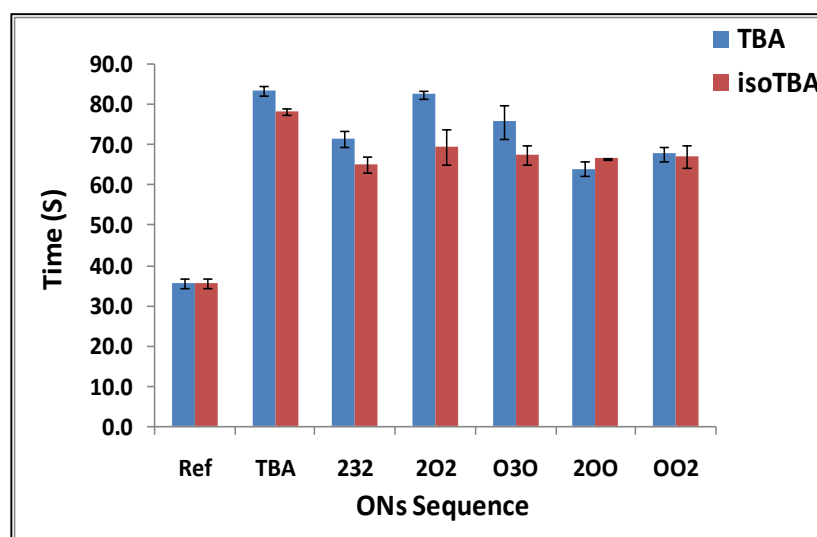


Figure 12: Antithrombin activity measurement using fibrinogen from human plasma and bovine thrombin. Error bars represent the standard deviation obtained from triplicate experiments. Ref indicates the clotting time measured with fibrinogen and thrombin in the absence of any added oligomer.

4.4.6 Stability of oligonucleotides towards exonuclease and endonuclease

In addition to improving the thermal stability and anticlotting ability of TBA, another aim of incorporating modified units into its sequence was to enhance the stability of the oligomers towards nuclease degradation. The 2'-5'-linked non-genetic DNA and RNA show high resistance to nuclease digestion compared with their natural 3'-5'-linked oligomers.²⁸ To examine the enzymatic stability of the quadruplex-forming mixed backbone, we exposed these aptamers to two kinds of nucleases, snake venom phosphodiesterase (SVPD) from *Crotalus adamanteus* (3' exonuclease) and S1 nuclease isolated from *Aspergillus oryzae* (endonuclease).

4.4.6.1 Exonuclease resistance

A comparative study of TBA002 and *iso*TBA002 against hydrolytic cleavage by SVPD was done. We exposed TBA, *iso*TBA, TBA002 and *iso*TBA002 oligomers to SVPD digestion at 37 °C. The progress of digestion was analysed by RP-HPLC by analyzing aliquots of the reaction at progressive time points (Figure 14a, 14b, 14c & 14d). The percent of intact oligomer was plotted versus time (Figure 13). The

homogeneous 2'-5'-linked *iso*TBA was found to be much stabler than any of the other oligomers studied. The half-life of *iso*TBA was found to be more than 50 min while *iso*TBA002 (studied as a representative oligomer) displayed a $t_{1/2} \sim 10$ min, while the $t_{1/2}$ of TBA oligomers TBA and TBA002 was < 2 min. Thus, compared to native TBA, *iso*TBA oligomers showed better stability to SVPD.

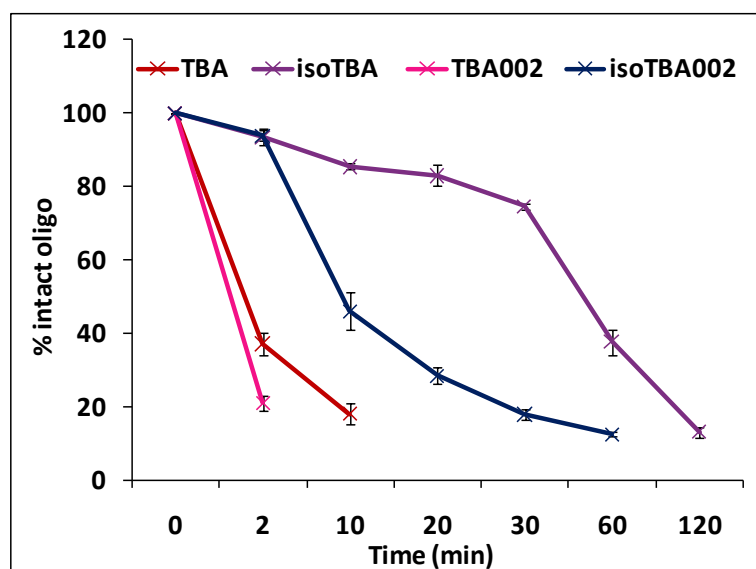


Figure 13: RP- HPLC at several times for SVPD (0.01 mg/mL) digestion of oligonucleotides TBA, *iso*TBA, TBA002, *iso*TBA002. Experiments were done in Duplicate and the error bars (standard deviation) are indicated.

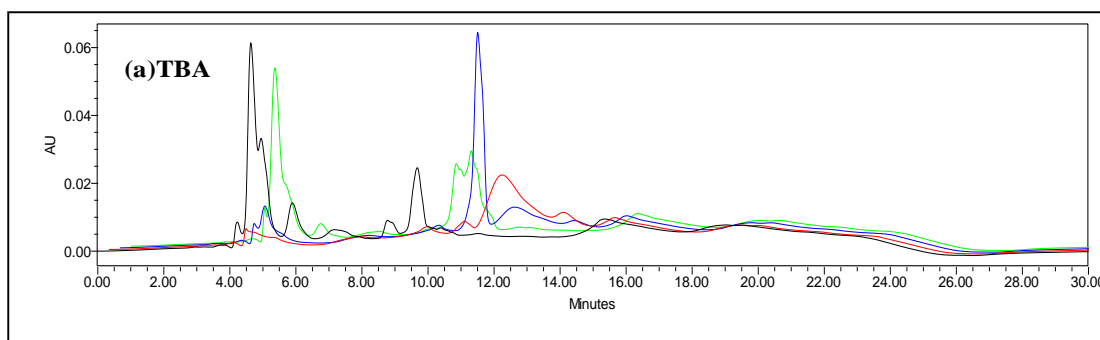


Figure 14a: RP-HPLC runs overlay of TBA towards SVPD nuclease at increasing time intervals
Red: without SVPD enzyme, Blue: 2 min, Green: 10 min, Black: 20 min

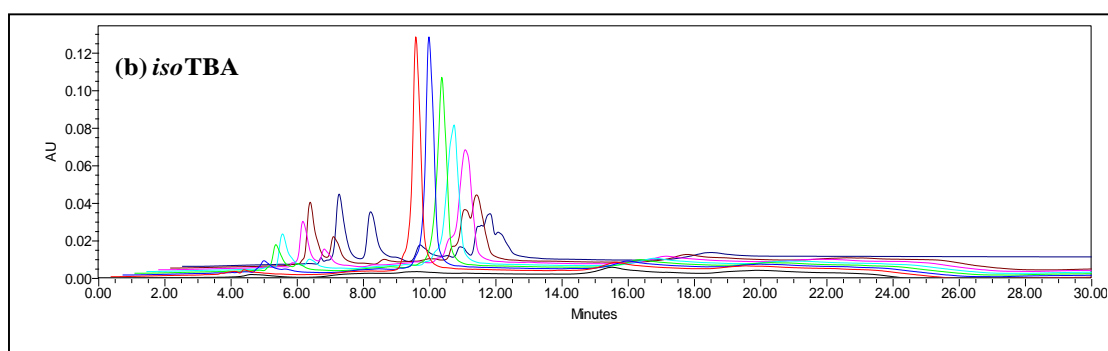


Figure 14b: RP-HPLC runs overlay of TBA towards SVPD nuclease at increasing time intervals Black: Buffer, Red: without SVPD enzyme, Blue: 2 min, Green: 10 min, Cyan: 20 min, Magenta: 30 min, Brown: 60 min, Dark blue: 120 min

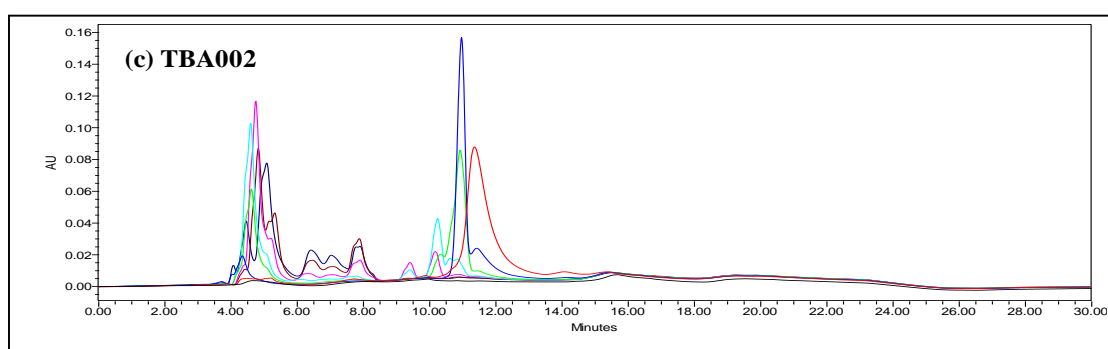


Figure 14c: RP-HPLC runs overlay of TBA002 towards SVPD nuclease at increasing time intervals Black: Buffer, Red: without SVPD enzyme, Blue: 2 min, Green: 10 min, Cyan: 20 min, Magenta: 30 min.

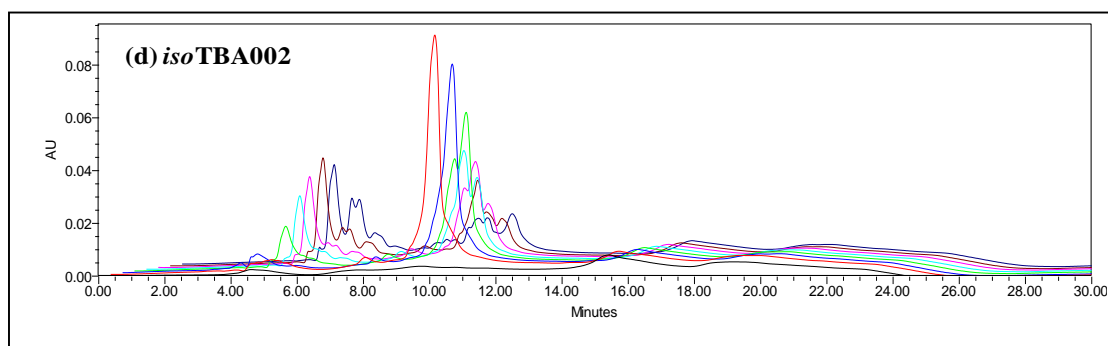


Figure 14d: RP-HPLC runs overlay of TBA towards SVPD nuclease at increasing time intervals Black: Buffer, Red: without SVPD enzyme, Blue: 2 min, Green: 10 min, Cyan: 20 min, Magenta: 30 min, Brown: 60 min, Dark blue: 120 min.

4.4.6.2 Endonuclease resistance

Formation of the G-quadruplex structure is reported to shield oligonucleotides from rapid nuclease degradation.²⁹ However, the loops are exposed and accessible to the certain nucleases, particularly endonucleases, for digestion. The shielding effect of

backbone modification was estimated by a comparative analysis of selected lateral TT loop modified oligomers by S1 nuclease that is an endonuclease. We exposed oligonucleotides TBA, *iso*TBA, TBA202 and *iso*TBA202 to S1 nuclease digestion at 37 °C, and monitored the progress with time by HPLC (Figure 15a, 15b, 15c & 15d). The percent of intact oligomer was plotted versus time (Figure 15). *iso*TBA202 (studied as a representative oligomer) displayed a $t_{1/2} \sim 15$ min, but was found to be intact even after 120 min, while the stability of TBA202 was extremely low, and was cleaved within 2 min. This proves the fact that oligomers in folded quadruplex form resist nuclease cleavage. The stability provided by the quadruplex stem seems to override the exposure of loop residues to endonucleolytic cleavage by S1 nuclease.

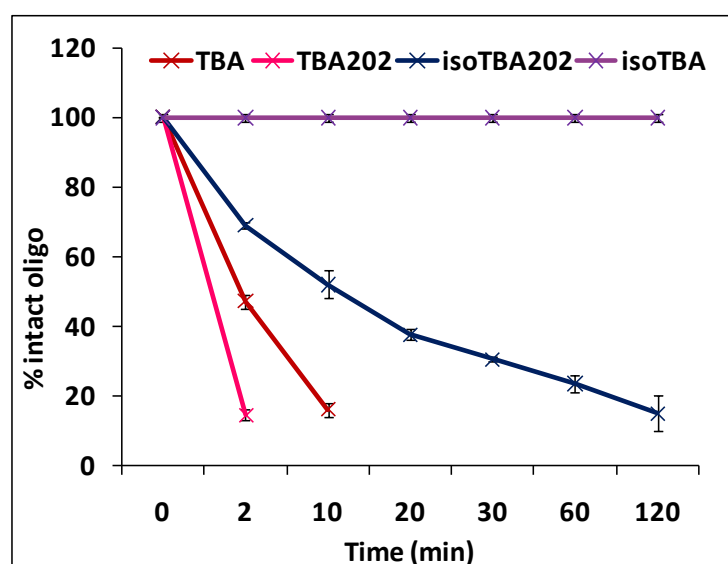


Figure 15: RP- HPLC at several times for S1endonuclease digestion of oligonucleotides TBA, TBA202, *iso*TBA 202, and *iso*TBA

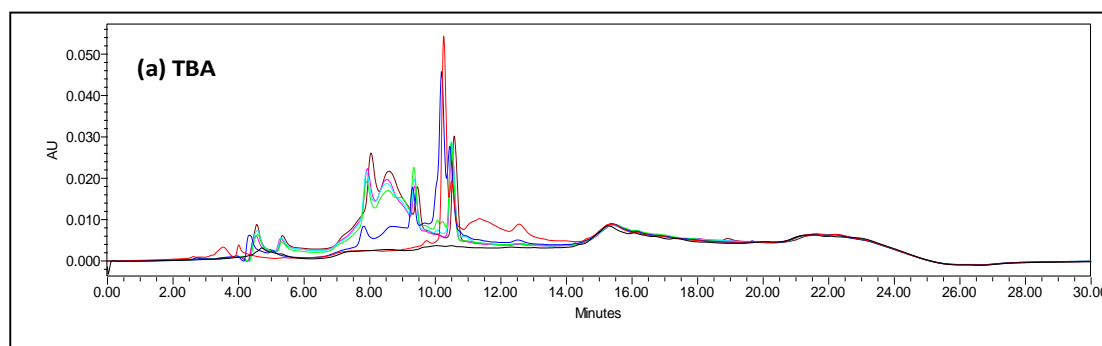


Figure 15a: RP-HPLC runs overlay of TBA towards SVPD nuclease at increasing time intervals. Black: Buffer, red: without S1 enzyme, Blue: 2 min, Green: 10 min, Cyan: 20 min, Magenta: 30 min

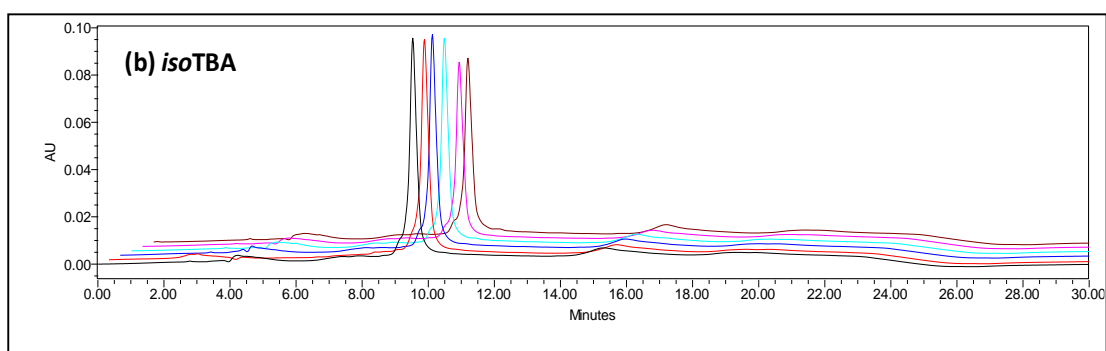


Figure 15b: RP-HPLC runs overlay of *isoTBA* towards SVPD nuclease at increasing time intervals. Black: without S1 nuclease enzyme, Red: 2 min, Blue: 10 min, Cyan: 30 min, Magenta: 60 min, Brown: 120 min

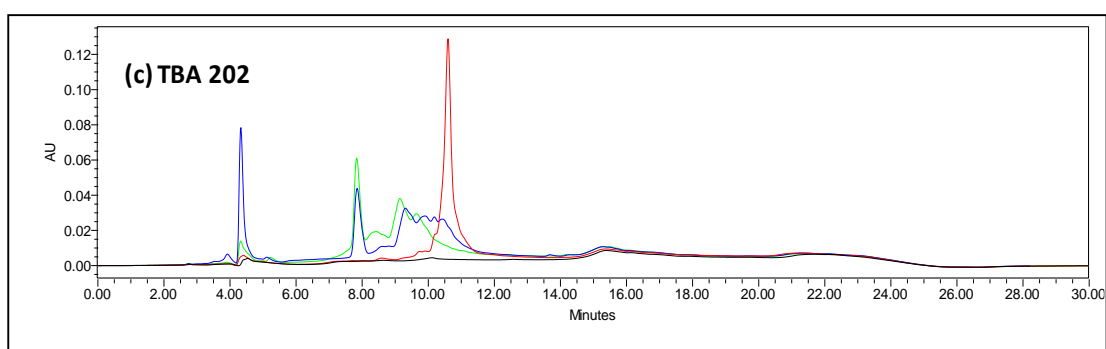


Figure 15c: RP-HPLC runs overlay of TBA202 towards SVPD nuclease at increasing time intervals. Black: Buffer, red: without S1 nuclease enzyme, Blue: 2 min, Green: 10 min

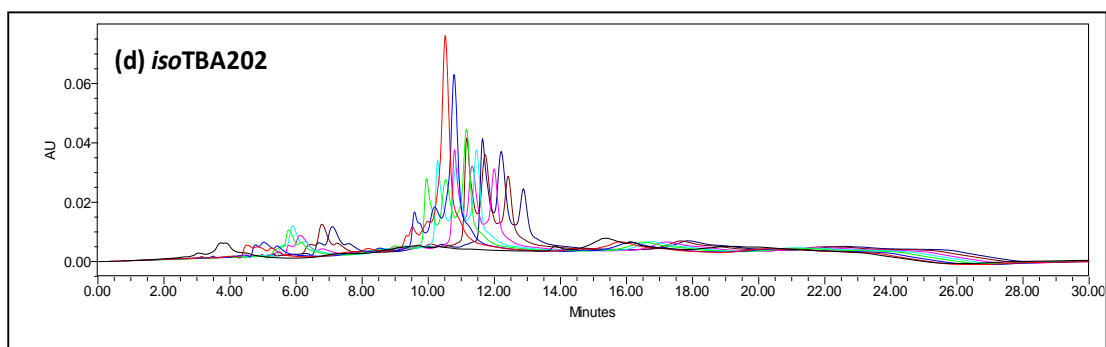


Figure 15d: RP-HPLC runs overlay of *isoTBA202* towards SVPD nuclease at increasing time intervals. Black: Buffer, red: without S1 nuclease enzyme, Blue: 2 min, Green: 10 min, Cyan: 20 min, Magenta: 30 min, Brown: 60 min, Dark blue: 120 min.

4.5 Key highlights of this study

- Chimeric variants of the thrombin-binding aptamer (TBA) and the isomeric *iso*TBA containing 2'-5'-backbone linkages, where the loop residues are linked by 2'-5'- or 3'-5'-phosphodiesterases respectively were synthesized.
- CD spectroscopy studies in the presence of K⁺, Na⁺ ions showed that all the oligomers studied in this work are able to form unimolecular antiparallel G-quadruplexes, similar to native TBA.
- Thrombin-binding studies brought out the chaperone effect of thrombin on the quadruplex topology of individual oligomers.
- Thrombin inhibition was examined, which revealed that TBA quadruplexes with extended 2'-5'- backbone in the loops showed greater anticlotting ability in comparison to their *iso*TBA counterparts.
- Enhanced stability to nucleases was shown by *iso*TBA oligomers compared to TBA and their TBA counterparts.

4.6 Conclusion

In conclusion, we developed a new class of chimeric thrombin-binding aptamers having extended backbone and studied the significant effect of the loop residue backbone on the topology and thermal stability of the quadruplexes. Chimeric TBA oligomers were found to be similar to the native DNA aptamer (TBA) both in terms of structure as well as function. Our finding demonstrates that the TT loops have a more pronounced effect on the thrombin-binding ability and the resulting anti-clotting effect. *Iso*TBA oligomers additionally have the feature of stability towards nucleases (both endo- and exo-), which could prove beneficial in applications in biological systems where a longer half-life is desired.

4.7 Experimental

4.7.1 Synthesis of oligonucleotides, purification and characterization

The regular procedures of oligonucleotide synthesis, their purification (High-performance liquid chromatography and Gel electrophoresis study) and MALDI-TOF characterization are same as discussed earlier in Chapter 2.

CD spectroscopy, Thrombin time measurements for clotting inhibition and Exonuclease stability study were carried out by using standard procedure. All the particulars of experiment are same as discussed previously in chapter 2.

4.7.2 Endonuclease stability

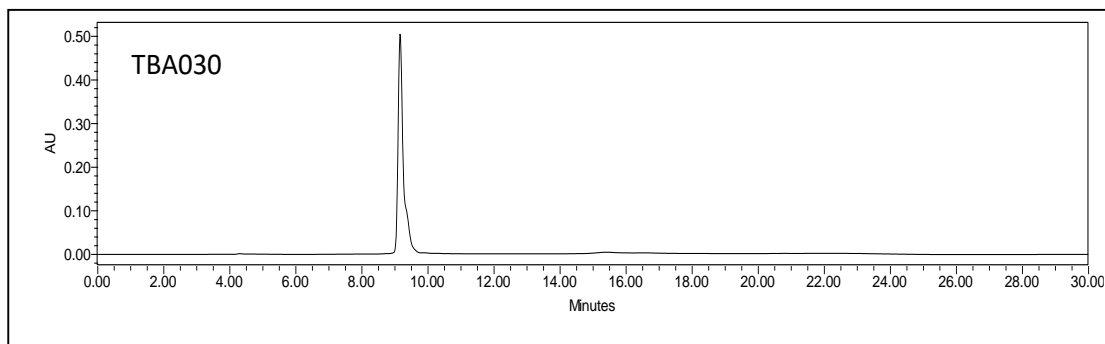
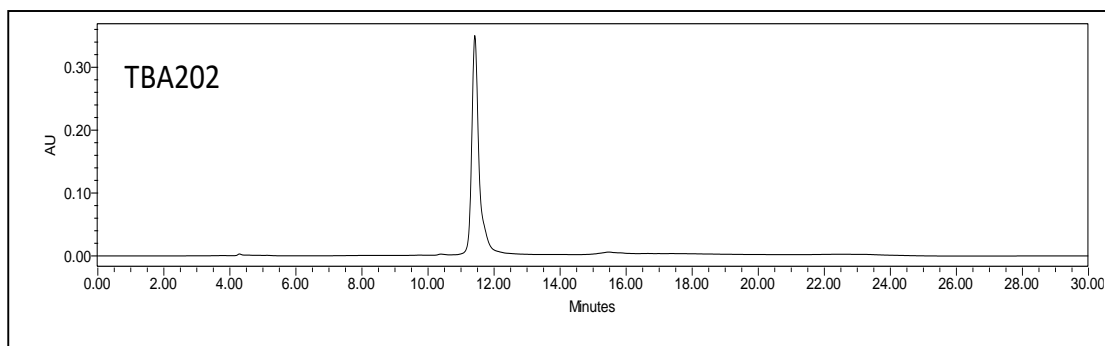
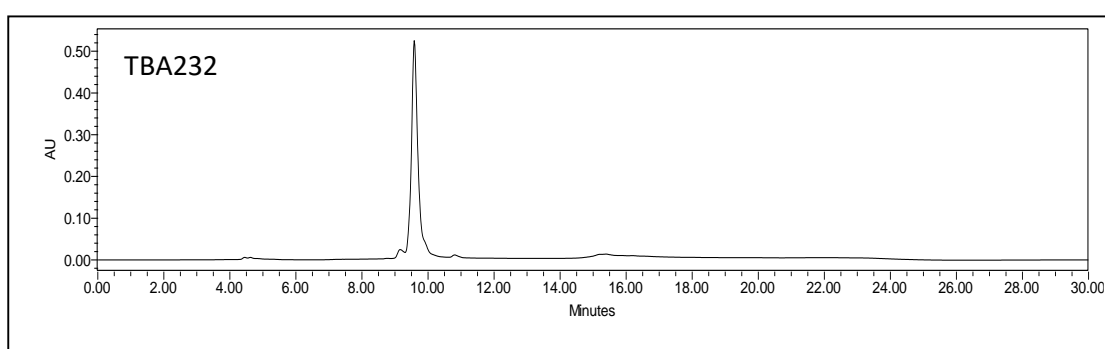
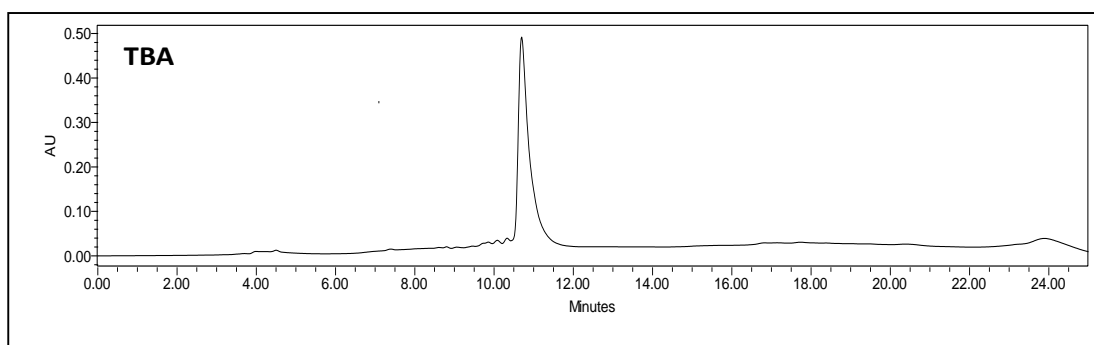
For S1 nuclease Digestion, 7.5 μ M oligonucleotides were dissolved in reaction buffer (pH 4.5) containing 0.5 M sodium acetate, 2.8 M NaCl, and 45 mM ZnSO₄. S1 nuclease 8.9 U/ μ L was added to the 100 μ L oligonucleotide at 37 °C, Aliquots were removed at successive time intervals of 2, 10, 20, 30, 60, 120 minutes. Aliquots were kept at 90 °C for 2 minutes to inactivate nuclease. Aliquots analysed by RP-HPLC using an increasing gradient of acetonitrile in triethylammonium acetate (A: 5% acetonitrile and B: 30% acetonitrile in 0.1N triethylammonium acetate, pH 7.0). The percent intact oligonucleotide (based on the peak area) was plotted against the time to show the degradation of oligomers with respect to time.

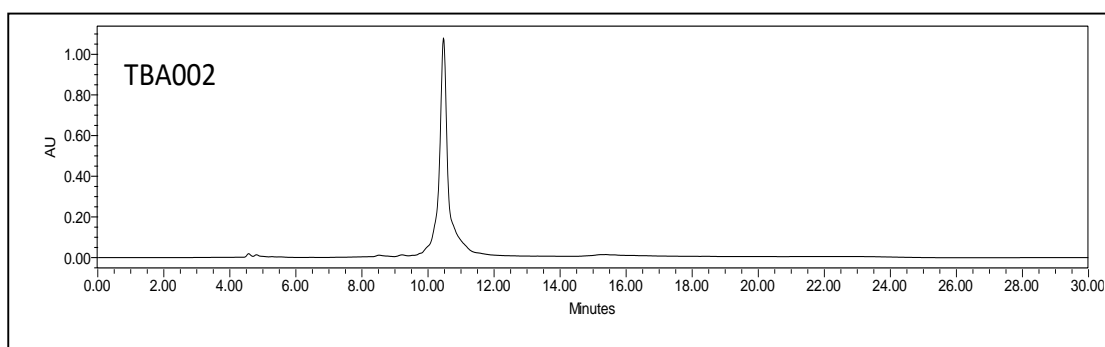
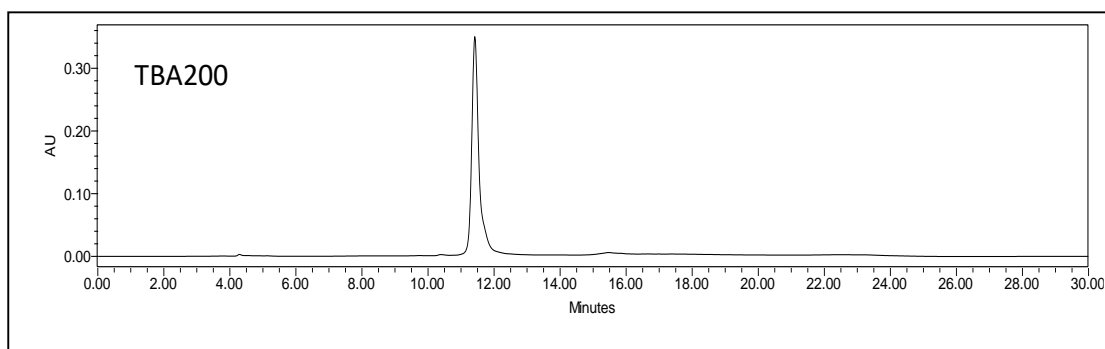
.

4.8 Appendix C

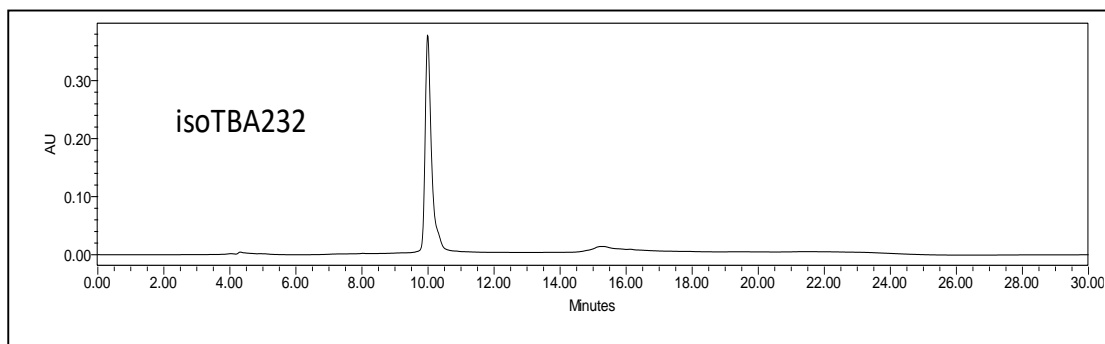
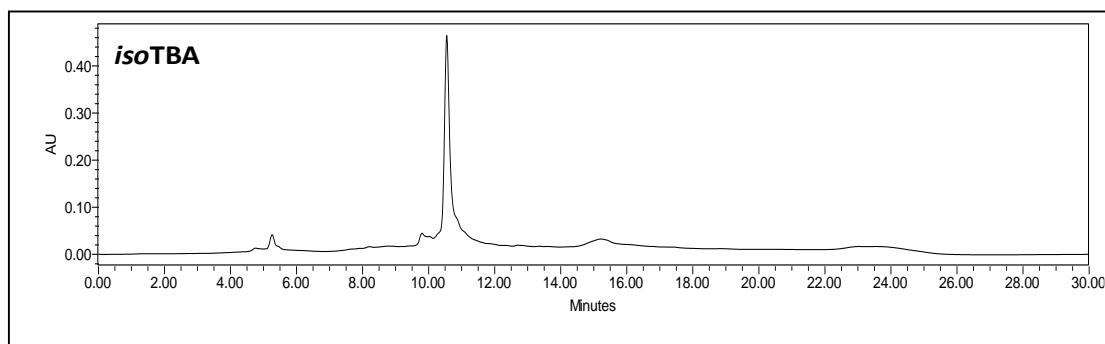
Description	Page No.
HPLC chromatogram of TBA oligomers	218-219
HPLC chromatogram of <i>iso</i> TBA oligomers	219-220
MALDI-TOF spectra of TBA oligomers	221-222
MALDI-TOF spectra of <i>iso</i> TBA oligomers	223-224

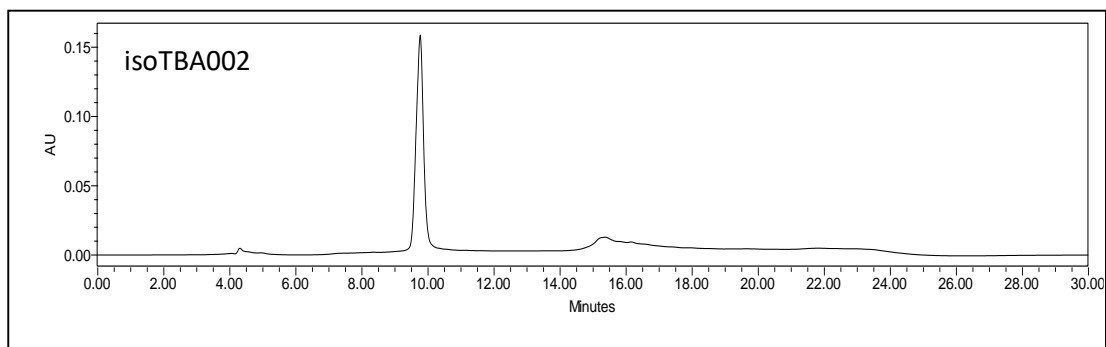
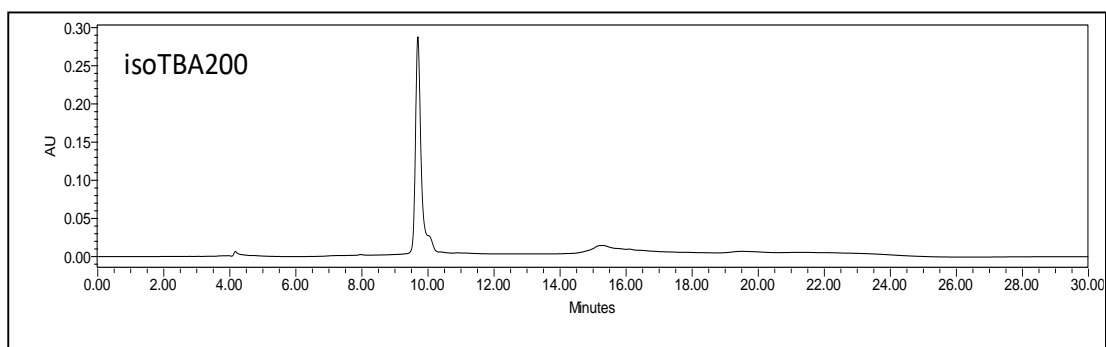
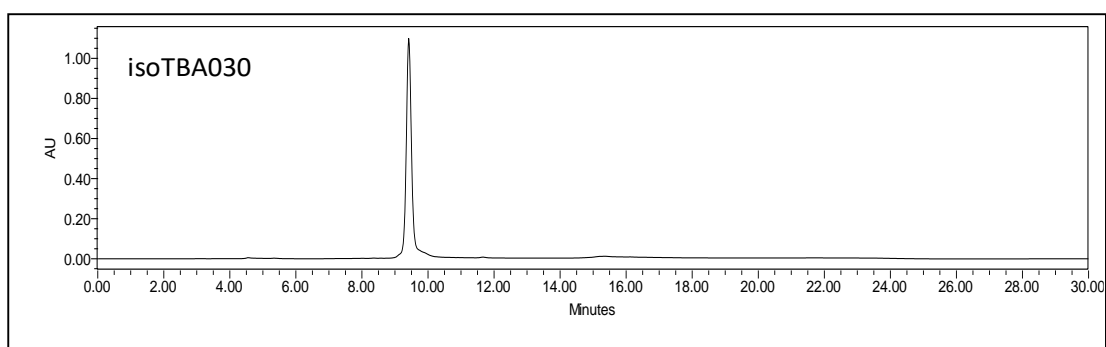
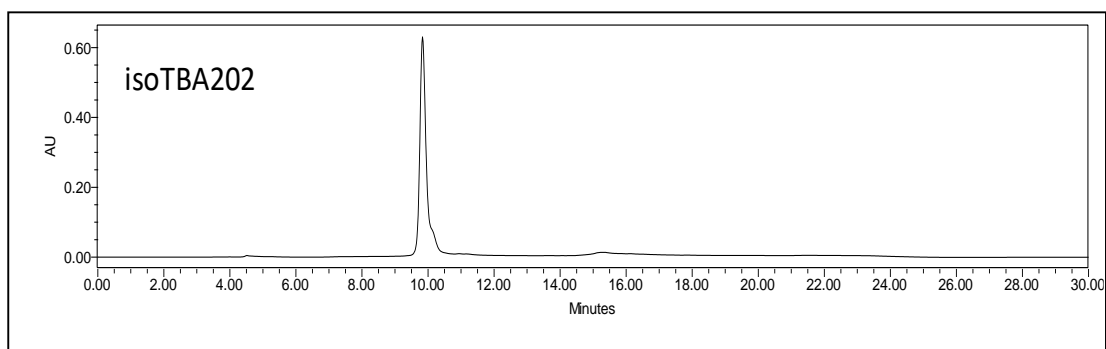
HPLC chromatograms of purified synthesized TBA oligomers



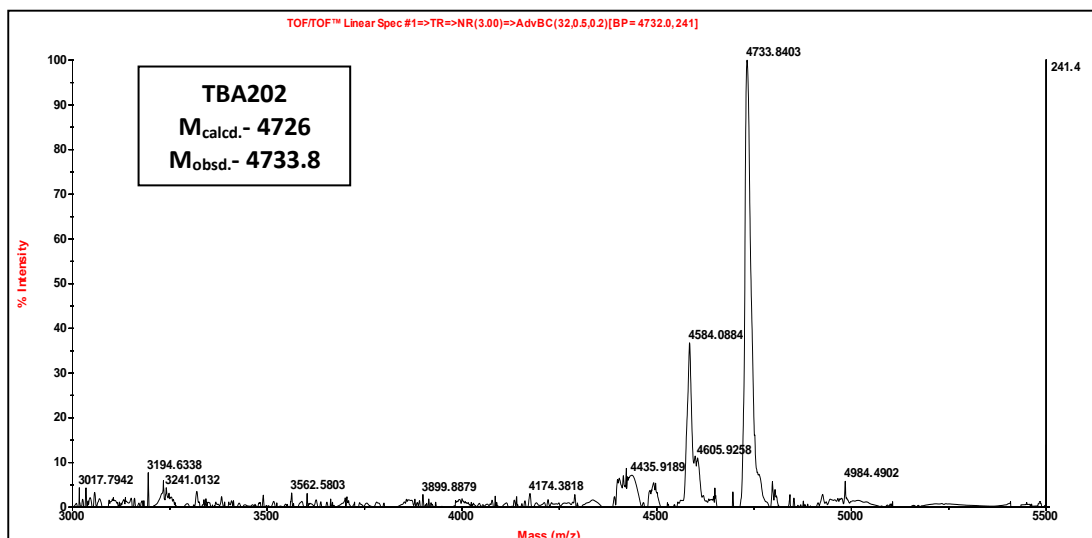
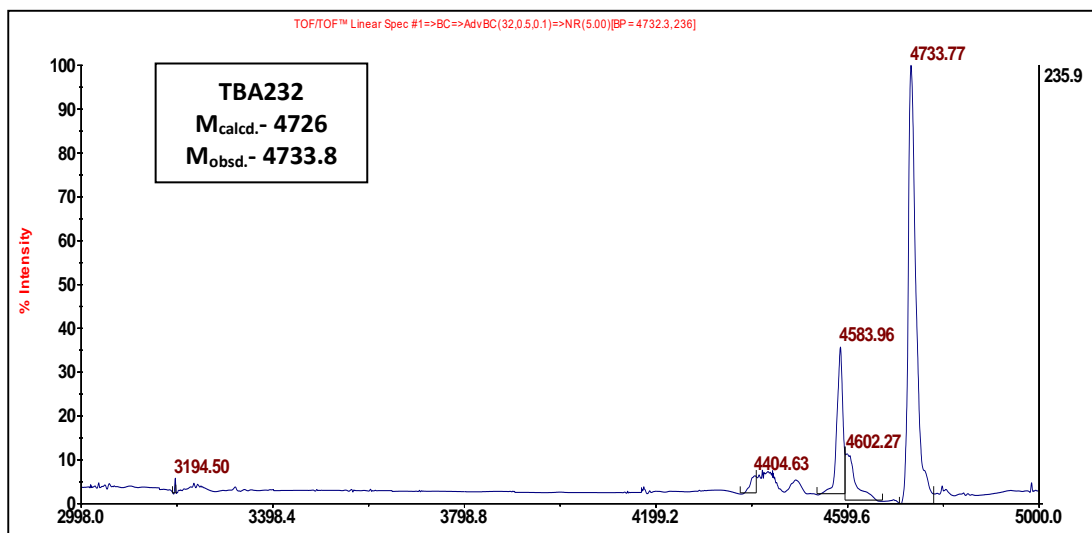
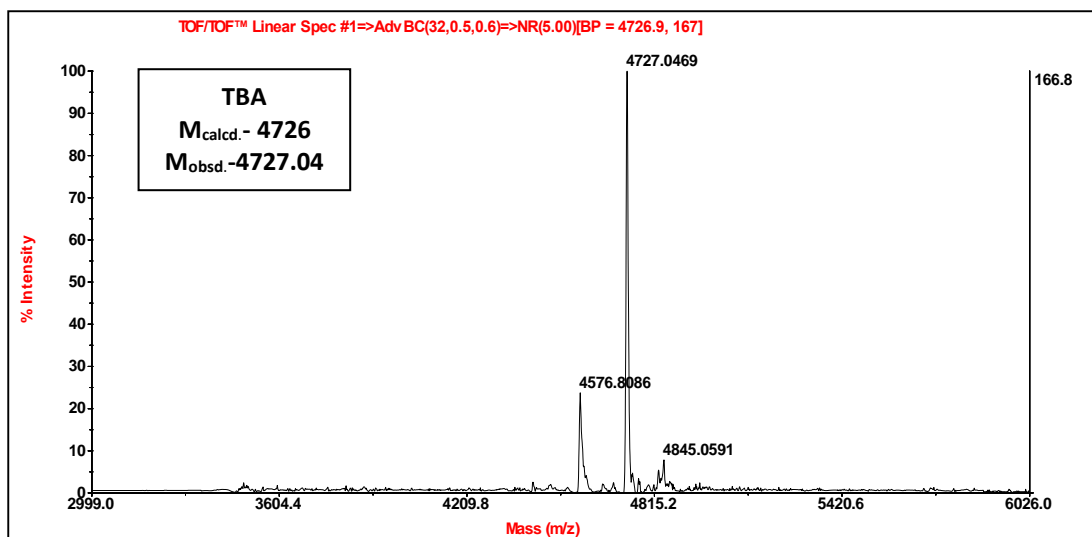


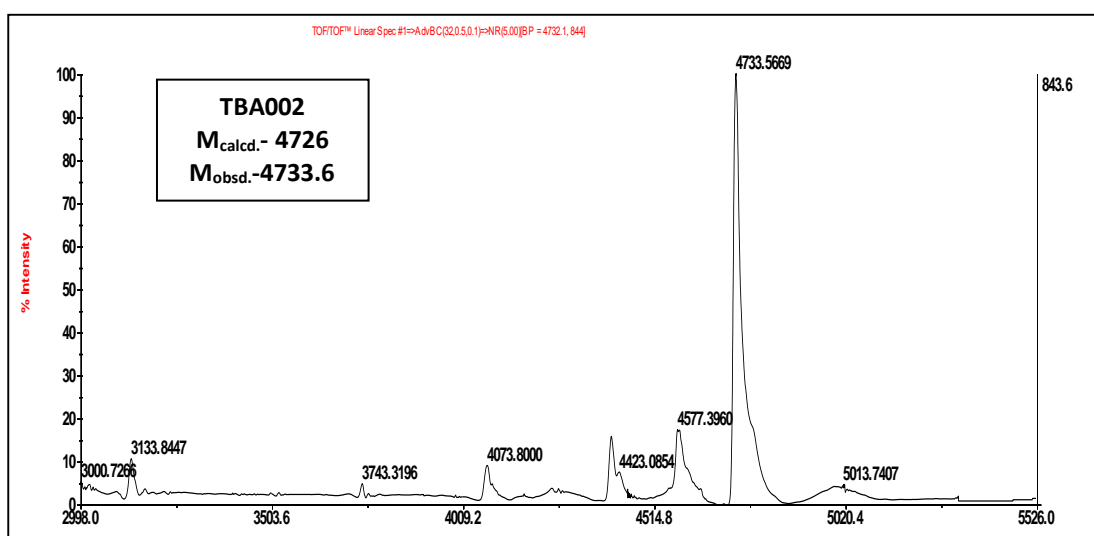
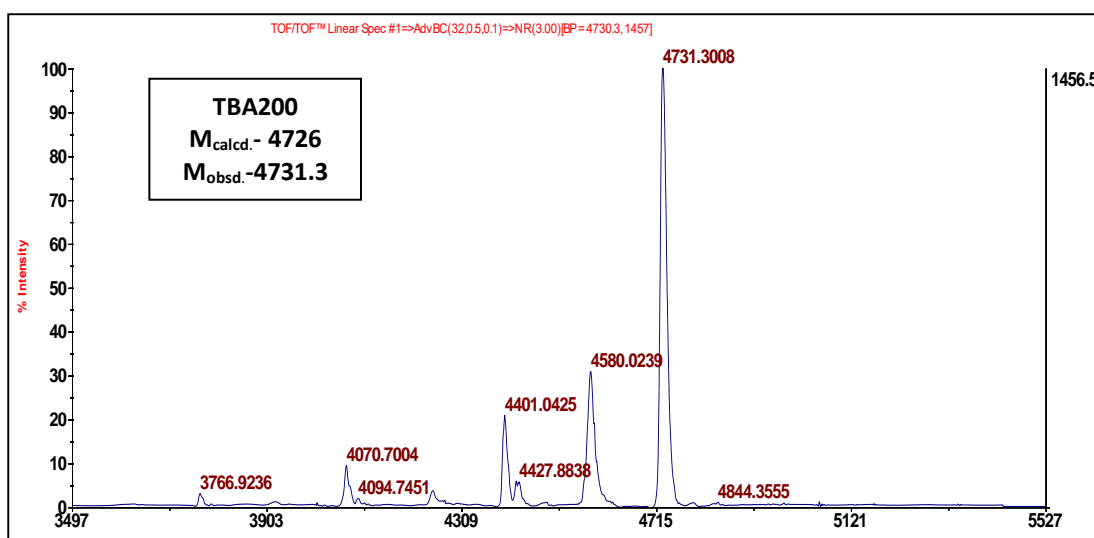
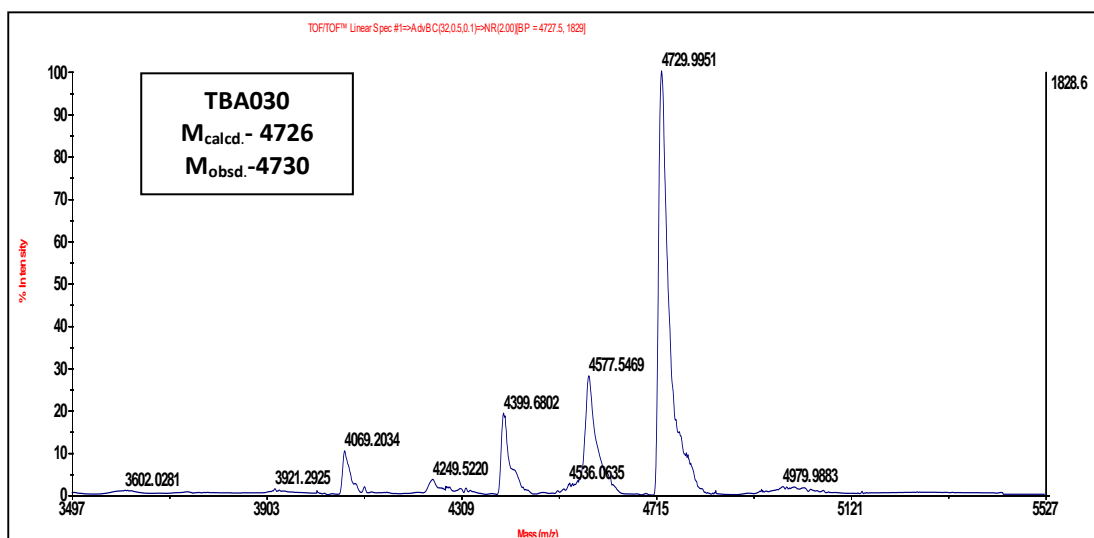
HPLC chromatograms of purified synthesized *iso*TBA oligomers

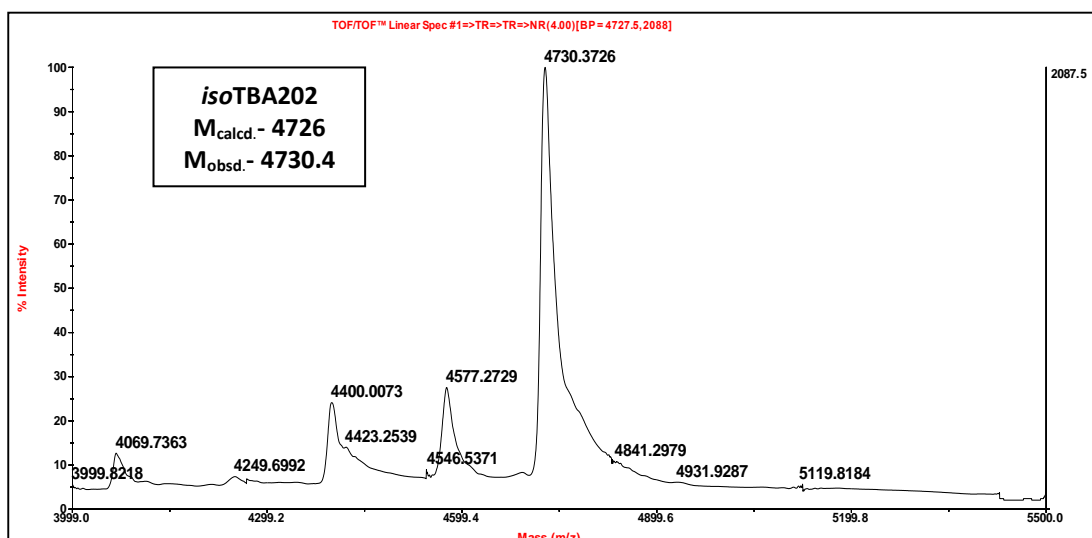
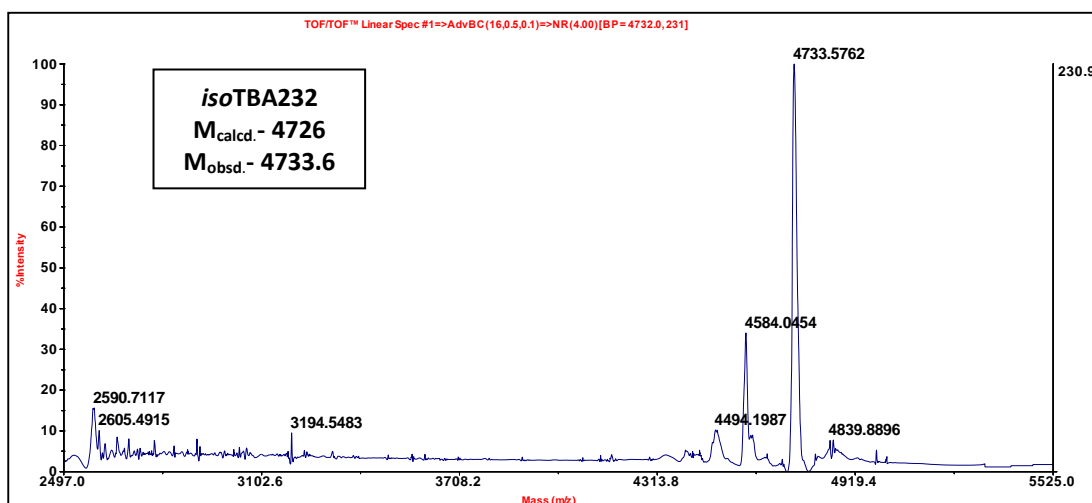
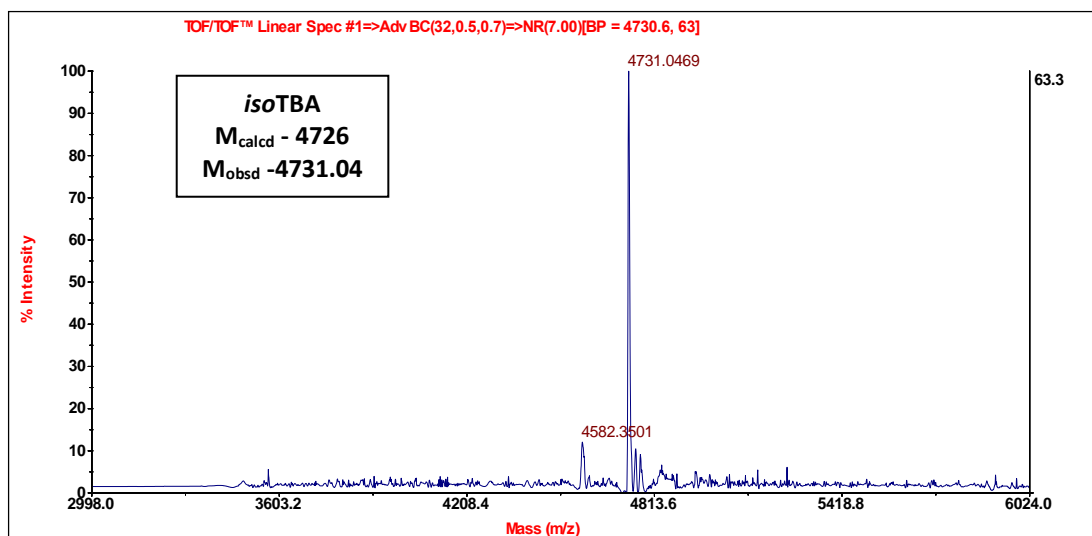


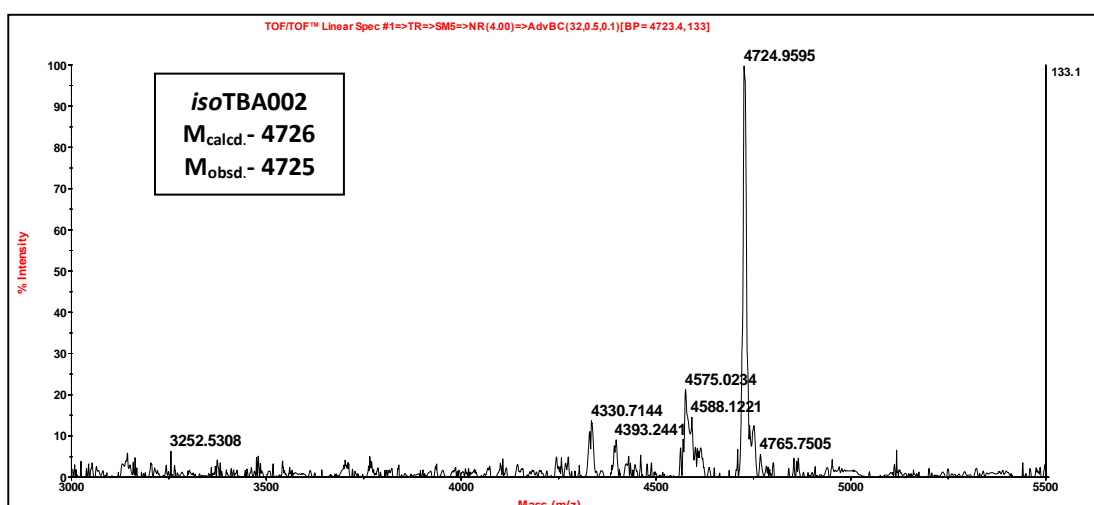
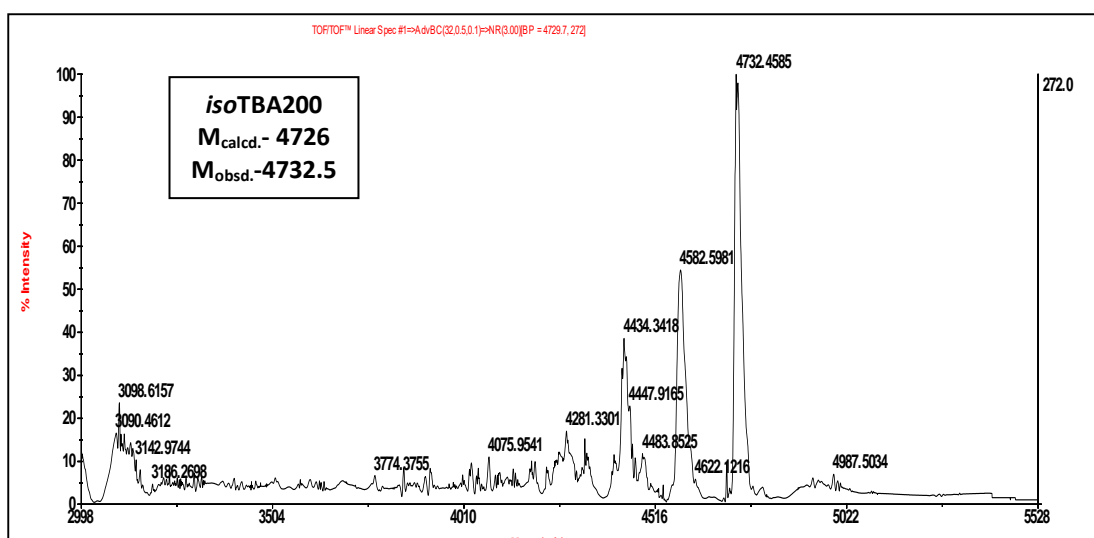
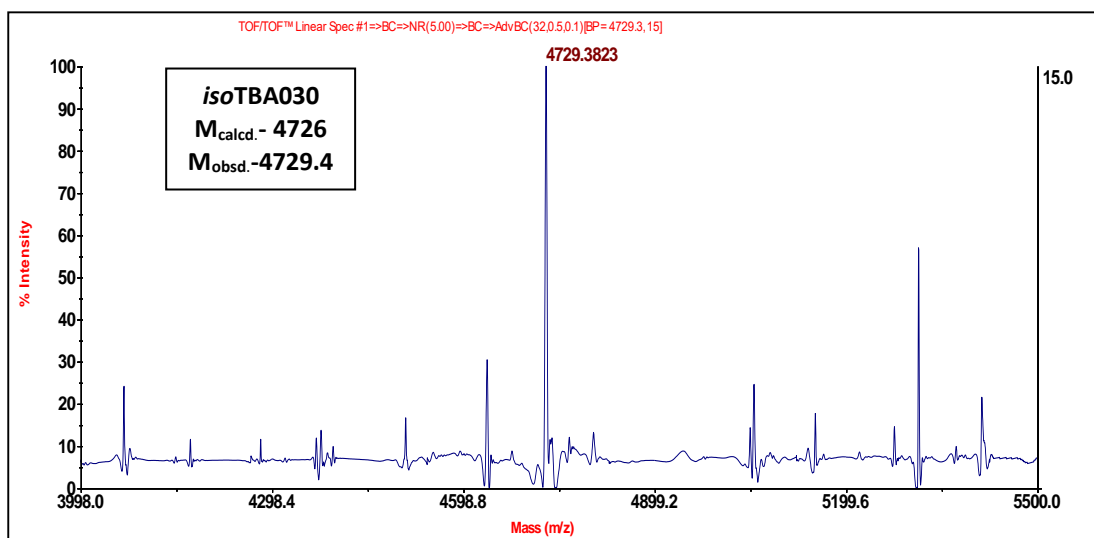


MALDI-TOF spectra of TBA oligomers





MALDI-TOF spectra of *iso*TBA oligomers



4.9 References

1. Dougherty, J. P.; Rizzo, C. J.; Breslow, R., Oligodeoxynucleotides that contain 2', 5' linkages: synthesis and hybridization properties. *J. Am. Chem. Soc.* **1992**, *114* (15), 6254-6255.
2. (a) Sheppard, T. L.; Breslow, R. C., Selective Binding of RNA, but Not DNA, by Complementary 2',5'-Linked DNA. *J. Am. Chem. Soc.* **1996**, *118* (40), 9810-9811; (b) Prakash, T. P.; Jung, K.-E.; Switzer, C., RNA recognition by the 2'-structural isomer of DNA. *Chem. Commun.* **1996**, (15), 1793-1794; (c) Jung, K.-E.; Switzer, C., 2', 5'-DNA containing guanine and cytosine forms stable duplexes. *J. Am. Chem. Soc.* **1994**, *116* (14), 6059-6061; (d) Giannaris, P. A.; Damha, M. J., Oligoribonucleotides containing 2', 5'-phosphodiester linkages exhibit binding selectivity for 3', 5'-RNA over 3', 5'-ssDNA. *Nucleic Acids Res.* **1993**, *21* (20), 4742-4749; (e) Premraj, B. J.; Raja, S.; Bhavesh, N. S.; Shi, K.; Hosur, R. V.; Sundaralingam, M.; Yathindra, N., Solution structure of 2', 5' d (G4C4) Relevance to topological restrictions and nature's choice of phosphodiester links. *Eur. J. Biochem.* **2004**, *271* (14), 2956-2966; (f) Erande, N.; Gunjal, A. D.; Fernandes, M.; Gonnade, R.; Kumar, V. A., Synthesis and structural studies of S-type/N-type-locked/frozen nucleoside analogues and their incorporation in RNA-selective, nuclease resistant 2'-5' linked oligonucleotides. *Org. Biomol. Chem.* **2013**, *11* (5), 746-757.
3. Sawai, H.; Seki, J.; Ozaki, H., Comparative Studies of Duplex and Triplex Formation of 2'-5' and 3'-5' Linked Oligoribonucleotides. *J. Biomol. Struct. Dyn.* **1996**, *13* (6), 1043-1051.
4. Damha, M. J.; Noronha, A., Recognition of nucleic acid double helices by homopyrimidine 2', 5'-linked RNA. *Nucleic Acids Res.* **1998**, *26* (22), 5152-5156.
5. Rhodes, D.; Lipps, H. J., G-quadruplexes and their regulatory roles in biology. *Nucleic Acids Res.* **2015**, *43* (18), 8627-8637.
6. Qi, H.; Lin, C.-P.; Fu, X.; Wood, L. M.; Liu, A. A.; Tsai, Y.-C.; Chen, Y.; Barbieri, C. M.; Pilch, D. S.; Liu, L. F., G-Quadruplexes Induce Apoptosis in Tumor Cells. *Cancer Res.* **2006**, *66* (24), 11808-11816.
7. Griffin, L.; Tidmarsh, G.; Bock, L.; Toole, J.; Leung, L., In vivo anticoagulant properties of a novel nucleotide-based thrombin inhibitor and demonstration of regional anticoagulation in extracorporeal circuits. *Blood* **1993**, *81* (12), 3271-3276.

8. Wyatt, J. R.; Vickers, T. A.; Roberson, J. L.; Buckheit, R. W., Jr.; Klimkait, T.; DeBaets, E.; Davis, P. W.; Rayner, B.; Imbach, J. L.; Ecker, D. J., Combinatorially selected guanosine-quartet structure is a potent inhibitor of human immunodeficiency virus envelope-mediated cell fusion. *Proc. Natl. Acad. Sci. USA* **1994**, *91* (4), 1356-1360.
9. Datta, B.; Bier, M. E.; Roy, S.; Armitage, B. A., Quadruplex Formation by a Guanine-Rich PNA Oligomer. *J. Am. Chem. Soc.* **2005**, *127* (12), 4199-4207.
10. Sacca, B.; Lacroix, L.; Mergny, J.-L., The effect of chemical modifications on the thermal stability of different G-quadruplex-forming oligonucleotides. *Nucleic Acids Res.* **2005**, *33* (4), 1182-1192.
11. Joachimi, A.; Benz, A.; Hartig, J. S., A comparison of DNA and RNA quadruplex structures and stabilities. *Bioorg. Med. Chem.* **2009**, *17* (19), 6811-6815.
12. Zhang, Y.; Hong, H.; Cai, W., Tumor-targeted drug delivery with aptamers. *Curr. Med. Chem.* **2011**, *18* (27), 4185-4194.
13. Bock, L. C.; Griffin, L. C.; Latham, J. A.; Vermaas, E. H.; Toole, J. J., Selection of single-stranded DNA molecules that bind and inhibit human thrombin. *Nature* **1992**, *355* (6360), 564.
14. Russo Krauss, I.; Merlino, A.; Randazzo, A.; Novellino, E.; Mazzarella, L.; Sica, F., High-resolution structures of two complexes between thrombin and thrombin-binding aptamer shed light on the role of cations in the aptamer inhibitory activity. *Nucleic Acids Res.* **2012**, *40* (16), 8119-8128.
15. (a) Bonifacio, L.; Church, F. C.; Jarstfer, M. B., Effect of locked-nucleic acid on a biologically active G-quadruplex. A structure-activity relationship of the thrombin aptamer. *Int. J. Mol. Sci.* **2008**, *9* (3), 422-433; (b) Aviñó, A.; Mazzini, S.; Ferreira, R.; Gargallo, R.; Marquez, V. E.; Eritja, R., The effect on quadruplex stability of North-nucleoside derivatives in the loops of the thrombin-binding aptamer. *Bioorg. Med. Chem.* **2012**, *20* (14), 4186-4193; (c) Peng, C. G.; Damha, M. J., G-quadruplex induced stabilization by 2'-deoxy-2'-fluoro-D-arabinonucleic acids (2'F-ANA). *Nucleic Acids Res.* **2007**, *35* (15), 4977-4988.
16. Zaitseva, M.; Kaluzhny, D.; Shchylkina, A.; Borisova, O.; Smirnov, I.; Pozmogova, G., Conformation and thermostability of oligonucleotide d

- (GGTTGGTGTGGTTGG) containing thiophosphoryl internucleotide bonds at different positions. *Biophys. Chem.* **2010**, *146* (1), 1-6.
17. He, G.-X.; Williams, J. P.; Postich, M. J.; Swaminathan, S.; Shea, R. G.; Terhorst, T.; Law, V. S.; Mao, C. T.; Sueoka, C.; Coutré, S.; Bischofberger, N., In Vitro and in Vivo Activities of Oligodeoxynucleotide-Based Thrombin Inhibitors Containing Neutral Formacetal Linkages. *J. Med. Chem.* **1998**, *41* (22), 4224-4231.
 18. Varizhuk, A. M.; Tsvetkov, V. B.; Tatarinova, O. N.; Kaluzhny, D. N.; Florentiev, V. L.; Timofeev, E. N.; Shchyolkina, A. K.; Borisova, O. F.; Smirnov, I. P.; Grokhovsky, S. L., Synthesis, characterization and in vitro activity of thrombin-binding DNA aptamers with triazole internucleotide linkages. *Eur. J. Med. Chem.* **2013**, *67*, 90-97.
 19. Tang, C.-F.; Shafer, R. H., Engineering the quadruplex fold: nucleoside conformation determines both folding topology and molecularity in guanine quadruplexes. *J. Am. Chem. Soc.* **2006**, *128* (17), 5966-5973.
 20. Gunjal, A. D.; Fernandes, M.; Erande, N.; Rajamohanan, P. R.; Kumar, V. A., Functional *iso*DNA aptamers: modified thrombin binding aptamers with a 2'-5'-linked sugar-phosphate backbone (*iso*TBA). *Chem. Commun.* **2014**, *50* (5), 605-607.
 21. Aher, M. N.; Erande, N. D.; Fernandes, M.; Kumar, V. A., Unimolecular antiparallel G-quadruplex folding topology of 2'-5'-*iso*TBA sequences remains unaltered by loop composition. *Org. Bio. Chem.* **2015**, *13* (48), 11696-11703.
 22. Polak, M.; Manoharan, M.; Inamati, G. B.; Plavec, J., Tuning of conformational preorganization in model 2',5'- and 3',5'-linked oligonucleotides by 3'- and 2'-O-methoxyethyl modification. *Nucleic Acids Res.* **2003**, *31* (8), 2066-2076.
 23. Gait, M. J., *Oligonucleotide synthesis: a practical approach*. Rev. repr. ed.; Oxford: IRL press: 1984.
 24. Karsisiotis, A. I.; Hessari, N. M. a.; Novellino, E.; Spada, G. P.; Randazzo, A.; Webba da Silva, M., Topological characterization of nucleic acid G-quadruplexes by UV absorption and circular dichroism. *Angew. Chem., Int. Ed. Engl.* **2011**, *50* (45), 10645-10648.
 25. Baldrich, E.; O'Sullivan, C. K., Ability of thrombin to act as molecular chaperone, inducing formation of quadruplex structure of thrombin-binding aptamer. *Anal. Biochem.* **2005**, *341* (1), 194-197.

26. Nagatoishi, S.; Tanaka, Y.; Tsumoto, K., Circular dichroism spectra demonstrate formation of the thrombin-binding DNA aptamer G-quadruplex under stabilizing-cation-deficient conditions. *Biochem. Biophys. Res. Commun.* **2007**, *352* (3), 812-817.
27. Mann, K. G.; Jenny, R. J.; Krishnaswamy, S., Cofactor proteins in the assembly and expression of blood clotting enzyme complexes. *Annu. Rev. Biochem.* **1988**, *57*, 915-956.
28. Kandimalla, E. R.; Manning, A.; Zhao, Q.; Shaw, D. R.; Byrn, R. A.; Sasisekharan, V.; Agrawal, S., Mixed backbone antisense oligonucleotides: design, biochemical and biological properties of oligonucleotides containing 2'-5'-ribo- and 3'-5'-deoxyribonucleotide segments. *Nucleic Acids Res.* **1997**, *25* (2), 370-378.
29. Cao, Z.; Huang, C.-C.; Tan, W., Nuclease resistance of telomere-like oligonucleotides monitored in live cells by fluorescence anisotropy imaging. *Anal. Chem.* **2006**, *78* (5), 1478-1484.

1. **Aher, M. N.;** Erande, N. D.; Fernandes, M.; Kumar, V. A., Unimolecular antiparallel G-quadruplex folding topology of 2'-5'-isoTBA sequences remains unaltered by loop composition. *Org. Biomol. Chem.* **2015**, *13* (48), 11696-11703.
2. **Aher, M. N.;** Erande, N. D.; Kumar, V. A.; Fernandes, M.; Gonnade, R. G., Influence of fluorine substitution on the molecular conformation of 3'-deoxy-3'-fluoro-5-methyluridine. *Acta Crystallogr., Sect. C: Struct. Chem.* **2020**, *76* (4), 346-352.
3. Varada, M.; **Aher, M.;** Erande, N.; Kumar, V. A.; Fernandes, M., Methoxymethyl Threofuranosyl Thymidine (4'-MOM-TNA-T) at the T7 Position of the Thrombin-Binding Aptamer Boosts Anticoagulation Activity, Thermal Stability, and Nuclease Resistance. *ACS Omega* **2020**, *5* (1), 498-506.
4. Awachat, R.; Wagh, A. A.; **Aher, M.;** Fernandes, M.; Kumar, V. A., Favorable 2'-substitution in the loop region of a thrombin-binding DNA aptamer. *Bioorg. Med. Chemistry Lett.* **2018**, *28* (10), 1765-1768.
5. Effect of 2'-5' and 3'-5' linkages in the loop region of in TBA and isoTBA respectively, on G quadruplex stability and function. *Manuscript under preparation.*
6. S/N-type frozen 3'-deoxy 3'-fluoro nucleosides in nongenetic 2'-5' linked thrombin binding aptamer (isoTBA). *Manuscript under preparation*

Cite this: *Org. Biomol. Chem.*, 2015, **13**, 11696

Unimolecular antiparallel G-quadruplex folding topology of 2'-5'-isoTBA sequences remains unaltered by loop composition†

Manisha N. Aher, Namrata D. Erande, Moneesha Fernandes and Vajjayanti A. Kumar*

Received 16th September 2015,
Accepted 9th October 2015
DOI: 10.1039/c5ob01923k
www.rsc.org/obc

A 2'-5'-linked isoTBA 15 mer sequence with (232) loop composition formed stable antiparallel quadruplex structures similar to the SELEX derived 15 mer TBA sequence with (232) loop composition. A parallel versus antiparallel topology of 3'-5'-G-quadruplexes is largely dictated by the loop length, and it is known that the truncated loops favour parallel quadruplexes. In contrast to TBA, systematic reduction of the loop length in isoTBA from (232) to (222), (131) or even (111) did not alter the antiparallel topology of the resulting 14 mer, 13 mer and 11 mer G-rich modified isoTBA-like sequences.

Introduction

G-quadruplexes have been gaining increasing attention in the recent past because of their abundance *in vivo* and their role in meiosis, telomere maintenance, gene regulation¹ and also as targets for cancer treatment.² The G-quadruplex structures, their folding mechanism, protein binding to the quadruplex structures and ligands targeting the quadruplex over duplex were extensively studied by various experimental and theoretical studies.³ Many therapeutically important G-quadruplex aptamers have been derived by SELEX and show high affinity towards biologically important targets. Examples include the thrombin-binding aptamer (TBA), anti-cancer and anti-HIV aptamers.⁴⁻⁶ The high affinity with the target is derived from the fitting of the three dimensional shape of the quadruplex to the binding site and an array of electrostatic/hydrogen bonding interaction possibilities created in the loop region, as a consequence of the folded structures.

The thrombin-binding aptamer (TBA; d[GGTGGTGTGG-TTGG]) binds to thrombin, a large protein involved in the blood coagulation cascade.⁷ The unimolecular structure of the G-quadruplex formed by TBA is well studied and is composed of two stacked G-quartets, two external TT loops and one central TGT loop, resulting in a chair-like conformation, stabilized by monovalent cations such as Na⁺ and K⁺.⁸ The TT loops were found to be sufficient to span the narrow grooves and the TGT loop sufficed to span the wider groove of the quadruplex.

The two TT loops of the quadruplex are currently believed to be interacting with thrombin anion exosite I in 1 : 1 stoichiometry.⁹ Several chemical modifications of TBA are reported in the literature in the view of further optimizing its binding to thrombin and also to improve its stability¹⁰ against cellular nucleases. The nucleotides in the loop region as well as the length of the loop control the topology and stability of the quadruplex structures in general and also in the case of TBA.^{11,12} Shorter loop lengths (less than total 6 nucleotides in the loop) are known to destabilize the intramolecular, antiparallel folded G-quadruplex of TBA and allow only the parallel intermolecular four-stranded G-quadruplex structures. As a consequence, the thrombin binding activity of TBA sequences in which the loops are short is adversely affected.¹² In contrast, releasing the rigidity in the loop region by introducing unlocked nucleic acid monomers at selective positions in the loop region of TBA, stabilized the intramolecular folded TBA quadruplex structure.¹³

The 3'-deoxy-2'-5'-linked non-genetic isoDNA (Fig. 1) exhibits high stability against cellular enzymes¹⁴ and therefore it could be a promising alternative nucleic acid for developing DNA therapeutics. Formation of duplex and triplex structures comprising isoDNA and complementary RNA are well-documented in the literature.^{15,23} In our previous study, we discovered that employing these nuclease resistant, homogeneous 2'-5' linkers in the sequence of TBA (isoTBA) could also form unimolecular folded G-quadruplex structures and could exhibit thrombin binding and anti-coagulant properties.¹⁶ In 3'-deoxy-isoDNA, the phosphodiester linkages are C2'-C5' instead of C3'-C5' linkages in native DNA (Fig. 1). This leads to an increase in the number of bonds between the O5' and 3'-O-phosphorus from six in DNA to seven in isoDNA. Also, the 2'-5' linkages maintain an extended backbone geometry, as

Organic Chemistry Division, CSIR-National Chemical Laboratory, Dr. Homi Bhabha Road, Pune 411008, India. E-mail: va.kumar@ncl.res.in
† Electronic supplementary information (ESI) available: Gel electrophoresis, representative CD-melting curves, CD-hysteresis curves, thrombin binding CD spectra and MALDI-TOF spectra. See DOI: 10.1039/c5ob01923k



Influence of fluorine substitution on the molecular conformation of 3'-deoxy-3'-fluoro-5-methyluridine

Manisha N. Aher,^{a,h} Namrata D. Erande,^c Vijayanti A. Kumar,^a Moneesha Fernandes^{a,b} and Rajesh G. Gonnade^{d,h*}^aOrganic Chemistry Division, CSIR-National Chemical Laboratory, Pune 411 008, India, ^bAcademy of Scientific and Innovative Research (AcSIR), Sector 19, Kailash Nagar, Ghaziabad, Uttar Pradesh 201002, India, ^cNational Centre for Cell Science, SPPU University Campus, Pune 411 007, India, and ^dCenter for Materials Characterization, CSIR-National Chemical Laboratory, Homi Bhabha Road, Pune 411 008, India. *Correspondence e-mail: rg.gonnade@ncl.res.in

Received 3 January 2020

Accepted 4 March 2020

Edited by A. Sarjeant, Bristol-Myers Squibb, New Brunswick, NJ, USA

Keywords: fluoro nucleoside; sugar puckering; pseudorotation parameter; crystal structure; uridine.

CCDC reference: 1988101

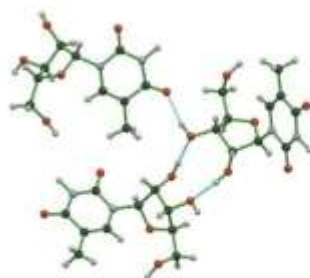
Supporting information: this article has supporting information at journals.iucr.org/c

Fluorine substitutions on the furanose ring of nucleosides are known to strongly influence the conformational properties of oligonucleotides. In order to assess the effect of fluorine on the conformation of 3'-deoxy-3'-fluoro-5-methyluridine (^RT^F), C₁₀H₁₃FN₂O₅, we studied its stereochemistry in the crystalline state using X-ray crystallography. The compound crystallizes in the chiral orthorhombic space group *P*2₁2₁2₁ and contains two symmetry-independent molecules (*A* and *B*) in the asymmetric unit. The furanose ring in molecules *A* and *B* adopts conformations between envelope (²E, 2'-*endo*, *P* = 162°) and twisted (²T₃, 2'-*endo* and 3'-*exo*, *P* = 180°), with pseudorotation phase angles (*P*) of 164.3 and 170.2°, respectively. The maximum puckering amplitudes, *v*_{max}, for molecules *A* and *B* are 38.8 and 36.1°, respectively. In contrast, for 5-methyluridine (^RT^{OH}), the value of *P* is 21.2°, which is between the ³E (3'-*endo*, *P* = 18.0°) and ³T₄ (3'-*endo* and 4'-*exo*, *P* = 36°) conformations. The value of *v*_{max} for ^RT^{OH} is 41.29°. Molecules *A* and *B* of ^RT^F generate respective helical assemblies across the crystallographic 2₁-screw axis through classical N—H···O and O—H···O hydrogen bonds supplemented by C—H···O contacts. Adjacent parallel helices of both molecules are linked to each other *via* O—H···O and O···π interactions.

1. Introduction

The five-membered furanose ring (C1'—C2'—C3'—C4'—O4'), which is centrally located in the sugar phosphate chains of nucleic acids, is not planar due to the flexibility offered by the C—C and C—O single bonds. This leads to two major conformations of the furanose ring, namely C2'-*endo* and C3'-*endo*. The C2' atom is *endo* when it lies on the same side of the ring plane as C5' and the sugar puckering is called south (S), whereas C3' is *endo* when it lies on the same side of the ring plane as C5' and the sugar puckering is called north (N) (Altona & Sundaralingam, 1972) (Fig. 1). Besides these two major conformations, the sugar can exist in a range of conformations, from E (envelope) to T (twist), according to the pseudorotational cycle of the furanose ring (see Fig. S5 in the supporting information) (Mathé & Périgaud, 2008). The conformation of the furanose ring can be described easily when the values of the pseudorotation phase angles (*P*) in combination with the maximum puckering amplitudes (*v*_{max}) (Hall *et al.*, 1970) are plotted in the pseudorotational cycle. The values of the phase angles are given in multiples of 36° and vary from 0 to 360°.

A switchover from S to N or *vice versa* of the furanose ring produces major structural changes in the naturally occurring



© 2020 International Union of Crystallography



Methoxymethyl Threofuranosyl Thymidine (4'-MOM-TNA-T) at the T7 Position of the Thrombin-Binding Aptamer Boosts Anticoagulation Activity, Thermal Stability, and Nuclease Resistance

Manojkumar Varada,^{§,§} Manisha Aher,^{§,§,#} Namrata Erande,^{§,#} Vaijayanti A. Kumar,^{§,#} and Moneesha Fernandes^{*,§,#}

[§]Organic Chemistry Division, CSIR-National Chemical Laboratory, Dr. Homi Bhabha Road, Pune 411008, India

[#]Academy of Scientific and Innovative Research (AcSIR), Ghaziabad 201002, India

Supporting Information

ABSTRACT: The synthesis of 4'-methoxymethyl threofuranosyl (4'-MOM-TNA) thymidine and derived oligomers of the G-rich thrombin-binding aptameric (TBA) sequence is reported. The G-quadruplex stability, anticoagulation activity, and the enzymatic stability of these oligomers bearing the 2'-3'-phosphodiester backbone as single substitutions in the loop regions are studied. Amongst all the oligomers, TBA-7T bearing the 4'-MOM-TNA unit at the T7 position formed a quadruplex with the highest thermal stability. It also resulted in enhanced anticlotting activity that allowed a one-third reduction in the dose, relative to TBA. Further, TBA-7T exhibited enhanced nuclease resistance properties to both endo- and exonucleases.



INTRODUCTION

The pentadecameric thrombin-binding aptamer¹ (TBA, 5'-G¹G²T³T⁴G⁵G⁶T⁷G⁸T⁹G¹⁰G¹¹T¹²T¹³G¹⁴G¹⁵) has been extensively studied and is well characterized. TBA folds into an intramolecular antiparallel G-quadruplex that consists of two G-quartets that are connected by two TT loops and a central TGT loop in a chair-like conformation. TBA is reported to interact with its target, thrombin, mainly through its loop regions, particularly the TT loops.² Owing to its promising potential as a heparin alternative in medicine, it has attracted the attention of researchers who strive to improve its nuclease- and thermal stability properties.^{3–5} However, most of the modifications failed to improve its thermal stability. Among the notable exceptions are the 3'-3' polarity inversion at the 3'-end,⁶ 5-fluoro-2'-deoxyuridine,⁷ and the unlocked nucleic acid (UNA),⁸ which also offered increased resistance to degradation by nucleases. UNA, by virtue of its "unlocked" flexible nature, could help to ease the strain in the loop regions of TBA and had a maximum stabilizing effect (T_m enhancement of 4 °C) and anticoagulation activity when incorporated at the T7 position in the TGT loop of TBA.⁸

We earlier reported the 2'-5'-phosphodiester-linked backbone (isoDNA, Figure 1), which also has increased nuclease resistance in comparison to the native 3'-5'-phosphodiester, in TBA.⁹ In contrast to other reports where backbone modifications were reported to significantly impact the structural topology of the resulting quadruplex,¹⁰ we found that the 2'-5'-linked isoTBA was able to retain the unimolecular antiparallel quadruplex topology of TBA and additionally exhibit thrombin-binding and anticoagulant properties⁹ even when the total number of loop residues was significantly reduced.¹¹ The 2'-3'-phosphodiester backbone

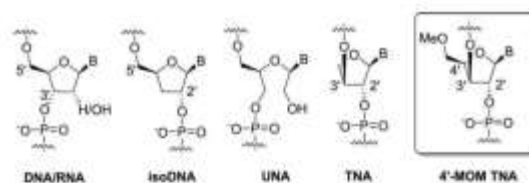


Figure 1. Structures of natural DNA/RNA, isoDNA, UNA, TNA, and 4'-MOM-TNA of the present work.

was reported in the (1, α -threofuranosyl nucleic acid (TNA)¹² (Figure 1). TNA was demonstrated to be capable of informational self-pairing and specifically hydrogen-bonding with complementary DNA and RNA. The quasi-diaxial nature of the 2'-3'-phosphodiester link ensured that the shortened 5-atom internucleotide distance was well tolerated in the formation of duplexes,¹² tertiary structures,¹³ and quadruplexes.¹⁴ Although S-type sugar pucker as in DNA are preferred in the loop regions of TBA over the N-type pucker, the shorter five-atom internucleotide link in TNA makes the backbone compact, similar to that seen in DNA with the S-type of sugar pucker, as reported in the X-ray structure of a B-type DNA duplex incorporating a single TNA residue, where only minimum perturbation of the backbone around the TNA residue¹⁵ was observed. Proposing to combine the advantages of TNA and a methoxy substituent, we envisioned the 4'-

Received: September 17, 2019

Accepted: December 11, 2019

Published: December 26, 2019



Contents lists available at ScienceDirect

Bioorganic & Medicinal Chemistry Letters

journal homepage: www.elsevier.com/locate/bmcl

Favorable 2'-substitution in the loop region of a thrombin-binding DNA aptamer



Ragini Awachat, Atish A. Wagh, Manisha Aher, Moneesha Fernandes*, Vaijayanti A. Kumar*

Organic Chemistry Division, CSIR-National Chemical Laboratory, Homi Bhabha Road, Pashan, Pune 411008, India
Academy of Scientific and Innovative Research (ACSIr), CSIR-NCL Campus, Pune 411008, India

ARTICLE INFO

Article history:

Received 26 February 2018

Revised 6 April 2018

Accepted 11 April 2018

Available online 13 April 2018

Keywords:

Thrombin binding aptamer

G-quadruplex

2'-O-methyl ribo-uridine

Fibrin polymerization

Thrombin time

ABSTRACT

Simple 2'-OMe-chemical modification in the loop region of the 15mer G-rich DNA sequence GGITGGTCTGGTTGG is reported. The G-quadruplex structure of this thrombin-binding aptamer (TBA), is stabilized by single modifications (T → 2'-OMe-U), depending on the position of the modification. The structural stability also renders significantly increased inhibition of thrombin-induced fibrin polymerization, a process closely associated with blood-clotting.

© 2018 Elsevier Ltd. All rights reserved.

The 15mer d(G₁G₂T₃T₄G₅G₆T₇G₈T₉G₁₀G₁₁T₁₂T₁₃G₁₄G₁₅) oligonucleotide is known as the thrombin-binding aptamer (TBA).¹ Its solution structure was solved by NMR studies² and 3D structure in the presence of K⁺ was elucidated by X-ray studies.³ The unimolecular G-quadruplex structure comprises two stacked G-quartets connected by two lateral thymine loops (T₇T₄ and T₁₂T₁₃) and a central (T₇G₈T₉) loop in a chair conformation (Fig. 1).

The binding of the aptamer to the protein, thrombin, is primarily due to its propensity to fold into the distinct 3-dimensional form of a G-quadruplex in the presence of univalent cations such as Na⁺ or K⁺. X-ray structural studies have shown that the lateral TT loops of the quadruplex are involved in binding to the charged surface of Exosite I in thrombin.³ This recent corrected crystal structure of thrombin complexed with TBA revealed an extended interface between thrombin Exosite I and the two TT loops of the G-quadruplex, and minimum interactions of thrombin with the TGT loop in TBA.³ The nucleotides in TBA are known to maintain the South (S) sugar pucker.⁴ The quadruplex structure of TBA is therefore highly sensitive to backbone modifications that affect the sugar pucker of the nucleosides.⁵ The fully modified ribo- or 2'-OMe-ribo-substituted TBA forms parallel, tetramolecular G-quadruplex structures⁶ that do not bind to thrombin. The TBA

sequence with a PNA backbone, on the other hand, could fold into the chair conformation of the TBA DNA G-quadruplex.⁷ The 2'-5'-linked isoTBA reported by us was also able to form this unimolecular G-quadruplex structure^{8,9} and could further show the chaperone effect by thrombin.¹⁰ Some designed modifications that stabilize the TBA G-quadruplex structure were reported recently,^{11–17} including introduction of UNA,¹¹ modified GNA,¹² 2'-fluoro-uridine,¹³ 2'-fluoro-2'-ara-uridine,^{14,15} 5-fluoro-2'-deoxyuridine¹⁶ substitutions or an abasic 3-C-spacer¹⁷ in the loop regions (Fig. 2). UNA substitution in the 15mer sequence was studied systematically by substituting a single position at a time.¹¹ Of the several sequences synthesized, only the one with the modification at T7 position improved the G-quadruplex stability and showed significant increase in thrombin time. Very recently it was also shown that an abasic C3-spacer in the TGT loop improved the stability of the TBA G-quadruplex and also improved thrombin-binding and anti-thrombin activity.¹⁷ It may be possible that these acyclic analogues adopt a suitable presentation other than that seen with the S-type sugar pucker of DNA in the loop region, thereby favorably affecting the overall geometry and resulting in quadruplex stabilization.

It was shown earlier that 2'-fluoro-substituted ara-uridine where the sugar adopts an intermediate S-type-envelope structure, stabilized the TBA quadruplex structure when used as a replacement in the loop, as well as, in G-tetrad-forming regions.^{14,15} It has been also shown that the 2'-ribo-fluoro-uridine with N-type sugar geometry when substituted in the TGT loop region, improved

* Corresponding authors at: Organic Chemistry Division, CSIR-National Chemical Laboratory, Homi Bhabha Road, Pashan, Pune 411008, India.

E-mail addresses: m.fernandes@ncl.res.in (M. Fernandes), va.kumar@ncl.res.in (V.A. Kumar).<https://doi.org/10.1016/j.bmcl.2018.04.027>

0960-894X/© 2018 Elsevier Ltd. All rights reserved.

Erratum

Erratum
